Czech University of Life Sciences, Prague
and
PC-Progress, s.r.o., Prague

Proceedings of the 4th International Conference

HYDRUS Software Applications to Subsurface Flow and Contaminant Transport Problems

March 21-22 2013

Prague, Czech Republic

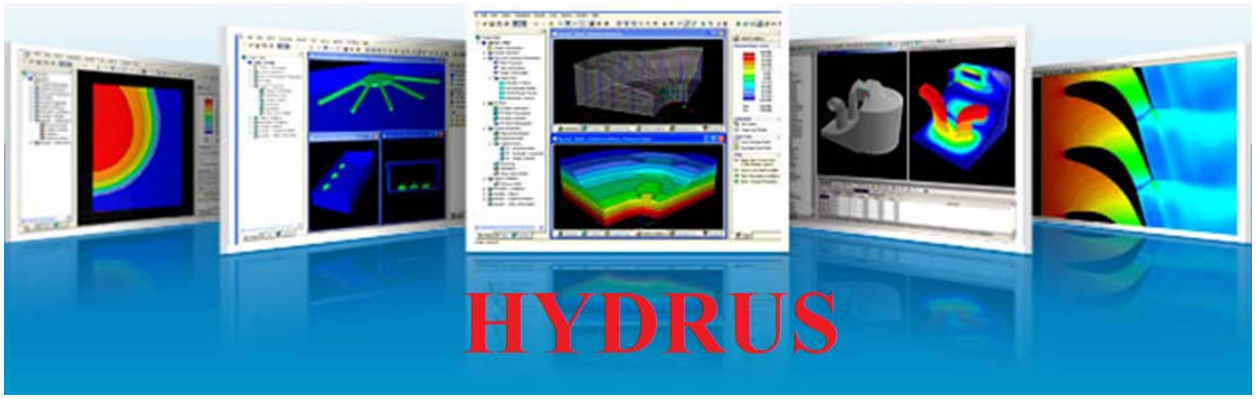

Czech University of Life Sciences, Prague
Faculty of Agrobiology, Food and Natural Resources
Kamýcká 129
165 21 Praha 6 – Suchdol
Czech Republic
http://www.af.czu.cz/en/

PC-Progress s.r.o.
Korunní 2569/108a
Prague, 101 00
Czech Republic
http://www.pc-progress.com/en/Default.aspx

ISBN: 978-80-213-2380-3

Table of Content

Please reference the **proceedings** as follows:
Šimůnek, J., M. Th. van Genuchten, and R. Kodešová (eds.), *Proceedings of the 4th International Conference "HYDRUS Software Applications to Subsurface Flow and Contaminant Transport Problems"*, March 21-22, 2013, Dept. of Soil Science and Geology, Czech University of Life Sciences, Prague, Czech Republic, ISBN: 978-80-213-2380-3, pp. 404, 2013.

Please reference the **individual papers** as follows (adjust highlighted text as needed):
Authors, Title, *Proceedings of the 4th International Conference "HYDRUS Software Applications to Subsurface Flow and Contaminant Transport Problems"*, edited by J. Šimůnek, M. Th. van Genuchten, and R. Kodešová, March 21-22, 2013, Dept. of Soil Science and Geology, Czech University of Life Sciences, Prague, Czech Republic, ISBN: 978-80-213-2380-3, pp. ??-??, 2013.

Preface

These proceedings document presentations given at the Fourth International Conference on "HYDRUS Software Applications to Subsurface Flow and Contaminant Transport Problems," held in Prague, Czech Republic, March 21-22, 2013. Previous conferences in this series were held in Utrecht in 2005, in Prague in 2008, and in Tokyo, also in 2008. The conferences focus on the development and application of advanced numerical models simulating variably-saturated flow, heat transport, and the transport of various contaminants or other solutes (such as nutrients, pesticides, heavy metals, radionuclides, and pathogenic microorganisms) in soils and groundwater. The conferences are designed to bring together users of the HYDRUS family of codes, as well as of related software, to review and exchange information on various aspects of the codes, future enhancements of the software, and their application to a range of soil, environmental, hydrological, ecological and agricultural problems.

Since the first workshop in 2005, the community of HYDRUS users has been continuously growing as evidenced by the number of downloads (over 10,000 times each of the past several years) and visits to the HYDRUS web pages (on average several hundred each day). Hundreds of journal articles have now been published in which the HYDRUS codes have been used. Feedback from users such as those attending the HYDRUS conference has been extremely important in identifying particular strengths and weaknesses of the codes, and for defining additional processes or features that should be included in the models. Feedback is also continuously obtained from several discussion forums on the HYDRUS website, where users can submit questions or suggestions about the models.

These proceedings contain 41 contributions from mostly HYDRUS software users, covering a range of topics from the very fundamental to important practical applications. These proceedings, as well as those of previous HYDRUS conferences, can be downloaded freely from the HYDRUS website at http://www.pc-progress.com.

We would like to thank the Czech University of Life Sciences and PC-Progress for hosting the conference in Prague. Our appreciation goes also to the many participants who travelled to Prague from all continents. Special thanks are due to those that contributed to these proceedings. Published studies in which the codes have been used always provide useful information for new users. We believe that the software tools have served, and will continue to serve, an important role in especially vadose zone research.

The Editors

Jirka Šimůnek
Rien van Genuchten
Radka Kodešová

The HPx Reactive Transport Models: Summary of Recent Developments and Applications

Diederik Jacques[1], Jiří Šimůnek[2], Dirk Mallants[3], and Martinus Th. van Genuchten[4]

[1]*Performance Assessments, Institute of Environment, Health and Safety, Belgian Nuclear Research Centre, Mol, Belgium, djacques@sckcen.be*
[2]*Department of Environmental Sciences, University of California Riverside, CA, USA*
[3]*Land and Water, CSIRO, Adelaide, Australia*
[4] *Department of Mechanical Engineering, Federal University of Rio de Janeiro, UFRJ, Rio de Janeiro, RJ, Brazil*

Abstract

The HPx reactive transport codes were developed to simulate flow and transport processes in variably-saturated porous media subject to a variety of low-temperature geochemical processes. The codes combine the HYDRUS models for flow and transport (HYDRUS-1D version 4.16, and HYDRUS 2D/3D version 2.02) with the generic thermodynamic and kinetic model PHREEQC-2.17. As such, HPx expands significantly the capabilities of the individual codes for multicomponent one-dimensional (HP1) and two-dimensional (HP2) transport problems. This paper provides a brief summary of recent developments and applications of HPx, such as (i) the inclusion of gas diffusion, (ii) extension to two-dimensional problems, (iii) inverse optimization, and (iv) feedback between changes in geochemical variables and transport properties. HPx is a flexible tool which can be applied to flow and transport problems involving relatively complex geochemical processes. A typical example is the geochemistry of mercury, which in a contaminated soil may be present in different forms and phases.

1. Introduction

The fate and transport of nutrients and contaminants in variably-saturated porous media is influenced by a range of interacting physical, chemical, and biological processes (Jacques et al., 2008). Transport in soil systems is often further complicated by a multitude of coupled biogeochemical reactions, the presence of spatially and temporally variable flow velocities, and spatial heterogeneities at different scales (for a review see Mallants et al., 2011). A numerical tool that integrates these various processes offers unique possibilities for advanced model building and improving process understanding, ranging from sensitivity analyses of processes and parameters, designing experiments, hypothesis testing by running virtual laboratories, conceptual model validation using experimental data, and evaluation of different management or remediation practices. Based on the HYDRUS suite of models for one-dimensional (Šimůnek et al., 2008) and multi-dimensional problems (Šimůnek et al., 2011), and the generic thermodynamic and kinetic geochemical model PHREEQC (Parkhurst and Appelo 1999), the HP1 (Jacques and Šimůnek, 2005) and HP2 (Šimůnek et al., 2012) modules were developed to handle water flow, multi-component solute transport, heat transfer, and biogeochemical reactions for a range of environmental soil quality applications. In this paper we provide a brief summary of recent developments and various applications of the HPx modules.

2. Conceptual Basis of HPx

The HPx codes considerably extend upon the capabilities of the individual codes. For example, the full range of water flow and solute transport formulations available in the standard HYDRUS codes are now combined with the different geochemical models available in PHREEQC.

Contrary to the conventional advection-dispersion-reaction equations forming the basis of the standard HYDRUS-1D and HYDRUS 2D/3D codes, the HPx modules account for interactions between different aqueous components to simulate intra-aqueous degradation, transformation or production processes, as well as heterogeneous equilibrium and kinetic processes. Using the capabilities of PHREEQC, HPx allows thermodynamic equilibrium calculations for

- aqueous speciation with different activity correction models (Davies, extended Truesdell-Jones, B-Dot, Pitzer, SIT - Specific ion Interaction Theory),
- multi-site ion exchange sites for different conventions (Gaines-Thomas, Vanselow, Gapon, or accounting for different selectivities considering the equivalent fraction occupied by the cation by the Rothmund-Kornfeld or the active fraction model),
- multi-site surface complexation sites with a non-electrostatic, the Dzombak and Morel, or the CD_MUSIC model and different options to calculate the composition of the diffuse double layer,
- mineralogical assemblages,
- solid-solutions consisting of multiple end members in an ideal solid solution or a binary non-ideal solid solution using the Guggenheim approach for determining the activity coefficients of the end members (Glynn and Reardon, 1990), and
- gas exchange.

Kinetic calculations are furthermore used to describe mineral dissolution/precipitation (e.g., based on transition state theories as shown by Lasaga (1998) and Brantley (2003)), non-equilibrium sorption processes, biogeochemical reactions, including first-order degradation networks (e.g., C-sequestration, see below), Monod kinetics, and Michaelis-Menten kinetics (e.g., solute-dependent plant uptake coupled with root exudation as shown by Raji et al. (2013)).

HPx allows one to select uniform or dual-porosity models for water flow, and uniform, mobile/immobile, or dual-porosity models for solute transport (Figure 1), as well as diffusive processes in the gas phase. As opposed to many other reactive transport codes, HPx also provides an option to account for the effects of root water and nutrient or contaminant uptake, including compensated water uptake and root growth (Šimůnek and Hopmans, 2008). Furthermore, the HPx simulators can accommodate complex boundary conditions including water and chemical exchange with streams and groundwater. Because geochemical gradients (e.g. changing redox conditions) are especially strong along such interfaces, only simulators that provide proper coupling between the various hydrological, geochemical and biological processes involved are capable of providing accurate system descriptions.

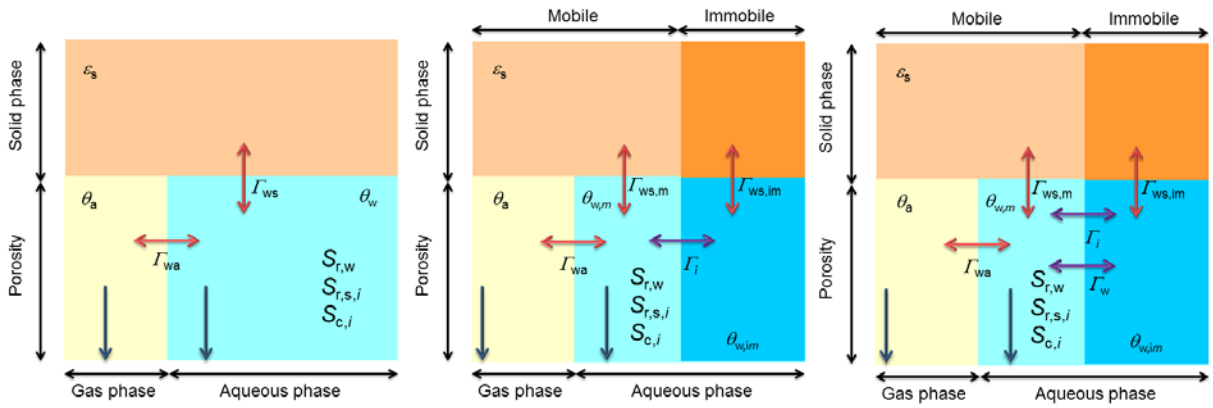

Figure 1. Schematic of possible coupled flow–transport–reaction models available within HPx: a uniform water flow and solute transport model (left), a uniform water flow model with a mobile/immobile solute transport model (middle), and a dual-porosity water flow model with a dual-porosity transport model (right). In the figure, ε_s is the volume fraction of solid phase, θ_a is the air content, θ_w is the water content, $\theta_{w,m}$ is the mobile water content, $\theta_{w,im}$ is the immobile water content, $S_{r,w}$ represents root water uptake, $S_{r,s,i}$ represents root uptake of solute i, $S_{c,i}$ is a sink or source term for solute i resulting from aqueous degradation or transformation processes, Γ_i and Γ_w are solute and water mass exchange terms between the mobile and the immobile water phases, respectively, and Γ_{wa}, Γ_{ws}, $\Gamma_{ws,m}$, and $\Gamma_{ws,im}$ are heterogeneous mass exchange terms between the water and air phases, the water and solid phases, the mobile water and solid phases, and the immobile water and the solid phases, respectively (after Šimůnek and van Genuchten, 2008).

3. Recent Developments and Applications

This section describes several recent improvements and applications of HPx. Additional examples are included in these proceedings for mercury transport and fate in soils (Leterme and Jacques, 2013), CO_2 production and transport in bare and planted mesocosmos (Thaysen et al., 2013), and active root nutrient uptake accounting for solution composition effects (Raji et al., 2013). The extension of the HPx code to two-dimensional flow and transport problems is described in another contribution to these proceedings (Šimůnek and Jacques, 2013).

3.1. Gas Diffusion Coupled to Organic Matter Degradation

A recent addition to HPx is diffusion of components in the gas phase. We present here an illustrative example that includes a process-based soil organic matter degradation model with three immobile organic carbon pools (litter, humus, and biomass), external input of C into the system, and an inorganic pool (CO_2). The model is based on previous work by Porporato et al. (2003) as illustrated in Figure 2 (see also Batlle-Aguilar et al., 2011). The model consists of a number of coupled nonlinear ordinary differential equations (see Fig. 2). There are several differences with the original model of Porporato et al. (2003). For example, water flow is modeled using the Richards equation with a root water uptake term (versus a probabilistic modeling approach in Porporato et al., 2003), while heat transport is also considered. Two inorganic pools are further included: $CO_{2(g)}$ and dissolved C, with thermodynamic exchange

between the two pools. We additionally consider the temperature dependence of rate parameters, and also included transport of inorganic C in the aqueous and gaseous phases.

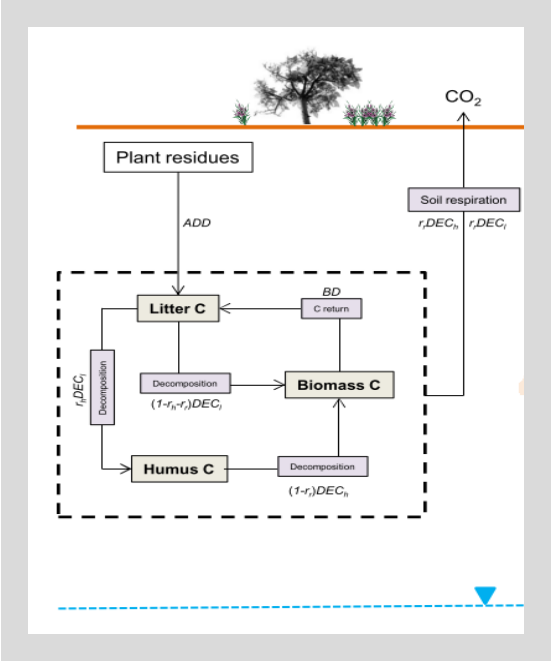

$$\frac{dC_l}{dt} = k_1 + k_2 C_b - k_3 C_b C_l$$

$$\frac{dC_h}{dt} = r_h k_3 C_b C_l - k_4 C_b C_h$$

$$\frac{dC_b}{dt} = (1 - r_h - r_r) k_3 C_b C_l + (1 - r_r) k_4 C_b C_h - k_2 C_b$$

$$\frac{dC_i}{dt} = r_r k_3 C_b C_l + r_r k_4 C_b C_h$$

C_l	Concentration of litter pool (gC / dm³)
C_h	Concentration of humus pool (gC / dm³)
C_b	Concentration of biomass pool (gC / dm³)
C_i	Concentration of CO_2 (gC / dm³)
k_1	Added litter
k_2	First-order biomass decay coefficient
k_3	First-order litter pool decomposition coefficient
k_4	First-order humus pool decomposition coefficient
r_r	Respiration coefficient
r_h	Humification coefficient

Figure 2. Schematic of the soil organic matter model (left), the set of coupled non-linear ordinary differential equations, and a list of symbols (after Porporato et al., 2003).

The rate parameters in Figure 2 for first-order decay and decomposition depend on the soil water content (described with the formulations of Porporato et al. (2003) and Manzoni and Porporato (2007)) and soil temperature. The latter effect is described using the temperature stress function from the RothC model of Coleman and Jenkinson (2005). The effects of water content and temperature stress were modeled as a multiplication of both factors. The combined effect of transient variations in the water content and temperature in a soil profile during one year on the stress factors is illustrated in Figure 3. Multiplication of the temperature and water content stress factors leads to considerable variation in organic matter decomposition rates during the year (Figure 3). Decomposition rates, relative to the reference rate value, range from zero (during dry periods near the surface) up to 3.5 (during wet and warm periods).

Evolutions of the organic C pools during one year are shown in Figure 4. The different curves follow smoothly the seasonal trends in temperature (and water content). The transformation and decomposition of the organic C pools is also reflected in the general trend of soil CO_2 gas. On the other hand, water content changes on the shorter temporal scale seem to influence variations in the soil CO_2 partial pressure.

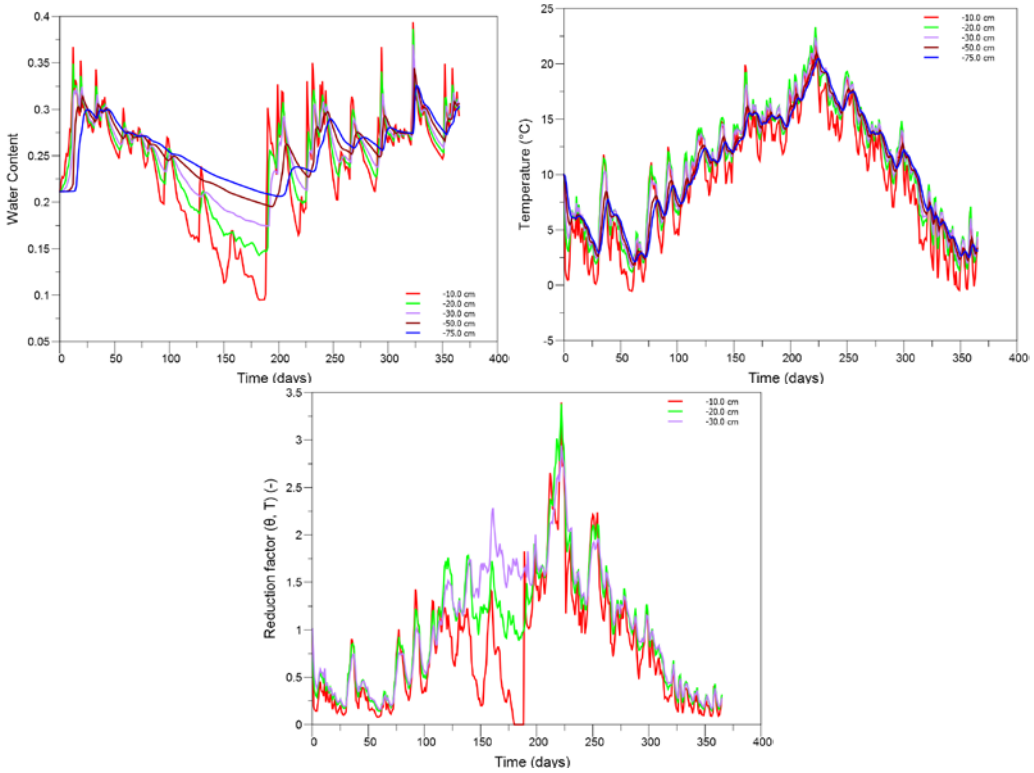

Figure 3. Temporal variations of water contents (top, left) and temperatures (top, right) in a soil profile during a one year simulation. Resulting stress factors (bottom) for the decay and decomposition rates.

3.2. Inverse Optimisation with UCODE

Coupled codes such as HP1 allow simultaneous optimization of various flow, transport, and geochemical parameters using inverse methods. A recent application with HP1 is given by Jacques et al. (2012), who combined HP1 with the general optimization tool UCODE (Poeter et al., 2005). The experimental data resulted from previously published laboratory experiments (Smiles and Smith, 2004) about the transport of major cations (Na, K, Mg, and Ca) during water absorption into horizontal soil columns, which were terminated at different times. Experimental data consisted of spatial distributions of the water content (θ), the Cl concentration, and total aqueous and sorbed concentrations of the major cations. In addition to selected flow and transport parameters (i.e., those describing the water retention and hydraulic conductivity functions, as well as the dispersivity), cation exchange coefficients for the major cations and the cation exchange capacity were estimated. Another new aspect of this study was that two different exchange models could be tested: the Gapon approach and a variable-selectivity model based on the Rothmund-Kornfeld approach. The latter enables stronger binding of a species at lower equivalent sorbed fractions (e.g., Bond, 1995). Calibrated profiles for Mg are shown in Figure 5. The Rothmund-Kornfeld approach was found to perform slightly better than the Gapon approach.

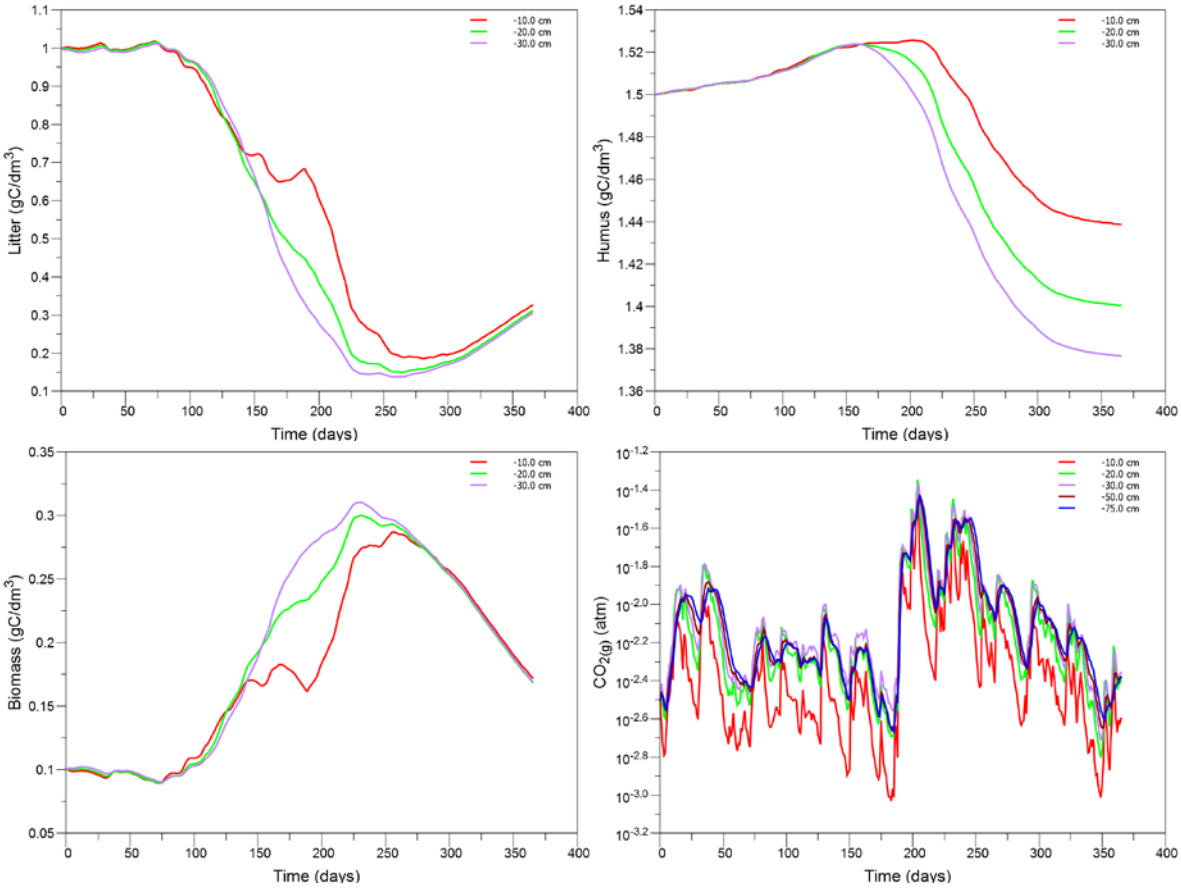

Figure 4. Time evolution of organic C pools (litter: top, left; humus: top, right; and biomass: bottom, left) and of gaseous CO_2 concentrations (in atm, bottom, right) in a soil profile during a one year simulation.

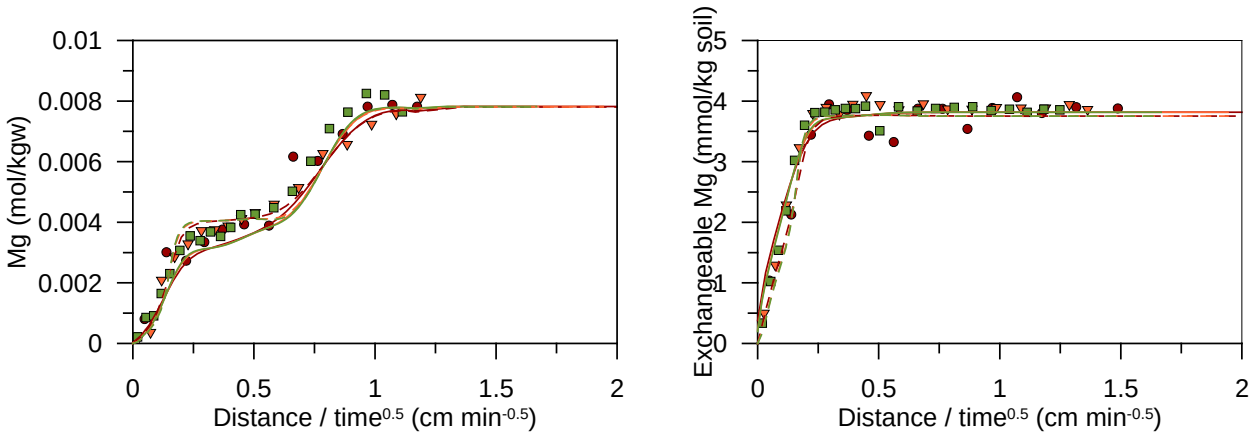

Figure 5. Simulated profiles of aqueous (left) and sorbed (right) Mg concentrations obtained with the Gapon approach [solid lines] or the Rohtmund-Kornfeld approach [dashed lines], compared with experimental data [symbols: circles - 36 min, triangles - 106 min, and squares - 144 min] from water absorption and solute transport experiments using piggery effluent (Smith and Smiles, 2004) (adapted from Jacques et al., 2012).

The HP1-UCODE study was supplemented with information content (Hill and Tiedeman, 2007) and surface contour analyses. As illustrated in Figure 6, the parameters of the Gapon exchange approach were better identifiable as compared to the parameters of the Rothmund-Kornfeld approach. Several parameters in the latter approach showed strong correlations. We refer to Jacques et al. (2012) for details.

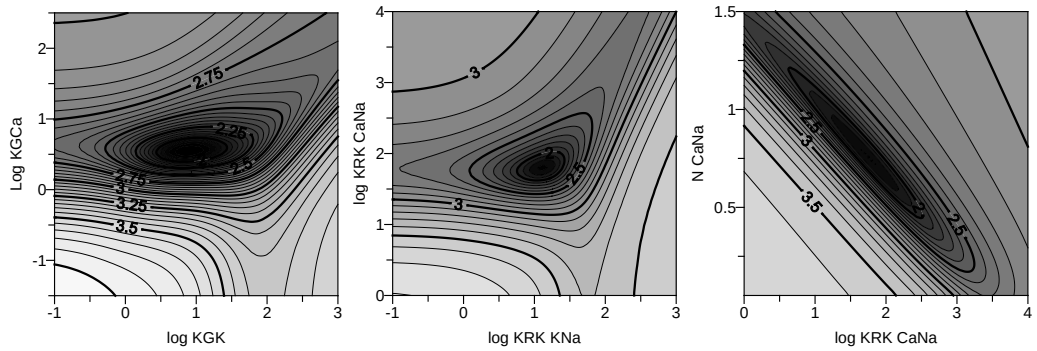

Figure 6. Contour plots of the objective function for (left) the exchange coefficient of K and Ca in the Gapon approach (K_{GK} and K_{GCa}), (middle) the exchange constant between K and Na (K_{RKKNa}), and between Ca and Na (K_{RKCaNa}) in the Rothmund-Kornfeld approach, and (right) the exchange constant (K_{RKCaNa}) and the nonlinear coefficient (N_{CaNa}) for exchange between Ca and Na in the Rothmund-Kornfeld approach (adopted from Jacques et al., 2012).

3.3. Coupling Between Geochemical Variables and Transport Properties

A useful new feature recently included in HP1 is an option to change the hydraulic and solute transport properties as a function of evolving geochemical state variables. HP1 makes it possible to account for changes in (i) the porosity (and hence the saturated water content), (ii) the hydraulic conductivity, (iii) a scaling factor for the pressure head, (iv) aqueous and gaseous phase pore geometry factors for calculating pore diffusion coefficients, (v) the dispersivity, (vi) the thermal capacity, (vii) the thermal conductivity, and (viii) the thermal dispersivity. HP1 does not provide any pre-defined conceptual or mathematical model to update the flow and transport parameters, but uses the flexibility of the embedded BASIC interpreter for this purpose. This permits users to define any user-specific relationship between the geochemical state variables and the transport properties.

A typical example, illustrated in Figure 7, is diffusive leaching from a porous medium in contact with more or less aggressive water. The example concerns leaching of a small concrete beam in contact with three types of water as indicated in the top part of Figure 7: (i) Rain W (wet deposition only), (ii) Rain B (wet and bulk deposition), which has higher ion concentrations, and (iii) Soil water with a higher inorganic carbon content as a result of soil microbiological processes. In terms of concrete performance, the soil water type should be the most detrimental since portlandite ($Ca(OH)_2$) dissolution proceeds rapidly due to leaching and carbonation (i.e., portlandite dissolution followed by calcite precipitation as show by Jacques et al. (2010)). At the same time, chemical dissolution of portlandite and precipitation of calcite change the physical properties such as porosity and tortuosity (e.g., Perko et al., 2010; Jacques et al., 2011).

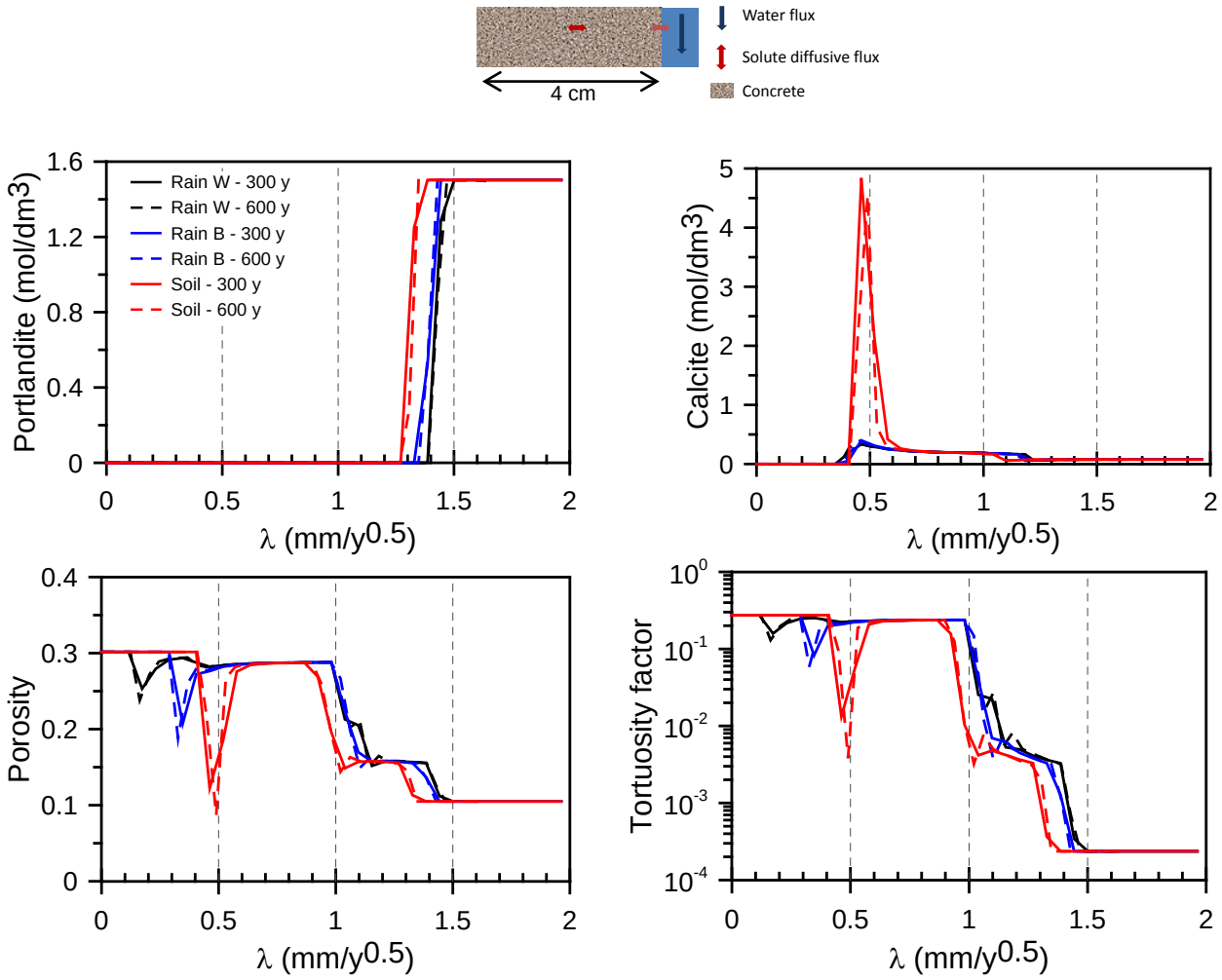

Figure 7. Example showing the effect of coupling transport parameters to geochemical variables. Results are for diffusive leaching of a small concrete beam. Shown are profiles of portlandite (top left), calcite (top right), porosity (bottom left), and the tortuosity factor (bottom right) as a function of the Boltzmann transform λ for three different water types and two different times.

Since calcite has a slightly larger molar volume than portlandite, porosity and tortuosity should decrease if calcite precipitation leads to pore blockage without generation of internal stresses and subsequent fracturing. Some of these processes are clearly evident from the results in Figure 7. The portlandite profiles as a function of the Boltzmann transform (which should collapse to a single curve in case of pure diffusive transport) are different among the three water types. In particular, the portlandite dissolution front has progressed slightly further for water with a presumably less aggressive solution composition (Rain W). On the other hand, enhanced calcite precipitation in the soil water case causes pore clogging and a strong reduction in the tortuosity and the diffusion coefficient. As a result, the portlandite dissolution front is retarded compared to the dissolution fronts when concrete is leached with the other two water compositions. A porosity decrease is also simulated for the Rain B case, mainly due to precipitation of Mg-bearing minerals.

References

Batlle-Aguilar, J., A. Brovelli, A. Porporato, and D. A. Barry, Modelling soil carbon and nitrogen cycles during land use change, A review, *Agron. Sustain. Dev.*, *31*, 251-275, 2011.

Bond, W. J., On the Rothmond-Kornfeld description of cation exchange, *Soil Sci. Soc. Am. J.*, *59*, 436-443, 1995.

Brantley, S. L., 5.03 Reaction kinetics of primary rock-forming minerals under ambient conditions, Treatise on Geochemistry, Elsevier, Volume 5, 73-117, 2003.

Coleman, K., and D. S. Jenkinson, RothC-26.3. A Model for Turnover of Carbon in Soil. Model Description and Windows User Guide, IACR-Rothamsted, Harpender, 2005.

Glynn, P. D., and E. J. Reardon, Solid-solution aqueous-solution equilibria: Thermodynamic theory and representation, *Am. J. Sci*., *290*, 164-201, 1990.

Hill, M. C., and C. R. Tiedeman, Effective Groundwater Model Calibration with Analysis of Data: Sensitivities, Predictions and Uncertainty, John Wiley & Sons, NJ, USA, 2007.

Jacques, D., and J. Šimůnek, User Manual of the Multicomponent Variably-Saturated Flow and Transport Model HP1, Description, Verification and Examples, Version 1.0, *SCK•CEN-BLG-998*, Waste and Disposal, SCK•CEN, Mol, Belgium, 79 pp., 2005.

Jacques, D., J. Šimůnek, D. Mallants, and M. Th. van Genuchten, Modeling coupled hydrological and chemical processes: Long-term uranium transport following phosphorous fertilization, *Vadose Zone J*., *7*,698-711, 2008.

Jacques, D., J. Šimůnek, D. Mallants, M. Th. van Genuchten, and L. Yu, A coupled reactive transport model for contaminant leaching from cementitious waste matrices accounting for solid phase alterations, Proceedings Sardinia 2011, Thirteenth International Waste Management and Landfill Symposium, 2011.

Jacques, D., C. Smith, J. Šimůnek, and D. Smiles, Inverse optimization of hydraulic, solute transport and cation exchange parameters using HP1 and UCODE to simulate cation exchange, *J. Cont. Hydrol*., *142-143*, 109-125, 2012.

Jacques, D., L. Wang, E. Martens, and D. Mallants, Modelling chemical degradation of concrete during leaching with rain and soil water types, *Cem. Concr. Res*., *40*, 1306-1313, 2010.

Lasaga, A.C., Kinetic Theory in the Earth Sciences, Princeton University Press, Princeton, New Jersey, 1998.

Leterme, B., and D. Jacques, Modeling Hg reactive transport in soil systems using HP1, (this issue), 2013.

Mallants D., M. Th., van Genuchten, J. Šimůnek, D. Jacques, and S. Seetharam, Leaching of contaminants to groundwater. In '*Dealing with Contaminated Sites'*, (Ed F Swartjens), pp. 787-850. DOI: 10.1007/978-90-481-9757-6_1, 2011

Manzoni, S., and A. Porporato, A theoretical analysis of nonlinearities and feedbacks in soil carbon and nitrogen cycles, *Soil Biol. Biochem*., *39*, 1542-1556, 2005.

Parkhurst, D. L., and C. A. J. Appelo, User's guide to PHREEQ C (Version 2) – A computer program for speciation, batch-reaction, one-dimensional transport and inverse geochemical calculations, Water-Resources Investigations, *Report 99–4259*, Denver, Co, USA, 312 pp., 1999.

Perko, J., D. Jacques, S. C. Seetharam, and D. Mallants, Long-term evolution of the near surface disposal facility at Dessel, NIROND-TR 2010-04 E, 2010.

Poeter, E. P., M. C. Hill, E. R. Banta, S. Mehl, and C. Steen, UCODE_2005 and six other computer codes for universal sensitivity analysis, calibration and uncertainty evaluation, *U.S. Geological Survey Techniques and Methods 6-A11*, 2005.

Porporato, A., P. D'Odorico, F. Laio, and I. Rodrigues-Iturbe, Hydrological controls on soil carbon and nitrogen cycles. I. Modelling scheme, *Adv. Water Resour.*, *26*, 45-58, 2003.

Raji, I., N. Lazarovitch, A. Ben-Gal, U. Yermiyahu, and D. Jacques, Accounting for solution composition in a plant roots active nutrient uptake model, (this issue), 2013.

Šimůnek, J. and J. W. Hopmans, Modeling compensated root water and nutrient uptake, *Ecological Modeling*, doi:10.1016/j.ecolmodel.2008.11.004, *220*(4), 505-521, 2009.

Šimůnek, J., and M. Th. van Genuchten, Modeling nonequilibrium flow and transport processes using HYDRUS, *Vadose Zone J.*, *7*(2), 782-797, 2008.

Šimůnek, J., M. Šejna, H. Saito, M. Sakai, and M. Th. van Genuchten, The HYDRUS-1D Software Package for Simulating the One-Dimensional Movement of Water, Heat and Multiple Solutes in Variably-Saturated Media, Version 4.08, *HYDRUS Software Series 3*, Department of Environmental Sciences, University of California Riverside, Riverside, California, USA, 2008.

Šimůnek, J., M. Th. van Genuchten, and M. Šejna, Development and applications of the HYDRUS and STANMOD software packages, and related codes, *Vadose Zone Journal*, *7*(2), 587-600, 2008.

Šimůnek, J., M. Th. van Genuchten, and M. Šejna, The HYDRUS Software Package for Simulating Two- and Three-Dimensional Movement of Water, Heat, and Multiple Solutes in Variably-Saturated Media, Technical Manual, Version 2.0, PC Progress, Prague, Czech Republic, pp. 258, 2011.

Šimůnek, J., D. Jacques, M. Šejna, and M. Th. van Genuchten, The HP2 Program for HYDRUS (2D/3D): A Coupled Code for Simulating Two-Dimensional Variably-Saturated Water Flow, Heat Transport, and Biogeochemistry in Porous Media, Version 1.0, PC Progress, Prague, Czech Republic, 76 pp., 2012.

Šimůnek, J., D. Jacques, and M. Šejna, HP2/3: Extensions of the HP1 reactive transport code to two and three dimensions, (this issue), 2013.

Smiles, D. E., and C. J. Smith, Absorption of artificial piggery effluent by soil: A laboratory study, *Austr. J. Soil Sci.*, *42*, 961-975, 2004.

Thaysen, E., E. Laloy, and D. Jacques, CO_2 fluxes to aquifers beneath cropland: Merging measurements and modeling, (this issue), 2013.

New Features of the HYDRUS Computer Software Packages

Jirka Šimůnek[1], Miroslav Šejna[2], Diederik Jacques[3], Günter Langergraber[4], Scott A. Bradford[5], and Martinus Th. van Genuchten[6]

[1]*Department of Environmental Sciences, University of California, Riverside, CA, USA, jiri.simunek@ucr.edu*
[2]*PC-Progress, Ltd., Prague 2, Czech Republic, m.sejna@pc-progress.cz*
[3]*Performance Assessments, Belgian Nuclear Research Institute, Mol, Belgium, djacques@sckcen.be*
[4]*Institute for Sanitary Engineering and Water Pollution Control, University of Natural Resources and Life Sciences, Vienna (BOKU University), Austria, guenter.langergraber@boku.ac.at*
[5]*U.S. Salinity Laboratory, USDA, ARS, Riverside, CA, USA, Scott.Bradford@ars.usda.gov*
[6]*Department of Mechanical Engineering, Federal University of Rio de Janeiro, UFRJ, Rio de Janeiro, RJ, Brazil, rvangenuchten@hotmail.com*

Abstract

The capabilities of the HYDRUS-1D and HYDRUS (2D/3D) software packages have been substantially expanded since two earlier HYDRUS workshops held in Prague, Czech Republic (March 2008) and Tokyo, Japan (June 2008). Multiple processes were added to both HYDRUS packages, including compensated root water and solute uptake models and triggered irrigation. Computational modules of both packages have been made about 2-3 times faster by using capabilities of advanced processors and compilers, such as using the loop vectorization. Major developments were introduced in version 2 of HYDRUS (2D/3D). This version can now handle for the first time complex, general, three-dimensional geometries, while domain properties, initial conditions, and boundary conditions can be specified on geometrical objects, rather than on the finite element mesh. Completely new modules accounting for processes not available in the standard HYDRUS version were introduced. These new modules include the HP2, C-Ride, DualPerm, UnsatChem, Wetland, and Fumigant modules. These new modules simulate flow and transport processes in two-dimensional transport domains and are fully supported by the HYDRUS graphical user interface. Several processes in these specialized modules of HYDRUS (2D/3D) have been made also part of HYDRUS-1D.

1. Introduction

The HYDRUS-1D and HYDRUS (2D/3D) programs (Šimůnek et al., 2008) are finite element models for simulating the one-, two- and three-dimensional movement of water, heat, and multiple solutes in variably saturated media. The standard versions of HYDRUS programs numerically solve the Richards equation for saturated-unsaturated water flow and convection-dispersion type equations for heat and solute transport. The flow equation incorporates a sink term to account for water uptake by plant roots. The heat transport equation considers movement by both conduction and convection with flowing water. The governing convection-dispersion solute transport equations are written in a very general form by including provisions for nonlinear nonequilibrium reactions between the solid and liquid phases, and linear equilibrium reaction between the liquid and gaseous phases. Hence, both adsorbed and volatile solutes, such as pesticides, can be considered. The solute transport equations also incorporate the effects of zero-order production, first-order degradation independent of other solutes, and first-order decay/production reactions that provide the required coupling between the solutes involved in the sequential first-order chain. The transport models also account for convection and dispersion in

the liquid phase, as well as diffusion in the gas phase, thus permitting the model to simultaneously simulate solute transport in both the liquid and gaseous phases. HYDRUS considers up to fifteen solutes, which can either be coupled in a unidirectional chain or move independently of each other. Physical nonequilibrium solute transport can be accounted for by assuming a two-region, dual porosity type formulation, which partitions the liquid phase into mobile and immobile regions. Attachment/detachment theory, including the filtration theory, is included to simulate transport of viruses, colloids, and/or bacteria.

Table 1. Selected new options in HYDRUS-1D (since 2008).

Version	New Options
4.04	• Option to specify the nonequilibrium phase concentration initially at equilibrium with the equilibrium phase concentration • Option to specify initial conditions in total (instead of liquid) concentrations • Option to print fluxes instead of temperatures for observation nodes
4.05	• HP1 – support of dual-porosity models • Linking of optimized parameters of different soil layers • Constant mobile water content in multiple layers (in the Mobile-Immobile Water Model) when optimizing immobile water content
4.06	• The Per Moldrup's tortuosity models (Moldrup et al., 1997, 2000) were implemented as an alternative to the Millington and Quirk (1960) model
4.07	• Surface energy balance (i.e., the balance of latent, heat, and sensible fluxes) for bare soils • Daily variations of meteorological variables can be generated by the model using simple meteorological models • Preliminary (at present rather simple) support of the HYDRUS package for MODFLOW
4.08	• Compensated root water and solute (passive and active) uptake based on Šimůnek and Hopmans (2009) • Executable programs made about three times faster due to the loop vectorization
4.12	• New additional output (e.g., solute fluxes for observation nodes and profiles of hydraulic conductivities (thermal and isothermal) and fluxes (liquid, vapor, and total))
4.13	• Version 2.1.002 of HP1, new GUI supporting HP1 • Conversions of the mass units for the threshold-slope salinity stress model from electric conductivity to osmotic head
4.15	• Input of sublimation constant and initial snow layer • New conversions of constants (EC, osmotic potential) for the salinity stress response function
4.16	• Option to set field capacity as an initial condition (Twarakavi et al., 2009) • Display of wetting hydraulic functions for hysteretic soils • Triggered irrigation • Interception can be considered with the standard HYDRUS input (without the need for meteorological input)

We continue to expand the capabilities of the HYDRUS-1D and HYDRUS (2D/3D) software packages and many new processes and options have been added since the two HYDRUS workshops held in 2008 in Prague, Czech Republic (in March) and Tokyo, Japan (in June). Multiple processes have been added to both HYDRUS packages since 2008, including the compensated root water and solute uptake model and/or triggered irrigation, and many others. Tables 1 and 2 list selected new processes and options that have been implemented in recent versions of HYDRUS-1D and HYDRUS (2D/3D), respectively. Note that we continue to expand the capabilities of the HYDRUS modeling environment (Table 2) by developing specialized

modules for more complex applications that cannot be solved using its standard versions. In this manuscript we list many of these changes and describe the new modules in more detail.

2. Specialized Modules

Completely new modules accounting for processes not available in the standard HYDRUS version were introduced. These new modules include the **HP2**, **C-Ride**, **DualPerm**, **UnsatChem**, **Wetland**, and **Fumigant** modules. All these modules simulate flow and transport processes in two-dimensional transport domains and are fully supported by the HYDRUS graphical user interface. Many processes included in these specialized modules of HYDRUS (2D/3D) are currently also available as part of HYDRUS-1D.

2.1. The HP1/HP2 Modules

The one-dimensional program **HP1**, which couples the **PHREEQC** geochemical code (Parkhurst and Appelo 1999) with **HYDRUS-1D**, was first released in 2005 (Jacques and Šimůnek 2005), and successfully used in many applications. This comprehensive simulation tool (HP1 is an acronym for **H**YDRUS-**P**HREEQC-**1**D) can simulate (1) transient water flow, (2) the transport of multiple components, (3) mixed equilibrium/kinetic biogeochemical reactions, and (4) heat transport in one-dimensional variably-saturated porous media (soils). **HP2** (Šimůnek et al., 2012d) is then a two-dimensional alternative of the HP1 module. Both HP1 and HP2 can simulate a broad range of low-temperature biogeochemical reactions in water, the vadose zone and/or ground water systems, including interactions with minerals, gases, exchangers and sorption surfaces based on thermodynamic equilibrium, kinetic, or mixed equilibrium-kinetic reactions. More details about both modules are presented in several papers of these proceedings (e.g., Jacques et al., 2013; Šimůnek et al., 2013).

2.2. The C-Ride Modules

The **C- Ride** module (Šimůnek et al., 2012c) simulates the transport of particle-like substances (e.g., colloids, viruses, bacteria, and nanoparticles) and colloid-facilitated solute transport (Šimůnek et al., 2006), the latter often observed for many strongly sorbing contaminants such as heavy metals, radionuclides, pharmaceuticals, pesticides, and explosives. These contaminants are predominantly associated with the solid phase, which is commonly assumed to be stationary. However, such contaminants may also sorb/attach to mobile and deposited colloidal particles (e.g., microbes, humic substances, suspended clay particles, and metal oxides), which then can act as pollutant carriers and thus provide a rapid transport pathway for the pollutants. This module fully accounts for the dynamics of colloid (attachment/straining) and solute (kinetic/equilibrium sorption to soil and mobile/deposited colloids) transfer between the different phases. The schematic of the colloid-facilitated solute transport model is shown in Figure 1.

Table 2. Selected new options in HYDRUS (2D/3D) (since 2008).

Version	New Options
1.09	• New more efficient algorithm for particle tracking
1.10	• Import of domain properties, initial and boundary conditions from another project with (slightly) different geometry or FE mesh (both 2D and 3D)
1.11	• The Per Moldrup's tortuosity models (Moldrup et al., 1997, 2000) were implemented as an alternative to the Millington and Quirk (1960) model
2.01	**Computational module:** • Initial conditions can be specified in the total solute mass (previously only liquid phase concentrations were allowed) • Initial equilibration of nonequilibrium solute phases with equilibrium solute phase • Gradient boundary conditions • A subsurface drip boundary condition (with a drip characteristic function reducing irrigation flux based on the back pressure) (Lazarovitch et al., 2005) • A surface drip boundary condition with dynamic wetting radius (Gärdenäs et al., 2005) • A seepage face boundary condition with a specified pressure head • Triggered Irrigation, i.e., irrigation can be triggered by the program when the pressure head at a particular observation node drops below a specified value • Time-variable internal pressure head or flux nodal sinks/sources (previously only constant internal sinks/sources) • Fluxes across meshlines in the computational module for multiple solutes (previously only for one solute) • HYDRUS calculates and reports surface runoff, evaporation and infiltration fluxes for the atmospheric boundary • Water content dependence of solute reactions parameters using the Walker's (1974) formula was implemented • An option to consider root solute uptake, including both passive and active uptake (Šimůnek and Hopmans, 2009) • An option to use a set of Boundary Condition records multiple times • Options related to the **Fumigant** transport (e.g., removal of tarp, temperature dependent tarp properties, additional injection of fumigant) • The **UNSATCHEM** module simulating transport of and reactions between major ions • The new **CWM1** constructed wetland module **GUI:** • Supports for complex general three-dimensional geometries (Professional Level) • Domain properties, initial conditions, and boundary conditions can be specified on "Geometric Objects" (defining the transport domain) rather than on the finite element mesh • Import of various quantities (e.g., domain properties, initial and boundary conditions) from another HYDRUS projects even with (slightly) different geometry or FE mesh • Geometric objects can be imported using DXF and TIN (triangular irregular network) files • Display of results using Isosurfaces • Support of **ParSWMS** (a parallelized version of SWMS_3D) (Hardelauf et al., 2006)
2.02	• The **DualPerm** module simulating flow and transport in dual-permeability porous media • The **C-Ride** module simulating colloid transport and colloid-facilitated solute transport • The **HP2** module (coupled HYDRUS and PHREEQC) for simulating biogeochemical reactions

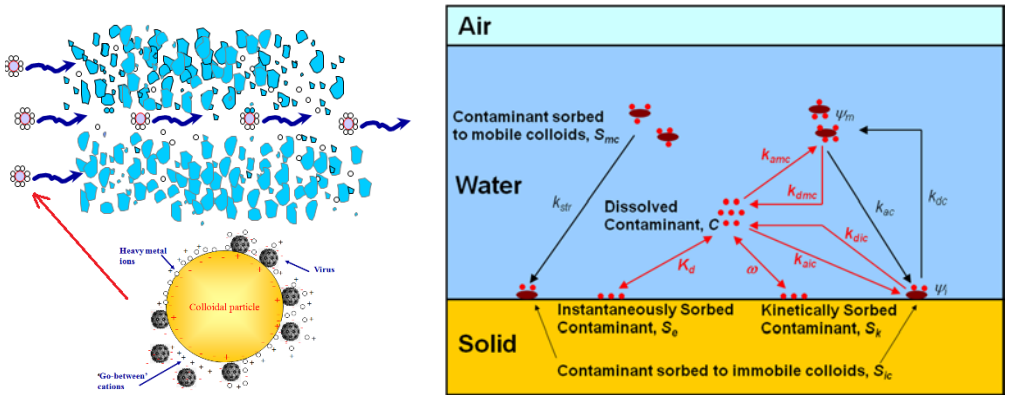

Figure 1. Schematic of the colloid-facilitated solute transport model.

2.3. The DualPerm Module

The **DualPerm** module (Šimůnek et al., 2012b) simulates preferential and/or nonequilibrium water flow and solute transport in dual-permeability media using the approach suggested by Gerke and van Genuchten (1993). The module assumes that the porous medium consists of two interacting regions: one associated with the inter-aggregate, macropore, or fracture system, and one comprising micropores (or intra-aggregate pores) inside soil aggregates or the rock matrix. Water flow can occur in both regions, albeit at different rates. Modeling details are provided by Šimůnek and van Genuchten (2008). An example of the pressure head profiles for a tension disc (with a disc radius of 10 cm) infiltration experiment in the transport domain, 50 cm wide and 150 cm deep, in the matrix and fracture domains for different ratios of the anisotropy coefficients (K_x^A/K_z^A=1, 10, and 0.1) is shown in Figure 2.

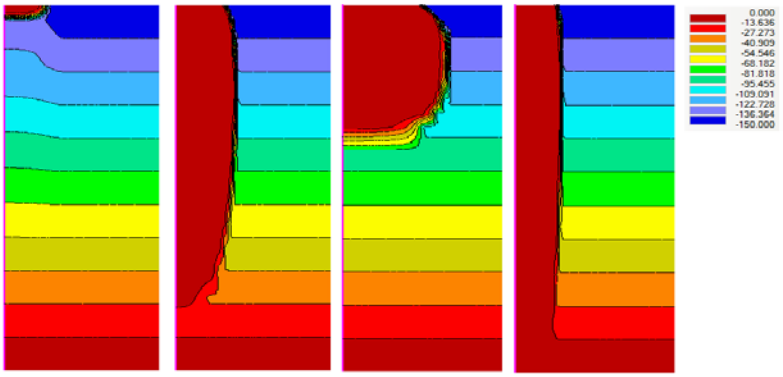

Figure 2. Pressure head profiles for the matrix (left), isotropic fracture, and fracture with K_x^A/K_z^A=10, and fracture with K_x^A/K_z^A=0.1 (right).

2.4. The UnsatChem Module

The geochemical **UnsatChem** module (Šimůnek et al., 2012a) has been implemented into both the one- and two-dimensional computational modules of Hydrus. This module simulates the

transport of major ions (i.e., Ca, Mg, Na, K, SO4, CO3, and Cl) and their equilibrium and kinetic geochemical interactions, such as complexation, cation exchange and precipitation-dissolution (e.g., calcite, gypsum, and/or dolomite). Possible applications include studies of the salinization/ reclamation of agricultural soils, sustainability of various irrigation systems, and the disposal of brine waters from mining operations. Since the computational driver for this module was developed some two decades ago (Šimůnek and Suarez, 1994), the UnsatChem module (especially its one-dimensional version) has found a wide use in many applications.

2.5. The Wetland Module

The **Wetland** module simulates aerobic, anoxic, and anaerobic transformation and degradation processes for organic matter, nitrogen, phosphorus, and sulphur during treatment of polluted wastewater in subsurface constructed wetlands (Langergraber and Šimůnek, 2012). Constructed wetlands are engineered water treatment systems that optimize the treatment processes found in natural environments. Constructed wetlands have become popular since they can be quite efficient in treating different types of polluted water and provide sustainable, environmentally friendly solutions. A large number of physical, chemical and biological processes are simultaneously active and may mutually influence each other. The Wetland module uses two biokinetic model formulations [CW2D of Langergraber and Šimůnek (2005) and CWM1 of Langergraber et al. (2009)] to account for complex conditions that may occur in various types of wetlands. An example of the application of the Wetland module to simulate the spatial distribution of heterotrophic organisms in a subsurface constructed wetland is shown in Figure 3.

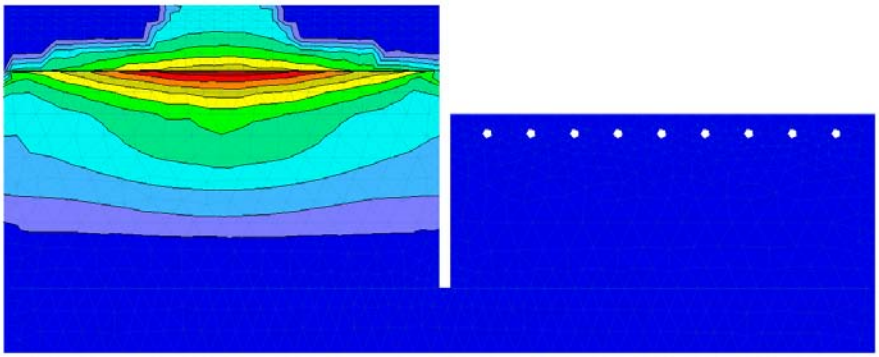

Figure 3. Steady-state distribution of heterotrophic organisms in a subsurface constructed wetland.

2.6. The Fumigants Module

The **Fumigants** module implements multiple additional options that are required to simulate processes related to fumigants applications and transport. This module allows users to specify an additional injection of fumigants into the transport domain at a specified location at a specified time and to consider the presence or absence of a surface tarp, a temperature dependence of tarp properties, and its removal at specified time. The Fumigants module has been recently used to investigate the effect of different application scenarios, such as tarped broadcast, tarped bedded

shank injection and a tarped drip line-source application and various factors (e.g., initial water content, tarp permeability) on fumigant volatilization (Fig. 4) (Spurlock et al., 2013).

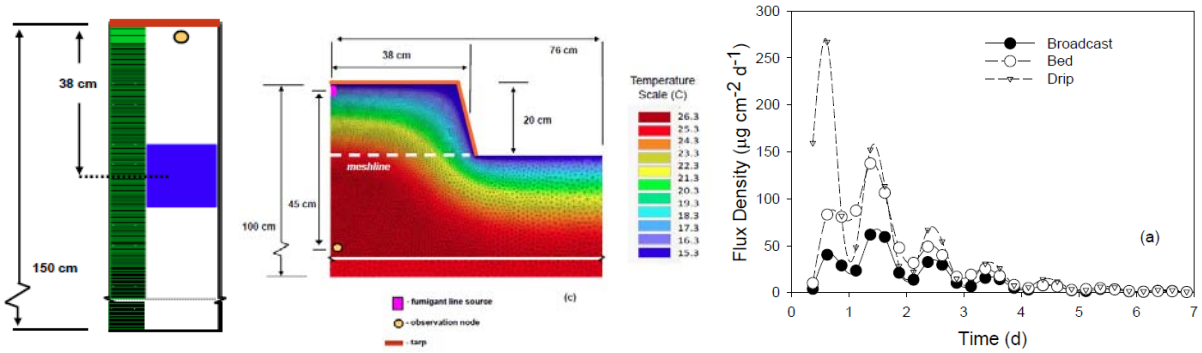

Figure 4. Tarped broadcast (left) and tarped bed drip scenarios (center). Volatilization fluxes for different scenarios (adopted from Spurlock et al., 2013).

3. Graphical User Interface (GUI) of HYDRUS (2D/3D)

3.1. Geometries in the Professional Level of HYDRUS (2D/3D)

The latest 3D-Professional Level of HYDRUS supports complex general three-dimensional geometries that can be formed from three-dimensional objects (**Solids**) of general shapes. Three-dimensional objects are formed by boundary **Surfaces**, which can be either **Planar** surfaces or **Curved** surfaces (**Quadrangle**, **Rotary**, **Pipe**, or **B-Spline**). Figure 5 provides examples of various curved surfaces, while Figure 6 shows how these individual objects can be combined to form complex three-dimensional geometries.

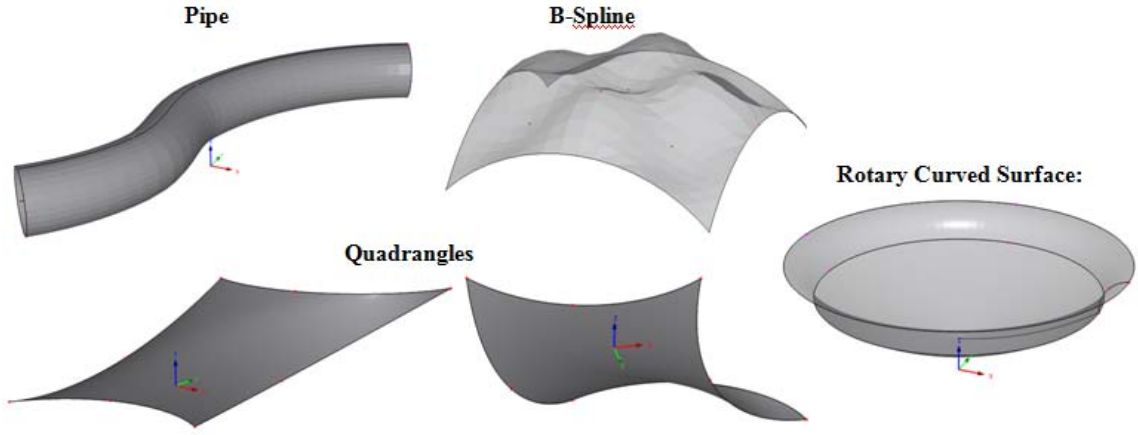

Figure 5. Examples of curved surfaces (Rotary, Pipe, B-Spline, and Quadrangle Surfaces).

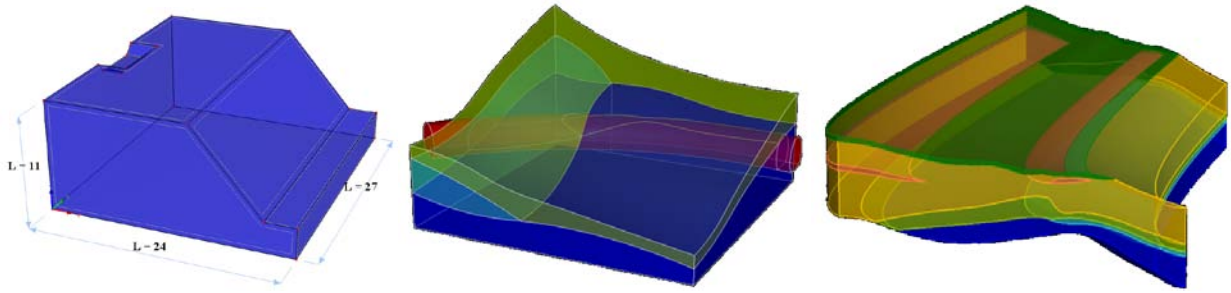

Figure 6. Transport domains formed using planar (left) or curved (center, right) surfaces.

3.2. Domain Properties, Initial Conditions, and Boundary Conditions Specified on Geometric Objects

Various spatially variable properties (e.g., material distribution, initial conditions, boundary conditions, domain properties, etc) can be specified in Version 2.0 of HYDRUS, either directly on the Finite Element Mesh (FEM) (as done in Version 1.0), or on Geometric Objects (e.g., boundary curves, rectangles, circles, surfaces, solids) (Fig. 7).

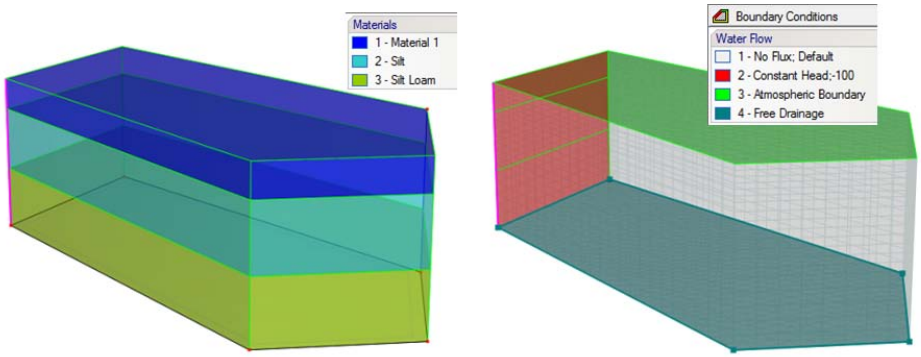

Figure 7. The transport domain with materials (left) and boundary conditions (right) specified on Geometric Objects.

3.3. Display of Standard and Alternative Variables

Many different spatially-variable properties can be displayed in the center "View" window of HYDRUS GUI, depending on what processes are being simulated. These variables are divided between standard variables, such as pressure heads, water contents, and/or liquid concentrations, and alternative variables, such as different types of water contents (mobile, immobile, and total) or concentrations (liquid, solid, gas, or total). While the standard variables can be selected from the "Data" tab of the Navigator bar, the alternative variables can be selected from the View tab of the Navigator bar (Fig. 8).

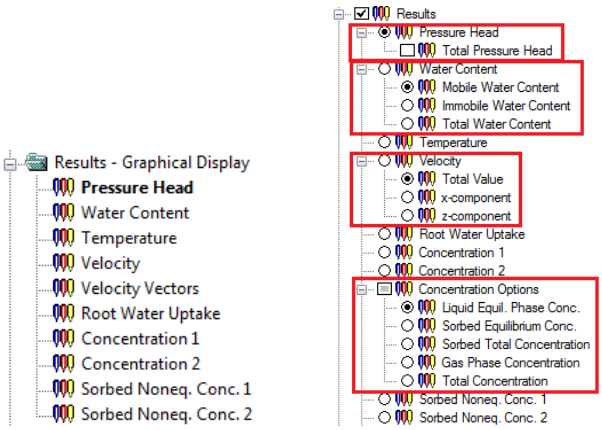

Figure 8. Standard and alternative variables that can be displayed in the View window.

4. Conclusions

The HYDRUS models have served, and are serving, an important role in vadose zone research. This is reflected by their frequent use in a variety of applications, many of them leading to peer-reviewed publications (HYDRUS website lists over one thousand references, in which HYDRUS has been used). The need for codes such as HYDRUS is further reflected by the frequency of downloading the program from the HYDRUS web site. For example, HYDRUS-1D was downloaded more than 10,000 times in 2012 by users from some 50 different countries. The HYDRUS web site receives on average some 700 individual visitors each day.

References

Gärdenäs, A., Hopmans, J. W., B. R. Hanson, and J. Šimůnek, Two-dimensional modeling of nitrate leaching for various fertigation scenarios under micro-irrigation, *Agricultural Water Management, 74*, 219-242, 2005.

Gerke, H. H., M. Th. van Genuchten, A dual-porosity model for simulating the preferential movement of water and solutes in structured porous media, *Water Resources Research*, *29*, 305-319, 1993.

Hardelauf, H., M. Javaux, M. Herbst, S. Gottschalk, R. Kasteel, J. Vanderborght, and H. Vereecken, PARSWMS: a parallelized model for simulating 3-D water flow and solute transport in variably saturated soils, *Vadose Zone Journal*, *6*(2), 255-259, 2007.

Jacques, D., and J. Šimůnek, User Manual of the Multicomponent Variably-Saturated Flow and Transport Model HP1, Description, Verification and Examples, Version 1.0, *SCK•CEN-BLG-998*, Waste and Disposal, SCK•CEN, Mol, Belgium, 79 pp., 2005.

Jacques, D., J. Šimůnek, D. Mallants, and M. Th. van Genuchten, The HPx reactive transport models: Summary of recent developments and applications, (this issue), 2013.

Langergraber, G., and J. Šimůnek, Modeling variably-saturated water flow and multi-component reactive transport in constructed wetlands, *Vadose Zone J.*, *4*(4), 924-938, 2005.

Langergraber, G., D. Rousseau, J. García, and J. Mena, CWM1 - A general model to describe biokinetic processes in subsurface flow constructed wetlands, *Water Sci. Technol.*, *59*(9), 1687-1697, 2009.

Langergraber, G., and J. Šimůnek, Reactive transport modeling of subsurface flow constructed wetlands, *Vadose Zone Journal*, *11*(2), doi:10.2136/vzj2011.0104, 14 pp., 2012.

Lazarovitch, N., J. Šimůnek, and U. Shani, System dependent boundary condition for water flow from subsurface source, *Soil Sci. Soc. Am. J.*, *69*(1), 46-50, 2005.

Millington, R. J., and J. M. Quirk, Permeability of porous solids, *Trans. Faraday Soc.*, *57*, 1200-1207, 1961.

Moldrup, P., T. Olesen, D. E. Rolston, and T. Yamaguchi, Modeling diffusion and reaction in soils: VII. Predicting gas and ion diffusivity in undisturbed and sieved soils, *Soil Sci*., *162*(9), 632-640, 1997.

Moldrup, P., T. Olesen, J. Gamst, P. Schjønning, T. Yamaguchi, and D. E. Rolston, Predicting the gas diffusion coefficient in repacked soil: water-induced linear reduction model, *Soil Sci. Soc. Am. J*., *64*, 1588-1594, 2000.

Parkhurst D. L., and C. A. J. Appelo, User's guide to PHREEQ C (Version 2) – A computer program for speciation, batch-reaction, one-dimensional transport and inverse geochemical calculations, Water-Resources Investigations, *Report 99–4259*, Denver, Co, USA, 312 pp., 1999.

Šimůnek, J., and D. L. Suarez, Two-dimensional transport model for variably saturated porous media with major ion chemistry, *Water Resources Research*, *30*(4), 1115-1133, 1994.

Šimůnek, J., Changming He, J. L. Pang, and S. A. Bradford, Colloid-facilitated transport in variably-saturated porous media: Numerical model and experimental verification, *Vadose Zone Journal*, *5*(3), 1035-1047, 2006.

Šimůnek, J. and J. W. Hopmans, Modeling compensated root water and nutrient uptake, *Ecological Modeling*, doi:10.1016/j.ecolmodel.2008.11.004, *220*(4), 505-521, 2009.

Šimůnek, J., and M. Th. van Genuchten, Modeling nonequilibrium flow and transport processes using HYDRUS, *Vadose Zone Journal*, *7*(2), 782-797, 2008.

Šimůnek, J., M. Th. van Genuchten, and M. Šejna, Development and applications of the HYDRUS and STANMOD software packages, and related codes, *Vadose Zone Journal*, *7*(2), 587-600, 2008.

Šimůnek, J., M. Šejna, and M. Th. van Genuchten, The UNSATCHEM Module for HYDRUS (2D/3D) Simulating Two-Dimensional Movement of and Reactions Between Major Ions in Soils, Version 1.0, PC Progress, Prague, Czech Republic, 54 pp., 2012a.

Šimůnek, J., M. Šejna, and M. Th. van Genuchten, The DualPerm Module for HYDRUS (2D/3D) Simulating Two-Dimensional Water Movement and Solute Transport in Dual-Permeability Porous Media, Version 1.0, PC Progress, Prague, Czech Republic, 32 pp., 2012b.

Šimůnek, J., M. Šejna, and M. Th. van Genuchten, The C-Ride Module for HYDRUS (2D/3D) Simulating Two-Dimensional Colloid-Facilitated Solute Transport in Variably-Saturated Porous Media, Version 1.0, PC Progress, Prague, Czech Republic, 45 pp., 2012c.

Šimůnek, J., D. Jacques, M. Šejna, and M. Th. van Genuchten, The HP2 Program for HYDRUS (2D/3D): A Coupled Code for Simulating Two-Dimensional Variably-Saturated Water Flow, Heat Transport, and Biogeochemistry in Porous Media, Version 1.0, PC Progress, Prague, Czech Republic, 76 pp., 2012d.

Šimůnek, J., D. Jacques, and M. Šejna, HP2/3: Extensions of the HP1 reactive transport code to two and three dimensions, (this issue), 2013.

Spurlock, F., J. Šimůnek, B. Johnson, and, A. Tuli, Sensitivity analysis of vadose zone fumigant transport and volatilization, *Vadose Zone Journal*, doi:10.2136/vzj2012.0130, (in press), 2013.

Twarakavi, N. K. C, M. Sakai, and J. Šimůnek, An objective analysis of the dynamic nature of field capacity, *Water Resources Research*, *45*, W10410, doi:10.1029/2009WR007944, 9 pp., 2009.

Walker, A., A simulation model for prediction of herbicide persistence, *J. Environ. Quality*, *3*(4), 396-401, 1974.

Investigating the Impact of the Irrigation Method on Profitability of Smallholder Gardening: Incorporating HYDRUS-1D into a Decision Support System

Adam Abramson[1], Eilon Adar[1], and Naftali Lazarovitch[2]

[1]*Dept of Environmental Hydrology and Microbiology, Zuckerberg Institute for Water Research,* adamab@bgu.ac.il *and* eilon@bgu.ac.il
[2]*Wyler Department of Dryland Agriculture, French Associates, Institute for Agriculture and Biotechnology of Drylands, The Jacob Blaustein Institutes for Desert Research, Ben-Gurion University of the Negev, Sede Boqer Campus, Midreshet Ben-Gurion, Israel,* lazarovi@bgu.ac.il

Abstract

Dry-season irrigation in tropical developing regions provides many households with both nutritional and monetary supplements. Optimizing production from these small-scale gardens is complicated by the unpredictability of water amounts available throughout the season, as well as the time, labor, and capital constraints common to subsistence livelihoods. Drip irrigation, known mostly for its high water use efficiency, holds additional benefits of time savings in comparison to a conventional hand-watering of smallholder gardens. The HYDRUS-1D software was incorporated into the Microsoft® Excel-based Decision Support System (DSS) to model and compare the economic performance of these two irrigation methods under a holistic range of agronomic, labor, and water parameter values. Results of this investigation suggest that, due to the tradeoff between capital costs and time-savings, drip irrigation does not always result in optimal net revenue as compared to hand-watering. We identified a linear relationship between the rate of revenue earned and the ratio between water and time availability for both irrigation methods. While these relationships are nearly identical, they reach a unique threshold value after which water becomes a limiting factor. The value of this threshold is lower for hand watering because the amount of water applied per unit of working time is less, thus labor becomes a limiting constraint at lower water supply levels. Drip irrigation allows labor to earn higher revenue at sufficient water supplies. Thus, it should be promoted where labor is relatively limiting.

1. Introduction

Dry-season irrigation in remote areas of tropical developing regions provides many households with both nutritional and monetary supplements. Often, smallholders depend on traditional (unimproved) water sources for meeting their irrigation needs, which are highly seasonal and many times unreliable throughout the length of the season: dams, ponds, ephemeral streams, or hand-dug shallow wells. Optimizing profits from these small-scale gardens is complicated by the unpredictability of water amounts available through the season as well as the time, labor, and capital constraints common to subsistence livelihoods. In resource-poor communities, labor commitments may replace cash payments for critical investments, such as water supplies, when coupled to income generating activities, such as irrigation (Abramson et al., 2011). Millions of smallholder farmers face the above challenges daily.

Low-cost drip irrigation has emerged as a means to address these challenges through increased water use efficiency, labor savings, and higher economic returns (Ngigi et al., 2005; Polak et al.,

2003; Friedlander et al., 2013). A recent study quantified the time savings and economic gains associated with drip irrigation for smallholders (Woltering et al., 2011). However, no studies have investigated the economic advantages of drip irrigation against traditional hand-watering while holistically considering all relevant constraints within a sufficiently robust modeling environment. These include agronomic factors as well as labor and water availability. This study's aim is to outline, through a representative scenario under a range of parameter values, the strategic niche of drip irrigation against hand-watering in smallholder gardens.

2. Materials and Methods

Figure 1 presents a comparison of the time and capital costs of hand-watering and drip irrigation.

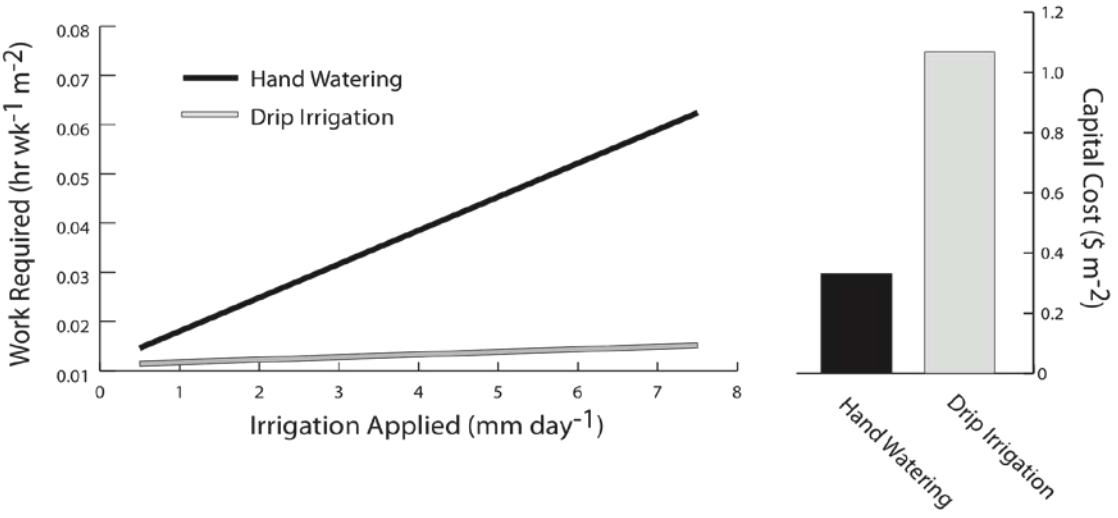

Figure 1. Relationship between work requirements, capital costs and irrigation method. Drip irrigation saves time, but requires more initial capital than hand watering. Work requirement data are adapted from Woltering (2011).

The HYDRUS-1D modeling environment (Šimůnek et al., 2008) was incorporated into a Microsoft® Excel-based Decision Support System (DSS) for investigating the economics of rural water development (Abramson, 2013). Modeled transpiration levels for field-grown tomato under a range of irrigation rates (mm day^{-1}) were obtained through a VBA-coded automation mechanism of the HYDRUS-1D software within Excel. These transpiration results were then translated into actual crop yields according to the yield-transpiration relationship investigated by Ben-Gal et al. (2003) for field-grown tomato. Various measures of time availability in the garden were input into the DSS. For 100 irrigation levels discretized between 10% and 150% of PET, total agricultural costs, comprised of capital and operation costs ($ m^{-2}), were calculated along with modeled yields(kg m^{-2}) and benefits ($ m^{-2}).

In the DSS optimization scheme, two main constraints exist for determining the revenue generated from irrigation: availability of labor (the time constraint) and the amount of available water for irrigation (the water constraint). Optimal net benefit occurs at the maximum of:

$$Net\ \ Benefit_i \left[Min\left(Time, Water\ \ Constra\,\text{int}\, s \right) \right]$$

where *i* is irrigation level (mm day^{-1}).

3. Results

In order to demonstrate the general trends of these factors, a single scenario was defined and imputed (Fig. 2).

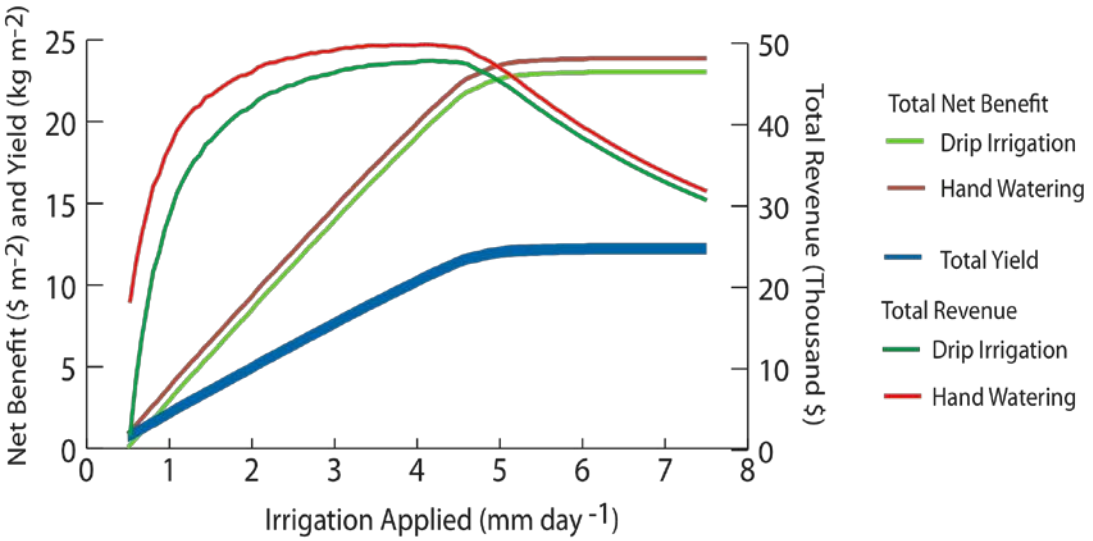

Figure 2. Yield, net benefit, and total revenue by irrigation method and application rate. In this scenario tomato is grown according to the yield-transpiration relationship derived by Ben-Gal (2003), PET is 5 mm, salinity is 0.1 dS m^{-1}, produce earns \$2 kg^{-1}, and irrigation is conducted over 3 seasons.

As expected, both total yield and net benefit increase linearly with irrigation application until roughly 100% of PET. Due to the tradeoffs illustrated in Figure 1, with increasing irrigation applications, work requirements also increase, resulting in less area that can be cultivated. The optimal revenue is achieved in light of these two opposing factors.

Figure 3 demonstrates that where the time constraint is the limiting factor (i.e., allows less irrigated area than available water), drip irrigation strongly outperforms hand watering. This is because of the time savings, which translates into higher irrigated areas and higher project revenues. Figure 4 presents a generalized representation of these trends.

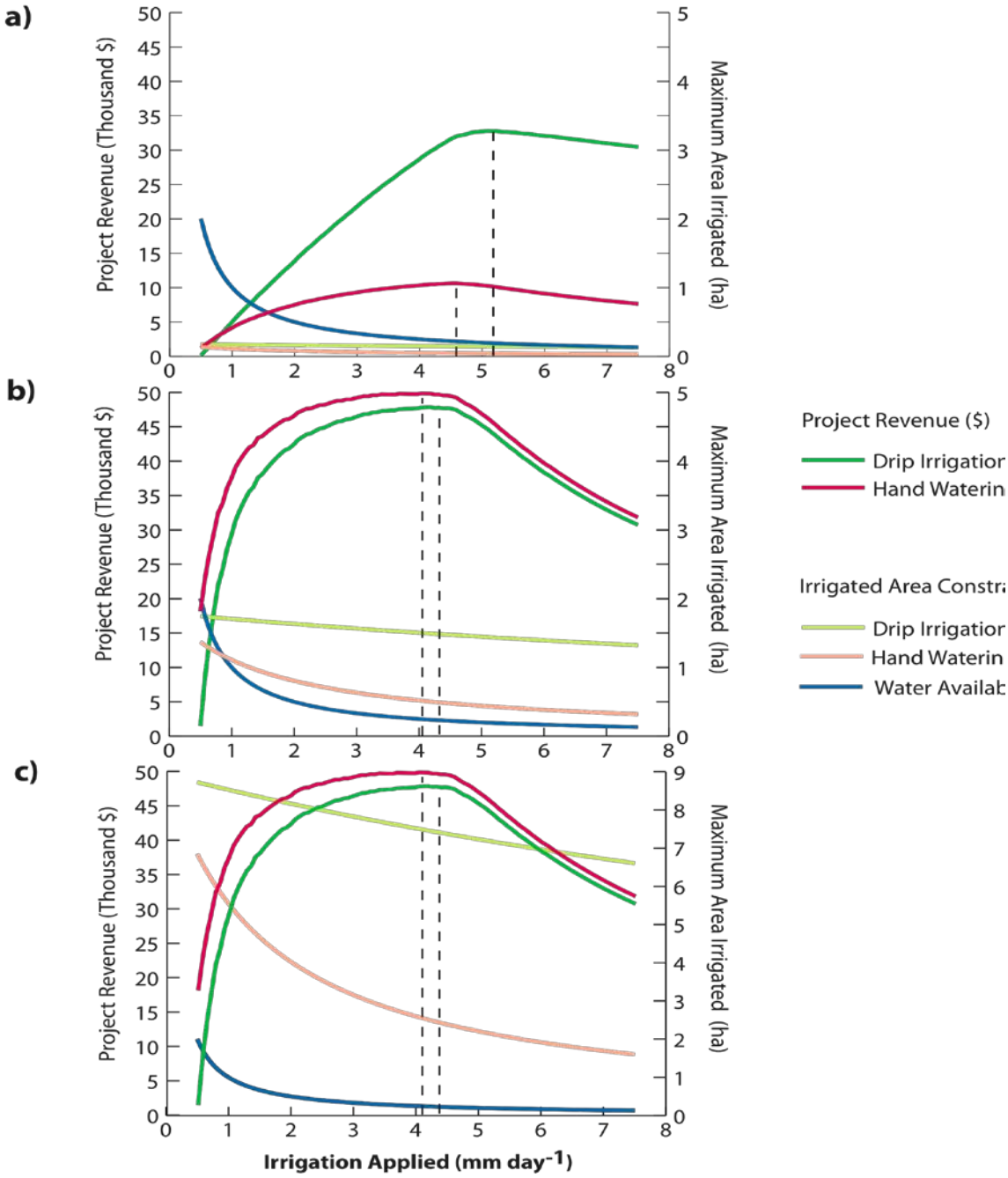

Figure 3. The relationship between irrigation application, labor availability, irrigation method, and project revenue for three scenarios: a) low (20 hr wk^{-1}); b) intermediate (100 hr wk^{-1}); and c) high (1,000 hr wk^{-1}) labor availability. Dotted lines represent the peak revenue achieved.

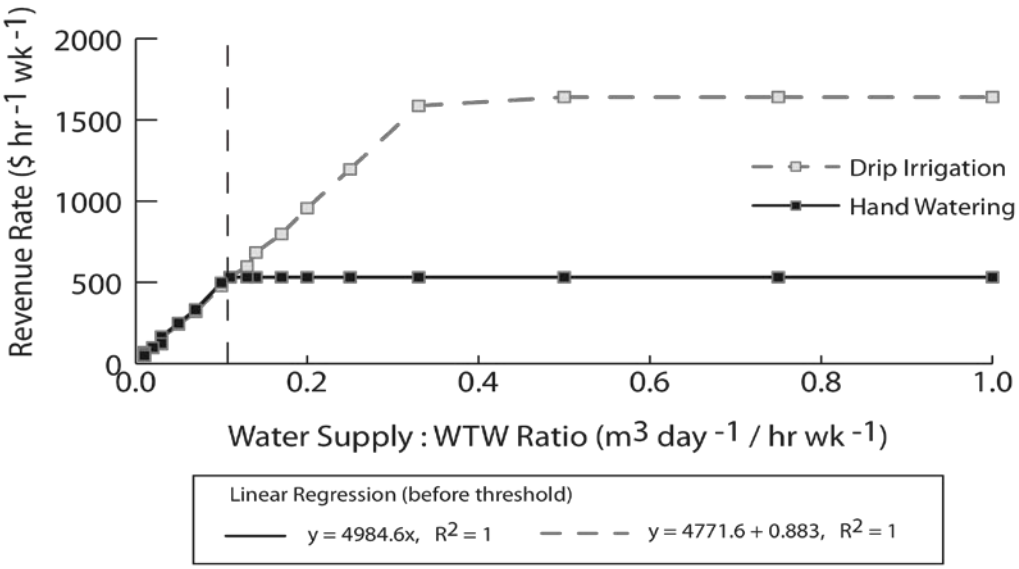

Figure 4. The relationship between available water and labor against revenue earned, expressed by the variation of the revenue rate by the ratio of available water-to-labor. Linear regression of the first (increasing) section of each line supports a constant, and nearly identical slope, which represents the revenue earned per daily water supply available ($ (m^{-3} day^{-1})). The area to the right of the vertical dotted line represents scenarios where drip irrigation is advantageous to hand watering, and vice versa. The nearly identical slopes of the two regression lines and the unitary values of R^2 indicate that these trends are explained entirely by the factors investigated.

As the available water-to-labor ratio increases, the revenue rate reaches a threshold. The value of this threshold is lower for hand watering because the amount of water applied per unit of time working is less, thus labor becomes a limiting constraint at lower water supply levels. Drip irrigation allows labor to earn higher revenue where water supplies are sufficiently high in relation to time commitments. Thus, it should be promoted where labor is relatively limiting. The exact values of these figures will change according to the scenario investigated, but these trends will remain.

4. Conclusions

These results demonstrate the following:

1) While drip irrigation certainly does demonstrate applicability in low resource smallholder economies, this may be limited to very water and/or labor scarce conditions. Given the time-capital tradeoffs associated with the transition from subsistence to 'developed' economic status, drip irrigation finds its niche in the latter stages of this transition. Other non-market benefits, however, such as increased water use efficiency, should be included in development strategies.
2) The HYDRUS-1D software can be effectively automated for conducting Excel-based analyses through simple algorithms.

References

Abramson, A., Decision Support System for assessing full cost recovery of water development in rural Africa, PhD Thesis, Ben Gurion University of the Negev, Israel, 2013. DSS Available online at www.outoftheground.org or https://dl.dropbox.com/u/24352729/DSS.zip

Abramson, A., N. Becker, Y. Garb, and N. Lazarovitch, Willingness to pay, borrow, and work for rural water service improvements in developing countries, *Water Resour. Res.*, *47*, W11512, doi:10.1029/2010WR010147, 2011.

Ben-Gal, A., L. Karlberg, P. Jansen, and U. Shani, Temporal robustness of linear relationships between production and transpiration, *Plant and Soil*, *251*(2), 211-218, 2003.

Friedlander, L., A. Tal, and N. Lazarovitch, Technical considerations affecting adoption of drip irrigation in sub-Saharan Africa, *Agricultural water management*, in press, 2013.

Ngigi, S., H. Savenije, J. N. Thome, J. Rockstrom, and F. Penning de Vries, Agro-hydrological evaluation of on-farm rainwater storage systems for supplemental irrigation in Laikipia district, Kenya, *Agricultural Water Management*, *73*, 21-41, 2005.

Polak, P., D. Adhikar, B. Nanes, D. Salter, and S. Suryawanshi, Transforming rural water access into profitable business opportunities, In: Proceedings of the *International symposium on Water, Poverty and Productive Uses of Water at the Household Level*, Muldersdrift, South Africa, 21-23 January, 2003.

Šimůnek, J., M. Th. van Genuchten, and M. Šejna, Development and applications of the HYDRUS and STANMOD software packages, and related codes, *Vadose Zone Journal*, *7*(2), 587-600, 2008.

Woltering, L., A. Ibrahim, D. Posternak, and J. Ndjeunga, The economics of low pressure drip irrigation and of hand watering for vegetable production in the Sahel, *Agricultural Water Management*, *99*, 67-73, 2011.

Simulation of Water and Air Distribution in Growing Media

Ruediger Anlauf[1] and Peter Rehrmann[2]

[1]*Faculty of Agricultural Sciences and Landscape Architectur, Osnabrueck University of Applied Sciences, Osnabrueck, Germany, r.anlauf@hs-osnabrueck.de*
[2]*Faculty of Agricultural Sciences and Landscape Architectur, Osnabrueck University of Applied Sciences, Osnabrueck, Germany, p.rehrmann@hs-osnabrueck.de*

Abstract

Understanding the water and air contents of growing media in plant containers is important for growers. To optimize crop growth, the relative effect of substrate type and irrigation strategy on water uptake of growing media must be known. Describing water uptake and distribution in the container with a dynamic simulation model may overcome the disadvantages of static parameters such as container capacity and air capacity. Water uptake and redistribution was investigated for an ebb-and-flow irrigation system with two different growing media, a coarse white peat and a fine seedling substrate, at two flooding depths (1 and 4 cm) and for three flooding durations (5, 10 and 15 min). The results were used to evaluate the use of HYDRUS-1D to describe water uptake and redistribution. The hydraulic functions (water retention and hydraulic conductivity curves) needed for the simulation model were determined in the laboratory. Hysteresis becomes especially important in irrigation systems where water is applied from the bottom of the container, such as in ebb-and-flow irrigation.

Preliminary simulations with HYDRUS-1D showed that hysteresis in the water retention curve must be taken into account for growing media to get reliable simulation results. Water retention drying curves were determined through the use of a standard sand box apparatus. Wetting curves were determined with equipment that allowed water contents of growing media to be measured in an experimental container with a constant flooding depth. Under the assumption that the water content at equilibrium is analogous to the water retention curve, the water content of the growing media above the water table will correspond to distinct pF values. Drying and wetting curves were parameterized to be used in HYDRUS-1D. The simulation was divided into a flooding cycle with a constant head lower boundary condition and a drainage cycle with a seepage phase boundary condition. The simulated water content at the end of the flooding cycle was used as the initial condition for the drainage cycle. The results show that HYDRUS-1D is able to describe water uptake and redistribution in containers filled with growing media sufficiently well, but only if hysteresis in the water retention curve is taken into account. This correct representation of the water balance in plant containers is an important basis for future work on oxygen concentration changes in growing media. Part of this study has been published elsewhere (Anlauf et al., 2012).

1. Introduction

Ebb-and-Flow irrigation is often used in horticultural practices to irrigate plant containers on concrete floors. The depth of water during irrigation is usually 1 to 2 cm but can be as much as 5 cm (Aendekerk, 1997; Raviv and Lieth, 2008). It is very important that the irrigation water is quickly and evenly distributed to realize a relatively uniform water level for all containers on the floor. The water is drained after about 10 to 20 min and collected in a storage tank (Raviv and Lieth, 2008).

It is known from practical experience that uneven water distributions in containers at different positions on a concrete floor occur frequently. One of the main reasons is the necessary slope of the concrete floor (0.2 to 0.4%) to realize quick drainage of water (Raviv and Lieth, 2008). Containers at a lower position will receive a higher irrigation depth and a longer irrigation time compared to containers at higher positions (example in Figure 1). This may result in either drought stress for the plants at some positions or too much moisture at others which then may cause aeration and disease problems.

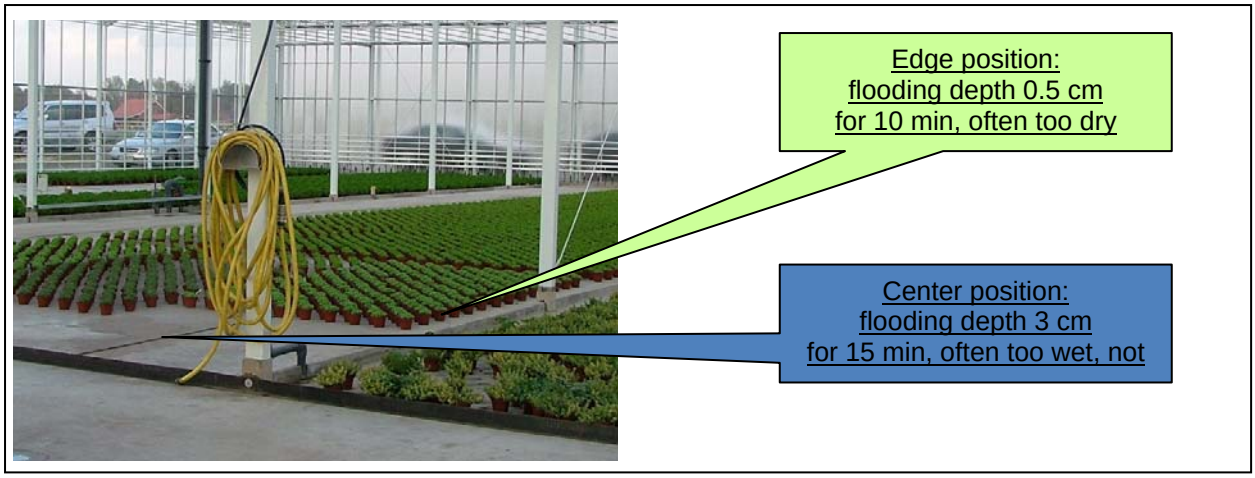

Figure 1. Example of uneven water distribution in containers at different positions on a concrete floor.

The physical properties of growing media describing the quality of the substrate for different horticultural uses are usually measured for standard conditions, such as container capacity and air capacity, both measured at a matric potential of -10 hPa. These methods are standardized (DIN EN 13041, 2010) and are widely accepted.

However, horticultural practices show that in some situations producers have problems related to low oxygen supply, even with growing media with a high air capacity, while in other cases plants with good growth and quality are produced using substrates of minor quality. This is not surprising because the standard parameters describe a static condition, whereas in horticultural practice a dynamic system exists in which the actual water and air contents fluctuate considerably with time, mainly due to the irrigation practices. Therefore, methods to describe the dynamic behavior of water and air in growing media, such as simulation models, seem to be promising tools to more realistically describe actual situations in a container (Fonteno, 1993; Heinen and de Willigen, 1995; Palla et al., 2008).

The use of simulation models to calculate water uptake and redistribution in plant containers depending on irrigation depth, time, and type of material could be a cost-effective method. Computer models are frequently and effectively used to simulate water movement in mineral soils. Model applications for growing media are much less frequent and the quality of the simulation is usually less good compared to mineral soils. Possible reasons are shrinking and

swelling processes and the hysteretic behavior of the hydraulic functions. Both processes are of much higher significance in growing media compared to mineral soils.

The objectives of this study were (i) to describe physical parameters related to water and gas transport in different growing media, and (ii) to test the ability of HYDRUS-1D to describe water content, water uptake, and redistribution in the two materials. The final goal was to develop a simple system to describe water and oxygen supply in growing media, based on a simulation model, usable under practical conditions for growers. Study details of the effect of flooding depth, flooding duration, and type of growing media on water uptake are given in Anlauf et al. (2012).

2. Materials and Methods

2.1. Water Retention Curve

The physical properties of growing media are described with different specific parameters. However, the use of these parameters is not always consistently used in literature. In this study, we used the following definitions (De Boodt and Verdonck, 1972; Raviv and Lieth, 2008): total porosity (TP) (combined volume of the liquid and gaseous phase of the medium), air capacity (AC) (volumetric percentage of the medium filled with air at a matric potential of 10 hPa, i.e., the difference between the water content at 10 hPa and the total porosity), container capacity (CC) (volumetric water content at 10 hPa), easily available water (EAW) (difference between the volumetric water contents at 10 and 50 hPa) and the water buffering capacity (WBC) (difference between the volumetric water contents at 50 and 100 hPa).

The basis for modeling the behavior of water in porous media is the media's pore structure, which is reflected in the water retention curve and the unsaturated hydraulic conductivity function. Both functions are necessary to simulate changes in the content and fluxes of water. After drying, poor rewetting of the growing medium is often observed. Thus, the water content of the substrate upon rewetting at a given matric potential will not reach its value measured before drying. This is due to air inclusions or wetting problems of the organic material and is called hysteresis in the water retention curve (Raviv and Lieth, 2008). Hysteresis becomes especially important in irrigation systems where the water is applied from the bottom of the container, such as ebb-and-flow irrigation (Wever et al., 1997).

Applications of unsaturated flow models often assume unique, non-hysteretic water retention and hydraulic conductivity functions to characterize the hydraulic properties of a material. Such a simplification may be acceptable for flow simulations in mineral soils; growing media usually require a more realistic description involving hysteresis in the soil hydraulic properties (Heinen and Raats, 1999; Naasz et al., 2005; Raviv and Lieth, 2008). The procedure for modeling hysteresis in the retention function in the HYDRUS model requires that both the main drying and main wetting curves are known. In that case θ_r, θ_s and n are assumed constant for the drying and wetting curves (Šimůnek et al., 2008). Thus, α is then the only parameter to change when describing the main wetting and drying curves.

2.2. Initial and Boundary Conditions for the HYDRUS-1D Simulations

The initial water content (or matric potential) for all depths must be specified at the start of the simulation. For the flooding cycle, a matric potential corresponding to the measured initial water content was specified for the depths above the water surface (-20 hPa or 32 % vol and -5000 hPa or 18.7 % vol for the seedling substrate and white peat, respectively). At the water surface during the flooding cycle (4 and 1 cm above the container bottom), a matric potential of 0 hPa was specified, and at the container bottom, a matric potential of +4 and +1 hPa, respectively. Between the container bottom and the water surface, a linear interpolation of the matric potential was carried out. For the drainage cycle, the simulated water content at the end of the flooding cycle was used as initial condition.

Due to the different physical conditions during flooding and drainage phases, different boundary conditions have to be used (Figure 2). For both the flooding and drainage cycles, a constant zero flux was used as the upper boundary condition, i.e. the assumption that there is no evaporation from the surface of the growing media during the short time period of 35 to 105 minutes.

The lower boundary condition during the flooding cycle is a constant matric potential of zero at the water surface. During the drainage cycle, the lower boundary condition changes to a seepage face boundary condition: as long as the lower end of the container is saturated, the pressure head becomes zero and water may leave the container. If the matric potential becomes negative (unsaturated conditions), no more water may leave the container and the flux becomes zero. Thus, the boundary condition changes from a constant zero potential to a constant zero flux (Šimůnek et al., 2008).

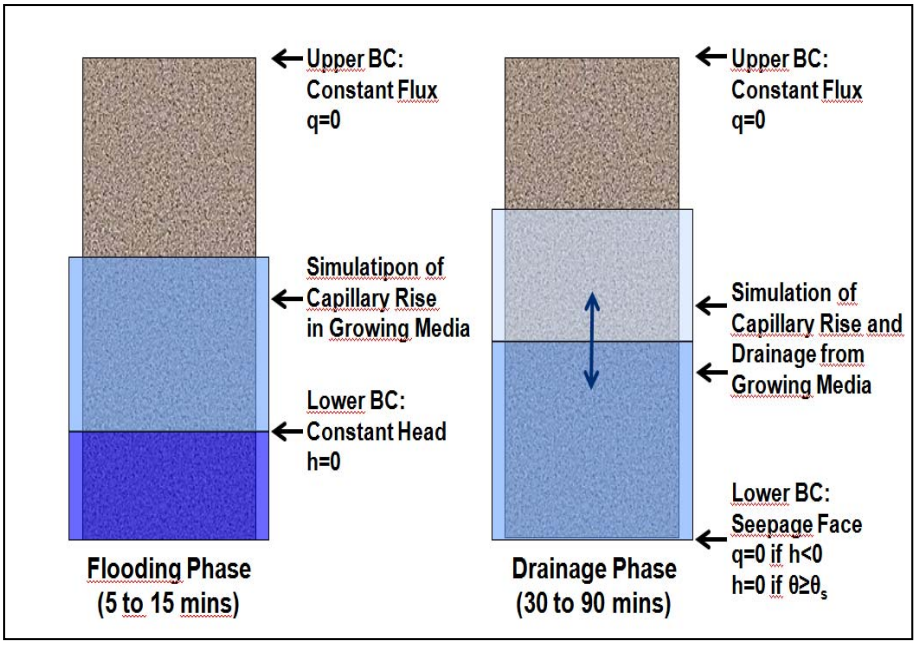

Figure 2. Boundary conditions for the simulation during flooding and drainage phase.

2.3. Model Quality Evaluation

To evaluate the quality of the simulations with HYDRUS-1D, different quality measures were applied: for a quick overview of the modeling quality, graphs measured against the simulated values were drawn together with the linear regression, the correlation coefficient, and the 1:1 line. The points of good quality simulations should lie close to the 1:1 line, the slope of the linear regression should be close to 1, and the correlation coefficient should be close to 1. Widely used measures of agreement between measured and simulated values are the root mean squared error (*RMSE*) and the modeling efficiency (*EF*) (Wallach, 2006):

$$RMSE = \sqrt{\frac{1}{N}\sum_{i=1}^{N}(X_i - P_i)^2} \qquad EF = 1 - \frac{\sum_{i=1}^{n}(X_i - P_i)^2}{\sum_{i=1}^{n}(X_i - X_{av})^2}$$

where N is the number of observations, X_i are the measured values, P_i the simulated (predicted) values and X_{av} the average of the measured values. *EF* calculates the advantage of model results compared to using one average value. If the model gives perfect results, the predicted values P_i will be equal to the measured values X_i and, thus, $EF = 1$. If the average of the measured values is used as a predictor for every case, $EF = 0$. A model which is a worse predictor than the average may result in $EF < 0$. A model with acceptable quality should have $EF > 0.5$.

2.4. Experimental Setup

The experimental container (Figure 3, left) is made up of six elements with an inner diameter of 10 cm. The total height is 15 cm, so that the shrinking of the substrate during irrigation and drying can be considered. The topmost ring is 5 cm high; the following five rings have a height of 2 cm each. The bottom of the container is replaced by a piece of gauze, which is stretched around the lower ring. The volume of the experimental container is 1.178 L. Three flooding times (5 min, 10 min, and 15 min), two flooding depths (1 cm and 4 cm), and 3 drainage durations (10 min, 30 min, and 90 min) were used. The flooding depths and durations were selected according to usual practice. Each treatment was carried out in four replications. To simulate the greenhouse floor, a specially made flooding tub is used (Figure 3, right).

Figure 3. Experimental containers with 10 cm inner diameter and 15 cm height.

2.5. Growing Media Used in the Study

Two types of substrate typically used in horticultural practice were chosen to carry out this investigation: Lithuanian white peat and a commercially available seedling substrate (Figure 4). The seedling substrate contains white peat, black peat and finely sieved cocos fiber. It is a substrate which is used especially for salinity sensitive ornamental seedlings in trays.

Figure 4. Growing media used: Coarse white peat (left) and seedling substrate (right).

The chemical properties of the substrates used in this study (EC 1:5, pH 1:5) were determined according to DIN EN 13037 (2009) and DIN EN 13038 (2009). Organic matter was determined as ignition loss (DIN EN 13039, 2009): air dried and ground substrate samples are burnt at 550°C for 24 h in a muffle furnace. The residue is considered as mineral material and the ignition loss as organic matter. Both are expressed as weight percent and related to dry matter content.

The particle size distribution of each substrate was determined using three 100 g oven dry samples. Each sample was placed on a series of 5 sieves (ranging from 4 to 0.5 mm) and shaken for 5 min at 160 shakes per min. Portions of substrate samples remaining on each screen were weighed and expressed as the percentage of total sample weight. The mean weight diameter (MWD) was calculated according to Kemper and Rosenau (1986). Bulk density was determined after VDLUFA (1991). Particle density (DP) was estimated from the gravimetric organic matter content and the gravimetric mineral matter content (DIN EN 13041, 2010). The saturated hydraulic conductivity was determined with an Eijkelkamp constant head infiltrometer (DIN 19683, 1998).

Water retention drying curves were determined using an Eijkelkamp standard sand box apparatus (Gabriels and Verdonck, 1991; DIN EN 13041, 2010) to measure the water content at pF 0.7, 1.0, 1.5 and 2.0. The TP was calculated as TP = (1 – DB/DP), where DB is bulk density ($g \cdot cm^{-3}$) and DP is the particle density ($g \cdot cm^{-3}$). The water retention curve was parameterized after van Genuchten (1980) from total porosity and the volumetric water content at the measured pF values.

As growing media are known to show intensive hysteretic behavior, water retention wetting curves were determined with the above mentioned experimental container made up of six

elements. The rings were filled with growing media with the same initial water content as in the experiments (-20 hPa or 32%vol and -5.000 hPa or 18.7%vol for the seedling substrate and white peat, respectively) and with the same bulk density. A flooding depth of 1 cm was installed (Figure 5). Under the assumption that the water content at equilibrium is analogous to the water retention curve (Raviv and Lieth, 2008), the water content of the media in the rings 2, 4, 6, and 8 cm above the water surface will correspond to pF log(2) [pF 0.3], pF log(4) [pF 0.6], pF log(6) [pF 0.78], and pF log (8) [pF 0.9]. The water retention wetting curve was parameterized by adjusting the parameter α (Šimůnek et al., 2008). The other van-Genuchten parameters were the same as in the drying curve.

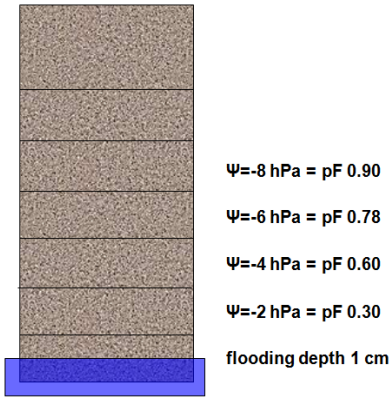

Figure 5. Experimental setup to determine the wetting water retention curve.

3. Results

3.1. Properties of the Growing Media

Table 1 shows some basic properties of the studied materials. The bulk densities of 0.130 and 0.139 $g \cdot cm^{-3}$ and the high organic matter content of 0.069 and 0.886 $g \cdot g^{-1}$ are typical for most growing media. The seedling substrate had a larger percentage of fine particles (< 2 mm; 88.2%) than the white peat (46.4%). The mean weight diameter was 1.15 mm for the seedling substrate and 5.65 mm for the white peat. Consequently, one can expect a higher percentage of small pores, more easily available water, and lower air capacity of the seedling substrate compared to the white peat. This should also be reflected in the water retention curve.

Table 1. Properties of the studied materials.

	pH	EC ($mS \cdot m^{-1}$)	DB ($g \cdot cm^{-3}$)	DP ($g \cdot cm^{-3}$)	OM ($g \cdot g^{-1}$)	FP (%)	MWD (mm)
White Peat	3.9	10	0.130	1.57	0.969	46.4	5.65
Seedling Substrate	5.5	25	0.139	1.63	0.886	88.2	1.15

pH (1:10), EC (1:10), DB: bulk density, DP: particle density,
OM: organic matter, FP: fine particles < 2 mm, MWD: Mean weight diameter

3.2. Water Retention Curves

Major differences were observed in the water holding parameters of the two substrates (Table 2). The total porosity and the water buffering capacity were nearly equal. The container capacity (CC; 0.88 and 0.71 $cm^3 \cdot cm^{-3}$) at 10 hPa and the easily available water (EAW; 0.44 and 0.26 $cm^3 \cdot cm^{-3}$) were significantly higher in the seedling substrate compared to the peat, while the air capacity (AC; 0.03 and 0.21 $cm^3 \cdot cm^{-3}$) was significantly lower for the seedling substrate compared to the white peat. This agrees well with the particle size distribution that showed a high percentage of small particles in the seedling substrate compared to the peat. The measured saturated hydraulic conductivity was slightly lower in the seedling substrate compared to the peat, which also agrees with the smaller particle size.

Table 2. Physical properties of the two materials.

Material	Total Porosity (TP) $cm^3 \cdot cm^{-3}$	Container Capacity (CC) $cm^3 \cdot cm^{-3}$	Air Capacity (AC) $cm^3 \cdot cm^{-3}$	Easily Avail. Water (EAW) $cm^3 \cdot cm^{-3}$	Water Buffering Capacity (WBC) $cm^3 \cdot cm^{-3}$	Sat. Hydraulic Conductivity (Ks) $cm \cdot s^{-1}$
White Peat	0.92	0.71	0.21	0.26	0.06	0.121
Seedling Substr.	0.91	0.88	0.03	0.44	0.05	0.097

Figure 6 shows the drying and wetting water retention curves for both media. The van-Genuchten parameters θ_r, α_w and n were fitted to the measured data by the least square regression, whereas θ_s was fixed as the water content at saturation. The van Genuchten parameters and the air entry values are given in Table 3.

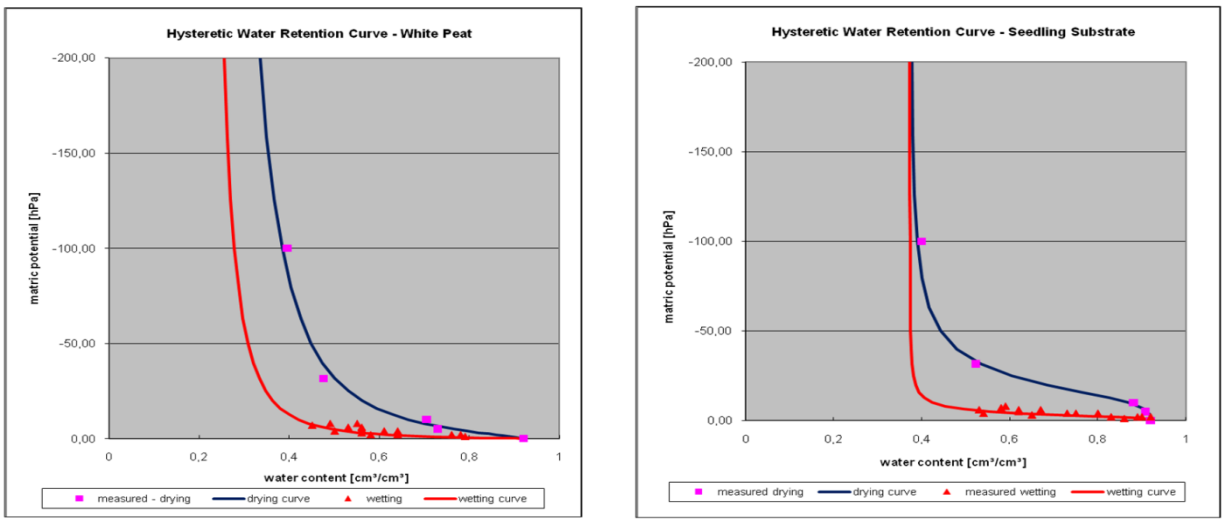

Figure 6. Water retention curves (drying and wetting curves) for the white peat and the seedling substrate.

Table 3. van Genuchten parameters for the water retention drying and wetting curves for the peat and the seedling substrate.

Parameter	White Peat	Seedling Substrate
θ_s [cm³·cm-³]	0.920	0.910
θ_r [cm³·cm-³]	0.187	0.373
α_d	0.232	0.055
α_w	1.600	0.320
α_w/α_d	6.90	5.82
n	1.411	3.022
Air entry value [hPa]	-1	-8

The air entry value (graphical determination according to Konyai et al., 2009) characterizes the matric potential at which the largest pores drain during drying, and air starts entering the material. The air entry value of the peat (-1 hPa) corresponds to a maximum pore size of approximately 3 mm (Hillel, 1998). The air entry value of the much finer seedling substrate (-8 hPa) corresponds to a maximum pore size of approximately 0.375 mm.

The residual water content θ_r of the van-Genuchten parameterization (0.37 and 0.19 $cm^3 \cdot cm^{-3}$ for the seedling substrate and the peat, respectively) also characterizes much higher water content at low matric potentials and thus lower air content. The wetting curves show a distinct hysteresis for both substrates (Figure 6). To describe hysteresis, the α values were fitted to the measured data by the least square regression (Table 3). The parameter α_w, describing the shape of the wet curve, was about 6 times larger than the parameter α_d describing the drying curve. The measured water content at high matric potentials (-5 to -10 hPa), where hysteresis shows its main effect, was about 20% higher for both growing media for the drying curve compared to the wetting curve. This corresponds well with investigations by other authors of hysteresis in peat substrates (Wever et al., 1997; Aendekerk, 1997).

3.3. Simulation Results

In the first step, the water uptake and redistribution was simulated without taking hysteresis into account. As an example, figures 7a and b show the results of the simulation for a flooding duration of 15 min, a flooding depth of 1 cm, and a drainage time of 90 min. Obviously, the simulated water content is much higher than the measured one. In the bottommost layer, the simulated water content exceeds the measured by 10 to 20%vol. In the topmost layer, the simulated water content is about 40 to 50%vol higher than the simulated one. Thus, the model highly over-estimates the amount of water entering the substrate by capillary forces. This fact is also reflected in the significantly different drying and wetting water retention curves. To describe water content and water uptake correctly with the model, the hysteresis of the water retention curve must be taken into account. Considering hysteresis, the simulation yields a completely different picture (Figures 7c and d). Due to hysteresis, the water uptake into the initially relatively dry substrate during the flooding period is much smaller. The measured and simulated values agree much better. Therefore, the simulations for all cases measured were carried out using the hysteretic water retention curves.

Table 4 shows numerical quality measures for the simulation of the water content in the containers. R^2 (0.96 and 0.91 for the white peat and seedling substrate, respectively) is high. The

slope of the regression line (1.15 and 1.20) however, indicates that there is a tendency that the model under-estimates low values and over-estimates high values. Similar but slightly better results can be seen for the water uptake, where R^2 is both 0.98 and the slope is 1.13 and 1.10 for the white peat and seedling substrate, respectively. *RMSE* for the 1 cm flooding depth is less than for a 4 cm flooding depth, and there are no big differences in the simulation quality between the two investigated growing media. The modeling efficiency *EF* ranges from 0.70 to 0.97, indicating a reasonable to very good simulation quality. The maximum total water uptake for the different measurements in the experimental containers is approximately 550 cm³. Similar to the simulation of the water content, the *RMSE* gives similar results for the simulated water uptake (Table 4): the simulation quality for 1 cm flooding depth is better than for a 4 cm flooding depth, and there are no big differences in the simulation quality between the two growing media. *EF* is very high, ranging from 0.95 to 0.99.

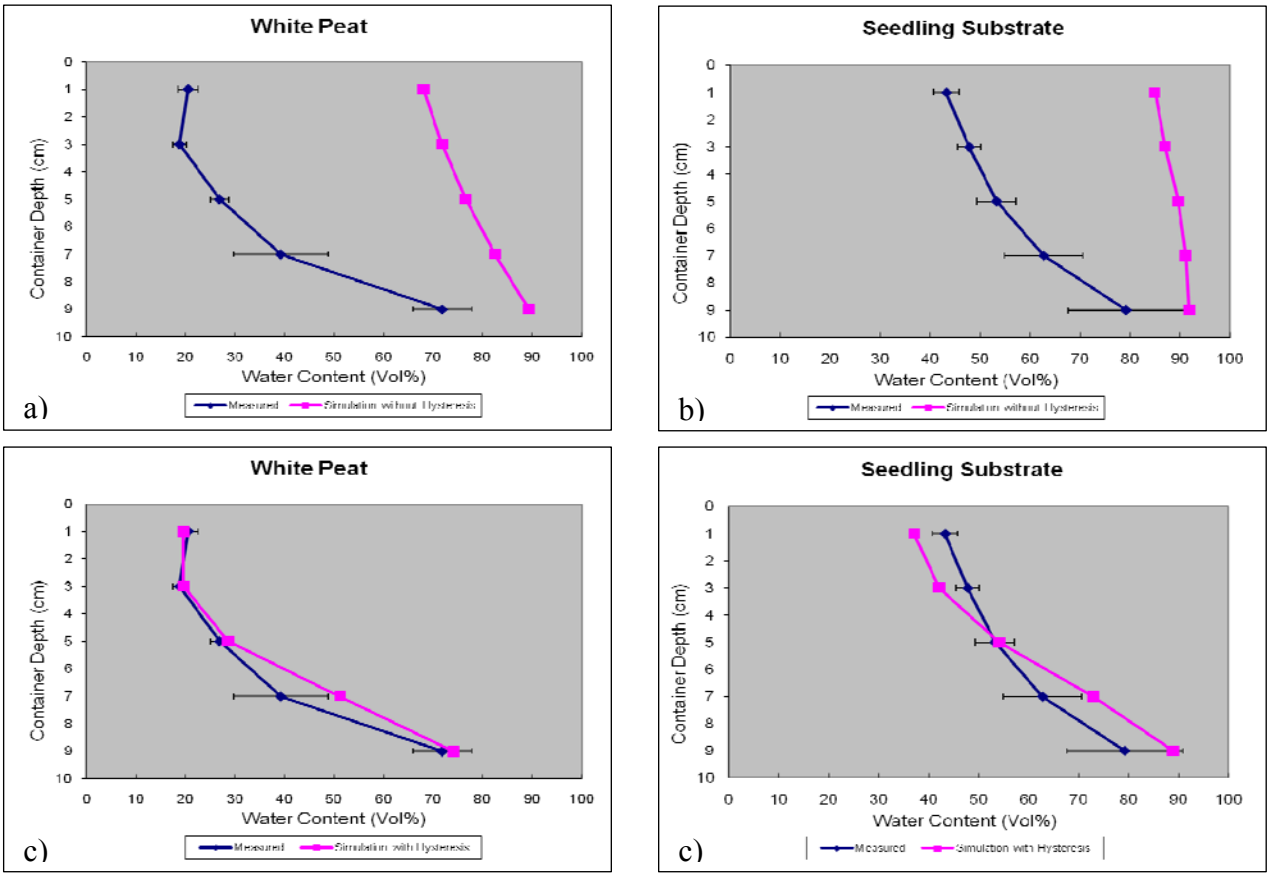

Figure 7. Water content (% vol) after 15 min of flooding, at a flooding depth 1 cm, and after 90 min of drainage, simulated without hysteresis (a, b) and with hysteresis (c, d) for the white peat and the seedling substrate.

Table 4. Quality measures for the simulation of the water content and water uptake.

Measure	White peat			Seedling substrate		
	1 cm flooding depth	4 cm flooding depth	All	1 cm flooding depth	4 cm flooding depth	All
	Simulation of water content					
R^2	0.977	0.956	0.961	0.920	0.868	0.910
Slope	1.040	1.225	1.150	1.211	1.139	1.197
RMSE (%vol)	6.67	8.36	7.56	3.56	8.96	6.81
EF	0.827	0.698	0.766	0.973	0.844	0.905
	Simulation of the water uptake					
R^2	0.988	0.983	0.982	0.974	0.988	0.981
Slope	1.020	1.156	1.129	1.035	1.122	1.103
RMSE (cm^3)	53.61	182.60	134.57	35.88	187.64	135.09
EF	0.994	0.966	0.975	0.994	0.948	0.958
RMSE: root mean squared error; *EF*: modeling efficiency						

4. Discussion and Conclusions

The model highly over-estimates the amount of water entering the substrate by capillary forces. This fact is also reflected in the drying and wetting water retention curves which differ significantly. To correctly describe water content and water uptake with the model, the hysteresis of the water retention curve must be taken into account. During the flooding period, the model mainly uses the wetting water retention curve, whereas during the drainage and redistribution phase, both curves and their connections are used: In the lower parts of the container, the water content mainly decreased during drainage and redistribution, resulting in the use of the drying curve, whereas in the upper part of the container, some capillary rise of water takes place, resulting in the use of the wetting curve.

The simulation results show that the simulation model, HYDRUS-1D is able to basically describe water uptake and redistribution in containers filled with the two investigated growing media. However, as these substrates show high hysteresis of the water retention curve, it is absolutely necessary that the model takes this hysteresis into account. The regression lines of the simulated against the measured values indicate that on average, the higher water contents are slightly over-estimated, whereas the lower water contents are under-estimated. A possible reason is that the hysteresis of the water retention curve is not completely correctly described because this hysteresis mainly governs the water uptake and distribution in the container. The description of hysteresis is simplified in two aspects: 1) the wetting curve is described only by changing the parameter α of the van-Genuchten parameterization while the other parameters are kept constant. This is done because the HYDRUS-1D version used has only this option to consider hysteresis, while other authors suggest that hysteresis of growing media needs a more complex formulation (Naasz et al., 2005); 2) the determination of the wetting curve was done in a very simple way to measure the water content in different layers after water uptake took place and then relating these values to the theoretical matric potential at equilibrium. This method should be evaluated and optimized in future investigations. However, the use of HYDRUS-1D seems to be a promising method to overcome the pure static description of physical properties of growing media, such as

available water capacity and air capacity, and moves toward a dynamic description of the water movement in containers, with the ultimate goal of optimizing the production of horticultural plants produced in growing media.

5. Outlook and Future Work

The final goal of the investigation was to develop a simple system to describe oxygen supply in growing media based on a simulation model. The basis for the simulation of oxygen in growing media is a correct simulation of water uptake and redistribution. The next step will be measuring and modeling the dependency of the oxygen diffusion coefficient on air content for different growing media in diffusion chambers with different bulk densities. Preliminary results show that the oxygen diffusion coefficient depends on water content and substrate density, which both influence air content of growing media. There is a stable dependency of the oxygen diffusion coefficient on air content, irrespective of the type of growing media (Schmitz et al., 2013). This relation can best be described by the function of Moldrup (1997).

Another important factor to describe oxygen supply is the oxygen consumption for different growing media, bulk densities, and water contents, which was determined by the Isermeyer method and showed high variability depending on water, nutrient, and pH status of the growing media (unpublished). Oxygen concentration profiles were measured for different growing media, different densities, and under different irrigation situations with optical O_2 sensors (unpublished). In a final step, the public domain HYDRUS source code will be modified to take the changes in the boundary conditions and the different ways to describe the oxygen diffusion coefficient into account.

References

Aendekerk T. G. L., Decomposition of peat substrates in relation to physical properties and growth of Chamaecyparis, *Acta Hort., 450*, 191-198, 1997.

Anlauf R., P. Rehrmann, and H. Schacht, Simulation of water uptake and redistribution in growing media during ebb-and-flow irrigation, *J Horticulture and Forestry, 4*, 8-21, 2012.

Bradford, S. A., J. Šimůnek, M. Bettahar, M. Th. van Genuchten, and S. R. Yates, Modeling colloid attachment, straining, and exclusion in saturated porous media, *Environmental Science & Technology*, *37*, 2242-2250, 2003.

De Boodt, M., and O. Verdonck, The physical properties of the substrates in horticulture, *Acta Hort.*, *26*, 37-44, 1972

DIN 19683, Methods of Soil Investigations for agricultural engineering – Physical laboratory tests – Part 9: Determination of the saturated hydraulic water conductivity in the cylindrical core-cutter (in German), Beuth, Berlin, 1998.

DIN EN 13037, Soil Improvers and growing media – Determination of pH, German Version prEN 13037:2009, Beuth, Berlin, 2009.

DIN EN 13038, Soil Improvers and growing media – Determination of electric conductivity, German Version prEN 13038:2009, Beuth, Berlin, 2009.

DIN EN 13039, Soil Improvers and growing media – Determination of organic content and ash. German Version prEN 13039:2009, Beuth, Berlin, 2009.

DIN EN 13041, Soil Improvers and growing media – Determination of physical properties – Dry bulk density, air volume, water volume, shrinkage value and total pore space, German Version prEN 13041:2010, Beuth, Berlin, 2010.

Fonteno, W. C., Problems and considerations in determining physical properties of horticultural substrates, *Acta Hort.*, *342*, 197-204, 1993.

Gabriels, R., and O. Verdonck, Physical and chemical characterization of plant substrates: towards a European standardization, *Acta Hort.*, *294*, 249-259, 1991.

Heinen, M., and P. de Willigen, Dynamics of water and nutrients in closed, recirculating sand bed systems: Modeling water flow, nutrient transport, root water and nutrient uptake, *Acta Hort.*, *401*, 501-508, 1995.

Heinen, M., and P. A. C Raats, Hydraulic properties of root zone substrates used in greenhouse horticulture, In: M. Th. Van Genuchten et al. (ed.) Proc. Int. Workshop on the characterization and measurement of the hydraulic properties of unsaturated porous media, Univ. of California, Riverside, 467–476, 1999.

Hillel D., Environmental Soil Physics, Academic Press, San Diego,1998.

Kemper W.D. and R.C. Rosenau, Aggregate stability and size distribution, In: Klute, A. (ed), Methods of soil analysis, Part 1. 2nd ed *Agron. Monogr. No 9*. ADSA and SSSA, Madison WI, 425-441, 1986.

Konyai, S., V. Sriboonlue, and V. Trelo-Ges, The effect of air entry values on hysteresis of water retention curve in saline soil, *American Journal of Environmental Sciences*, *5*, 341-345, 2009.

Moldrup, P., T. Olesen, D. E. Rolston, and T. Yamaguchi, Modeling diffusion and reaction in soils: VII. Predicting gas and ion diffusivity in undisturbed and sieved soils, *Soil Science*, *162*, 632-640, 1997.

Naasz, R., J. C. Michel, and S. Charpentier, Measuring hysteretic hydraulic properties of peat and pine bark using a transient method, *Soil Sci. Soc. Am. J.*, *69*, 13-22, 2005.

Palla, A., L. G. Lanza, and P. La Barbera, A green roof experimental site in the Mediterranean climate, Proc. 11th Conf. on Urban Drainage, Edinburgh, UK, 31. Aug.-5. Sept., 2008.

Raviv, M. and J. H. Lieth, Soilless Culture: Theory and Practice, Elsevier, 2008.

Schmitz, D., R. Anlauf, and P. Rehrmann, Effect of air content on the oxygen diffusion coefficient of growing media, *Am. J. Plant Sci.*, 2013 (in press).

Šimůnek, J., M. Šejna, H. Saito, M. Sakai, and M. T. van Genuchten, The HYDRUS-1D Software Package for Simulating the Movement of Water, Heat, and Multiple Solutes in Variably Saturated Media, Version 4.0, HYDRUS Software Series 3, Department of Environmental Sciences, University of California Riverside, Riverside, California, USA, 2008.

van Genuchten, M. T., A closed form equation for predicting the hydraulic conductivity of unsaturated soils, *Soil Sci. Soc. Am. J.*, *49*, 12-19, 1980.

VDLUFA, Bestimmung der Rohdichte (Volumengewicht) von gaertnerieschen Erden und Substraten ohne sperrige Komponenten. Methodenbuch Band I: Die Untersuchung von Boeden. Darmstadt, 1991.

Wallach, D., Evaluating Crop models. In: Wallach, D., D. Makowski, J. W. Jones (Ed.), Working with dynamic crop models, Elsevier, 11-53, 2006.

Wever, G., A. A. van Leeuwen, and M. C. van der Meer, Saturation rate and hysteresis of substrates, *Acta Hort.* , *450*, 287-295, 1997.

Application of the HYDRUS (2D/3D) Inverse Solution Module for Estimating the Soil Hydraulic Parameters of a Quaternary Complex in Northern Bulgaria

Dimitar Antonov[1], Dirk Mallants[2], Jirka Šimůnek[3], and Doncho Karastanev[1]

[1]*Geological Institute, Bulgarian Academy of Sciences, Sofia, Bulgaria, dimia@geology.bas.bg, doncho@geology.bas.bg*
[2]*CSIRO Land and Water, Urrbrae, South Australia, Dirk.Mallants@sciro.au*
[3]*Department of Environmental Sciences, University of California Riverside, CA, USA, jiri.simunek@ucr.edu*

Abstract

Characterizing hydraulic properties of the unsaturated zone at spatial scales commensurate with the numerical model grid size is key to reliable predictive modeling of the fate and transport of contaminants in the environment. We used the HYDRUS (2D/3D) model and inverse modeling to determine the hydraulic properties of a 10-m deep vadose zone from borehole infiltration tests. The investigated soil profile is located in the Pleistocene loess complex near the town of Kozloduy, Northern Bulgaria, in the vicinity of the Kozloduy Nuclear Power Plant (NPP). Four constant-head infiltrometer tests were carried out several meters below the ground surface to determine the unsaturated hydraulic properties of a silty loess, clayey loess, clayey gravel, and a highly carbonated layer. Infiltration tests provided data on cumulative infiltration and the movement of the wetting front in the initially unsaturated sediments surrounding the infiltrometer. A cylindrical TRIME-IPH/T3 time-domain reflectometry probe was used to measure water content variations with time during the movement of the wetting front. An axisymmetric model was developed in HYDRUS (2D/3D) for each of the four infiltrometer tests. The inverse optimization routine implemented in HYDRUS (2D/3D) was used to determine field-scale soil hydraulic parameters θ_r, θ_s, α, n, and K_s for all layers of interest. Results suggest the size of the affected volume of soil was large enough to reduce the effect of spatial variability and to produce effective field-scale hydraulic parameters that are relevant for prediction of large-scale, variably-saturated water flow and radionuclide migration pathways at the Kozloduy NPP site.

1. Introduction

At present, only one nuclear power plant (NPP) is in operation in Bulgaria. Two reactors out of six are still in operation near the town of Kozloduy, while the remaining four were shut down in December 2002 (units 1 and 2) and December 2006 (units 3 and 4). A National Repository for Low and Intermediate Level Radioactive Waste (LILW) from all the units is foreseen to be built in the vicinity of the Kozloduy NPP. The investigated area represents an undulating landscape developed on Pliocene clay covered with loess sediments, with the groundwater table usually located in a clay formation at a depth of about 30 m (Antonov, 2002). For the purposes of a safety assessment for the LILW repository, an evaluation of radionuclide migration through variably-saturated, geological strata should be performed.

The fate and transport of contaminants in the geosphere is a multi-process phenomenon. It usually involves the combination of several physical and chemical processes, such as convective

mass transport, hydrodynamic dispersion, molecular diffusion, adsorption/desorption, ionic exchange, precipitation/dissolution, radioactive decay, etc. (Jacques et al., 2008; Mallants et al., 2011). Hence, the relevant numerical simulators should incorporate all the above processes. The most popular approaches to the mathematical description of water flow and mass transport incorporate the Richards equation for variably-saturated flow and the Fickian-based convection-dispersion equation for solute transport (Mallants et al., 2011). Therefore, the characterization of hydrological parameters and subsequent numerical modeling of water flow in the vadose zone is a key component in any contaminated site risk assessment. Accurate analysis of the unsaturated flow regime requires an investigation of the stratification in soil and sediment profiles and determination of layer-specific hydraulic parameters by either laboratory or field tests. When the soil is characterized by a complicated structure and texture, the results of laboratory tests carried out on small samples may not fully capture properties of the unsaturated zone (Mallants et al., 1997). Examples of successful determination of the soil hydraulic parameters via different types of field experiments, including for the purposes of migration analyses, can be found in Kodešová et al. (1999) and Gvirtzman et al. (2008). This paper discusses the use of the HYDRUS (2D/3D) (Šimůnek et al., 2006) computer code to determine by inverse modeling hydraulic parameters of the vadose zone from borehole infiltration tests. The investigated 10-m deep soil profile is located in the Pleistocene loess complex near the town of Kozloduy, Northern Bulgaria.

2. Theory and Methods

Water flow in variably-saturated soils is described using the Richards equation. A one-dimensional form is given as follows:

$$\frac{\partial \theta}{\partial t} = \frac{\partial}{\partial z}\left[K(h)\left(\frac{\partial h}{\partial z} + 1 \right) \right] \tag{1}$$

where θ is the volumetric soil water content [L^3L^{-3}], t is time [T], z is the vertical coordinate (from a reference level) [L], K is the unsaturated hydraulic conductivity [LT^{-1}], and h is the soil water pressure head [L]. Numerical solution of Eq. (1) requires the knowledge of two highly nonlinear functions, namely the soil water retention curve, $\theta(h)$, and the unsaturated hydraulic conductivity function, $K(h)$. One of the most popular and flexible equations describing $\theta(h)$ was developed by van Genuchten (1980). When coupled with the statistical pore size distribution model of Mualem (1976), it gives a closed-form equation for $K(h)$:

$$\theta(h) = \begin{cases} \theta_r + \dfrac{\theta_s - \theta_r}{\left(1 + \left(\alpha |h|\right)^n\right)^m} & h < 0 \\ \theta_s & h \geq 0 \end{cases} \tag{2}$$

$$K(h) = \begin{cases} K_s K_r(h) & h < 0 \\ K_s & h \geq 0 \end{cases} \tag{3}$$

where

$$K_r = S_e^l \left[1 - \left(1 - S_e^{1/m} \right)^m \right]^2 \tag{4}$$

and where θ_r and θ_s are, respectively, the residual and saturated water contents [L^3L^{-3}], α [L^{-1}], n [−], and m (m=1−1/n) are empirical constants defining the shape of the curves, h is the soil water pressure head [LT^{-1}], l is an empirical constant [-], assumed equal to 0.5, K_r is the relative hydraulic conductivity [-], K_s is the saturated hydraulic conductivity [LT^{-1}], and S_e is the saturation degree given by:

$$S_e = \frac{\theta - \theta_r}{\theta_s - \theta_r} \tag{5}$$

According to the van Genuchten-Mualem model, knowledge of the five parameters θ_r, θ_s, α, n, and K_s allows quantification of the two functions $\theta(h)$ and $K(h)$ (van Genuchten, 1980). The values of these parameters for a given soil can be determined using field and/or laboratory tests (Mallants et al., 2007; Antonov et al., 2012). The software code HYDRUS (2D/3D) incorporates the above-mentioned relations (Šimůnek et al., 2006). The automatic parameter optimization routine implemented in HYDRUS (2D/3D) was used to optimize the parameters α and K_s (*see further*). The HYDRUS code adopts the minimization of the sum of squared residual (SSQ):

$$SSQ = \sum_{i=1}^{N} \left(q_{p,i} - q_{o,i} \right)^2 \tag{6}$$

where N is the number of the calibration points (note that here only the cumulative fluxes are used), $q_{p,i}$ is the ith predicted value, and $q_{o,i}$ is the ith observed value. The HYDRUS code uses the Marquardt-Levenberg optimization algorithm to minimize the objective function (6).

3. Field Infiltration Tests – Results and Discussion

Constant-head infiltration tests were carried out for determining the field-scale soil hydraulic properties. Four such tests were carried out down to a depth of 10 m in the unsaturated Pleistocene loess complex. Infiltration tests provided data on cumulative infiltration and progression of the wetting front in the initially unsaturated sediments surrounding the infiltrometers. A cylindrical time-domain reflectometry TRIME-IPH/T3 probe operated by the TRIME-HD device was used to measure water content variations with time during the progression of the wetting front. Special polycarbonate access tubes for the TRIME probe were installed at 0.3 to 0.5 m from the infiltrometers. A more detailed description of the field and technical equipment layout could be found in Mallants et al. (2007). By means of an inverse optimization routine implemented in the finite element code HYDRUS (2D/3D), field-scale soil hydraulic parameters θ_r, θ_s, α, and n were derived for particular layers, namely silty loess, clayey loess, clayey gravel, and a highly carbonated zone. For cemented layers, such as the clayey gravel and the carbonated zone, collection of classical soil cores is not possible, leaving only field determination as a reliable option for determining hydraulic properties (Fig. 1). The inverse optimization is based on simulating the expected soil water redistribution history while adjusting

the soil hydraulic parameters until the best possible agreement is obtained between measured and calculated cumulative infiltration and soil moisture profiles. An axisymmetric model was developed in HYDRUS (2D/3D) for each of the four infiltrometers (Fig. 2).

Figure 1. Carbonate concretions in the carbonated zone (left) and gravel concretions from the gravel layer (right).

The vertical dimension of the model was limited to the soil layers that would be immediately influenced by infiltrating water (Fig. 2). The simulation starts with "guess" or "trial" values of the soil hydraulic properties; these values may be estimated using pedotransfer functions based on particle size data, or by using some other prior information, e.g., laboratory tests data.

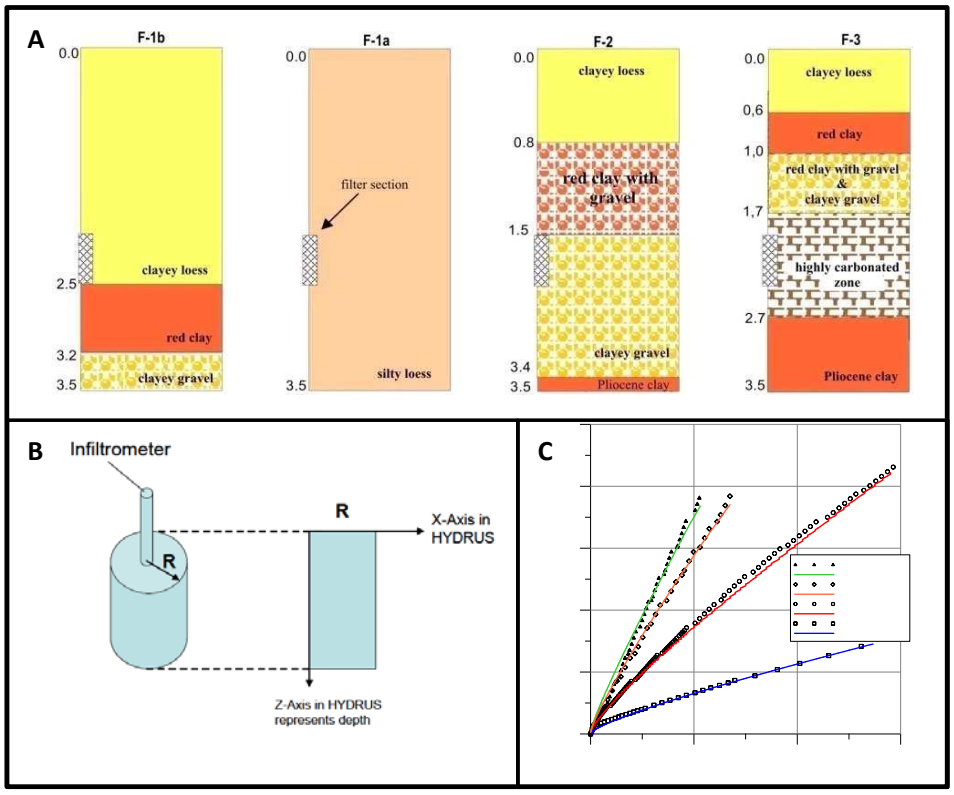

Figure 2. A) Conceptual models used in flow calculations. Vertical dimensions (in m) refer to model coordinates. B) An axisymmetrical quasi-3D model. C) Observed and calculated cumulative infiltrations.

An initial optimization with three parameters, α, K_s, and n, showed a high correlation between α and K_s, and a high standard error coefficient for n, indicating non-uniqueness of the solution. Therefore, the n parameter was excluded from optimization. The parameter optimization routine provided in HYDRUS (2D/3D) was invoked to further optimize the parameters α and K_s. The n parameter was kept constant at its initial value of 2 (obtained from initial trial runs). The results from parameter optimization for each of the modeled infiltrometers F-1b, F-1a, F-2, and F-3 are shown on Table 1. Overall good fits were obtained with hydraulic parameters being representative of several cubic meters of soil.

Table 1. Parameter values obtained by an inverse optimization using HYDRUS (2D/3D).

Soil description	Parameter	Best fitted value	S.E. coefficient	Lower 95%	Upper 95%
Clayey loess*	α [m^{-1}]	0.351	0.0354	0.281	0.490
	K_s [ms^{-1}]	6.03E-07	0.00144	0.0492	0.0549
	SSQ	0.0119	-	-	-
	R^2	0.997	-	-	-
Red clay	α [m^{-1}]	0.497	0.450	-0.395	1.39
	n [-]	4.29	-	-	-
	K_s [ms^{-1}]	6.89E-07	0.0229	0.0140	0.105
	SSQ	0.0118	-	-	
	R^2	0.997	-	-	-
Silty loess*	α [m^{-1}]	0.0586	0.00849	0.0418	0.0754
	K_s [ms^{-1}]	5.20E-07	0.00068	0.0436	0.0463
	SSQ	0.00281	-	-	-
	R^2	0.999	-	-	-
Clayey gravel*	α [m^{-1}]	3.00	1.17	0.701	5.30
	K_s [ms^{-1}]	1.06E-06	0.000739	0.089	0.0927
	θ_s [cm^3cm^{-3}]**	0.431	0.00011	0.411	0.416
	SSQ	0.00251 (0.000605)**	-	-	-
	R^2	0.999 (0.999)**	-	-	-
Highly carbonated zone*	α [m^{-1}]	2.68	2.29	-1.85	7.21
	K_s [ms^{-1}]	1.88E-07	0.000246	0.0158	0.0168
	θ_s [cm^3cm^{-3}]	0.354	0.0229	0.308	0.399
	SSQ	0.00391	-	-	-
	R^2	0.998	-	-	-

*Parameter n is fixed at 2; ** when θ_s fitted separately.

4. Conclusions

Field investigations have been performed in order to characterize the unsaturated zone in the Pleistocene loess sediments near the town of Kozloduy, Northern Bulgaria. The values of the van Genuchten model parameters have been derived from a series of field borehole infiltration tests using an inverse optimization with the computer code HYDRUS (2D/3D). Due to the small measurement scale of the laboratory test and the inability to obtain core samples from strongly cemented layers, the use of a field-scale approach is the preferred option for obtaining hydraulic flow parameters representative of larger soil volumes typically used as grid elements in numerical models. Field-scale hydraulic parameters obtained at different locations were

consistent, showing only little special variability. The use of a field infiltrometer set-up, in which a relatively large volume of soil is affected by the constant head infiltration process, averages out the effects of special variability. The use of field infiltration data in an inverse optimization routine of the computer code HYDRUS (2D/3D) is a practical and reliable methodology to obtain field-scale hydraulic characteristics. Additional modeling work is required in the implementation of the TRIME probe data into the objective function of the minimization procedure.

References

Antonov, D., Loess near Kozloduy NPP as a medium for low and intermediate level radioactive waste disposal, PhD Thesis, Geological Institute – BAS, 167 pp., 2002.

Antonov, D., D. Karastanev, D. Mallants, Determination of soil hydrologic parameters for multi-layered loess sediments using HYDRUS-2D and field infiltration experiments, *Comptes endus de l`Academy bulgare des Sciences*, *65*(12), 1717-1724, 2012.

Gvirtzman, H., E. Shalev, O. Dehan, and Y. Hazor, Large-scale infiltration experiments into unsaturated stratified loess sediments: monitoring and modeling, *Journal of Hydrology*, *349*, 214-229, 2008.

Jacques, D., J. Šimůnek, D. Mallants, and M. Th. Van Genuchten, odeling coupled hydrologic and chemical processes: Long-term Uranium transport following Phosphorus fertilization, *Vadose Zone Journal*, *7*(2), 698–711, 2008.

Kodešová, R., S. E. Ordway, M. M. Gribb, and J. Šimůnek, Estimation of soil hydraulic properties with the cone permeameter: Field studies, *Soil Science*, *164*(8), 527-541, 1999.

Mallants, D., B. P. Mohanty, D. Jacques, and J. Feyen, Spatial variability of hydraulic properties in a multi-layered soil profile, *Soil Science*, *161*, 167–181, 1996.

Mallants, D., B. P. Mohanty, A. Vervoort, and J. Feyen, Spatial analysis of saturated hydraulic conductivity in a soil with macropores, *Soil Technology*, *10*, 115–131, 1997.

Mallants, D., D. Karastanev, D. Antonov, and J. Perko, Innovative in-situ determination of unsaturated hydraulic properties in deep loess sediments in North-West Bulgaria, Proceedings of the *11th International Conference on Environmental Remediation and Radioactive Waste Management*, Bruges, ICEM2007–7202, 733–740, 2007.

Mallants, D., M. Th. van Genuchten, J. Šimůnek, D. Jacques, and S. Seetharam, Leaching of contaminants to groundwater, Chapter 18, In: *Dealing with Contaminated Sites. From Theory towards Practical Application* (ed. F. A. Swartjes), Dordrecht, the Netherlands, Springer, ISBN: 978-90-481-9756-9, 787–850, 2011.

Mualem, Y., A new model for predicting the hydraulic conductivity of unsaturated porous media, *Water Resources Research*, *12*, 513–522, 1976.

Šimůnek, J., N. J. Jarvis, M. Th. Van Genuchten, and A. Gärdenäs, Review and comparison of models for describing non-equilibrium and preferential flow and transport in the vadose zone, *Hydrology Journal*, *272*, 14–35, 2003.

Šimůnek, J., M. Th. van Genuchten, and M. Šejna, *The HYDRUS Software Package for Simulating Two- and Three-Dimensional Movement of Water, Heat, and Multiple Solutes in Variably-Saturated Media*, Technical Manual, Version 1.0, PC Progress, Prague, Czech Republic, pp. 241, 2006.

van Genuchten, M. Th., A closed-form equation for predicting the hydraulic conductivity of unsaturated soils, *Soil Science Society of America Journal*, *44*, 892–898, 1980.

Using Hydrus-HP1 to Estimate 226Ra Transport in Soils Following the Use of Phosphogypsum in Agriculture

Camila R. Bezerra Coelho[1], Márcia S. Batalha[1], Maria Claudia Barbosa[1], Diederik Jacques[2], and Martinus Th. van Genuchten[3]

[1]*Department of Civil Engineering, Federal University of Rio de Janeiro, UFRJ, Rio de Janeiro, RJ, Brazil*
camila.rosabz@gmail.com, marciabatalha.nunes@gmail.com, mclaudia@coc.ufrj.br
[2]*Performance Assessments, Institute of Environment, Health and Safety, Belgian Nuclear Research Centre, Mol, Belgium, djacques@sckcen.be*
[3]*Department of Mechanical Engineering, Federal University of Rio de Janeiro, UFRJ, Rio de Janeiro, RJ, Brazil, rvangenuchten@hotmail.com*

Abstract

Agricultural soils generally require the use of fertilizers and soil conditioners for optimal production. Phosphate fertilizers produced from igneous phosphate rock often contain small amounts of natural radionuclides (most notably ^{238}U and ^{232}Th), while the byproduct phosphogypsum (dihydrated calcium sulfate) is enriched in ^{226}Ra and ^{210}Pb. Our study focused on the long-term (200 year) subsurface fate of ^{226}Ra when phosphogypsum (PG) is applied annually for 27 years as an amendment to a typical Brazilian Cerrado soil profile, after which PG applications ceased but agriculture continued. Expected water flow and solute transport processes were estimated first using the standard HYDRUS-1D software package assuming linear equilibrium transport, followed by simulations using the HP1 module of HYDRUS-1D. Analyses with HP1 considered a range of geochemical and physical parameters affecting ^{226}Ra transport in the vadose zone, especially the effects of varying calcium concentrations resulting from the PG applications. Several aspects related to the modeling approach, such using daily versus monthly averaged weather data and assuming long-term steady-state flow conditions, are discussed also.

1. Introduction

Natural radioactivity is common in most or all soils and rocks. This natural radioactivity may change when fertilizers or amendments are used in agricultural operations to improve crop production. For example, phosphate fertilizers often contain small amounts of radionuclides from the uranium (^{238}U) and thorium (^{232}Th) decay chains. During the phosphate production process, the naturally occurring U and Th decay series in the host rock are disrupted and some of the radionuclides tend to accumulate in both the fertilizer itself (approximately 86% of ^{238}U and 70% of ^{230}Th) and the by-product phosphogypsum (about 80% of ^{226}Ra and its daughter products) (Mazzilli et al., 2000; Papastefanou et al., 2006, Saueia and Mazzilli, 2006). For every ton of phosphoric acid being produced (the basic constituent for the production of phosphate fertilizers), about 4.8 tons of phosphogypsum (PG) is being generated. Because of its ^{226}Ra content, PG in many countries is considered a waste and stockpiled in very large quantities.

In Brazil, a major agricultural production area is the Cerrado region. Cerrado soils typically are highly weathered, slightly acidic, leached, have a relatively low cation exchange capacity, and are poor in nutrients such as P, Ca and Mg. Natural gypsum has long been used as an amendment or soil conditioner for such situations. Since PG is rich in P, Ca and Mg, many studies have

advocated the use of PG as both a fertilizer and soil conditioner to reduce subsoil acidity and Al toxicity, as well as to promote sodic soil reclamation and reduce soil erosion (Oster, 1982; Oates and Caldwell, 1988; Embrapa, 2005; among others).

Detailed analyses are needed to understand the possible accumulation of radionuclides when fertilizers and/or phosphogypsum are being applied routinely over long periods of time to the same field (Jacques et al., 2008; Batalha et al. 2011b). For this purpose we used the HYDRUS-1D flow and transport simulator (Šimůnek et al., 2008) to predict the long-term fate and transport of ^{226}Ra present in PG into and through the vadose zone to groundwater, assuming linear equilibrium transport. Rather than considering one single application, which should have very little impact on the environment (e.g., Rothbaum et al., 1979; Zielinski et al., 1997), the application is assumed to be repeated once every year for 27 years to a typical soil profile in the Cerrado region of Brazil. The transport of ^{226}Ra in the vadose soil is subsequently followed for another 170 years.

A recent study by Jacques et al. (2008) shows that radionuclide transport in soils is affected by a range of physical and geochemical processes. Their study focused on the transport of uranium following the long-term use of phosphate fertilizers, as opposed to radium in this study. Since radium and calcium released from applied PG may compete for the same sorption sites, several simulations were performed using the HP1 (Jacques and Šimůnek, 2010) multicomponent transport module of HYDRUS-1D. The module was obtained by coupling HYDRUS-1D with the PHREEQC biochemical code (Parkhurst and Appelo, 1999). We were especially concerned about the possible effects of varying calcium concentrations on ^{226}Ra transport. Several aspects related to the modeling approach, such as the use of daily versus monthly weather data and the effect of assuming different transport regimes in the vadose zone (notably transient versus long-term steady-state flow) are discussed also. Additional details of the simulations are presented elsewhere (Batalha et al., 2011, 2012).

2. Simulation Methodology

The scenario of concern is the repeated application of phosphogypsum to the same Cerrado soil profile, and resultant ^{226}Ra accumulation and transport in the vadose zone, and possibly into underlying groundwater. We considered a 2-m deep physically and chemically uniform soil profile, without any preferential water flow. Since contaminant transport is very much affected by the rates of water flow into and through the soil profile as a function of local weather conditions, transient precipitation and evaporation conditions were evaluated. Phosphogypsum was assumed to be applied once each year for 27 years to the soil surface in the form of a short pulse with known composition. Free drainage conditions were imposed at the bottom of the profile. In this study we did not consider any uptake of water and solutes by plant roots.

Water flow in the soil profile is described using the standard Richards equation (Šimůnek et al., 2008):

$$\frac{\partial \theta(h)}{\partial z} = \frac{\partial}{\partial z}\left[K(h)\left(\frac{\partial h}{\partial z} + 1\right)\right] \tag{1}$$

where h is the soil water pressure head [L], θ is volumetric water content [L^3L^{-3}], t is time [T], z is the spatial coordinate (positive upward in this study) [L], and K is the hydraulic conductivity [LT^{-1}].

The volumetric water content (θ) and the hydraulic conductivity (K) in Equation (1) are strongly nonlinear functions of the pressure head, h. These functions are described here using the constitutive relationship of van Genuchten (1980) as follows:

$$S_e(h) = \frac{\theta - \theta_r}{\theta_s - \theta_r} = \begin{cases} \left(1 + |\alpha h|^n\right)^{-m} & h < 0 \\ 1 & h \geq 0 \end{cases} \tag{2a}$$

$$K(h) = K_s S_e^l \left[1 - (1 - S_e^{1/m})^m\right]^2 \tag{2b}$$

where S_e is effective saturation [L^3L^{-3}], θ_r and θ_s are the residual and saturated volumetric soil water contents, respectively [-], K_s is the saturated hydraulic conductivity [LT^{-1}], and α [L^{-1}], n>1 [-], m=1-1/n [-] and l [-] are mostly empirical shape factors. Following van Genuchten (1980), the pore-connectivity parameter l was fixed at a value of 0.5.

Radionuclide transport was simulated initially with HYDRUS-1D using the standard linear equilibrium advection-dispersion equation:

$$\frac{\partial(\theta RC)}{\partial t} = \frac{\partial}{\partial z}\left(\theta D \frac{\partial C}{\partial z} - qC\right) - \mu\theta RC \tag{3}$$

where C is the solution concentration [ML^{-3}], R the retardation factor [-], D is the dispersion coefficient [L^2T^{-1}], q is the Darcy-Buckingham volumetric flux [LT^{-1}], and μ is the decay coefficient [T^{-1}] for the particular radionuclide being considered (in our case ^{226}Ra). Since the half-life of ^{226}Ra (1600 years) is much greater than the time period of our study (200 years), radioactive decay will not be considered here (i.e., μ=0). The parameters R and D in Eq. (3) are given by:

$$R = 1 + \frac{\rho_b K_d}{\theta} \tag{4}$$

$$D = D_d \tau + \lambda \frac{|q|}{\theta} \tag{5}$$

in which ρ_b is the bulk density of the soil [ML^{-3}], K_d is the distribution coefficient for linear sorption [L^3M^{-1}], λ is the longitudinal dispersivity [L], D_d is the diffusion coefficient in free water [L^2T^{-1}], and τ is the porous medium tortuosity factor [-] given by $\theta^{7/3}\theta_s^{-2}$ (Millington and Quirk, 1961).

Geochemical transport involving phosphogypsum was represented by a system of N_m reaction equations for the primary (or master) species, in canonical form given by

$$\sum_{j=1}^{N_m} \nu_{ji} A_j = A_i \tag{6}$$

and correspondent mass action equations assuming equilibrium:

$$K_i = \gamma_i C_i \prod_{j=1}^{N_m} (\gamma_j C_j)^{-\nu_{ji}} \tag{7}$$

where N_m the number of master aqueous species, A_j and A_i are the chemical equations for the master and secondary species, respectively, ν_{ji} are stoichiometric coefficients of the reaction, K_i is the equilibrium constant of a reaction, γ_i is the activity coefficient of the aqueous complex, and γ_j is the activity coefficient for the j^{th} master species in solution.

Transport of each species is represented in the above manner by a set of N_m multicomponent reactive transport equations of the form (Jacques et al., 2008):

$$\frac{\partial(\theta C_j)}{\partial t} = \frac{\partial}{\partial z}\left(\theta D \frac{\partial C_j}{\partial z} - q C_j\right) + R_{0,j} \tag{8}$$

where $R_{0,j}$ is the reaction term representing the sources/sinks for each aqueous component, C_j is the total concentration of master species j

$$C_j = c_j + \sum_{i=1}^{N_s} \nu_{ji} c_i \tag{9}$$

in which N_s the number of secondary aqueous species, and c_i is the concentration of secondary species i.

For ^{226}Ra sorption we assumed a relatively simple equilibrium approach that lumps all of the sorption processes onto the solid phase into a single linear isotherm in which the distribution coefficient is a nonlinear function of the calcium concentration, as described in Batalha (2011b).

$$K_d = K_{d0} C_{Ca}^{p} \tag{10}$$

in which K_d is the reference distribution coefficient for ^{226}Ra when the calcium activity is 1, C_{Ca} is the calcium activity in soil solution, and p is an empirical parameter whose value was fixed at -0.4 as deduced from data in USEPA (2004).

3. Cerrado Soils and PG Application Data

Flow boundary conditions at the soil surface were defined by meteorological data (rainfall and temperature) obtained from a weather station in the western part of Minas Gerais state in Brazil (17^o 25′ 11″ S, 46^o 88′ 64″ W) for the period 1982-2005. These values were repeated many times for the long-term (200 year) simulations. Daily potential evapotranspiration rates were calculated with the Hargreaves equation (e.g. Jensen et al., 1997) from available weather data and the geographic location of the site. Data of the rainwater composition were taken from Maier et al. (1992) and adapted for use in HP1 module: pH 6.3; 5.59 10^{-5} mol/L of Ca and 6.05 10^{-5}mol/L of Mg. The soil chosen for the study is a typical Brazilian Cerrado oxisol, whose physical and chemical data were obtained from Oliveira (2008). Chemical parameters are listed in Table 1.

The granulometric composition of the soil was 16% sand, 63% fine sand, 5% silt and 16% clay. Values of the soil hydraulic parameters needed for the water flow simulations were estimated from the soil textural data using the Rosetta neural network based pedotransfer functions of Schaap et al. (1998) as implemented in HYDRUS-1D. The soil bulk density was taken to be 1.50 g/cm^3. For solute transport we used a diffusion coefficient in free water (D_d) of 1.0 cm^2/d, while a dispersivity (λ) of 20 cm was used for the simulations involving transient flow and 30 cm for the steady-state flow regime.

Table 1. Soil chemical parameters of the Cerrado oxisol.

	P	Ca^{2+}	K^+	Mg^{2+}	Al^{3+}
pH	mmol/L				----
5.3	0.081	0.500	0.410	0.100	0.333

Simulations of the cumulative flux leaving the bottom of the 2m soil profile over a period of 27 years assuming transient water flow were used to define the recharge rate (0.152 cm/d) used for the long-term simulations assuming steady-state flow. Equation (1) for this purpose must be augmented with a set of initial and boundary conditions. For Equation (1) we assumed an initial pressure head of -100 cm, the presence of atmospheric boundary conditions at the soil surface (i.e., given precipitation and calculated potential evapotranspiration data), and a free drainage condition (dh/dx=0) at the bottom of the profile.

For the phosphogypsum and ^{226}Ra transport calculations we considered PG application rates that are common in Brazil (1.000 kg/ha year). The annual application was pulsed in 1 cm of rainwater in the wet season (November). Measurements of the amount of ^{226}Ra in the PG were carried out at the Poços de Caldas Laboratory of the Brazilian Nuclear Energy Commission (CNEN). Results indicated an activity of 252±26 Bq per kg of PG. Mass balance calculations produced values of 73.45 mmol/L of $CaSO_4$ and 3.04 x 10^{-13} mol/L of ^{226}Ra when applied in 1 cm of rainwater for the transient simulations, and values of 483.2 mmol/L of $CaSO_4$ and 20 x 10^{-10} mmol/L of ^{226}Ra when simulating the constant flow regime using an averaged flux of 0.152 cm/day. A distribution coefficient (K_d) of 2000 cm^3/g was used for radium based on data provided by ISAM (1999) as described in Batalha (2011a).

4. Results and Discussion

Figure 1 shows calculated net infiltration fluxes (actual evaporation minus precipitation) into the soil profile for nine years using transient conditions of precipitation and potential evaporation. Results indicates two main seasons (wet and dry) during the year. The simulations using daily weather data from Minas Gerais state (Brazil) revealed no run-off.

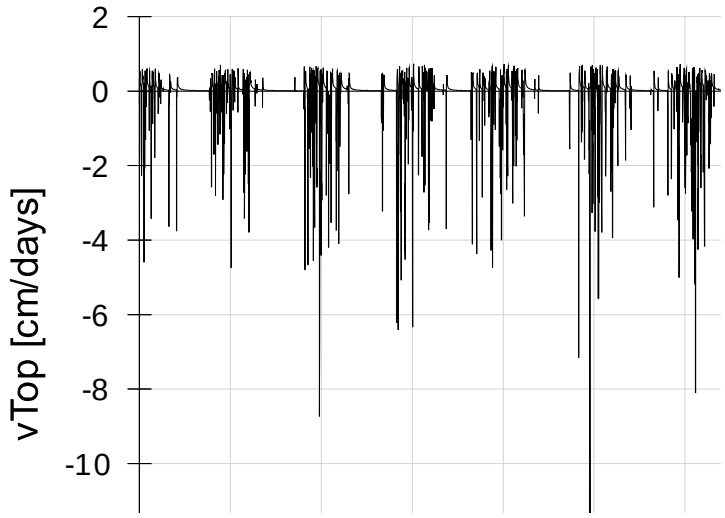

Figure 1. Net fluxes across the soil surface during the first 9 years of the simulations (negative fluxes are downward into the soil profile).

Cumulative drainage fluxes from the soil profile are showed in Figure 2. Results are for both transient flow using daily weather data (left) and monthly averaged precipitation and evaporation data (right). The importance of using daily weather data can be evaluated by the slopes of the two plots. The results indicate an average recharge rate of 0.152 cm/day when using daily weather data, and a nearly 50% lower value of 0.079 cm/d when monthly averaged values for precipitation and potential evaporation are used. This means that time-averaging weather data (especially precipitation) can lead to significantly lower estimates of the recharge rate.

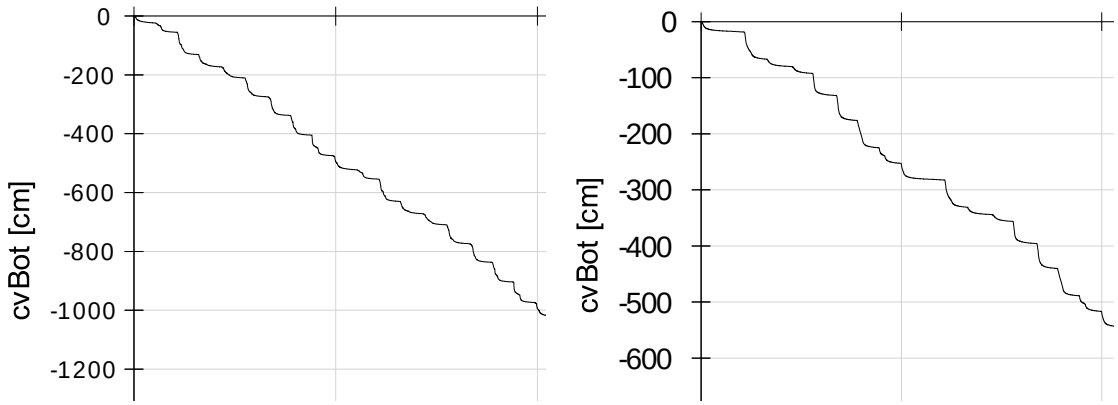

Figure 2. Calculated cumulative recharge rates from the soil profile during 27 years using daily (left) and monthly averaged (right) weather data.

Figure 3 compares calculated ^{226}Ra concentration distributions in the soil profile assuming transient (left) and steady-state (right) flow conditions. Results for transient flow were obtained using observed daily weather data, while those for steady-state flow assumed a constant long-time average recharge rate of 0.152 cm/d as deduced from the transient simulations (Fig. 2, left). Since the transient regime produced a slightly more dispersed contaminant front, a higher longitudinal dispersivity (D_L = 30 cm) for the steady flux scenario was used. The results in Figure 3 indicate that long-term predictions can be based equally well assuming steady-state water flow, rather than transient flow, provided the correct long-term deep drainage (recharge) rate is used for the steady-state simulations.

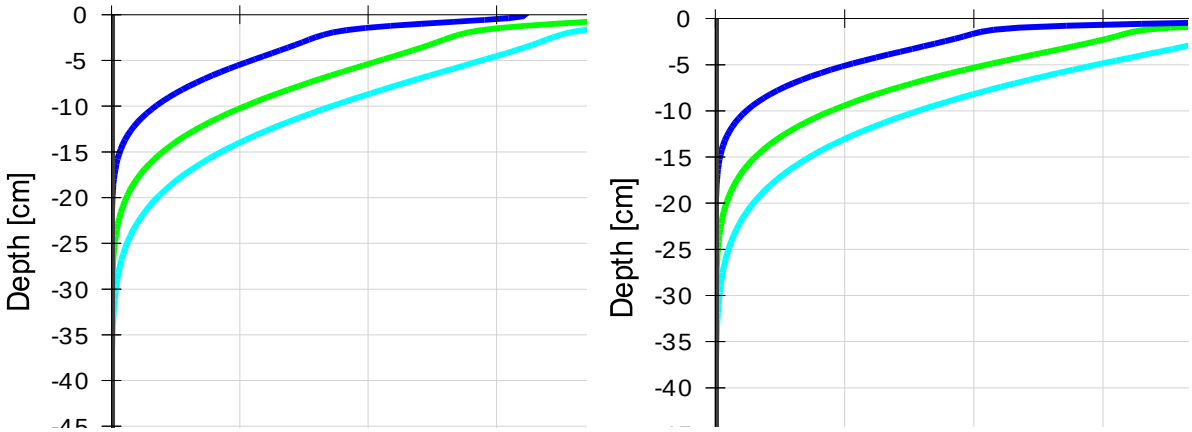

Figure 3. Calculated ^{226}Ra concentrations after T_0= 0, T_1=9, T_2=18, and T_3=27 years assuming transient weather data (left) and a constant long-term average recharge rate (right).

Figure 3 shows that after 27 years of PG application, essentially no ^{226}Ra had reached a depth of about 30 or 40 cm. Subsequent transport after PG applications ceased, but while maintaining the same water flow conditions, remained equally slow. This is shown in Figure 4 which presents calculated ^{226}Ra distributions in the soil profile after 27, 100 and 200 years. The plots show very little movement into the lower part of the profile, with essentially no ^{226}Ra reaching a depth of 1 m after 200 years. Cumulative amounts leached beyond 40 cm depth after 100 and 200 years were estimated to be 3.58 x 10^{-13} and 1.85 x 10^{-12} mmol/cm^2. Also notice that the maximum concentrations in the upper part of the profile decreased substantially with time.

Figure 5 shows the influence of the calcium concentration on ^{226}Ra transport after 9, 18 and 27 years of phosphogypsum application. The plots compare simulations for a constant distribution coefficient, Kd (left) and for a distribution coefficient that varies as a function of Ca^{2+} activity (right). Results indicate that Ca^{2+} resulting from the PG application has a major effect on both the transport rate of ^{226}Ra and the solution concentration. However, this trend is only present initially. Once the PG is no longer applied (after 27 years), calculated ^{226}Ra curves slowly converged to the point that after 100 or 200 years they became very similar (results not further shown here).

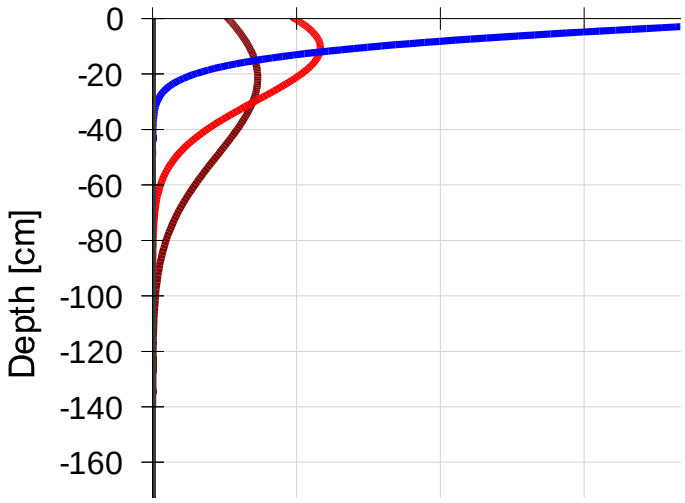

Figure 4. Calculated ^{226}Ra concentrations after T_0= 0, T_1=27, T_2=100, and T_3=200 years (left).

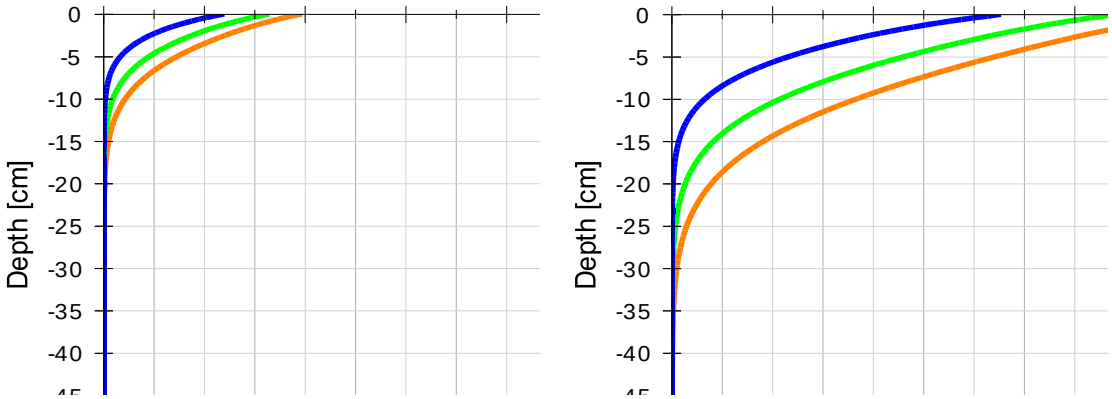

Figure 5. Calculated ^{226}Ra concentrations after T_1= 9, T_2=18, and T_3=27 years, without (left) and with (right) accounting for the effect of the Ca^+ activity on the K_d of ^{226}Ra.

5. Conclusions

In this paper we analyzed the fate and transport of ^{226}Ra present in phosphogypsum when applied for many years as an amendment to a typical Brazilian Cerrado soil used for crop production. The main factors that influenced water flow and radionuclide transport were the deep drainage flux determined by rainfall and evaporation and the use of daily precipitation and potential evaporation data. Results indicate that for the assumed long-term transport scenario (200 years and having relatively low ^{226}Ra activities), steady-state flow conditions could be assumed without

significantly affecting the predictions. Most of the ^{226}Ra remained in the upper 40 cm of the soil profile.

The effect of PG derived calcium was important by decreasing the effective distribution coefficient of ^{226}Ra, and as such increasing the transport rate. All of the simulations in this study assumed equilibrium water flow and solute transport conditions. We did not consider preferential flow or nonequilibrium transport, or any other non-ideal transport process (such as colloid-facilitated transport). These processes could all lead to much higher rates of transport in the soil profile (e.g., Šimůnek and van Genuchten, 2008).

In conclusion, we believe that modeling efforts such as those in this study using HYDRUS-1D and HP1 are essential for detailed environmental assessment of the long-term use of phosphogypsum or other naturally occurring radioactive materials (NORMs). They are especially needed for scenarios that cannot be easily monitored and/or occur over relatively long periods of time.

References

Batalha, M. S., Multicomponent transport of contaminants released in the environment due to phosphogypsum use, MS dissertation in Mechanical Engineering, COPPE/UFRJ, Rio de Janeiro, RJ, Brazil., 86 pp., 2011a (in Portuguese).

Batalha, M. S., C. R. Bezerra, M. C. Barbosa, D. Jacques, E. M. Pontedeiro and M. Th. van Genuchten, Multicomponent transport of ^{226}Ra present in phosphogypsum applied to a Brazilian Cerrado soil. VI Brazilian Symposium on Geosynthetics, REGEO2011, Belo Horizonte, MG, Brazil, Nov. 21-14, 2011b (in Portuguese).

Batalha, M. S., C. B. Bezerra, D. Jacques, M. C. Barbosa, E. M. Pontedeiro, and M. Th. van Genuchten, Multicomponent transport predictions of 226Ra in soil following the use of phosphogypsum, WasteEng 2012,14th Int. Conf. on Engineering for Waste and Biomass Valorization, Oporto, Portugal, 2012.

Embrapa, *Uso de Gesso Agrícola nos Solos do Cerrado*, Empresa Brasileira de Pesquisa Agropecuária, Planaltina, *Circular Técnica 32*, 18 p., 2005.

Jacques, D., J. Šimůnek, D. Mallants, and M. Th. van Genuchten, Modeling coupled hydrological and chemical processes: Long-term uranium transport following phosphorous fertilization, *Vadose Zone J*., *7*,698-711, 2008.

Jacques, D. and J. Šimůnek, Notes on HP1, a software package for simulating variably-saturated water flow, heat transport, solute transport, and biogeochemistry in porous media, HP1 Version 2.2., Open Report, *SCK•CEN-BLG-1068*, Mol, Belgium, 129 p., 2010.

Jensen, D. T., G. H. Hargreaves, B. Temesgen, and R. G.Allen, Computation of ETo under nonideal conditions, *J. Irrig. Drain. Eng.*, ASCE, *123*(5), 394-400, 1997.

Maier, M. H., M. Takino, and L. L. Miyamaru, Alguns aspectos da composição da água da chuva, *Acta Limnol. Brasil.*, IV, 247-254, Brazil, 1992

Mazzili, B., V. Palmiro, C. Saueia, and M. B. Nisti, Radiochemical characterization of Brazilian phosphogypsum, *J. Environ. Radioactivity*, *40*, 113-122, 2000.

Millington, R. J., and J. M. Quirk, Permeability of porous solids, *Trans. Faraday Soc., 57*, 1200-1207, 1961.

Oates, K. M., and A. G. Caldwell, Use of by-product gypsum to alleviate soil acidity, *Soil Sci. Soc. Am J*., *49*, 915-918, 1988

Oliveira, K. A. P., Aplicação do fosfogesso na agricultura do Cerrado e suas implicações radiológicas, Dissertação de Mestrado, CDTN/CNEN, Belo Horizonte, MG, Brazil, 2008.

Oster, J. D., Gypsum usage in irrigated agriculture: A review, *Fertilizer Res.*, *3*, 73-89, 1982.
Papastefanou, C., S. Stoulos, A. Ioannidou, and M. Manolopoulou, The application of phosphogypsum in agriculture and the radiological impact, *J. Environ. Radioactivity*, *89*, 188-198, 2006.
Parkhurst, D. L., and C. A. J. Appelo, User's guide to PHREEQC (Version 2), A computer program for speciation, batch-reaction, one-dimensional transport, and inverse geochemical calculations, *Water Resources Investigations Report 99-4259*, Denver, CO, 1999.
Rothbaum, H. P., D. A. McGaveston, T. Wall, A. E. Johnston, and G. E. G. Mattingly, Uranium accumulation in soils from long-continued applications of superphosphate, *J. Soil Sci. 30*, 147-153, 1979.
Saueia, C. H. R., and N. P. Mazzilli, Distribution of natural radionuclides in the production and use of phosphate fertilizers in Brazil, *J. Environ. Radioactivity*, *89*, 229-239, 2006.
Schaap, M. G., F. J. Leij, and M. Th. van Genuchten, Neural network analysis for hierarchical prediction of soil hydraulic properties, *Soil Sci. Soc. Am. J.*, *62*, 847-855, 1998.
Šimůnek, J., and M. Th. van Genuchten, Modeling nonequilibrium flow and transport processes using HYDRUS, *Vadose Zone J.*, *7*(2), 782-797, 2008.
Šimůnek, J., M. Šejna, H. Saito, M. Sakai, and M. Th. van Genuchten, The HYDRUS-1D Software Package for Simulating the Movement of Water, Heat, and Multiple Solutes in Variably Saturated Media, Version 4.0, *HYDRUS Software Series 3*, Department of Environmental Sciences, Univ. of California, Riverside, CA, 2008.
U.S. Environmental Protection Agency, Understanding Variation in Partition Coefficient, Kd, Values. Vol III, *EPA 402-R-04-002C*, EPA, Washington, DC, 2004
van Genuchten, M. Th., A closed-form equation for predicting the hydraulic conductivity of unsaturated soils, *Soil Sci. Soc. Am. J.*, *44*, 892-898, 1980.
Zielinski, R.A., S. Asher-Bolinder, A. L. Meier, C. A. Johnson, and B. J. Szabo, Natural or fertilizer-derived Uranium in irrigation drainage: A case study in southeastern Colorado, *Appl. Geochem.*, *12*, 9-21, 1997.

Optimization of Triggered Irrigation Using a System-Dependent Boundary Condition in HYDRUS (2D/3D)

Sharon Dabach[1], Jiří Šimůnek[2], Alon Ben-Gal[3], Jianchu Shi[4], and Naftali Lazarovitch[5]

[1]*Seagram Center for Soil and Water Sciences, The Robert H. Smith Faculty of Agriculture, Food and Environment, The Hebrew University of Jerusalem, Rehovot, Israel.*
[2]*Department of Environmental Sciences, University of California Riverside, Riverside, California.*
[3]*Soil, Water and Environmental Sciences, Agricultural Research Organization, Israel*
[4]*Department of Soil and Water Sciences, College of Resources and Environment, China Agricultural University*
[5]*The Jacob Blaustein Institutes for Desert Research, Ben-Gurion University of the Negev, Sede Boqer Campus, Ben-Gurion, Israel.*

Abstract

Improving the sustainability of irrigation systems requires the optimization of relevant operational parameters, such as the irrigation threshold, the irrigation amount, and the sensor location. However, little work has been done to investigate the relationship between irrigation scheduling, irrigation threshold, water salinity, irrigation amount, and their dependence on the sensor location. Optimization of these parameters using field experiments would require numerous experiments, time, and work. Instead, in this paper, we propose the use of the HYDRUS (2D/3D) model as a tool for investigating different scenarios that occur in the field.

1. Introduction

Efficiency of water use in agriculture can be increased by improving irrigation scheduling, i.e., by optimizing the timing and amounts of water applications over the growing season. However, executing an efficient irrigation plan is challenging, due to many variables that must be taken into consideration, including climate, crop type, irrigation method, salinity, and various system constraints (Howell, 1996). Several approaches can be used to initiate and terminate irrigation. The most common approach is to initiate irrigation for a certain amount of time or by applying a certain water volume when a predetermined threshold is reached. Automated closed loop irrigation systems, based on a threshold of soil pressure head or water content, have been shown to save water while maintaining high yields (Phene and Howell, 1984). Determining the proper irrigation threshold has been studied extensively (e.g., Taylor, 1965; Phene and Howell, 1984; Hodnett et al., 1990; Thompson et al., 2000; Hoppula and Salo, 2007). Nevertheless, most of these studies are empirically based and are valid only for a specific experimental setup: a crop type, soil type, climatic conditions, location of the measuring device, irrigation method, irrigation salinity, and the volume of applied water for each irrigation episode. However, for different soils, climate, and vegetation, different combinations of a threshold and an irrigation amount will yield different ranges of water available for plants, different root water uptake rates, and different water losses below the root zone. Optimization of these parameters, aimed at achieving better water use efficiency, should take into consideration the crop water uptake rate and water application rates.

In this study, we examined the relationship between irrigation thresholds and applied amounts of water for different soils and climates using the HYDRUS (2D/3D) (Šimůnek et al., 2008) code that numerically solves the Richards equation describing water flow and plant water uptake in homogeneous or heterogeneous soils. HYDRUS has previously been utilized to study optimal irrigation management (e.g., Cote et al., 2003; Lazarovitch et al., 2009). Additionally, we studied the effect of sensor location in a heterogeneous soil on measurement variability and the effect of water salinity on the performance of a feedback irrigation system.

2. Materials and Methods

The HYDRUS (2D/3D) model was used for three different scenarios to evaluate (i) the effect of the irrigation threshold on the quantity of applied water, (ii) the dependence of the variability of observation (irrigation triggering) points' measurements on their location (depth and distance) relative to a dripper, and (iii) the effect of salinity of irrigation water on water use efficiency of crops. The triggered irrigation option in the HYDRUS (2D/3D) code was used for two hypothetical soils, silt and clay loam (Carsel and Parrish, 1988), to determine an optimal irrigation threshold that maximizes water use efficiency. The triggered irrigation option switched a time-variable flux boundary condition, representing a surface dripper, from no flux to constant flux for a certain time duration when the pressure head in a predetermined observation point reached the irrigation threshold (Dabach et al., 2013).

Scenario 1: For an irrigation amount of 10 mm, two hypothetical soils (silt and clay loam), and increasingly larger potential transpiration rates (2, 4, 6, 7, and 10 mm d^{-1}), the irrigation threshold was adjusted until the ratio between irrigation and potential transpiration (IT_p^{-1}) reached a value of 1. The simulations included irrigation and root water uptake processes.

Scenario 2: The effect of sensor placement on the performance of an automated irrigation system was also investigated. Specifically, the variability of measurements by a sensor placed at various distances from a subsurface dripper, the total volume of applied water, and bottom drainage were studied. The HYDRUS (2D/3D) software numerically simulated two-dimensional water flow and root water uptake in a heterogeneous sandy loam soil (Carsel and Parrish, 1988) with a subsurface dripper. Twelve heterogeneity realizations in soil hydraulic properties were created using random fields of scaling factors (Vogel et al., 1991) with a standard deviation of 0.5 and a correlation length of 5 cm in both *x* and *z* directions. Three pairs of observation points were defined in the flow domain on each side and at distances of 10, 20, and 30 cm from the dripper. Each simulation was run for a different observation point, i.e., for every heterogeneity realization, six simulations were performed. In each simulation, irrigation events were triggered by a different observation point when the irrigation threshold was -60 cm. The irrigation amount was 5 mm per irrigation pulse. The coefficients of variation were calculated for observation points located at the same distance from the dripper (two in each realization times twelve realizations).

Scenario 3: Triggered irrigation was additionally simulated with saline water in a sandy loam soil (Carsel and Parrish, 1988). The simulation was axisymmetric with a surface drip source and a duration of 90 days. Various levels (from 0 to 4 mmol cm^{-3}) of irrigation salinity were applied

from a surface drip source. The irrigation threshold was -80 cm, and the potential transpiration rate was 4 mm day^{-1}. Water use efficiency (WUE) was calculated from root water uptake (RWU) divided by a total irrigation amount for the simulation duration.

3. Results and Discussion

Figure 1 shows the thresholds that yielded an IT_p^{-1} value of 1 for silt and clay loam soils, as a function of different potential transpiration rates, when a water volume of 10 mm per irrigation pulse was used. The higher the daily potential transpiration rate, the higher the irrigation threshold needed to achieve the IT_p^{-1} value of 1. As plants grow during the season, their transpiration rate increases and so does their water demand. Therefore, the irrigation threshold has to be raised in order to compensate for an increasing water demand during the growing season. Keeping the irrigation threshold constant while the potential transpiration rates rise would result in more irrigation events since the threshold would be reached faster. Nevertheless, this would not produce a sufficient supply of water since the rate of the pressure head decrease depends on water fluxes in the soil and is limited by the hydraulic conductivity. Therefore, to achieve optimal automatic triggering of irrigation via pressure head measurements, the irrigation threshold must be adjusted according to changing potential transpiration rates.

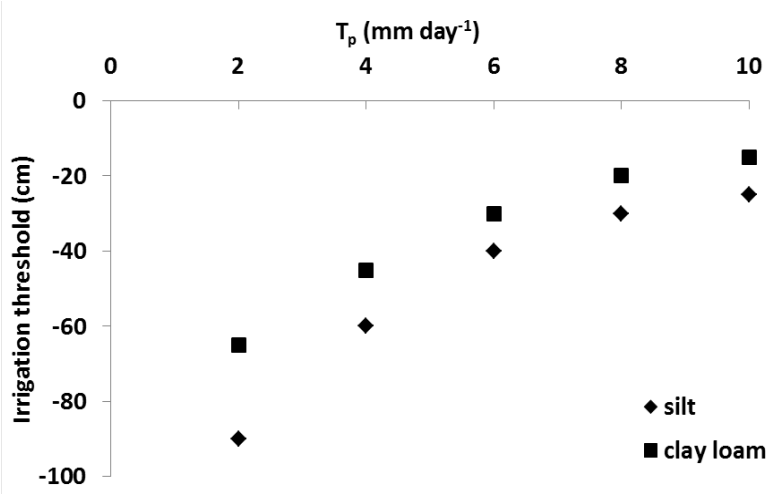

Figure 1. Irrigation thresholds that yielded IT_p^{-1} [-] values of 1 as a function of potential transpiration for silt and clay loam soils with a water volume per irrigation equal to 10 mm.

Coefficients of variation for simulated pressure head measurements are presented in Figure 2 for each of the three distances of the observation points from the dripper. The coefficient of variation was increasing when water contents were changing rapidly in the soil. For observation points located further away from the dripper, the water front did not reach them in all realizations at the same time, and as a result the variation in measurements increased. On the other hand, as observation points were placed further away from the dripper, the coefficient of variation decreased because the rise in the pressure head due to irrigation was smaller. However, the coefficient of variation of the total quantity of applied water increased considerably with the

distance of the observation point away from the dripper (results not shown). If the pressure head in the measurement location does not rise above the irrigation threshold after the irrigation pulse, then another irrigation pulse is triggered. Even though the variability in pressure head measurements was lower as the distance of the observation point increased, the hydraulic conductivity of the soil between the dripper and the observation point varies depending on the location of the observation point relative to the dripper. This variation in the hydraulic conductivity affects the travel time of the water front from the dripper to the observation point, thus causing the variability in total applied water.

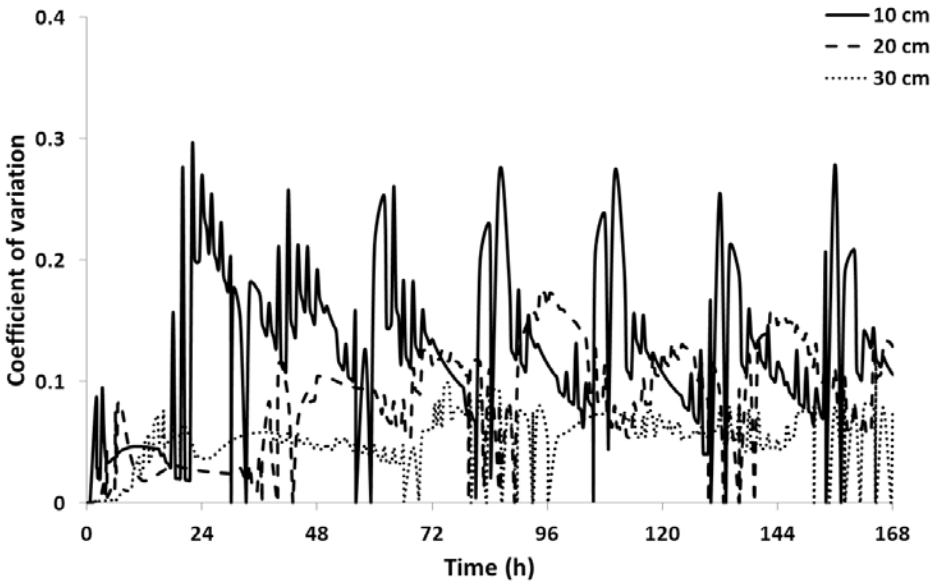

Figure 2. The coefficient of variation of simulated pressure heads at three distances (10 cm, 20 cm, and 30 cm) from the dripper during a 1-week simulation.

As the salinity of irrigation water increased, WUE decreased (Figure 3). Salinity affects root water uptake of plants, and indeed, simulations showed a steady decrease in RWU as salinity increased. The drop in RWU resulted in a slower decrease in the pressure head, which resulted in fewer irrigation events and hence less applied water while drainage was only slightly higher. This combination of factors and processes converged to an undesirable result, in which the decrease in RWU caused fewer irrigation events, which further raised soil salinity and decreased RWU. The decrease in RWU was steeper than the decrease in the quantity of applied irrigation water, and consequently, WUE declined with salinity. When irrigating with saline water, the tensiometer alone cannot efficiently be used to control irrigation. An additional sensor that monitors salinity is necessary in order to provide data needed for the decision to leach excess salts from the root zone.

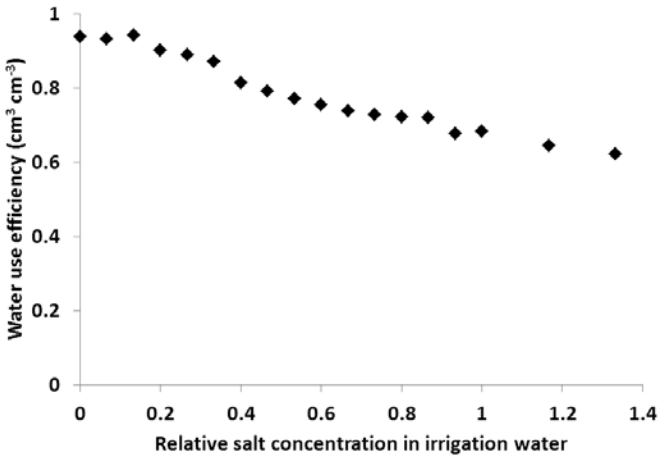

Figure 3. Water use efficiency (root water uptake divided by irrigation) as a function of the relative salinity of irrigation water (water salinity divided by the C_{50} (3 mmol cm^{-3}) parameter of van Genuchten (1987).

4. Conclusions

Optimization and adjustment of the irrigation threshold throughout the growth season is needed to accommodate changing water uptake rates of the plants in systems that use pressure head measurements to trigger irrigation. The HYDRUS (2D/3D) code can be utilized to optimize irrigation threshold values for specific boundary conditions and plant types. The boundary conditions can be updated during the growing season, and used to determine new irrigation thresholds to compensate for increasing root water uptake by plants.

Variability of matric head measurements substantially increases during changes in soil water status. When a rapid change in soil water contents occurs, whether naturally or artificially, it will not occur at all locations simultaneously, and therefore variability will increase during times of change. Irrigation systems, which operate based on data from tensiometers, sometimes use an algorithm that turns off irrigation when the pressure head rises above a preset value. Our results suggest that this algorithm should be avoided because of the increase in variation of the tensiometer measurements during irrigation. Instead, we recommend using an algorithm that stops irrigation after a fixed volume of water has been applied.

When irrigating with saline water, a decrease in plant water uptake results in higher pressure heads in the soil and hence fewer irrigations, which in turn causes higher soil salinity. Therefore, when this is an issue, irrigation cannot be based only on sensors measuring the soil water status, but must be complemented with salinity monitoring.

A numerical model is a good tool for optimizing irrigation regimes. However, many parameters are involved in simulating triggered irrigation systems, and the operation of the numerical model requires relatively extensive knowledge (i.e., root spatial distribution, soil spatial variability, dripper wetting patterns, uptake fluxes), to which most farmers do not have access or realize only at the end of the season. Additional work is necessary in order to standardize and simplify the

decision making process regarding sensor location, the value of the irrigation threshold, and the volume of applied water in each irrigation pulse according to changing spatial variability, irrigation methods, and crop conditions.

References

Carsel, R. F., and R. S. Parrish, Developing joint probability-distributions of soil-water retention characteristics, *Water Resources Research*, *24*, 755-769, 1988.

Cote, C. M., K. L. Bristow, P. B. Charlesworth, F. J. Cook, and P. J. Thorburn, Analysis of soil wetting and solute transport in subsurface trickle irrigation, *Irrigation Science*, *22*,143-156, 2003.

Dabach, S., N. Lazarovitch, J. Šimůnek, and U. Shani, Numerical investigation of irrigation scheduling based on soil water status, *Irrigation Science*, *31*, 27-36, 2011.

Hodnett, M. G., J. P. Bell, P. D. A. Koon, G. C. Soopramanien, and C. H. Batchelor, The control of drip irrigation of sugarcane using index tensiometers - Some comparisons with control by the water-budget method, *Agricultural Water Management*, *17*, 189-207, 1990.

Hoppula, K. I., and T. J. Salo, Tensiometer-based irrigation scheduling in perennial strawberry cultivation, *Irrigation Science*, *25*, 401-409, 2007.

Howell, T. A., Irrigation scheduling research and its impact on water use, *in*: C. R. Camp, et al. (eds.) Evapotranspiration and Irrigation Scheduling, San Antonio Convention Center, San Antonio, Texas, pp. 1-15, 1996.

Lazarovitch, N., M. Poulton, A. Furman, and A. W. Warrick, Water distribution under trickle irrigation predicted using artificial neural networks, *Journal of Engineering Mathematics*, *64*, 207-218, 2009.

Maas, E. V., and C. J Hoffman, Crop salt tolerance – current assessment, *ASCE Journal of Irrigation and Drainage Division*, *103*, 115-134, 1977.

Phene, C. J., and T. A. Howell, Soil sensor control of high-frequency irrigation systems, *Transactions of the ASAE*, *27*, 392-396, 1984.

Šimůnek, J., M. T. van Genuchten, and M. Šejna, Development and applications of the HYDRUS and STANMOD software packages and related codes, *Vadose Zone Journal*, *7*, 587-600, 2008.

Taylor, S. A., Managing irrigation water on the farm, *Transactions of the ASAE*, *8*, 433-436, 1965.

Thompson, T. L., T. A. Doergo, and R. E. Godin, Nitrogen and water interactions in subsurface drip-irrigated cauliflower: 1.Plant response, *Soil Science Society of America Journal*, *64*, 406-441, 2000.

van Genuchten, M. Th., A numerical model for water and solute movement in and below the root zone, *Research Report No 121*, U.S. Salinity Lab, ARS USDA, Riverside, CA, 1987.

Vogel, T., M. Cislerova, and J.W. Hopmans, Porous media with linearly variable hydraulic propertie, *Water Resourse research*, *27*, 2735–2741, 1991.

Modeling Non-equilibrium Water Flow in Multistep Outflow and Multistep Flux Experiments

Efstathios Diamantopoulos[*1], Sascha C. Iden[*2], and Wolfgang Durner[*3]

[*]*Institut für Geoökologie, Technische Universität Braunschweig, Braunschweig, Germany,*
[1]ediamant@tu-bs.de, [2]s.iden@tu-bs.de, [3]w.durner@tu-bs.de

Abstract

During the last 50 years, experimental observations have shown that the soil hydraulic properties estimated under static and dynamic flow conditions can substantially differ. These observations are often described by the terms "dynamic non-equilibrium" or "dynamic effects." The way in which hydraulic non-equilibrium is expressed in experimental data depends on experimental boundary conditions. During experiments with controlled pressure head boundary conditions, non-equilibrium effects appear as a relaxation in the cumulative outflow / system-averaged water content data, while the pressure head in the soil column indicates hydrostatic equilibrium. For experiments with flux boundary conditions, non-equilibrium effects appear as a relaxation of the pressure head while the flux density and macroscopic water content distribution appear static. These phenomena are often attributed to processes such as air-water-interface reconfiguration, pore-water blockage, air entrapment, dynamic contact angles, among others. We have developed a model to quantitatively describe hydraulic non-equilibrium during variably saturated flow. The model considers two continua at the macroscopic scale: one continuum is described by the Richards equation and the second, associated with non-equilibrium water flow, by an extended Richards equation using the non-equilibrium approach of Ross and Smettem. The new model called DNE was implemented by extending the Hydrus-1D code. Numerical simulations with the DNE model demonstrate its ability to describe the dynamic effects occurring in transient flow experiments very well.

1. Introduction

The Richards equation is the most widely used model for describing water flow in the unsaturated zone. It has a clear physical basis and its applicability has been proved in various experimental studies in the laboratory and the field. The use of the Richards equation for the purpose of prediction requires knowledge of the soil-water characteristics, i.e. the water retention and the hydraulic conductivity curve. The water retention curve relates the water content θ with the pressure head h and is parameterized by a monotonous function $\theta(h)$, which is easily used in numerical simulations. Traditional theory assumes that the water retention curve is independent of the soil water flow regime. However, observations reveal that water retention curves determined under static equilibrium and dynamic conditions can differ. For this reason, the Richards equation often cannot describe observations of soil water dynamics in laboratory experiments. These observations are often described as dynamic non-equilibrium (NE) effects and are known since the work of Topp et al. (1967).

Diamantopoulos and Durner (2012) presented a comprehensive review on this phenomenon that focused on dynamic NE observations, hypothesized causes and modeling approaches. In this contribution, we review only the key studies concerning NE. Topp et al. (1967) performed laboratory experiments in sandy soils and measured the water retention curves (drainage) for

three different flow cases: static, steady–state and dynamic. They drained their sample by controlling the pressure in the gas phase. They found that although the retention curves were almost the same for static equilibrium and steady state flow experiments, the dynamic retention curves significantly differed. Specifically, for the same pressure head value, the water content was higher in the case of transient experiments compared with the other two cases. Similar water dynamics are also observed in multistep outflow experiments (MSO). Figure 1 shows experimental results for an MSO experiment presented by Diamantopoulos et al. (2012). After an applied pressure step at the lower boundary, the pressure head in the soil quickly reaches the equilibrium state. However, the time series of cumulative outflow shows two stages. During the first stage, immediately after the change in the applied pressure head, a large volume of water quickly flows out from the soil column. This is followed by a second stage with a much slower flow in the column toward hydraulic equilibrium. The crucial point is that these data cannot be described by the Richards equation because it cannot predict different equilibration times for θ and h due to the tight coupling by the retention curve.

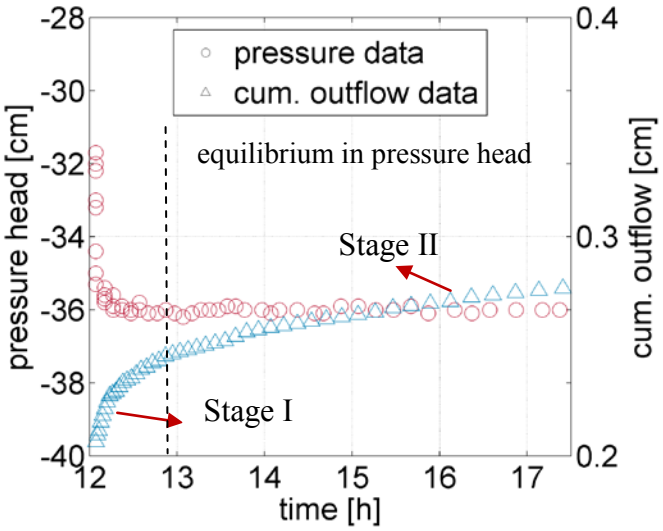

Figure 1. Non-equilibrium water flow during an MSO experiment. After a pressure head change at the boundary, the pressure head in the soil quickly equilibrates whereas outflow of water continues.

Poulovassilis (1974) investigated the effect of water flow on the water retention curve by conducting constant flux infiltration experiments in a soil column equipped with five tensiometers. After achieving uniform steady-state flow and uniform water content and pressure head throughout the soil column, he sealed both ends of the soil column and placed it horizontally. He observed that all tensiometers recorded a pressure head increase (suction decrease) while the water content inside the column remained constant. Recently, Weller et al. (2011) presented an automated method for direct measurements of hydraulic conductivity by a succession of unit-gradient experiments. They applied constant fluxes at the upper boundary of the soil column and set the pressure head at the lower boundary equal to the pressure head of water near the surface. Under these conditions, the hydraulic conductivity equals the applied flux density. Their experiments started with a saturated soil column and the applied fluxes were

decreased in steps. As was expected, pressure head measured in the soil dropped immediately after each applied step, but rose to higher levels afterwards, even though the column-averaged water content remained constant. Weller et al. (2011) also observed this phenomenon for increasing fluxes, but in this case the pressure head decreased during the relaxation period. Similar to what has been stated earlier, the observations of Poulovasillis (1974) and Weller et al. (2011) cannot be described by the Richards equation because of its inherent assumption of a flux-invariant θ-h-K relationship.

The above studies reveal that for a given pressure head boundary condition, dynamic NE effects appear as a relaxation in the cumulative outflow data (or water content), whereas for a given flux boundary condition, they appear as a relaxation of the pressure head. Diamantopoulos et al. (2012) proposed a model for describing dynamic NE water flow in the case of MSO experiments. The model assumes two continua at the macroscopic scale. In the first continuum, water flow is described by the Richards equation, whereas in the second continuum, water flow is described by the Ross and Smettem (2000) model. In this article, we investigate the possibility of describing the two major dynamic NE observations outlined above with this model.

2. Model

2.1. Richards Equation

Variably saturated water flow in homogeneous porous media is generally described by the Richards equation:

$$\frac{\partial \theta}{\partial t} = \frac{\partial}{\partial z}\left[K\left(\frac{\partial h}{\partial z}\right) - 1 \right] \tag{1}$$

where θ [L^3 L^{-3}] is the water content, t [T] is time, z [L] is the vertical coordinate, positive downwards, h [L] is the pressure head and K [L T^{-1}] is the unsaturated hydraulic conductivity.

2.2. Dual–Fraction Non-Equilibrium Model (DNE)

The DNE model assumes two fractions of water in the same porous system, one fraction f_{eq} in instantaneous equilibrium with the local pressure head, and the second fraction f_{ne} for which the equilibration of water content is time dependent. By assuming that the pressure heads in the two regions quickly equilibrate relative to the movement of water in the main flow direction, the main equation describing water flow becomes (Diamantopoulos et al., 2012):

$$(1 - f_{ne})\frac{\partial \theta_{eq}}{\partial t} + f_{ne}\frac{\partial \theta_{ne}}{\partial t} = \frac{\partial}{\partial z}\left[K(\theta)\left(\frac{\partial h}{\partial z} - 1\right)\right] \tag{2}$$

with

$$\frac{\partial \theta_{ne}}{\partial t} = \frac{\left(\theta_{eq} - \theta_{ne}\right)}{\tau} \tag{3}$$

where τ describes the equilibration of water content in the non-equilibrium region [T], and K is a function of the water content θ. For more information about the model, the reader is referred to Diamantopoulos et al. (2012).

2.3. Parameterization of Hydraulic Properties

The unsaturated soil hydraulic properties are parameterized with the van Genuchten–Mualem (VGM) model (van Genuchten, 1980). The retention function and the hydraulic conductivity function (as a function of water content θ) are given by:

$$\theta(h) = \begin{cases} \theta_r + (\theta_s - \theta_r) \cdot (1 + |\alpha h|^n)^{-m}, h < 0 \\ \theta_s, h \geq 0 \end{cases} \quad (4)$$

$$S_e = \frac{\theta - \theta_r}{\theta_s - \theta_r} \quad (5)$$

$$K(S_e) = K_s \cdot S_e^{\ l} \left[1 - (1 - S_e^{\ 1/m})^m\right]^2 \quad (6)$$

where, θ_s and θ_r [L^3 L^{-3}] are saturated and residual water contents, respectively, α [L^{-1}], n [-], m [-] and l [-] are shape parameters and $m = 1 - \frac{1}{n}, n > 1$.

2.4. Inverse Modeling

The laboratory experiments were evaluated by inverse modeling. The objective function used for determining the unknown parameters p from measurements of cumulative outflow and pressure head data in the case of the MSO experiment and pressure head data in the case of the multistep flux experiment is given by:

$$O(p) = \sum_{j=1}^{M} w_j \sum_{i=1}^{N_j} r_{ij}(p)^2 \quad (7)$$

where M is the number of the data groups used in the objective function ($M = 2$ for MSO and $M = 1$ for multistep flux experiments), N_j is the number of data for each group and r_{ij} are the residuals, i.e. the differences between observed and model–predicted data. The estimation of the model parameters is done by minimizing Eq. (7) with respect to the parameter vector p. This was achieved by the globally convergent evolutionary scheme SCE–UA (Duan et al., 1992). Numerical simulations with both the Richards equation and the DNE model were done with a modified version of Hydrus-1D (Šimůnek et al., 2008).

3. Material and Methods

3.1. Multistep Outflow (MSO) Experiment

The DNE model was tested against experimental results from an MSO experiment presented by Diamantopoulos et al. (2012). In that experiment, an undisturbed soil column 7.2 cm in height was collected from the subsoil horizon (35–45 cm) of a Luvisol (Schelle et al., 2011). The column was placed on a 0.7 cm thick porous plate that was covered by a fine–pored diaphragm. A tensiometer (T5, UMS Munich) was installed at a 1.8 cm depth measured from the top to record pressure head. The sample was slowly saturated from the bottom. The initial water content was calculated from the water content at the end of the experiment, and the cumulative water loss throughout the experiment. The bulk density, porosity and initial water content were 1.67 g cm^{-3}, 0.371 cm^3 cm^{-3} and 0.334 cm^3 cm^{-3}, respectively. The saturated hydraulic conductivity of the plate (K_p) and soil (K_s) were 1.0 cm h^{-1} and 2.7 cm h^{-1}, respectively. In the inverse simulations with the Richards equation and the DNE model, both saturated conductivities were fixed to these measured values.

3.2. Multistep Flux (MSF) Experiment

We tested the DNE model against experimental data from MSF experiments presented by Weller et al. (2011). They obtained direct measurements of unsaturated hydraulic conductivity by imposing gravity flow to one sandy undisturbed soil column as was described in the introduction. For more information about the material type or the experimental procedure, the reader is referred to Weller et al. (2011).

4. Results

4.1. MSO

Figure 2 illustrates results of a sensitivity analysis in which the effect of the non-equilibrium parameters τ and f_{ne} for a multistep outflow and inflow experiment were analyzed for a sandy material. The first case (blue line) represents equilibrium flow described by the Richards equation. Figure 2a shows the prediction of the DNE model for a drainage–imbibition experiment and for increasing values of parameter τ (2, 4 and 8 h) when all the water is assumed to be in non-equilibrium (f_{ne} = 1). This corresponds to the Ross and Smettem (2000) NE model, which obviously is able to predict the basic observation that after an abrupt change in the applied pressure head at the lower boundary, the pressure head in the soil equilibrates faster than the cumulative outflow data. However, the equilibration dynamics always follow an exponential form, which is in contrast to the observations. As described previously, outflow data often show an equilibration in two stages. After each applied step, there is a quick outflow followed by a period with slower outflow. As shown in Figure 2b, this can be simulated by the DNE model. Figure 2b shows that the greater the value of f_{ne}, the smaller the amount of water that leaves the soil column after each applied pressure head.

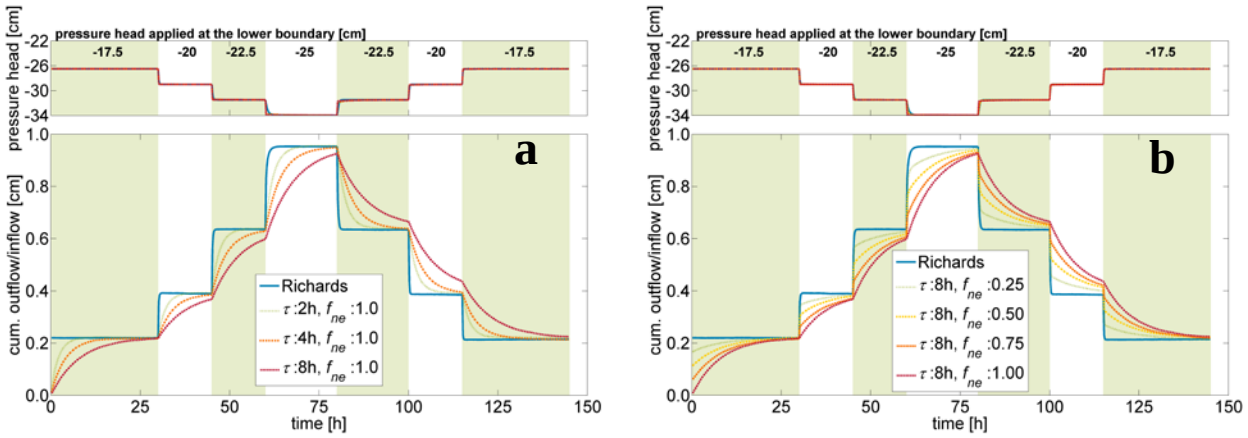

Figure 2. Sensitivity analysis of DNE model for MSO experimental type.
(a): the effect of τ parameter; (b): the effect of f_{ne} parameter

Figure 3 shows measured and fitted outflow and pressure head data for a MSO experiment for a loamy sand soil. The experimental data show that after each pressure change at the lower boundary, the equilibration of the pressure head data in the column is quicker than that of the cumulative outflow data. The blue line illustrates that this cannot be described by the Richards equation since it assumes simultaneous equilibration between pressure head and water content (or cumulative outflow). Accordingly, any attempt to describe the data leads to misfits. On the contrary, the DNE model describes both the pressure head and outflow data very well. Any remaining discrepancies between measured and simulated outflow data, especially in the second and third step, can be attributed to the limited flexibility of the van Genuchten-Mualem model of the soil hydraulic properties. The fitted parameter τ and f_{ne} were 3.2 h and 0.76, respectively.

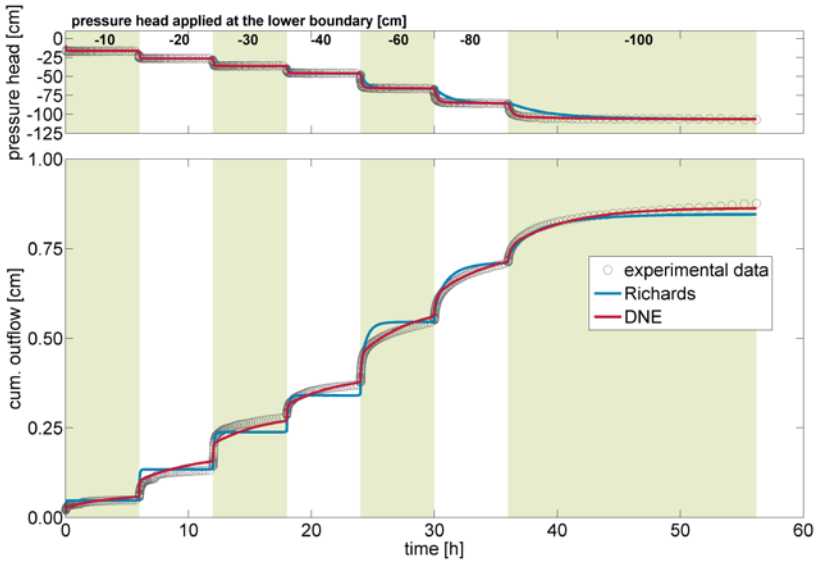

Figure 3. Observed and simulated cumulative outflow and pressure head data for an undisturbed loamy sand. The fitted data are calculated using the Richards equation and the dual-fraction non-equilibrium (DNE) model.

4.2. MSF

Figures 4a and b show results of a sensitivity analyses for both non-equilibrium parameters of the DNE model for an MSF experiment. At the beginning, we assume a series of steady fluxes decreasing stepwise corresponding to a drainage experiment; after 150 hours, we assume increasing fluxes corresponding to an imbibition experiment. The Richards equation predicts that after an applied flux at the upper boundary, water content and pressure head in the soil immediately change and assume the relationship defined by the soil water retention curve. Figure 4a shows that the DNE model can predict the capillary overshoot presented by Weller et al. (2011) in both the drainage and imbibition sequence of the MSF experiment. At a constant value of the f_{ne} parameter, increasing τ values result in slower equilibration of the pressure head after each applied flux. Additionally, the magnitude of the pressure head drop after each flux change is controlled by parameter f_{ne} (Figure 4b).

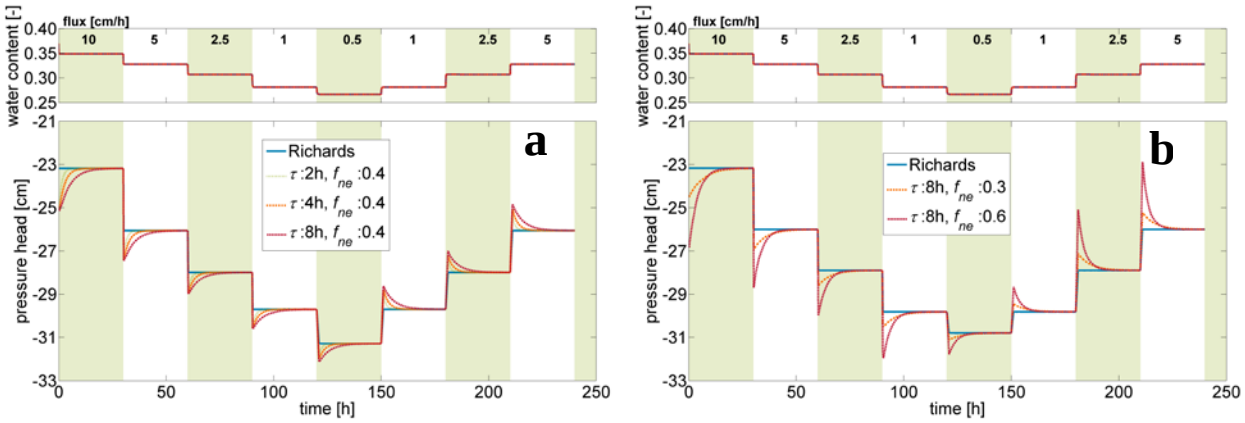

Figure 4. Sensitivity analysis of DNE model for MSF experimental type.
(a): the effect of τ parameter; (b): the effect of f_{ne} parameter

Figure 5 shows the experimental and simulated data from the study of Weller et al. (2011). The experimental data were digitized from figure 4 in Weller et al. (2011). Figure 5 shows that after a stepwise change of the applied flux at the upper boundary, the pressure head drops as expected (drainage), but then it rises again to a higher value. The Richards equation predicts that after the establishment of steady state flux with constant water content in the soil, the pressure head remains constant as well and corresponds to the pressure head value obtained from the retention curve. This contradicts the experimental findings. In contrast, the DNE model predicts the observed slow equilibration of the pressure head data even if the water content remains constant and the agreement between fitted model predictions and experimental data is excellent. The fitted parameter τ and f_{ne} were 19 h and 0.37, respectively.

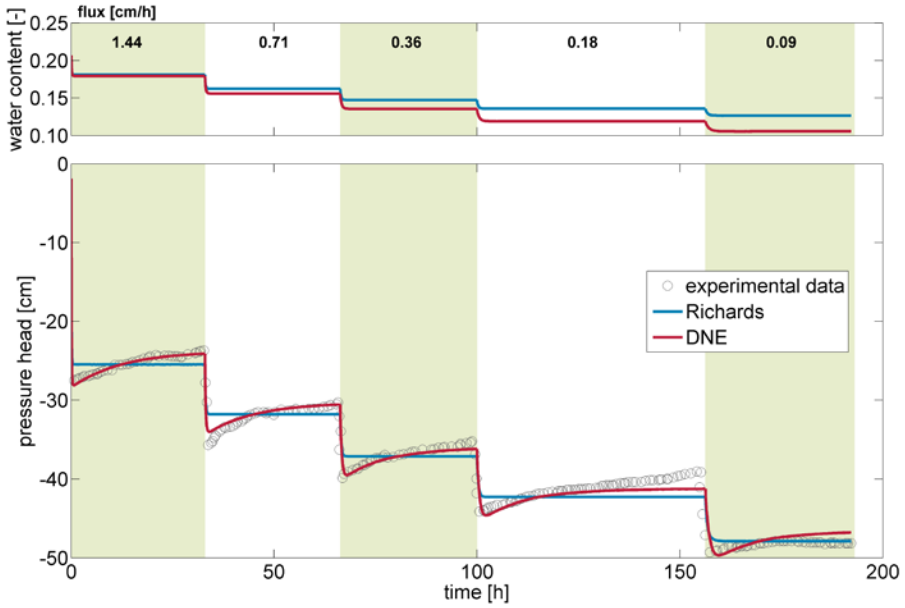

Figure 5. Observed and simulated pressure head data for an undisturbed sand (Weller et al., 2011). The fitted data are calculated using the Richards equation and the dual–fraction non-equilibrium (DNE) model. The experimental data were digitized from Figure 4 in Weller et al. (2011).

References

Diamantopoulos, E., and W. Durner, Dynamic non-equilibrium of water flow in porous media – A review, *Vadose Zone Journal*, *11*(3), doi:10.2136/vzj2011.0197, 2012.

Diamantopoulos, E., I. C. Iden, and W. Durner, Inverse modeling of dynamic non-equilibrium in water flow with an effective approach, *Water Resources Research, 48*, W03503, doi:10.1029/2011WR010717, 2012.

Duan, Q., S. Sorooshian, and V. Gupta, Effective and efficient global optimization for conceptual rainfall-runoff models, *Water Resources Research*, *28*, 1015-1031, 1992.

Poulovassilis, A., The uniqueness of the moisture characteristics, *Soil Science, 25*, 27-33, 1974.

Ross, P. J., and K. R. J. Smettem, A simple treatment of physical nonequilibrium water flow in soils, *Soil Science Society of America Journal, 64*, 1926-1930, 2000.

Schelle, H., S. C. Iden, and W. Durner, Combined transient method for determining soil hydraulic properties in a wide pressure head range, *Soil Science Society of America Journal*, *75*(5), 1-13, 2011.

Šimůnek, J., M. Th. van Genuchten, and M. Šejna, Development and applications of the HYDRUS and STANMOD software packages, and related codes, *Vadose Zone Journal*, *7*(2), 587-600, 2008.

Topp, G. C., A. Klute, and D. B. Peters, Comparison of water content-pressure head data obtained by equilibrium, steady state, and unsteady-state methods, *Soil Science Society of America Proceedings*, *31*, 312-314, 1967.

van Genuchten, M. Th., A closed-form equation for predicting the hydraulic conductivity of unsaturated soils, *Soil Science Society of America Proceedings*, *44*, 892-898, 1980.

Weller, U., O. Ippisch, J. M. Köhne, and H. J. Vogel, Direct measurement of unsaturated hydraulic conductivity in sandy soil including temporal dynamics, hydraulic non-equilibrium and hysteresis, *Vadose Zone Journal*, *10*, 654-661, 2011.

Dual-Drip Subsurface Irrigation Systems: Can it Act as a Hydraulic Barrier?

Mohammad El-Nesr, N. B.[1], Abdurrahman Alazba[1], and Jiří Šimůnek[2]

[1]*Alamoudi Chair for Water Researches, King Saud University, Riyadh, Saudi Arabia (drnesr@gmail.com).*
[2]*Department of Environmental Sciences, University of California Riverside, Riverside, CA, USA.*

Abstract

Subsurface drip irrigation systems, compared to other irrigation systems, enhance delivery of water and chemicals directly into the root zone. However, in light-textured soils, certain quantities of water may percolate below the root zone due to the subsurface position of drip lines. The main objective of this paper is to evaluate three technologies to enhance a spatial distribution of water and solutes in the root zone and to limit downward leaching. The three technologies include a) a physical barrier, b) a dual-drip system with concurrent irrigation, and c) a dual-drip system with sequential irrigation. To achieve this objective, we performed computer simulations and field experiments. Numerical simulations were carried out using the HYDRUS (2D/3D) software for both bare and cultivated soils. The results indicate that the physical barrier is more efficient than dual-drip systems in enhancing the water distribution in the root zone while preventing downward leaching.

1. Introduction

Surface and subsurface drip irrigation systems are increasingly being used in arid regions with limited water resources to irrigate agricultural crops. The subsurface drip irrigation (SDI) systems, have an especially promising future due to their many advantages. The main advantages of SDI, compared to surface drip irrigation (DI), include: a) a significant reduction of evaporation, b) a direct injection of water and fertilizers into the root zone, and c) an easier and for drip lines, safer, operation of machinery.

The proper design of SDI systems requires knowledge of the water distribution patterns around the emitters that match the root extraction patterns and minimizes wetting of the soil surface and deep percolation (Kandelous et al., 2011). The exact shape of the wetted volume and water distribution depends on many factors, including soil hydraulic characteristics, initial soil conditions, discharge rate, application frequency, root characteristics, evaporation, and transpiration (Subbaiah, 2013). Additionally, the wetting pattern depends on the location of the emitter with respect to the soil surface. The wetting pattern is hemi-ellipsoidal or ellipsoidal when the dripper is located on the soil surface or in the subsurface, respectively.

Generally, plants have higher root densities in the upper part of the root zone. Majumdar (2004) indicated that in a soil profile with a uniform water content most plants extract about 40, 30, 20, and 10% of their water needs from corresponding quarters of the root zone (Figure 1a). Despite a similar wetting pattern under DI and SDI systems (Figure 1bc), a considerable amount of water escapes from the root zone by percolating downwards or dispersing laterally in the soil beyond

the reach of roots. Figure 1 indicates that the wetting pattern for the DI system is more similar to the root distribution than for the SDI system, while more water leaches below the root zone in the SDI system than in the DI system. El-Berry (1989) reported that the main avenue for water losses under SDI is deep percolation, which is highest during the seedling stage and declines with the growth of the root system.

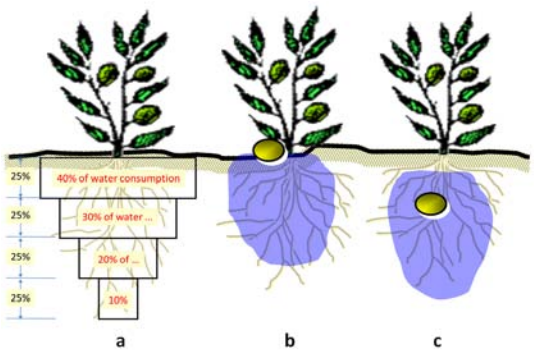

Figure 1. A wetting pattern in the root zone: a) a distribution of a root water extraction, b) a wetting pattern for a surface dripper, and c) a wetting pattern for a subsurface dripper.

Several investigators have tried to adjust the shape of the wetted zone to better match the root extraction pattern (e.g., Phene et al., 1987; Barth, 1995; Welsh et al., 1995; Ismail et al., 2006). Phene et al. (1987) showed that the wetted pattern around the buried emitter can be managed by adjusting the irrigation frequency and that more water moves toward the soil surface when the irrigation frequency is increased. Other investigators (e.g., Barth, 1995; Welsh et al., 1995) have suggested placing an impermeable barrier below the lateral drip lines. This barrier can be made of polyethylene (Barth, 1995) or metal (Welsh et al., 1995). However, there are some problems concerning this physical barrier. For example, there are technical and economical problems with digging a wide and deep trench to install the physical barrier.

Ismail et al. (2006) attempted to modify the wetting pattern by burying a secondary drip line beneath the primary one, and by dividing the required water volume between the two drip lines. This approach depends on the fact that water moves faster into the dry soil (due to a higher pressure head gradient) than into the moist soil, and thus, when the secondary drip line moistens the soil below the primary drip line, it forces water from the upper drip line to redistribute upward and laterally, rather than moving downward. Hence, they called this technique "a hydraulic barrier". This technique requires no wider trenching than the normal SDI trenching. Their results showed that when applied in the field, the hydraulic barrier increased the total and marketable yields of the Jerusalem artichokes by 12 and 48%, respectively, while the physical barrier increased the yields by 131 and 138%, respectively (Ismail et al., 2006). These results clearly document the benefits of using such techniques to increase crop yields.

In order to efficiently design and manage SDI systems, several models (analytical and empirical) have been developed to describe water flow from an emitting source (a point or line source) in the soil (surface or subsurface) (e.g., Brandt et al., 1971; Warrick, 1985; Khalifa et al., 2004; Sing et al., 2006). One of the most complete packages for simulating water, heat, and solute movement in both two- and three-dimensional, variably-saturated, porous media is the HYDRUS software package (Šimůnek et al., 2008). Many investigators have used this model to evaluate

either field or laboratory experiments, or other mathematical models (e.g., Skaggs et al., 2004; Provenzano, 2007; Kandelous et al., 2011). The HYDRUS model enables its users to trace the movement of water and solutes and the wetting patterns in both simple and complex geometries for homogeneous or heterogeneous soils, and for different combinations of initial and boundary conditions.

The main objectives of this study therefore are (a) to simulate water flow for an SDI system while considering both the physical barrier and the dual-drip system using the HYDRUS package, (b) to numerically evaluate how these alternative techniques affect the movement of water, and (c) to evaluate whether or not the dual-drip system can act as a hydraulic barrier for movement of water.

2. Material and Methods

2.1. Modeled Scenarios

To address our main objectives, we have chosen to evaluate the following alternative scenarios:

1. Two soil textures (sand and loam).
2. Different water applications:
   a. A single emitter without a physical barrier
   b. Two emitters operating concurrently
   c. Two emitters operating sequentially
   d. A single emitter with a physical barrier

Simulations were carried out for soils representing two textural classes: sand and loam. Soil hydraulic parameters for the two textural classes were taken from the soil catalog provided by the HYDRUS software (Carsel and Parish, 1988).

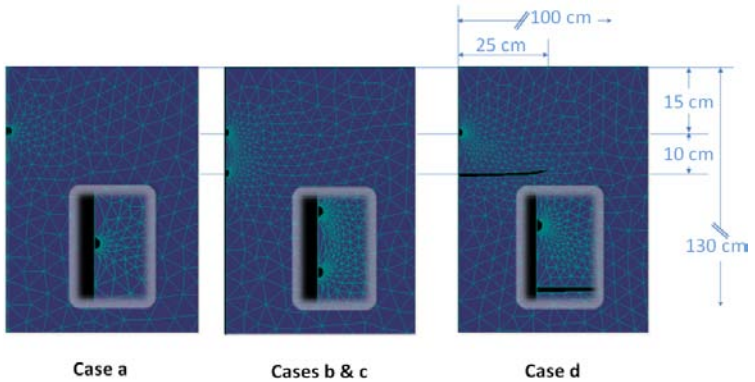

Figure 2. Location of the emitters and the physical barrier in the transport domain considered in Hydrus simulations: a domain around a dripper is magnified in excerpts.

2.2. Initial and Boundary Conditions

The Hydrus (2D/3D) software package (version 2.02) (Šimůnek et al., 2008) is used in numerical simulations for all modeled scenarios. The transport domain for all scenarios was considered to be axisymmetrical around a vertical axis. Figure 2 shows the detail of the upper left corner of the

transport domain, in which the emitters and a physical barrier are located. The transport domain was 100 cm wide (radius) and 130 cm deep (depth). The (upper) emitter was located 15 cm below the soil surface (Figure 2, left), while the secondary emitter (in scenarios b and c) was 25 cm below the soil surface (Figure 2, center). The physical barrier (when considered, scenario d) was placed 27 cm below the soil surface and was considered to have a radius of 25 cm (Figure 2, right).

Figure 3 shows the boundary conditions (BCs) considered in different scenarios in this study. Boundary conditions that are placed in parenthesis are used only in some cases. In all simulated scenarios, the upper boundary of the transport domain was subjected to atmospheric conditions, while the lower boundary of the domain was free drainage. Boundaries at both vertical sides were assigned a "No Flux" boundary condition. Emitters were represented in all cases as half circles with a radius of 1 cm, located on the left vertical boundary of the transport domain. The upper emitter was assigned a "Variable Flux 1" BC. In scenarios b and c, in which two emitters were considered, the second emitter was assigned a "Variable Flux 2" BC. In scenario d, the physical barrier was simulated as a 1-cm thick impermeable barrier 25 cm wide with a "No Flux" BC, (Figure 2d and Figure 3). Simulations were carried out for 2,880 minutes (i.e., 2 days).

Time-variable boundary conditions were used to simulate drip irrigation. The dripper discharge (Q) was considered to be 7.5 L/h, which is equivalent to a boundary flux (q) of about 10 cm/min In scenarios with a single emitter (cases a and d), the irrigation flux was 10 cm/min. In scenarios with two emitters (cases b and c), the irrigation flux at each emitter was 5 cm/min, thus maintaining the same total discharge in all scenarios.

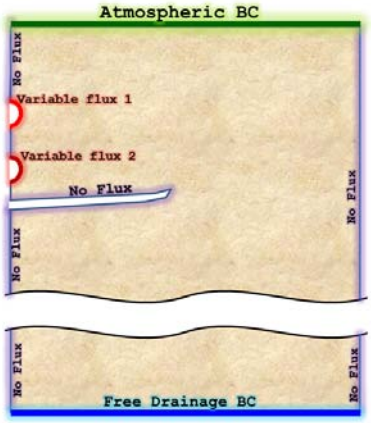

Figure 3. The transport domain with applied boundary conditions.

The operation sequence of different emitters in different scenarios is shown in Figure 4. In cases a and d with only one emitter, this emitter operates for 60 minutes every two days. In case b with two emitters, the two emitters have the same duration of operation, but with only 50% flux applied to each of them. Finally, for cases c, c_u, and c_d with two emitters operating sequentially, Figure 4 shows the pattern of each sequential operation. The secondary (deeper) emitter starts operating either 30 or 120 minutes before the main (upper) emitter in cases c and c_d, respectively, or 120 minutes after the upper emitter in case c_u. Again, n these sequential scenarios, the irrigation flux to each emitter is i half of the flux in cases a and d.

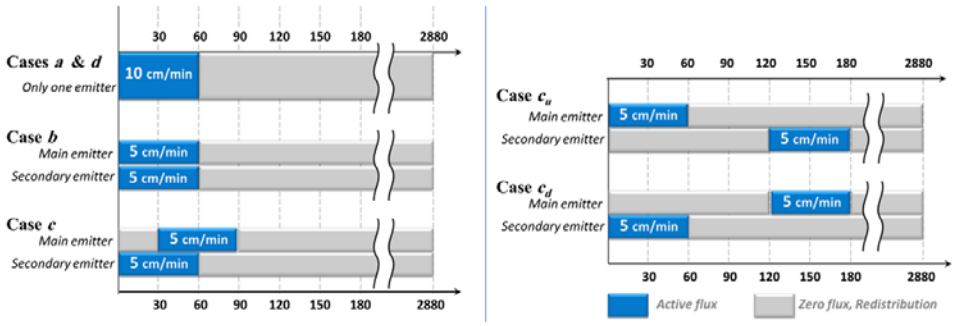

Figure 4. Irrigation fluxes applied in different scenarios.

In the 'Results and Discussion' section below, we will provide graphical outputs for pressure heads along vertical and horizontal cross-sections throughout the transport domain. Five horizontal cross-sections are at depths of 5, 10, 15, 25, and 35 centimeters, while seven vertical cross-sections are at distances of 5, 10, 15, 20, 30, 40, 50, and 60 cm away from the axis of symmetry.

3. Results and Discussion

3.1. Simulation Results for Water Flow

In this section, we will discuss the results of numerical simulations for scenarios a, b, c, and d, for both the loam- and sand-textured soils. For each soil texture we will discuss both water content profiles along horizontal and vertical cross-sections. Each figure will show water content profiles for nine output times at an increasing time interval, i.e., 1, 5, 20, 60, 90, 360, 720, 1440, and 2880 min after the beginning of infiltration. These water content profiles thus cover both the infiltration and redistribution parts of the numerical experiment.

3.1.1. Bare Loamy Soil

Water Distribution along Vertical Cross-Sections

Figure 5 shows the vertical water content distributions at five vertical cross-sections at distances of 5, 10, 15, 25, and 35 cm from the emitter(s) for the bare loamy soil for four analyzed scenarios (a, b, c, and d). Multiple curves represent outputs at different times.

The irrigation scheme can be clearly identified from the water content profiles after 1 min in the 5 cm from the emitter cross-section (Fig. 5; left). While water content profiles for cases a and d clearly show infiltration from a single emitter, for case b they show infiltration from two emitters, and for case c only from the bottom emitter, since the upper emitter starts operating only after 30 minutes. In case a, the area around the emitter (depths of 8-25 cm) at a distance of 5 cm reached saturation before 5 min. This area (at a 5-cm distance from the emitter) continues to widen until almost the entire root zone is saturated at the end of irrigation. The water content profile after 60 min already reflects the redistribution process, since the irrigation flux stops at 60 min in all cases except c (as shown in Figure 4).

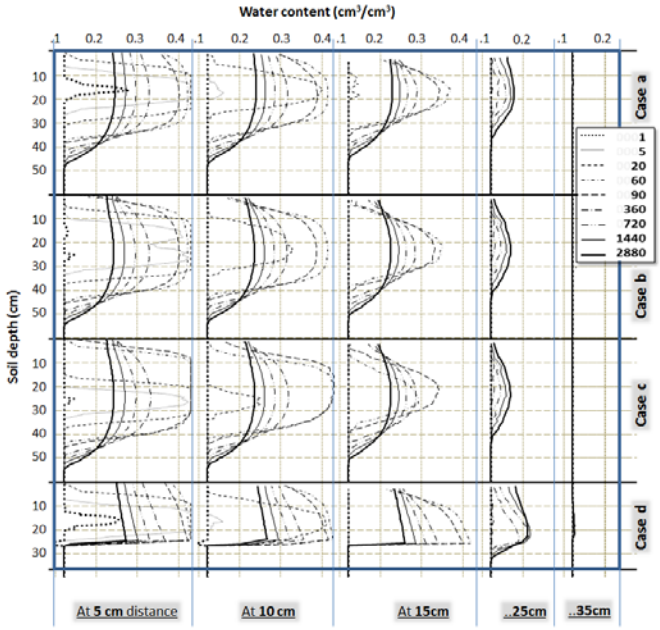

Figure 5. Vertical water content distributions at different distances (5, 10, 15, 25, and 35) away from the dripper for different irrigation scenarios for a bare loamy soil.

Water content profiles are quite similar at a 10-cm distance from the emitter, except in case d, which shows some small differences in the upper 25 cm. Maximum water contents are reached in case c at times of 60 and 90 min. At a 15-cm distance from the emitter, the highest water contents are reached in case d in the upper 25 cm, while the three other cases are quite similar. At a 25-cm distance, only small increases in water contents can be observed over time. While the first increase in the water content is observed only after 60 min in cases b and c, this occurs earlier (after 20 min) in cases a and d, due to the higher irrigation flux from a single emitter.

Interestingly, at a 25-cm distance, water content values appear in reverse order versus time compared to water content values at shorter distances. While at this distance, water contents are increasing for larger times, at shorter distances they are decreasing. This is due to the redistribution process, which both vertically and laterally drives water to distances further from emitters. Finally, notice that water did not reach the 35-cm distance, except in case d between depths of 10 and 25 cm.

Water Distribution along Horizontal Cross-Sections

Water content distributions for four analyzed cases are shown in Figure 6 at seven horizontal cross-sections and at depths of 5, 10, 20, 30, 40, 50, and 60 cm. The same output times as in Figure 5 are shown. The highest water contents are found at a depth of 20 cm, i.e., between the main and secondary emitters, which are placed at depths of 15 and 25 cm, respectively. In this depth, the soil stays saturated to a horizontal distance of about 20 cm for up to about 90 min in case c. In case d, water contents are highest compared to other scenarios at all times at depths of 5, 10, and 20 cm, while only a small amount of new water appears at a 30-cm depth at the far end of the physical barrier at later times (at about 360 min). This is due to the redistribution process, which is demonstrated in Figure 7. Figure 7 shows that the physical barrier is very effective in

preventing leaching of water to deeper depths, as only small quantity of water flows around the barrier.

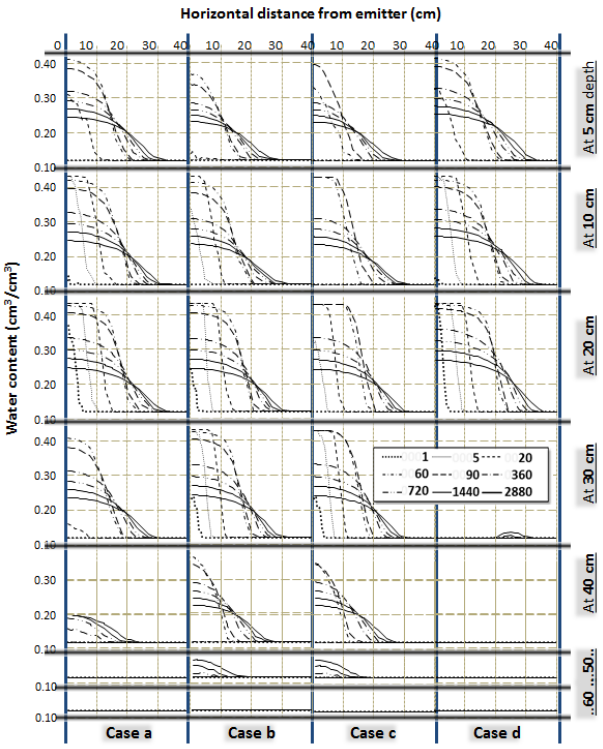

Figure 6. Horizontal water content distributions at different depths (5, 10, 20, 30, 40, 50, and 60) for different irrigation scenarios for a bare loamy soil.

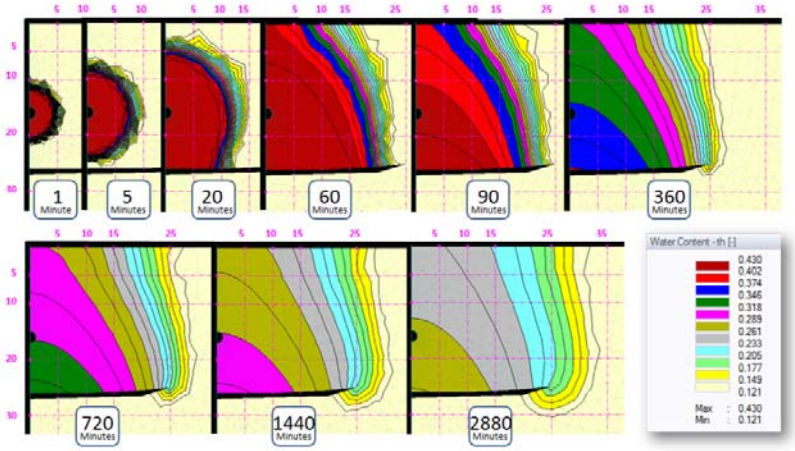

Figure 7. Water content distributions at different times for case d for a bare loamy soil.

While water content profiles for the first three cases a, b, and c are quite similar in the top 30 cm (Figure 6), substantial differences occur at a depth of 40 cm and below. While in case a, at a depth of 40 cm the maximum water content is only about 0.2, in both cases b and c, water contents are as much as 0.38 at 90 min and 0.3 at 360 min. Only cases b and c show increases in

water contents (up to 0.20) at later times due to the redistribution process (at times of 720, 1440, 2880 min). None of the analyzed cases delivered water down to a 60-cm depth.

3.1.2. Bare Sandy Soil

Water Distribution along Vertical Cross-Sections

Sandy soils have significantly higher hydraulic conductivities and infiltration rates than loamy soils and significantly lower macroscopic capillary length. This causes water to move deeper and much less laterally into the sandy soil profile than in the loamy soil. Our simulations clearly show that in Figure 8. In cases b and c, water infiltrated down to 60 and 90 cm at a 5-cm distance at times of 60 and 2880 min, respectively. On the other hand, the rest of the profile is much less saturated. Although water contents around emitters are higher than 0.40, water quickly redistributes when irrigation stops. The highest water contents around the emitter at all times can be observed in case d, because of the physical barrier, which prevents redistribution of water downwards, while physical properties of the sandy soil prevent lateral redistribution. In case c, the highest water contents are reached at 90 min when irrigation from the primary emitter stops.

There are only small differences in water content profiles between the first three cases after 360 min. This shows that none of the analyzed cases, except case d, improve the wetting pattern once redistribution in the sandy soil starts. The same phenomena can be observed at cross-sections at distances of 10 and 15 cm. On the other hand, in case d one can observe accumulation of water above the physical barrier, as well as its bypassing during the redistribution process (at the 25- and 35-cm cross-sections). This shows that the physical barrier indeed enhances water redistribution in the root zone.

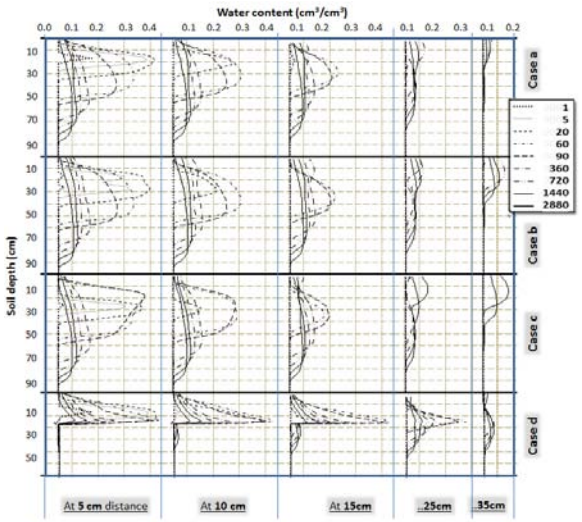

Figure 8. Vertical water content distributions at different distances (5, 10, 15, 25, and 35) away from the dripper for different irrigation scenarios for a bare sandy soil.

Water Distribution along Horizontal Cross-Sections

One of the main benefits of the subsurface drip irrigation is that it keeps a dry soil surface. This helps to reduce the loss of water due to evaporation and prohibits the growth of weeds at the soil surface. Cases b and c have the lowest water contents in the top 5 cm of the soil profile (Figure

9). This is caused mainly by the lower value of the discharge (5 cm/min) of the upper emitter in the case of the dual-drip system compared to the single-drip system (10 cm/min). This may be considered one of the benefits of the dual-drip system.

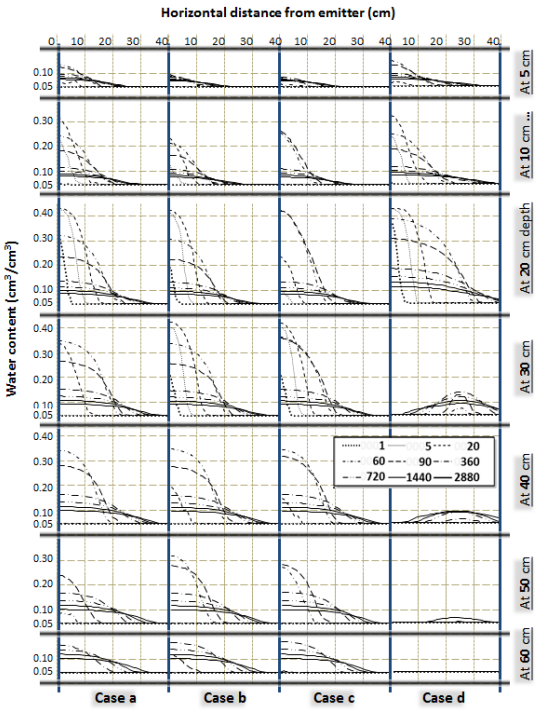

Figure 9. Horizontal water content distributions at different depths (5, 10, 20, 30, 40, 50, and 60) for different irrigation scenarios for a bare sandy soil.

At a 10-cm depth, the highest water contents for cases a and d occur at 20 min, while for case c the highest water contents occur at times of 60 and 90 min. No noticeable differences are visible between cases a, b, and c from time 360 min to 2880 min. In case d water laterally spreads laterally both above (at higher values) and below the physical barrier, moving more than 40 cm at times of 1440 and 2880 min, while in other cases the lateral spreading is at most 30 cm. At a 20-cm depth, the highest water contents were obtained in case d at almost all times. This reflects the role of the physical barrier. Case c has the second highest water contents with a near-saturation state for up to 90 minutes. This reflects the effect of the sequential operation of the dual-drip system. At depths of 30 and 40 cm, the highest water contents were obtained in case c at 90 min, while the lowest water contents were obtained in case d due to the existence of the physical barrier at a depth of 27 cm. In case d, there was almost no water content increase at a depth of 50 cm and no increase at all at a depth of 60 cm. On the other hand, the dual-drip scenarios (cases b and c) show a better distribution of water at a depth of 50 cm than case a.

4. Conclusions

Numerical simulations carried out in this study show that the application of a dual-drip system or the installation of a physical barrier can significantly alter both the wetting pattern and spatial distribution of applied solutes. Physical barriers simply prevent downward movement of all substances (e.g., water, nutrients, and other chemicals) and thus their usefulness depends on

whether we want to retain these substances in the root zone or if we prefer to flush them out. A dual-drip system represents a powerful tool for manipulating the distribution of solutes in the root zone, especially if the two emitters can be operated sequentially. Such a system allows growers to control which solute to retain in the root zone and which one to discard by simply altering the operation of the two drippers. However, this technology requires much more research through the evaluation of larger numbers of possible scenarios involving different solutes, different soils, and different operation scenarios, and especially, through evaluation under field conditions.

Acknowledgments

The authors wish to express their gratitude to the National Plan of Science and Technology at King Saud University for funding this research by the research project (10-WAT985-02). Thanks are also due to Alamoudi Chair for Water Research, where this research is being carried out.

References

Barth, H. K., Resource conservation and preservation through a new subsurface irrigation system, Proc. of the 5th International Microirrigation Congress, Florida, ASAE, 168-174, 1995.

Brandt A., E. Bresler, N. Dinar, I. Ben-Asher, J. Heller, and D. Goldberg, Infiltration from trickle source: I. Mathematical model, *Soil Sci. Soc. Am. J. Proc*., *35*, 675-682, 1971.

Carsel, R. F., and R. S. Parrish, Developing joint probability distributions of soil water retention characteristics, *Water Resour. Res.*, *24*, 755-769, 1988.

El-Berry, A. M., Design and utilization of subsurface drip irrigation system for fodder production in arid lands, *Misr J. Agr. Eng.*, *6*(2), 153-165, 1989.

Ismail, S. M., T. K. Zien El-Abedin, M. M. Wassif, and M. N. El- Nesr, Physical and hydraulic barriers under surface and subsurface drip irrigation systems, The 14th annual conf. of *Misr J. of Agr. Eng. MSAE*, *23*(4), 1021-1034, 2006.

Kandelous, M. M., J. Šimůnek, M. Th. van Genuchten, and K. Malek, Soil water content distributions between two emitters of a subsurface drip irrigation system, *Soil Science Society of America Journal*, *75*(2), 488-497, 2011.

Khalifa H. E., A. M. El-Gindy, G. A. Sharaf, and Kh. A. Allam, Simulating water movement in sandy soil under surface point source emitter. I. Model development, *Misr J. Ag. Eng.*, *21*(2), 341-361, 2004.

Majumdar, D. K., *Irrigation Water Management: Principles and Practice*, PHI Learning Pvt. Ltd, 2004.

Phene, C. J., K. R. Davis, R. B. Hutmacher, and R. L. McCormick, Advantages of subsurface drip irrigation for processing tomatoes, *Acta Horticulture*, *200*, 101-113, 1987.

Provenzano, G., Using HYDRUS-2D simulation model to evaluate wetted soil volume in subsurface drip irrigation systems, *J. Irrig. Drain. Eng.*, *133*, 342–349, 2007.

Šimůnek, J., M. Th. van Genuchten, and M. Šejna, Development and applications of the HYDRUS and STANMOD software packages, and related codes, *Vadose Zone Journal*, *7*(2), 587-600, 2008.

Singh, D. K., T. B. S. Rajput, D. K. Singh, H. S. Sikarwar, R. N. Sahoo, and T. Ahmad, Simulation of soil wetting pattern with subsurface drip irrigation from line source, *Agricultural Water Management*, *83*(1-2), 130–134, 2006.

Skaggs, T. H., T. J. Trout, J. Šimůnek, and P. J. Shouse, Comparison of HYDRUS-2D simulations of drip irrigation with experimental observations, *J. Irrig. Drain. Eng.*, *130*, 304–310, 2004.

Subbaiah, R., A review of models for predicting soil water dynamics during trickle irrigation, *Irrigation Science*, *31*(3), 225-258, 2011.

Warrick, A. W., Point and line infiltration calculation of the wetted soil surface, *Soil Sci. Soc. Am. J. Proc*., *49*, 1581-1583, 1985.

Welsh, D. F., U. P., Kreuter, and J. D. Byles, Enhancing subsurface drip irrigation through vector flow, Proc. of the 5th International Microirrigation Congress, Florida, ASAE, 688-693, 1995.

Numerical Modeling of Water Flow and Nitrate Dynamics in Zero Tension Plate Lysimeters Using HYDRUS-2D

Filipović Vilim[1], Radka Kodešová[2], and Dragutin Petošić[1]

[1]*Department of Soil Amelioration, Faculty of Agriculture, University of Zagreb, Svetošimunska 25, 10000 Zagreb, Croatia, vfilipovic@agr.hr*

[2]*Department of Soil Science and Soil Protection, Faculty of Agrobiology, Food and Natural Resources, Czech University of Life Sciences, Kamýcká 129, Prague 6, Czech Republic, kodesova@af.czu.cz*

Abstract

Lysimeter experiments attempt to represent as closely as possible actual field conditions. The ability of zero tension plate lysimeters, installed in silty clay soils, to represent real field conditions, as well as the ability of the HYDRUS-2D software package to simulate water flow and nitrate dynamics in these conditions, were evaluated in this study. The relatively poor performance of the lysimeters during the vegetative period was mostly caused by a high water demand of the crops and possible diversion of water to the sides of the zero tension plate lysimeter when the groundwater table was deep. The HYDRUS-2D model was able to reproduce observed outflows to some degree. Water and solute diverged from the plate towards the drier unsaturated soil when groundwater table was deep. Simulated distributions of the pressure heads and nitrate concentrations around the lysimeter plate illustrated that the lysimeter plate had a significant impact on the water regime and nitrate dynamics in the soil. This paper summarizes some of the results published earlier by Filipović et al. (2013).

1. Introduction

Numerical simulations of water flow and urea-ammonium-nitrate reactions and transport in the vadose zone, while simultaneously accounting also for root water and nutrient uptake, can improve our understanding of the dynamic nature of these processes under field conditions. This insight could then be used to improve fertilizer application strategies. Many computer models have been developed over the years to solve the problems of water, heat, and pollutant movement in the vadose zone. Two of the most advanced and most widely used numerical models are HYDRUS-1D (Šimůnek et al., 2008) and HYDRUS 2D/3D (Šimůnek et al., 2011). These programs have been used successfully to simulate fertigation and the transport of nitrogen (Hanson et al., 2006). Simulations were used also to optimize fertigation (with urea) and to reduce fertilizer applications by 30% (Ravikumar et al., 2011). Experiments used to validate mathematical models are frequently performed in the laboratory under controlled conditions generally not typical of natural field conditions. Lysimeters may also be used to evaluate solute transport models (Schoen et al. 1999), and to monitor the fate and mobility of contaminants (Ludwig et al., 2000). The goal of this study was to evaluate the efficiency of zero-tension plate lysimeters to collect soil water samples and to assess soil water regime and nitrate leaching in soils influenced by a high groundwater table. Four zero-tension plate lysimeters were tested in relatively fine-textured soils (silty clay) in 2007, 2008, 2009, and 2010. The ability of HYDRUS-2D to reproduce observed water and nitrate outflows (collected by lysimeters) was also assessed. Results were published by Filipović et al. (2013). Here we show data only for 2010.

2. Materials and Methods

2.1. Input Data and Soil Hydraulic Properties

The research area is located near Bid Field in Eastern Croatia between 18º15' to 19º00' east longitude and 44º45' to 45º20' north latitude. Climatic data were collected from the Gradište meteorological station (45°09' N and 18°42' E). The study was performed at 4 locations. Soil types were classified as follows: Luvic Stagnic Phaeozem Siltic (Horizons: Ap-Bt-Bg-C) at locations L1 and L2, Haplic Fluvisol Eutric Siltic (Horizons: Ap-A/Bw-Cg-Cr) at location L3, and Haplic Gleysol Calcaric Eutric Siltic (Horizons: Ap-Bg-Cr-Cg) at location L4. Measured soil textures are shown in Table 1.

Table 1. Soil texture, bulk density, and van Genuchten soil hydraulic parameters for the four lysimeters L1 through L4 (Filipović et al., 2013).

Location	Depth (cm)	Sand (%)	Silt (%)	Clay (%)	Bulk density (g cm^{-3})	θ_s (cm^3 cm^{-3})	θ_r (cm^3 cm^{-3})	K_s (cm day^{-1})	α (cm^{-1})	n
L1	0-40	13	65	22	1.59	0.38	0	11	0.0026	1.18
	40-75	4	63	33	1.57	0.37	0	15	0.0026	1.17
L2	0-30	9	67	24	1.56	0.36	0	17	0.0018	1.26
	30-75	2	61	37	1.55	0.37	0	12	0.00017	1.25
L3	0-40	6	60	34	1.49	0.37	0	14	0.0016	1.20
	40-90	6	60	34	1.55	0.38	0	9	0.0029	1.18
L4	0-30	5	54	41	1.37	0.42	0	12	0.0014	1.20
	30-70	3	54	43	1.55	0.41	0	14	0.0021	1.18

Table 2. Information about crops, sowing and harvest dates, and fertilizer applications (Filipović et al., 2013).

Year	Location	Crop	Sowing date	Harvest date	Application date	Fertilizer
2010	L2	Barley	13.11.2009	15.07.2010	01.04.2010	NPK 15:15:15 260 kg/ha, Urea 180 kg/ha
	L3	Corn	04.05.2010	10.10.2010	04.05.2010	NPK 15:15:15 700 kg/ha, Urea 180 kg/ha
	L4	Corn	01.05.2010	03.10.2010	01.05.2010	NPK 15:15:15 600 kg/ha, Urea 180 kg/ha

2.2. Lysimeter Experiment

One zero tension lysimeter was installed at each location at a depth of 50 cm. Nitrate concentrations were determined with a continuous flow analyzer San+ (Skalar), while outflows were collected manually. Daily elevations of the groundwater table were monitored using two water level limnigraphs (Orphimedes-OTT Hydrometry). We recorded also all agricultural activities in the experimental fields, including sowing and harvesting dates, and the date and

amount of fertilizer application (Table 2). Location L1 was not used for the solute transport simulations because only an organic fertilizer was applied at this location.

2.3. Model Description

The HYDRUS-2D model was used to simulate water flow and solute transport. The Richards equation, which describes isothermal Darcian flow in a variably-saturated rigid porous medium, is solved numerically by the software. This equation may be written in a general form as follows:

$$\frac{\partial \theta}{\partial t} = \nabla \left(K \nabla H \right) - S_w \tag{1}$$

where θ is the volumetric water content [L^3L^{-3}], K is the unsaturated hydraulic conductivity [LT^{-1}], H is the hydraulic head [L], S_w is a sink term accounting for plant water uptake [T^{-1}], ∇ is the spatial gradient operator, and t is time (T).

Soil hydraulic functions were described using the van Genuchten-Mualem model (van Genuchten, 1980). Table 1 lists the parameters values. Of these, the saturated water content, θ_s, was measured, while the remaining parameters of the soil water retention curve (θ_r, α, and n) were optimized using the RETC software (van Genuchten, 1991) by fitting the measured retention data. Unsaturated hydraulic conductivities were predicted using the θ_s, θ_r, and n values, the measured values of saturated hydraulic conductivity, K_s, and assuming the pore connectivity parameter to be equal to the average of many soils (l=0.5) as suggested by Mualem (1976).

The governing solute transport equations, which solve the transport of each chemical species separately, were simplified as follows:

For urea:

$$\frac{\partial \theta c_1}{\partial t} = \nabla \left(\theta D \nabla c_1 \right) - \nabla \left(q c_1 \right) - \mu_a \theta c_1 - S_w c_1 \tag{2}$$

For ammonium:

$$\frac{\partial \theta c_2}{\partial t} + \rho \frac{\partial s_2}{\partial t} = \nabla \left(\theta D \nabla c_2 \right) - \nabla \left(q c_2 \right) - \mu_v \theta c_2 - \mu_n \theta c_2 + \mu_a \theta c_1 - S_w c_2 \tag{3}$$

For nitrate:

$$\frac{\partial \theta c_3}{\partial t} = \nabla \left(\theta D \nabla c_3 \right) - \nabla \left(q c_3 \right) + \mu_n \theta c_2 - S_w c_3 \tag{4}$$

where c_i is the liquid phase concentration of chemical species i (the subscripts 1, 2, and 3 represent urea, ammonium, and nitrate, respectively) [ML^{-3}], D is the dispersion coefficient tensor [L^2T^{-1}], q is the volumetric flux density[LT^{-1}], ρ is the bulk density of the soil [ML^{-3}], s_2 is the adsorbed concentration of ammonium [MM^{-1}], μ_a is a first-order rate constant [T^{-1}] representing nitrification of urea to ammonium, μ_v is a first-order rate constant [T^{-1}] representing

volatilization of ammonium to ammonia and μ_n is a first-order reaction rate constant [T^{-1}] representing nitrification of ammonium to nitrate.

The parameters needed for simulating the transport of the various nitrogen species were set as follows. The longitudinal dispersivity along the direction of flow was taken as 5 cm and the transverse dispersivity as 0.5 cm. Molecular diffusion was neglected. The first-order reaction constant representing nitrification of urea to ammonium (μ_a) was taken as 0.38 per day (Hanson et al., 2006), the reaction constant representing nitrification of ammonium to nitrate (μ_n) was set at 0.2 per day (Hanson et al., 2006), and the reaction constant for volatilization of ammonium to ammonia (μ_v) was set at 0.0552 per day (Bolado Rodriguez et al., 2005). The distribution coefficient for ammonium (K_d) was assumed to be 3.5 cm^3g^{-1} (Hanson et al., 2006). The bulk density was measured using undisturbed soil samples (Table 1).

The model was used to simulate the water regime and solute transport above and around the lysimeter plate assuming a radially symmetric flow domain. The assumed 2D transect was 150 cm wide radially, and 150 cm deep, with the lysimeter plate (Ø 50 cm) at a depth of 50 from the soil surface. Initial conditions were defined as a hydrostatic equilibrium pressure head distribution with the value of the pressure head at the bottom being zero (a groundwater table). Atmospheric conditions with surface runoff were selected at the top. A seepage face was applied at the top of the lysimeter plate. Root water uptake was calculated assuming potential evapotranspiration, a given root depth and density, and using the Feddes water stress response function (Filipović et al., 2013).

The initial ammonium and nitrate contents in soils were set in terms of nitrogen concentrations in soil water (expressed in mmol cm^{-3}). No flux was considered at both lateral boundaries, and the sides and bottom of the lysimeter plate. A third-type boundary condition was used at remaining boundaries. The concentration fluxes of nitrogen for all 3 applied species (urea, ammonium, or nitrate) were calculated assuming molar mass and a number of atoms for each molecule (Filipović et al., 2013).

3. Results and Discussion

3.1. Water Flow

Observed and simulated results are shown in Figure 1. The simulated results depended upon precipitation events, the transpiration intensity and the position of the groundwater table. The water table in particular was found to have a major effect on pressure head distributions around the lysimeter plate. No outflow was simulated when the water table was deep. Cumulative outflow was then strongly affected by water diverging around the lysimeter, without any water flowing through the lysimeter plate. The reason is that outflow will occur only when the soil above the plate is fully saturated (e.g., the pressure head in the soil above the plate must reach a positive value). Outflows were simulated only after intensive rainfalls when the soil above the plate became saturated from below (i.e., when the water table was high and the soil profile mostly saturated due to capillary rise from the water table).

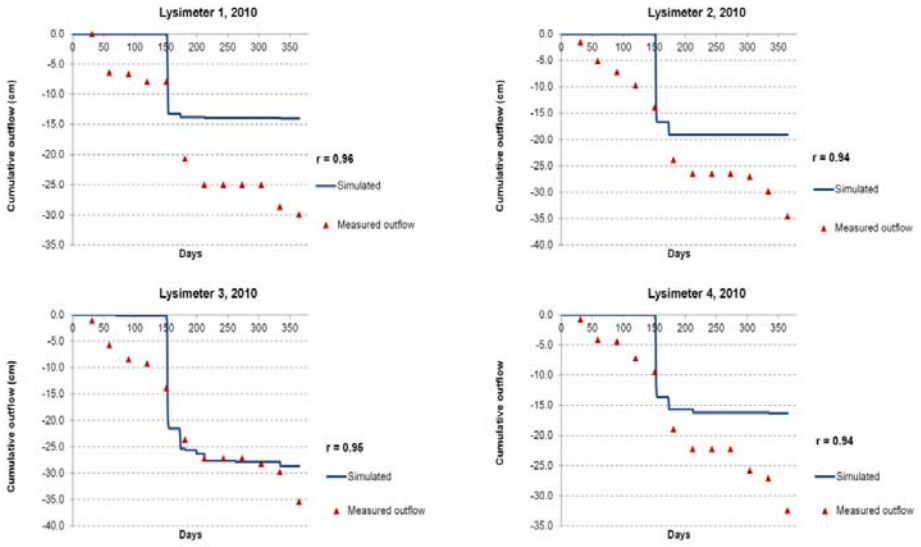

Figure 1. Observed and simulated cumulative outflows from the four lysimeters in 2010. The correspondence between measured and simulated values is expressed using the correlation coefficient, *r* (Filipović et al., 2013).

The spatial distributions of the pressure head clearly indicate that water was diverging around the plate towards the dryer surrounding soil (as also discussed by Peters and Durner, 2009) and that water could also be supplied by capillary rise from the water table. Two examples of the pressure head distribution are shown in Figure 2. Figure 2a shows pressure heads within a two-dimensional transect (i.e., around the lysimeter plate) after rainfall when no outflow was simulated. Figure 2b similarly shows pressure heads within the two-dimensional transect after rainfall when considerable outflow was simulated. The figures clearly show either low or high pressure heads above the plate, which resulted into either no or high outflows, respectively.

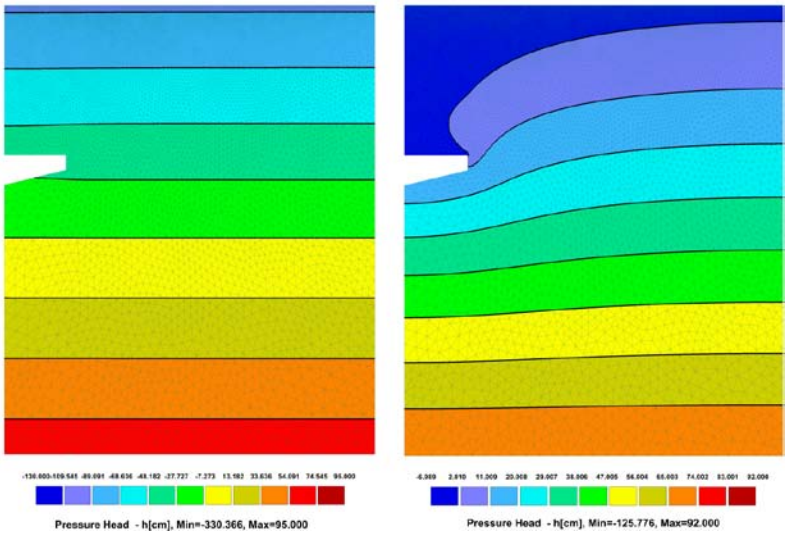

Figure 2. Simulated pressure heads within the two-dimensional transect of lysimeter 4, 2010, day 71 (a, left) and 152 (b, right) (after Filipović et al., 2013).

3.2. Nitrate Transport

Cumulative nitrate outflow measured in different lysimeters and simulated using HYDRUS-2D are presented in Figure 3. Values reflect cumulative water outflow rates (Fig. 2) and actual nitrate concentrations above the lysimeter plate. Therefore, the correspondence between observations and model outputs varies. This is reflected by the *r* values in Figure 3, which range from 0.72 to 0.89. No outflow of urea was simulated because of root uptake and rapid conversion into nitrate (urea and NPK are highly reactive fertilizers that start reacting immediately after their dissolution in percolating water). Figure 4 shows the nitrate concentrations (79 days after the fertilizer application) after an extreme rainfall event in 2010. A considerable amount of nitrate passed in this case below the lysimeter plate due to large and intensive rainfall. Clearly, the amount of precipitation and its intensity strongly influenced the nitrate leaching process and its dynamics in the observed soil profile. These are the most dominant processes determining nitrate transport and distributions in the soil.

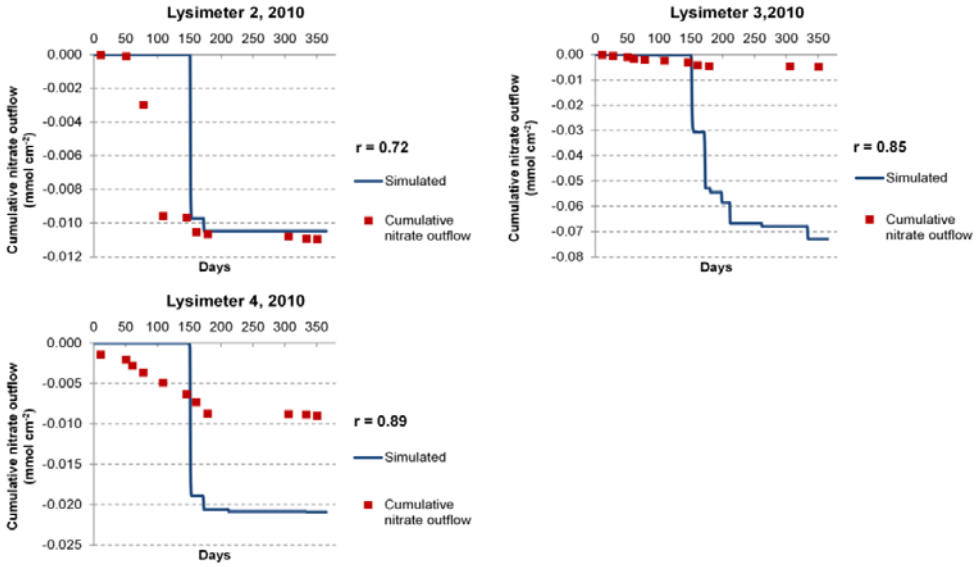

Figure 3. Observed and simulated cumulative nitrate outflows from the three lysimeters in 2010. The correspondence between measured and simulated values is expressed using the correlation coefficient, *r* (after Filipović et al., 2013).

4. Conclusions

The ability of zero-tension plate lysimeters to collect soil water samples and to assess soil water regimes and nitrate leaching in soils influenced by the groundwater table was evaluated in this study. A poor efficiency during the vegetation period was caused mostly by high plant water demand and possible lateral diversion of water when the groundwater table was deep. The simulated water and nitrate outflows showed that the water regime was affected significantly by the groundwater table, which was monitored in the field. Outflow was simulated only when the soil above the plate was saturated from below, and during intensive rainfall periods.

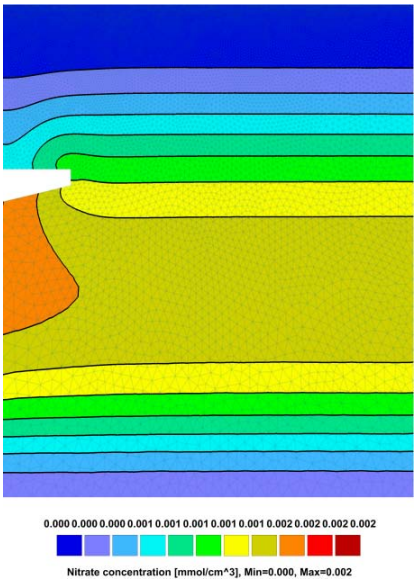

Figure 4. Simulated nitrate concentrations within a two-dimensional transect of lysimeter 4, day 200 (Filipović et al., 2013).

Nitrate outflow always reflected the simulated outflow of water and the actual nitrate concentrations above the lysimeter plate. The lysimeter plate generally acted as a barrier for water flow and also solute transport. The HYDRUS-2D software package was able to reproduce to some degree the observed water and nitrate outflows. Our results indicate that HYDRUS can be very helpful for understanding and estimating the dynamics of water flow and nitrate transport under real field conditions.

References

Bolado-Rodriguez, S., A. Alonso-Gaite, and J. Álvarez-Benedi, Characterization of nitrogen transformations, sorption and volatilization processes in urea fertilized soils, *Vadose Zone J., 4,* 329-336, 2005.

Filipović, V., R. Kodešová, and D. Petošić, Experimental and mathematical modeling of water regime and nitrate dynamics on zero tension plate lysimeters in soil influenced by high groundwater table, *Nutrient Cycling in Agroecosystems, 95,* 23-42, 2013.

Hanson, B. R., J. Šimůnek, and J. W. Hopmans, Numerical modeling of urea-ammonium-nitrate fertigation under microirrigation, *Agricultural Water Management, 86,* 102-113, 2006.

Ludwig, C., C. A. Johnson, M. Käppeli, A. Ulrich, and S. Riediker, Hydrological and geochemical factors controlling the leaching of cemented MSWI air pollution control residues: A lysimeter field study, *J. Contam. Hydrol., 42,* 253-272, 2000.

Mualem, Y., A new model for predicting the hydraulic conductivity of unsaturated porous media, *Water Resour. Res., 12*(3), 513-522, 1976.

Peters, A., and W. Durner, Large zero-tension plate lysimeters for soil water and solute collection in undisturbed soils, *Hydrol. Earth System Sci. Discussions, 6,* 4637-4669, 2009.

Ravikumar, V, G. Vijayakumar, J. Šimůnek, S. Chellamuthu, R. Santhi, and K. Appavu, Evaluation of fertigation scheduling for sugarcane using a vadose zone flow and transport model, *Agric. Water Manage., 98,* 1431-1400, 2011.

Schoen, R., J. P. Gaudet, and D. E. Elrick, Modelling of solute transport in a large undisturbed lysimeter, during steady-state water flux, *J. Hydrol.*, *215*, 82-93, 1999.

Šimůnek, J., M. Šejna, H. Saito, M. Sakai, and M. Th. van Genuchten, The HYDRUS-1D Software Package for Simulating the Movement of Water, Heat, and Multiple Solutes in Variably Saturated Media, Version 4.0, *HYDRUS Software Series 3*, Department of Environmental Sciences, University of California Riverside, Riverside, California, USA, pp. 315, 2008.

Šimůnek, J., M. Th. van Genuchten, and M. Šejna, The HYDRUS Software Package for Simulating Two- and Three-Dimensional Movement of Water, Heat, and Multiple Solutes in Variably-Saturated Media, Technical Manual, Version 2.0, PC Progress, Prague, Czech Republic, 258 p, 2011.

van Genuchten, M. Th., F. J. Leij, and S. R. Yates, The RETC Code for Quantifying the Hydraulic Functions of Unsaturated Soils, Version 1.0, *EPA Report 600/2-91/065*, U.S. Salinity Laboratory, USDA, ARS, Riverside, California, 1991.

van Genuchten, M. Th., A closed form equation for predicting the hydraulic conductivity of unsaturated soils, *Soil Sci. Soc. Am. J., 44*(5), 892–898, 1980.

Single and Double Porosity Modeling of Solute Transport in Intact Soil Columns – Effects of Texture, Slurry Placement, and Intermittent Irrigation

Nadia Glæsner[1,2,3] and Horst H. Gerke[3]

[1]*Faculty of Science, University of Copenhagen, Frederiksberg, Denmark, nadia.glaesner@gmail.com*
[2]*Faculty of Science and Technology, Aarhus University, Tjele, Denmark,*
[3]*Leibniz-Zentrum für Agrarlandschaftsforschung (ZALF) e.V., Müncheberg, Germany, hgerke@zalf.de*

Abstract

We investigated using single and double porosity models implemented in HYDRUS-1D numerical code, solute transport and solute mass exchange between pore water regions in intact soil columns (20 cm diameter, 20 cm high) under variably-saturated flow conditions during injection and surface application of dairy slurry manure in three soil textures, and during continuous and intermittent irrigation. All models tested were able to describe breakthrough curves of nonreactive slurry components (Br tracer applied to slurry) and a tritium tracer applied with irrigation water for all experimental conditions. Simulation of intermittent irrigation with HYDRUS software was limited by the option of a fixed bottom seepage face value, which could not be changed in time according to experimental conditions. The problem was provisionally fixed by restarting the program with the modified bottom conditions at experimentally defined times using the calculated final distribution of state variables as new initial conditions. Both single and double porosity water flow and mobile-immobile solute transport models predicted decreased solute mass exchange when injecting slurry into the soil profile compared with surface application in a loam, but not in the more coarse-textured soils. These results suggest protection of slurry compounds when placed inside the soil matrix in finer-textured soils compared with placement of slurry at the soil surface. Introducing rainfall interruptions (and variably-saturated flow) led to higher leaching of injected slurry compounds compared with steady flow conditions. These results were explained by increased mass exchange from immobile to mobile pore water regions during interruptions. The model based analysis suggests considering more natural boundary conditions when trying to obtain improved understanding of nutrient leaching after slurry application.

1. Introduction

Leaching of plant nutrients from agricultural fields is causing eutrophication problems of surface waters worldwide. Nutrient losses especially occur from fields subjected to land application of animal manure in areas of high livestock production (Coelho et al., 2007; Kronvang et al., 2009). In order to minimize leaching of agricultural chemicals to the subsurface and aquatic environments, the effects of different soil management strategies are being evaluated (e.g., Maguire et al., 2011).

Injection of animal slurry into arable topsoil was proposed as an alternative to surface application to reduce ammonia gas emissions (Webb et al., 2010). Injection of dairy slurry has additionally been shown to reduce leaching of slurry components (Glæsner et al., 2011a,b) in loamy soils when compared with surface application; the effect was less obvious for the sandy soils. Early tracer appearance in the loam indicated the effects of preferential flow (e.g., Flühler et al., 1996; Gerke, 2006) and physical non-equilibrium solute transport (e.g., van Genuchten and Dalton, 1986). Physical non-equilibrium in the loamy soil could be explained by the existence of a two-domain pore system (van Genuchten and Wierenga, 1976) characterized by a mobile and an immobile (aggregate or less mobile soil matrix) pore water region.

Solute transport in column experiments has often been studied assuming steady-flow conditions (de Jonge et al., 2004; Glæsner et al., 2011a), thereby simplifying model analysis by neglecting soil hydraulic properties. Under steady flow conditions, breakthrough curves (BTCs) of percolation experiments can be analyzed with analytical solutions of the convection-dispersion equation (CDE); for instance, with the program CXTFIT (Toride et al., 1995). Transfer of steady flow laboratory column experimental data to field conditions however, can be criticized because the steady flow assumption rarely occurs. It is more realistic to have rain infiltration periods followed by dry periods, generating variably-saturated flow of water and locally varying pore water velocities (Wehrer and Totsche, 2003). While diffusion-limited solute mass transfer can already occur under steady-flow conditions, an additional mass exchange by transfer of water between the mobile and immobile pore regions has to be considered for intermittent flow conditions with physical non-equilibrium (e.g., Gerke, 2006; Jarvis, 2007).

This study aims at identifying the possible role of mass exchange between mobile and immobile pore regions during different slurry placements (surface application and injection) and irrigation regimes (steady-flow and intermittent irrigation). Based on the description of a set of soil column percolation experiments, the aim is achieved by a stepwise increase in model complexity using an analytical CDE model and numerical single and double porosity models. The analysis required i) choosing the most appropriate flow and transport model types, ii) determining parameters for each model type (again from simple to more complex), iii) identifying limitations given by experimental data at certain modeling steps, and iv) defining particular initial conditions and treatment of the boundary conditions for the injection case. The final aim was to couple experimental results with detailed understanding of the underlying mechanisms of leaching losses of slurry compounds.

2. Experimental Design and Modeling Approach

2.1. Experimental Design

Although experimental conditions are thoroughly described in the papers of Glæsner et al. (2011a,c), a short description is given here. Intact soil columns (20 cm diameter, 20 cm height) were excavated from the plough layer of an agricultural field in Denmark with a natural gradient of clay content; loamy sand, sandy loam, and loam. The effects of no slurry application, surface application of slurry, and injection of slurry were all studied (Glæsner et al., 2011a). The finer-textured loamy soil with injected slurry was furthermore studied during continuous irrigation and

intermittent irrigation at a rate of 2 mm h^{-1} (Glæsner et al., 2011c). The experiments were carried out in triplicate.

All intact soil columns, excavated at field capacity, were initially saturated and subsequently drained on tension tables to -100 cm. The columns were then transferred to an irrigation/leaching setup; irrigation was initiated, and a suction of -5 cm was applied at the lower boundary after 2.5 – 12.5 h irrigation to ensure unsaturated conditions. Experiments were carried out for approximately 5 days, and during intermittent irrigation, suction was increased to -20 cm during irrigation interruptions.

Dairy slurry manure was initially homogenized and spiked with KBr (2.69 g L^{-1}), and then applied to the soil columns 52–53 h prior to initiation of the leaching experiment at an amount corresponding to 25 t ha^{-1}. Slurry was either evenly distributed at the soil surface or injected in a 1 cm wide and 10 cm long band, placed 5 cm from the edge of the cylinder and 8 cm below the soil surface. The columns received a pulse of 2.5 mm ^3H_2O after steady outflow was reached.

2.2. Modeling Approach

For simulating tracer movement (^3H_2O), we used the equilibrium (EQ) and non-equilibrium (NEQ) convection-dispersion equations (CDE); model parameters were fitted using the CXTFIT program (Toride et al., 1995) as implemented in STANMOD software (Šimůnek et al., 2008).

For simulating solute transport under steady-state (continuous irrigation) and variably-saturated flow conditions (intermittent irrigation), we used: i) the single porosity model for uniform equilibrium-type flow and solute transport (SP-EQM), in which the volumetric water content, θ (cm^3 cm^{-3}), the solute concentration, c (g L^{-1}), and the solute mass, $c\theta$, are defined for a single porosity soil, ii) the combination of equilibrium water flow (EQ water) with mobile-immobile solute transport (SP-MIM solute), and iii) the double porosity model for non-equilibrium mobile-immobile type water flow and solute transport (DP-MIM) (cf., Šimůnek and van Genuchten, 2008). These models were numerically solved as implemented in the HYDRUS-1D program (Šimůnek et al., 2008).

The double porosity and MIM approaches partition the bulk soil into fractions for mobile and immobile pore-water regions for the volumetric water content, θ, and the solute mass as $\theta = \theta_{im} + \theta_m$ and $c\theta = c_{im}\theta_{im} + c_m\theta_m$, respectively. Equations and parameters used in this paper are as in Toride et al. (1995) and Šimůnek et al. (2008).

2.2.1. Stepwise Parameter Estimation

The parameter estimation was carried out stepwise as illustrated in Figure 1. The ^3H_2O-BTCs were first analyzed with CXTFIT. The EQM model was used to fit an initial value of D to the ^3H_2O-BTCs for all columns, assuming a retardation factor of $R = 1$. These initial D values were used in the NEQM to further optimize the values of D, β, and ω to obtain λ, as well as θ_{im}, and α_s to be used in HYDRUS. The best fit was based on the lowest possible MSE (mean square error), low correlation between parameters, and low 95% confidence intervals as calculated in CXTFIT.

The β parameter (mobile water fraction) was used in the DP-MIM transport simulation (see below).

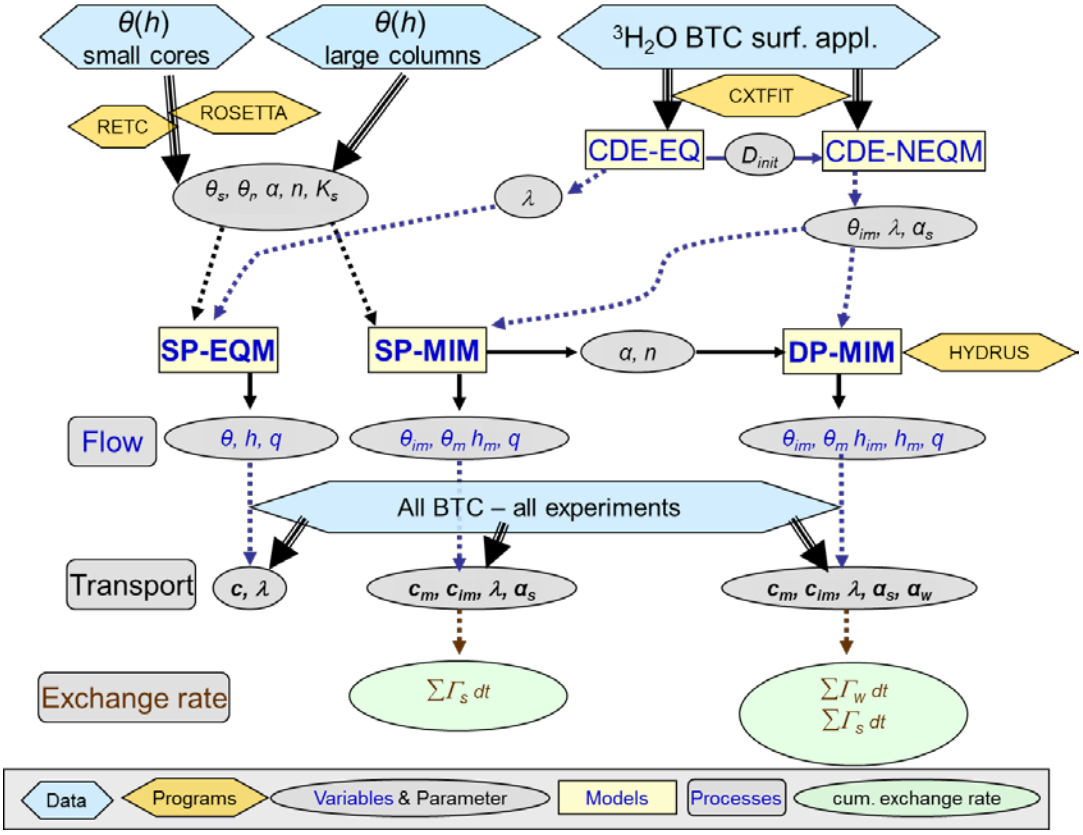

Figure 1. Overview of the complex stepwise analysis of mass exchange in the leaching experiments, illustrating the data input from small cores and larger intact columns, breakthrough curves (BTC) for ^3H_2O and Br for steady flow (top row), variably-saturated flow and transport during surface application and injection (of slurry) for intermittent irrigation (bottom), and the resulting exchange rates and the used programs, models, flow and transport parameter derivations.

Soil Hydraulic Model Parameters

From the experimental conditions (Glæsner et al., 2011a, b, c), the volumetric water contents at -5 and -100 cm from each intact soil column as well as eight values of the water retention curve from 100 cm^3 intact core samples were available for each soil texture-type in the pressure head range between -4 and -300 cm. Two approaches were carried out to find optimized single porosity vGM (van Genuchten, 1980) soil hydraulic parameters:

A) Soil hydraulic functions were estimated using pedotransfer functions with the ROSETTA program (Schaap et al., 2001) as implemented in HYDRUS. ROSETTA estimates were based on data of texture, bulk density, and water content at -100 cm, which we used instead of that at -330 cm. Since the ROSETTA fit did not match the two retention values at -5 and -100 cm available for each soil column, the value of θ_s was manually adjusted based on the vGM equation (van Genuchten, 1980), such that the fitted matched the

observed θ-value at -5 cm. With the manually fitted θ_s and the ROSETTA fitted θ_r, n and α values as initial estimates, the α-values of the vGM function were again optimized using the RETC program (van Genuchten et al., 1991), assuming m=1-1/n to fit the retention values at -5 and -100 cm. The values of K_s were fitted such that $K(h)$ function (van Genuchten, 1980) matched the observed K-value at h =-5 cm.

B) The water retention data from 100 cm^3 soil cores of each texture were fitted with the RETC program using the optimized vGM-parameters from step A) as initial estimates. The value of θ_s was fixed, and θ_r, n, and α were fitted. For the loam, the optimized values for n were not allowed to drop below n = 1.2 (fixed minimum) to avoid numerical problems. The resulting α and n values based on soil core retention data were applied to all columns of each texture class, whereas θ_s and θ_r values were adjusted to match the measured water contents at -100 cm and -5 cm of each individual column using the vGM equation (van Genuchten, 1980).

The parameter sets were finally tested by describing the experiments with the vGM parameters in HYDRUS, such that simulated θ-values were matching the measured ones during drainage (at -100 cm) and irrigation (at -5 cm) for each column.

For the double porosity flow model parameters, the identical values of α and n obtained from above were used for both mobile and immobile pore water regions in order to minimize parameter identification. The fractions θ_m and θ_{im} were obtained from CXTFIT results (above). For the loamy sand and the sandy loam columns, the mobile pore water region θ_{sm} and θ_{rm} were defined as 0.9-times, and the immobile region θ_{sIm} and θ_{rIm} as 0.1-times the values of the vGM parameters. For the loam, θ_{sm} and θ_{rm} were 0.4-times, and θ_{sIm} and θ_{rIm} were 0.6-times the values of the vGM parameters. Values of the water exchange coefficient, α_w, were fitted using the optimization routine provided in the HYDRUS program.

Solute Transport and Mass Exchange Parameters

The transport parameter θ_{im} obtained with CXTFIT from ^3H_2O solute transport was not further fitted; however, λ and α_s of columns subjected to injection were fitted in HYDRUS using the average values of the parameters from columns of the same texture that were subjected to surface application as initial values. For analyzing Br leaching, we used the parameters obtained from ^3H_2O as initial estimates in all columns and then fitted the values of λ and α_s for Br in HYDRUS. For intermittent irrigation, solute transport parameters, λ and α_s, obtained during steady flow, were used as initial estimates in HYDRUS and then fitted to the effluent data of the respective soil columns.

2.2.2. Initial and Boundary Conditions

Conditions in HYDRUS were different for columns subjected to surface application or injection of slurry (mixed with Br). Surface application of slurry was treated as a flux boundary condition with a flux rate of 32.4 cm d^{-1} for 10 min, assuming that a pulse of 70 mL of water in applied slurry per column was mixed within the first 1 cm layer for 10 min after application at day 11 (2 days prior to irrigation).

Slurry injection as an initial condition was assumed to be fully mixed with the soil of a vertical layer of 2.5 cm in 6.5 - 9 cm depth for the loamy sand and the sandy loam, and a layer of 7 cm thickness in 4 - 11 cm depth for the loam columns. The full mix of slurry and soil in the layers of the whole column was required when assuming a 1D vertical model. The slurry injection introduced Br and additional water. This application-induced increase in water contents was considered proportional to the available water storage porosity, hence the vertical thickness of the injection layer was chosen the smallest layer possible that could store the additional slurry water without exceeding the porosity. Due to a larger fraction of smaller pores in the loam (Glæsner et al., 2011a), the higher water-filled porosity at -100 cm at the time of slurry injection resulted in the assumed larger layer for the loam in which slurry was mixed as compared to the other two soils.

Upper boundary conditions in HYDRUS were set to atmospheric with a surface layer. The lower boundary was set to a seepage face condition of 0 cm when irrigation was initiated; hereafter, a seepage face condition of -5 cm was imposed after 2.5 - 12.5 hours. These changes of lower boundary conditions required us to split the simulation runs in a series of interrupted model periods per run. Hence, end conditions of a previous period were applied as initial conditions in the subsequent period during each simulation run. Transport of $^{3}H_2O$ was described as concentration flux at the upper boundary and with zero concentration gradient at the lower boundary, whereas Br was described (see above) in the initial condition in the form of a resident concentration. The flow domain was spatially discretized using 200 nodes.

3. Leaching of Irrigation Tracer ($^{3}H_2O$)

Simulations using ROSETTA-derived parameters for $^{3}H_2O$ transport yielded only small differences as compared to those results obtained with the optimized RETC retention parameter set (data not shown). We, therefore, used optimized RETC retention parameters in all solute transport simulations.

The NEQM in CXTFIT fitted the $^{3}H_2O$ BTCs before slurry application better than the EQM in all soil textures (Fig. 2), even though the NEQM fit improved more with increased clay content, as the degree of nonequilibrium transport increased with increasing clay content observed by earlier breakthrough and larger tailing (e.g., Flühler et al., 1996). In HYDRUS, applying DP-MIM did, however, not improve the fitting of $^{3}H_2O$ in an injected column during continuous irrigation compared with the simpler models (Fig. 3, left).

Simulations of intermittent irrigation conditions improved with increasingly complex models from SP-EQ to SP-MIM to DP-MIM (Fig. 3, right). One explanation for improved simulation with increasingly complex models for the increased complex experimental setup during intermittent conditions could be the inclusion of solute and water exchange in the more complex models, as increased exchange of solute as well as of water is expected as new pressure and concentration gradients arise within the soil when pores are emptied for water during interruptions.

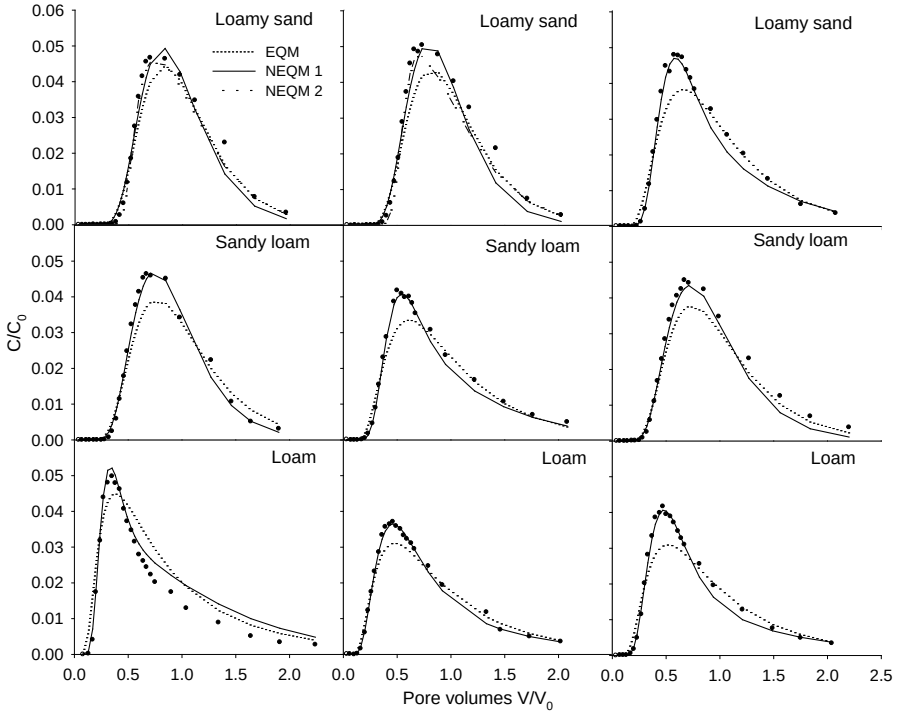

Figure 2. ^3H_2O BTCs in surface applied triplicate columns from the three soil textures using EQM and NEQM in CXTFIT for curve fitting for steady flow (continuous irrigation).

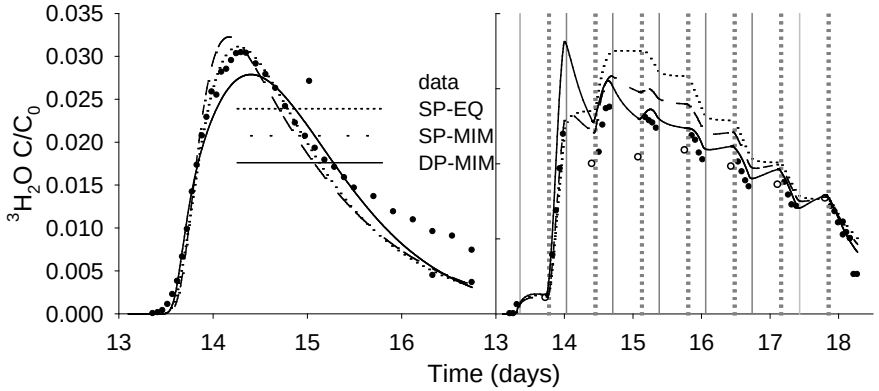

Figure 3. ^3H_2O BTCs after injection with continuous (left) and intermittent (right) irrigation using SP-EQ (dotted line), SP-MIM (dashed line), and DP-MIM (solid line) in HYDRUS. Only one column from each experiment is shown. Open symbols represent samples collected during interruptions; vertical solid lines represent interruptions; and vertical dotted lines represent initiation of irrigation.

Water exchange during continuous irrigation occurred only from mobile to immobile pore water regions (positive values) (Fig. 4). Water exchange during intermittent irrigation occurred from mobile to immobile pore regions during irrigation and from immobile to mobile pore regions (negative values) during irrigation interruptions (Fig. 4), resulting in lower cumulative mass exchange of water from mobile to immobile pore regions during intermittent conditions.

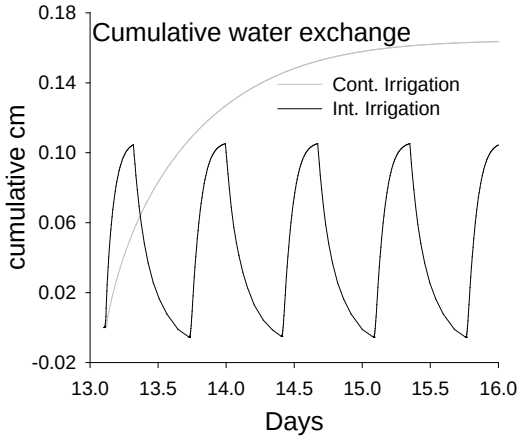

Figure 4. Cumulative water exchange for continuous and intermittent irrigation using the DP-MIM approach.

The importance of water exchange for solute transport is evident, as a substantially larger exchange of ^3H_2O occurred when applying DP-MIM compared with SP-MIM (Fig. 5). This is explained by the additional advective solute mass exchange of ^3H_2O caused by assuming water exchange between the pore regions in the DP-MIM. However, for solute exchange, higher cumulative ^3H_2O exchange from mobile to immobile pore regions is recorded for intermittent irrigation as compared with continuous irrigation, which is due to "diffusive" mass exchange of ^3H_2O being the main mechanism for ^3H_2O exchange caused by concentration differences between pore regions compared to "advective" exchange of ^3H_2O with water caused by pressure head gradients. The high fluctuations in cumulative water exchange (Fig. 4) are therefore not so evident in the cumulative ^3H_2O exchange (Fig. 5). This was further confirmed by decreased mass recovery of leached ^3H_2O when changing the boundary conditions from continuous (86.6 %) to intermittent (76.4 %) irrigation (Glæsner et al., 2011c).

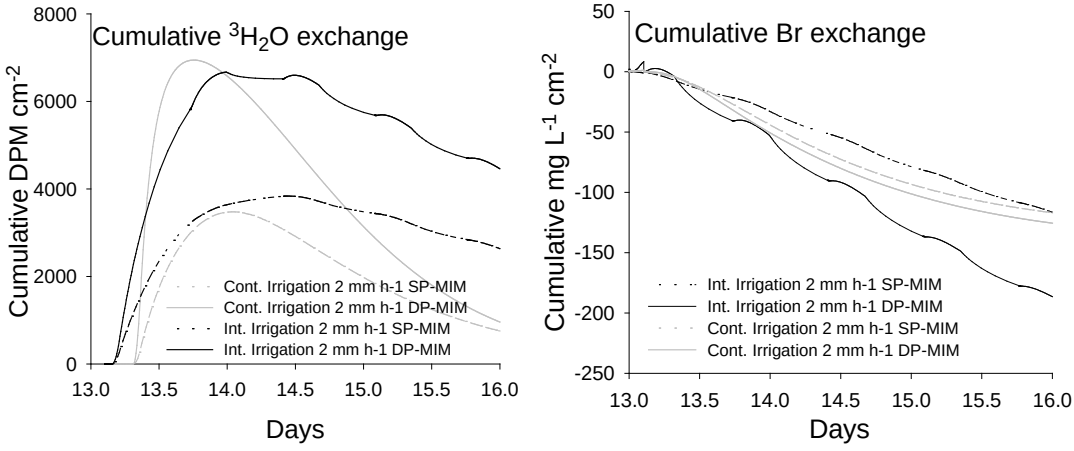

Figure 5. Cumulative ^3H_2O and Br exchange for continuous and intermittent irrigation simulated with the SP-MIM and DP-MIM approaches.

4. Leaching of Slurry Tracer (Bromide)

Bromide BTCs, when slurry was applied both to the soil surface and injected into the soil, were simulated less well than ^3H_2O, but the models still gave good simulation fits (Fig. 6). That BTCs of Br were less well fitted compared with ^3H_2O reflects that Br was applied with slurry which has a different consistency and viscosity than water (Kumar et al., 1972; Frey et al., 2012).

Injection of slurry decreased mass recovery of bromide (60.2 %) compared with surface application (80.6 %) in the loam soil, but not in the other soils (Glæsner et al., 2011a). The authors suggested this to be due to protection of solutes from the few preferential flow paths in the more fine-textured soil. This hypothesis was confirmed in this study by lower cumulative mass exchange from immobile to mobile pore regions during injection compared with surface application in the loam, whereas no difference was observed in the loamy sand and sandy loam when using SP-MIM, even though no statistical significance was found (Table 1). The highly heterogeneous nature of the different columns challenges statistical analysis of the results.

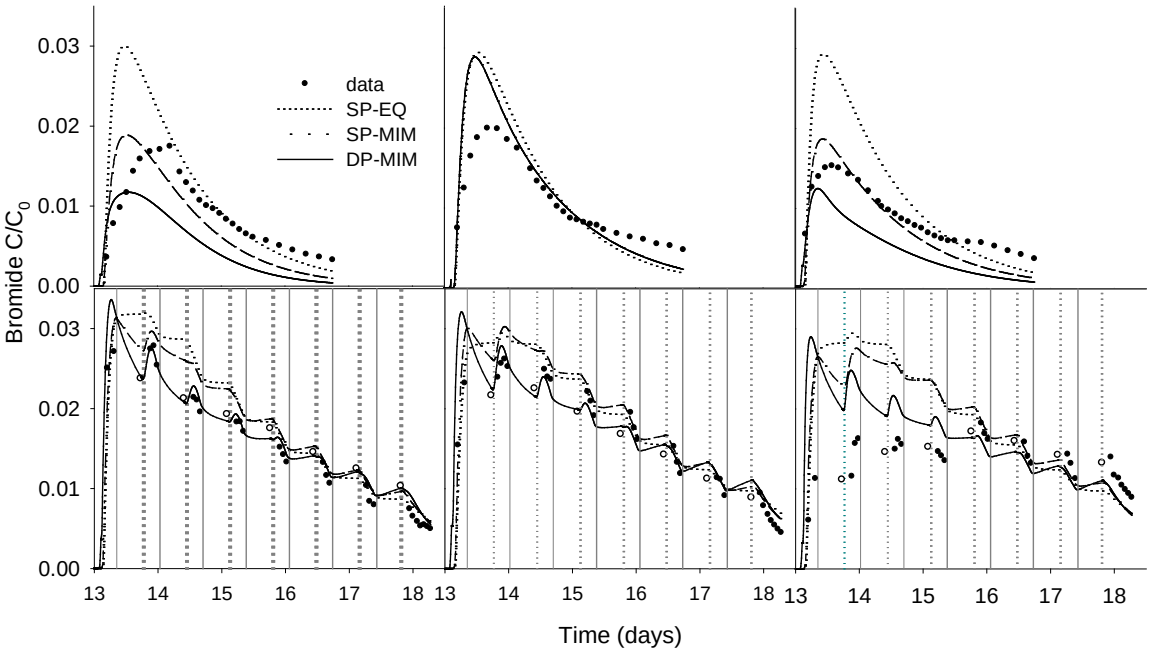

Figure 6. Bromide BTCs after injection with continuous (upper) and intermittent irrigation (lower) using SP-EQ (dotted line), SP-MIM (dashed line), and DP-MIM (solid line) in HYDRUS. Open symbols represent samples collected during interruptions; vertical solid lines represent interruptions; and vertical dotted lines represent initiation of irrigation.

Table 1. Averaged cumulative mass exchange of Br after 1.2 eluted PV using SP-MIM and DP-MIM. Positive values represent exchange from mobile to immobile pore regions, whereas negative values represent exchange from immobile to mobile pore regions. Statistical differences at the 5% level are given by different letters.

Experiment	**SP-MIM**	**DP-MIM**
	mg L^{-1} cm^{-2}	mg L^{-1} cm^{-2}
Loamy sand – surface application	-0.01 (0.00)[a]	-16.79 (13.7)[a]
Loamy sand – injection	-0.61 (0.49)[a]	-3.11 (1.04)[a]
Sandy loam – surface application	-0.01 (0.00)[a]	-17.91 (14.4)[a]
Sandy loam – injection	-4.64 (1.14)[a]	-1.42 (0.81)[a]
Loam – surface application	-127.45 (28.4)[a]	-140.27 (8.46)[a]
Loam – injection	-58.46 (0.13)[a]	-124.21 (8.59)[a]
Loam – injection - continuous	-127.73 (21.5)[a]	-170.23 (47.1)[a]
Loam – injection - intermittent	-175.02 (3.18)[a]	-272.56 (4.20)[a]

During intermittent conditions, in similarity to ^3H_2O, simulation fits increased with increased model complexity (Fig. 6). The Br mass exchange values were all negative (Fig. 5), indicating that exchange of injected Br is only directed from the immobile to the mobile pore water region, which corresponds well with Br being placed within the intact columns at -100 cm, when only pores <30 µm were saturated. Though the water content of the slurry added to higher pore classes being saturated, Br was assumed to diffuse into the water-filled porosity at the time of application, hence the immobile region. Mass recovery of Br in the effluent during continuous irrigation (45.5% ± 2.5) was lower than during intermittent irrigation (59.3% ± 5.2) (Glæsner et al., 2011c). This is fully supported by the cumulative exchange analysis, demonstrating higher mass exchange from immobile to mobile pore regions during intermittent irrigation (Fig. 5), thereby resulting in higher effluent mass recovery.

5. Conclusions

The role of mass exchange was analyzed using different models implemented in HYDRUS-1D. Both single and double porosity water flow and mobile-immobile solute transport models described the data well. However, as experimental conditions became more complex, the more complex models described the data better by including solute and water exchange between pore water regions. Injection decreased leaching of solutes compared with surface application in a loam, but not in the more coarse-textured soils, which could be described by decreased solute exchange from immobile to mobile pore regions in the loam by the model based analysis. Introducing rainfall interruptions (and variably-saturated flow) led to higher leaching of injected slurry compounds compared with steady flow conditions, explained by increased mass exchange from immobile to mobile pore water regions during interruptions in the model based analysis. The results suggest considering more natural boundary conditions when trying to obtain improved understanding of nutrient leaching after slurry application.

References

Coelho, B. R. B., R. C. Roy, E. Topp, and D. R. Lapen, Tile water quality following liquid swine manure application into standing corn, *Journal of Environmental Quality*, *36*, 580–587, 2007.

De Jonge, L. W., P. Moldrup, G. H. Rubæk, K. Schelde, and J. Djurhuus, Particle leaching and particle-facilitated transport of phosphorus at field scale, *Vadose Zone Journal*, *3*, 462-470, 2004.

Flühler, H., W. Durner, and M. Flury, Lateral solute mixing processes - A key for understanding field-scale transport of water and solutes, *Geoderma*, *70*, 165-183, 1996.

Gerke, H. H., Preferential flow descriptions for structured soils, *Journal of Plant Nutrition and Soil Science*, *169*, 382-400, 2006.

Glæsner, N., C. Kjaergaard, G. H. Rubæk, and J. Magid, Interacting effects of soil texture and placement of dairy slurry application. I. Flow characteristics and leaching of nonreactive components, *Journal of Environmental Quality*, *40*, 337-343, 2011a.

Glæsner, N., C. Kjaergaard, G. H. Rubæk, and J. Magid, Interacting effects of soil texture and placement of dairy slurry application. II. Leaching of phosphorus forms, *Journal of Environmental Quality*, *40*, 344-350, 2011b.

Glæsner, N., C. Kjaergaard, G.H . Rubæk, and J. Magid, Effect of irrigation regimes on mobilization of nonreactive tracers and dissolved and particulate phoshorus in slurry-injected soils, *Water Resources Research*, *47*, W12536, 2011c.

Jarvis, N. J., A review of non-equilibrium water flow and solute transport in soil macropores: principles, controlling factors and consequences for water quality, *European Journal of Soil Science*, *58*, 523–546, 2007.

Kronvang, B., G. H. Rubæk, and G. Heckrath, International Phosphorus Workshop: Diffuse phosphorus loss to surface water bodies - Risk assessment, mitigation options and ecological effects in river basins, *Journal of Environmental Quality*, *38*,1924-1929, 2009.

Kumar, M., H. D. Bartlett, and N. N. Mohsenin, Flow properties of animal manure, *Transactions ASAE*, *15*, 718-722, 1972.

Maguire R. O., P. J. A. Kleinman, C. J. Dell, D. B. Beegle, R. C. Brandt, J. M. McGrath, and Q. M. Ketterings, Manure application technology in reduced tillage and forage systems: A review, *Journal of Environmental Quality*, *40*, 292-301, 2011.

Schaap, M. G., F. J. Leij, and M. Th. van Genuchten, ROSETTA: a computer program for estimating soil hydraulic parameters with hierarchical pedotransfer functions, *Journal of Hydrology*, *251*, 163-176, 2001.

Šimůnek, J., and M. Th. van Genuchten, Modeling nonequilibrium flow and transport processes using HYDRUS, *Vadose Zone Journal*, *7*(2), 782-797, 2008.

Šimůnek, J., M. Th. van Genuchten, and M. Šejna, Development and applications of the HYDRUS and STANMOD software packages, and related codes, *Vadose Zone Journal*, *7*(2), 587-600, 2008.

Toride, N., F. J. Leij, and M. Th. van Genuchten, The CXTFIT code for estimating transport parameters from laboratory or field tracer experiments, Version 2.0, *Research Report No. 137*, US Salinity Laboratory, USDA, ARS, Riverside, CA, USA, 1995.

van Genuchten, M. Th., A closed-form equation for predicting the hydraulic conductivity of unsaturated soils, *Soil Science Society of America Journal*, *44*, 892-898, 1980.

van Genuchten, M. Th., and P. J. Wierenga, Mass-transfer studies in sorbing porous-media. 1. Analytical solutions, *Soil Science Society of America Journal*, *44*, 473-480, 1976.

van Genuchten, M. Th., and F. N. Dalton, Models for simulating salt movement in aggregated field soils, *Geoderma*, *38*, 165-183, 1986.

Van Genuchten, M. Th., F. J. Leij, and S. R. Yates, The RETC code for quantifying the hydraulic functions of unsaturated soils, Version 1.0, *EPA Report 600/2-91/065*, US Salinity Laboratory, USDA, ARS, Riverside, CA, USA, 1991.

Webb. J., B. Pain, S. Bittman, and J. Morgan, The impacts of manure application methods on emissions of ammonia, nitrous oxide and on crop response – a review, *Agriculture, Ecosystem and Environment*, *137*, 39-46, 2010.

Wehrer, M., and K. U. Totsche, Detection of non-equilibrium contaminant release in soil columns: delineation of experimental conditions by numerical solutions, *Journal of Plant Nutrition and Soil Science*, *166*, 475-483, 2003.

The Use of HYDRUS-1D for Groundwater Recharge Estimation in Boreal Environments

Sergey O. Grinevskiy[1] and Sergey P. Pozdniakov[2]

[1]*Hydrogeology division, Geological Department, Moscow State University, Leninskie Gory, MSU, Moscow, Russia, sogrin@geol.msu.ru*

[2] *Hydrogeology division, Geological Department, Moscow State University, Leninskie Gory, MSU, Moscow, Russia, sppozd@geol.msu.ru*

Abstract

The well-known package HYDRUS-1D (Šimůnek et al., 2009) was used for groundwater recharge simulations based on long term meteorological data with daily resolution. For a boreal climate with a long winter period, initial meteorological data such as precipitation cannot be used directly as the atmospheric boundary condition in HYDRUS. This data must be preprocessed to take snow accumulation and snow melting, evaporation from snow and vegetation cover, and soil freezing-defrosting processes into account. For this purpose, SurfBal (Grinevskii and Pozdnyakov, 2010), a special preprocessing code for simulating surface water and energy balances and generating upper boundary conditions for HYDRUS-1D was developed. SurfBal calculates surface water balance using known daily values of precipitation, solar radiation, and maximum and minimum temperatures. It calculates interception by canopy, surface (leaf and snow) evaporation, snow accumulation, consolidation of snowpack and its melting and surface runoff, as well as initial potential values of evaporation, transpiration, and input water fluxes for HYDRUS-1D. The results of water balance and groundwater recharge simulations using SurfBal and HYDRUS-1D for climate conditions of the south-western part of Moscow Artesian Basin show the principal role of the spring-period surface-soil water budget for groundwater recharge under various landscapes and soil cover, and the effects of various groundwater level depths.

1. Introduction

The methodological principles of regional estimation of groundwater recharge (GWR) by atmospheric water infiltration are based on simulation of the water balance on the land surface and unsaturated flow inside the soil cover and vadose zone to groundwater level (GWL). These processes are generally identical for the uniform, typical natural conditions of GWR, which are characterized by a combination of meteorological conditions, type of surface and vegetation, soil and underlying vadose zone properties, as well as GWL depth. So the results of simulation of GWR, obtained for each type (combination) of such conditions, may be extrapolated for the corresponding part of the river basin (Crosbie et al., 2010; Grinevskii and Pozdnyakov, 2010).

In small-scale, regional consideration, the typical conditions of GWR are formed by the complex of meteorological, landscape, vegetation, soil and hydrogeological factors, which jointly influence the recharge heterogeneity (Fig. 0).

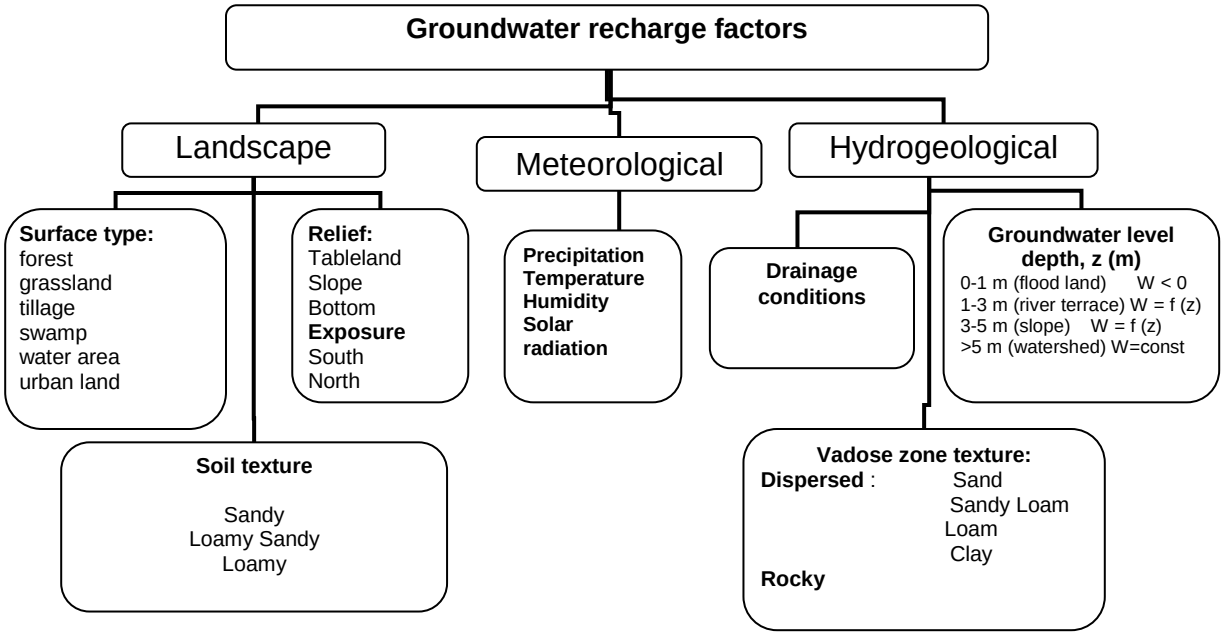

Figure 1. Main regional factors of groundwater recharge.

Main features of boreal climate with regard to GWR processes are:

- the total precipitation exceeds total potential evapotranspiration, so the dry index is less than one;
- the long winter season with temperatures below zero causes a high amount of solid precipitation, accumulated in snow cover;
- winter thaws are usually very short and rare, and the upper part of the soil is frozen, so the water seepage into the soil is negligible during winter season;
- the snow melting period is usually short and intensive, which causes the high volume of snowmelt runoff.

All these features result in special variable upper boundary meteorological and flow conditions for unsaturated flow simulations using HYDRUS-1D. The program code SurfBal was developed to simulate the processes of precipitation and heat energy transformations on the land surface in order to generate the upper boundary meteorological conditions for HYDRUS.

2. Model of Precipitation and Heat Energy Transformations on the Land Surface (SurfBal)

The SurfBal integrates the next water budget equation at the surface:

$$\frac{dV}{dt} = P - E_{LS} - S - v_p\,; \quad V=V_S + V_L; \quad E_{LS} = E_L + E_S \tag{1}$$

where V is the total volume of water accumulated on vegetation (V_L) and in snowpack (V_S), P is the precipitation rate, E_{LS} is the total surface evaporation, including evaporation from canopy

(E_L) and snow cover (E_S), S is the surface runoff, and v_p is the potential infiltration into the soil profile. Solution of Eq. (3) with daily time step gives a value of v_p^i for *i-th day*, which is passed to HYDRUS-1D as the upper boundary condition:

$$v_p^i = P^i \pm \Delta V_S - \Delta V_L - S^i - E_S^i - E_L^i \tag{2}$$

where ΔV_S and ΔV_L equal daily changes of water volumes, accumulated in snow and on leaves, respectively.

Tracking the temperature records, SurfBal calculates the interception of liquid precipitation by the canopy P_L (if the mean daily air temperature is above zero) as the well-known bucket model (Vinogradov, 1988):

$$P_L^i = \Lambda^i \left[1 - \exp\left(\frac{P^i}{\Lambda^i} \right) \right], \quad \Lambda^i = P_{\max}^i - V_L^i, \quad P_{\max}^i = K_L LAI^i \tag{3}$$

According to this approach, total intercepted water is less than maximum storage P_{max}, depending on the daily value of *LAI* and water retention constant K_L = 0.2 mm (Liang et al., 1994). So, a daily variation of water accumulated by canopy depends on interception as well as leaf evaporation E_L, which is proportional to potential evapotranspiration ET^0 (Liang et al., 1994):

$$\Delta V_L^i = V_L^i - V_L^{i-1} = P_L^i - E_L^i \; ; \quad E_L^i = ET_i^0 \left(\frac{V_L^i}{P_{\max}^i} \right)^{2/3} \tag{4}$$

Daily values of potential evapotranspiration ET^0 are calculated based on air temperature and net solar radiation data by the Penman-Montheith or Priestley-Taylor methods (Allen, 2001).

The modified model of Gelphan and Kuchment (Kuchment and Gelfan, 1996) is used to calculate snow depth dynamic and the release of melting water at the soil surface. Dynamics of the snow depth H_S at the surface is simulated by depth-averaged equations for the snow state, considered as a three-phase system that includes solid phase ice with the density ρ_i, water with density ρ_w, and void space. The model takes into account accumulation of snow during precipitation when air temperature T <0, snowmelt, snow metamorphism, sublimation, refreezing of melting water, and its flow to the soil surface through snowpack:

$$\begin{aligned} \frac{dH_s}{dt} &= \left[P_s \chi_0 - \left(L + E_S \right) \chi I^{-1} \right] - V_\rho \\ \frac{d}{dt}\left(IH_s \right) &= \chi \left(P_s - L - E_S + S_i \right) \\ \frac{d}{dt}\left(\theta H_s \right) &= \left(P_r + L - V_m - E_W - S_i \right) \end{aligned} \tag{5}$$

where I and θ are parts of ice and water in snow volume, $\chi_0 = \rho_w \rho_{s0}^{-1}; \chi = \rho_w \rho_i^{-1}$, P_s and P_r are snowfall and rainfall rates, respectively, and S_i is the rate of refreezing of melt water for $T<0$, which is calculated as:

$$S_i = K_i \sqrt{|T|} \tag{6}$$

where $K_i \approx 4.5$ mm/ deg^{0,5}/day is the empirical coefficient of water-ice phase transformations.

The total sublimation of ice E_S and evaporation of liquid water E_W from snowpack depends on potential evapotranspiration ET^0 (Budagovskii, 1981):

$$(E_S + E_W)_i = \begin{cases} \beta^i ET_i^0, & \text{when} \quad V_S^i > \beta^i ET_i^0 \\ V_S^i, & \text{when} \quad V_S^i < \beta^i ET_i^0 \end{cases}; \beta^i = \exp(-\delta\, LAI^i); \quad 0.45 < \delta < 0.55 \tag{7}$$

V_ρ is the snowpack self-compression rate due to its weight:

$$V_\rho = 0.5 K_v \rho_s H_s^2 \exp\left(\xi_1 T - \xi_2 \rho_s\right) \tag{8}$$

The snow melting rate L depends on the temperature and the current snow density ρ_s with the empirical coefficient of snow melting K_s:

$$L = \begin{cases} 0; & T < 0 \\ K_s \rho_s T; & T \geq 0 \end{cases} \tag{9}$$

V_m is the release rate of melting water to the soil surface due to gravity-dominated flow of water through the unsaturated snowpack:

$$V_m = \begin{cases} K_f \overline{\theta}^{3.5}; \quad \overline{\theta} = \dfrac{\theta - \theta_{\max}}{1 - I - \theta_{\max}}; & \theta \geq \theta_{\max} \\ 0; & \theta < \theta_{\max} \end{cases} \tag{10}$$

where K_f is the snow hydraulic conductivity, and $\theta_{\max}$ is the maximum water retention by snow.

The current snow density is:

$$\rho_s = \frac{\rho_i I + \rho_w \theta}{H_s} \tag{11}$$

and fresh snow density ρ_{s0} is the function of air temperature:

$$\rho_{s0} = \begin{cases} \rho_{\min}; & T < T_{\min} \\ \rho_{\min} + (\rho_{\max} - \rho_{\min}) \dfrac{T - T_{\min}}{|T_{\min}|}; & T_{\min} \le T < 0 \\ \rho_{\max}; & T \ge 0 \end{cases} \quad (12)$$

The well-known curve number method (USDA, 1985) is used for calculations of daily surface runoff. When T<0, daily curve number value CN depends on thawed or frozen status of topsoil (Schroeder et al., 1993). The beginning of soil defrosting may be identified by a reverse weighed average of air temperature for the last ten days T_{th}>0 and a current snowpack thickness H_s<0.2 m, with the empirical delay factor ε:

$$T_{th} = \int_{t-t_l}^{t} T(\tau) \exp(-\varepsilon(t-\tau)) d\tau \quad (13)$$

Because potential evapotranspiration ET^0 characterizes total available water losses to atmosphere due to energy limits of the landscape, the remaining daily part of ET^0, except for losses by snow E_S and leaf E_L evaporation, can be estimated:

$$ET_p^0 = ET^0 - E_S - E_L \quad (14)$$

This value is the limit for soil evaporation and plant transpiration, which can be divided into their potential values E_p^0 и TR_p^0 (Budagovskii, 1981):

$$E_p^0 = \beta ET_p^0 \ , \quad TR_p^0 = (1-\beta) ET_p^0 \quad (15)$$

where β is obtained from eq. (7).

The results of SurfBal calculations - daily values of inflow v_p, and potential evaporation E_p^0 and transpiration rates TR_p^0 - describe upper boundary conditions for the soil profile and are passed to HYDRUS-1D as the atmospheric boundary condition.

3. Site and Data Description and GWR Model Parameters

With a total area of 49 600 km^2, the investigated region is the south-western part of Moscow Artesian Basin (MAB) and is located in the center of the European part of Russia. This is the periphery, the edge of MAB, where the regional recharge of carboniferous aquifers takes place. Mean annual precipitation varies in a south-north direction from 600 to 700 mm; mean air temperature ranges from 5.0^{o}C to 4.6^{o}C. These differences are correlated with river runoff, which also changes from 160 mm to 200 mm per year from south to north. For further investigations, the observed daily values of total precipitation, mean, and minimum and maximum air temperatures from 6 meteorological stations for a period of about 50 years were

used. The representative weather stations for different major river basins of the region were selected by the statistical analysis and correlation between precipitation and river runoff.

The areal division of the region using the typical recharge conditions, including landscape, vegetation and soil type, as well as the dominant texture of the underlying vadose zone and mean annual GW level depths, was made. And for each type of GWR conditions, the model of surface and vadose zone water balance was developed for a fifty year simulation period.

The main parameters of the surface water balance model (SurfBal) are presented in Table 1. CN values in the curve number method reflect the mean areal runoff properties of the catchment. Typical curve numbers were used as preliminary values and then were verified by river runoff observations on stream gage stations.

Table 1. Main parameters of the SurfBal model.

Model parameter		**Landscape type**	
		Field	**Forest**
LAI, min-max, [-]		0-3	2-8
Snow melting rate, K_s [cm^4/deg/g/day]		4-6	1.5-3.5
Snow melting delay, ε, day^{-1}		1	3
δ, [-]		0.45	0.55
Curve number, CN, [-]	sandy soil	70	40
	loamy soil	88	83
	clayey soil	94	90

The snowpack dynamic model allows calibration of its parameters by comparing simulated and observed snow depth during winter (Fig. 2). Main fitting parameters in this simulation stage are K_v, K_s, K_f and ξ_1, ξ_2 in eqs. (8-10).

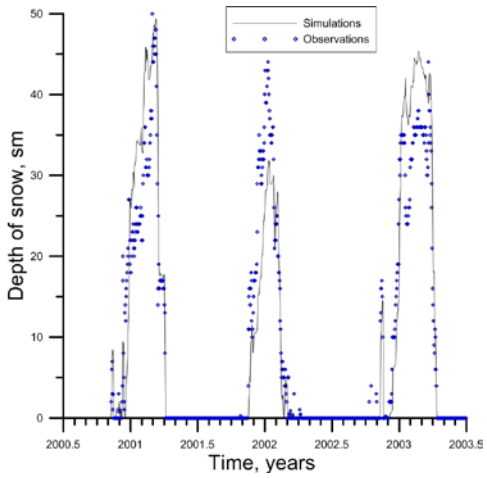

Figure 2. Simulated (lines) and observed (dots) snow depths for the 3-year period.

The soil profile for the unsaturated flow simulation consists of three model layers, which reflect an average typical structure of the vadose zone (Grinevskii, 2010). The upper layer is the soil

horizon of the A type (humus horizon) and has the maximum variability of soil properties. Moreover, water retention curve (WRC) characteristics not only depend on the lithological texture, but also on the type of surface vegetation. The second soil layer, the illuvial soil horizon of the B type, usually has a lower permeability than expected for such soil texture because of the inflow of the organic matter from topsoil. The third model layer simulates the underlying parent rock material (horizon C), whose properties are almost unchanged by pedogenic processes and well-corresponded to the soil texture. Vertical model distribution of this layer is limited by GWL depth.

Average characteristics of WRC van Genuchten equations (van Genuchten, 1980) for three simulated soil profile layers, depending on soil texture and type of vegetation cover (for the upper layer) were calculated using the well known program, Rosetta (Schaap et al., 2001) and numerous soil data (Grinevskii, 2010), and were used for GWR simulation (Table 2). Data in Table 2 show that WRC parameters for the top soil differ depending on the type of vegetation cover. Besides this, the influence of vegetation cover leads to anomalous values of parameter α, which decrease from loamy to sandy soil, unlike those for the underlying layers.

Table 2. Average van Genuchten WRC parameters for different soil layers, soil texture and types of surface landscape (Grinevskii, 2010).

Soil texture / Landcape	θ_r -	θ_s -	α, m^{-1}	n -	K_s, m/d
Layer 1– Soil horizon A					
Loam / Forest	0,041	0,525	1,00	1,388	0,562
Loam / Field	0,054	0,525	1,17	1,352	0,049
Loamy sand / Forest	0,038	0,532	0,79	1,486	0,73
Loamy sand / Field	0,033	0,500	1,08	1,494	0,27
Sand / Forest	0,029	0,482	0,34	2,280	3,85
Sand / Field	0,030	0,413	0,55	1,744	1,50
Layer 2 – Soil horizon B					
Loam	0,055	0,427	0,60	1,352	0,07
Sandy Loam	0,038	0,412	0,90	1,442	0,21
Sand	0,022	0,366	1,25	1,578	1,21
Layer 3 – Soil horizon C					
Clay	0,057	0,380	0,74	1,145	0,007
Loam	0,052	0,383	0,49	1,269	0,04
Sandy Loam	0,034	0,379	1,39	1,361	0,20
Sand	0,018	0,370	2,06	1,581	2,96

For root water uptake calculations, the S-shape function, which describes the water uptake stress response function $\varphi(h)$ in HYDRUS-1D (Šimůnek et al., 2008), was used:

$$\varphi(h) = \frac{1}{1 + \left(h/h_{50}\right)^{\tau}} \tag{16}$$

where h_{50} represents the pressure head at which the root water extraction rate is reduced by 50%, and τ is an empirical parameter. The beginning of decreasing root water extraction ($\varphi(h) <1$) due

to drying conditions in dependence of WRC and it's specific points (field capacity and wilting point) was defined by Li et al. (2006). Following this, values of h_{50} for different soil and vegetation types were calculated (Table 3) using average WRC parameters (Table 2) as (Grinevskii, 2011):

$$\frac{\sqrt{h^* \theta^*}}{\overline{TR_p^0}/(TR_p^0)_{\max}} = 0.5 \;\; ; \;\; h^* = \frac{h_{50} - h_{wp}}{h_{fc} - h_{wp}} \;\; ; \; \theta^* = \frac{\theta_{50} - \theta_{wp}}{\theta_{fc} - \theta_{wp}} \qquad (17)$$

where θ_{fc} and θ_{wp} are water content at field capacity and wilting point, h_{fc} and h_{wp} are corresponding pressure heads, $\overline{TR_p^0}$ and $(TR_p^0)_{\max}$ equals average and maximum potential transpiration rate during the vegetation period. In eq. (17) h_{fc} = -3.36 m and h_{wp} = -153 m, and the corresponding θ_{fc} and θ_{wp} were calculated from WRC. Values of τ, which reflect different rates of decreasing root water extraction ability due to drying conditions for trees and grasses, were obtained by the best fit of calculated and observed $\varphi(h)$ curves (Sudnitsyn, 1979). The exponent tau was set smaller for trees produce a slower decreasing $\varphi(h)$ curve, due to the trees' best adaptability to water stress conditions.

The root distribution model takes into account the differences in root zone structure and depth for various vegetation and soil textures. The exponential function (Gale and Grigal, 1987) of the root distribution with depth was used for trees with bar root system. For grass vegetation with a fibrous root system we used another root distribution function, offered by Hoffman and van Genuchten (Šimůnek et al., 2008). Parameters of the root water uptake model thus reflect the type of vegetation as well as soil texture (Table 3).

Table 3. Parameters of the root water uptake model (Grinevskii, 2011).

Vegetation type	**Soil**	**h_{50}, m**	**τ**	**Average root depth, m**
Trees	Loam	-37.3	2	1.0
	Loamy sand	-33.3		1.5
	Sand	-15.0		2.0
Grass	Loam	-45.5	4	0.15
	Loamy sand	-31.9		0.3
	Sand	-24.0		0.5

4. Simulation Results and Discussion

Using daily precipitation and temperature data and SurfBal and HYDRUS-1D parameters for different types of vegetation cover and soil and vadose zone textures, as presented above, daily and mean annual values of GWR (for the 50 year period) for each type of natural conditions were calculated. These mean annual GWR values were extended to areas with similar GWR conditions across the investigated region (Grinevskii and Pozdnyakov, 2010). Differences in landscape, soil and groundwater conditions cause significant variability of mean annual GWR rates – from 15 to 144 mm/year (Figure 3).

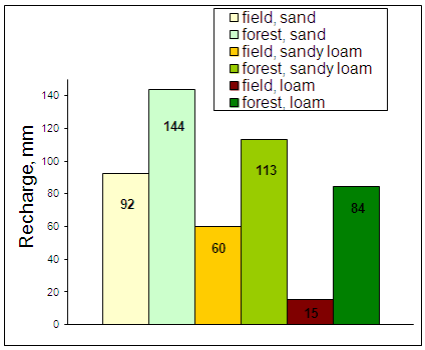

Figure 3. Differences in simulated mean annual GWR due to landscape and soil conditions (for GWL depth >5 m).

Simulation results also show the strong landscape and soil type influence on seasonal surface and vadose zone water balance variations (Fig. 4). The total sum of annual evapotranspiration is almost the same, but for woody vegetation, the main part is the plant transpiration. In field landscapes, the main part is evaporation. The principal differences for various landscapes are in spring surface runoff, which forms during a short snow melting period (Grinevskii and Novoselova, 2011). There is an intensive peak of water seepage to the soil in forest landscapes, where snow isn't melting as fast. Exactly during this period the upper inflow to the soil is strongly variable and differs from precipitation data. This is the main reason for the landscape differences in annual GW recharge and its seasonal variability (Fig. 4).

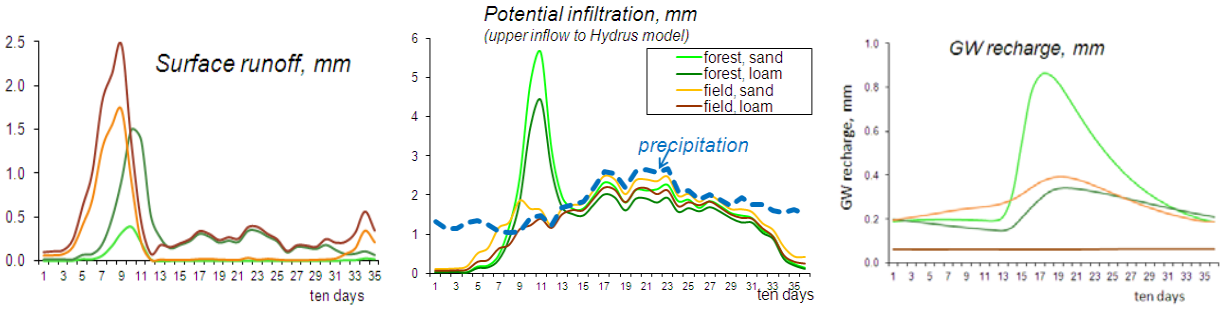

Figure 4. Simulated mean seasonal variations of surface runoff, potential infiltration to the soil and GWR due to landscape and soil conditions (for GWL depth >5 m).

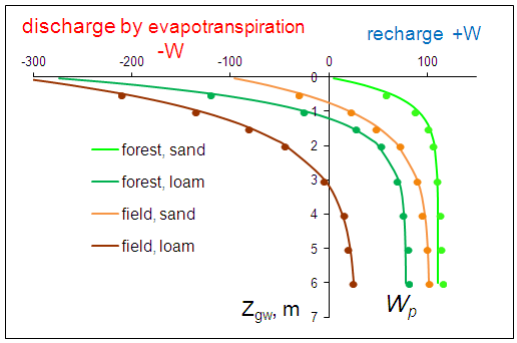

Figure 5. Mean annual GWR (W) as a function of GWL depth (Z) for different landscapes and soil types.

Landscape and soil conditions also influence the relationship between mean annual GWR and GWL depth (Fig. 5). Simulation results show that mean annual GWR increases with depth only to a certain limit, w_p, and can be approximated with the Pashkovskii equation (Shestakov et al., 1982):

$$w(z) = w_p - \left(w_p - w_0\right)\exp\left(-z/\gamma\right) \tag{18}$$

where w_0 and γ are fitted parameters. For shallow groundwater levels, the mean annual GWR becomes negative as a rule, which means that the upward flow in the vadose zone by the evapotranspiration processes dominates the downward flow. This means groundwater discharge by evapotranspiration. The w_0 is thus an asymptotic negative value, where GWL depth z=0, and is close to ET^0. The critical GWL depth z^0, where mean annual GWR $w(z)$=0, can be obtained from eq. (18). Therefore, for every landscape and soil type, $z < z^0$ means GW evapotranspiration discharge ($w(z) < 0$) and vice versa: when $z > z^0$, $w(z) > 0$, which means recharge conditions.

Acknowledgments. This work was supported by RBRFoundation via grants 11-05-00478-a

References

Allen R. G., REF-ET calculation software for FAO and ASCE standardized equations, Kimberly, University of Idaho, 86 p., 2001.

Budagovskii, A. I., Soil water evaporation, In "Physics of soil water", Moscow, "Nauka", p. 13-95, 1981, (in Russian).

Crosbie R. S., J. L. McCallum and G. R. Walker, Modeling climate-change impacts on groundwater recharge in the Murray-Darling Basin, Australia, *Hydrogeology J.*, *18*, 1639–1656, 2010.

Gale M. R., and D. F. Grigal, Vertical root distributions of northern tree species in relation to successional status. *Can. J. For. Res.*, *17*, 829–834, 1987.

Grinevskii, S. O., Structure and parameter schematization of the vadose zone for groundwater recharge modeling, *Moscow University Geology Bulletin*, *65*(6), 387–398, 2010.

Grinevskii, S. O., Modeling root water uptake when calculating unsaturated flow in the vadose zone and groundwater recharge, *Moscow University Geology Bulletin*, *66*(3), 189–201, 2011.

Grinevskii, S. O., and M. V. Novoselova, Regularities in the formation of groundwater infiltration recharge, *Water Resources*, *38*(2), 175–186, 2011.

Grinevskii, S. O., and S. P. Pozdnyakov, Principles of regional estimation of infiltration groundwater recharge based on geohydrological models, *Water Resources*, *37*(5), 638–652, 2010.

Kuchment, L. S., and A. N. Gelfan, The determination of the snowmelt rate and the meltwater outflow from a snowpack for modeling river runoff generation, *J. Hydrol.*, *179*, 23–36, 1996.

Li, K. Y., R. De Jong, T. R. Coe, and N. Ramankutty, Root-water uptake based upon a new water stress reduction and an asymptotic root distribution function, *Earth Interact.*, *10*(14), 1-22, 2006.

Liang, X., D. P. Lettenmaier, E. F. Wood, and S. J. Burges, A Simple hydrologically based model of land surface water and energy fluxes for general circulation models, *J. Geophys. Res.*, *99*(D7), 14415–14428, 1994.

Schaap, M. G., F. J. Leij, and M. Th. van Genuchten, Rosetta: A computer program for estimating soil hydraulic parameters with hierarchical pedotransfer functions, *J. of Hydrology*, *251*, 163–176, 2001.

Shestakov, V. M., I. S. Pashkovskii, and A. M. Soyfer, Hydrogeological investigations on irrigated areas, Moscow, "Nedra", 244 p, 1982, (in Russian).

Shestakov, V. M., S. P. Pozdnyakov, *Geohydrology*, Moscow. "Akademkniga", 173 p., 2003, (in Russian).

Schroeder, P. R., T. S. Dozier, P. A. Zappi, B. M. McEnroe, J. W. Sjostrom, and R. L. Peyton, The Hydrologic Evaluation of Landfill Performance (HELP) Model: Engineering Documentation for Version 3, EPA/600/R-94/168b, September 1994, U.S. Environmental Protection Agency Office of Research and Development, Washington, DC, 116 p., 1994.

Šimůnek J., M. Šejna, H. Saito, M. Sakai, and M. Th. van Genuchten, The HYDRUS-1D Software Package for Simulating the One-Dimensional Movement of Water, Heat, and Multiple Solutes in Variably-Saturated Media. Ver. 4.08, Dept. of Environ. Sci., University of California Riverside, California, 296 p., 2009.

Sudnitsyn, I. I., Movement of soil water and root water uptake, Moscow, MSU, 255 p., 1979, (in Russian).

van Genuchten, M. Th. A closed-form equation for predicting the hydraulic conductivity of unsaturated soils, *Soil Sci. Soc. Am. J.*, *44*, 892–898, 1980.

Vinogradov, J. B., Runoff mathematical simulation. Experience of critical analysis, Leningrad, "Gidrometeoizdat ", 1988, (in Russian).

USDA, Soil Conservation Service, National engineering handbook, Section 4, Hydrology, US Government Printing Office, Washington, D.C., 1985.

Simulation of Uranium Tailing Leaching using VS2DRT

Sosina S. Haile and Broder J. Merkel

Department of Geology, Technische Universität Bergakademie Freiberg, Gustav-Zeuner-Str. 12, 09596 Freiberg/Sa., Germany, wedatnsos@yahoo.com and merkel@geo.tu-freiberg.de

Abstract

Uranium contamination of surface and ground waters from uranium tailings is a serious environmental problem in many countries that have uranium mining. Reactive transport models can be used to predict the potential environmental impacts of new uranium tailing sites, as well as to assess a level of contamination from existing uranium tailing sites. Hence, reactive transport models are useful tools to visualize potential threats, as well as to emanate dangerous situations, and to design preventive and remedial measures to protect and rehabilitate water resources. In the present study, a newly developed, two-dimensional, multi-species coupled reactive transport model, VS2DRT, is used to simulate uranium tailing leaching. The problem was adapted from HYDROGEOCHEM 5.0 and HP2 manuals and deals with the release and subsequent migration of uranium from a uranium tailing pile toward ground water and a nearby river. The simulation does not involve redox reactions and shows the application of VS2DRT in simulating uranium migration in the subsurface.

1. Introduction

Uranium is a natural, radioactive and hazardous element which exists in three isotope forms of U^{238}, U^{235}, and U^{234} in trace amounts in the environment. The discovery of radium by Marie Curie led to uranium mining in the first half of the 20^{th} century for the production of radium (Carvalho, 2012). After World War II, uranium was mined widely for production of nuclear weapons and later for nuclear power plants to produce energy. The radioactive and hazardous nature of waste materials from uranium mining and milling was poorly recognized during the first uranium boom in the 1940s to 1960s (Robinson, 2004).

Uranium tailing refers to a uranium ore residue, which contains the radioactive decay products of uranium and heavy metals that are deposited in ponds. There is a huge volume of tailing waste around the world, with an estimated volume of 938 million cubic meters produced at more than 4000 mines (IAEA, 2004). Living in a uranium mining area may lead to exposure to radionuclides from mining, mill tailings, dust, and contaminated water and foodstuff (Matias, 2008). Although the major environmental impacts of uranium tailings are the failure of tailing dams and exposure to radiation, contamination of groundwater and/or surface water by leakage of contaminated water from tailing ponds is a serious concern. For example, in Australia in 1994, the uranium tailing Olympic Dam released up to 5 million m^3 of contaminated water into the soil (IAEA, 2004). More recently, in 2012 in Sotkamo, Kainuu province, Finland, leakage from a gypsum pond resulted in higher uranium concentrations in the nearby Snow River, exceeding more than tenfold the allowable threshold level (http://www.wise-uranium.org/mdaf.html).

Reactive transport modeling of contaminants from uranium tailing dams or ponds could be used as a predictive tool to estimate the extent of contamination and to take remedial measures to rehabilitate the site. Hence, reactive transport models such as HYDROGEOCHEM 5.0 (Yeh et al., 2004), HP2 (Šimůnek et al., 2012), and VS2DRT (Haile, 2013) could be useful tools to simulate possible leaching of uranium from passive as well as active tailing sites. In this paper, we introduce a new reactive transport model, VS2DRT, which could be used to simulate leaching of uranium and other heavy metals from uranium tailings. The HP2 test example involving leaching of uranium tailing is adapted here to show the applicability of VS2DRT for such cases.

2. VS2DRT Simulation of Leaching of Uranium Tailings

2.1. Description of VS2DRT

VS2DRT is a new reactive transport model for variably-saturated porous media. VS2DRT couples the single solute transport program, VS2DT (Healy R., 1990), and the heat transport program, VS2DH (Healy and Ronan, 1996), with the hydro-geochemical program, PHREEQC (Parkhurst and Appelo, 1999). VS2DRT uses a non-iterative operator splitting approach to couple the programs. This approach involves solving the transport and chemical reactions sequentially in one time step. VS2DRT has capabilities to simulate the flow of water, heat transport, multi-solute transport, various equilibrium reactions such as cation exchange, adsorption, dissolution/precipitation, and various kinetic reactions in variably-saturated porous media. However, VS2DRT does not consider gas phase flow, the effect of chemical reactions on hydraulic properties, and the density of water.

2.2. The Case of Leaching of Uranium Tailings

This problem was adapted from the HYDROGEOCHEM 5.0 and HP2 manuals. The problem deals with a hypothetical case of a uranium mill-tailing disposal and a subsequent release and migration of uranium to groundwater and a river. The schematic representation of the domain of simulation is presented on Figure 1. The tailings pile is located on a flat surface which slopes down to a river. The hydraulic properties of soil and tailing are presented in Figure 2. The surface of the tailing pile was defined as the flux boundary with an infiltration rate of 0.0139 m/day. The top boundary, except for the surface of the tailing pile, has a flux boundary condition with an infiltration rate of 0.00139 m/day. The bottom boundary is considered to be impervious. The left side of the simulation domain below the water table has a 5 m pressure head. The river bottom and the vertical nodes on the right side of the river have a 4 m pressure head boundary condition. The initial pressure head and uranium profiles are presented in Figures 3 and 4, respectively. The light green color on the top right corner in Figure 3 is out of the simulation domain.

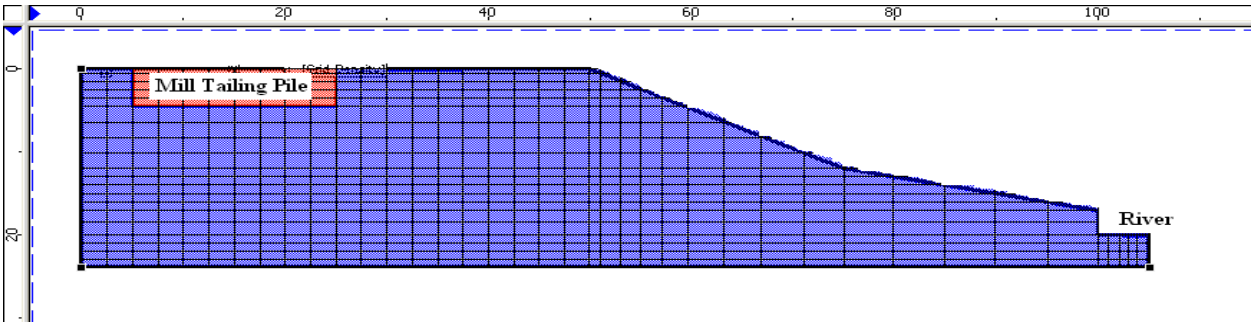

Figure 1. Schematic representation of the uranium tailing problem.

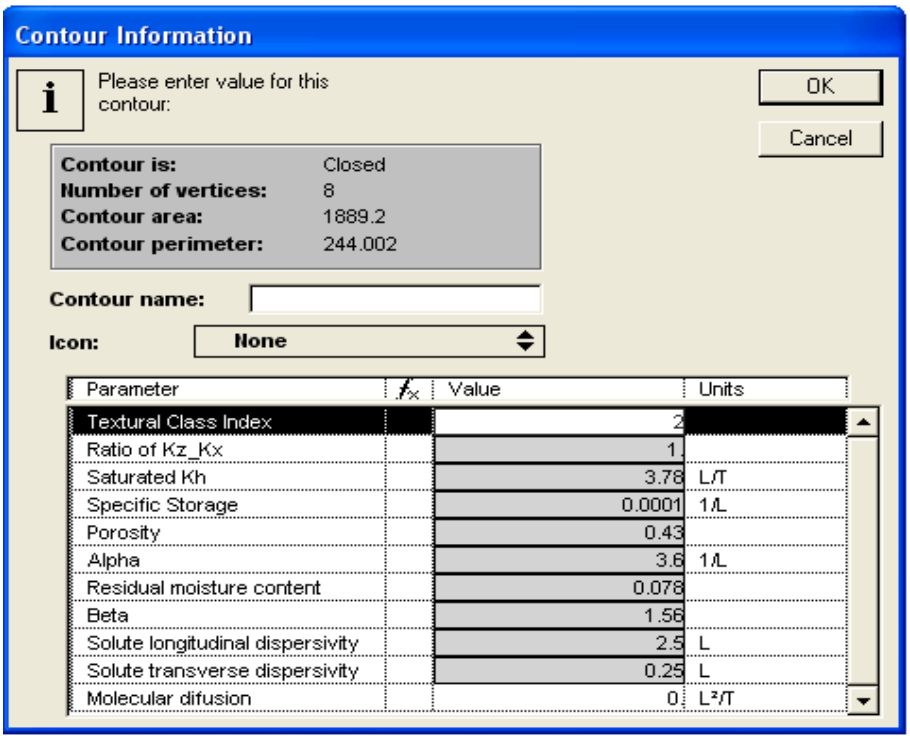

Figure 2. van Genuchten hydraulic parameters used for the soil and tailing piles.

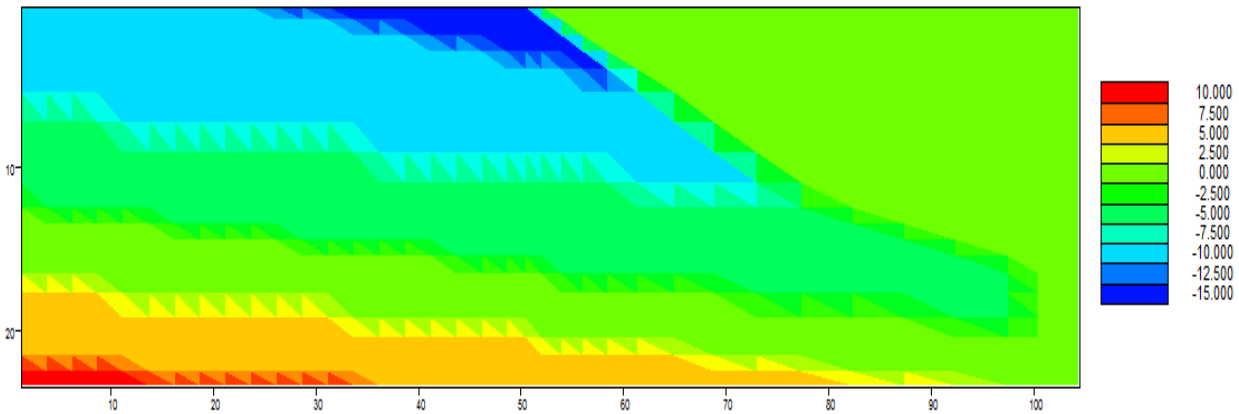

Figure 3. The pressure head profile at the beginning of the simulation (0 days).

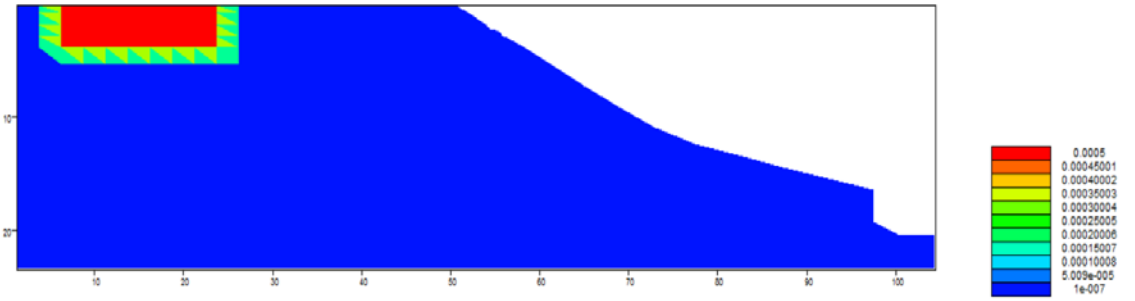

Figure 4. The uranium (mole/ kg of water) profile at the beginning of the simulation (0 days).

The list of chemical reactions and their thermodynamic equilibrium constants considered for this case are presented in Table 1. The simulation here does not consider redox reactions. The aqueous solution inside the tailing piles, outside the tailing, and at the boundaries are presented in Table 2. The simulation was conducted for 1000 days with a time step of 1 day.

Table 1. Reactions and log K used for a uranium tailing problem (Šimůnek et al., 2012).

Reaction	**No**	**Log *K***
Aqueous Complexation Reactions considered		
$H_2O \leftrightarrow H^+ + OH^-$	R1	-14
$Ca^{2+} + CO_3^{2-} \leftrightarrow CaCO_3$	R2	3.22
$Ca^{2+} + H^+ + CO_3^{2-} \leftrightarrow CaHCO_3^+$	R3	11.43
$Ca^{2+} + SO_3^{2-} \leftrightarrow CaSO_3$	R4	2.31
$Ca^{2+} + 2H^+ + PO_4^{3-} \leftrightarrow CaH^2PO_4^+$	R5	20.96
$Ca^{2+} + PO_4^{3-} \leftrightarrow CaPO_4^-$	R6	6.49
$Ca^{2+} + H^+ + PO_4^{3-} \leftrightarrow CaHPO_4$	R7	15.08
$Ca^{2+} + H_2O \leftrightarrow H^+ + CaOH^-$	R8	-12.58
$Fe^{2+} + SO_4^{2-} \leftrightarrow FeSO_4$	R9	2.2
$Fe^{2+} + H_2O \leftrightarrow H^+ + FeOH^-$	R10	-9.5
$Fe^{2+} + 2H_2O \leftrightarrow 2H^+ + Fe(OH)_2$	R11	-20.57
$Fe^{2+} + 3H_2O \leftrightarrow 3H^+ + Fe(OH)_3^-$	R12	-31.00
$Fe^{2+} + 4H_2O \leftrightarrow 4H^+ + Fe(OH)_4^{2-}$	R13	-43.00
$UO_2^{2+} + H_2O \leftrightarrow H+ + (UO_2)(OH)^+$	R14	-5.3
$2UO_2^{2+} + 2H_2O \leftrightarrow 2H+ + (UO_2)_2(OH)_2^{2+}$	R15	-5.68
$3UO_2^{2+} + 4H_2O \leftrightarrow 4H+ + (UO_2)_3(OH)_4^{2+}$	R16	-11.88
$3UO_2^{2+} + 5H_2O \leftrightarrow 5H+ + (UO_2)_3(OH)_5^+$	R17	-15.82
$4UO_2^{2+} + 7H_2O \leftrightarrow 7H+ + (UO_2)_4(OH)_7^+$	R18	-21.9
$3UO_2^{2+} + 7H_2O \leftrightarrow 7H+ + (UO_2)_3(OH)_7^-$	R19	-28.34
$UO_2^{2+} + CO_3^{2-} \leftrightarrow (UO_2)(CO_3)$	R20	9.65
$UO_2^{2+} + 2CO_3^{2-} \leftrightarrow (UO_2)(CO_3)_2^{2-}$	R21	17.08
$UO_2^{2+} + 3CO_3^{2-} \leftrightarrow (UO_2)(CO_3)_3^{4-}$	R22	21.7
$2UO_2^{2+} + CO_3^{2-} + 3H_2O \leftrightarrow 3H+ + (UO_2)_2(CO_3)(OH)_3^-$	R23	-1.18
$UO_2^{2+} + SO_4^{2-} \leftrightarrow (UO_2)(SO_4)$	R24	2.95
$UO_2^{2+} + 2SO_4^{2-} \leftrightarrow (UO_2)(SO_4)_2^{2-}$	R25	4.0
$2H^+ + UO_2^{2+} + PO_4^{3-} \leftrightarrow H_2(UO_2)(PO_4)^+$	R26	23.2
$3H^+ + UO_2^{2+} + PO_4^{3-} \leftrightarrow H_2(UO_2)(PO_4)^{2+}$	R27	22.90
$Ca^{2+} + 4H^+ + UO_2^{2+} + 2PO_4^{3-} \leftrightarrow CaH_4(UO_2)(PO_4)_2^{2+}$	R28	45.24

$Ca^{2+} + 5H^{+} + UO_2^{2+} + 2PO_4^{3-} \leftrightarrow CaH_5(UO_2)(PO_4)_2^{3+}$	R29	46.00
$H^{+} + CO_3^{2-} \leftrightarrow HCO_3^{-}$	R30	10.32
$2H^{+} + CO_3^{2-} \leftrightarrow H_2CO_3$	R31	16.67
$H^{+} + SO_4^{2-} \leftrightarrow HSO_4^{-}$	R32	1.99
$H^{+} + PO_4^{3-} \leftrightarrow HPO_4^{2-}$	R33	12.32
$2H^{+} + PO_4^{3-} \leftrightarrow H_2PO_4^{-}$	R34	19.55
$3H^{+} + PO_4^{3-} \leftrightarrow H_3PO_4$	R35	21.74
Precipitation-Dissolution Reactions		
$Ca^{2+} + SO_4^{2-} \leftrightarrow CaSO_4$ (s)	R36	4.62
$Ca^{2+} + CO_3^{2-} \leftrightarrow CaCO_3$ (s)	R37	8.48
$Ca^{2+} + 3PO_4^{3-} + H_2O \leftrightarrow H^{+} + Ca_5(OH)(PO_4)_3$(s)	R38	40.47
$Fe^{2+} + CO_3^{2-} \leftrightarrow FeCO_3$ (s)	R39	10.50
$Ca^{2+} + 2UO_2^{2+} + 2PO_4^{3-} \leftrightarrow Ca(UO_2)_2(PO_4)_2$(s)	R40	48.61
$4Ca^{2+} + H^{+} + 3PO_4^{3-} \leftrightarrow CaH(PO_4)_3$(s)	R41	48.20
$Ca^{2+} + H^{+} + PO_4^{3-} \leftrightarrow CaH(PO_4)$ (s)	R42	19.30
$Ca^{2+} + 2H_2O \leftrightarrow 2H^{+} + Ca(OH)_2$ (s)	R43	-21.90
$3Fe^{2+} + 2PO_4^{3-} \leftrightarrow Fe_3(PO4)_2$(s)	R44	33.30
$Fe^{2+} + 2H_2O \leftrightarrow 2H^{+} + Fe(OH)_2$ (s)	R45	-12.10
$UO_2^{2+} + 2H_2O \leftrightarrow 2H^{+} + (UO_2)(OH)_2$ (s)	R46	-5.40
$UO_2^{2+} + CO_3^{2-} \leftrightarrow (UO_2)(CO_3)$ (s)	R47	14.11
$Fe^{2+} + 2UO_2^{2+} + 2PO_4^{3-} \leftrightarrow Fe(UO_2)_2(PO4)_2$(s)	R48	46.00
$H+ + UO_2^{2+} + PO_4^{3-} \leftrightarrow H(UO_2)(PO4)_2$(s)	R49	25.00

Table 2. Initial and boundary solutions for a uranium tailing problem (Šimůnek et al., 2012).

Species	Inside the Tailing (mole/kg of water)	Outside the Tailing (mole/kg of water)	Boundary solution (mole/kg of water)
Ca^{2+}	1.0×10^{-2}	1.0×10^{-2}	1.0×10^{-3}
CO_3^{2-}	1.0×10^{-2}	1.5×10^{-3}	1.5×10^{-3}
UO_2^{2+}	5.0×10^{-4}	1.0×10^{-7}	1.0×10^{-8}
PO_4^{3-}	1.0×10^{-6}	1.0×10^{-6}	1.0×10^{-6}
SO_4^{2-}	2.0×10^{-1}	2.0×10^{-2}	1.0×10^{-4}
H^{+}	3.5×10^{-2}	1.0×10^{-7}	1.0×10^{-7}
Fe^{2+}	2.0×10^{-1}	1.0×10^{-3}	1.0×10^{-3}

3. Result and Discussion

The results of the VS2DRT simulation are presented in Figures 5, 6, and 7 for uranium at 250, 500, and 1000 days, respectively. At 250 days, the uranium plume spreads toward the ground water, which is located at a depth of about 12 m. At 500 days, the uranium plume continues to spread in ground water and moves toward the river, which is located about 100 m along the *x*-axis. At 1000 days, ground water is completely polluted with uranium with concentrations as high as 0.0004 mole/kg of water. Uranium continues spreading toward the river with a concentration of 0.00005 mole/kg of water.

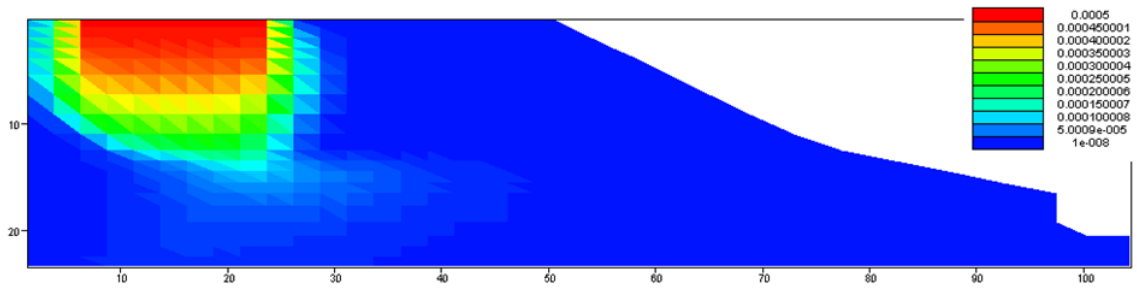

Figure 5. The uranium (mole/ kg of water) profile at 250 days.

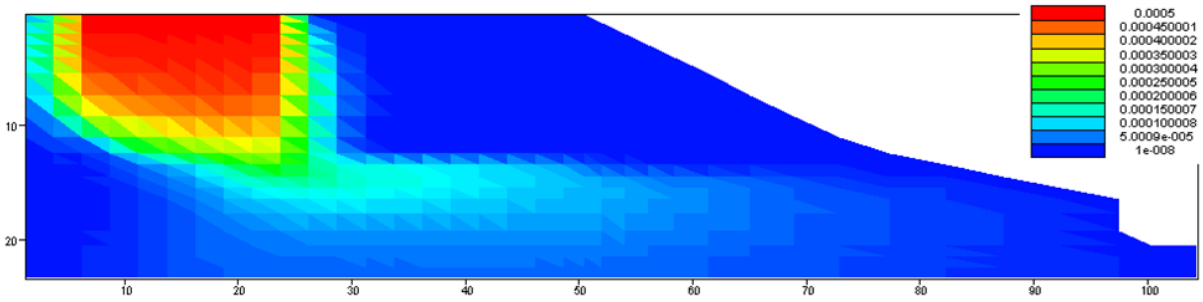

Figure 6. The uranium (mole/kg of water) profile at 500 days.

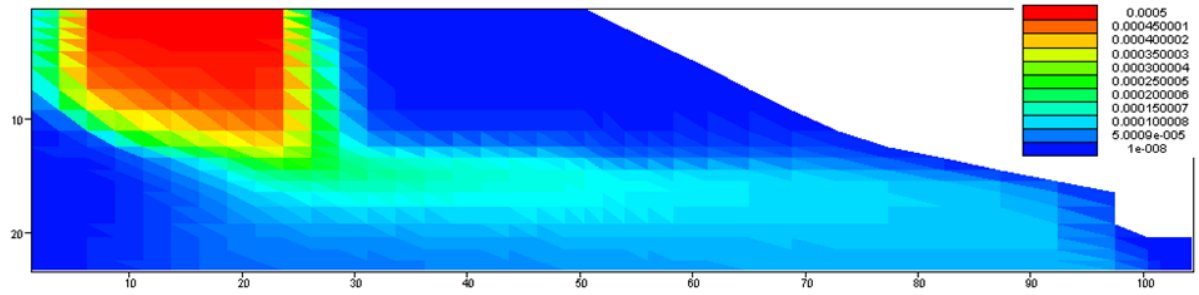

Figure 7. The uranium (mole/kg of water) profile at 1000 days.

Figure 8 shows the uranium profile at 250 and 500 days based on the HP2 simulation. The uranium plumes show similar patterns for both HP2 and VS2DRT models. The difference between HP2 and VS2DRT simulation results could be due to spatial and temporal discretizations used. HP2 uses a finite element method, and for the current problem, it used a time step of 0.0001 day. However, VS2DRT uses a finite difference method, and for the current problem, it used a time step of 1 day. The effect of the pumping well considered in the HP2 simulation is also not included in VS2DRT.

Generally, both HP2 and VS2DRT can be used for 2D reactive transport modeling in variably-saturated porous media. The advantage of VS2DRT is that it is a public domain program while HP2 is a commercial one.

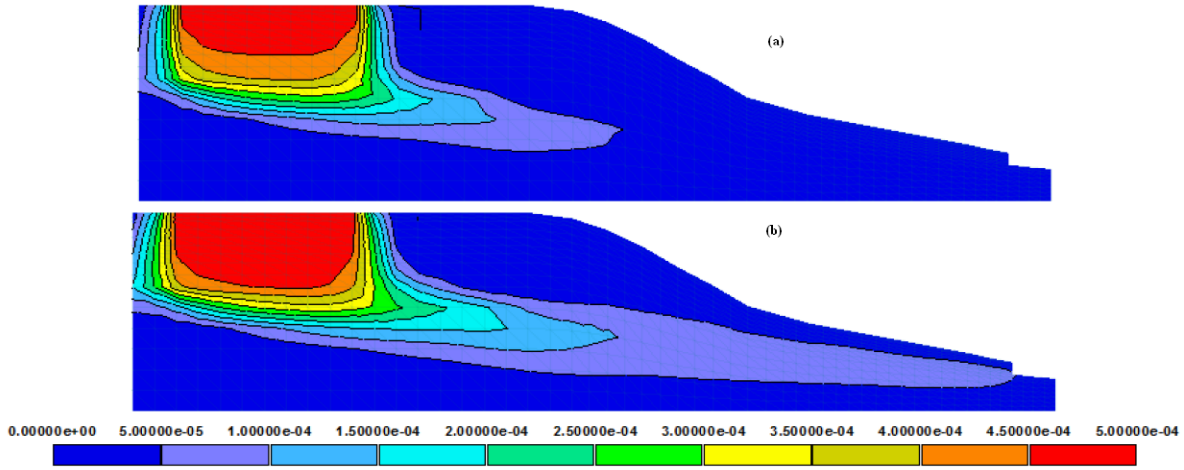

Figure 8. Uranium (mole/kg of water) profiles at (a) 250 days and (b) 500 days based on the HP2 simulation (Šimůnek et al., 2012).

4. Conclusions

Reactive transport programs such as VS2DRT are useful tools to visualize the possible spatial and temporal distributions of contaminants in the subsurface. Coupling of VS2DT and VS2DH with PHREEQC has boosted the applicability of VS2DT to simulate multi-solute transport with a wide variety of equilibrium and kinetic reactions. The hypothetical case presented here shows that VS2DRT can be used to predict the uranium plume pattern at variable times. In real world applications, the accuracy of the simulation depends on the hydraulic and chemical properties and the initial and boundary conditions for flow and chemical solutions. Moreover, the grid size and the time steps used for the numerical simulations play a huge role. It is good practice to verify the numerical simulations with measured or observed values whenever possible in order to have more confidence in the obtained results and in decisions made based on numerical simulations.

References

Carvalho, F. P., Marie Curie and the Discovery of Radium. In Merkel, B., and M. Schipek (eds.), The New Uranium Mining Boom, pp. 3-17, Berlin, Springer, 2012.

Haile, S. S., VS2DRT: Variably Saturated Two Dimensional Reactive Transport, Freiberg, Saxony, Germany, 2013.

Healy, R., Simulation of solute transport in variably saturated porous media with supplemental information on modifications to U.S. Geological Survey's Computer Program VS2D, Denver, Colorado, U.S. Geological Survey, 1990.

Healy, R., and A. Ronan, Documentation of Computer Program VS2DH for simulation of energy transport in Variably saturated porous media--modification of the US Geological Survey's computer program VS2DT, Denver, Colorado, U.S. Geological Survey, 1996.

IAEA, The long term stabilization of uranium mill tailings, Vienna, International Atomic Energy Agency, 2004.

Matias, O. N., Assessment of groundwater quality and contamination problems ascribed to an abandoned uranium mine (Cunha Baixa region), *Environ Geol*., 1799–1810, 2008.

Parkhurst, D., and C. Appelo, User's guide to PHREEQC (version-2) a computer program for speciation, batch-reaction, one-dimensional transport, and inverse geochemical calculations, Denver, Colorado, U.S. Geological Survey, 1999.

Robinson, P., Uranium Mill Tailings Remediation Performed by the US DOE: An Overview, US DOE, 2004.

Šimůnek, J., D. Jacques, M. Šejna, and M. Th. van Genuchten, The HP2 Program for HYDRUS (2D/3D): A Coupled Code for Simulating Two-Dimensional Variably-Saturated Water Flow, Heat Transport, and Biogeochemistry in Porous Media, Version 1.0, PC Progress, Prague, Czech Republic, 76 pp., 2012.

Yeh, G.-T., J. Sun, P. M. Jardine, W. D. Burgos, Y. Fang, M.-H. Li, and M. D. Siegel, HYDROGEOCHEM 5.0: A Three-Dimensional Model of Coupled Fluid Flow, Thermal Transport, and HYDROGEOCHEMical Transport through Variably Saturated Conditions - Version 5.0, US DOE, 2004.

http://www.wise-uranium.org/mdaf.html

Infiltration Into a Stony Soil: Modeling of the Process Using HYDRUS Codes

Hana Hlaváčiková, Viliam Novák, and Marek Rodný

Institute of Hydrology, Slovak Academy of Sciences, Račianska 75, 83102 Bratislava, Slovakia
hlavacikova@uh.savba.sk

Abstract

Stony soils are composed of fractions (rocks and fine particles) with different hydrophysical characteristics. Consequently, effective hydrophysical characteristics are needed for simulations of water flow in stony soils. In the following contribution, the effective hydraulic conductivity of a stony soil was estimated using the HYDRUS-2D numerical experiment. Next, infiltration into soils with different stoniness was performed using the derived effective characteristics and the HYDRUS-1D model. Ponded and rainfall infiltrations were modeled (with the rainfall intensity lower than the saturated hydraulic conductivity of a stony soil) with the aim of evaluating the influence of different stoniness on the process of water flow in stony soils.

1. State of the Art

Soils containing a significant fraction of rocks (stones, skeleton), generally denoted as stony soils, are located mainly in forest and mountainous areas. According to Poesen and Lavee (1994), Western Europe contains about 30% of such soils; in the Mediterranean region stony soils cover around 60% of the territory. According to Šály (1976), the major portion of Slovak forest soils (up to 80%) contain stones, while the stone content increases with depth. Furthermore, about 47% of Slovak agricultural soils are referred to as stony soils (Hraško and Bedrna, 1988). Shape, size, degree of weathering, and geological origin of the soil skeleton can strongly influence the soil hydrophysical properties, mainly the retention capacity and hydraulic conductivity. Therefore, it is important to characterize the properties of the stony skeleton and its distribution in the soil profile. Obtained information could be used to elucidate the influence of stones on soil water transport processes. It can be expected that the stone content in soils will reduce the effective cross-sectional area through which water flows. Furthermore, an increase in stoniness results in higher tortuosity of soil pores, which consequently leads to a lower hydraulic conductivity of the stony soil (Ravina and Magier, 1984, Childs and Flint, 1990; Novák et al., 2011; Bouwer and Rice, 1984; Ma et al., 2010). On the other hand, the shrinking-swelling phenomena could lead to the presence of temporal lacunar pores (voids along soil/stone interface), which could consequently cause the presence of preferential flow, and thus an increase in the saturated hydraulic conductivity (Sauer a Logsdon, 2002; Shi et al., 2008; Verbist et al., 2009; Zhou et al., 2009). Moreover, it could be hypothesized that the degree of preferential flow in such soils will be proportionally related to the stone content and its spatial distribution.

In this study we present an original method for estimating the effective hydraulic conductivity of stony soils (K_{se}) based on the HYDRUS-2D numerical simulations. Moreover, HYDRUS-1D simulations were performed for soils with different stoniness under different infiltration

conditions. Simulated upper and bottom boundary fluxes for soils with different stoniness were evaluated and discussed.

2. Soil Characteristics

2.1. Effective Saturated Hydraulic Conductivity of a Stony Soil

Effective saturated hydraulic conductivities and retention curves need to be estimated for a quantitative description of soil water movement in stony soils. The representative elementary volume (REV) used for the determination of the above-mentioned soil hydraulic properties is dependent on the size of rock fragments. For example, for a soil containing stones with an average diameter of 10 cm, a REV of 1 m^3 is needed. Since it is extremely technically difficult to perform physical experiments with this size of soil sample, solutions based on virtualization of classical laboratory experiments are taking place. In this study, a classical Darcy´s experiment was simulated using the HYDRUS-2D model (Šimůnek et al., 2008b). Impermeable stones of a spheroidal shape (approximated as circles in a 2D cross-sectional area) were equally distributed in the virtual soil sample with a volume of 1 m^3. Furthermore, steady-state water flow was simulated using the unit hydraulic gradient (1 cm of water pressure head was applied as the upper and bottom boundary conditions). The rate of water flow through the REV therefore equals the effective saturated hydraulic conductivity K_{se} (Novák et al., 2011). Results of the numerical experiments were used to adjust the formula of Ravina and Magier (1984) to the form presented in Novák et al. (2011):

$$K_{se} = (1 - a.R_v)K_{fe} \tag{1}$$

where K_{se} is the effective saturated hydraulic conductivity [cm h^{-1}], K_{fe} is the saturated hydraulic conductivity of a fine-textured soil fraction [cm h^{-1}], a is a parameter that incorporates the hydraulic resistance of the rock fragments to water flow and depends on soil texture and dimensions of rock fragments [-] (e.g., a = 1.1 was estimated for sandy loam and spherical rock fragments of a 10-cm diameter), and R_v stands for a relative volume fraction of stones [cm^3cm^{-3}] (stoniness).

2.2. Effective Water Retention Curve of a Stony Soil

The relationship between water contents and pressure heads for stony soils can be estimated using the method presented by Bouwer and Rice (1984). In this method, the bulk volumetric water content of a stony soil is expressed from the volumetric water content of a fine soil fraction alone (eq. 2). Bouwer and Rice (1984) have neglected the retention capacity of the rock fragments.

$$\theta_{se} = (1 - R_v)\theta_{fe} \tag{2}$$

where θ_{se} is the bulk volumetric water content of a stony soil [cm^3cm^{-3}], θ_{fe} is the volumetric water content of a fine soil fraction alone [cm^3cm^{-3}], and R_v is the relative volume fraction of stones [cm^3cm^{-3}].

3. Infiltration into Soils with Different Stoniness

The impact of different stoniness on the upper and bottom boundary water fluxes during infiltration through the stony soil was evaluated using HYDRUS-1D (Šimůnek et al., 2008a). Two qualitatively different upper boundary conditions were used to evaluate the stony soil behavior during infiltration. A Dirichlet boundary condition with a 2 cm layer of water ponded on the soil surface was used to simulate ponded infiltration. The second case involved simulating infiltration from precipitation with an 80 mm/h rainfall intensity and three hours duration (an extremely high rainfall event). However, the rainfall intensity was lower than the saturated hydraulic conductivity of a stony soil with 50% stoniness. Under this condition, surface runoff did not occur. Furthermore, the effective hydraulic properties were determined for the sandy loam soil from the study site Červenec (1500 m a.s.l.) located in the Western High Tatra Mts. Infiltration was modeled using the standard (single domain) description of hydraulic properties (van Genuchten, 1980; Mualem, 1976).

Infiltration into four virtual soil profiles with a depth of 95 cm and different stoniness (R_v = 0, 10, 30, and 50%) were modeled. During the simulation, evaporation from the soil surface and the water retention of the rock fragments were neglected. For all modeled soil profiles, the initial conditions were set as vertically uniform (h = -1000 cm). The bottom boundary was defined as a free drainage boundary. The spatial distribution of rock fragments in the soil profile was assumed to be uniform in order to be compatible with ideas presented in the HYDRUS-2D numerical experiment.

4. Results and Discussion

The parameters of effective retention curves and effective saturated hydraulic conductivities reflecting different stoniness are presented in Table 1. As can be seen in Figure 1, under ponded conditions the infiltration rates are negatively correlated with the amount of stones present in the soil (stoniness). As is demonstrated in Figures 2 and 3, cumulative infiltration rates and fluxes through the bottom boundary under saturated conditions are lower for stony soils in comparison with soil without stones (0% stoniness). This is due to the fact that rock fragments reduce the effective cross-sectional area through which water flows. Hydraulic conductivities of the matrix soil fraction in forest stony soils are usually high. Therefore, it can be expected, even in the case of heavy rains, that surface runoff will rarely occur in the mild temperate climatic zone. This fact was already confirmed by a study of Holko et al. (2011) for the same catchment.

Table 1. Effective soil hydraulic parameters determined for the Červenec study site.

	Rv 0%	Rv 10%	Rv 30%	Rv 50%
θ_r (-)	0.05	0.045	0.035	0.025
θ_s (-)	0.495	0.4455	0.346	0.2475
α (-)	0.01809	0.0181	0.0174	0.0181
n (-)	1.09439	1.09439	1.0949	1.09439
K_s (cm.h^{-1})	19.79	17.61	13.26	8.91

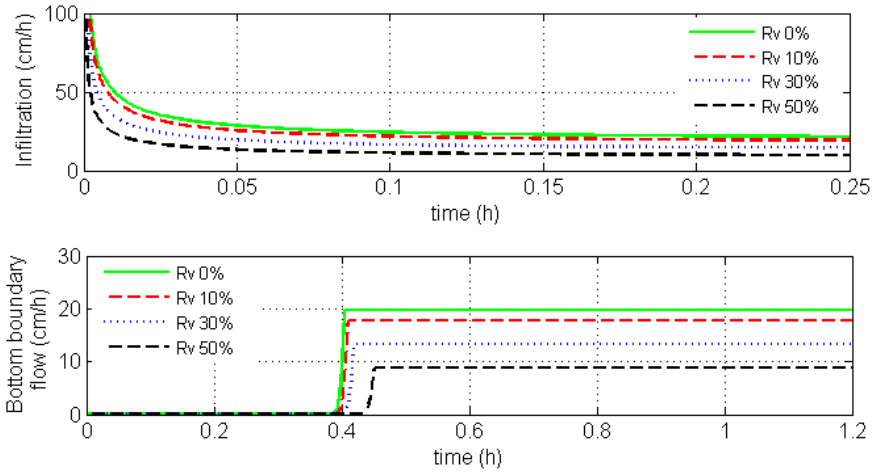

Figure 1. Modeled infiltration rates and bottom boundary fluxes for soils with different stoniness under ponded conditions.

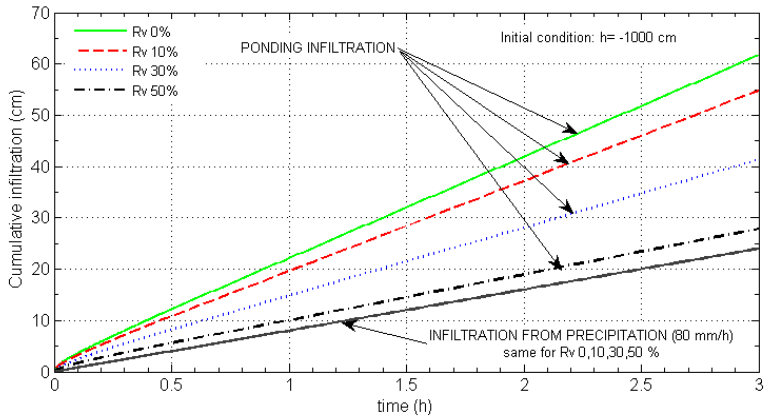

Figure 2. Modeled cumulative infiltration amounts for soils with different stoniness.

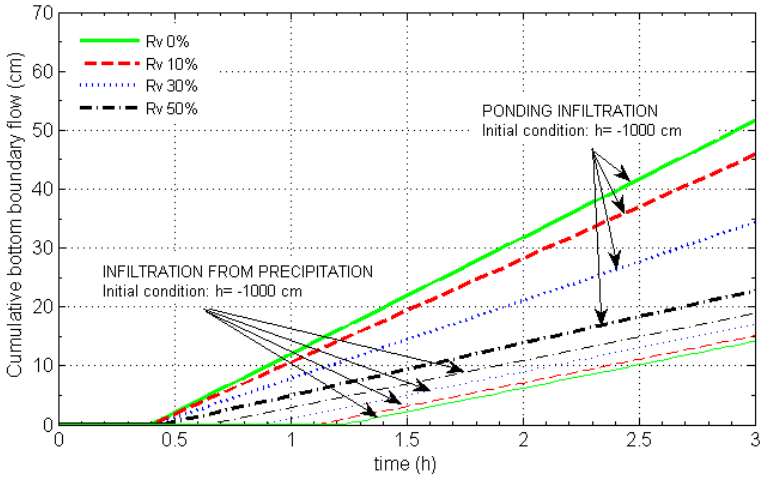

Figure 3. Cumulative outflow through the bottom boundary of a soil layer 95 cm thick, during infiltration shown in Figure 2. Outflow rates for soils with different stoniness (R_v) are shown using color lines.

The situation is completely different if infiltration under unsaturated conditions (the rainfall intensity is lower than the saturated hydraulic conductivity) is modeled (compare Figs. 4 and 5). As a result, an increase in the penetration depth of the infiltration front (Figure 5), and also in the bottom boundary flux (Figs. 3 and 6), is higher for stony soils compared to the soil without stones. Moreover, the penetration depth and bottom outflow are positively correlated with the stone content (Figs. 4 and 5). These phenomena could be explained by reduced water retention capacity of a stony soil. Since stones present in the soil limit the volume of fine soil matrix, less infiltrating water is needed to increase the water content in the matrix of the stony soil and its related unsaturated hydraulic conductivity. Consequently, a faster movement of pollutants into deeper soil layers could be expected for soils with high stone content.

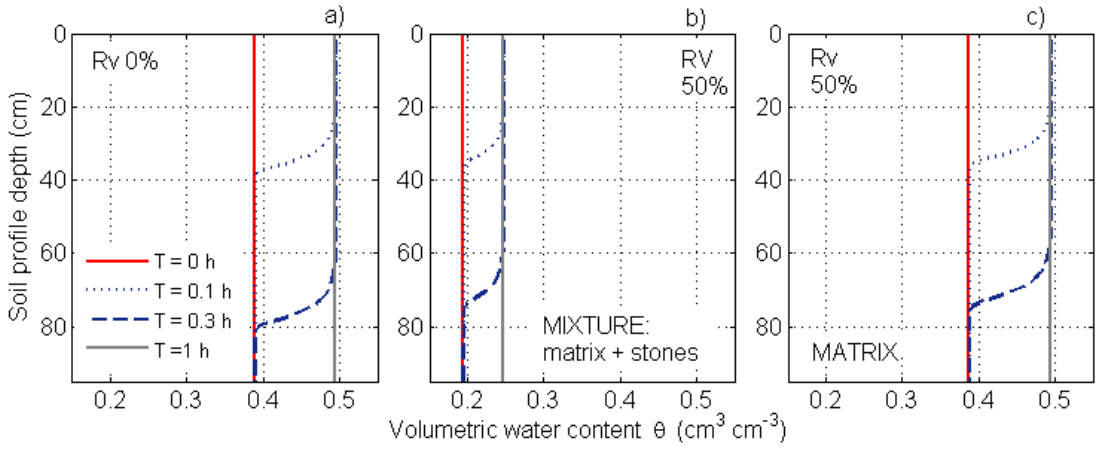

Figure 4. Soil water content profiles during ponded infiltration with the initial soil matrix water pressure head h= -1000 cm and θ_i = 0.38. a) a homogeneous soil without stones, (R_v = 0.), b) a stony soil with stoniness of 50% (R_v = 0.5), a total water content, and c) a stony soil with stoniness of 50% (R_v = 0.5), a matrix water content.

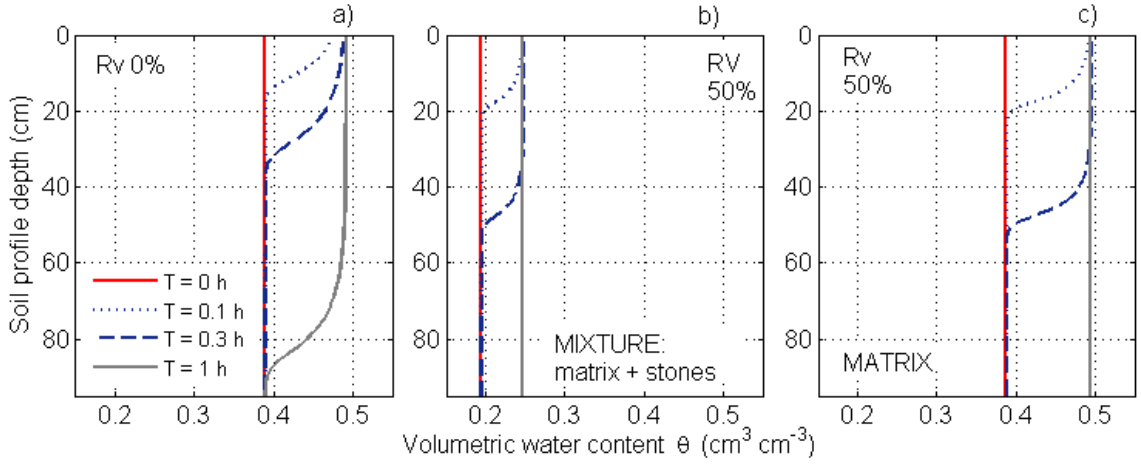

Figure 5. Soil water content profiles during rainfall infiltration. Rain intensity was 80 mm/h, rain duration 3 h, the initial soil matrix water pressure head h= -1000 cm and water content θ_i = 0.38. a) a homogeneous soil without stones, (R_v = 0.), b) a stony soil with stoniness of 50% (R_v = 0.5), a total water content, and c) a stony soil with stoniness of 50% (R_v = 0.5), a matrix water content.

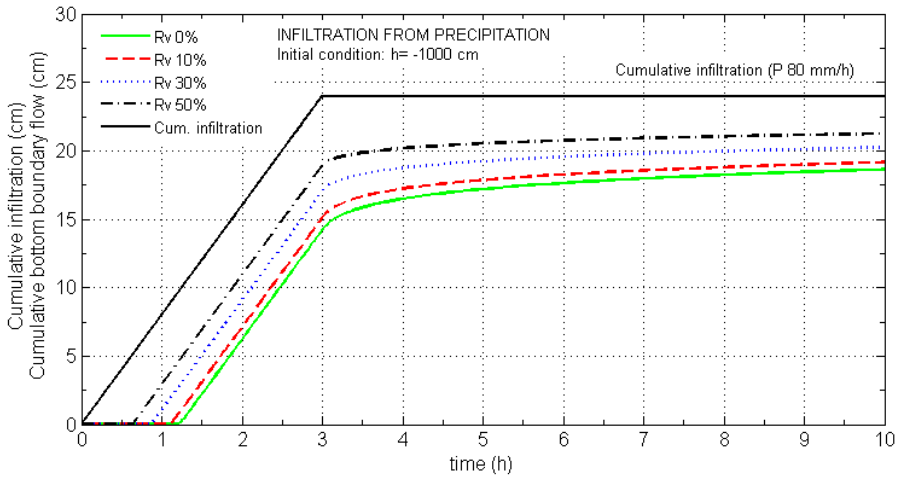

Figure 6. Cumulative rain infiltration (full line, rain duration 3 h) into a stony soil and cumulative outflows (color lines) from the bottom boundary of a soil with different stoniness (R_v).

5. Conclusions

In this paper, the effective saturated hydraulic conductivities reflecting different soil stoniness were calculated by the HYDRUS-2D numerical model, which was used to simulate the classic Darcy's experiment. Furthermore, soil water retention curves for stony soils were estimated under an assumption of zero retention capacity of the rock fragments. Obtained effective hydraulic characteristics were then used to simulate the infiltration process using HYDRUS-1D.

Calculated cumulative infiltration rates during ponded infiltration were lower for stony soils compared to a soil without stones (0% stoniness). When an infiltration from rainfall was modeled (on the assumption that the rainfall intensity was lower than the saturated hydraulic conductivity of a stony soil), a faster penetration of the infiltration front and higher cumulative bottom fluxes were calculated for soils containing stones. Moisture front penetration depths and related bottom fluxes were positively correlated with the stone content.

Acknowledgement
This contribution was partially supported by grant agency of the Slovak Academy of Sciences VEGA, project No. 2/0032/13 and is the result of the project implementation ITMS 26240120004 Centre of excellence for integrated flood protection of land supported by the Research & Development Operational Programme funded by the ERDF.

References

Bouwer, H., and R. C. Rice, Hydraulic Properties of Stony Vadose Zones, *Ground Water*, *22*(6), 696-705, 1984.

Childs, S. W., A. L. Flint, Physical properties of forest soils containing rock fragments. In: Gessel, S. P., D. S. Lacate, G. F. Weetman, and R. F. Powers, R.F. (Eds.), Sustained productivity of forest soils,

Proceedings of the 7th North American forest soils conference. University of British Columbia, Faculty of Forestry Publication, Vancouver, Canada, 95–121, 1990.
Hraško, J., and Z. Bedrna, Applied Soil Science, Priroda Publ. House, Bratislava, pp. 474, 1998 (in Slovak).
Holko, L., Z. Kostka, and M. Šanda, Assessment of frequency and areal extent of overland flow generation in a forested mountain catchment, *Soil & Water Res., 6*(1), 43-53, 2011.
Ma, D. H., M. A. Shao, J. B. Zhang, and Q. J. Wang, Validation of an analytical method for determining soil hydraulic properties of stony soils using experimental data, *Geoderma*, *159*, 262-269, 2010.
Mualem, Y., A new model for predicting the hydraulic conductivity of unsaturated porous media, *Wat. Resour. Res., 12*(3), 513-522, 1976.
Novák, V., K. Kňava, and J. Šimůnek, Determining the influence of stones on hydraulic conductivity of saturated soils using numerical method, *Geoderma*, *161*, 177-181, 2011.
Ravina, I., and J. Magier, Hydraulic conductivity and water retention of clay soils containing coarse fragments, *Soil Sci. Soc. Am. J., 48*, 736–740, 1984.
Poesen, J., and H. Lavee, Rock fragments in top soils: significance and processes, *Catena, 23*, 1–28, 1994.
Sauer, T. J., and S. D. Logsdon, Hydraulic and physical properties of stony soils in a small watershed, *Soil Sci. Soc. Am. J. 66*, 1947-1956, 2002.
Shi, Z., Y. Wang, P. Yu, L. Xu, W. Xiong, and H. Guo, Effect of rock fragments on the percolation and evaporation of forest soil in Liupan Mountains, China, *Acta Ecologica Sinica, 28*(12), 6090-6098, 2008.
Šály, R., Soil - basic component of forest production, *Príroda,* Bratislava, p. 235, 1978 (in Slovak).
Šimůnek, J., M. Šejna, HYDRUS (2D/3D), Software Package for Simulating Two- and Three-Dimensional Movement of Water, Heat, and Multiple Solutes in Variably-Saturated Media, User Manual, Version 1.02, PC Progress, Prague, Czech Republic, pp. 203, 2007.
Šimůnek, J., M. Šejna, H. Saito, M. Sakai, and M. Th. van Genuchten, The HYDRUS-1D Software Package for Simulating the One-Dimensional Movement of Water, Heat, and Multiple Solutes in Variably-Saturated Media, Version 4.0, Hydrus Series 3, Department of Environmental Sciences, University of California Riverside, Riverside, CA, USA, pp. 281, 2008a.
Šimůnek, J., M. Th. van Genuchten, and M. Šejna, Development and applications of the HYDRUS and STANMOD software packages, and related codes, *Vadose Zone Journal*, *7*(2), 587-600, 2008b.
van Genuchten, M. Th., A closed-form equation for predicting the hydraulic conductivity of unsaturated soils, *Soil Sci. Soc. Am. J., 44*, 987-996, 1980.
Verbist, K., J. Baetens, W. M. Cornelis, D. Gabriels, C. Torres, and G. Soto, Hydraulic conductivity as influenced by stoniness in degraded drylands of Chile, *Soil Sci. Soc. Am. J., 73*(2), doi: 10.2136/sssaj2008.0066, 471-484, 2009.
Zhou, B., M. Shao, and H. Shao, Effects of rock fragments on water movement and solute transport in a Loess Plateau soil, *C.R. Geoscience, 341*, doi: 10.1016/j.crte.2009.03.009, 462-472, 2009.

Simulations of the Impact of Different Rainfall Intensities on Reactive Transport of Metal Contaminants from Mine Tailings

Fatemeh Izadi Tame[1], Ali Motalebi Damuchali[2], Gholamreza Asadollah Fardi[3], and Ahmad Khodadadi[4]

[1]*Civil Engineering Department, Kharazmi University, Tehran, Iran, fateme.izadi66@gmail.com, fardi@tmu.ac.ir*
[2]*Environmental Engineering, Kharazmi University, Tehran, Iran; a.m.damuchali@gmail.com*
[3]*Civil Engineering Department of Kharazmi University, Tehran, Iran; fardi@tmu.ac.ir*
[4]*Engineering Faculty, Tarbiat Modares University, Tehran, Iran; akdarban@modares.ac.ir*

Abstract

Contamination of aquifers underlying mining areas is one of many environmental problems that can be evaluated using numerical models in order to delineate possible measures minimizing contamination of groundwater and neighboring river systems. Interpreting the geochemistry of the system and achieving a good understanding of the processes involved is necessary to mitigate environmental damage. Extensive internal risk prediction models often fail to predict where catastrophes will arise. In this study, the potential risk of metal contamination around mining sites is evaluated, and the sensitivity of reactive transport of metals to different leachate fluxes is estimated. The numerical model PHREEQC was used to simulate the transport of three metals (Cd, Ni and Mn) from zinc leaching plant tailings in Zanjan, Iran, with variable leachate fluxes during 30 days. The simulations showed that different rainfall rates induce different metal speciations. Decreasing water contents lowered the soil solution pH and produced new cation exchange conditions. The simulation results were generally in good agreement with experimental data. Incompatibility of modeled and experimental data for some scenarios may be attributed to the assumption of linear cation retardation in PHREEQC. Of the three metals considered, modeled Ni concentrations differed the most from experimental results of the different scenarios. We conclude that variations in water fluxes can significantly influence metal mobility and availability, and hence that specific risk assessments for past and present hydrological regimes are needed for mining disposal sites.

1. Introduction

Soil and groundwater contamination by heavy metals released from mining activities is a worldwide environmental problem. Heavy metals and other contaminants may be released from mining sites, especially from waste dumps or tailing ponds. Uncontrolled releases of these pollutants will contaminate soil and groundwater, which in turn poses serious threats to both the environment and human health because of toxicity and non-degradability of the metals.

The migration of contaminants from a waste disposal site usually involves one or more of the following processes: (1) advective, dispersive, and diffusive mass transport through the tailings, (2) chemical reactions within the soil solution, (3) interaction between the soil solution and the soil solids, such as adsorption, ion exchange, and precipitation, and (4) biodegradation.

Heavy metals in tailings exist in different forms, such as exchangeable or adsorbed, with the specific form having an important effect on their mobility and bioavailability. Heavy metals in available forms (i.e., exchangeable or adsorbed to the surface of clays, organic matter, or oxides

with weak bonding strength) are easily moved and dispersed in an ecosystem. On the other hand, metals bound with organic ligands or held within a crystal lattice are not easily separated and moved (Fletcher et al., 1981). Therefore, areas near the mines should be continuously monitored using observation wells to control and prevent groundwater pollution. Such monitoring is quite expensive and time consuming. Due to these economic reasons and the complexity of geochemical processes affecting metal reactive transport, various mathematical simulation models have been developed for assessing groundwater vulnerability to contamination and water resources management. These models have been found to be promising tools to unravel the complex interactions between soil physical and biogeochemical processes for all types of problems, including the impact of natural processes and anthropogenic activities on soil evolution (Jacques et al., 2008).

Seuntjens et al. (2002) studied how physical and chemical properties affected field-scale Cd transport in a heterogeneous soil profile. Using Monte Carlo simulations, they demonstrated that variations in field-scale Cd fluxes were dominated by variations in the deposition rate and the parameters of the Freundlich sorption isotherm. Using geochemical analyses and investigations of samples from mine tailings and water resources adjacent to the Piscinas River in Sardinia, Italy, Concas et al. (2005) concluded that a decrease in the pH will increase metal dissolution and transport from mine tailings. Tipping et al. (2006) used the CHUM-AM model to investigate the behavior of atmospherically-deposited metals (Ni, Cu, Zn, Cd and Pb) in Cumbria, UK, and concluded that the main processes controlling cationic metals are competitive partitioning to soil organic matter, chemical interactions in solution, and chemical weathering. Michel et al. (2007) applied mathematical and empirical models to investigate nickel and cadmium transport in silty and sandy soils in north Germany and concluded that lower pH level increases metal transport in acidic soils.

In another study, Van der Grift and Griffioen (2008) investigated Cd and Zn leaching from a polluted soil using saturated and unsaturated zone flow and reactive transport models. They concluded that metal contamination depended on the surface water loadings, the geohydrologic and geologic structure of the site, soil type and the dominant land use. Hanna et al. (2007) used PHREEQC to study the transport of zinc and lead in soils and concluded that the model can predict metal transport in acidic conditions, and that decreasing pH increases metal transport. Gordon et al. (2009) used geochemical modeling of Ni and Cd transport and found that decreasing pH levels will cause an increase in Ni and Cd mobility in silt and sandy soils. Horvath et al. (2009) in another study employed column leaching tests to investigate metal transport from mine tailings to water resources and showed that the adopted method was suitable for metal transport analyses.

The Zanjan zinc leaching plant, located 12 km from Zanjan, Iran, processes ore from the affiliated Anguran mine into zinc sheet metal. Tailings or “cake” of this operation are enriched in nickel (Ni) and cadmium (Cd). The objective of our study was to determine how different rainfall rates affected nickel (Ni), cadmium (Cd), and manganese (Mn) transport from these tailings, using the PHREEQC geochemical model.

2. Materials and Methods

2.1. Simulations

This section defines some of the governing equations for the physical and biogeochemical processes used in the reactive transport code. PHREEQC2 (Parkhurst and Appelo, 1999) was used to simulate different scenarios with different flow rates for a period of 30 days. PHREEQC is a geochemical model that can be used for water and soil environments. The code has the capability to model several one-dimensional transport processes, including diffusion, advection, advection and dispersion, and advection and dispersion with diffusion into stagnant zones. All of these processes can be combined with equilibrium and kinetic chemical reactions. The software uses the Advection-Reaction-Dispersion (ARD) equation to simulate transport as follows

$$\frac{\partial C}{\partial t} = -v\frac{\partial C}{\partial x} + D_L\frac{\partial^2 C}{\partial x^2} - \frac{\partial q}{\partial t} \tag{1}$$

where C, t, v, x, q, and D_L are concentration in water (mol/kgw), time (s), pore water flow velocity (m/s), distance (m), concentration in the solid phase (expressed as mol/kgw in the pores) and the hydrodynamic dispersion coefficient (m^2/s), respectively. The first term on the right side of (1) represents advective transport, the second term dispersive transport, and the third term the change in concentration in the solid phase due to reactions.

The relationship between the hydrodynamic dispersion coefficient, the effective diffusion coefficient (D_e) and the dispersivity (λ_L) is as follows:

$$D_L = D_e + \lambda_L v \tag{2}$$

The usual assumption is that v and D_L are equal for all solute species, so that C can be the total dissolved concentration of an element, including all redox species. The transport part of equation (1) is solved with an explicit finite difference scheme that is forward in time, central in space for dispersion, and upwind for advective transport (Parkhurst and Appelo, 1999). The chemical interaction term for each element is calculated separately from the transport part for each time step and is the sum of all equilibrium and non-equilibrium reaction rates. The numerical approach follows the basic components of the ARD equation in a split-operator scheme (Yanenko, 1971).

The process of metals cation exchange can be modeled effectively with the software for one-dimensional transport. However, it is not possible to directly enter the initial flow rate into the software. Hence, the leached solution from the tailing columns corresponds to the flow rate and needs to be described in the software for each transport procedure. This approach substantially prolongs the run times.

2.2. Simulation Efficiency

The modeling efficiency (*EF*), a measure of correspondence between measured and modeled results, is calculated using the equation (Loague and Green, 1990):

$$EF = \frac{\sum_{i=1}^{n}\left(x_i - x_n\right)^2 - \sum_{i=1}^{n}\left(y_i - x_i\right)^2}{\sum_{i=1}^{n}\left(x_i - x_n\right)^2} \quad (3)$$

where x_i, y_i, x_n, and n are measured values, modeled predictions, the arithmetic mean of measured values, and the number of measured and modeled values, respectively. When modeled predictions perfectly match the measured ones, *EF* is equal to 1. A negative value indicates that the modeled predictions describe the data less well than the mean of the observations.

2.3. Ni-Cd Cake Compounds

The deposited waste material was studied using the X-ray fluorescence test (XRF). Its physical properties were reported by Hashem Zadeh (2003) and Sedaghat (2007). Elemental analysis indicated that the waste material contains high concentrations of metals: 40.4% Zn, 11.2% Cd, 3.3% Ni, 1.4% Cu, and 0.8% Pb. Table 1 shows the types and quantities of elements in a 100 g Ni-Cd cake sample. A 1 kg sample was sieved by Sedaghat (2007) using 18, 35, 60, 80, 100, 120, 140, 170, 200, 230, and 270 mesh sieves.

Table 1. Quantities of elements in 100 g Ni-Cd Cake.

Compounds	Percentage	Elements	Percentage
Na_2O	10.94	Cd	11.1
MgO	0.57	Ni	3.34
Al_2O_3	0.19	Cu	1.40
SiO_2	0.36	Zn	40.4
SO_3	8.40	Pb	0.80
CaO	0.31	LOI	22.1
MnO	0.17		

Sedaghat (2007) worked experimentally on the same site and conducted 30-day leaching tests on 1,441 g of the Ni-Cd cake in each of the three 6-cm internal diameter columns. The columns were 50 cm long, with the tailings in each column occupying 40 cm. The effluent of each column was analyzed after 1, 3, 7, 13, 20, and 30 days. Parameters and their different levels used in the simulation scenarios are summarized in Table 2. The experimental data of Sedaghat (2007), and the same parameters and boundary conditions, were used also in this study.

Table 2. Simulation parameters.

Compounds	Level 1	Level 2	Level 3
Flow (cc/min)	0.5	1	2
Time (day)	1	13	30

2.4. Using the PHREEQC Model

Input into the PHREEQC code is identified using special Keywords. Using the SOLUTION keyword one can define types and concentrations of elements and their composition in the columns. The exchange reactions and one-dimensional transport parameters can be simulated using the EXCHANGE and TRANSPORT keywords, respectively. Equilibrium and exchange constants for chemical species of the tailing columns were taken from the MINTEQ database (Allison et al., 1990).

3. Results and Discussion

As mentioned earlier, understanding and modeling multicomponent reactive transport at the field scale is necessary for the design of remediation strategies in groundwater pollution problems and for risk assessment evaluations. While numerical and analytical methods are generally available to address multicomponent reactive transport problems at the local scale, it is not clear whether these methods can be extended to the field scale. The simulation results of this study will be evaluated and compared against the experimental results.

Three flow rates (low, moderate, and high) were selected to simulate natural processes. While a flow rate of 0.5 cc/min (cc stands for cubic centimeters), which produces laminar flow , was the lowest rate that could be reliably established in the laboratory, the 2 cc/min rate was the highest flow rate since ponding occurred at higher flow rates (Sedaghat, 2007). Also, the Meteorological Organization of the Islamic republic of Iran reported a maximum daily rainfall rate of 55 mm/day for Zanjan. The number of time steps was defined for each flow rate in PHREEQC.

Cadmium leaching concentrations were found to decrease with increasing flow rates. Cadmium concentrations declined with time during the 30-day period. Leaching concentrations were decreasing dramatically during the first 7 days and then only gradually as illustrated in Figure 1.

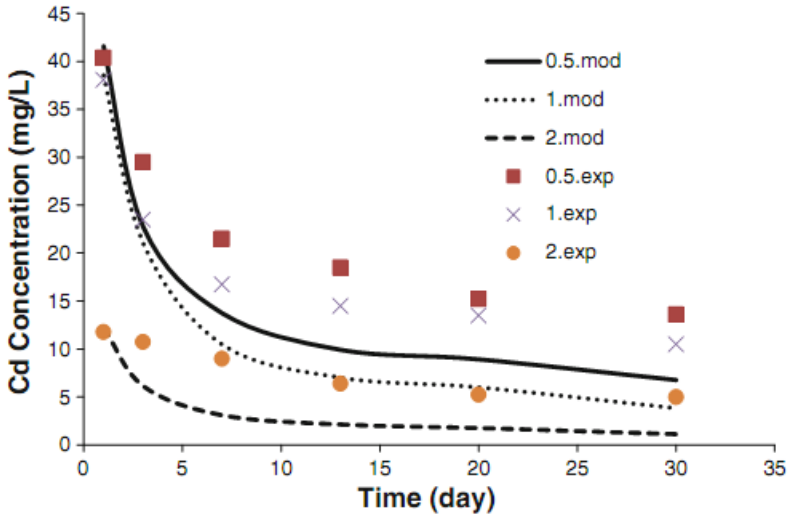

Figure 1. Simulated and measured leaching cadmium concentrations for various flow rates.

Figure 2 compares the modeled and measured nickel concentrations. Leached nickel concentrations also decreased with increasing flow rates. Similarly as for cadmium, the nickel concentrations dropped quickly during the first 7 days and then more gradually at later times.

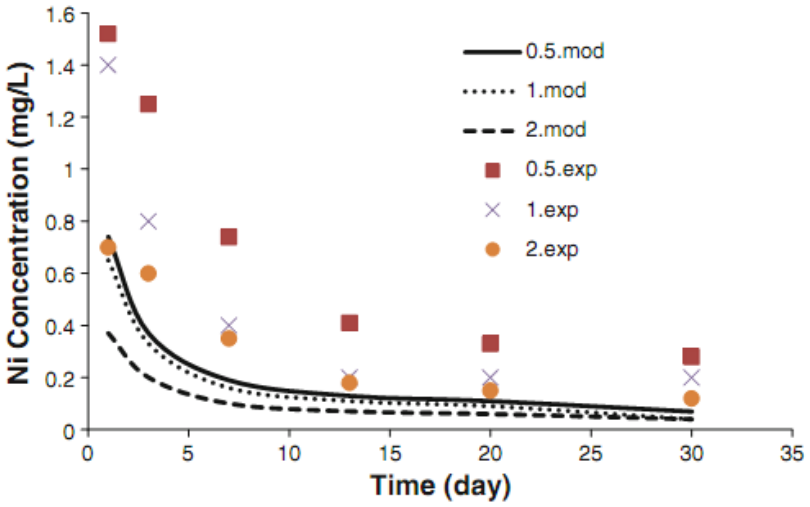

Figure 2. Simulated and measured leaching nickel concentrations for various flow rates.

The removal of manganese from tailing columns is presented in Figure 3. The behavior of manganese for various flow rates was similar to that of the other heavy metals. Higher inflow in general produced lower manganese leaching concentrations. The leached Mn concentrations decreased over time for all flow rate scenarios. Simulation efficiencies for the various flow rate scenarios are presented in Table 3.

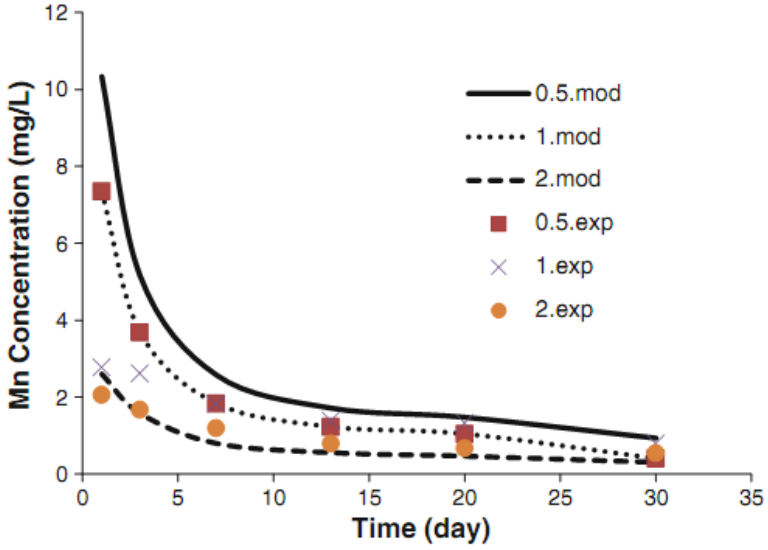

Figure 3. Simulated and measured leaching manganese concentrations for various flow rates.

Table 3. Simulation efficiencies for the different flow rate scenarios.

Flow rate (cc/min)	0.5	1	2
Cadmium	0.22	0.61	0.21
Nickel	0.2	0.3	0.62
Manganese	0.74	0.44	0.7

Michel et al. (2007) investigated the removal of Ni and Cd from acidic sandy and silty soils using empirical and mathematical modeling. The simulation efficiency in their study was between 0.35 and 0.85 for different scenarios, while the effects of chemical and other parameters were not considered. In a study of the effect of increasing pore water flow on zinc and lead transport using PHREEQC, Hanna et al. (2007) observed poor correspondence between predicted and measured results. They concluded that the differences were due to the inability of the software to consider the strong metal-binding capacity of the soil.

In our study we found good agreement between model predictions and experimental results for most scenarios. However, the ratio of the leached volume of water to the pore volume of the tailing columns was high for all scenarios, which may explain observed differences between simulated results and experimental data. Several reasons may have contributed to the poor correspondence between measured and simulated concentrations of some of the scenarios. One is the assumption of linear cation retardation in PHREEQC. Retardation reflects the activity of a cation species in an exchange reaction, which in PHREEQC is defined as

$$R = \frac{1 + CEC}{C} \tag{4}$$

where R is the retardation, CEC is the cation exchange capacity expressed in mol/kg water) and C is the species concentration (mol/kg water). In some scenarios, for example at lower pH, chemical reactions could compensate for the effects of linear retardation and improve the correspondence between modeled and measured data.

The differences between simulated and experimental results can be explained in part also by simplification of the problem to a one-dimensional domain, and ignoring possible heterogeneities in the porous medium. Large scale transport in spatially heterogeneous field systems is usually different from transport observed in homogeneous media, and more often of a non-Fickian nature. Realistic hydro-geological applications must directly or indirectly account for this heterogeneity. Under certain conditions, the asymptotic large scale transport of conservative species can be described by the advection-dispersion equation (ADE) with upscaled transport parameters (Dagan, 1989; Gelhar, 1993). The asymptotic limit is typically given by time, after which the species distribution is spread out over a volume whose dimensions are much larger than the largest heterogeneity scale. At pre-asymptotic times, however, which are relevant for most hydrogeological problems, data (e.g., Adams and Gelhar, 1992) often display what is known as anomalous (non-Fickian) or nonergodic (Kitanidis, 1998) behavior. This implies that concentrations then are not easily simulated using an ADE, even when allowing for upscaled parameters (Carrera, 1993). Different nonlocal methods have been developed to describe the effective transport of conservative species at intermediate distances, such as continuous time

random walks (CTRW) (Berkowitz and Scher, 1998; Berkowitz et al., 2006), fractional advection-dispersion equations (fADE) (Benson et al., 2000), multi-rate mass transfer (MRMT) formulations (Haggerty and Gorelick, 1995; Silva et al., 2009), and memory functions (Carrera et al., 1998). Regardless of using nonlocal methods, the same problem as considered in this study could be solved using other similar software, such as the HYDRUS family of programs or the coupled reactive transport code HP1.

4. Conclusions

The transport of heavy metals was evaluated in our study using PHREEQC for various flow rate scenarios. The modeled results matched experimental data collected on laboratory columns fairly well, which suggests that geochemical modeling may be an alternative and economic method to investigate metal transport from mine tailings for various environmental situations. In all cases, lower flow rates produced higher concentrations of metals leached from the Zanjan tailings. Of the three metals considered, the modeled Ni concentrations were least similar to collected data for different leaching scenarios.

Acknowledgment
The first author would like to express her appreciation to Dr. Jirka Šimůnek, Dr. Diederik Jacques, and Miss Elnaz Siami for their kind help and guidance.

References

Adams, E. E., and L. W. Gelhar, Field study of dispersion in a heterogeneous aquifer: 2. Spatial moment analysis, *Water Resour. Res.*, *28*(12), 3293–3308, 1992.

Allison, J. D., D. S. Brown, and K. J. Novo-Gradac, MINTEQA2/PRODEFA2 - A geochemical assessment model for environmental system - version 3 user's manual, Environmental Research Laboratory, Office of Research and Development, U.S. Environmental Agency, Athens, Georgia, 106 p, 1990.

Benson, D. A., S. W. Wheatcraft, and M. M. Meerschaerdt, The fractional-order governing equation of Lévy motion, *Water Resour. Res.*, *36*(6), 1413–1423, 2000.

Berkowitz, B., and H., Scher, Theory of anomalous chemical transport in fracture networks, *Phys. Rev. E.*, *57*(5), 5858–5869, 1998.

Berkowitz, B., A. Cortis, M. Dentz, and H. Scher, Modeling non-Fickian transport in geological formations as a continuous time random walk, *Rev. Geophys.*, *44*, RG2003, 2006.

Carrera, J., An overview of uncertainties in modelling ground water solute transport, *J. Contam. Hydrol.*, *13*(1-4), 23–48, 1993.

Carrera, J., X. Sánchez-Vila, I. Benet, A. Medina, G. Galarza, and J. Guimera, On matrix diffusion: Formulations, solution methods and qualitative effects, *Hydrogeol. J.*, *6*(1), 178–190, 1998.

Concas, A., C. Ardou, A. Cristini, P. Zuddas, and G. Cao, Mobility of heavy metals from tailings to stream waters in a mining activity contaminated site, *Chemosphere*, *63*, 244-253, 2005.

Dagan, G., *Flow and Transport in Porous Formations*, Springer, Berlin, 1989.

Fletcher, W. K., *Handbook of Exploration Geochemistry 1*, Elsevier Science Publishers B.V, Amsterdam, Oxford, New York, 1981.

Gelhar, L. W., *Stochastic Subsurface Hydrology*, Prentice Hall Publication, Old Tappan, New York, 1993.

Gordon, G. W., T. W. Lyons, G. L. Arnold, J. Roe, B. B. Sageman, and A. D. Anbar, When do black shales tell molybdenum isotope tales, *Geology*, *37*(6), 535–538, 2009.

Hanna, K., L. Lassabatere, and B. Bachet, Zinc and Lead transfer in a contaminated road soil: experimental study and modeling, *J. Hazard. Materials*, *161*, 1499-1505, 2007.

Haggerty, R., and S. M. Gorelick, Multiple-rate mass transfer for modeling diffusion and surface reactions in media with pore scale hetero geneity, *Water Resour. Res.*, *31*(10), 2383–2400, 1995.

Hashemzadeh, M., Study of the machinery methods for quantity and quality analysis of mineral, MSc Thesis, Tarbiat Modares University, Tehran, Iran, 2003.

Horvath, E., G. Jordan, U. Fugedi, A. Bartha, L. Kuti, G. Heltai, J. Kalmar, I. Waldmmann, I. Napradean, and G. Damian, Risk assessment of heavy metals in abandoned mine lands as significant contamination problem in Romania, *Geophys. Res. Abstracts*, 11, p. 8916, EGU General Assembly, 2009.

Islamic Republic of Iran Meteorological Organization, Climate Statics. http://www.irimo.ir, accessed Nov. 20 2012.

Jacques, D., J. Šimůnek, D. Mallants, and M. Th. van Genuchten, Modelling coupled water flow, solute transport and geochemical reactions affecting heavy metal migration in a podzol soil, *Geoderma*, *145* (3-4), 449-461, 2008.

Kitanidis, P. K., Prediction by the method of moments of transport in a heterogeneous formation, *J. Hydrol.*, *102*, 453–473, 1998.

Loague, K., and R. E. Green, Statistical and graphical methods for evaluating solute transport models: overview and application, *J. Contam. Hydrol.*, *7*(1-2), 51-73, 1990.

Michel, K., M. Roose, and B. Ludwig, Comparison of different approaches for modelling heavy metal transport in acidic soils, *Geoderma*, *140*, 207-214, 2007.

Parkhurst, L. B., and C. A. J. Appelo, User guide to PHREEQC (version 2), A computer Program for Speciation, Batch Reaction, One Dimensional Transport, and Inverse Geochemical Calculations, *USGS Water-Resources Investigation Report 99-4259*, Washington DC, USA, 1999.

Sedaghat, B., Investigation of effective parameters for hazardous material transport from zinc leaching plants to environment, MSc thesis, Tarbiat Modares University, Tehran, Iran, 2007.

Seuntjens, P., D. Mallants, J. Šimůnek, J. Patyn, and D. Jacques, Sensitivity analysis of physical and chemical properties affecting field-scale transport in a heterogeneous soil profile, *J. Hydrol., 264*, 185-200, 2002.

Silva, O., J. Carrera, S. Kumar, M. Dentz, A. Alcolea, and M. Willmann, A general real-time formulation for multi-rate mass transfer problems, *Hydrol. Earth Syst. Sci.*, *13*(8), 1399–1411, 2009.

Tipping, E., A. J. Lawlor, S. Lofts, and L. Shotbolt, Simulating the long term chemistry of an upland UK catchment: Heavy metals, *Environ. Pollution*, *141*, 139-150, 2006.

Van der Grift, B., and J. Griffioen, Modelling assessment of regional ground water contamination due to historic smelter emission of heavy metals, *J. Contam. Hydrol.*, *96*, 48-68, 2007.

Yanenko, N., *The Method of Fractional Steps*, Springer, New York, 1971.

Investigating the Effect of Acidic Rain on Reactive Transport of Metal Contaminants in Groundwater

Fatemeh Izadi Tame[1], Gholamreza Asadollah Fardi[2], Ahmad Khodadadi[3], Mohammad Faridzad[4]

[1]*Civil Engineering Department, Kharazmi University, Tehran, Iran; fateme.izadi66@gmail.com,*
[2]*Civil Engineering Department of Kharazmi University, Tehran, Iran; fardi@tmu.ac.ir*
[3]*Engineering Faculty, Tarbiat Modares University, Tehran, Iran; akdarban@modares.ac.ir*
[4]*School of Civil Engineering, Sharif University of Technology, Tehran, Iran; m.farizdad@yahoo.com*

Abstract

Multicomponent reactive transport in porous media is a complex process owing to a combination of variability in the processes involved and the inherent heterogeneity of nature. In recent years, various multicomponent reactive transport models have been developed to study the mobility of potentially toxic heavy metals in the subsurface. Heavy metals and other contaminants may be released from mining sites, especially from waste dumps and tailing ponds. Soil and groundwater contamination due to mining activities is an important environmental problem worldwide. Because of their abundance and potential toxicity, Pb^{2+}, Zn^{2+}, and Cd^{2+} figure prominently among inorganic contaminants of greatest concern in mine tailings. This study investigated the effect of pH on the transport of these metals through lead and zinc leaching plant tailings in Lakan, Iran. The HP1 model and PHREEQC database were used to simulate the transport of the metals through a saturated soil at the laboratory column scale during a 15-day time period. The simulations assumed local equilibrium. As expected, a lower pH increased metal transport. However, although the simulation results generally agreed well with results of the column study, they indicated that physical and chemical parameters must be carefully determined for use in the simulations. Improvements in the results are expected when using multi-dimensional models and a kinetic modeling approach for the reactions involved.

1. Introduction

Despite significant progress in science and technology, environmental problems are increasing at the national, regional, and international levels. Correlations between industrial activities and environmental contamination make it difficult to expect substantial industrial development without some impact on the environment. The production of inorganic wastes in mining operations has always been an important issue and a threat to the environment, especially the subsurface. These wastes often contain high levels of heavy metals, which constitute a major threat to human populations, aquatic species, plants, ecosystems, and groundwater quality in general because of their biological non-degradability and stability in the environment. Large-scale mining can especially adversely affect the environment. Iran, as a developing country, still needs to develop much of its mining activities. Unfortunately, a lack of necessary standards for proper processing and waste burial make environmental pollution more probable in Iran. Leaching of heavy metals from surface soils to deeper layers, and the risk of groundwater pollution, depend on the retention, mobilization, and transport of heavy metals in soils. Specific adsorption, ion exchange, and precipitation of various solid phases are the main processes responsible for the retention of heavy metals. Previous studies indicate that the pH is one of the most important factors affecting the transport and sorption of heavy metals (Chotpantarat et al.,

2011). Changes in the chemical composition or pH of the soil solution may impact the sorption of elements on organic matter or iron oxides.

Decision makers need predictions of the fate of heavy metals in soils to design management strategies that minimize adverse environmental impacts. Accurate simulations of pollutant transport require a coupled reactive transport code that integrates the physical processes of water flow and advective-dispersive solute transport with a range of biogeochemical processes. Many models have been developed to simulate and predict the fate and transport of pollutants in porous media (e.g., Šimůnek, 2007; Šimůnek et al., 2008b). The most commonly-used models are based on advection-dispersion equations and consider such mechanisms as advection, dispersion, sorption, and degradation.

Wu et al. (1998) showed that at lower pH levels, Cd and Pb precipitation will cause a sharp decrease in their external concentrations. Pang et al. (2002) showed that the breakthrough curves (BTCs) of Cd, Zn, and Pb in gravel columns with pore water velocities ranging from 3 to 60 m/day displayed long tailing, suggesting that non-equilibrium sorption conditions occurred in the gravel columns due to high pore water velocities. Using geochemical analyses and investigations of samples from mine tailings and water resources adjacent to the Piscinas River in Sardinia, Italy, Concas et al. (2005) concluded that a decrease in the pH level increased metal dissolution and transport from mine tailings. Pot et al. (2005) used different physical and chemical equilibrium and non-equilibrium transport models to simulate the impact of various rainfall intensities on herbicide transport. Their study showed that physical/chemical non-equilibrium conditions were dominant. Michel et al. (2007) used mathematical and empirical models to investigate nickel and cadmium transport in silty and sandy soils and concluded that a decrease in the pH will increase the transport of heavy metals in acidic soils. Using HP1 model, Jacques et al. (2008) further showed that reducing the inflow intensity will cause a decrease in the pH level, thereby promoting monovalent cations to sorb on the cation exchange complex, and bivalent cations to desorb into the soil solution. Simulating the effect of pH on Pb, Mn, Zn, and Ni transport using HYDRUS-1D, Chotpantarat et al. (2011) found that increasing the pH of the inflow solution will increase the retardation of heavy metals. They also showed that the use of a two-site model (TSM) for sorption produced a better match with measured heavy metal BTCs than linear or nonlinear Langmuir type equilibrium models.

The main objective of this research was to investigate the effect of aqueous pH conditions on the sorption and transport of three heavy metal ions, Cd^{2+}, Pb^{2+}, and Zn^{2+}, using the HP1 numerical model, to evaluate the model's utility in simulating the transport of heavy metals in soil columns, and to investigate the sorption behavior of heavy metals in soil columns.

2. Materials and Methods

2.1. General Features of Study Area

The Lakan lead and zinc processing plant is located 46 km Southwest of Arak City in the Markazi Province, Iran. The geographical location of this site is 33°42'5"N latitude and 49°43'26"E longitude. The Lakan plant is located in a temperate mountainous zone with hot

summers and cold winters. Annual variations in temperatures are very high, ranging from -20 ºC in the winter to +35 ºC in the summer.

2.2. Soil Physical and Chemical Properties

The deposited waste material had been studied previously by Marzban (2008) using X-ray fluorescence (XRF) tests. Table 1 shows the types and quantities of elements in a 100 g sample.

Table 1. Quantities of elements in a 100 g sample.

Compounds	Percentage	Compound/Element	Percentage
Na_2O	0.5	MnO	0.3
MgO	0.8	Ni	0.0146
AL_2O_3	3.5	Zn	1.15
SiO_2	66.6	Pb	1.5
SO_3	4.5	Cd	0.005
K_2O	0.7	P_2O_5	0.9
CaO	9.5	Fe_2O_3	2.9
BaO	0.4	LOI	6.73

Using tailings from the same site, Marzban (2008) conducted 15-day leaching tests on 180 g samples in three 2.7-cm internal diameter columns in which the tailings occupied heights of 21 cm. The effluent from each column was analyzed after 3, 7, 10, and 15 days. Physical properties of the tailing dam soil as reported by Marzban (2008) are presented in Table 2.

Table 2. Physical properties of tailing dam soil.

Soil Property	Unit	Value
Bulk Volume	(mL)	150
Weight	(g)	221.77
Pore Volume	(mL)	40
Specific Volume	(mL)	110
Bulk density	(g/mL)	1.48
Specific density	(g/mL)	2.02
Solid fraction	-	0.73
Porosity	-	0.27

2.3. Transport Model

All calculations in this paper were carried out using version 2.2 of HP1 (Jacques et al., 2010). The HP1 reactive transport simulator, obtained by weak coupling of HYDRUS-1D and PHREEQC-2, was developed and designed to address multicomponent geochemical transport processes in the vadose zone. The software integrates a broad range of physical and biogeochemical processes, as described in the original manuals of HYDRUS-1D (Šimůnek et al., 2008ab), PHREEQC-2 (Parkhurst and Appelo, 1999), and HP1 (Jacques et al., 2010). HYDRUS-1D was originally designed mostly for simulating water flow, solute transport, and heat transport

in soils from the soil column scale to the field scale. The program can numerically solve the Richards equation for saturated-unsaturated water flow and the advection-dispersion equation for solute and heat transport. In this software, the solute transport module also considers equilibrium and non-equilibrium advection-dispersion in the liquid phase, and nonlinear equilibrium physical and chemical sorption. Important to note is that both the HYDRUS-1D and HP1 models account for soil heterogeneity at the macroscopic scale by using scaling factors (Vogel et al., 1991), and at the microscopic scale by using dual-porosity or mobile/immobile type flow models (Šimůnek et al., 2003). HP1 implements a weak coupling method in which the governing equations for water flow, heat transport, and solute transport are solved sequentially. The multicomponent reactive transport equations are solved using a non-iterative sequential approach, meaning that the physical part is solved first without any chemical interactions, while the chemical reactions that are uncoupled in space and coupled over the components are solved subsequently (Jacques et al., 2008). A flow chart of the operator-splitting approach used in HP1 was given in Jacques et al. (2006). Although operator-splitting errors may occur with this approach, Jacques et al., (2006, 2008) showed that very accurate results can be obtained by carefully selecting the spatial and temporal discretizations.

2.3.1. Soil Hydraulic Properties

Six analytical models are available in HP1 to describe the soil hydraulic properties, including the function of Brooks and Corey (1964), van Genuchten (1980), and Vogel and Cislerova (1988). In this study the van Genuchten-Mualem model (van Genuchten, 1980) was used to describe the water retention and hydraulic conductivity ($K(h)$) functions:

$$\theta(h) = \begin{cases} \theta_r + \dfrac{\theta_s - \theta_r}{[1+|\alpha h|^n]^m} & h < 0 \\ \theta_s & h \geq 0 \end{cases} \tag{1}$$

$$K(h) = K_s S_e^l [1 - (1 - S_e^{1/m})^m]^2 \tag{2}$$

$$S_e(h) = \frac{1}{[1+|\alpha h|^n]^m} \tag{3}$$

where $\theta(h)$ is the soil water content [-] as a function of the pressure head, h [L], θ_s is the saturated water content [-], θ_r is the residual water content [-], K_s is the saturated hydraulic conductivity [LT^{-1}], S_e is the effective water content [-], α, m, and n are empirical parameters of the retention curve (m=1-1/n for n>1), and $K(h)$ is the unsaturated hydraulic conductivity [LT^{-1}]. The pore connectivity/tortuosity factor (l) used in the simulations was set to 0.5 for all simulation scenarios. This value was recommended by Mualem (1976) and is a default value used for soils in the HYDRUS software.

2.3.2. Water Flow Equation

A combination of the mass balance equation with the Darcy-Buckingham law results in the Richards equation describing water flow in variably-saturated porous media. The one-dimensional form of the Richards equation can be written as:

$$\frac{\partial \theta(h)}{\partial t} = \frac{\partial}{\partial z}\left[K(h)\left(\frac{\partial h}{\partial z} + \cos\alpha \right) \right] - S(h) \tag{4}$$

where h is the water pressure head [L], θ is the volumetric water content [-], t is time [T], z is the spatial coordinate [L] (positive upward), S is the sink term [$L^3L^{-3}T^{-1}$], α is the angle between the flow direction and the vertical axis, and K is the unsaturated hydraulic conductivity [LT^{-1}].

2.3.3. Solute Transport Equation

Solute transport in porous media can be described with the one-dimensional convective-dispersive equation (CDE):

$$\frac{\partial \theta C}{\partial t} + \frac{\partial \rho_b S}{\partial t} = \frac{\partial}{\partial z}\left(\theta D \frac{\partial C}{\partial z} \right) - \frac{\partial q_w C}{\partial z} \tag{5}$$

in which C is the solute concentration in solution [ML^{-3}], S is the sorbed solute concentration [MM^{-1}], ρ_b is the soil bulk density, q_w is the volumetric water flux [LT^{-1}], and D is the effective dispersion coefficient [L^2T^{-1}]. The effective dispersion is given by Bear (1972):

$$D\theta = \lambda_L \left| q_w \right| + \theta \tau D_0 \tag{6}$$

where λ_L is the longitudinal dispersivity [L], D_0 is the aqueous ionic or molecular diffusion coefficient of a solute in water [L^2T^{-1}], and τ is the tortuosity factor given by (Milington and Quirk, 1961):

$$\tau = \frac{\theta^{7/3}}{\theta_s^2} \tag{7}$$

By manipulating Equation (5), the modified convective-dispersive equation is obtained as follows:

$$R\frac{\partial C}{\partial t} = D\frac{\partial^2 C}{\partial z^2} - v\frac{\partial C}{\partial z} \tag{8}$$

where R is the retardation factor given by the following equation:

$$R = \frac{1 + \rho_b K_d}{\theta} \tag{9}$$

in which K_d is the partitioning coefficient of solute [L^3M^{-1}] and v the average pore water velocity [LT^{-1}].

2.3.4. Numerical Simulations

The water flow and solute transport equations were solved numerically using the HP1 code (Jacques et al., 2010). The upper and lower boundary conditions for water flow were assumed to

be a constant pressure head, and for solute transport to be a concentration flux BC (third type) and a zero concentration gradient (free drainage), respectively. In the HP1 model, the Galerkin finite element method with a space weighting scheme was selected, while the time derivatives for the solute transport solution were approximated using a Crank-Nicholson finite difference scheme. All simulations were conducted over a period of 15 days. The column height was 21 cm and the inflow rate 1 cc/min (cc stands for cubic centimeters), while acid concentrations were 0, 0.12, and 0.29 g/L. Selected parameter values (Levels 1, 2, and 3) used in the simulation scenarios are summarized in Table 3.

Table 3. Simulation parameters and levels.

Compounds	Level 1	Level 2	Level 3
pH	7	6	5
Time (day)	3	10	15

2.3.5. Modeling Efficiency

The modeling efficiency (*EF*) was calculated for the measured and modeled data using (Loague and Green, 1990)

$$EF = \frac{\sum_{i=1}^{n}\left(x_i - x_n\right)^2 - \sum_{i=1}^{n}\left(y_i - x_i\right)^2}{\sum_{i=1}^{n}\left(x_i - x_n\right)^2} \tag{10}$$

where x_i, y_i, x_n and n are measured values, model predictions, arithmetic means of the measured values, and the number of measured and modeled values, respectively. When model predictions perfectly match the measured data, *EF* is equal to 1. A negative value indicates that the predictions describe the data less than the mean of the observations.

3. Results and Discussion

The effects of pH on the transport of Cd, Zn, and Pb are shown in Figure 1. Taking into account the fact that the pH of rain in the Arak city is 5.5, three input solutions with pH values of 5, 6, and 7 were selected for the study, similarly as in the experiments carried out by Marzban (2008) and Darban et al. (2012). Maximum removal of Cd, Zn, and Pb was achieved after three days using the input solution with pH of 5. The removal concentrations of these three metals were 0.4, 16.38, and 1.21 mg/L, respectively. The lower removal concentrations of Cd and Pb, compared to Zn, is likely due to precipitation of Cd and Pb species, especially at lower pH levels. The higher removal of metals with decreasing pH is reasonable, since higher pH indicates lower quantities of H^+ ions and an increase in the retardation factor of heavy metals as shown by Chotpantarat et al. (2011), among many others. The removal concentrations of the three metals after 15 days are shown in Table 4.

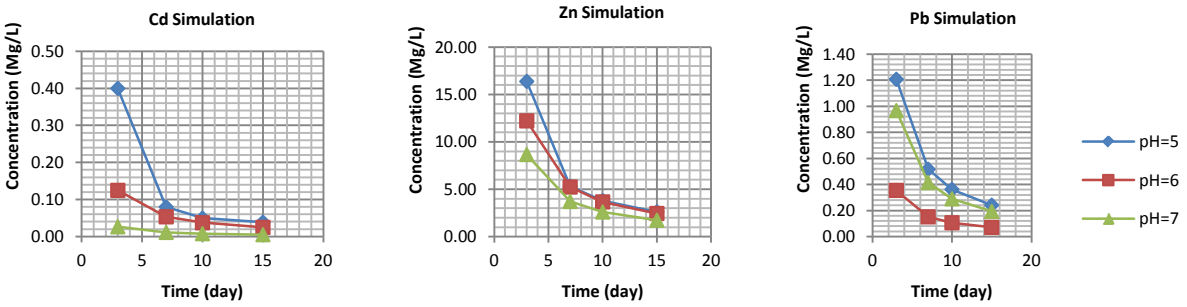

Figure 1. Effect of pH on Cd, Zn, and Pb transport and removal.

Table 4. Removal concentrations of heavy metals in mg/L after 15 days.

Element/pH	pH=5	pH=6
Cd	0.04	0.02
Zn	2.62	2.44
Pb	0.24	0.07

Allowable limits for concentrations of zinc, lead, and cadmium in groundwater according to the U.S. Environmental Protection Agency (US EPA, 1993) are 5, 0.005, and 0.01 ppm, respectively. The results in Table 4 indicate that the concentrations of Cd and Pb in solution exceeded the EPA limits. They also exceeded the Iranian standard for drinking water (Standard No. 1053). Similar findings were reported by Darban et al. (2012). Heavy metal mobility followed the order $Zn^{2+} > Pb^{2+} > Cd^{2+}$. The same results for similar conditions were reported by Wu et al. (1998), except for Pb. This difference can be attributed to the lower simulation efficiency for Pb in our study. As reported also by Wu et al. (1998), Darban et al. (2012), and Nguyen at al. (2010), the removal concentrations were lower for neutral solutions, as compared to more acidic solutions, because of precipitation of metals under neutral aquatic conditions.

Experimental and simulated concentrations for Cd, Zn, and Pb after 7 days are presented in Table 5, while the simulation efficiencies for different pH levels are listed in Table 6. Comparing the simulated and the experimental results, the highest efficiency was achieved for Cd removal concentrations, followed by Zn and Pb.

Table 5. Experimental and simulated removal concentrations of heavy metals (in mg/L).

Element	pH=6 (Experiment)	pH=6 (Simulation)	pH=5 (Experiment)	pH=5 (Simulation)
Cd	0.041	0.054	0.053	0.08
Zn	4.47	5.24	5.46	5.32
Pb	0.039	0.15	0.078	0.052

Table 6. Modeling efficiencies for the heavy metals removal concentrations at two pH values.

Element/pH	pH=6	pH=5	Average
Cd	0.80	0.69	0.75
Zn	0.77	0.5	0.63
Pb	0.79	0.29	0.54

Brown et al. (1998) attributed the differences in their observed and simulated results to the local equilibrium assumption. They indicated that due to the slow reaction kinetics and limited interactions of solid phase surfaces with solutes, the dominant process could not be effectively described using the assumption of local equilibrium in their simulation. Pot et al. (2005) concluded that the physical/chemical non-equilibrium models were also more effective in simulating herbicide transport. Michel et al. (2007) investigated the removal of Ni and Cd from acidic sandy and silty soils using empirical and mathematical modeling. They found the simulation efficiencies between 0.35 and 0.85 for different scenarios. The effects of different chemicals or other transport and reaction parameters were not considered.

Jacques et al. (2008) found that decreasing the pH level will increase bivalent cations removal concentrations. A comparison of our results with results reported by Motalebi et al. (2012) shows that the PHREEQC and HP1 models had approximately the same efficiency for Cd reactive transport, perhaps because of the saturated flow conditions in both studies.

Relatively good agreement between model predictions and experimental results was obtained in our study. Some small differences between the experimental and simulated results were observed only during the first few days of the simulations. The presence of dissolved organic matter (DOM) may have influenced the mobility and retention of heavy metals in soils. The formation of complexes with DOM can be especially important for Pb (Weng et al., 2002; Tipping et al., 2003). The lower simulated removal concentrations of metals may be attributed to the formation of complexes during the first few days of simulation.

Another possible reason for the differences may be the fact that the soil hydraulic conductivity was assumed to be constant during the simulations. In reality, the hydraulic conductivity changes with changes in pH, which should affect the heavy metal precipitation rate. In general, disagreement between the model and the data (lower modeling efficiencies) of some of the scenarios can be attributed also to uncertainty in the value of some parameters, simplification of the transport process to a one dimension, ignoring the effects of macropores and other transport processes in natural soil (such as bioturbation), and/or local physical or chemical non-equilibrium processes.

4. Conclusions

In this study, the effects of pH on reactive transport of Cd, Zn, and Pb from Lakan mine tailings were investigated using the HP1 model. Metal removal concentrations were predicted using the HP1 model. Simulation results were compared with previously published experimental results and the results of other researchers. Overall, the HP1 model successfully simulated water flow and solute transport in the columns, considering the limitations in the experimental data.

Using different pH levels for the inflow solution, the following conclusions were reached:

- The retardation of heavy metals followed the order $Zn^{2+}>Pb^{2+}>Cd^{2+}$
- Decreasing pH values produced higher metal removal concentrations
- The removal concentrations of Cd and Pb exceeded the allowable EPA and Iranian's 1053 standard thresholds
- The simulations for Cd had the highest modeling efficiency, followed by Zn and Pb

- Predicted early removal concentrations did not successfully match the observed data, likely due to the presence of sharp solute fronts, failure to establish local equilibrium, insufficient time for complete soil solid phase and soil solution reactions, or temporal variations in the physical properties. Some of the differences could be attributed also to the formation of complexes at the beginning of simulations.
- Differences between modeling and experimental results for some scenarios could also be attributed to uncertainty in the values of some parameters, simplification of the transport process to 1D, ignoring the effects of macropores and other transport mechanisms occurring in soils (such as bioturbation), local physical/chemical non-equilibrium, or uncertainty in the dominant chemical processes and their parameters.
- PHREEQC and HP1 models had approximately the same modeling efficiency for the Cd reactive transport simulations.

More research is needed to explore the various physico-chemical and biological processes that control the potential solubility of toxic metals from mine tailings. The use of two- and three-dimensional models, as well as kinetic modeling, is recommended to more accurately simulate reactive transport in actual field conditions.

Acknowledgments
The authors give heartfelt thanks to Dr. Jirka Šimůnek for his kind help and guidance during the time of this research.

References

Brooks, H., and A. T. Corey, Hydraulic properties of porous media, Colorado State Univ. Hydrol. Paper, No. 3, 27 pp. Fort Collins, CO, 1964.

Brown, J. G., R. L. Bassett, and P. D. Glynn, Analysis and simulation of reactive transport of metal contaminants in ground water in Pinal Creek Basin, Arizona, *J. Hydrol. 209*, 225-250, 1998.

Chotpantarat, S., S. K. Ong, Ch. Sutthirat, and Kh. Osathaphan, Effect of pH on transport of Pb^{2+}, Mn^{2+}, Zn^{2+} and Ni^{2+} through lateritic soil: Column experiments and transport modeling, *J. Environ. Sci.*, *23*(4), 640-648, 2011.

Concas, A., C. Ardou, A. Cristini, P. Zuddas, and G. Cao, Mobility of heavy metals from tailings to stream waters in a mining activity contaminated site, *Chemosphere*, *63*, 244-253, 2005.

Darban A., A. Khodadadi, S. Koleini, M. Marzban, and R. Yong, Study of leachability of heavy metals from Zinc flotation plant tailings dam sediments, ASTM standard, Contaminated Sediments, 5th volume, Restoration of Aquatic Environment, *STP1554*, 2012.

Jacques, D., J. Šimůnek, D. Mallants, and M. Th. van Genuchten, Operator-splitting errors in coupled reactive transport codes for transient variably saturated flow and contaminant transport in layered soil profiles, *J. Contam. Hydrol.*, *88*, 197-218, 2006.

Jacques, D., J. Šimůnek, D. Mallants, and M. Th. van Genuchten, Modelling coupled water flow, solute transport and geochemical reactions affecting heavy metal migration in a Podzol Soil, *Geoderma*, *145*(3-4), 449–461, 2008.

Jacques, D., and J. Šimůnek, Notes on HP1 - A software Package for Simulating Variably-Saturated Water Flow, Heat Transport, Solute Transport, and Biogeochemistry in Porous Media, Version 2.2. *SCK•CEN-BLG-1068,* Waste and Disposal, SCK•CEN, Mol, Belgium, 113 pp., 2010.

Marzban, M., Study of effective parameters on transport of hazardous waste from Lakan sulfide Zinc flotation plant to environment, MSc thesis, Tarbiat Modares University, Tehran, Iran, 2008.

Michel, K., M. Roose, and B. Ludwig, Comparison of different approaches for modelling heavy metal transport in acidic soils, *Geoderma*, *140*(1-2), 207-214, 2007.

Millington, R., and P. J. Quirk, Permeability of porous media, *Trans. Faraday Soc.*, *57*(7), 1200-1207, 1961.

Motalebi, A., G. Asadollahfardi, and A. Khodadi, Effective Parameter Predictions in Metals Transport from the Zanjan Zinc Mine Tailings using PHREEQC, *Mine Water and the Environment*, *31*(4), 339-343, 2012.

Mualem, Y., A new model for predicting the hydraulic conductivity of unsaturated porous media, *Water Resour. Res.*, *12*(3), 513-522, 1976.

Nguyen, T. H., M. Ohtsubo, L. Li, T. Higashi, and M. Kanayama, Heavy metal characterization and leachability, *Int. J. Soil, Sediment Water*, *3*(1), 1-21, 2010.

Pang, L., M. Close, D. Schneider, and G. Stanton, Effect of pore water velocity on chemical nonequilibrium transport of Cd, Zn, and Pb in alluvial gravel columns, *J. Contam. Hydrol.*, *57*, 241-258, 2002.

Parkhurst, D. L., and C. A. J., Appelo, User's guide to PHREEQC (version 2), A Computer Program for Speciation, Batch-Reaction, One-Dimensional Transport, and Inverse Geochemical Calculations, *Water Resources Investigation, Report 99–4259*, Denver, Co, USA, 312 p., 1999.

Pot, V., J. Šimůnek, P. Benoit, Y. Coquet, A. Yra, and M. L. Martinez-Cordon, Impact of rainfall intensity on the transport of two herbicides in undisturbed grassed filter strip soil cores, *J. Contam. Hydrol.*, *81*(1-4): 63-88, 2005.

Šimůnek, J., N. J. Jarvis, M. Th. van Genuchten, and A. Gärdenäs, Review and comparison of models for describing non-equilibrium and preferential flow and transport in the vadose zone, *J. Hydrol.*, *272*, 14-35, 2003.

Šimůnek, J., Models for Soil Pollution Risk Assessment, *Proc. of NATO Advanced Research Workshop "Air, Water and Soil Quality Modelling for Risk and Impact Assessment*", Eds. A. Ebel and T. Davitashvili, NATO Security through Science Series, C: Environmental Security, Springer, ISBN-10 1-4020-5876-4 (PB), 221-233, 2007.

Šimůnek, J., M. Šejna, H. Saito, M. Sakai, and M. Th. van Genuchten, The HYDRUS-1D Software Package for Simulating the Movement of Water, Heat, and Multiple Solutes in Variably Saturated Media, Version 4.0, *HYDRUS Software Series 3*, Department of Environmental Sciences, University of California Riverside, Riverside, California, USA, pp. 315, 2008a.

Šimůnek, J., M. Th. van Genuchten, and M. Šejna, Development and applications of the HYDRUS and STANMOD software packages, and related codes, *Vadose Zone Journal*, doi:10.2136/VZJ2007.0077, *7*(2), 587-600, 2008b.

Tipping, E., J., Rieuwerts, G. Pan, M. R. Ashmore, S. Lofts, M. T. R. Hill, M. E. Farago, and I. Thornton, The Solid-Solution partitioning of heavy metals (Cu, Zn, Cd, Pb) in upland soils of England and Wales, *Environ. Pollution*, *125*, 213-225, 2003.

U.S. EPA, Clean Water Act, Standards for the use and disposal of sewage sludge, *Code of Federal Regulations (CFR) Part 503*, 58(32). U.S. Environmental Protection Agency, Washington, DC, 1993.

van Genuchten, M., Th., A closed form equation for predicting the hydraulic conductivity of unsaturated soils, *Soil Sc. Soc. Am. J.*, *44*(5), 892-898, 1980.

Vogel, T., and M. Cislerova, On the reliability of unsaturated hydraulic conductivity calculated from the moisture retention curve, *Transport Porous Media*, *3*, 1-15, 1988.

Vogel, T., M. Cislerova, and J. W. Hopmans, Porous media with linearly variable hydraulic properties, *Water Resour. Res.*, *27*, 2735-2741, 1991.

Weng, L. P., E. J. M. Temminghoff, S. Lofts, E. Tipping, and W. H. Riemsdijk, Complexation with dissolved organic matter and solubility control of heavy metals in a sandy soil, *Environ. Sci. Techn.*, *36*, 4804-4810, 2002.

Wu, G., and L. Y. Li, Modeling of heavy metal migration in sand/bentonite and the leachate pH effect, *J. Contam. Hydrol.*, *33*(3-4), 313-336, 1998.

Comparison of Two Numerical Modeling Codes for Hydraulic and Transport Calculations in the Near Field

Jan Kalin[1], Borut Petkovšek[1], Philippe Montarnal[2], Alain Genty[2], Estelle Deville[2], Jure Krivic[3]

[1] *Slovenian National Building and Civil Engineering Institute, Ljubljana, Slovenia, jan.kalin@zag.si, borut.petkovsek@zag.si*
[2] *CEA/Saclay, DM2S, Gif-sur-Yvette, France, philippe.montarnal@cea.fr, alain.genty@cea.fr, estelle.deville@cea.fr*
[3]*Geolgical Survey of Slovenia, Ljubljana, Slovenia, jure.krivic@geo-zs.si*

Abstract

In past years, the Slovenian PA/SA team has performed many generic PA/SA studies for the future Slovenian LILW repository, most recently a Special Safety Analysis (SSA) for the Krško site. The modeling approach taken was to split the problem into three parts: near-field (detailed model of the repository), far-field (i.e., geosphere) and biosphere. In the SSA, the code used to perform near-field calculations was HYDRUS-2D. Recently, the team has begun to cooperate with CEA/Saclay and, as a result of this cooperation, began investigations into using the Alliances numerical platform for near-field calculations in order to compare the overall approach and calculated results. This article presents the comparison between these two codes for a silo-type repository that was considered in the SSA. We will present the physical layout and characteristics of the repository and develop and implement a hydraulic and transport model of the repository in Alliances. Some analysis of the sensitivity to mesh fineness and to a simulation timestep has been performed and will also be presented. The compared quantity will be the output flux of radionuclides on the boundary of the model. We will compare the results and comment on differences/similarities.

1. Introduction

In the previous years the Slovenian Performance Analysis/Safety Assessment (PA/SA) team has performed many studies for the future low and intermediate level waste repository. The most recent one was a Special Safety Analysis (SSA) (Petkovšek et al., 2006) for three proposed preliminary designs, including a silo-type subsurface repository.

In the SSA, the code used to perform near-field calculations was HYDRUS-2D (HYDRUS, 2013). However, the team investigated the possibility of using Alliances (Montarnal et al., 2006) - a numerical platform co-developed by CEA, ANDRA and EDF for the numerical simulation of nuclear waste disposal - to perform near-field transport and other calculations. In the decision process one of the tasks was to repeat the near-field calculations for the silo-type repository with Alliances and compare results with those obtained with HYDRUS.

2. System Description

The silo-type subsurface repository is buried in a silty soil. It is a cylindrical concrete structure with a 12.8 m inner radius, 0.9 m thick walls and an inner height of 33 m after closure. The space inside the repository is filled with layers of 70 waste-containing concrete blocks with external

dimensions 2.45m × 2.45m × 3.2m. Any remaining space between the blocks and silo walls is filled with drainage gravel. The whole of the repository lies underneath the water table so the hydraulic conditions in the soil and in the repository are saturated. There is a general horizontal hydraulic gradient of 0.00118 in the aquifer.

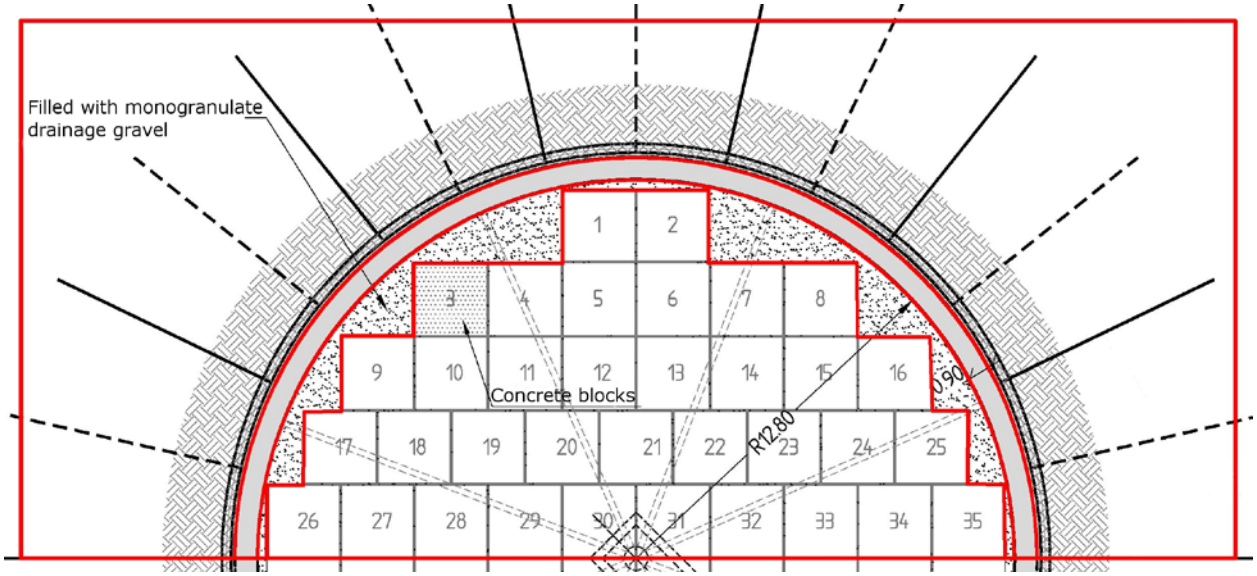

Figure 1. Horizontal section through repository.

Since the hydraulic flow is driven by an external horizontal gradient and the repository is completely below the water table, the end effects of top and bottom of the silo can be neglected and the model simplifies to horizontal flow in 2D. The red rectangle in figure 1 marks the boundary of the 40 m × 20 m modeled domain. The other three red lines mark the boundaries between different regions of the repository; from the center outwards: the boundary between waste containing blocks and drainage gravel, the boundary between drainage gravel and a silo wall, and the boundary between a silo wall and silt. The direction of the gradient was chosen so that the water flows from left to right.

3. Hydraulic Calculations

The hydraulic conditions are saturated, so the only parameters needed are the saturated hydraulic conductivities of materials, listed in Table 1.

Barrier degradation was simulated by artificially changing the hydraulic conductivities of materials at specified times. Up to 10,000 years, there is no degradation. It is assumed that between 10,000 and 100,000 years, the silo wall degrades. This is simulated by increasing the hydraulic conductivity of the silo wall to that of the silt. After 100,000 years, the containers also degrade so that their hydraulic conductivity increases to that of the silt.

Table 1. Saturated hydraulic conductivities of materials.

Material	K_s **[m/s]**
Silt	10^{-7}
Concrete (silo and containers)	10^{-10}
Drainage Gravel	10^{-3}

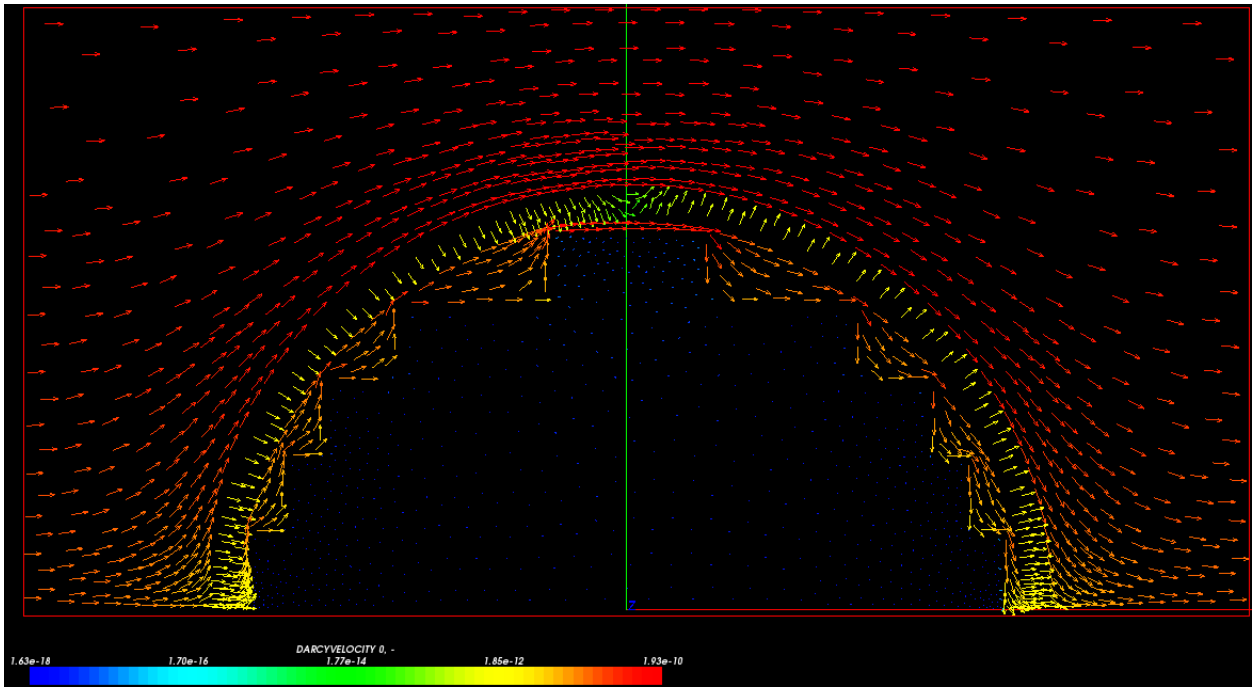

Figure 2. Darcy velocity field in m/s, no degradation, Alliances result.

Figure 2 shows the Darcy velocity field in the un-degraded state. The velocity field looks right, but when the Darcy velocities in the middle of the repository were compared, there were large discrepancies between the Alliances and HYDRUS results, as can be seen in Table 2.

Table 2. Darcy velocities (in m/s) in the middle of the repository.

Degradation	**Alliances**	**HYDRUS**
0	4.96×10^{-18}	1.74×10^{-13}
1	6.32×10^{-16}	5.44×10^{-13}
2	6.31×10^{-13}	1.19×10^{-10}

It turned out that the calculations for the SSA were simplified. In the attempts to calculate the hydraulic field and transport with HYDRUS, the team ran into problems. The difference between hydraulic conductivities of drainage gravel and concrete is 7 orders of magnitude. This caused numerical instabilities on the boundaries between these two materials, especially in the bottom right corner region of the repository. The team worked around this by assigning the hydraulic conductivity of silt to the drainage gravel, effectively substituting the drainage gravel with silt and reducing the difference to 3 orders of magnitude.

The hydraulic field was recalculated with the two hydraulic conductivities that were used for the SSA. As shown in Table 3, the comparison between Darcy velocities in the middle of the repository shows a much better agreement between Alliances and HYDRUS.

Table 3. Darcy velocities (in m/s) in the middle of the repository, 2 hydraulic conductivities.

Degradation	Alliances	HYDRUS	Ratio
0	3.95×10^{-14}	1.74×10^{-13}	4.4
1	1.94×10^{-13}	5.44×10^{-13}	2.8
2	1.18×10^{-10}	1.19×10^{-10}	1.0

4. Transport Calculations

The processes considered were advection, diffusion, dispersion, sorption and radioactive decay (including chains). The total radionuclide flux through the downstream (right) boundary of the modeled domain was measured, and the height and position of the flux peak compared to the results obtained with HYDRUS.

Of all the radionuclides in the inventory, only those whose half-lives are long enough that they stand a chance of exiting from the repository were considered. The full inventory and transport parameters for the considered radionuclides can be found in (Kalin et al., 2010).

The calculations in SSA stopped at 10^6 years because that was all that was required for the study and because of the slow calculation speed of HYDRUS. However, since peaks for some radionuclides were not reached, it was decided to run calculations up to 10^{10} years. By that time, all the radionuclides have either decayed or have been washed out of the system. It is assumed that the waste is uniformly spread between the containers and within each container and that it is completely dissolved in water at the beginning of the simulation. This is unrealistic, since in reality, the radionuclides would first need to be leeched from solids, but it is conservative. A previous unpublished study determined that all concentrations everywhere are far below solubility limits, so these are reasonable assumptions.

4.1. Mass Balance and Timestep Sensitivity Analysis

All the timesteps were performed using the fully implicit scheme (Press et al., 2007), which is unconditionally stable - one can increase timestep between successive steps (and decrease the real time for simulations) almost arbitrarily. But there's a trade-off in the loss of accuracy. To determine the optimum balance between computational speed and accuracy, a timestep sensitivity analysis was performed.

A strongly sorbed radionuclide, ^{129}I, was used to check accuracy. Decay was turned off, which means that at the end of the simulation, the cumulative flux (time integral of flux) exiting the model must match the amount put in the repository at the start of simulation.

Figure 3 shows the results of calculations. The vertical axis is the ratio of cumulative flux to starting amount. One can see that even with relatively large timesteps, the mass balance is off only by 15%. In most other cases the accuracy is better than 3%. For further calculations, such a discretization was chosen that the mass balance for ^{129}I is accurate to 0.5% (far above what's needed for the comparison), but still relatively little real time is needed to perform the calculations.

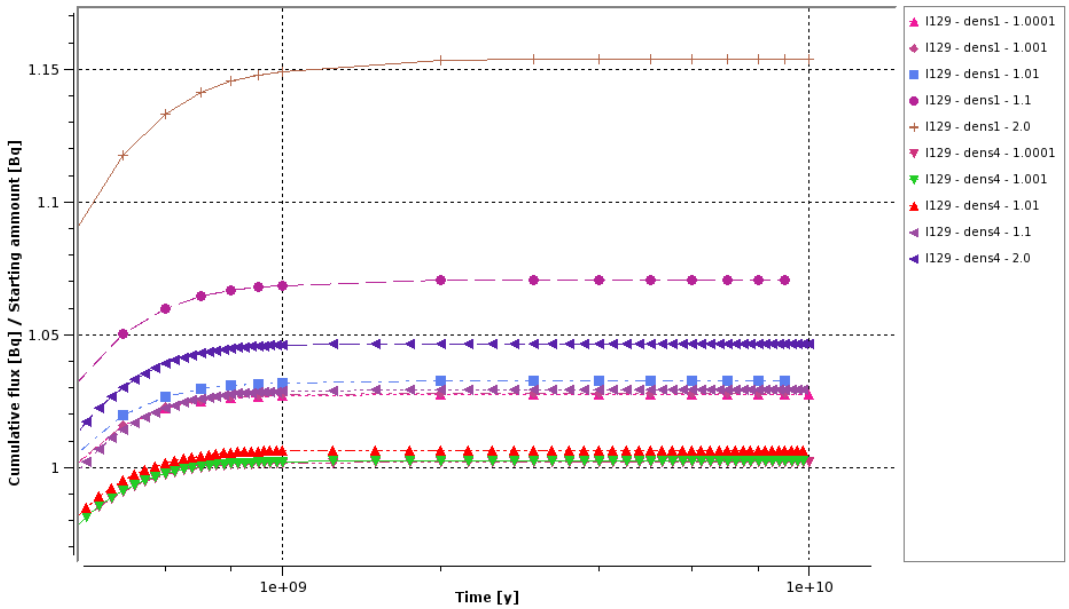

Figure 3. Timestep sensitivity.

4.2. Results and Comparison

First, the mass balances were checked by turning off the decay. All the cumulative fluxes were within 1% of the input activities.

Figure 4 shows the results with decay and Table 4 contains the numerical comparison between results obtained with Alliances and with HYDRUS. The "Ratio" column is the ratio of HYDRUS peak flux height versus Alliances peak flux height.

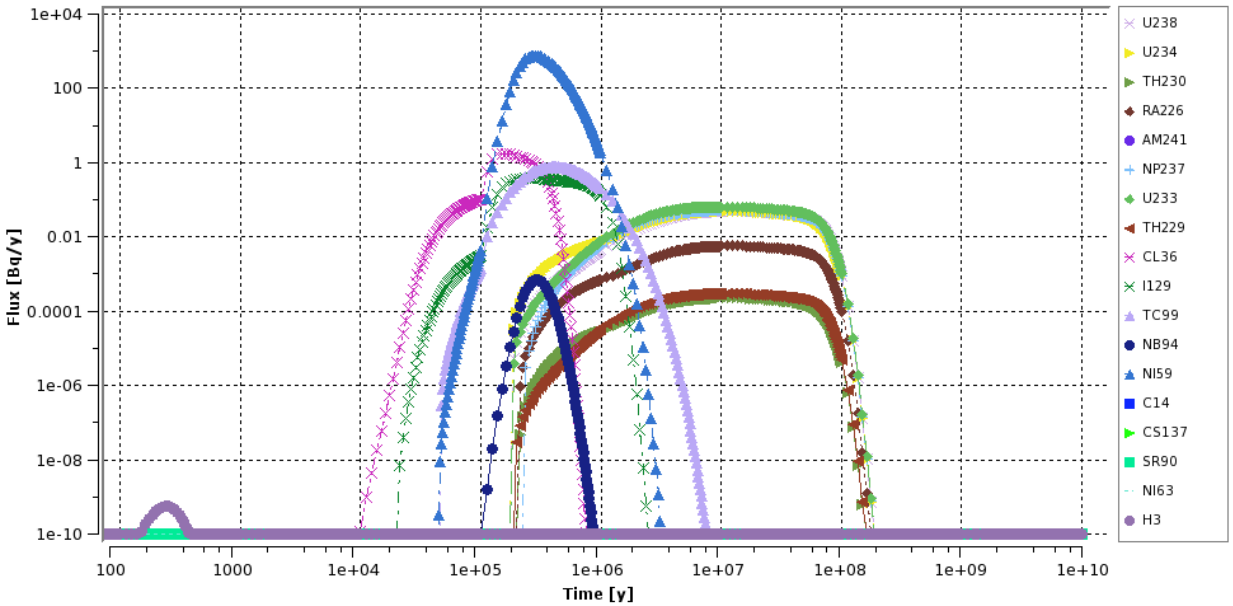

Figure 4. Transport results.

Table 4. Transport comparison.

		Alliances		HYDRUS		
RN	**Half+life [y]**	**Max [bq/y]**	**At [y]**	**Max [bq/y]**	**At [y]**	**Ratio**
^{238}U	$4.50\times10^{+09}$	5.03×10^{-02}	$1.25\times10^{+07}$	2.35×10^{-06}	$6.10\times10^{+05}$	4.68×10^{-01}
^{234}U	$2.45\times10^{+05}$	5.03×10^{-02}	$1.25\times10^{+07}$	5.83×10^{-06}	$6.45\times10^{+05}$	1.16×10^{-01}
^{230}Th	$7.68\times10^{+04}$	2.30×10^{-04}	$1.25\times10^{+07}$	2.23×10^{-08}	$7.61\times10^{+05}$	9.68×10^{-01}
^{226}Ra	$1.59\times10^{+03}$	5.74×10^{-03}	$1.25\times10^{+07}$	5.51×10^{-07}	$7.63\times10^{+05}$	9.60×10^{-01}
^{241}Am	$4.29\times10^{+02}$	8.86×10^{-52}	$5.50\times10^{+03}$			
^{227}Np	$2.14\times10^{+06}$	5.24×10^{-02}	$1.13\times10^{+07}$	4.55×10^{-08}	$3.96\times10^{+05}$	8.69×10^{-01}
^{233}U	$1.59\times10^{+05}$	6.49×10^{-02}	$1.13\times10^{+07}$	1.08×10^{-10}	$3.96\times10^{+05}$	1.66×10^{-01}
^{229}Th	$7.33\times10^{+03}$	2.95×10^{-04}	$1.13\times10^{+07}$	9.20×10^{-25}	$6.86\times10^{+02}$	3.11×10^{-01}
^{36}Cl	$3.10\times10^{+05}$	$1.78\times10^{+00}$	$1.50\times10^{+05}$	$3.66\times10^{+01}$	$1.64\times10^{+05}$	20.54
^{129}I	$1.59\times10^{+07}$	3.81×10^{-01}	$2.75\times10^{+05}$	8.30×10^{-01}	$3.23\times10^{+05}$	2.18
^{99}Tc	$2.10\times10^{+05}$	7.61×10^{-01}	$4.13\times10^{+05}$	5.06×10^{-01}	$7.35\times10^{+05}$	0.67
^{94}Nb	$2.00\times10^{+04}$	6.99×10^{-04}	$2.88\times10^{+05}$	6.59×10^{-03}	$2.81\times10^{+05}$	9.42
^{59}Ni	$7.59\times10^{+04}$	$7.70\times10^{+02}$	$2.88\times10^{+05}$	$1.40\times10^{+03}$	$3.37\times10^{+05}$	1.82
^{14}C	$5.70\times10^{+03}$	4.13×10^{-11}	$1.63\times10^{+05}$	1.42×10^{-17}	$9.44\times10^{+05}$	3.44×10^{-07}
^{137}Cs	$3.00\times10^{+01}$	3.54×10^{-181}	$2.00\times10^{+04}$			
^{90}Sr	$2.90\times10^{+01}$	2.31×10^{-41}	$7.00\times10^{+02}$			
^{63}Ni	$9.99\times10^{+01}$	6.28×10^{-32}	$1.38\times10^{+03}$			
^{3}H	$1.20\times10^{+01}$	5.47×10^{-10}	$2.50\times10^{+02}$	5.71×10^{-07}	$2.13\times10^{+02}$	1045.47

As noted earlier, the calculations in the SSA were done only for the first 10^6 years. Considering that the peaks in the case of the ^{238}U chain occur at 1.25×10^7y in Alliances results, these sets of results cannot be compared. Similarly in the case of the ^{241}Am chain, the peaks in Alliances results occur at 1.13×10^7y (except for the ^{241}Am itself, which rapidly decays into ^{237}Np), so again the results cannot be compared.

The fluxes of ^{137}Cs, ^{90}Sr, and ^{63}Ni are so low that they can be neglected; indeed, in the SSA they were not even considered.

The difference in ^{14}C peak fluxes is over 7 orders of magnitude, but this can be explained by decay. The peak in Alliances results occurs at 7.8×10^{5}y before peak in HYDRUS results, while the half-life of ^{14}C is 5.7×10^{3}y. The difference in peak times is thus 136 half-lives, and much more ^{14}C decays in the HYDRUS case.

In any case, the peak fluxes for ^{14}C are very low - on the order of 10^{-11}bq/y for Alliances and 10^{-17}bq/y for HYDRUS. At values this low, there's already a chance of numerical problems, not to mention that values this low are completely undetectable in nature and pose absolutely no problem as far as doses are concerned

Next are the ^{36}Cl and ^{94}Nb, where the HYDRUS results are around an order of magnitude higher. No immediate explanation was found for this.

Values for ^{129}I, ^{99}Tc and ^{59}Ni, however, match very well - within a factor of two. This is very good for the purposes of PA/SA, as ^{129}I and ^{59}Ni are exactly the two radionuclides that contribute the most to the total dose.

This leaves us with ^{3}H, where the difference is three orders of magnitude. ^{3}H is not sorbed, i.e., not retarded. Additionally, it has a short half-life of only 12y, so a small difference of 5% in peak position (at around 220 y) can alter the peak height by a factor of two. Recalling also that there's still an appreciable difference in hydraulic conductivities between different regions and that these differences caused problems in HYDRUS, it was decided to investigate the effect of mesh on ^{3}H transport.

5. Sensitivity to Mesh Density

To check sensitivity to mesh density, the whole calculation (from mesh generation onwards) was repeated with two finer meshes. Figure 5 shows the details of the mesh in the critical region — the bottom right corner of the repository.

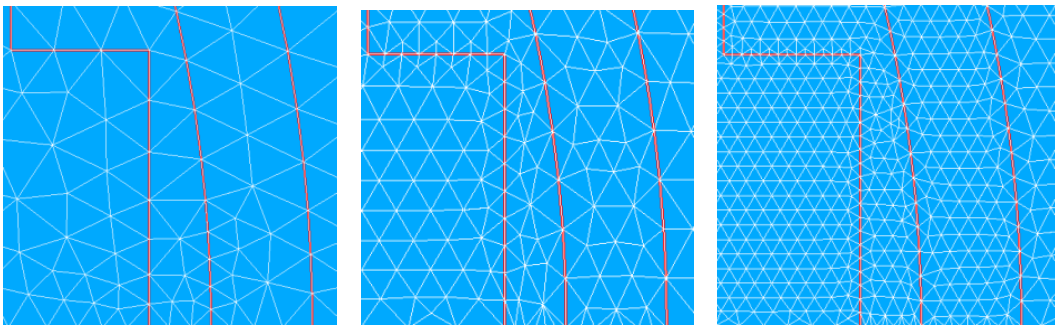

Figure 5. Mesh details.

From left to right the following meshes are depicted: "NetGen2D, very fine mesh" ("NGv", the mesh used for the calculations so far), "Triangles, fine mesh" ("TRf") and "Triangles, very fine mesh" ("TRv"). The calculations were run for 1000 years for ^{3}H and for 10^{10} years for ^{129}I.

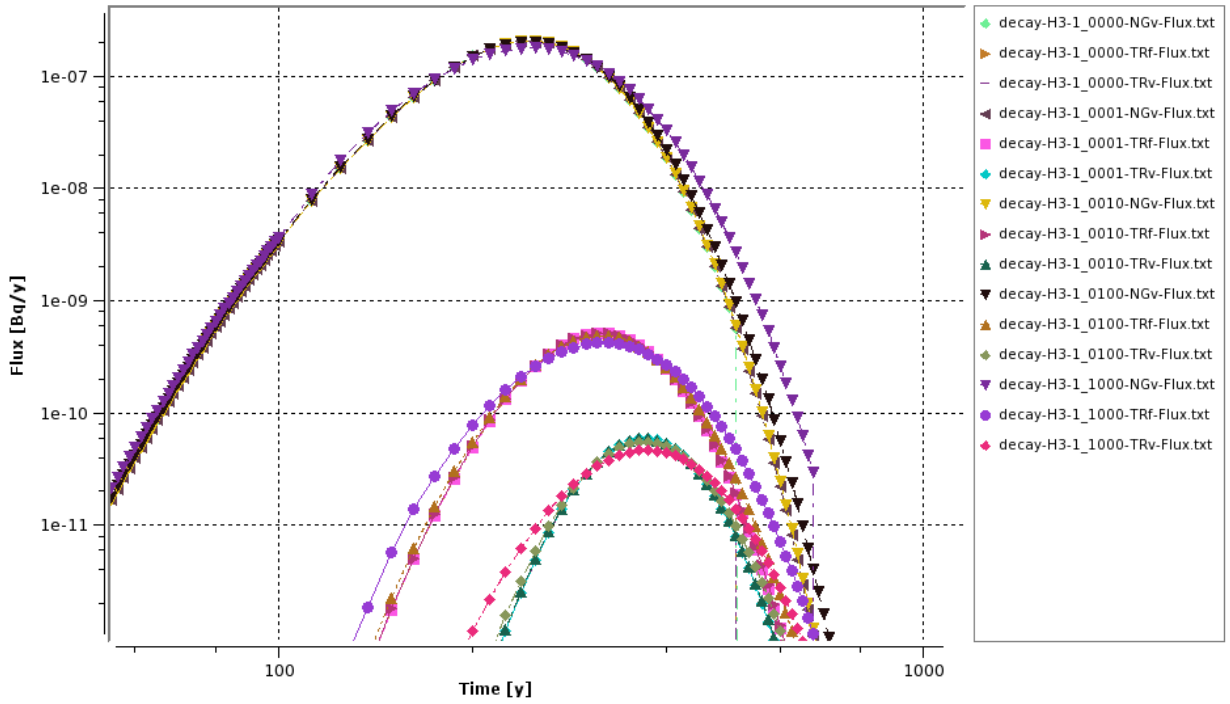

Figure 6. Mesh sensitivity for ^{3}H.

Figure 6 shows the effects of different meshes for ^{3}H. Different timestep discretizations were tried, but this did not appreciably affect the results. However, the position and height of the peak are strongly influenced by the mesh details. It seems that the finer the mesh is, the later the peak occurs. In other words, the coarser mesh appears to overestimate the Darcy velocities.

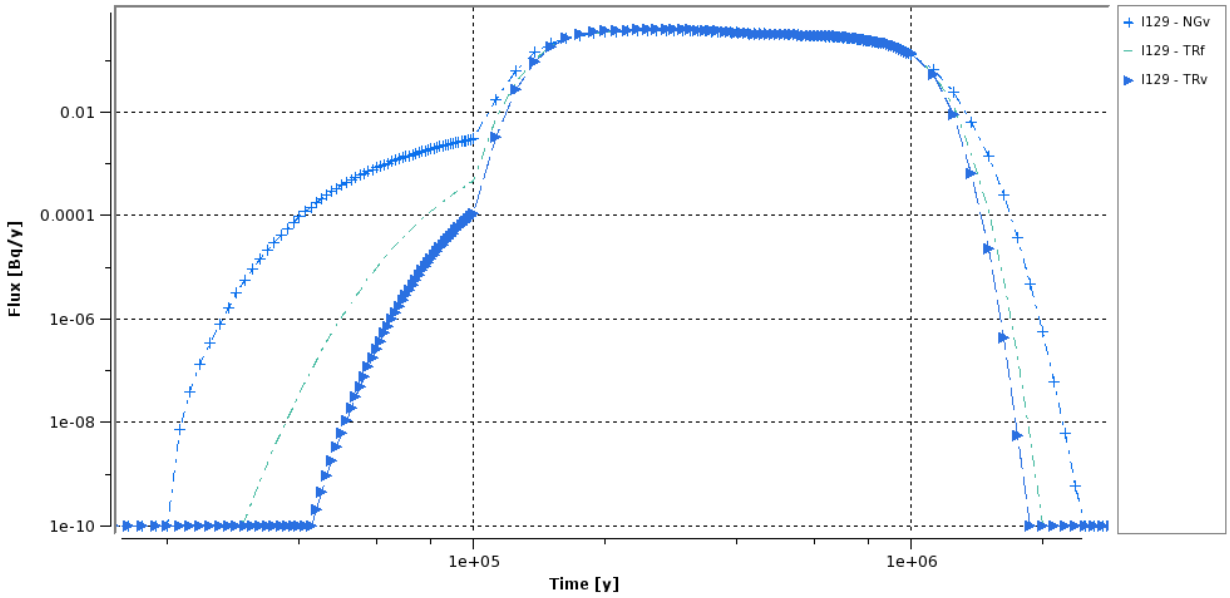

Figure 7. Mesh sensitivity for ^{129}I.

Figure 7 shows the effects of different meshes for ^{129}I. Note that in this case, only the default timestep discretization was used, as the calculation for the TRv mesh took almost five days on an Intel 2 GHz Core 2 Duo with 800 MHz FSB and 2 GB of memory.

The coarser mesh again has the effect of allowing a contaminant to appear earlier (and to dis-appear later). The position of the peak does not change (this cannot be verified in the figure, but was checked in the output data). This is understandable, as the majority of the contaminant appears after 10^5y, when the barriers have all degraded and there is no difference in hydraulic conductivities.

6. Conclusions and Further Work

From the study of mesh sensitivity we can conclude that, especially for the short-lived radionuclides, the mesh details can have a strong influence on the results. For future calculations, the density of the mesh should be increased in the critical areas (around the boundaries between materials) and kept about the same elsewhere. It would be impractical to use the TRv mesh, as the transport calculations for all radionuclides would take around three months.

On the other hand, for the significant radionuclides (^{59}Ni and ^{129}I), the results are very close to the ones obtained by HYDRUS, meaning that in some cases the coarser mesh may be adequate. In any case, the sensitivity to mesh details needs to be investigated further before performing "real" calculations.

It would also be interesting to run transport calculations with the hydraulic fields from three hydraulic conductivities and compare them with results with two hydraulic conductivities. If anything, the mesh details should be even more influential, as the differences between hydraulic conductivities are much bigger.

Last, but not least, Alliances had an enormous advantage in speed for this type of problem, i.e., the calculation of Darcy velocity field and transport in saturated conditions. It took a few days of calculations to produce results for 10^6 years with HYDRUS and a few hours to produce results for 10^{10} years with Alliances - an advantage of 10^5 in the ratio of real time to simulation time.

At the time when the comparison was performed, HYDRUS did not have any means to automate transitions between degradations - human intervention was necessary to save radionuclide concentration fields produced with one level of degradation, calculate Darcy velocity field for the next level of degradation, and use the saved concentration fields as the initial conditions for concentrations. Since Alliances uses Python (Python, 2013) as the underlying language, it was easy to automate the transitions, thus no human intervention was necessary to obtain final results. This capability was used in an unpublished study and allowed us to perform sensitivity analysis, not only to physical parameters, but also to the mesh, as it is possible to programmatically generate mesh .

References

HYDRUS 2D/3D for Windows, http://www.pc-progress.com/en/Default.aspx?HYDRUS-3d, retrieved on 27/03/2013.

Kalin, J., et al., Comparison of two numerical modelling codes for hydraulic and transport calculations in the near-field, *Nucl. Eng. Des.*, doi:10.1016/j.nucengdes.2010.04.026, 2010.

Montarnal, Ph, A. Bengaouer, C. Chavant and L. Loth, ALLIANCES: Simulation Platform for Nuclear Waste Disposal, proceedings of CMWR'06, Copenhagen, Denmark, http://proceedings.cmwr-xvi.org/getFile.py/access?contribId=205&sessionId=10&resId=0&materialId=paper&confId=a05, 2006.

Petkovšek, B., J. Kalin, J. Krivic, G. Omahen, P. Pavšič, R. Ratej. Izdelava ocene lastnosti in varnosti odlagališča v sklopu PVA za potencialno lokacijo Vrbina (T2226-1): revizija 1. Ljubljana: Zavod za grabeništvo Slovenije, 2006.

Press, W. H., S. A. Teukolsky, W. T. Vetterling and B. P. Flannery, Numerical Recipes: The Art of Scientific Computing, 3rd. ed., p.1045 Cambridge University Press, 2007.

Python Programming Language – Official Website, http://www.python.org/, retrieved on 27/03/2013.

Characterization and Modeling of Water Movement and Salts Transfer in a Semi-arid Region of Tunisia

Sabri Kanzari[1*], Mohamed Hachicha[1], Rachida Bouhlila[2], and Jorge Battle-Sales[3]

[1]*National Institute of Research of Rural Engineering, Waters and Forests of Tunis, Tunisia*
[2]*National Engineering School of Tunis, Modeling in Hydraulic and Environment Laboratory, Tunisia*
[3]*University of Valencia - Department of Plant Biology, Valencia, Spain*
[*]*Corresponding author, sabri.kanzari@gmail.com*

Abstract

The semi-arid region of Bou Hajla (Kairouan – Central Tunisia) is exposed to the risk of salinization of soils and aquifers. A characterization of water movement using TDR probes installed down to a depth of 4 m and salts transport using soil sampling was conducted to highlight this risk. At the same time, climatic parameters were monitored. The results were collected over a time period of approximately one year (from June 12, 2006 to May 08, 2007). Water movement and salts transport were simulated using the Hydrus-1D model. Inverse modeling was used to optimize the required soil hydraulic parameters. It was found that the simulated profiles of the volumetric water content and the electrical conductivity were close to those measured. The calculated *RMSE* values were low, indicating the reliability of Hydrus-1D to simulate the hydro-saline dynamics under field conditions.

Keywords: Soil, Salinization, Hydrus-1D, Aquifer, Semi-arid region, Tunisia.

1. Introduction

Besides the scarcity of water resources and their often poor quality in arid regions, there is a potential shortage of these resources that could be exacerbated by climate change; especially when irrigation is a determinant factor of the agricultural intensification (Mermoud et al., 2005; Khan et al., 2006). In several regions, this intensification led to the endoreisation of the hydropedologic watershed (Mhiri et al., 1998). In addition, the use of saline waters in these areas induces, in the short-term, salinization of soils and, over time, the salinization of aquifers. Modeling of water movement and solute transport is useful for analyzing the effects of irrigation with saline water and predicting its impacts on soils, crops, and groundwater, as well as for developing sustainable management practices for irrigation and fertilization (Gonçalves et al., 2006).

Considerable progress has been made in recent decades in numerical modeling (van Genuchten and Šimůnek, 2004). The most commonly used models use a deterministic approach, which is based primarily on the numerical solution of the Richards equation for variably-saturated water flow and the advection-dispersion equation for solute transport. These models are important tools for analyzing water and solute dynamics in the vadose zone. However, their use in the field remains limited (Suarez and Šimůnek, 1997; Gonçalves et al., 2006) due to the large amount of critical input data they require, such as the soil hydraulic properties, solute transport parameters, and climatic data.

In the context of arid regions that are essentially endorheic and depend on saline aquifers, it is necessary to prevent soil salinization and the contamination of these aquifers. Risk assessment of the salinization process is usually based on a quantitative approach, which requires an understanding of salts transport phenomena, which are driven by water movement through the unsaturated soil zone to the aquifer (Milnes and Perrochet, 2005).

Tunisia has limited water resources (4.8 billion of m^3), which are very often salted. Over half of available water resources, essentially those of Central Tunisia, have a salinity of more than 3 g l^{-1}. Besides the scarcity and poor quality, overexploitation of groundwater results in the depletion of these resources. In the region of Bou Hajla on the plain of Kairouan in Central Tunisia, salinization of soils and aquifers is a widespread phenomenon, making groundwater resources unsuitable for irrigation (with saline water of about 6 g l^{-1}) (Hachicha et al., 2005). In the short term, the impact of salinity on soils and crops occurs particularly in summer when evaporation is high. In the long-term, irrigation with saline water can degrade the overall system formed by the soil and groundwater.

The objectives of this paper are (a) to evaluate water movement and salt transport in the soil profile by studying variations of water and salt profiles as they depend on weather events, (b) to highlight the risk of salinization of the aquifers, and (c) to calibrate and validate Hydrus-1D (Šimůnek et al., 2005) for modeling the hydro-saline dynamics in the semi-arid context of Central Tunisia.

2. Materials and Methods

2.1. The Plot, Soil and Irrigation Water

The region of Bou Hajla is located about 30 km southeast of the city of Kairouan in central Tunisia. It is situated between a mountain range to the west and an area of sabkhas (salt flats) in the east and south, receiving surface waters and groundwater flowing from the mountains. The region is characterized as having an arid climate and a temperate winter. Rainfall is highly variable with an annual average of about 250 mm. Evapotranspiration is about 1600 mm per annum. An experimental plot (35°15'47.58''N; 10°4'17.16''E) was selected from a farmer's field about 9 km south of the village of Bou Hajla, having surface soils of sandy texture (0-0.6 m) and a high clay content to a depth of 2 m. Below this depth, the texture is sandy to sandy-silty (Table 1). Irrigation water comes from a surface well about 20 m deep, with a pumping rate of approximately 3 l s^{-1}, and a water quality corresponding to a *TDS* (total dissolved solids) of 6.5 g l^{-1}, an EC_i (electric conductivity of irrigation water) of 7 dS m^{-1}, and an *SAR* (sodium adsorption ratio) of about 7.5.

Table 1. Soil particle size analysis.

Depth (m)	Clay (%)	Loam (%)	Sand (%)	Texture
0 – 0.6	11.5	4.5	81.5	Sand
0.6 – 1.1	15.5	6.5	77.5	Sand clay
1.1 – 1.8	13.0	6.0	70.5	Sand clay
2 – 2.5	4.0	8.0	81.0	Sand
2.5 – 3	10.0	14.0	76.0	Sand loam
3 – 3.5	11.0	14.0	56.0	Sand loam
3.5 – 3.7	10	19.0	55.0	Sand loam
3.7 –4	17.0	22.7	47.5	Sand clay

2.2. Experimental Methods

The analysis of soil and aquifer salinization was performed by monitoring the soil water content using time domain reflectometry (TDR), and the soil salt content by using soil sampling.

- Water content monitoring: Water content was monitored using TDR probes installed at depths of 0.1, 0.5, 1, 1.5, 2, 3, and 4 m. Monitoring of the soil water profile in situ by the TDR sensors was launched at the time of installation (Apr/05/2006).
- Soil salt content monitoring: Soil salt profiles were monitored to a depth of 4 m. Soil salinity was determined using soil samples and the method of the soil diluted extract (soil/water ratio of 1/5). A relationship established by Hachicha (2005) has been used to convert $EC_{(1/5)}$ into the electrical conductivity of the saturated paste extract: EC_e=7.4*$EC_{(1/5)}$. Three salt profiles were observed on the following dates: December 26, 2006, February 2, 2007, and May 8, 2007.
- Monitoring climate parameters: An automated weather station from the Campbell Company has been installed in Bou Hajla since April, 2004. It includes a set of sensors and a communication interface for data transfer, which includes an anemometer for measuring speed and wind direction, a bucket rain gauge, a temperature sensor, a relative humidity device, and a pyranometer for measuring solar radiation. Monitoring of each parameter is done hourly, and daily data is obtained by averaging data collected over 24 hours. An ET_0 software (Raes, 2007) was used to estimate daily evapotranspiration (ET_0) from the collected data.

2.3. Input Parameters of Hydrus-1D

The soil hydraulic parameters were determined from the particle size distribution and the bulk density of the soil using the Rosetta model (Schaap et *al*., 2001) implemented in Hydrus-1D. Values obtained by pedotransfer functions were adjusted to volumetric water content and electrical conductivity values measured in the field using inverse modeling described by Šimůnek et al. (2005), as a method of optimizing parameters by matching results of numerical solutions with experimental data. Inverse modeling has been used for the determination of the shape parameters α and n, and the saturated hydraulic conductivity (K_s), the most sensitive parameters to water flow according to Lu and Zhang (2002). Initial values of the soil hydraulic parameters are presented in Table 2. The residual water content, θ_r, and the saturated water

content, θ_s, were estimated from the particle size distribution using the Rosetta (Schaap et al., 2001) pedotransfer functions.

As for solute transport parameters, dispersions coefficients (Disp) were taken from the literature (Vanderborght and Vereecken, 2007) for each type of texture. The adsorption coefficients (K_d) of salts were determined using the batch experiment for different layers. The upper boundary condition was set to the atmospheric boundary condition (BC) with a surface water layer, which requires an input of rainfall and evaporation calculated from climate data. Free drainage was used as the lower BC. Concentration flux BC was used as the upper boundary condition for solute transport. The results of the model were evaluated by both graphical and statistical methods. In the graphical approach, the measured and simulated volumetric water contents and soil salinities were plotted as a function of the soil depth at different times. The statistical approach involved the calculation of the root mean square error (*RMSE*):

$$RMSE = \sqrt{\frac{\sum_{i=1}^{n}(p_i - m_i)^2}{n}} \times \frac{1}{\overline{m}} \tag{5}$$

where p_i are the predicted values, m_i are the measured values, $\overline{m}$ is the average value of observed data, and n is the number of observations.

3. Results

3.1. Characterization of Water Movement and Salt Transport

All water content profiles have the same distinct shape, from which four layers can be distinguished: two layers with high variations of water contents and two layers with small changes in water contents (Fig. 1).

The layers with high variations in water contents are characterized by the following:

- In the topsoil, primarily between depths of 0 and 0.7 m, the soil water content varies between the field capacity (36%) and the permanent wilting point (14%) in the silty sand material. This layer is directly exposed to evaporation, rainfall, and irrigation (absent during this period).
- In the deep layer, located at a depth of approximately 2 m, the water content varies between the field capacity (35%) and the permanent wilting point (14%) in the silty clay material (Musy and Soutter. 1991). Variations in water contents in the deep soil layer can be explained by deep drainage and the influence of the clay material on top.

The layers with minimal changes in water contents correspond to the following:

- The soil stratum with a thickness of about 1 m, located between the topsoil and the soil layer starting at a depth of 2 m. This layer is a first zero-flux plane, which retains low levels of water. The texture is similar to the one found at the soil surface, i.e., a very permeable silty sand.

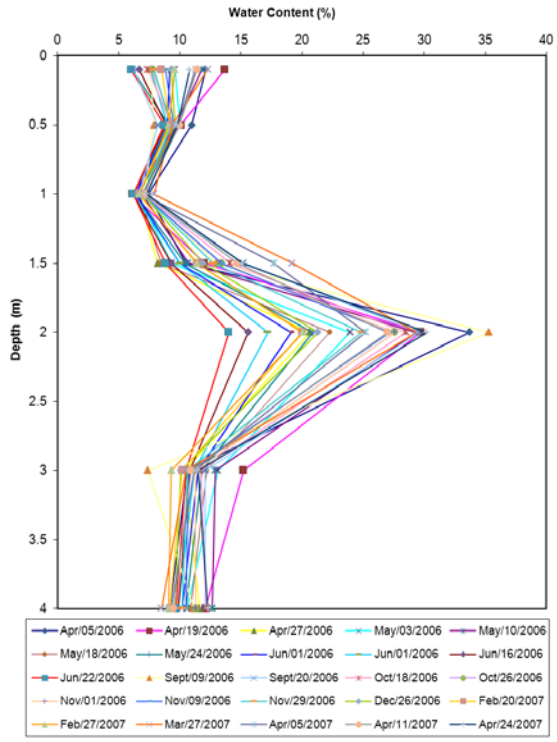

Figure 1. Soil water content profiles at different times.

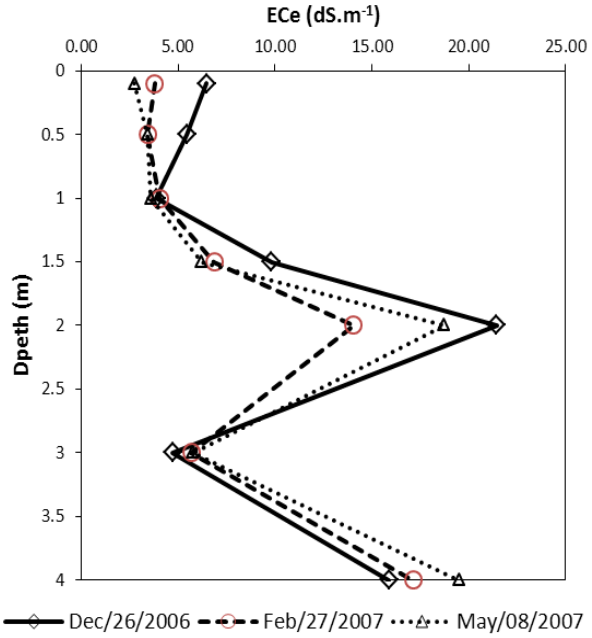

Figure 2. Variations of the soil salinity profiles at different times.

- The soil layer at a depth of about 3 m, located between the soil layer at 2 m and the one at depths greater than 4 m. This layer is a second zero-flux plane that moderately retains water. The texture is sandy-silty and is also quite permeable.

Five layers, corresponding to the four layers distinguished above in the examination of water contents, can be identified from the three available saline profiles (Fig. 2):

- In the topsoil, between depths of 0 and 0.7 m, salinity (EC_e) varies between 3 and 7 dS m^{-1}. The high salinity value is due to the winter planting season in 2006, when a barley crop was irrigated with water having a salinity of 7 dS m^{-1}. Fall rains appear to have completely leached salts.
- The soil layer located about 2 m deep is a very salted layer, with an EC_e higher than 20 dS m^{-1}. The silt-clay material reduces water infiltration, leading to the accumulation of salts. Rainfall also influences the content of salts in this layer, which allows for the transfer of salts to greater depths (Alimi-Ichola and Gaidi, 2006).
- The soil layer between depths of 0.7 and 1 m, which corresponds with the first zero-flux plane, is comprised of a highly permeable sandy-silty material, which does not appear to retain salt, but is a salts transfer zone.
- The soil layer down to a depth of 3 m, the second zero-flux plane with average salinity, seems to retain a portion of the salts arriving from the above saline layer. Although the soil layer located at a 4-m depth does not appear as a place for water retention, the EC_e reached excessive levels equivalent to the soil layer located at approximately 2 m. However, this soil

layer differs from the 2 m layer, because it remains salinized and accumulates salts, while the 2 m layer is desalinized. Although it is difficult to make further conclusions without further information regarding the constitution of the soil, it seems likely that a soil layer similar to that of the 2 m layer exists, playing a similar role in water retention and accumulation of salts. This soil layer seems to be located at a deeper level and may reach a degree of salt accumulation comparable to the previous level. The salt storage calculated for different dates shows an export of salts below the 4 m depth during the winter period (-0.623 t ha^{-1}). An infiltration test was accompanied by an import of salts, which is reflected in the saline storage on May 08, 2007. This highlights the risk of salinization of the aquifer.

3.2. Modeling the Hydrosaline Dynamics

Calibration of Hydrus-1D was performed for a time period of 134 days, with a daily time step (from December 26, 2006 to May 08, 2007). Inverse modeling was used in the calibration of Hydrus-1D against the water content profiles. The solute transport parameters (dispersion and adsorption coefficients) were adjusted several times in order to find an adequate match between the measured and simulated salinity profiles. The print times were set to 57^{th} and 134^{th} days to match the salinity profiles measured on February 27, 2007 and May 8, 2007, respectively. The initial profiles of the volumetric water content and soil electrical conductivity are those of December 26, 2006. The depth of the soil profile is 4 m. There are five distinct soil strata, identified through the characterization of the dynamics of water contents and salinities in Sections 3.1 and 3.2. The depths of different soil layers are as follows: 0 - 0.7, 0.7 - 1, 1 - 2, 2 – 3, and 3 - 4 m. Observation points were added to depths that correspond to the locations of TDR probes (0.1, 0.5, 1.5, 2, 3, and 4 m). The soil hydraulic parameters (θ_r, θ_s, α, n, and K_s) were determined by inverse modeling with a correlation coefficient, r^2, between measured data (volumetric water contents and electric conductivities) and modeling results, equal to 0.94. Optimized values of the dispersion and adsorption coefficients for each soil material are given in Table 2.

Validation of calibrated results was performed on the water content and electrical conductivity profiles measured on July 22, 2008. The same input data were used, and only the upper boundary conditions were changed. Values of evaporation and precipitation were extended to day 577 in this simulation.

Table 2. Input parameters of Hydrus-1D.

	Soil hydraulic parameters				**Solute transport parameters**			
Depth (m)	θ_r $cm^3\ cm^{-3}$	θ_s $cm^3\ cm^{-3}$	α cm^{-1}	n -	K_s $cm\ d^{-1}$	B_d $cm^3\ g^{-1}$	Disp cm^{-1}	K_d -
0-0.7	0.0543	0.372	0.0254	1.77	128.	1.38	17	0.10
0.7-1	0.0536	0.373	0.0195	1.62	97.	1.35	6	0 .1
1-2	0.0454	0.382	0.0474	1.61	142.	1.60	40	0.3
2-3	0.055	0.386	0.01892	1.37	21.	1.54	17	0.05
3-4	0.055	0.386	0.0173	1.375	54.	1.60	40	0.03

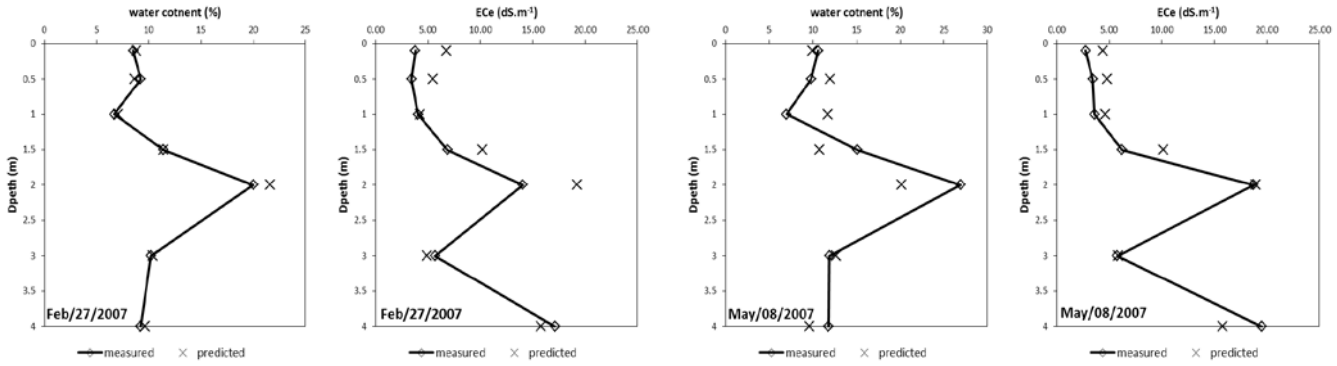

Figure 3. Measured and predicted water content and salinity profiles for calibration times.

The water content and salinity profiles measured and simulated for the two calibration times are shown in Figure 3. Calibrated results showed a strong correlation between simulated and measured values. The *RMSE* values calculated for the 57th and 134th days of simulation are 0.06 cm^3cm^{-3} and 0.028 cm^3cm^{-3} for water content profiles, and 0.35 dS m^{-1} and 0.26 dS m^{-1} for salinity profiles, respectively.

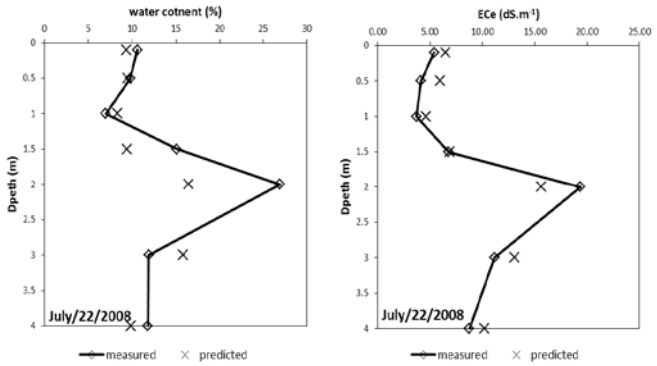

Figure 4. Measured and predicted water content and EC_e profiles on 577th day of the simulation.

Similar results were found in the validation stage. Good agreement between simulated and measured soil water contents and electrical conductivities were found for the 577th day of the simulation (Figure 4). The *RMSE* value for the water content profile was 0.043 cm^3cm^{-3}, and for the electrical conductivity profile it was 0.21 dS m^{-1}. These values are close to 0, which indicates the reliability of the model for the reproduction of water movement and transfer of salts under the field conditions.

3.3. Discussion

The Hydrus-1D model was able to simulate the dynamics of water and salts, as indicated by low values of *RMSE*. The inverse parameter estimation method was able to optimize the soil hydraulic parameters and to achieve a good correlation between measured and simulated data. However, it was unable to provide precise values of these parameters, due to the effects of spatial heterogeneity and the soil microstructure organization. An increase in the number of measurement points in time and space is suggested in order to better understand the variation of

soil water and salts contents (Köhne et al., 2009). The characterization of these parameters and the use of a hydro-structural approach for modeling the water and solute dynamics in the soil, as utilized in the Kamel model (Braudeau et al., 2009), can be a good alternative to our approach and could also demonstrate the limits of the approach used in this paper.

The salts balance, calculated at a depth of 4 m, is additive, which increases the risk of aquifer contamination. It is essential to monitor the groundwater level and the aquifer quality in order to determine possible contamination of groundwater by irrigation with saline water and to assess this risk. Also, the consideration of cultures and the design of some irrigation management scenarios for the farmers in the region are needed, in order to better assess the magnitude of the secondary salinization and to find appropriate management strategies (Forkutsa et al., 2009). Finally, it will be interesting to study the effects of torrential rains on the leaching of salts in the semi-arid region of Bou Hajla. These rains may have a regulatory role on the salts dynamic in the topsoil (Armstrong et al., 1998). All these recommendations will be considered in future research work and papers.

4. Conclusions

The effect of irrigation with saline water on soils and aquifers was studied in an experimental plot in Bou Hajla, central Tunisia. Deep characterization and simulation of salt and water content of the soil over the course of one year reveals the significant effects of infiltration after rainfall. As changes in climate affect soil evaporation at certain layers, it can be seen that the infiltration effect is dependent upon climate. The greatest effect is seen at depths greater than 3 m, and at a clay layer at 2 m, which is surrounded by sandy loam materials. This particular layer appears to play a major role in the movement of water and in the transfer of salts. Indeed, the salinity profiles highlight the phenomenon of reversibility of salts movement toward the soil surface, but also its accumulation in the clay layer where the value of electrical conductivity exceeds 20 dS m^{-1}. This layer reduces the transfer of salts into the aquifer, but does not seem to prevent them altogether. Thus, the region of Bou Hajla is subject to the salinization of its soils, which is further aggravated by aquifer over-exploitation and a decrease in aquifer piezometric levels. This may result in a reversal of the direction of groundwater flow, and thus exacerbate the intrusion of saline waters from surrounding sabkhas (salt flats).

References

Alimi-Ichola, I., and L. Gaidi, Influence of the unsaturated zone of soil layer on the solute migration, *Engineering Geology*, *85*, 2-8, 2006.

Armstrong, A. S. B., T. W. Tanton, and D. W. Rycroft, The effect of ped size. simulated rainfall duration and frequency on the leaching of salts from clay topsoils, *Agricultural Water Management*, *37*, 133-143, 1998.

Braudeau, E., R. H. Mohtar, N. E. Ghezal, M. Crayol, M. Salahat, and P. Martin, A multi-scale "soil water structure" model based on the pedostructure concept, *Hydrol. Earth Syst. Sci. Discuss.*, *6*, 1111–1163, 2009.

Forkutsa, I., R. Sommer, Y. P. Shirokova, J. P. A. Lamers, K. Kienzler, C. Tischbein, P. L. Martius, and G. Vlek, Modeling irrigated cotton with shallow groundwater in the Aral Sea Basin of Uzbekistan: II. Soil salinity dynamics, *Irrig. Sci.*, *27*, 319-330, 2009.

Gonçalves, M. C., J. Šimůnek, T. B. Ramos, J. C. Martins, M. J. Neves, and F. P. Pires, Multicomponent solute transport in soil lysimeters irrigated with waters of different quality, *Water Resources Research*, *42*, W08401, doi:10.1029/2006WR004802, 17 pp., 2006.

Hachicha, M., M. Mansour, S. Rejeb, R. Mougou, H. Askri, and J. Abdelgawad, Applied Research for the Utilization of Brackish/Saline Water in Center of Tunisia: water use. salinity evolution and crop response. salinity evolution and crop response, *Proceedings of International Salinity Forum*, Riverside, 25-27 April 2005, 213-216, 2005.

Khan, S., R. Tariq, C. Yuanlai, and J. Blackwell, Can irrigation be sustainable? *Agricultural Water Management*, *80*, 87-99, 2006.

Köhne, J. M., S, Köhne, and J. Šimůnek, A review of model applications for structured soils: a) Water flow and tracer transport, *Journal of Contaminant Hydrology*, *104*, 4-35, 2009.

Lu, Z., and D. Zhang, Stochastic Analysis of transient flow in heteregeneous variably saturated porous media: The van Genuchten-Mualem constitutive model, *Vadose Zone Journal*, *1,* 137-149, 2002.

Mermoud, A ., T. D. Tamini, and H. Yacouba, Impact of different irrigation schedules on the water balance components of an onion crop in semi-arid zone, *Agricultural Water Management*, *77*, 282-295, 2005.

Mhiri, A., J. Tarhouni, M. Hachicha, and F. Lebdi, Approche systématique des risques de salinisation par endoréisation anthropique, *Revue Etude et gestion des sols*, *5*(4), 257-268, 1998.

Milnes, E., and P. Perrochet, Direct simulation of solute recycling in irrigated areas, *Advances in Water Resources*, *29*, 1140-1154, 2005.

Raes, D., The ET0 calculator – Reference Manual, K. U. Leuven University, *Belgium*, 36 pp., 2007.

Schaap, M. G., F. J. Leij, and M. Th. van Genuchten, Rosetta: A computer program for estimating soil hydraulic parameters with hierarchical pedotransfer functions, *J. Hydrol.*, *251*, 163-176, 2001.

Šimůnek, J., K. Huang, M. Šejna, and M. Th. van Genuchten, The HYDRUS-1D Software Package for Simulating the One-Dimensional Movement of Water, Heat, and Multiple Solutes in Variably-Saturated Porous Media, International Ground Water Modeling Center, Colorado School of Mines, Golden, Colorado, 162 pp., 2005.

Suarez, D. L., and J. Šimůnek, UNSATCHEM: Unsaturated water and solute transport model with equilibrium and kinetic chemistry, *Soil Sci. Soc. Am. J.*, *61*, 1633–1646, 1997.

Vanderborght, J., and H. Vereecken, Review of Dispersivities for Transport Modeling in Soils, *Vadose Zone Journal*, *6*, 29–52, 2007, 2007.

van Genuchten, M. Th., and J. Šimůnek, Integrated modeling of vadose zone flow and transport processes, in *Unsaturated Zone Modelling: Progress, Challenges and Applications*, Frontis Ser. vol. 6, edited by R. A. Feddes, G. H. de Rooij, and J. C. van Dam, 37–69, Springer, New York, 2004.

Characterization and Modeling of Water and Salt Dynamics in a Sandy Soil Under the Effects of Surface Drip Irrigation

Sabri Kanzari[1*], Ibrahima Bâ[2], Mohamed Hachicha[1], and Rachida Bouhlila[2]

[1]*National Institute of Research of Rural Engineering, Waters and Forests of Tunis, Tunisia*
[2]*National Engineering School of Tunis, Modeling in Hydraulic and Environment Laboratory, Tunisia*
[*]*Corresponding author, sabri.kanzari@gmail.com*

Abstract

In the global context of water scarcity and salinization, there is a more pressing need for an efficient use of irrigation water through alternative, localized irrigation techniques. Experimental characterization and two-dimensional modeling of water movement and salts transport is important for managing such irrigation systems. However, experimental observations rarely accompany most numerical modeling studies of two-dimensional water flow and solute transport under drip irrigation. For this purpose, two sandy soil monoliths were instrumented with TDR probes to monitor water contents and Watermark sensors to monitor soil pressure heads. Soil salinity was measured using the method of the soil diluted extract (soil/water ratio of 1/5). Preliminary tests on small monoliths were carried out to determine soil hydraulic parameters of this soil. The two monoliths were saturated with either distilled or saline waters (with electrical conductivity of 4 dS m^{-1}). Experimental results show important vertical movement of water and the formation of a saline bulb around a depth of 20 cm.

Modeling of water movement and solute transport was performed with Hydrus-2D. Four sets of soil hydraulic parameters were evaluated against data from the monolith irrigated with distilled water. The best results were obtained with the parameters estimated using the RETC software and the retention curve data measured by the evaporation method. Model validation was performed on the data obtained from the monolith irrigated with saline water. Modeling results showed a good agreement between measured and predicted values. A scenario highlighting the effect of significant evaporation (8 mm day^{-1}) during an irrigation cycle revealed a potential for soil salinization with the formation of a saline bulb of medium salinity (3.5 dS m^{-1}) around the emitter. This bulb extends to a depth of 30 cm. In the long-term, after several cycles of irrigation, the salinity risk can be aggravated and affect the soil physical properties and consequently, crops production.

1. Introduction

In arid and semi-arid regions, soil salinity remains one of the most crucial and widespread environmental problems in agriculture, in addition to an increasing demand on water resources and water quality degradation. To cope with these twin problems, a wide range of irrigation systems, including surface drip irrigation, have been developed. Surface drip irrigation is widely used in agriculture in recent decades because of its many advantages in terms of water economy, water efficiency, and limitation of soil salinization. Thus, increasing water demand, water quality degradation, and soil salinization have aroused a great interest in understanding the processes governing water movement and solute transport in unsaturated soils through numerical modeling. This requires a reliable characterization of soil hydraulic properties and solute transport parameters. However, measuring these parameters is expensive and often difficult to implement.

Indirect methods and laboratory measurements are increasingly used by researchers. Meanwhile, several numerical models have been developed to study water and salts dynamics under drip irrigation (Al-Qinna and Abu-Awwad, 2001). For example, Skaggs et al. (2004) compared measured values of water contents under surface drip irrigation to those simulated using Hydrus-2D. Zhou et al. (2007) also compared simulated values of water contents by Hydrus-2D with those simulated by a two-dimensional model APRI under the dripper. However, these days there are only few studies that focus on soil salinization risks with surface drip irrigation. In Tunisia, there is also a lack of studies that focus on numerical modeling in the management of water and soil salinity under drip irrigation.

The objectives of this paper are to experimentally characterize and model two-dimensional water and solute dynamics in a sandy soil under surface drip irrigation and to study the effects of high evaporation on the distribution of water content and soil salinity.

2. Materials and Methods

2.1. Experimental Design and Measurements

Two monoliths of a sandy soil (93% sand, 4% silt and 3% clay) were used (Fig. 1). Their dimensions were: 60 cm along the *x*-axis, 60 cm along the *z*-axis, and 10 cm along the *y*-axis. In each monolith, given the symmetry of the problem, five TDR probes were placed on the right side at the following coordinates: one probe 45 cm below the emitter axis, two probes at a depth of 30 cm at $x = 0$ cm and $x = 15$ cm, and two probes at a depth of 10 cm depth at $x = 0$ cm and $x = 15$ cm. The dripper was placed in the center ($x = 0$ cm, $z = 0$ cm) at the surface of the monolith. The first monolith was irrigated at a flow rate of 0.316 L h^{-1} with fresh water (0.5 dS m^{-1}) and the second monolith at a flow rate of 0.490 L h^{-1} with saline water (4 dS m^{-1}). Water was applied for 4 h 45 min and 4 h 25 min to the first and second monoliths, respectively. The water content was monitored using TDR probes. The 2001 Trase model from the Soil Moisture Corp Company was used. The TDR probes were adapted to salinity and previously calibrated. The salinity of the soil was determined on soil samples using the method of the soil diluted extract (soil/water ratio of 1/5) at the same measurement points.

2.2. Modeling of Water Movement and Solute Transport

Only the right side of the monolith was simulated using Hydrus-2D (Šimůnek et al., 1999). The geometric domain is defined for the two monoliths as before: width = 30 cm and height = 60 cm. The emitter, represented by a quarter of a circle with a radius of 1 cm, is placed 1 cm below the origin of the coordinate system, i.e., in the center, 1 cm below the surface of the monolith. The simulations were carried out over periods of 2,685 min and 2,800 min, respectively, for the first and second monolith. The first monolith was used to evaluate the model with four different sets of soil hydraulic parameters, and the second to validate the model. As an initial condition, the average water contents measured by TDR probes in each depth were used. The average water content for the probes located at a depth of 10 cm was 12%. This value was assigned uniformly to the portion of the soil between the soil surface and a depth of 20 cm. The same approach was used for the following 20-cm thick soil layer by taking the average of probes located at a depth

of 30 cm. For the soil profile between depths of 40 and 60 cm, the water content value measured by a probe located at a 45-cm depth was used. The initial electrical conductivity was assumed to be uniform and equal to 0.5 dS m^{-1}.

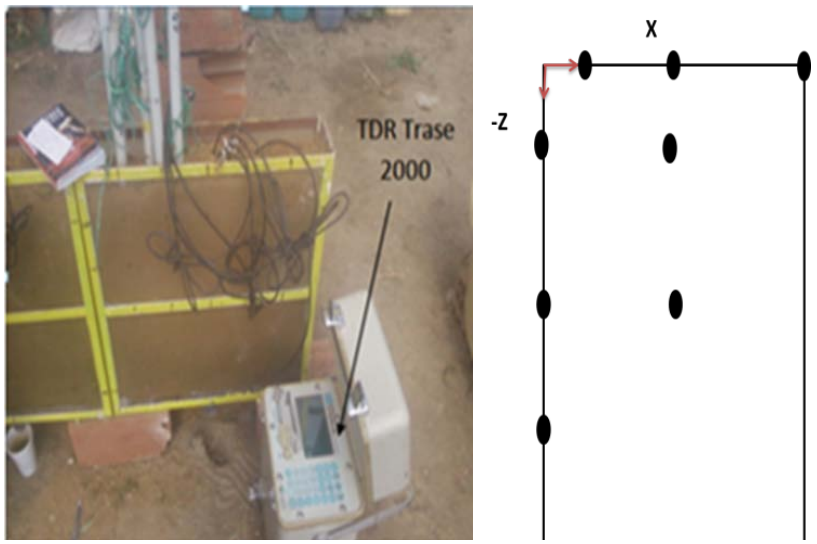

Figure 1. Monolith and measurement points.

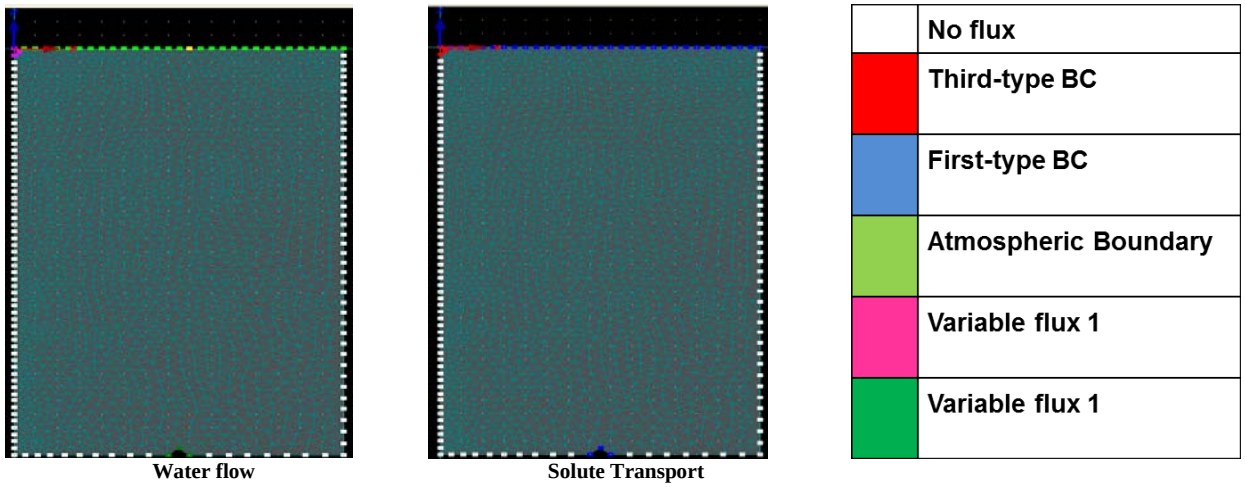

Figure 2. Water flow (left) and solute transport (middle) boundary conditions.

Soil hydraulic properties were estimated using either:

- the van Genuchten catalog (1991) (denoted as vG)
- Rosetta pedotransfer functions (Schaap at al., 2001) (denoted as R), and
- the evaporation method (Kanzari et al., 2012), using fresh water (0.5 dS m^{-1}) (denoted as FW) and saline water (4 dS m^{-1}) (denoted as SW).

Table 1. Soil hydraulic parameters determined by the four methods.

Source	θ_s (cm^3cm^{-3})	θ_r (cm^3cm^{-3})	α (cm^{-1})	n (-)	K_s ($cm\ d^{-1}$)
vG	0.43	0.0001	0.036	1.56	24.9
R	0.43	0.0001	0.145	2.68	24.9
FW	0.749	0.134	0.00959	4.34	712.8
SW	0.831	0.0444	001086	2.75	712.8

The results of model simulations were evaluated using graphical and statistical methods. In the graphical approach, the measured and simulated volumetric water contents and soil salinities were plotted as a function of soil depth using Surfer 8.0. The statistical approach involved the calculation of the root mean square error (*RMSE*).

3. Results

3.1. Characterization of Water Movement and Solute Transport

Figure 3 below shows the distribution of the water content and soil salinity for the two monoliths at different times. The vertical movement of water is more important than the lateral movement. For monolith 2, the salts bulb extends down to a depth of 30 cm.

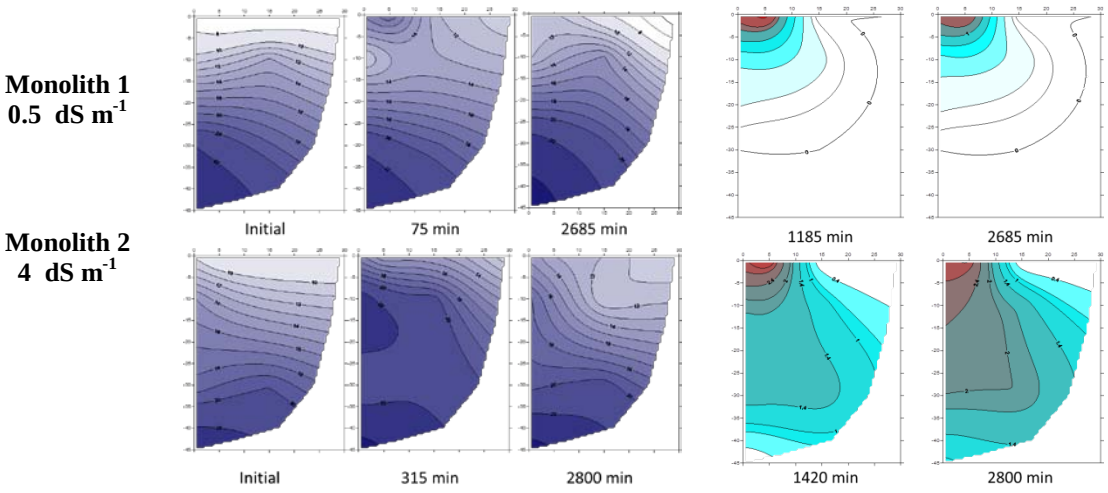

Figure 3. Measured water contents (left) and soil salinities (right) for the two monoliths.

3.2. Hydrus-2D Calibration

Hydrus-2D was calibrated against the experimental data on water and salts dynamics in monolith 1 using four different sets of hydraulic properties. According to the graphical and statistical evaluation, the parameters estimated using the evaporation method with fresh water provided the best agreement between predicted and measured values.

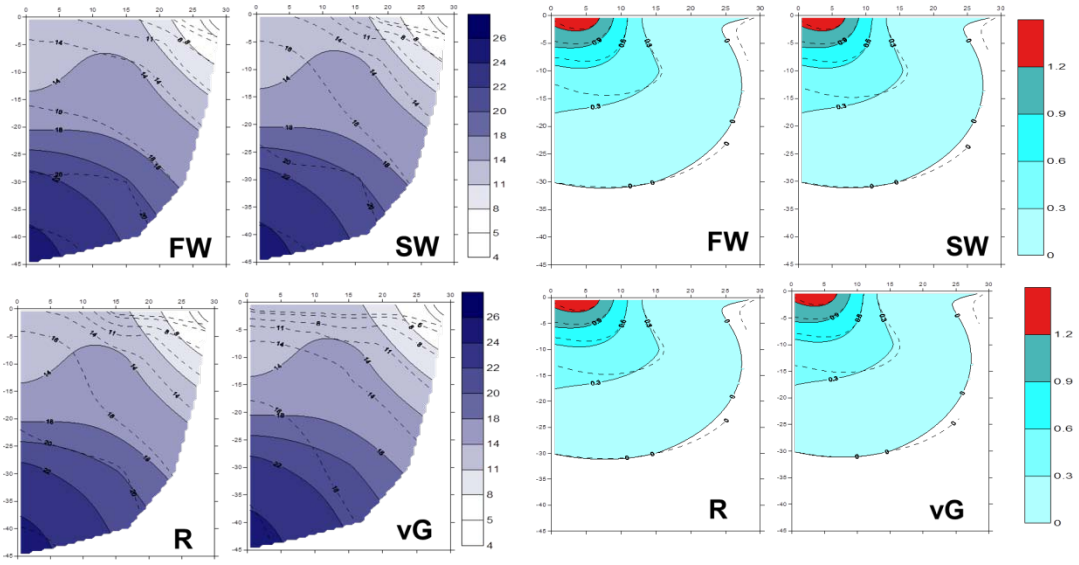

Figure 4. Measured and simulated (using four different sets of soil hydraulic parameters) water content and soil salinity distributions for Monolith 1.

Table 2. *RMSE* Values.

Value	FW	SW	R	vG
RMSE: Water Contents	0.140	0.206	0.199	0.256
RMSE: EC_e	0.379	0.372	0.388	0.374

3.3. Hydrus-2D Validation

Validation of Hydrus-2D was carried out using the experimental results from Monolith 2. Good agreement between measured and simulated values was obtained. The wetting bulb and salts accumulation were more important. At the end of the irrigation cycle, the soil was dry and low soil salinity around the dripper was observed.

3.4. Effects of High Evaporation

A scenario with a high evaporation rate (8 mm day^{-1}) was studied numerically using the same input parameters for monolith 2 during a 3 month long irrigation cycle (1 irrigation per week) with a 25 mm irrigation volume of 4 dS m^{-1} saline water. 25 mm is approximately the irrigation volume applied to the second monolith. The results show that at the end of the irrigation, soil salinity is low under the dripper down to a depth of about 10 cm and that salts migrated to a depth of 30 cm with an EC_e of 3.5 dS m^{-1}.

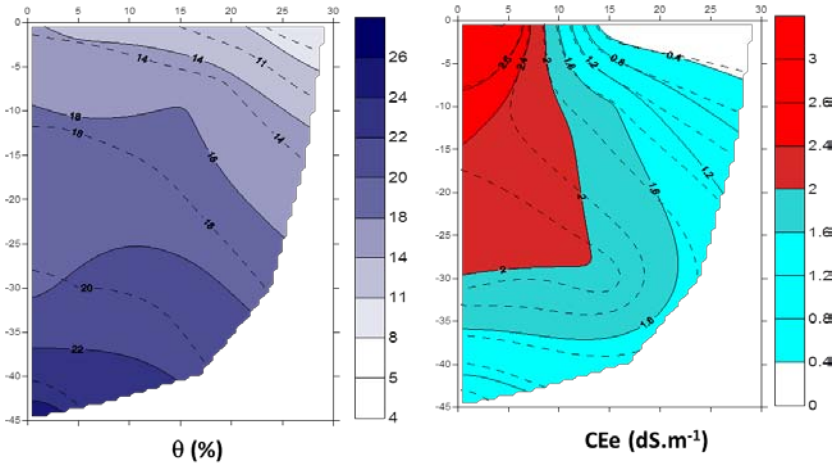

Figure 5. Simulated and measured water and salts distributions for Monolith 2.

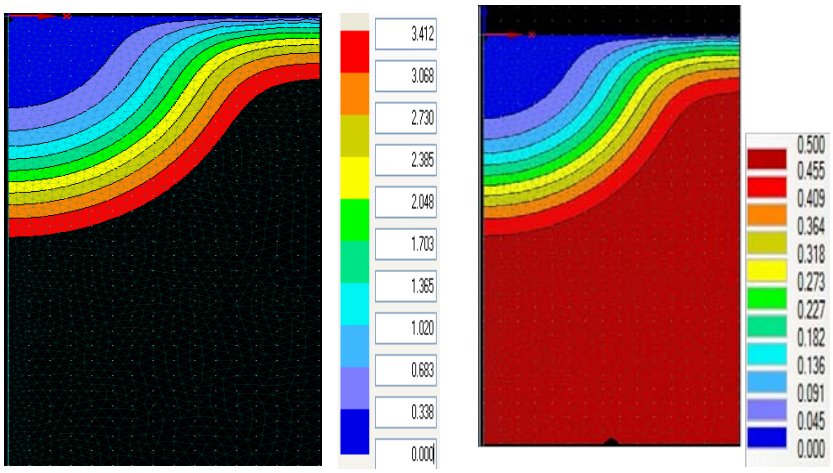

Figure 6. Soil salinity and water content profile under a high evaporation rate.

4. Conclusions

In this study, a good agreement between simulated and measured soil water contents and salt contents was found using Hydrus-2D. The effect of high evaporation (8 mm day^{-1}) during an irrigation cycle revealed a risk of soil salinization. In the long term, after several irrigation cycles, this risk can be aggravated and affect the soil physicochemical properties and crop growth.

References

Al-Qinna, M. I., and A. M. Abu-Awwad, Soil and water: Wetting patterns under trickle source in arid soils with surface crust, *Journal of Agricultural Engineering Research*, *8*(3), 301-305, 2001.

Kanzari S., M. Hachicha, and R. Bouhlila, Laboratory method for estimating soil water retention properties of an unsaturated soils, *Walailak Journal of Science and Technology*, *9*(4), 361-367 2012.

Schaap, M. G., F. J. Leij, and M. T. van Genuchten, ROSETTA: A computer program for estimating soil hydraulic parameters with hierarchical pedotransfer functions, *Journal of Hydrology*, *251*, 163-176, 2001.

Šimůnek J., M. Šejna, and M. Th. van Genuchten, The Hydrus-2D Software Package for Simulating Two-Dimensional Movement of Water, Heat, and Multiple Solutes in Variably Saturated Media, Version 2.0, *IGWMC-TPS-53*, International Ground Water Modeling Center, Colorado School of Mines, Golden, Colorado, 251pp., 1999.

Skaggs, T. H.,T. J. Trout, J. Šimůnek, and P. J. Shouse, Comparison of HYDRUS-2D simulations of drip irrigation with experimental observations, *ASCE Journal of Irrigation and Drainage Engineering*, *130*(4), 304–310, 2004.

Zhou Q., S. Kang, L. Zhang, and L. Fusheng, Comparison of APRI and Hydrus-2D models to simulate soil water dynamics in a vineyard under alternate partial root zone drip irrigation, *Plant and Soil*, *291*(1-2), 2007.

van Genuchten, M. Th., A closed-form equation for predicting the hydraulic conductivity of unsaturated soils, *Soil Sci. Soc. Am. J.*, *44*, 892-898, 1980.

Hydraulic Properties and Reduction of COD, Phosphorus and Nitrogen in a Sand Filter used for Greywater Treatment – Simulation and Verification

Susanna Ciuk Karlsson[1], Sahar Dalahmeh[2], Cecilia Lalander[3], and Håkan Jönsson[4]

Department of Energy and Technology, Swedish University of Agricultural Sciences, Uppsala, SWEDEN,
[1]susanna.ciuk.karlsson@slu.se, [2]sahar.dalahmeh@slu.se, [3]Cecilia.Lalander@slu.se, [4]Hakan.Jonsson@slu.se

Abstract

A vertical flow sand filter is a simple, effective and inexpensive system for treating greywater. The performance of sand filters treating artificial greywater was tested in the laboratory over a time period of 113 days. The filters consisted of columns (0.2 m diameter) filled with sand to a height of 0.6 m. The hydraulic properties of the filters were measured as well as the inflow and outflow concentrations of COD, BOD_5, total and phosphate phosphorus and total-, ammonia- and nitrate nitrogen. To get a better quantitative understanding of the treatment processes inside the filters, the HYDRUS-CW2D computer software was used to simulate the filters. The simulation of water flow through the filter could be well fitted to the measured flow by adjusting three model parameters: the air entry value, the pore size distribution index, and the pore connectivity parameter. For the COD reduction the simulated results agreed well with experimental data after an adjustment of the microbial lysis parameters of HYDRUS-CW2D. The simulated reduction of COD was 65 %, while a 72 % reduction was measured for the filters in the lab. Simulated reduction of phosphorus in the sand filter effluent corresponded well to the measured reduction: the simulated reduction of phosphorus was 72 % while the experimental filters achieved a 79 % reduction. Also, the simulated effluent concentrations of nitrate compared quite well to the measured values. Almost no reduction (4 %) in total nitrogen took place in the experimental filters, which agreed with the simulated reduction (0 %). For the phosphorus and nitrate components in HYDRUS-CW2D, so far no changes have been made to the default parameters.

1. Introduction

Physical water scarcity affects one fifth of the world's population today, and over the coming years water scarcity is likely to increase (Molden, 2007). About 90 % of the globally produced wastewater is left untreated, resulting in extensive pollution of natural water resources (Drechsel et al., 2010). An estimated 5.4 billion people have access to pit toilets or no toilet, which means their household wastewater is constituted of greywater (water from bath, shower and wash) (WHO, 2006). Greywater contains suspended solids, various household chemicals, oil, and to some extent, pathogenic microorganisms. Source-separated greywater is, however, usually less polluted than common wastewater or industrial wastewater (Morel and Diener, 2006). Greywater can, after suitable treatment, be a sustainable resource for irrigation, cleaning and strengthening the groundwater by infiltration (WHO, 2006). A vertical flow sand filter could prove to be a simple, effective and inexpensive system for treating greywater.

The performance of a sand filter treating artificial greywater was tested in the laboratory over a time period of 113 days. The filter consisted of a column (0.2 m diameter) filled with sand to a

height of 0.6 m. Duplicates of the sand filter were simultaneously tested. The filters were intermittently loaded three times a day; the loading was performed as a rapid flush emerging from sprinklers installed on top of the filter columns. The size and timing of the loadings were intended to correspond to the greywater yield of a typical rural community household in Jordan (Abu Ghunmi et al., 2008). The hydraulic properties of the filters were measured as well as the inflow and outflow concentrations of COD, BOD_5, total and phosphate phosphorus, and total-, ammonia- and nitrate nitrogen.

To get a better quantitative understanding of the treatment processes inside the filters, the HYDRUS-CW2D computer software (Langergraber and Šimůnek, 2005) was used to simulate the filters. The simulation results were compared to the measured observations for verification. The idea was to verify if HYDRUS-CW2D could simulate the capacity of a system using vertical flow sand filters for treatment of household greywater.

The simulation of water flow through the filter could be well fitted to the measured flow by adjusting three model parameters: the air entry value (α, [cm^{-1}]), the pore size distribution index (n, [-]), and the pore connectivity parameter (l, [-]). The simulation of reactive transport of nutrients within the filter compared quite well to the experimental observations. The simulated reduction of COD was 65 % while a 72 % reduction was measured for the filters in the lab (Table 5). Simulated reduction of phosphorus in the sand filter effluent corresponded well to the measured reduction: the simulated reduction of phosphorus was 72 % while the experimental filters achieved a 79 % reduction (Table 5). Also, the simulated effluent concentration of nitrate compared quite well to the measured values. Almost no reduction (4 %) in total nitrogen took place in the experimental filters, which agreed with the simulated reduction (0 %) (Table 5).

HYDRUS-CW2D was to a large extent successfully used to simulate the capacity of a system using vertical flow sand filters for the treatment of household greywater. Using HYDRUS-CW2D for running simulations has so far improved our understanding of the lab scale sand filters by elucidating that some water bypasses the filter by running alongside the filter column walls. The simulations also indicated that the biological activity and COD reduction mainly took place in the very top of the filter, thereby agreeing with experimental observations.

2. Materials and Methods

The experimental setup consisted of a column (0.2 diameter) filled with sand up to 60 cm. Several characteristics of the sand were measured (Table 1). To facilitate drainage and distribution of loadings, a 0.1 m layer of coarse gravel was placed at the bottom of the column. Some large pieces of gravel were placed on top of the sand to even out the distribution of incoming greywater. The loadings were set to be automatically conducted as short, intermittent bursts following the same schedule (Table 2) each day for 113 days.

The artificial greywater was prepared by mixing standard nutrient broth, dishwashing gel, shampoo, washing powder and maize oil with tap water. To include indigenous bacterial flora, a small amount of wastewater from a nearby Swedish municipal sewage treatment plant was also added. Various characteristics of the artificial greywater were measured (Table 3).

Table 1. Characteristics of the sand filter material used in the experiment set up (Dalahmeh et al., 2012).

Parameter	**Sand**
pH [SU]	7.9
Loss on ignition [%]	<1
Effective size [mm]	1.4
Uniformity coefficient [-]	2.2
Bulk density [kg m^{-3}]	1690
Particle density [kg m^{-3}]	2570
Porosity [%]	34
Surface area [$m^2 g^{-1}$]	0.136
Hydraulic conductivity [cm h^{-1}]	360

Table 2. Loading schedule for the irrigation of the filter.

Time	9:00	16:00	20:00
Amount of water [L]	0.7	0.1	0.2

Table 3. Characteristics of the artificial greywater used in the experiment set up (Dalahmeh et al., 2012).

Parameter	**Concentration in artificial greywater**
pH [SU]	7.8 ± 0.3
Electrical conductivity, *EC*, [µS cm^{-2}]	1960 ± 140
Biochemical oxygen demand, BOD_5, [mgL^{-1}]	425 ± 56
Chemical oxygen demand, COD, [mgL^{-1}]	890 ± 130
Total organic carbon, TOC, [mgL^{-1}]	304
Methylane blue activity substances, MBAS, [mgL^{-1}]	30 ± 10
Total phosphorus, Tot-P, [mgL^{-1}]	4.2 ± 0.2
PO_4-P, [mgL^{-1}]	2.1 ± 0.4
Total nitrogen, Tot-N, [mgL^{-1}]	75 ± 10

The filter effluent was collected in a bucket placed on top of a digital scale connected to a computer that recorded the weight once a minute. Weight and time recorded in this manner gave a thorough estimate of the cumulated effluent flow of the filter. Samples from both influent greywater and filter effluent were collected and analyzed regularly during the experiment.

To get a better quantitative understanding of the treatment processes inside the filter, the HYDRUS-CW2D computer software was used to simulate the filter. HYDRUS-CW2D was first used to model the hydraulics of the filter. A large number of simulations with varied empirical coefficients α, n, and l were carried out and compared to the experimental data. The areas between simulated curves and measured curve for cumulative water flow were calculated and used as a measure to determine the best fit (Table 4), as the least area indicates the best fit.

After a good fit to measured values had been established, the reactive transport of nutrients was also modeled. Some assumptions were made to adjust the concentrations of pollutants in the artificial greywater (Table 3) to values of the components in CW2D. COD in CW2D is divided into three fractions: readily biodegradable soluble COD (CR); slowly biodegradable soluble

COD (CS) and inert soluble COD (CI). It was assumed that CR equals measured BOD_5 (Table 3). BOD_u was taken into consideration to determine the CS fraction. BOD_u can be expected to equal the total amount of biodegradable COD (Ghunmi, 2011). It was assumed that BOD_u could be determined from the measured BOD_5 by dividing BOD_5 with a factor 0.7, according to literature values (Ghunmi, 2011). The calculation of CR, CS, and CI was thereafter done by:

$$CR = BOD_5 \quad (1)$$

$$CS = BOD_5/0.7\text{-}CR \quad (2)$$

$$CI = COD\text{-}CR\text{-}CS \quad (3)$$

To evaluate the performance of the filters, the efficient % reduction ($\%red$) was calculated for each parameter with available data by using:

$$\%red = \frac{c_{in} - c_{out}}{c_{in}} * 100 \quad (4)$$

where c_{in} is the influent concentration and c_{out} is the filter effluent concentration.

3. Results

3.1. Hydraulic Model

When configuring the empirical coefficients, different sets of values of coefficients α, n, and l, gave a broad variety to the outcome of the simulated cumulative flow. The values that were finally judged to give a good enough fit of simulated data onto the experimental data are presented in Table 4.

Table 4. Values of empirical coefficients used in the final simulation.

Empirical coefficients	**Estimated best fit values**
Air entry value, α [cm^{-1}]	0.06
Pore size distribution index, n [-]	2.68
Pore connectivity parameter, l [-]	1

Observations from the duplicate sand filter showed that there were some variations in the hydraulic behavior between the same type of filters (Figure 1). The simulated cumulative water flux was deemed as a good enough intermediate fit to the two sets of experimental data, although the simulated water flux deviated somewhat from the measured flux after the second loading (Figure 1).

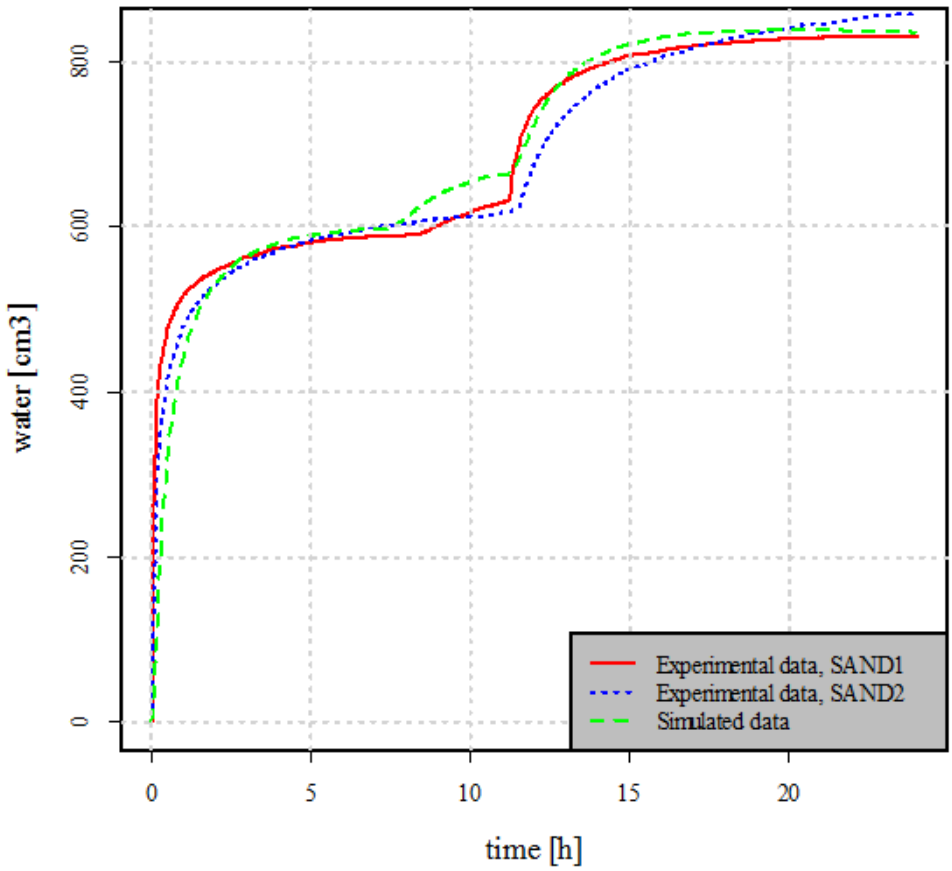

Figure 1. Cumulative water fluxes: simulated data compared to experimental data from the main sand filter (SAND1) and its duplicate (SAND2).

3.2. Reactive Transport Model

The simulated heterotrophic bacteria appeared to grow continuously (Fig. 2a) while the autotrophic bacteria appeared to reach a steady state of constant growth after 30 days. The simulated microorganisms appeared to be concentrated to the top 20 cm of the filter, with the largest concentrations (17.6 mg COD g^{-1} DW; 12 µg COD g^{-1} DW and 13 µg COD g^{-1} DW for heterotrophic bacteria, Nitrosomonas, and Nitrobacter, respectively) at the very top of the filter (Figure 2b).

From the empirical experiment, the measured values of effluent pollutant concentrations were considered as steady state values. To compare measurements with simulated observations, the mean values of the simulated effluent pollutant concentrations were calculated for days 56-113 (Table 5). CR, CS, and CI concentrations in the simulated inflow (Table 5) were calculated based on the concentrations in the artificial greywater (Table 3), according to equations 1-3.

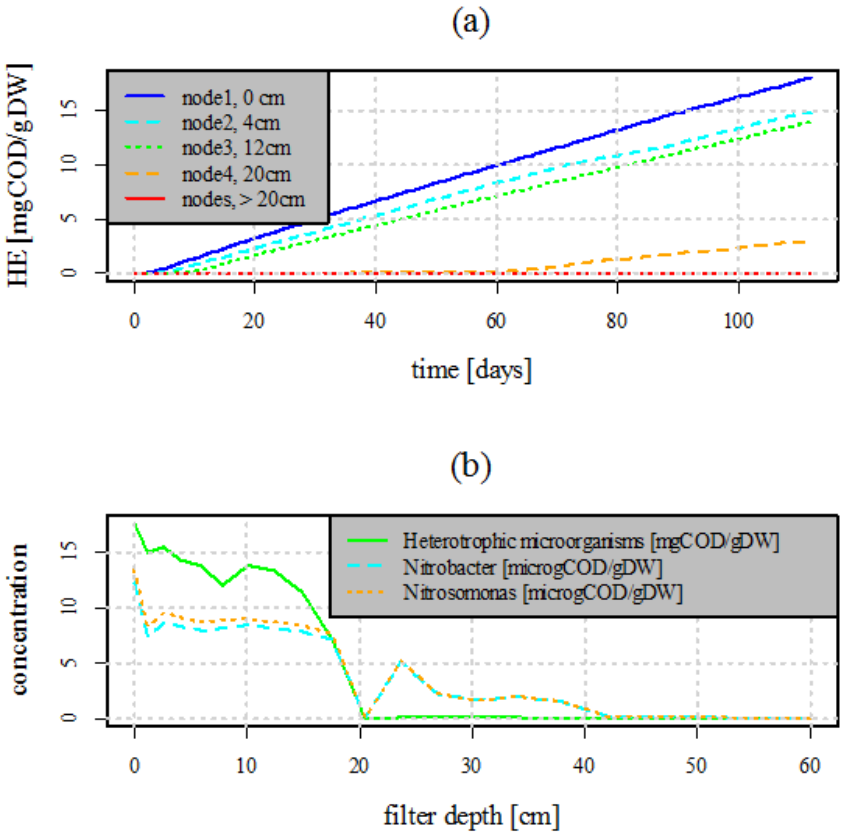

Figure 2. (a) Growth of heterotrophic microorganisms at different depths in the filter, 0 cm being the top of the filter. (b) Amount of microorganisms over a filter depth during day 113 of the simulation.

Table 5. Simulated and measured mean values of the filter effluent concentrations of pollutants (from simulation timespan 56-113 days).

Parameter	**Simulated greywater concentrations [mgL^{-1}]**	**Measured filter effluent concentrations [mgL^{-1}]**	**Simulated filter effluent concentrations [mgL^{-1}]**	**Measured *%red* [%]**	**Simulated *%red* [%]**
CR	425	108	0	75	99.9
CS	180	46	0	74	100
CI	278	91	308	67	-
COD	885	245	308	72	65
IP	2	0.4	0.5	83	78
TP	4.2	0.9	1.2	79	72
NO3N	1	57	47	-	-
NH4N	0.5	4	0.1	-	79
NO2N*	-	-	0	-	-
TN**	75	72	-	4	-

* NO2N was not measured

**simulated TN could not be established within the model

4. Discussion

The simulation of flow dynamics was considered successful since a close fit of simulated and measured data was achieved for the cumulative flux. It was demonstrated that calibration of empirical coefficients α, n, and l was necessary to achieve a good fit. The coefficients were chosen by matching the curves of simulated and measured cumulative fluxes, similar to a study of the simulation of a subsurface vertical flow constructed wetland for CSO treatment (Dittmer et al., 2005). It is possible that a measured retention curve for the sand used as filter material could provide further insight on which empirical coefficient values to use (van Genuchten, 1980).

The measurements on the physical filter indicated that the filter operated under pseudo steady state conditions because the observed concentrations of pollutants in the filter effluent did not vary from day to day. However, the simulations demonstrated constant growth of heterotrophic microorganisms in the filter (Fig. 2a), which contradicts the observed behavior of the physical filter. In order to calibrate the simulated growth of biomass, some quantitative measurements of biomass should be performed on the physical filter. A study of microbial biocoenosis has been carried out on vertical subsurface flow constructed wetlands treating municipal wastewater (Tietz et al., 2006). The result of the study by Tietz et al. (2006) was used further in a comparative study of measured and simulated distributions of microbial biomass in subsurface vertical flow constructed wetlands (Langergraber et al., 2007). In the study, carried out by Langergraber et al. (2007), different heterotrophic lysis rate constants were varied to fit simulated data to measured data of biomass, which proved successful. A similar attempt to calibrate the simulated biomass growth in vertical flow sand filters treating greywater would be a suitable continuation in order to correct the current model.

Regardless of the inconsistency of the constant growth of biomass in the simulations, the simulated performance matched the performance of the physical filter quite well. The simulated reduction of COD was 65 % while a 72 % reduction was measured for the physical filter (Table 5). Simulated reduction of phosphorus in the sand filter effluent corresponded well to the measured reduction: the simulated reduction of phosphorus was 72 %, while the physical filter achieved a 79 % reduction (Table 5). Also, the simulated effluent concentrations of nitrate compared quite well to the measured values. Almost no reduction (4 %) in total nitrogen took place in the physical filter, thereby agreeing with the simulated reduction (0 %) (Table 5).

References

Abu Ghunmi, L., G. Zeeman, J. V. Lier, and F. Fayyed, Quantitative and qualitative characteristics of grey water for reuse requirements and treatment alternatives: The case of Jordan, *Water Science & Technology*, *58*(7), 1385-1396, 2008.

Dalahmeh, S., M. Pell, B. Vinnerås, L. Hylander, I. Öborn, and H. Jönsson, Efficiency of bark, activated charcoal, foam and sand filters in reducing pollutants from greywater, *Water Air Soil Pollut.*, Published online: 29 March 2012.

Dittmer, U., D. Meyer, and G. Langergraber, Simulation of a subsurface vertical flow constructed wetland for CSO treatment, *Water Science & Technology*, *51*(9), 225-232, 2005.

Drechsel, P., C. A. Scott, L. Raschid-Sally, M. Redwood, and A. Bahri, A. (eds.), Wastewater irrigation and health: Assessing and mitigating risks in low-income countries, *Earthscan-IDRC-IWMI*, UK, *404*, 475-478, 2010.

Ghunmi, L. A., G. Zeeman, M. Fayyad, and J. B. van Lier, Grey water biodegradability, *Biodegradation*, *22*, 163-174, 2011.

Langergraber, G. and J. Šimůnek, Modeling variably-saturated water flow and multi-component reactive transport in constructed wetlands, *Vadose Zone Journal*, *4*(4), 924-938, 2005.

Langergraber, G., A. Tietz, and R. Haberl, Comparison of measured and simulated distribution of microbial biomass in subsurface vertical flow constructed wetlands, *Water Science & Technology*, *56*(3), 233-240, 2007.

Molden, D. (Ed), Water for food, Water for life: A Comprehensive Assessment of Water Management in Agriculture, *Earthscan/IWMI*, p. 11, 2007.

Morel, A, and S. Diener, Greywater Management in Low and Middle Income Countries, Sandec, Eawag, Switzerland, ISBN: 978-3-906484-37-2, 2006.

Tietz, A., A. Kirschner, G. Langergraber, K. Sleytr, and R. Haberl, Characterization of microbial biocoenosis in vertical subsurface flow constructed wetlands, *Science of Total Environment*, *380*, 163-172, 2007.

van Genuchten, M. Th., A closed-form equation for predicting the hydraulic conductivity of unsaturated soils, *Soil Science Society of America Journal*, *44*, 892-898, 1980.

WHO, Guidelines for the safe use of wastewater, excreta and greywater, *Vol. IV. Excreta and Greywater Use in Agriculture*, Geneva: World health organization, 2006.

Predicting Soil CO_2 Dynamics in Arable Land of Andisol in A Western Suburb of Tokyo

Chihiro Kato[1], Taku Nishimura[1], Hiromi Imoto[1], and Tsuyoshi Miyazaki[2]

[1]*Graduate School of Agricultural and Life Sciences, The University of Tokyo, Tokyo, JAPAN,*
kato@soil.en.a.u-tokyo.ac.jp
[2]*Professor Emeritus at the University of Tokyo, Tokyo, JAPAN*

Abstract

Recently, carbon capture and storage by soils is recognized as an important function of agricultural fields. When discussing global warming mitigation such as proper agricultural practices and/or an appropriate depth of composting in agricultural lands for soil carbon storage, not only CO_2 efflux, but also profiles of CO_2 concentrations in soil air are important. In this study, we evaluated the performance of the SOILCO2 model in predicting soil CO_2 dynamics, especially CO_2 concentrations at various depths in an arable bare land of Andisol. We attempted to experimentally determine two soil parameters required for the CO_2 production model, the optimal CO_2 production rate and the parameter of a depth-dependent CO_2 production function, by measuring CO_2 efflux from the surface and a vertical distribution of concentrations of dissolved organic carbon, respectively. Soil CO_2 concentrations, water contents, and temperatures were continuously monitored for about a half year at three different depths. Simulated results were compared with the observed data for model validation. We concluded that the soil parameters were properly determined, especially for the upper layer, and that the soil CO_2 dynamics in the arable bare land could be well predicted using the SOILCO2 model.

1. Introduction

Soil retains two to three times more carbon (C) than the atmosphere (Sundquist, 1993). Soil is an important source and sink of C, and soil respiration plays an important role in soil CO_2 dynamics. Recently, it has become more and more important and necessary to predict the soil CO_2 dynamics in agricultural lands. Carbon capture and storage (CCS) are recognized as important functions of agricultural fields, and the capacity for the C storage of agricultural lands has been discussed. For example, the application of compost to agricultural fields has been attempted to increase the C storage in soils (Ministry of Agriculture, Forestry and Fisheries of Japan, 2008). Effects of various management practices, such as drainage, tillage, and fertilizer applications on the soil organic C dynamics have been investigated in various parts of the world (e.g., Lal and Kimble, 1997).

When predicting the soil C storage and discussing global warming mitigations such as proper agricultural practices and/or an appropriate depth of composting in agricultural lands, both CO_2 fluxes and profiles of CO_2 concentrations in soil air are important. However, most previous studies dealing with modeling of soil CO_2 dynamics have focused on predicting the soil CO_2 efflux, and few have evaluated the model performance with respect to simulated profiles of soil CO_2. It is mainly because of the two following difficulties remaining in simulating vertical distributions of soil CO_2 concentrations.

First, there is no acceptable way of determining parameters describing the soil CO_2 production and transport. There are many ways to empirically describe the vertical distribution of the CO_2 production rate, which varies with land use such as agricultural fields and forests. Uncertainty in soil hydraulic parameters were also said to have strong impact on simulated CO_2 dynamics, because the volumetric water content directly affects the soil respiration rate, and indirectly CO_2 diffusion (Buchner et al., 2008).

Second, lack of monitoring data for model validation has been problematic for predicting soil CO_2 dynamics. Validation of models simulating soil CO_2 dynamics has been done mainly using the data of CO_2 flux from the soil surface rather than continuously monitored data of CO_2 at various depths. Recently, a gas permeable resin, which allows gas to pass but excludes liquid water from outside, has been used to monitor soil gas without disturbing the soil air phase. Kato et al. (2013) reduced the size and improved responsiveness of the CO_2 monitoring system to conduct continuous monitoring at various depths.

The purpose of this study is to predict the soil CO_2 dynamics, which includes both CO_2 fluxes from the soil surface and profiles of CO_2 concentrations in the arable bare land in the western suburb of Tokyo, using the SOILCO2 module of HYDRUS-1D (Šimůnek et al., 2008). In this study, we tried to experimentally determine two CO_2 production parameters dealing with the amount and distribution of the respiratory substrate in soil. Continuous monitoring of soil CO_2 concentrations was conducted over half a year to obtain data for evaluating the model performance. Soil water contents and temperatures were also monitored and simulated results were compared with observed values.

2. Materials and Methods

2.1. Study Site and Field Monitoring

For model validation, continuous monitoring was conducted at the Institute for Sustainable Agro-ecosystem Services of the University of Tokyo (ISAS-UT; N 35°44′13″, E 139°32′30″) in Nishi-Tokyo City, a western suburb of Tokyo, for approximately half a year from 28th Aug., 2010 to 31st March, 2011. The soil between depths of 0 and 35 cm was Kuroboku andisol (soil texture: Loam), and between depths of 35 and 100 cm was Tachikawa loam andisol (soil texture: Light Clay). A 10-m^2 area was kept bare until the end of the monitoring using weed management.

Time-domain reflectometry (TDR) sensors (self-made) and copper-constantan type thermocouples were used to monitor soil water contents and soil temperatures, respectively, at depths of 3, 5, 7, 10, 20, 30, 50, and 80 cm. TDR sensors were connected to the TDR100 Time-domain reflectometer (Campbell Scientific Inc., United States) and both TDR100 and thermocouples were connected to a CR10X data logger (Campbell Scientific Inc., United States) (Kato et al., 2011). Non-Dispersive Infrared type CO_2 sensors GMM 221 (Vaisala Co. Ltd., Finland) were used for measuring soil CO_2 concentrations at depths of 10, 20, and 50 cm. Each CO_2 sensor (GMM221) was sealed in a gas-permeable silicone tube (Kato et al., 2013). These CO_2 sensors were connected to a CR1000 data logger (Campbell Scientific Inc., United States).

All data were collected every 20 minutes. CO_2 efflux from the surface during daytime was measured with a closed chamber method in both summer (28th Jul., 2011) and winter (20th Dec., 2010). Meteorological data was obtained from the ISAS-UT and AMeDAS (Automated Meteorological Data Acquisition System, Japan Meteorological Agency) weather stations located in the city of Fuchu, about 10 km south from the experimental field.

2.2. Numerical Models

The SOILCO2 model first calculates soil water flow and heat transport since the CO_2 production is sensitive to both soil water contents and soil temperatures. The governing equation for one-dimensional water flow in bare fields is the Richards equation. Heat transport can be described with the convection-dispersion equation when the effects of water vapor diffusion are neglected:

$$\frac{\partial C_p T}{\partial t} = \frac{\partial}{\partial z}\left[\lambda(\theta_w)\frac{\partial T}{\partial z}\right] - C_w\frac{\partial q_w T}{\partial z} \tag{1}$$

where C_p and C_w are volumetric heat capacities of the moist soil and liquid water, respectively. λ is the thermal conductivity of the moist soil and q_w [L T^{-1}] is soil water flux.

In SOILCO2, the one-dimensional CO_2 transport in bare fields can be described as follows:

$$\frac{\partial\left(c_a\theta_a + c_w\theta_w\right)}{\partial t} = \frac{\partial}{\partial z}\theta_a D_{dif\_s}\frac{\partial c_a}{\partial z} + \frac{\partial}{\partial z}\theta_w D_{disp\_s}\frac{\partial c_w}{\partial z} + \frac{\partial}{\partial z}q_w c_w + P \tag{2}$$

where c_a and c_w are the volumetric concentrations of CO_2 in the gas and dissolved phase [L^3L^{-3}], respectively, D_{dif_s} is the effective soil matrix diffusion coefficient of CO_2 in the gas phase [L^2T^{-1}], D_{disp_s} is the effective soil matrix dispersion coefficient of CO_2 in the dissolved phase [L^2T^{-1}], and θ_a and θ_w are the volumetric fractions of air and water [L^3L^{-3}], respectively. P is the CO_2 production term. The term on the left-hand side of eq. (2) represents changes in the total CO_2 concentration in the soil. The first, second, and third terms of the right-hand side correspond to gaseous soil CO_2 flux by diffusion, dissolved CO_2 flux by water dispersion, and by convection, respectively. In this study, convective transport of CO_2 in response to the total pressure gradient was assumed to be negligible compared to diffusion.

The total dissolved CO_2 concentration, c_w, defined as the sum of aqueous $CO_{2(aq)}$ and H_2CO_3, is related to the CO_2 concentration in the gas phase by Henry's law as follows:

$$c_w = K_{CO_2} R T c_a \tag{3}$$

where K_{CO2} is the Henry's law constant [$MT^2M^{-1}L^{-2}$], R is the universal gas constant (=8.314 JK^{-1} mol^{-1}) [$ML^2T^{-2}K^{-1}M^{-1}$], and T is the absolute temperature [K]. The dispersion coefficient D_{disp_s} and the diffusion coefficient D_{dif_s} are defined according to Millington and Quirk (1961):

$$D_{disp\_s} = D_{disp\_w}\tau_w + \lambda_w\left|\frac{q_w}{\theta_w}\right| = D_{disp\_w}\frac{\theta_w^{7/3}}{p^2} + \lambda_w\left|\frac{q_w}{\theta_w}\right| \tag{4}$$

$$D_{dif\_s} = D_{dif\_a}\tau_a = D_{dif\_a}\frac{\theta_a^{7/3}}{p^2} \quad (5)$$

where D_{disp_w} and D_{dif_a} are the dispersion coefficient of CO_2 in the aqueous phase and the diffusion coefficient of CO_2 in the air, respectively, τ_w and τ_a are the tortuosity factors [LL^{-1}] in both phases, respectively. p is the porosity [L^3L^{-3}], which is assumed to be equal to the saturated water content θ_s, and λ_w is the dispersivity in the water phase [L].

Soil CO_2 in bare fields is assumed to be produced by soil microorganisms. In this study, respiration by plant roots was ignored.

$$P = \gamma_s = \gamma_{s0}\prod_i f_{si} \quad (6)$$

$$\prod_i f_{si} = f_1(z)f_2(T)f_3(c_a)f_4(h) \quad (7)$$

where γ_s [$L^3L^{-3}T^{-1}$] is the CO_2 production rate by soil microorganisms, which is calculated as the reduced optimal production rate γ_{s0} by soil microorganisms for the entire soil profile at 20°C under optimal water, solute, and CO_2 concentration conditions, with the various environmental factors described by reduction coefficients f_{si}. In this study, four environmental factors were taken into account; $f_1(z)$ for depth, $f_2(T)$ for temperature, $f_3(c_a)$ for the CO_2 concentration or O_2 concentration, and $f_4(h)$ for soil moisture.

The reduction coefficient for depth, $f_1(z)$, represents a profile of the potential CO_2 production rate or respiration rate by soil microorganisms when other conditions such as moisture and temperature are vertically uniform. In SOILCO2, the exponential function is used:

$$f_1(z) = ae^{-az} \quad (8)$$

where a is an empirical constant [L^{-1}]. The exponential function is multiplied by the constant a to insure that the integral from the soil surface to the infinite depth of the function $f_1(z)$ is equal to unity.

The dependence of the soil CO_2 production, $f_2(T)$, on temperature is described using the Arrhenius equation:

$$f_2(T) = \exp\left[\frac{E(T - T_{20})}{RTT_{20}}\right] \quad (9)$$

where $f_2(T) = 1$ when temperature is $T_{20} = 293.15$ and K = 20°C. R is the universal gas constant, and E is the activation energy of the reaction [$ML^2T^{-2}n^{-1}$], which was treated as a constant in this study.

In SOILCO2, the impact of O_2 deficiency $f_3(c_a)$ is not described as a function of soil moisture but of the CO_2 concentration using the Michaelis-Menten equation:

$$f_3(c_a) = \frac{c_b}{c_b + K_M} = \frac{0.21 - c_a}{0.42 - c_a - K_m^*} \tag{10}$$

where K_M is the Michaelis constant [$L^3L^{-3}T^{-1}$] for O_2, that is, O_2 concentration c_b at which the oxygen uptake rate q is equal to 1/2 q_{max}, which is half of the maximum oxygen uptake rate [$L^3L^{-3}T^{-1}$], and K^*_m is the Michaelis constant for the CO_2 concentration. Because $f_3(c_a)$ is not equal to unity when $c_a = 0$, the value of the optimal production γ_{s0} must be adjusted accordingly (Šimůnek and Suarez, 1993).

Since SOILCO2 describes the effects of O_2 stresses using $f_3(c_a)$, no reduction in the coefficient, $f_4(h)$, occurs even close to saturation:

$$\begin{aligned} f_4(h) &= 1 && h \in (h_2, \infty) \\ f_4(h) &= \frac{\log|h| - \log|h_3|}{\log|h_2| - \log|h_3|} && h \in (h_3, h_2) \\ f_4(h) &= 0 && h \in (-\infty, h_3) \end{aligned} \tag{11}$$

where h_2 and h_3 are the pressure heads when the CO_2 production is optimal and when it ceases [L], respectively. More details about the model description can be found in Šimůnek and Suarez (1993).

2.3. Determinations of Parameters

2.3.1. Soil Hydraulic and Thermal Properties

The soil profile was divided into three layers based on the soil texture and the dry bulk density; overlying Kuroboku andisol between 0 and 35-cm depths was subdivided into two layers, "Plowed" for depths of 0~15 cm, and "Hardpan" for depths of 15~35 cm, and underlying "Tachikawa loam andisol" for the soil layer deeper than 35 cm below the soil surface. The Durner-Mualem model (Durner, 1994) was used for predicting water retention curves and unsaturated hydraulic conductivities for each soil:

$$S_e = \frac{\theta - \theta_r}{\theta_s - \theta_r} = w_1\left(1 + |\alpha h|^{n_1}\right)^{-m_1} + w_2\left(1 + |\alpha_2 h|^{n_2}\right)^{-m_2} \tag{12}$$

$$K(S_e) = K_s\left(w_1 S_{e1} + w_2 S_{e2}\right)^l \times \frac{\left(w_1\alpha_1\left[1 - (1 - S_{e1}^{1/m})^m\right] + w_2\alpha_2\left[1 - (1 - S_{e2}^{1/m2})^{m2}\right]\right)^2}{\left(w_1\alpha_1 + w_2\alpha_2\right)} \tag{13}$$

where θ_r is the residual volumetric water content [L^3L^{-3}], K_s is the saturated hydraulic conductivity [LT^{-1}], S_e is the effective saturation [dimensionless], α_i [L^{-1}] , l, m_i (=1-1/n_i), and n_i [dimensionless] are empirical parameters, and w_i are weighing factors (i=1,2). These hydraulic parameters in eq. (12) and (13), θ_r, K_s, α_i , l, n_i, and w_i for "Plowed" and "Hardpan" layers were determined using an inverse analysis and the evaporation method (Šimůnek et al., 1998). Since

Kuroboku andisol is highly aggregated and it is difficult to reproduce the behavior of the undisturbed field soil on disturbed repacked soil samples (Kato et al., 2011), undisturbed soil cores sampled from each layer were used for the evaporation experiments.

The saturated volumetric water content, θ_s, plays an important role in predicting CO_2 diffusion through air-filled pores in a variably-saturated soil. In this study, porosity of the field soil was assumed to be equal to θ_s. The modified version of SOILCO2 was used so that we could conduct calculations using the Durner-Mualem model. Soil thermal properties, i.e., soil thermal conductivities and volumetric heat capacities of Kuroboku and Tachikawa loam andisols were obtained from Kato et al. (2011).

2.3.2. CO_2 Production and Transport Parameters

Several laboratory experiments have shown that the soil respiration rate positively correlates with the amount of dissolved organic carbon (DOC) (e.g., Sato and Seto, 1999). In this study, a profile of the DOC concentration was measured in order to determine the parameter "a" in $f_1(z)$, assuming that DOC can represent "readily decomposable organic matter" in soil. Field soil was sampled at 12 different depths between 0 and 90 cm. DOC of each soil sample was extracted with deionized water at the soil-water ratio of 1:5 and then the total organic carbon (TOC) of the extracts was analyzed using the TOC analyzer (TOC-VCPH, SHIMADZU Co. Ltd, Japan).

The optimal CO_2 production rate by soil microorganisms for the entire profile at 20^{o}C, γ_{s0}, was determined based on the measured soil CO_2 efflux from the soil surface in the field at daytime on 28th July, 2010, assuming that the rate of the CO_2 production of the entire soil profile is equal to the CO_2 efflux. Since the air temperature at that time was about 28^{o}C, the measured value was corrected for the temperature difference using the reduction function of temperature $f_2(T)$ (eq. (12)) and then divided by $f_3(c_a=0) = 0.91$. Other parameters needed to simulate the CO_2 transport and production were obtained from Suarez and Šimůnek (1993) and Buchner et al. (2008). In the simulation, the CO_2 production and transport parameters were assumed to be constant through a year.

2.4. Initial and Boundary Conditions

In the simulation, the soil profile was considered to be 1000 cm deep with a spatial discretization of 1 cm, assuming that the underlying Tachikawa loam layer was distributed down to 1000 cm. Since the exact distributions of soil water contents, temperatures, and CO_2 concentrations on the first day of the simulation period were unknown, initial conditions, at midnight of 1st Jan. 2010, were determined by a 1-yr preliminary simulation (Kato et al., 2011), assuming that the initial distribution of the soil water pressure head and temperature for the preliminary simulation was -100 cm H_2O and 20^{o}C, respectively. The initial condition for the soil CO_2 concentration at the surface in the preliminary simulation was set at 0.035%, which is the average atmospheric CO_2 concentration. The soil CO_2 concentration then linearly increased to the measured value at a depth of 50 cm at 24:00 on 31st Dec., 2010 (=0.45 %). The deeper layer had the same initial CO_2 concentrations as those at a depth of 50 cm.

Boundary conditions (BCs) for water movement at the soil surface were hourly precipitations observed at ISAS-UT and daily potential evaporation rates, which were obtained from the MeteoCrop data base (Kuwagata et al., 2011). A free drainage condition was used at the bottom of the soil profile. Continuous surface temperatures, calculated using the sinusoidal function and daily maximum and minimum soil surface temperatures, were used as the upper BC for heat transport calculations. These temperatures were independently simulated using HYDRUS-1D ver. 4.14 (Šimůnek et al., 2008; Kato et al., 2011). A zero temperature gradient was used as the bottom BC. The upper BC for CO_2 transport at the soil surface was the constant CO_2 concentration at the atmospheric value of 0.035%. The lower BC was also a zero CO_2 concentration gradient (Suarez and Šimůnek, 1993; Buchner et al., 2008).

3. Results and Discussion

Estimated water retention curves and unsaturated hydraulic conductivities of each soil layer are shown in Figure 1.

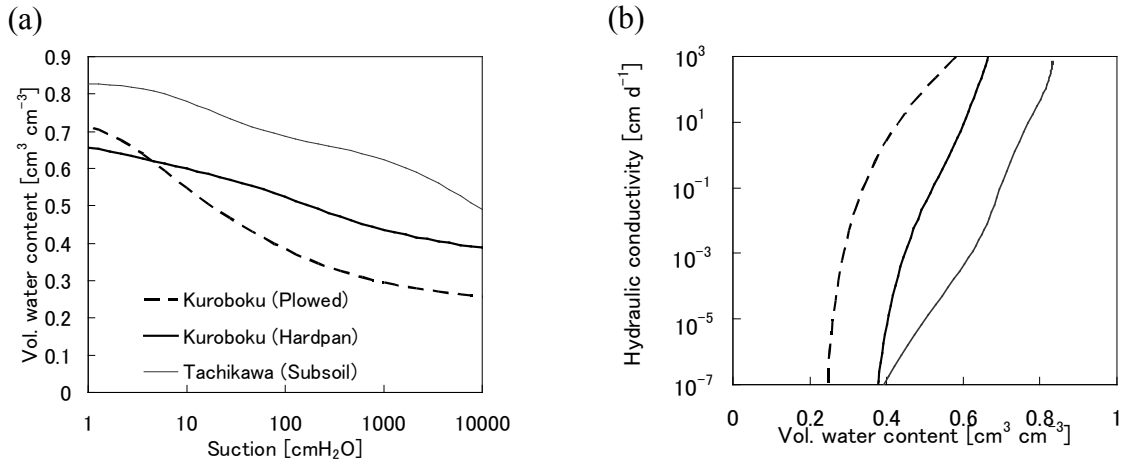

Figure 1. Estimated (a) water retention curves and (b) unsaturated hydraulic conductivities of each soil.

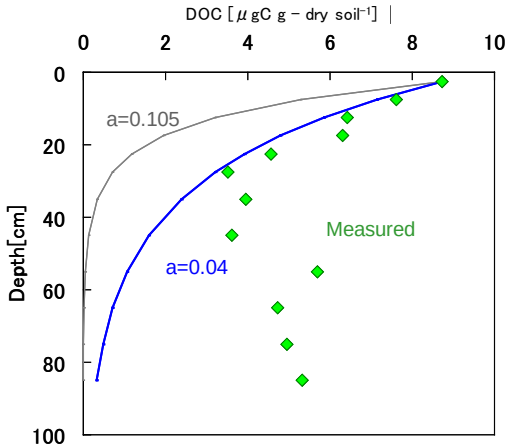

Figure 2. Comparison of the measured profile of DOC concentrations and depth-dependent functions of CO_2 production rates for different a coefficients, $f_1(z)$.

The profile of measured soil DOC concentrations per unit of soil mass is shown in Figure 2. It decreases with depth from the surface to a depth of 30 cm, and is almost constant in the Tachikawa loam layer. In Figure 2, the profile of measured DOC was compared with $f_1(z)$. Here, since $f_1(z)$ is the normalized function, $f_1(z)$ was multiplied by the ratio of measured and calculated values at a depth of 2.5 cm. Since the parameter "a" in $f_1(z)$ is empirical and there is no common method to determine its value, first, a=0.105, after Suarez and Šimůnek (1993) and Buchner et al. (2008), was employed. In this case, a decrease in $f_1(z)$ with increasing depth was more rapid than expected from the measured DOC profile. Since a smaller "a" gives larger values of $f_1(z)$ in deeper layers, a value of 0.04 was employed as "a" in an attempt to fit the measured DOC. Again, $f_1(z)$ was multiplied by the ratio of measured and calculated values at a depth of 2.5 cm (Fig. 2). When a=0.04, the model described the decrease in the vertical distribution of the measured DOC profile in the upper 30-cm-thick soil layer well, though the calculated values were still smaller than measured ones below a depth of 40 cm. In simulations presented in this study, both values of 0.04 and 0.105 were employed as "a" and their results were compared.

Figure 3a shows a comparison of observed and simulated soil water contents at depths of 10, 20, and 50 cm. Data could not be obtained due to sensor and/or datalogger problems from 22nd Sept. till 14th Oct., 2010. The model described fluctuations in the soil water content well, reflecting rainfall and evaporation. Although there was no rainfall for 47 days from 24th Dec., 2010 to 8th Feb., 2011, except for rains of 0.3 mm on 25th Jan. and 0.1 mm on 27th Jan., 2011, the measured soil water content at depths of 10 and 20 cm decreased very little, and the model underestimated the soil water content during this period. It is possible that air temperatures were below a freezing point and ice occurred in the soil profile, while the SOILCO2 model does not take freezing and frost into account (Kato et al., 2011).

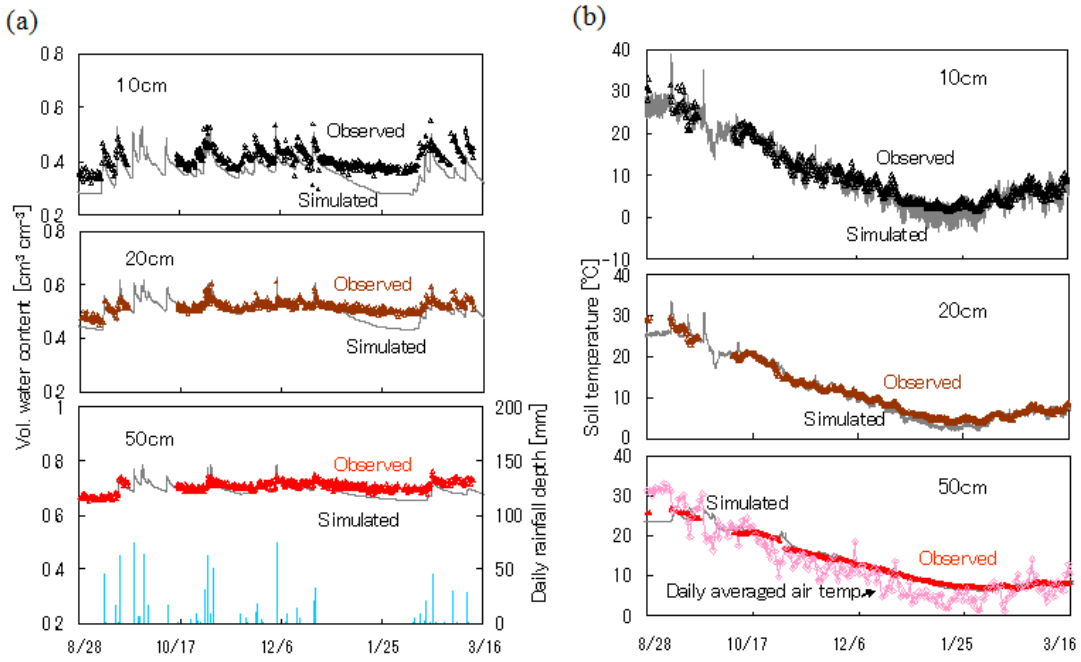

Figure 3. Comparison of observed and simulated (a) soil water contents and (b) soil temperatures at depths of 10, 20, and 50 cm.

Simulated soil temperatures at depths of 10, 20, and 50 cm are compared with observed data in Figure 3b. The simulated results agreed with the observed values fairly well. Soil temperatures, especially those at depths of 10 and 20 cm, were underestimated in winter. The upper boundary condition for soil heat transport was surface temperature, which was independently calculated with the HYDRUS-1D model using the energy balance equation. The underestimation of temperatures seems to coincide with the underestimation of soil water contents. A lack of consideration of the latent heat of freezing and the heat capacity of ice in the heat flow equation presumably resulted in the underestimation of the soil temperature in winter and thus inputted surface temperatures in winter likely led to the underestimation of soil temperatures.

Figure 4 shows a comparison of observed and simulated soil CO_2 concentrations at depths of 10, 20, and 50 cm. Daily rainfall depth is also shown. Seasonal changes in CO_2 concentrations were observed at all three depths in the field monitoring. This seasonal variation was associated with seasonal changes in soil temperature, e.g., soil CO_2 concentrations decreased with decreasing soil temperatures. Observed CO_2 concentrations suddenly increased when rainfall occurred. This could be because the rise in the soil water content following rainfall events (Fig. 3a) enhanced activities of microorganisms and decreased the diffusion coefficient (Kato et al., 2013). The model could describe these seasonal variations and responses to rainfall well.

When the experimentally determined value of 0.04 was employed for a in $f_1(z)$, simulated results agreed well with the observed soil CO_2 concentrations at both depths of 10 and 20 cm, while the model underestimated soil CO_2 concentrations at a depth of 20 cm when a literature-based a=0.105 was used.

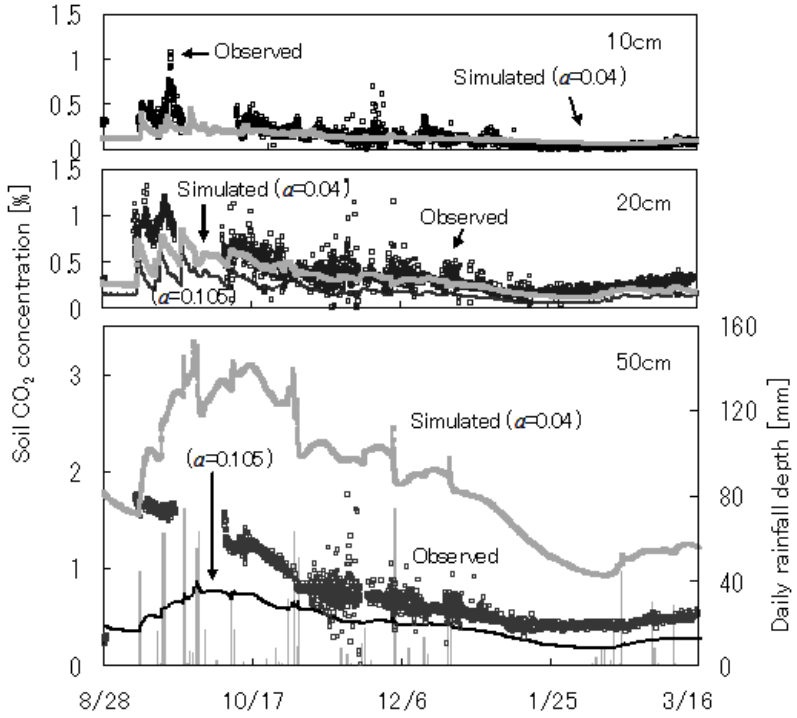

Figure 4. Comparison of observed and simulated soil CO_2 concentrations at depths of 10, 20, and 50 cm.

The CO_2 concentration at a depth of 50 cm was overestimated when the experiment-based a=0.04 was employed. This result suggests that the CO_2 production from the soil layer below 50 cm may be smaller than that expected from the DOC distribution. Not only the quantity of DOC, but also its quality may determine the respiration rate by soil microorganisms. Boyer and Groffman (1996) investigated the vertical distribution of the water extractable DOC (WEDOC) and biodegradable DOC (BDOC). They showed that WEDOC diminished with depth and, furthermore, the percentage of BDOC to the total WEDOC pool decreased with depth. Wagai and Sollins (2002) compared the biodegradability of WEDOC and leachable DOC in forest soils, and their results suggest that the leachable DOC was not always labile. In the experimental field, some of DOC in the deeper layer must have been leached from the surface layer and less labile, and thus the CO_2 production rate of deeper soil is small.

4. Conclusions

In this study, we evaluated the performance of the SOILCO2 model in predicting soil CO_2 dynamics, especially soil CO_2 concentrations at various depths in arable bare land. For the simulation, we have tried to experimentally determine two parameters that are related to the respiratory substrate of the soil. The optimal CO_2 production rate, "γ_{s0}" was determined using the CO_2 efflux from the soil surface measured during the summer season. The parameter of the depth dependent coefficient, "a", which describes a profile of respiratory substrate, was determined from a measured profile of the dissolved organic carbon (DOC). For the model validation, the soil CO_2 concentrations, soil water contents, and soil temperatures were continuously monitored for approximately half a year at three different depths. Seasonal and daily changes in soil water contents and soil temperatures, which both affect the production and transport of soil CO_2, were well described with the SOILCO2 model. Simulated behavior of the soil CO_2 concentration, such as seasonal variations and responses to rainfall, agreed well with the observed values, especially in upper layers.

The model tended to overestimate the soil CO_2 concentration in deeper layers when an experiment-based parameter "a" was employed, although soil water contents and temperatures were properly predicted. It may be because labile DOC tends to degrade rapidly and some of the DOC present in deeper layers could have been leached from the surface and not highly labile. We concluded that the soil CO_2 dynamics in arable bare land could be predicted well using the SOILCO2 model. To improve simulation results of CO_2 concentrations, especially in deeper layers, it may be necessary to consider the relationship between the water extractable DOC (WEDOC) and the biodegradable DOC (BDOC) in soil.

Acknowledgement
This study was partly supported by JSPS Research Fellowships for Young Scientists and Research Program on Climate Change Adaptation (RECCA) of Ministry of Education, Culture, Sports, Science and Technology. We appreciate Mr. S. Hatano, Mr. H. Kubota, and Mr. K. Yatsuda of ISAS-UT for their help in using the field and meteorological data. We would also like to thank Prof. Šimůnek for his help in using a modified version of the SOILCO2 program.

References

Boyer, J. N., and P. M. Groffman, Bioavailability of water extractable organic carbon fractions in forest and agricultural soil profiles, *Soil Biol. Biochem.*, *28*, 783-790 , 1996.

Buchner, J. S., J. Šimůnek, J. Lee, D. E. Rolston, J. W. Hopmans, A. P. King, and J. Six, Evaluation of CO_2 fluxes from an agricultural field using a process-based numerical model, *J. of Hydrol.*, *361*, 131-143, 2008.

Durner, W., Hydraulic conductivity estimation for soils with heterogeneous pore structure, *Water Resour. Res.*, *30*, 211-223, 1994 .

Lal, R., and J. M. Kimble, Conservation tillage for carbon sequestration, *Nutr. Cycl. Agroecosys.*, *49*, 243-253, 1997.

Kato, C., T. Nishimura, H. Imoto, and T. Miyazaki, Predicting soil moisture and temperature of Andisol under monsoon climate in Japan, *Vadose Zone J.*, *10*, 541-551, 2011.

Kato, C., H. Imoto, T. Nishimura, and T. Miyazaki, Investigation of changes in soil CO_2 concentration by using compact buried tubing soil gas monitoring system, *Jpn. Soc. Soil phys.*, 2013, in print (in Japanese with English abstract)

Kuwagata, T., M. Yoshimoto, Y. Ishigooka, T. Hasegawa, M. Utsumi, M. Nishimori, Y. Masaki, and O. Saito, MeteoCrop DB: An agrometeorological database coupled with crop models for studying climate change impacts on rice in Japan, *J. Agric. Metrorol.*, *67*, 209-224, 2011.

Millington R. J. and J. M. Quirk, Permeability of porous solids, *Trans. Faraday Soc.*, *57*, 1200-1207, 1961.

Ministry of Agriculture, Forestry, and Fisheries, Government of Japan, 2012/10/31 http://www.maff.go.jp/j/press/kanbo/kankyo/pdf/080321-02.pdf (in Japanese)

Sato, A., and M. Seto, Relationship between rate of carbon dioxide evolution, microbial biomass carbon, and amount of dissolved organic carbon as affected by temperature and water content of a forest and an arable soil, *Commun. Soil Sci. Plan. Anal.*, *30*, 2593-2605, 1999.

Šimůnek, M., M. Th. van Genuchten, and M. Šejna, Development and applications of the HYDRUS and STANMOD software package and related codes, *Vadose Zone J.*, *7*, 587-600, 2008

Šimůnek, J., and D. L. Suarez, Modeling of carbon dioxide transport and production in soil: 1. Model development, *Water Resour. Res.*, *29*, 487-497, 1993.

Šimůnek, J., O. Wendroth, and M. Th. van Genuchten, Parameter estimation analysis of the evaporation method for determining soil hydraulic properties, *Soil Sci. Soc. Am. J.*, *62*, 894-905, 1998.

Suarez, D. L., and J. Šimůnek, Modeling of carbon dioxide transport and production in soil: 2. Parameter selection, sensitivity analysis and comparison of model predictions to field data, *Water Resour. Res.*, *29*, 499-513, 1993.

Sundquist, E., The global carbon dioxide budget, *Science*, *259*, 934-941,1993.

Wagai, R., and P. Sollins, Biodegradation and regeneration of water soluble carbon in a forest soils: leaching column study, *Biol. Fertil. Soils*, *35*, 18-26, 2002.

Flow at Low Water Contents: A Simple Approach for Inverse Estimation of van Genuchten-Mualem Soil Hydraulic Parameters

Marcel Bawindsom Kébré[1,2], Fabien Cherblanc[1], François Ouédraogo[2], Jean-Claude Bénet[1], and François Zougmoré[2]

[1]*LMGC, CNRS, Université Montpellier 2, Place Eugène Bataillon 34000 Montpellier, France,* mkebre@hotmail.com
[2]*LAME, UFR-SEA, Université Ouagadougou, Avenue Charles de Gaulle 03 BP 7021, Burkina Faso*

Abstract

The unsaturated soil hydraulic properties (the soil water characteristic and relative permeability curves) are key hydrodynamic parameters in the fields of soil science and civil engineering. Because of the strong dependency of these properties on water content, their determination is subject to considerable experimental and numerical problems. Difficulties increase when the soil approaches oven-dry conditions, a situation often encountered in arid and semi-arid areas. Moreover, computational costs of estimating the hydrodynamic properties can be relatively high also. After a short review of alternative modeling approaches for the hydraulic functions from saturation to oven-dryness, we present a theoretical-numerical approach, along with a relatively simple, robust and inexpensive experimental method for inverse determination of van Genuchten/Mualem soil hydraulic parameters. For gravimetric water contents greater than 0.04, numeral results agreed well with experimental data, while some discrepancies were observed at very low water contents.

1. Introduction

The process of water flow in soils has been the focus of intensive research in the fields of agronomy, hydrology and geomechanics. The amount and energy status of water in a soil can affect considerably the soil hydraulic properties. While knowledge of the two extreme states of water in a soil (saturated and very dry conditions) seems well advanced, the unsaturated state at medium to low water contents deserves further investigation. This condition is usually encountered in soil surface layers where strong interactions occur between soil and roots, microorganisms or building foundations. In arid and semi-arid zones, precise knowledge of physical flow processes at low water contents would allow development of more effective tools for water resources management.

The Richards equation is commonly used to describe water flow in the unsaturated zone of soils. Other formulations based on thermodynamics (Fremond and Nicolas, 1990) and/or the thermodynamics of irreversible processes (Bénet, 1981) lead to similar equations. Application of these equations in all cases requires initial and boundary conditions, as well as relationships between the gravimetric or volumetric water content (w in $kg.kg^{-1}$, and θ in $m^3.m^{-3}$, respectively) and the water flow rate. One can show that the suction or matric potential ψ (in Pa) and the matric head h (in m), both widely used in soil hydrology, are closely related to the chemical potential μ ($J.kg^{-1}$) (Bénet et al., 2012). The relationship between matric potential, chemical

potential and matric head is given by $\mu=\psi/\rho_w=gh$, where ρ_w is the density of water, taken as 1000 $kg.m^{-3}$, and g the acceleration of gravity ($m.s^{-2}$). These relationships reflecting the soil hydraulic properties are conventionally expressed using two functions, namely the water retention function denoted by $w(\mu)$ and the hydraulic conductivity function $K(\mu)$ or $K(w)$. Additional processes may be included in the flow equation such as liquid-gas phase change (or evaporation), which is important especially in arid regions.

All of the above functions and processes must be known from saturation to oven-dry conditions where measurements are especially challenging (Sakai et al., 2009). Physical and technical difficulties include possible cavitation of tensiometers (limiting their use up to about 80 $J.kg^{-1}$) and lack of continuity in the liquid phase of the soil when a saturated porous plate is used beyond 500 $J.kg^{-1}$ (e.g., using the axis translation procedure as implemented by Baker and Frydman, 2009). In addition, acquisition of the data can be very time consuming and costly. For these reasons most studies are limited to situations between saturation and some intermediate state of soil water, corresponding to the range of operation of the most common experimental devices (Sakai et al., 2009; Fujimaki and Inoue, 2003; Fujimaki et al., 2004).

Inverse methods are now increasingly used to identify the hydraulic properties of unsaturated porous media. They offer a very flexible approach by allowing a range of numerical optimization algorithms (e.g., Levenberg-Marquart, conjugate gradient methods, genetic algorithms and neural network approaches). In soil hydrology, the approach generally used for inverse problems is solution of the Richards equation in conjunction with some infiltration/drainage or evaporation/condensation experiment (Durner et al., 1999; Fujimaki et al, 2004; Peters and Durner, 2008; Schindler et al., 2010; Sakai et al., 2009). A major difficulty of inverse problems is to find analytical or empirical models that accurately represent the hydraulic properties at very low water contents.

In this paper, we first review the problem of obtaining accurate descriptions of the soil hydraulic properties (the soil water characteristic and relative hydraulic conductivity curves) over the full range of water contents, but especially at relatively low water contents. The soil water characteristic curve is a representation of the relationship between soil water suction and water content. For suction ψ (Pa), we prefer to use the equivalent concept of water chemical potential μ ($J.kg^{-1}$), which provides a link between the physics of water in porous media and thermodynamically open systems. We next propose a theoretical-numerical model for isothermal water flow, which will be used in the inverse problem formulation. The selected state variables are the gravimetric water content, w, and the water vapor pressure, p_v. A simple, robust and very cheap experimental method for the inverse determination of the soil hydraulic properties is then presented. The soil hydraulic functions in this study are based on the van Genuchten model (1980) for the soil water characteristic and the van Genuchten (1980) - Mualem (1976) model for the unsaturated hydraulic conductivity. The ROSETTA code (Schaap et al., 2001) is further used to provide initial estimates of the model parameters. Various scenarios with regard to the residual water content, w_r, Mualem's tortuosity parameter, L, and the saturated hydraulic conductivity, K_{sat}, will be simulated and discussed.

2. Characterization of Soil Hydraulic Properties at Low Water Contents

2.1. The Soil Water Characteristic

Despite the relatively small amounts of water retained, accurate representation of soil water characteristic curves at the dry end is important for modeling biological processes including plant water uptake and microbial activity in arid environments (Tuller and Or, 2005). Accurate measurement over the full range of water contents is a delicate task. Most or all methods for measuring the water potential have limitations, especially at intermediate and very low values of the water content (its pendular and hygroscopic states). Very often the curve is completed by extrapolation, which can lead to instabilities in numerical codes (Lu et al, 2008). Experimental methods (infiltration and/or drainage, evaporation and condensation) associated with inverse problems also suffer from shortcomings, including in the instrumental devices, and are mostly robust only at the higher water contents (i.e., the funicular state) where the liquid phase is continuous. All this raises the question of the validity at low water contents of the matric head - water content relationship, h - θ, usually a key function to describe the physics of unsaturated flow. Indeed, this range of the water content comprises the pendular state where the liquid and vapor phases presumably are discontinuous, and the hygroscopic state where only the gas phase is continuous, while water is being strongly adsorbed onto the solid phase. This is why we prefer the use of the water chemical potential to describe the movement of water in all of its states. One of the fundamental properties of the chemical potential stipulates that at local thermodynamic equilibrium, the potential of a component present in two phases should be the same (Callen, 1985). Experimentally well-defined methods (e.g., Bénet et al., 2012) should apply to all important parts of the soil water characteristic curve, from saturation to oven dryness.

The models most commonly used in the literature to represent the soil water characteristic curve (Brooks and Corey, 1964; van Genuchten, 1980) often fail to reproduce experimental data at very low water contents (Sakai et al., 2009). Many researchers therefore developed new models or extended existing models to the full range of water contents. Campbell and Shiozawa (1992) used data at very high chemical potentials (in absolute value) to establish an equation reflecting the phenomenon of water adsorption on the surface of particles in the soil matrix. They modified the model of van Genuchten (1980) to improve the calibration of data at low water contents. The adsorption equation (Campbell and Shiozawa, 1992) was used later also by others (e.g., Fayer and Simmons, 1995; Khlosi et al., 2006) as an additional correction to the classical models at the low water contents. Fredlund and Xing (1994) opted for a different mathematical expression to better fit experimental data in this range. Junction models are now also available (e.g., Rossi and Nimmo, 1994; Webb, 2000; Zhang et al., 2011). Recent evaluations have highlighted the strengths and weaknesses of the various models. For example, Sillers and Fredlund (2001) noted that the Fayer and Simmons (1995) correction of van Genuchten's (1980) soil water characteristic model with m = 1.0 gave excellent results for about 200 soils from the USDA database over the entire range of moisture contents, while avoiding the controversial concept of residual water content. Using data from 137 soils of the UNSODA database, Khlosi et al. (2008) compared eight analytical models describing the complete soil water characteristic curve. They found that the model of Khlosi et al. (2006) with four fitting parameters was most consistent for soils covering a broad range of densities, organic matter contents and textures.

2.2. The Unsaturated Hydraulic Conductivity

Unlike the soil water characteristic curve, very few studies have been devoted to the hydraulic conductivity over the full range of water contents (Zhang, 2011). One problem involves the physical processes that govern the flow of water at low water contents. While capillary models based on theories by Purcell (1949), Childs and Collis (1950), Burdine (1953), Kunze (1968) and Mualem (1976) for estimating the unsaturated hydraulic conductivity are generally fairly accurate at high water contents, they often underestimate the permeability at low water contents (Sakai et al. 2009). Hydraulic conductivity expressions that have been validated over the full range of water contents often are relatively complex and sometimes difficult to use within an inverse optimization program. As for the physical flow phenomena at low water contents, Tuller and Or (2001), Peters and Durner (2008) and Zhang (2011) use the concepts of film flow at low water contents to establish hydraulic conductivity models over the full range of water contents. The model of Tuller and Or (2001) is mathematically very complex and not easily associated with one of the classical models for the soil-water characteristic curve. Those of Peters and Durner (2008) and Zhang (2011) add an extra term accounting for capillary flow according to the theories of Mualem (1976) and Burdine (1953), and another term describing film flow around solid particles in the soil matrix. However, some of these models remain very complex, especially when used in an inverse procedure.

3. Theoretical-Numerical Model for Water Flow in Arid Soils

A natural soil can be idealized as a triphasic porous medium by considering a solid, a liquid and a gaseous phase, with the gaseous phase consisting of two components: dry air and water vapor. From an experimental point of view, appropriate state variables for water flow modeling are the gravimetric water content, w, defined as the ratio between the apparent mass densities of liquid, ρ_l, and solid ρ_s (i.e., $w= \rho_l/\rho_s$), and the vapor partial pressure of the gas phase, p_v (Pa) linked to the apparent density of vapor, ρ_v, through the ideal gas law:

$$p_v = \frac{\rho_v}{\phi_g}\frac{RT}{M_w} \tag{1}$$

where R (J.kg^{-1}) is the ideal gas constant and M_w (kg.mol^{-1}) the molar mass of water. The volume fraction of the gas phase ϕ_g is related to the water content w by:

$$\phi_g = \frac{V_g}{V} = 1 - \frac{\rho_s}{\rho_s^*} - w\frac{\rho_s}{\rho_l^*} \tag{2}$$

Three elementary processes are considered: liquid flow governed by capillary and gravity effects, vapor diffusion in the gas phase, and liquid-gas phase changes of water. The main assumptions are that the temperature is uniform and constant, the solid skeleton is rigid, the total gas pressure is constant and uniform, and hence also that convective flow in the gas phase is negligible.

Fundamental mass balance equations for water in liquid and gas phases are then written as:

$$\rho_s \frac{\partial w}{\partial t} + \nabla.\left(\rho_l \mathbf{v}_l\right) = -\hat{\rho} \tag{3}$$

$$\frac{M_w}{RT}\frac{\partial}{\partial t}\left(\phi_g p_v\right) + \nabla.\mathbf{J}_v = +\hat{\rho} \tag{4}$$

The liquid filtration flux, denoted by $\rho_l \mathbf{v}_l$ in Equation (3) is described with Darcy's law extended to unsaturated conditions. Extension of the above description to very low water contents is questionable since the concept of liquid pressure is meaningless (Nitao and Bear, 1996). An alternative proposed by Bénet et al. (2012) is to rely on the chemical potential, which is defined over the full range of water contents. This thermodynamic potential is a function of the water content described by the soil-water retention curve obtained by merging measurements using classical tensiometry and sorption isotherms. Therefore, water flow can be governed by the equation:

$$\rho_l \mathbf{v}_l = -K_{sat} k_r \frac{\rho_l^*}{g}\left(\nabla \mu_l - \mathbf{g}\right) \tag{5}$$

where μ_l (J.kg^{-1}) is the mass chemical potential of liquid water, $\mathbf{g}$ (m.s^{-2}) is the gravity acceleration vector, k_r is the relative permeability function and K_{sat} (m.s^{-1}) the hydraulic conductivity at saturation. The mass density of water ρ_l^* is taken to be 1000 kg.m^{-1}.

The vapor diffusion flux, denote by $\mathbf{J}_v$ in Equation (4), is classically described using a first-order Fick's law of the form:

$$\mathbf{J}_v = D_{vs} \nabla \rho_v^* \tag{6}$$

in which D_{vs} is the effective vapor diffusion coefficient in the soil:

$$D_{vs} = \tau \phi_g D_{va} \tag{7}$$

where τ is the tortuosity, which can be described using functions given by Penman (1940), Millington and Quirck (1961) or Moldrup et al. (1997), and D_{va} the free diffusion coefficient of vapor in air. Standard correlations give a value of 26.1×10^{-6} m.s^{-2} for D_{va} at 30°C.

From thermodynamic considerations of liquid-gas phase changes, it can be shown that the volumetric rate of phase change is proportional to the chemical potential difference of water between the liquid and vapor states. A detailed theoretical development of this phase change has been given by Bénet et al., (2009).

The nonlinear equations (3) and (4) are strongly coupled through the phase change term $\hat{\rho}$, as well as through the soil physical characteristics that depend on the water content: $\phi_g(w)$, $D_{vs}(w)$, and $k_r(w)$. The governing equations were discretized using a finite-volume formulation on a one-dimensional regular mesh, with the unknowns w and p_v located at the center of grid blocks. A first-order upstream scheme was used to describe the convective term appearing in liquid mass balance Equation (3). Temporal integration was performed based on a fully implicit scheme to ensure numerical stability. Nonlinearities were dealt with by using a Newton-Raphson method which produced accurate convergence with relatively moderate time steps.

4. Materials and Methods

4.1. Morphological Characteristics and Soil Moisture

The material under investigation is a natural soil from Nasso, Burkina-Faso. The soil sample was taken from the top layer of soil (0-30 cm depth). The analysis by dry sieving after washing (standard NF P94-056) for particles having diameters greater than 80 µm and a sedimentation analysis (standard NF P94-057) for smaller particles, indicated that the soil contained 95% sand, 2% silt and 3% clay (USDA classification). Soil texture is hence sand. The dry soil density measured at the site gave an average value of 1688 kg.m^{-3}. Points of the soil water characteristic (desorption data) were obtained by combining two methods: using a pressure plate apparatus at constant temperature (30°C) for water in the funicular state (saturations up to μ = -500 J.kg^{-1}) and a desorption device (using saturated solutions at equilibrium) to complete the curve in the hygroscopic state (from -5000 to -3×10^5 J.kg^{-1}). Figure 1 shows the measured data as well as the relationship between the chemical potential and the water content based on the model of van Genuchten (1980) as identified using the RETC code of van Genuchten et al. (1991).

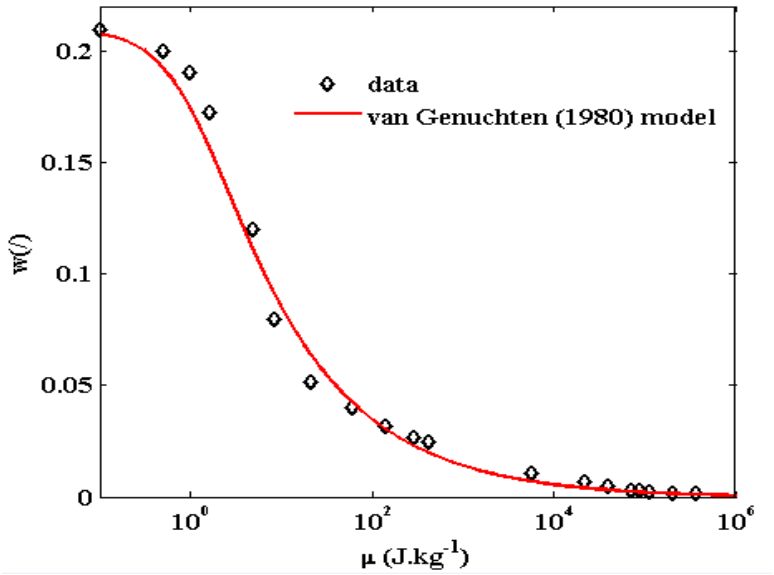

Figure 1. Measured and fitted soil water characteristic curves (gravimetric water content, w, as a function of the chemical potential, μ).

4.2. Measured Water Content Profiles

The objective of the experimental study was to establish profiles of water content in a homogeneous soil column. The upper half of the PVC column used for this purpose (20 cm high and 7.5 cm inner diameter) was packed with soil having a desired initial gravimetric water content of 0.06, and the lower half with soil having a gravimetric water content of 0.02. Both parts of the column were compacted to the field-measured dry density. The sealing ends of the columns were coated with a thick plastic film. Crafted columns were stored in a thermo-regulated chamber. Evaporative phenomena were negligible. The mass of the column was assumed to be constant. The experiment consisted in a redistribution of water on both sides of the interface due to the gradient of the moisture content (or chemical potential). A destructive method was used for measurement of gravimetric water contents by weighting after oven-drying at 105°C for 48 hours. The soil columns for this purpose were sliced using a mechanical device to determine the distributions of the water content along the column at given time intervals. The mechanical device permitted slices of soil of only 5 mm thick. Ideal conditions of the experiment were such that only the physical phenomenon of water flow in the column occurred (e.g., flow of water in the liquid phase from the top part). Phase changes could be neglected since air within the column was presumably saturated.

4.3. Inverse Analysis

The inverse analysis was based on solutions of the theoretical model given by Equations (3) and (4) using a nonlinear Newton-Raphson method. The chemical potential as a function of the water content was described using the model van Genuchten (1980) and the relative permeability function using the van Genuchten (1980) - Mualem (1976) equation as follows:

$$S_e = \frac{w(\mu) - w_r}{w_{sat} - w_r} = \left[1 + \left(|\alpha\mu|\right)^n\right]^{-m} \tag{8}$$

$$k_r(S_e) = S_e^L \left[1 - \left(1 - S_e^{1/m}\right)^m\right]^2 \tag{9}$$

where w_r and w_{sat} are the residual and saturated gravimetric water contents, respectively, α (> 0 in kg.J^{-1}), n (> 1) and L are fitting parameters, m=1-1/n as suggested by van Genuchten and Nielsen (1985), and S_e is effective saturation. In this study we selected the above original van Genuchten equations rather than the complicated modified expressions advocated by Schaap and van Genuchten (2006).

Two minimization programs were used next in the inverse analysis to find optimal hydraulic parameter values based on obtaining the minimum average squared difference between measured and calculated values: one based on the Levenberg-Marquardt (1963) algorithm, and another using the Nelder-Mead Downhill Simplex method (Nelder and Mead, 1965). All optimizations produced a value of zero for the residual water content (w_r = 0), while the saturated water contents w_{sat} was fixed at 0.208 kg.kg^{-1} as estimated from the measured porosity of the soil.

Since laboratory saturated permeability tests (rigid-wall or flexible-wall permeameters) often show considerable errors (e.g., Chapuis, 2012) with predicted values sometime deviating considerably from measured values due to macroporosity or other effects (Schaap and Leij, 2000; Schaap and van Genuchten, 2006), we decided to keep K_{sat} as a free (adjustable) parameter in the inverse analysis.

Table 1. Assumed optimization scenarios and imposed parameter constraints

Scenario	Free parameters	Fixed parameters	Lower bond	Upper bound
S1	K_{sat} (m.s^{-1})	$w_r = 0$, α, n, $m = 1\text{-}1/n$, $L = 0.5$	10^{-10}	10^{-3}
S2	n, m, K_{sat} (m.s^{-1})	$w_r = 0$, α, $L = 0.5$	$n>1$, $m>0$	$n<10$, $m<1$
S3	K_{sat} (m.s^{-1})	$w_r = 0$, α, n, $m = 1\text{-}1/n$, $L = -6.5$	10^{-10}	10^{-3}
ROS	α, n, K_{sat} (m.s^{-1})	$w_r = 0$, $L = 0.5$	-//-	-//-

Several optimization scenarios were considered as summarized in Table 1. Scenario S1 corresponds to an optimization of the saturated permeability (K_{sat}) with the model parameters $w(\mu)$ deduced from the fitted soil water characteristic curve in Figure 1. Scenario S2 considered both m and K_{sat}, to be the optimization parameters. The parameter m in Equation (9) is in that case independent of n in Equation 8. In a third scenario, S3, following the work of Schaap and Leij (2000), Peters et al. (2011), Peters and Durner (2008) and Zhang (2011), we fixed L at a negative value (-6.5) and focused on the optimization of K_{sat}. The other parameters kept the values associated with Figure 1. In a fourth scenario, denoted ROS, we optimized all parameters of Equations 8 and 9. The initial values were estimated from textural properties and the density using the ROSETTA code (Schaap and al., 2001). Parameter constraints were further introduced to ensure realistic physical descriptions of the hydraulic functions. Inspired by the work of van Genuchten and Nielsen (1985); Ippisch et al. (2006) and Peters et al. (2011), we used the following constraints: $1<n<10$, $0<m<1$, and $0<\alpha<15$. Following Schaap and Leij (2000) and Schaap and van Genuchten (2006), we further imposed the constraint $10^{-10}<K_{sat}<10^{-3}$ on the saturated hydraulic conductivity of our sandy soil.

5. Results and Discussion

Table 2 summarizes the estimated values for optimization scenarios (S1, S2, S3, ROS), including values of the Root Mean Square Error (*RMSE*). Figures 2 and 3 show the experimental and simulated profiles according to the scenarios presented in Table 1. Figure 2 is for scenario S1, while Figure 3 shows results for all scenarios at different times (1, 3, 5 and 13 days).

Table 2. Optimized values of van Genuchten/Mualem model parameters.

Scenario	α	n	m	K_{sat}	*RMSE*
	kg.J^{-1}	-	-	m.s^{-1}	
S1	0.9527	1.3922	1- 1/n	$3.6946.10^{-5}$	0.002652
S2	0.9527	1.3922	0.6288	$2.3698.10^{-7}$	0.002068
S3	0.9527	1.3922	1- 1/n	10^{-10} +	0.006482
ROS	13.1034	1.0 *	1- 1/n	$4.3277.10^{-5}$	0.002286

+ minimum limit imposed

* minimum limit imposed, $n_{opt} = 0.86735$

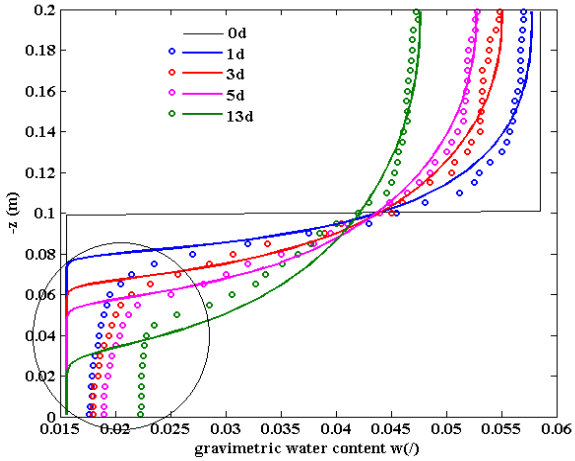

Figure 2. Experimental and simulated water content profiles for scenario S1.

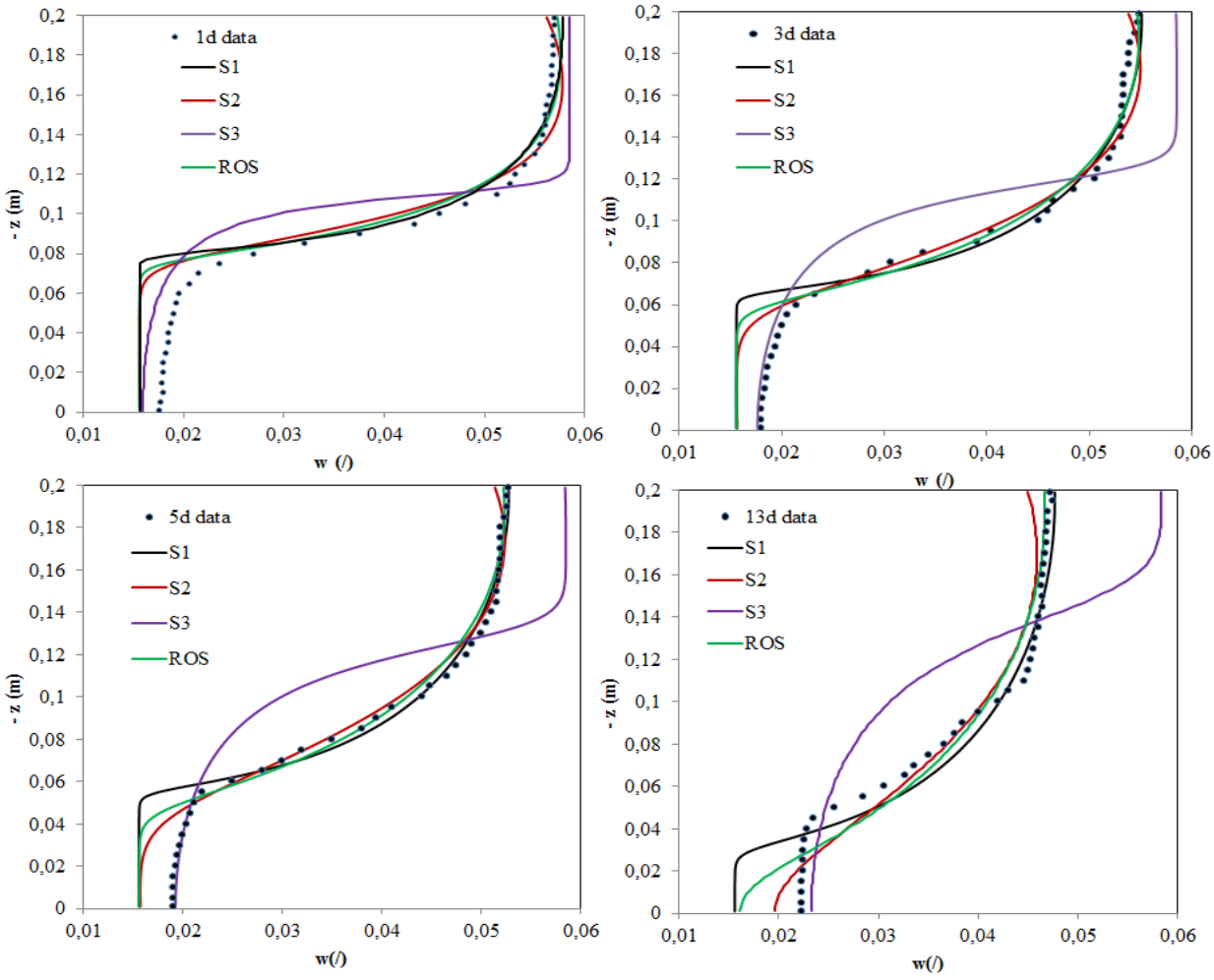

Figure 3. Experimental and simulated water content profiles for optimization scenarios S1, S2, S3, and ROS at different times (1, 3, 5 and 13 days).

The results presented in Table 2 and Figures 2 and 3 show that the inverse analysis in conjunction with the assumed numerical model (section 3) leads to a good match with the experimental data. The inverse procedure based on the Levenberg Marquart method was found to be quite robust by producing unique solutions. The computational time depended on the number of parameters to be optimized and the invoked initial values. The Nelder-Mead method (1985), on the other hand, was found to be very time-consuming.

Except for case S3, all scenarios using the van Genuchten model for $w(\mu)$ and the van Genuchten-Mualem model for the unsaturated hydraulic conductivity accurately described the flow of water at relatively high water contents. Below 0.03, however, significant discrepancies are apparent in Figure 2. When the parameter n of Equation 8 was optimized along with m (kept independent of n) and K_{sat} (i.e., scenario S2), the inverse analysis gave the best results in terms of yielding the lowest value of *RMSE*. However, the optimized value for K_{sat} (2.3698×10^{-7} ms^{-1}) was very small compared to typical values for a sandy soil, as can be observed in the work of Schaap and Leij (2000). Taking into account the textural properties of the soil, optimizing all parameters (α, n, $m = 1\text{-}1/n$, K_{sat}) and using initial estimates provided by ROSETTA (Schaap et al., 2001) produced excellent results (*RMSE* = 0.002286). This case may well prove the most promising for characterizing the hydraulic properties of unsaturated soils. The cost of the method is very small considering the simplicity of the experimental method, including the use of initial estimates as predicted with ROSETTA from soil texture.

Optimizing K_{sat} according to scenario S3 produced the lowest value of the saturated hydraulic conductivity ($K_{sat} = 10^{-10}$ ms^{-1}), while only a fair match was obtained at the lower water contents. This case also failed to reproduce the observed gradients in the moisture profile in the centre of the column at intermediate water contents.

6. Conclusion

Determining the unsaturated soil hydraulic properties at very low water contents is still a major challenge. Existing numerical and experimental methods have many limitations in the very dry range. The theoretical model we proposed in this paper is based on the chemical potential, which provides a fundamental thermodynamic link between the physics of water flow in porous media and the thermodynamics of open systems. A numerical inverse procedure was developed to identify the parameters associated with the models of van Genuchten (1980) for the soil-water characteristic curve and the van Genuchten (1980) - Mualem (1976) formulation for the unsaturated hydraulic conductivity. Experimental water content profiles were obtained using a very simple experimental setup. The optimized parameters remained within their physical limits, in agreement with literature values. They closely described the results as shown by relatively small *RMSE* values. However, discrepancies were still observed at very low water contents. An alternative is to rely on the general model of van Genuchten and Nielsen (1985) with independent m and n values, which gives more flexibility to match the experimental results in the low water content range

References

Baker, R., and S. Frydman, Unsaturated soil mechanics. Critical review of physical foundations, *Eng. Geol.*, *106*, 26-39, 2009.

Bénet, J.-C., A. Ramirez-Martinez, F. Ouédraogo, and F. Cherblanc, Measurement of the chemical potential of a liquid in porous media, *J. Porous Media*, *15*, 1019-1029, 2012.

Bénet, J.-C., A.-L Lozano, F. Cherblanc, and B. Cousin, Phase change of water in hygroscopic porous medium. phenomenological relation and experimental analysis for water in soil, *J. Nonequi. Thermodyn.*, *34*, 133-153,2009.

Bénet, J. C., Contribution à l'étude thermodynamique des milieux poreux non saturés avec changement de phase, *Thèse*, Université des Sciences et Techniques du Languedoc, Montpellier, 1981.

Callen, H. B., Thermodynamics and an Introduction to Thermostatistics, *John Wiley & Sons*, 1985.

Campbell, G. S., and S. Shiozawa, Prediction of hydraulic properties of soils using particle-size distribution and bulk density data. In: M. Th. van Genuchten et al. (eds.), *Proc. Int. Workshop on Indirect Methods for Estimating Hydraulic Properties of Unsaturated Soils*, Riverside, CA, 11-13 Oct. 1989, p. 317-328, Univ. of California, Riverside, 1989.

Chapuis, R. P., Predicting the saturated hydraulic conductivity of soils: a review, *Bull Eng. Geol. Environ.*, *71*, 401–434, 2012.

Durner, W., B. Schultze, and T. Zurmuhl, State-of-the-art in inverse modeling of inflow/outflow experiments, In: M. Th. van Genuchten, F.J. Leij, and L. Wu (eds.), *Proc. Int. Workshop on Characterization and Measurement of the Hydraulic Properties of Unsaturated Porous Media*, Riverside, CA, 22-24 Oct, 1997, p. 661-681, 1999.

Fayer, M. J., and S. C. Simmons, Modified soil water retention functions for all matric suctions, *Water Resour. Res.*, *31*(5), 1233–1238, 1995.

Fredlund, D. G., and A. Xing, Equations for the soil-water characteristic curve, *Can. Geotechn. J.*, *31*(4), 521–532, August 1994.

Fremond, M., and P. Nicolas, Macroscopic thermodynamics of porous media, *Continuum Mech. Thermodyn.*, *2*, 119-139, 1990.

Fujimaki, H., M. Inoue, and K. Konishi, A multi-step inflow method for estimating hydraulic conductivity at low pressure under the wetting process, *Geoderma*, *120*, 177–185, 2004.

Fujimaki, H., and M. Inoue, A transient evaporation method for determining soil hydraulic properties at low pressure, *Vadose Zone J.*, *2*, 400–408, 2003.

Ippisch, O., H.-J. Vogel, and P. Bastian, Validity limits for the van Genuchten–Mualem model and implications for parameter estimation and numerical simulation, *Adv. Water Resour.*, *29*, 1780–1789, 2006.

Khlosi, M., W. M. Cornelis, A. Douaik, M. Th. van Genuchten, and D. Gabriels, Performance evaluation of models that describe the soil water retention curve between saturation and oven Dryness, *Vadose Zone J.*, *7*, 87–96, 2008.

Khlosi, M., W. M. Cornelis, D. Gabriels, and G. Sin, Simple modification to describe the soil water retention curve between saturation and oven dryness, *Water Resour. Res.*, *42*, W11501, 2006.

Kosugi, K., General model for unsaturated hydraulic conductivity for soils with log-normal pore-size distribution, *Soil Sci. Soc. Am. J.*, *63*, 270–277, 1999.

Lu, S., T. R. Y. Gong, and R. Horton, Evaluation of three models that describe soil water retention curves from saturation to oven dryness, *Soil Sci. Soc. Am. J.*, *72*(6), 1542 - 1546, 2008.

Nelder, J. A. and R. Mead, A simplex method for function minimization, *The Computer J.*, *7*, 308-313, 1965.

Nimmo, R. J., Experimental testing of transient unsaturated flow theory at low water content in a centrifugal field, *Water Resour. Res.*, *26*, 1951–1960, 1990.

Nitao, J. J., and J. Bear, Potentials and their role in transport in porous media, *Water Resour. Res.*, *32*, 225-250, 1996.

Peters, A., W. Durner, and G. Wessolek, Consistent parameter constraints for soil hydraulic functions, *Adv. Water Resour.*, *3,* 1352–1365, 2011.

Peters, A., and W. Durner, Simplified evaporation method for determining soil hydraulic properties. *J. Hydrol.*, *356*(1-2), 147–162, 2008.

Rossi, C., and J. R. Nimmo, Modeling of soil water retention from saturation to oven dryness, *Water Resour. Res.*, *30*, 701–708, 1994.

Sakai, M., N. Toride, and J. Šimůnek, Water and vapor movement with condensation and evaporation in a sandy column, *Soil Sci. Soc. Am. J.*, *73*(3), 707, 2009.

Schaap, M. G., and M. Th. van Genuchten, A Modified Mualem–van Genuchten formulation for improved description of the hydraulic conductivity near saturation, *Vadose Zone J.*, *5*, 27–34, 2006.

Schaap, M. G., F. J. Leij, and M. Th. van Genuchten, *ROSETTA:* A computer program for estimating soil hydraulic parameters with hierarchical pedotransfer functions, *J. Hydrol.*, *251,* 163-176, 2001.

Schaap, M. G., and F. J. Leij, Improved prediction of unsaturated hydraulic conductivity with the Mualem – van Genuchten model, *Soil Sci. Soc. Am. J.*, *64*, 843-851, 2000.

Schindler, U., W. Durner, G. von Unold, and L. Müller, Evaporation method for measuring unsaturated hydraulic properties of soils: Extending the measurement range, *Soil Sci. Soc. Am. J.*, *74*(4), 1071, 2010.

Sillers, S. W, and D. G. Fredlund, Statistical assessment of soil-water characteristic curve models for geotechnical engineering, *Can. Geotechn. J.*, *38*(6), 1297–1313, 2001.

Tokunaga, T. K., Hydraulic properties of adsorbed water films in unsaturated porous media, *Water Resour. Res., 45*, W06415, 2009.

Tuller, M., and D. Or, Hydraulic conductivity of variably saturated porous media - Film and corner flow in angular pore space, *Water Resour. Res.*, *37*, 1257–1276, 2001.

van Genuchten, M. Th., F. J. Leij, and S. R. Yates, The RETC Code for Quantifying the Hydraulic Functions of Unsaturated Soils, Version 1.0., *EPA Report 600/2-91/065*, U.S. Salinity Laboratory, USDA, ARS, Riverside, California, 1991.

van Genuchten M. Th., and D. R. Nielsen, On describing and predicting the hydraulic properties on unsaturated soils, *Annales Geophysicae*, *3*(5), 615-628, 1985.

van Genuchten M. Th., A closed form equation for predicting the hydraulic conductivity of unsaturated soils, *Soil Sci. Soc. Am. J.*, *44*(5), 1980.

Webb, S. W., A simple extension of two-phase characteristic curves to include the dry region, *Water Resour. Res.*, *36*, 1425–1430, 2000.

Zhang, Z. F., Soil water retention and relative permeability for conditions from oven-dry to full saturation, *Vadose Zone J.*, *10*(4), 1299-1308, 2011.

Estimating Saturated Hydraulic Conductivity from Surface Ground-Penetrating Radar Monitoring of Infiltration

Emmanuel Léger[1], Albane Saintenoy[2], and Yves Coquet[3]

[1] *Université Paris Sud, UMR8148 IDES, Orsay, France, emmanuel.leger@u-psud.fr*
[2]*Université Paris Sud, UMR8148 IDES, Orsay, France, albane.saintenoy@u-psud.fr*
[3]*Université Orléans, ISTO/OSUC.,Orléans, France, yves.coquet@univ-orleans.fr*

Abstract

In this study we used Hydrus-1D to simulate water infiltration from a ring infiltrometer. We generated water content profiles at each time step of infiltration, based on a particular value of the saturated hydraulic conductivity while knowing the other van Genuchten parameters. Water content profiles were converted to dielectric permittivity profiles using the Complex Refractive Index Method relation. We then used the GprMax suite of programs to generate radargrams and to follow the wetting front using arrival time of electromagnetic waves recorded by a Ground-Penetrating Radar (GPR). Theoretically, the depth of the inflection point of the water content profile simulated at any infiltration time step is related to the peak of the reflected amplitude recorded in the corresponding trace in the radargram. We used this relationship to invert the saturated hydraulic conductivity for constant and falling head infiltrations. We present our method on synthetic examples and on two experiments carried out on sand. We further discuss the possibility of estimating two other van Genuchten parameters, n and α, in addition to the saturated hydraulic conductivity.

1. Introduction

Soil hydraulic properties, represented by the soil water retention $\theta(h)$ and hydraulic conductivity $K(h)$ functions, dictate water flow in the vadose zone, as well as partitioning between infiltration and runoff. Their evaluation has important implications for modeling available water resources and for flood forecasting. It is also crucial in evaluating the soil capacity to retain chemical pollutants and in assessing the potential for groundwater pollution.

The determination of parameters defining the van Genuchten soil water retention function (van Genuchten, 1980) is usually done using laboratory experiments, such as the hanging water column (Dane and Hopmans, 2002). On the other hand, the hydraulic conductivity can be estimated either in the laboratory, or *in situ* using infiltration tests. Among the large number of existing infiltration tests (Angulo-Jaramillo, 2002), the single (Müntz et al., 1905) or double ring infiltrometers (Boivin et al., 1987) provide the field saturated hydraulic conductivity by applying a positive pressure on the soil surface, while the disk infiltrometer (Perroux et White, 1988; Clothier and White, 1981) allows for reconstruction of the hydraulic conductivity curve by applying different pressures smaller than or equal to zero. For infiltration tests, the volume of infiltrated water versus time is fitted to infer the soil hydraulic conductivity at or close to saturation. These tests are time-consuming and difficult to apply to landscape-scale forecasting of infiltration. Furthermore, their analysis involves various simplifying assumptions, partly due to the ignorance of the shape of the infiltration bulb.

Geophysical monitoring methods, mainly electrical (Battle-Aguilar et al., 2009) and electromagnetic methods, have been carried out during the infiltration process. Among them, the Ground-Penetrating Radar (GPR) is based on electromagnetic (EM) wave propagation. It is highly sensitive to variations in water contents, which are directly related to the dielectric permittivity (Huismann et al., 2003). This method thus appears to be an accurate tool for monitoring the wetting front movement during infiltration (Saintenoy et al., 2008).

2. Methods

We studied infiltration of a 5-cm thick water layer inside of a single ring infiltrometer in a sandy soil. The schematic of the apparatus is presented in Figure 1. The single ring infiltrometer is a 1-mm thick aluminum cylinder of a 60-cm diameter, approximately 20-cm high, buried in the soil to a depth of 10 cm. We set up a GPR antennae (namely the transmitter T and the receiver R) at a variable distance from the edge of the cylinder, labeled *x* in Figure 1. In all of our field experiments, we used a Mala RAMAC system with antennae centered on 1600 MHz, shielded at the top. We then covered the inner part of the cylinder with a plastic waterproof sheet. The plastic sheet allowed us to fill the cylinder with water and create an initial 5-cm thick water layer, while preventing infiltration into the sand before starting data acquisition. The beginning of the acquisition was launched by pulling away the plastic sheet to trigger water infiltration. The GPR system was set to acquire a trace every 10 s. With this apparatus, we performed two types of infiltration: i) a falling head infiltration consisting of pulling away the plastic sheet and leaving water to infiltrate into the sand freely with no additional refill, and ii) a constant head infiltration, when water was continuously added to the ring to maintain a 5-cm thick water layer during the infiltration experiment. In the following examples we will show how we can use the GPR data acquired every 10 s during the infiltration experiment to estimate the saturated hydraulic conductivity.

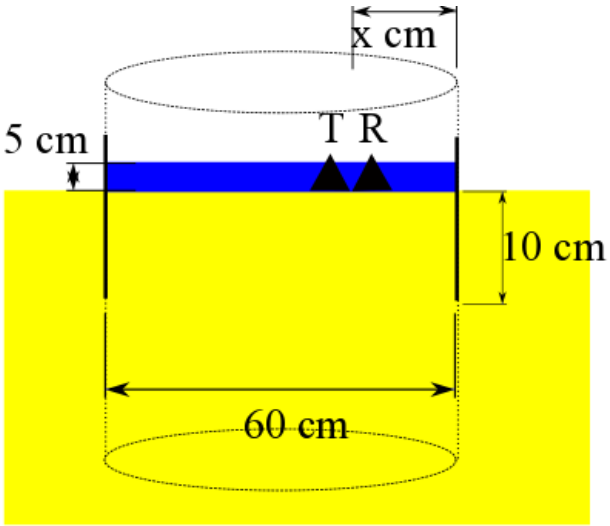

Figure 1. Schematic of the apparatus at its initial state.

3. Falling Head Infiltration

3.1. Numerical Example

3.1.1. Forward Modeling

The falling head infiltration experiment was simulated using Hydrus-1D (Šimůnek et al., 1996, 2008; Šimůnek and van Genuchten, 1996). The soil profile was 50 cm deep, was assumed to be homogeneous, and was divided into 1001 layers. To describe the soil hydraulic properties of the medium, we used the van Genuchten-Mualem (van Genuchten, 1980) hydraulic conductivity and water retention functions, which require 5 parameters, namely the saturated water content, θ_s, the residual water content, θ_r, two fitting parameters, α and n, and the saturated hydraulic conductivity, K_s. For our numerical example, we set θ_s=0.43, θ_r=0.07, α=0.019 cm^{-1}, n=8.67, and K_s=0.120 cm/min. We used an atmospheric boundary condition (BC) with no rain and no evaporation at the soil surface and a free drainage BC at the bottom. To simulate the 5-cm layer of water, the initial condition was set to a 5 cm pressure head in the top node. We simulated the first 10 minutes of the experiment with a time step of 10 s, i.e., with 60 water content snapshots. Using the CRIM relation (Birchak et al., 1974; Roth et al., 1990), each water content snapshot was converted to permittivity profiles (made of 1001 points), considering a three-phase media: sand (considered as pure silica), water, and air. Each one of these permittivity profiles (Fig. 2a) were the input for the GprMax2D program (Giannopoulos, 2004), based on finite difference time domain modeling, the output of which is one simulated GPR trace acquired at the antenna position (set at the surface of the medium, in the middle with X=0.3 m in Fig. 1). The simulated GPR monitoring of the infiltration process is shown in Figure 2b. The horizontal axis is the number of traces simulated by GprMax2D, two traces being separated by 10 seconds, as Hydrus-1D profiles are. The vertical axis is the Two-Way Travel time (TWT) of the EM wave amplitude coming back to the receiver.

On the profile presented in Figure 2b, we denote one particular reflection, labeled A. Its arrival time is increasing as the wetting front moves deeper. This reflection is interpreted as coming from the wetting front. The reflections labeled A' and A" are primary and secondary multiples of reflection A. The reflection labeled B is the wave traveling in the air directly between the two antennae. After the 40th trace, the 5-cm layer of water has been infiltrated and drainage is starting. As a consequence, the permittivity of the upper part of the medium decreases. The EM wave velocity is inversely proportional to the square root of permittivity (Huisman et al., 2003). Then the TWT of the reflection A increases more slowly, creating a change of slope in the reflection time curve (Fig. 2b). In Figure 2c, we display two curves: the TWT of the maximum peak of a reflection A (obtained from Fig. 2b) and the TWT calculated by a ray-path algorithm, going from the GPR antennae to the inflection point of $\varepsilon(z)$ curves (indicated by crosses in Fig. 2a), as proposed by Saintenoy and Hopmans (2011). We attribute the difference between these two curves to some numerical dispersion of the signal, a problem that we will address later.

3.1.2. Inversion

We used the TWT obtained from the radargram of Figure 2b as data to be fitted to derive the saturated hydraulic conductivity, assuming the other 4 parameters are known. Using Hydrus-1D, we generated 60 water content snapshots using the saturated hydraulic conductivity in the range from 0.01 to 1 cm/min, with a step of 0.001 cm/min. For each value of K_s, we calculated the TWT by the ray-path algorithm from the surface to the inflection point of the $\varepsilon(z)$ curves. We computed the Root Mean Square Error (*RMSE*) between these times and the data. The *RMSE* was minimized for K_s=0.129 cm/min, which is higher than the value used for simulating the data, i.e., K_s=0.120 cm/min.

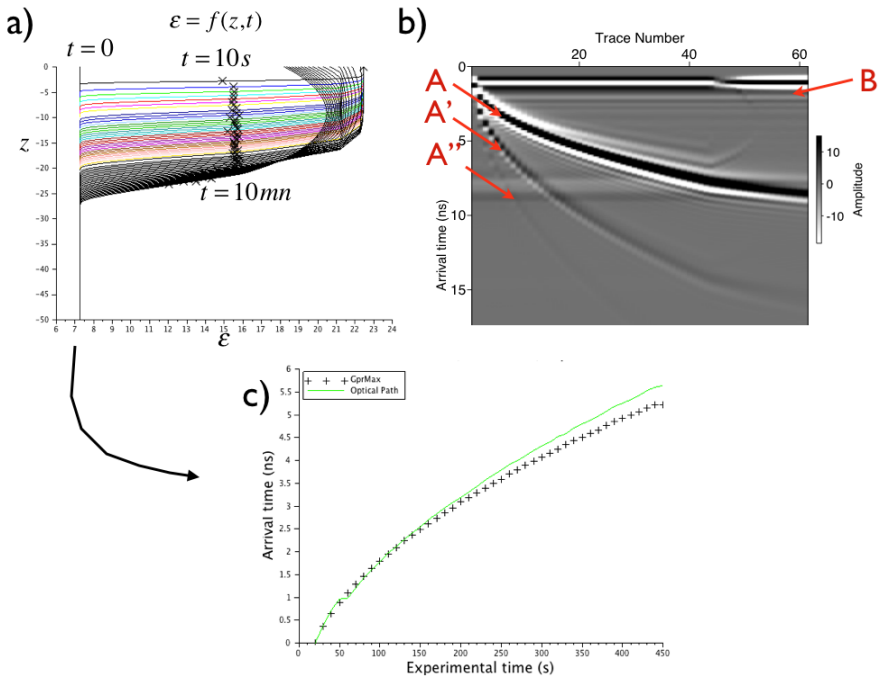

Figure 2. Falling head infiltration from a 5-cm thick water layer. a) Permittivity profiles: each curve is plotted every 10 s; crosses represent the inflection points of each curve. b) Radargram simulated with GprMax2D; reflection A is coming from the wetting front, B is the direct wave, A' and A" are multiples of reflection A. c) TWT computed with an optical path algorithm, directly from the permittivity profiles.

3.2. Experimental Example

3.2.1. Experimental Data and its Analysis

The experiment took place in a quarry of Fontainebleau sand in Cernay-La-Ville (Yvelines, France). The middle of the antennae was positioned 11 cm away from the cylinder wall (x = 11 cm in Fig. 1). The 5-cm water layer was fully infiltrated after about 10 minutes, although in certain areas of the soil surface this time has been slightly shorter. The recorded GPR data are shown in Figure 3. We recorded during 30 minutes, with a time window of 15 ns, transmitting

and receiving each 10 seconds (stacking 4 measurements). We subtracted the average trace and applied an Automatic Gain Control to the data. The sand parameters have been determined in laboratory by several classical hanging water column experiments, fitted by the van Genuchten retention curve. Assuming a 5% uncertainty of the optimized parameters, we obtained θ_r=0.062 ±0.003, θ_s=0.39±0.01, α=0.023±0.001, and n=6.7±0.3. We considered in our model that the sand was homogeneous. Gravimetric measurements on field samples gave us an initial volumetric water content of θ_i=0.09±0.01. In the profile presented in Figure 3, we denote three particular reflections. The one interpreted as coming from the infiltration front, labeled A, is visible during the first 30 minutes of the acquisition, with an arrival time varying from 2 ns down to 9 ns. The other reflections are interpreted in Léger and Saintenoy (2012). We determined the arrival time of the A reflection peak and inverted the saturated hydraulic conductivity using the same algorithm as for the synthetic case. We obtained the minimum of the objective function for K_s=0.131 cm/min. In parallel, we also carried out disk infiltrometer experiments using the multi-potential method (Ankeny et al., 1991; Reynolds and Elrick, 1991). We obtained a value of the saturated hydraulic conductivity of K_{Disk}=0.108±0.01 cm/min.

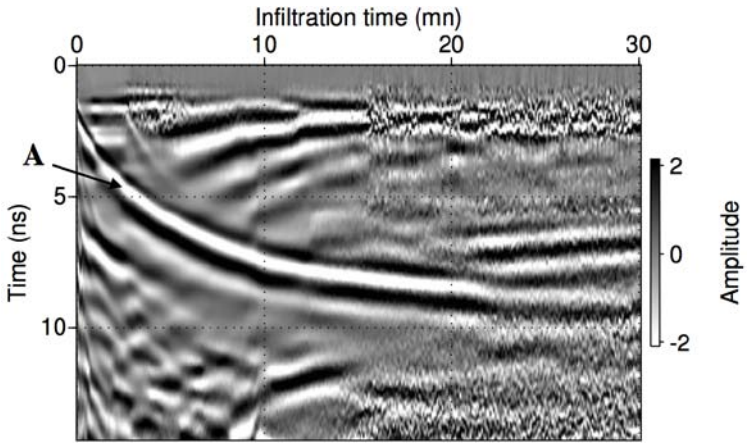

Figure 3. Experimental GPR data acquired during the falling head infiltration (from a 5 cm initial water layer). Reflection A is the reflection coming from the wetting front.

3.2.2. Uncertainty Analysis

We assumed a 5% relative uncertainty of four van Genuchten parameters and the initial water content of the sand. These parameters directly influence the arrival time curves used to compute the misfit function. Figure 4 shows variations associated with each of these parameters. It appears that the uncertainty in α has the strongest influence on the arrival time curves. As an attempt to evaluate the uncertainty in the saturated hydraulic conductivity retrieved from GPR data fitting, we made some quadratic error summation associated with each of the parameters. The total quadratic error has the expression of $\delta_{tot} = \sqrt{\delta_{ti}^2 + \delta_{tr}^2 + \delta_{ts}^2 + \delta_{\alpha}^2 + \delta_n^2 + \delta_{gpr}^2 + \delta_{A\lg o}^2}$, where δ_{ti}, δ_{tr}, δ_{ts}, δ_{α}, and δ_n are *RMSE* due to uncertainties in θ_i, θ_r, θ_s, α, and n. The *RMSE* is the summation of the two curves for each parameter, presented in Figure 4. δ_{gpr} =0.1 ns is assumed to be the error on picking, and δ_{A1go}=0.01 ns is the *RMSE* between the arrival times generated by the optical path-algorithm and the GprMax modeling (Fig. 2c). The total quadratic error was

estimated at δ_{tot}=0.101 ns. From the objective function curve, all K_s in the interval [0.04; 0.263 cm/min] have a misfit value to our data of less than 0.111 ns, with the minimum at 0.131 cm/min. We think that this wide interval of possible K_s is over-estimated by our rough error determination.

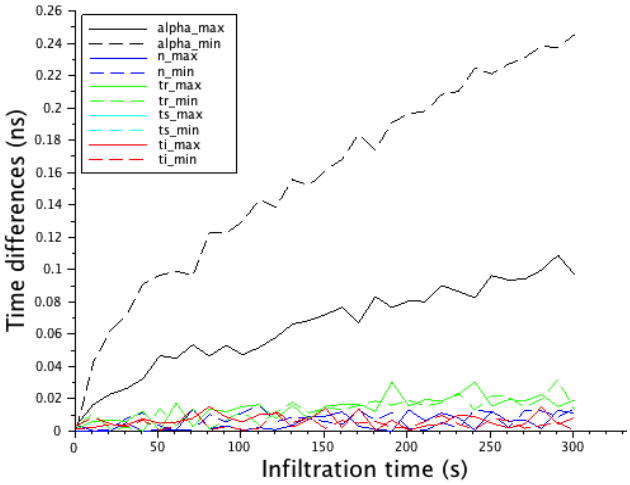

Figure 4. Influence of the parameter uncertainties on the arrival time difference, between the arrival time generated with each parameter and the arrival time generated with optimal parameters.

4. Constant Head Infiltration

4.1. Numerical Example

In the second case, a water layer of 5 cm above the ground is kept constant during the entire experiment. Similarly as above, using the same van Genuchten parameters as in the first synthetic example (θ_s=0.43, θ_r=0.07, α=0.019 cm^{-1}, n=8.67, and K_s=0.120 cm/min), we modeled infiltration of water inside a ring infiltrometer by applying a constant pressure head of 5 cm to the top node during 10 minutes. The permittivity profiles are presented in Figure 5a, with each curve plotted every 10 s as in the previous case. Figure 5b shows the radargram simulated with GprMax2D. As can be seen, the reflection labeled A, describing the position of the infiltration front, is returning at increasing times because infiltration is being constantly fed by the constant ponding depth, contrary to the previous falling head case. In Figure 5c, we computed the TWT of the wetting front, using the ray path algorithm and the picking of A reflection coming from the radargram in Figure 5b.

Assuming the four van Genuchten parameters θ_r, θ_s, α, and n are known, we inverted for the saturated hydraulic conductivity by minimizing the differences between the arrival times of the wetting front reflection obtained by the ray path-algorithm and the arrival times picked from the radargram in Figure 5b. The objective function was minimized for K_s=0.128 cm/min, which is again larger than the value used for simulating the data: K_s=0.120 cm/min.

4.2. Experimental Example

The experiment took place in the same quarry of Fontainebleau sand as the previous experiment. The middle of antennae was positioned in the middle of the ring (x = 30 cm in Fig. 1). The recorded GPR data are shown in Figure 6. We recorded during 80 minutes, with a time window of 30 ns (in Fig. 6, we only present a part of the radargram), transmitting and receiving each 5 seconds and with no stacking. In the radargram in Figure 6, we subtracted the average trace and applied an AGC gain to the data. We used the van Genuchten parameters determined in the laboratory using the hanging column experiments, and we measured on sand samples an initial volumetric water content of θ_i=0.07±0.02.

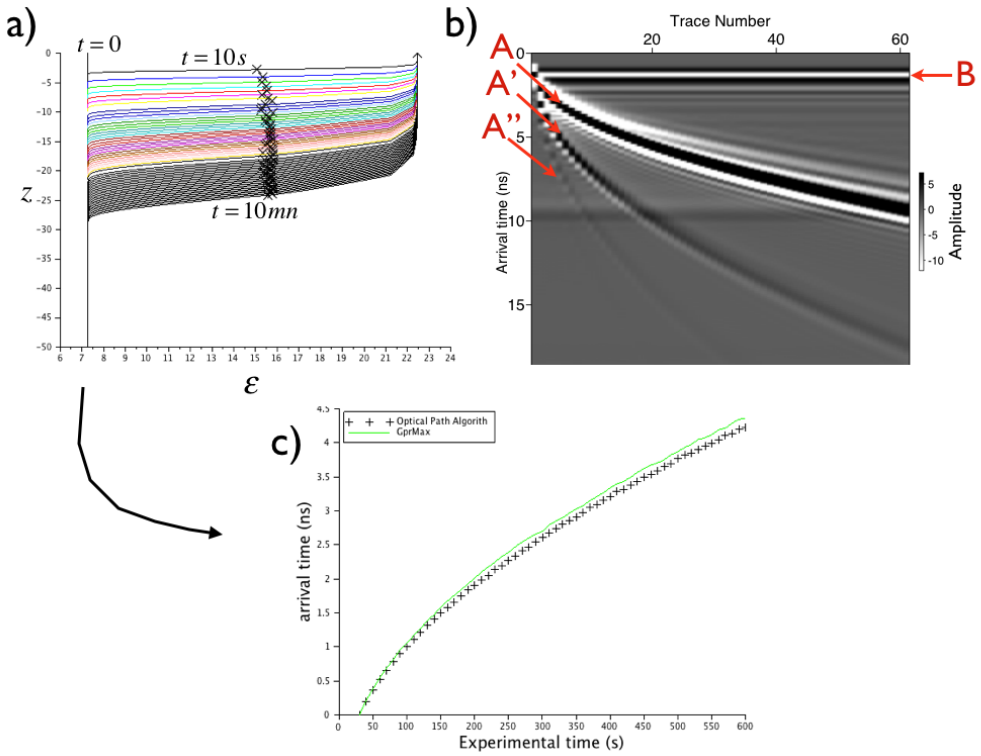

Figure 5. Constant head infiltration with 5 cm of water. a) Permittivity profiles, each curve is plotted every 10 s. Crosses represent the inflection points. b) Radargram simulated with GprMax2D, reflection A is the wetting front, B is the direct wave, A' and A" are multiples. c) Two Way Travel Time, computed with an optical path algorithm directly from the permittivity profiles.

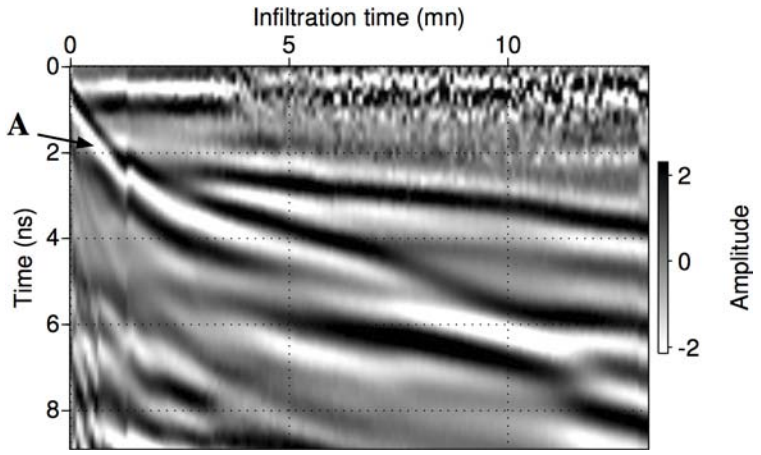

Figure 6. GPR data acquired during a constant head (5 cm) infiltration. Reflection A is the reflection coming from the wetting front.

In the profile presented in Figure 6, the arrival time of reflection A ranges from 0 at the beginning of the experiment to about 6 ns after 10 min. We picked the arrival time of the reflection A peak and computed the objective function using the same procedure as described before. We obtained the minimum of the objective function for K_s=0.110 cm/min. This value has to be again compared with the one obtained by the disk infiltrometer experiment, K_{Disk}=0.108±0.01 cm/min. Using the same procedure as presented in the earlier field example, we found a total quadratic error of δ_{tot} =0.131 ns, which gives a range of possible values for the saturated hydraulic conductivity, K_s =[0.035; 0.213] cm/min.

5. Toward a Three Parameter Inversion

From our uncertainty analysis (Fig. 4), we pointed out the high sensitivity of our inversion to the parameter α. The solution may be in inverting our GPR measurements for α and n in addition to K_s, assuming θ_s and θ_r known. We computed misfit diagrams of the arrival times, to analyze which parameters can be easily inverted by our algorithm and which cannot. The procedure of calculating misfit diagrams is presented in Figure 6d. We carried out this analysis for both infiltration cases. We set one of the three parameters and plotted the misfit diagram for the two others. In Figure 6, we present the misfit diagrams obtained for the constant head infiltration. In Figure 6, we present similar diagrams for the falling head infiltration. When Hydrus-1D did not converge for a given combination of parameters, we set the misfit equal to 10 (dark red areas in Figures 6abc). The misfit diagram (K_s,α) in Figure 6b does not exhibit a correlation between those two parameters, and informs us about the possibility of inverting (K_s,α) while knowing n. The two other diagrams show the difficulty of obtaining the correct value of n. Indeed, this parameter is directly related to the slope of the retention curve $\partial\theta/\partial h$, and thus also to $\partial\theta/\partial z$ at the infiltration front. This information is not present in the TWT of the inflection points used for the misfit computations.

Figure 7 presents misfit diagrams for the falling head infiltration, calculated using the same procedure as above. The upper boundary condition in Hydrus-1D was set to a variable pressure

head. Note again that each time when Hydrus-1D did not converge, the misfit was set equal to 10 (dark red zones in the graph). Graphs 7a and 7c are completely different than in the previous case. They imply that having information on the evolution of the water layer thickness from the experiment itself is providing additional information that can help resolve the uniqueness problem for the *n* parameter. This case needs to be explored in the future in more detail.

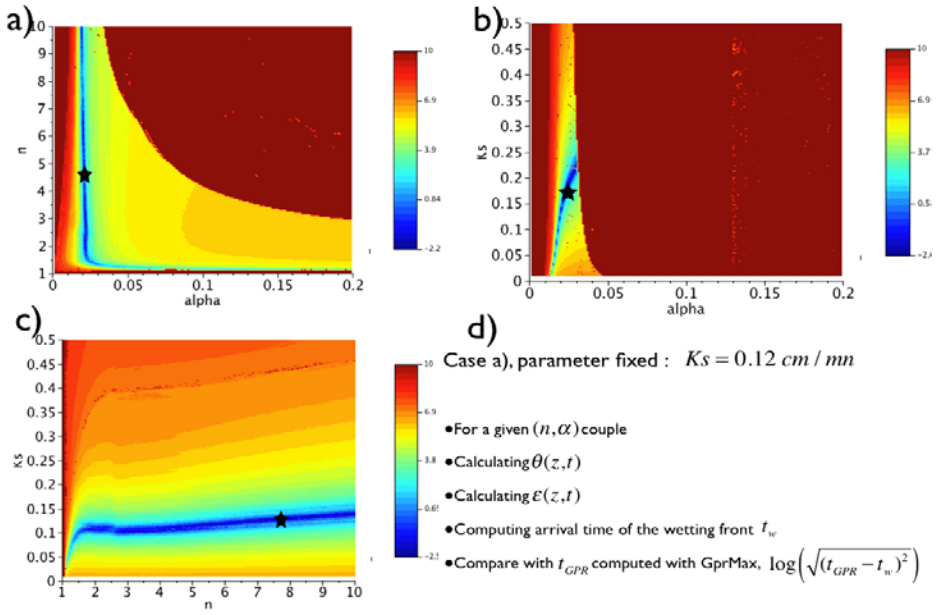

Figure 7. Misfit diagrams for the constant head boundary condition: a) n-α diagram, b) K_s-α diagram, and c) K_s-n diagram. Black stars represent minimum.

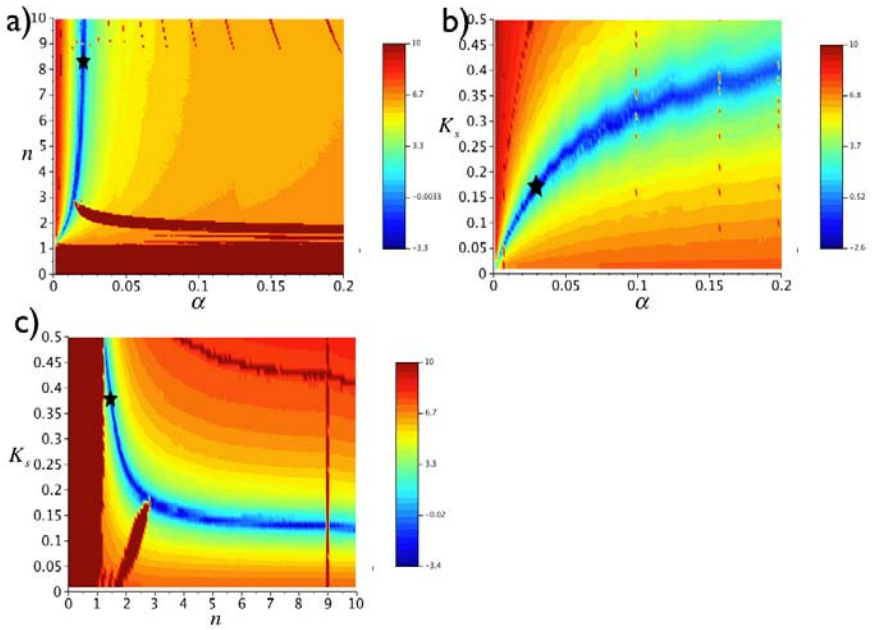

Figure 8. Misfit diagrams for the falling head boundary condition: a) n-α diagram, b) K_s-α diagram, and c) K_s-n diagram. Black stars represent minimum.

References

Angulo-Jaramillo, R., J. Vandervaere, S. Roulier, J. Thony, J. Gaudet, and M. Vauclin, Field measurement of soil surface hydraulic properties by disc and ring infiltrometers. a review and recent developments, *Soil and Tillage Research*, *55*, 1–29, 2000.

Ankeny, M. D., M. Ahmed, T.C. Kaspar, and R. Horton, Simple field method for determining unsaturated hydraulic conductivity, *Soil Sci. Soc. Am. J.*, *55*, 467-470, 1991.

Battle-Aguilar, J., S. Schneider, M. Pessel, P. Tucholka, Y. Coquet, and P. Vachier, Axisymmetrical infiltration in soil imaged by non-invasive electrical resistivimetry, *Soil Sci. Soc. Am. J.*, *73*(2), 510–520, 2009.

Birchak, J. R., C. G. Gardner, J. E. Hipp, and J. M. Victor, High dielectric constant microwave probes for sensing soil moisture, *Proceedings of the IEEE*, *62*, 93–98, 1974.

Boivin, P., J. Touma, and P. Zante, Mesure de l'infiltrabilité du sol par la méthode du double anneau. 1-Résultats expérimentaux, *Cahiers Orstom, série Pédologique*, *24*(1), 17-25, 1987.

Clothier, B. E., and I. White, Measurement of sorptivity and soil water diffusivity in the field, S*oil Sci. Soc. Am. J.*, *45*, 241–245,1981.

Dane, J. H., and J. W. Hopmans, Hanging water column, In: *Methods of Soil Analysis, Part 4, Physical Methods,* Eds. J. H. Dane and G. C. Topp, Third edition, SSSA, Madison, WI, pp. 680–684, 2002.

Giannopoulos, A., Modelling ground penetrating radar by GprMax, *Construction and Building Materials*, *19*(10), 755–762, 2005.

Huisman, J. A., S. S. Hubbard, J. D. Redman, and A. P. Annan, Measuring soil water content with ground-penetrating radar: A review, *Vadose zone journal*, *2*, 476–491, 2003.

Léger, E., and A. Saintenoy, Surface ground-penetrating radar monitoring of water infiltration inside a ring infiltrometer, In *14th International Conference on Ground Penetrating Radar*, Shanghai, 2012.

Müntz, A., L. Faure, and E. Laine, Etudes sur la perméabilité des terres, faites en vue de l'arrosage, *Ann. De la Direction de l'Hydraulique*, vol. f33, pp. 45–53, 1905.

Perroux, K. M., and I. White, Designs for disc permeameters, *Soil Sci. Soc. Am. J.,* 52:1205–1215, 1988.

Reynolds, W. D., and D. E. Elrick, Determination of hydraulic conductivity using a tension infiltrometer, *Soil Sci Soc. Am. J.*, *55*, 633-639, 1991.

Saintenoy, A., and J. W. Hopmans, Ground Penetrating Radar: Water Table Detection Sensitivity to Soil Water Retention Properties, *Selected Topics in Applied Earth Observations and Remote Sensing, Journal of IEEE*, *4*(4), 748,753, 2011.

Saintenoy, A., S. Schneider, and P. Tucholka, Evaluating ground penetrating radar use for water infiltration monitoring, *Vadose Zone Journal*, *7*, 208–214, 2008.

Šimůnek, J., and M. Th. van Genuchten, Estimating unsaturated soil hydraulic properties from tension disc infiltrometer data by numerical inversion, *Water Resour. Res*., *9*, 2683–2696, 1996.

Šimůnek, J., M. Šejna, and M. Th. van Genuchten, *The HYDRUS-2D Software Package for Simulating Water Flow and Solute Transport in Two-Dimensional Variably-Saturated Porous Media*, Version 1.0. Int. Ground Water Model. Ctr., Colorado School of Mines, Golden, 1996.

Šimůnek, J., M. Th. van Genuchten, and M. Šejna, Development and applications of the HYDRUS and STANMOD software packages, and related codes, *Vadose Zone Journal*, *7*(2), 587-600, 2008.

van Genuchten, M. Th., A closed form equation for predicting the hydraulic conductivity of unsaturated soils, *Soil Sci. Soc. Am. J.*, *44*, 892– 898, 1980.

Modeling Hg Reactive Transport in Soil Systems Using HP1

Bertrand Leterme and Diederik Jacques

Performance Assessments, Institute Environment, Health and Safety, Belgian Nuclear Research Centre, Mol, Belgium, bleterme@sckcen.be, djacques@sckcen.be

Abstract

We developed a reactive transport model for simulating mercury (Hg) fate and transport in the unsaturated zone, in order to gain insight into the environmental fate of Hg originating from contaminated soil. The code was implemented using the module HP1 (Jacques et al., 2006; 2008), which couples HYDRUS-1D (Šimůnek et al., 2008) for water and solute transport with PHREEQC (Parkhurst and Appelo, 1999) for geochemical reactions. The main processes accounted for in the model are Hg aqueous speciation (including complexation with dissolved organic matter (DOM), humic and fulvic acids (HA and FA), and thiol groups), Hg sorption to solid organic matter (SOM, while also distinguishing between humic and fulvic acids and thiol groups), dissolution of solid phase Hg (e.g., cinnabar $HgS_{(s)}$), dissolution of Hg non-aqueous phase liquid (NAPL), sunlight-driven Hg^{II} reduction to Hg^0, Hg^0 diffusion in the gas phase and volatilization, and DOM sorption to soil minerals. Using a 50-year time series of daily weather data from Dessel (Belgium) and a 1-m deep sandy soil with deep groundwater (free drainage, oxic conditions), we implemented a sensitivity analysis using the elementary effects method (Morris, 1991). The most sensitive parameters determining Hg leaching or retardation were found to be the equilibrium constant for Hg sorption to humic and fulvic acids (i.e., the most abundant sorption sites in SOM), the initial concentration of Hg, and the concentration of DOM in the soil solution.

1. Introduction

Mercury (Hg) poses threats to human health and the environment, notably due to its persistence in the environment and its ability to bioaccumulate in ecosystems and the food chain. Anthropogenic sources are major contributors to the release of mercury into the atmosphere, water and soil. Soil contamination not only results from direct spills, but also indirectly, for example via deposition of prior atmospheric emissions. The main sources of mercury in soils are mercury mining activities, gold and silver mining (Hg^0 is used to amalgamate the metal), manufacturing (e.g., chlor-alkali plants, or manometer spills), wood preservation, and cemeteries (release of mercury from dental amalgams).

Mercury in soils can be present in different phases: the solid phase (most frequently cinnabar (HgS) and montroydite (HgO)), the solution phase (mainly Hg^{2+} bound to organic or inorganic ligands, but also methylmercury CH_3Hg^+ and dissolved Hg^0), the gas phase (Hg^0 or dimethylmercury $(CH_3)_2Hg$), and the non-aqueous liquid phase (NAPL), which may contain especially elemental mercury Hg^0 and is more dense than water. This complexity of multiple phases makes modeling of mercury transport in soils a particularly challenging task. As such, knowing the history of a given contaminated site is important because Hg species present in soils are closely related to the type of industry or activity that caused the contamination. The age of an Hg contaminated site is also important since the kinetics of phase transformations and retention processes may be relatively slow.

This study is focused on Hg fate and transport in the unsaturated zone following direct soil contamination from human activities. Our main objective was to develop a reactive transport model in order to gain insight into the fate and transport processes of Hg in soils under oxic conditions. The relative importance of different processes and parameters is assessed by means of with a sensitivity analysis based on the Morris (1991) method of elementary effects. The analysis is carried out for different initial speciations (dissolved, solid phase or NAPL) of Hg contamination.

2. Conceptual Model and Numerical Implementation in HP1

Figure 1 shows the conceptual model implemented in the HP1 simulator (Jacques et al., 2006; 2008). Aqueous complexation is treated using the database IM003_THERMODDEM (Blanc et al., 2012), augmented with some Hg speciation data from Skyllberg (2012). However, complexation with organic ligands is not included in IM003_THERMODDEM. Therefore, four hypothetical organic compounds (Ya, Yb and Yc representing oxygen sites of humic and fulvic acids, and Ys representing thiol groups) were added (Table 1, left column). Based on exchange capacity data, approximately 99% of the dissolved organic matter (DOM) ligands were modeled as humic and fulvic acids (88%, 11% and 1% for Ya, Yb and Yc, respectively), and about 1% as thiols (Gustafsson, 2001; Skyllberg, 2008).

Colloidal transport of Hg (Sen and Khilar, 2006; Zhu et al., 2012) is implicitly considered by the transport of Hg bound to DOM. While numerical solutions exists for simulating more realistically colloid formation and migration exist (Šimůnek et al., 2006), they generally demand numerous specific parameters that were not available for the present case.

For Hg sorption to soil organic matter (SOM) we used the EXCHANGE command of PHREEQC for simulating multiple proton/ion exchangers. Similarly to Hg complexation with DOM, four reactive surface sites were considered (Table 1, right column): Xa, Xb, Xc (representing the ~99% oxygen exchange sites from fulvic and humic acids) and Xs (representing ~1% thiol exchange sites). Sorption of DOM on soil minerals was modeled using the PHREEQC function SURFACE for surface complexation, with a Langmuir isotherm and parameters fitted by Kothawala et al. (2008).

Starting with Hg^{2+} in the aqueous phase, mercury volatilization requires two steps: (i) reduction of Hg^{II} to Hg^0, and (ii) a phase change from Hg^0(aq) to Hg^0(g). Our model at present was developed for oxic conditions, which thermodynamically does not favor volatilization. For this reason we decided to implement a (pseudo-first-order) kinetic reaction in HP1 for the reduction of Hg^{II} to Hg^0(aq) (cf. Figure 1).

Two other kinetic reactions were necessary to allow dissolution of cinnabar ($HgS_{(s)}$) and NAPL (cf. Figure 1). Cinnabar dissolution is dependent upon DOM (Waples et al., 2005) and represented by a zero-order rate equation, while NAPL dissolution is modeled by means of a first-order rate law (this was done somewhat arbitrarily due to the absence of data on Hg NAPL dissolution).

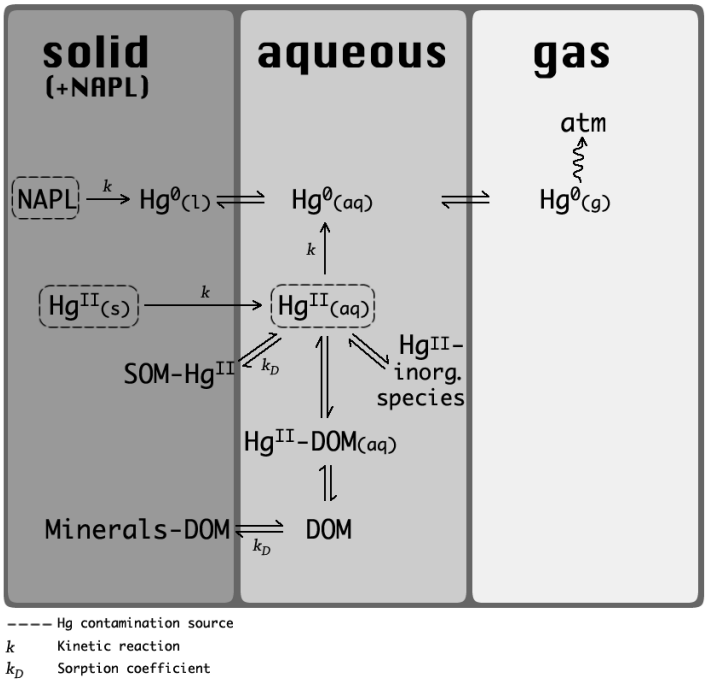

Figure 1. Conceptual model of Hg speciation and reactions in the solid, aqueous and gas phases. Initial mercury contamination can be simulated as non-aqueous phase liquid (NAPL), solid, or aqueous phase.

Table 1. Equilibrium constants for Hg-DOM complexes (left column) and for sorption of Hg to SOM (ion exchange assemblage; right column).

Complexation Hg-DOM	**Log k**	**Sorption Hg-SOM**	**Log k**
$HYa + 0.5Hg^{2+} = Hg_{0.5}Ya + H^+$	−1.1[(a)]	$Hg^{2+} + 2Xa^- = HgXa_2$	3.5[(a)]
$HYb + .5Hg^{2+} = Hg_{0.5}Yb + H^+$	−7.6[(a)]	$Hg^{2+} + 2Xb^- = HgXb_2$	4.3[(a)]
$HYc + .5Hg^{2+} = Hg_{0.5}Yc + H^+$	−1.8[(a)]	$Hg^{2+} + 2Xc^- = HgXc_2$	5.08[(a)]
$HYa + HgOH^+ = HgOHYa + H^+$	−3[(a)]	$HgOH^+ + Xa^- = HgOHXa$	7.7[(a)]
$HYb + HgOH^+ = HgOHYb + H^+$	1.8[(a)]	$HgOH^+ + Xb^- = HgOHXb$	7.7[(a)]
$HYc + HgOH^+ = HgOHYc + H^+$	2.0[(a)]	$HgOH^+ + Xc^- = HgOHXc$	10.2[(a)]
$2HYs + Hg^{2+} = HgYs_2 + 2H^+$	22.0[(b)]	$Hg^{2+} + 2HXs = HgXs_2 + 2H+$	15.4[(b)]

[(a)] Bessinger and Marks (2010)
[(b)] Skyllberg (2008)

Within the context of Hg contamination from anthropogenic sources, mercury uptake by vegetation and atmospheric wet and dry deposition could be ignored since they generally generate relatively small Hg fluxes compared to those included in our model.

3. Sensitivity Analysis

We applied Hg reactive transport model to a synthetic case, consisting of a 1-m course-textured soil having a uniform SOM content in the top 30 cm, initial Hg contamination in the top 10 cm, and a grass cover with uniform rooting depth until 30 cm (no Hg uptake). The soil surface hydraulic boundary condition consisted of atmospheric input (precipitation and potential evapotranspiration rates) obtained from a 50-year time series of daily observations in Dessel (Belgium). The lower hydraulic boundary condition was set to free drainage in order to ensure oxic conditions.

Given these assumptions, a sensitivity analysis (SA) was performed using the elementary effects method of Morris (1991). Sampling trajectories were randomly designed across parameter space (each parameter range being divided into p levels), with successive deviations in the trajectories resulting in quantification of the elementary effects. One computes then μ (the average elementary effect) which assesses the overall influence of the factor on the output, and also σ (standard deviation) which estimates the ensemble of the factor's higher order effects (i.e., non-linear and/or interaction effects). Campolongo et al. (2007) further proposed the use of μ^* (the mean of the absolute value of elementary effects) as an indicator of parameter sensitivity to identify model non-monoticity (i.e. when for a given factor elementary effects of opposite signs cancel each other in the measure of μ).

Thirteen parameters were included in the SA (Table 2), while the following model outputs were selected: leached Hg, Hg still in the originally polluted horizon, and Hg below the top 30-cm thick horizon (all expressed as % of the initial Hg contamination). The SA was repeated at three different simulation times (after 5, 25 and 50 years) and with three different contamination sources (cinnabar, Hg NAPL and aqueous mercuric chloride). Only a few representative results are presented hereafter.

Figure 2 shows plots of μ vs. σ and μ^* vs. σ for the percentage of Hg being leached after 50 years in case of cinnabar being the contamination source. Among the parameters tested, X_4 (DOM concentration of infiltrating rainwater) had the highest sensitivity. This is due to (i) Hg^{II} migration occurring mainly via Hg-DOM complexes and (ii) cinnabar dissolution rate depending upon the DOM concentration of soil water. Other parameters showing a high sensitivity were X_1 (initial cinnabar concentration) and X_8 (log k Hg-DOM (thiols)). For X_1, the high sensitivity was partly explained by the model output being expressed in a relative way (% of initial Hg), and by incomplete cinnabar dissolution over the simulation time.

Figure 3 shows plots of the concentration of Hg^{II} in the leachate over time, obtained from one SA simulation using cinnabar as the contamination source. Results indicate that Hg^{II} leaching occurs after only about 30 years. Also, after the initial breakthrough, the variability in the Hg^{II} concentration spans about two orders of magnitude. These are important findings, for example within the context of designing a sampling strategy, or for planning (temporal) objectives of soil remediation and/or risk assessment.

Table 2. List of parameters included in the sensitivity analysis, and their lower and upper bounds (uniform distributions).

Factor		Unit	Lower bound	Upper bound
X_1	Initial Hg concentration	mg kg^{-1}	135	13500
X_2	Cinnabar dissolution rate	day^{-1} g_{OC}^{-1}	4.59×10^{-4} [(a)]	1.42×10^{-2} [(a)]
X_3	Hg^{II} reduction rate	day^{-1}	6.91×10^{-7}	6.91×10^{-5}
X_4	DOM (in rainwater boundary solution)	mg L^{-1}	9 [(c,d)]	90 [(c,d)]
X_5	Exchange capacity of HA and FA (SOM top 30 cm)	meq dm^{-3}	7.95	159
X_6	Exchange capacity of thiols (SOM top 30 cm)	meq dm^{-3}	0.0705	1.41
X_7	log k complexation Hg-DOM (HA and FA)	-	$HgYa_2$ −2.2 $HgYb_2$: −15.2 $HgYc_2$: −3.6 HgOHYa: −6.0 HgOHYb :0.9 HgOHYc : 1.0	−0.55 −3.8 −0.9 −1.5 3.6 4.0
X_8	log k complexation Hg-DOM (thiols)	-	11.0	44.0
X_9	log k sorption Hg-SOM (HA and FA)	-	$HgXa_2$: 1.75 $HgXb_2$: 2.15 $HgXc_2$: 2.54 HgOHXa: 3.85 HgOHXb: 3.85 HgOHXc: 5.1	7.0 8.6 10.16 15.4 15.4 20.4
X_{10}	log k sorption Hg-SOM (thiols)		7.7	30.8
X_{11}	K_L sorption DOM to soil minerals	-	5.6×10^{-4}	1.23×10^{-2} [(g)]
X_{12}	S_{max} max. adsorption capacity of DOM to minerals	mg kg^{-1}	109 [(g)]	601 [(g)]
X_{13}	NAPL dissolution rate	day^{-1}	8.64×10^{-5}	8.64×10^{-3}

[(a)] Waples et al. (2005)
[(b)] Scholtz et al. (2003)
[(c)] Mertens et al. (2007)
[(d)] Don and Schulze (2008)
[(e)] Skyllberg (2008)
[(f)] Bessinger and Marks (2010)
[(g)] Kothawala et al. (2008)

Figure 4 presents results for the percentage of Hg still present in the top horizon (0-10 cm) after 50 years, with Hg NAPL being the contamination source. Parameter X_9 (log k Hg-SOM (HA, FA)) was the most sensitive parameter. The corresponding parameter for thiols, X_{10}, showed no sensitivity due to the high proportion of HA and FA sites compared to thiols. Factor X_1 (Hg initial concentration) was the second most important parameter. This parameter is characterized by μ values indicating non-monotonic behavior of the model. Nonlinearities and interactions with other parameters are also important for X_9 and X_1 (high σ values).

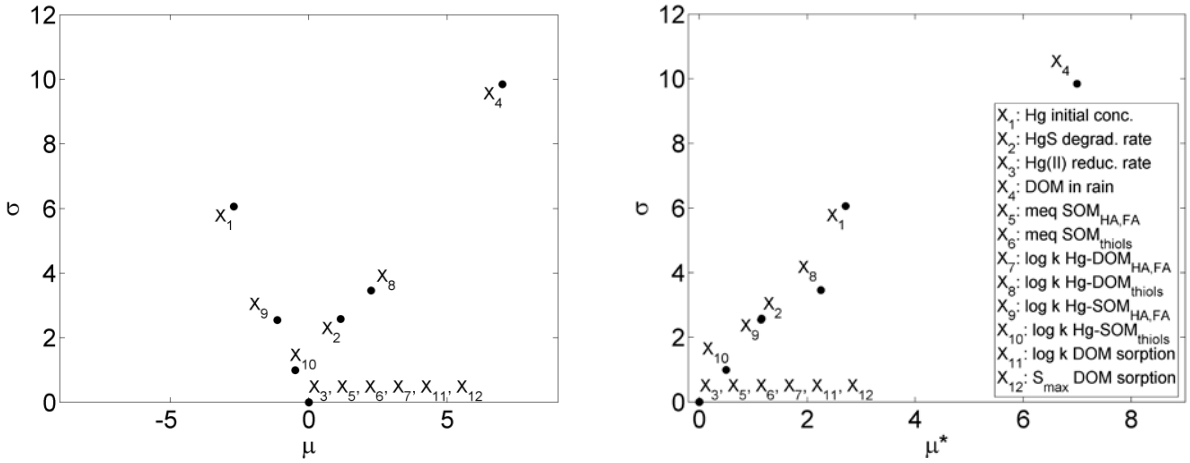

Figure 2. Plots of μ vs. σ and μ^* vs. σ for elementary effects of the percentage Hg leaching after 50 years, using 5 trajectories and cinnabar ($HgS_{(s)}$) was the contamination source.

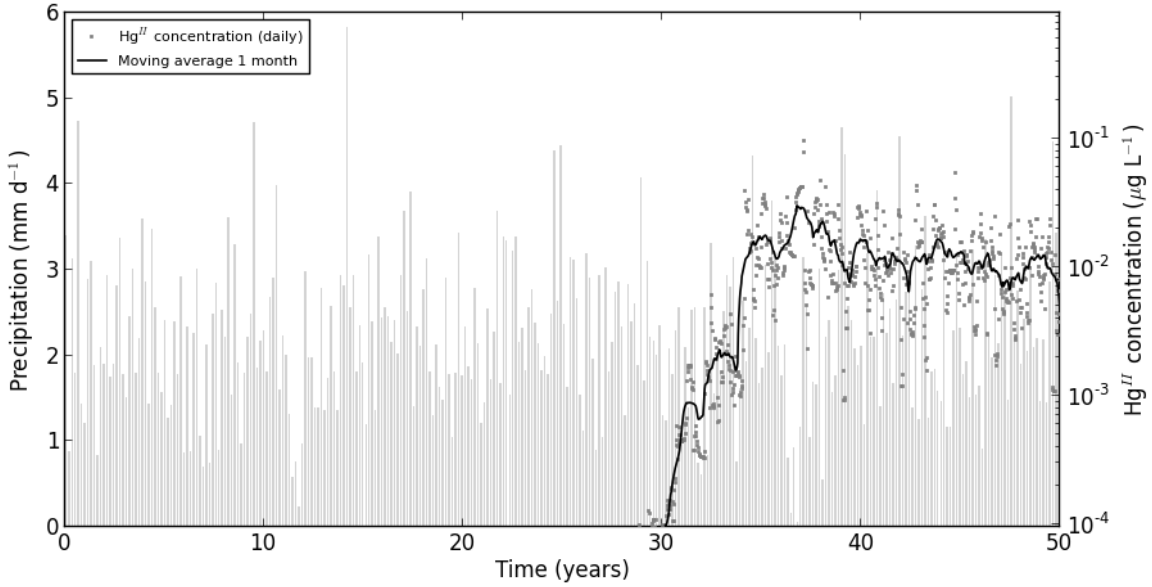

Figure 3. Hg^{II} concentration (μg L^{-1}) in the leachate over time, from one of the 60 HP1 runs of the sensitivity analysis using cinnabar ($HgS_{(s)}$) as the contamination source.

Two simulations illustrating model nonlinearity and the interaction effects are shown in Figure 5. Figure 5a indicates that no more Hg is present in the top horizon (0-10 cm) after 50 years, while the percentage is still 32.5% of the initial Hg in Figure 5b (= the maximum of all simulations of the 5 trajectories). Both simulations were carried out using the same initial concentration (X_1) and a low value of X_9. Differences between the two simulations is mainly due to interactions between X_1 and X_6 (exchange capacity of thiols). Even though thiol sorption sites are less abundant than HA and FA sites, the interaction of low X_1 and high X_6 in Figure 5b means that thiols in SOM are sufficient to retain a significant percentage of the initial Hg in the topsoil.

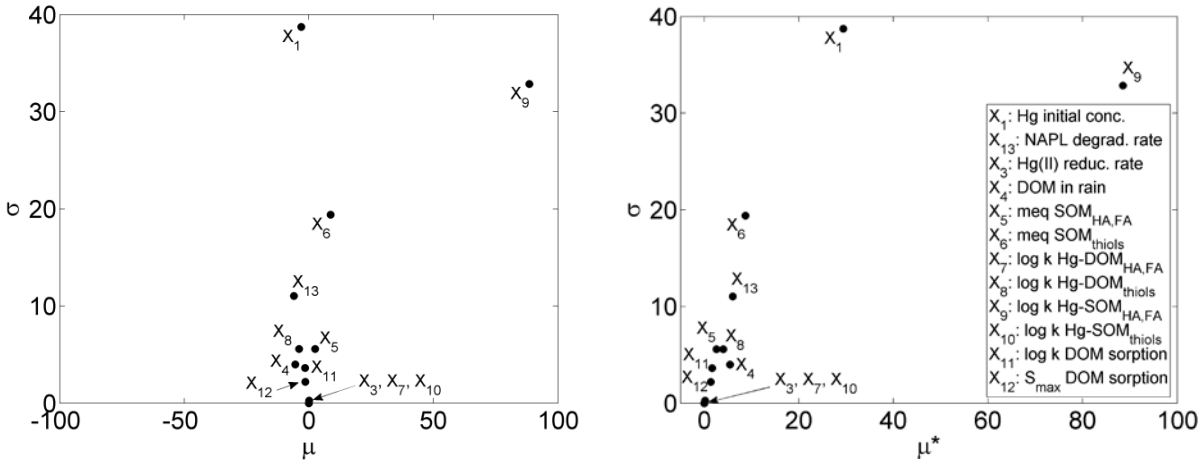

Figure 4. Plots of μ vs. σ and μ^* vs. σ for elementary effects of the percentage Hg still in the surface horizon initially polluted after 50 years, using 5 trajectories and Hg NAPL as contamination source.

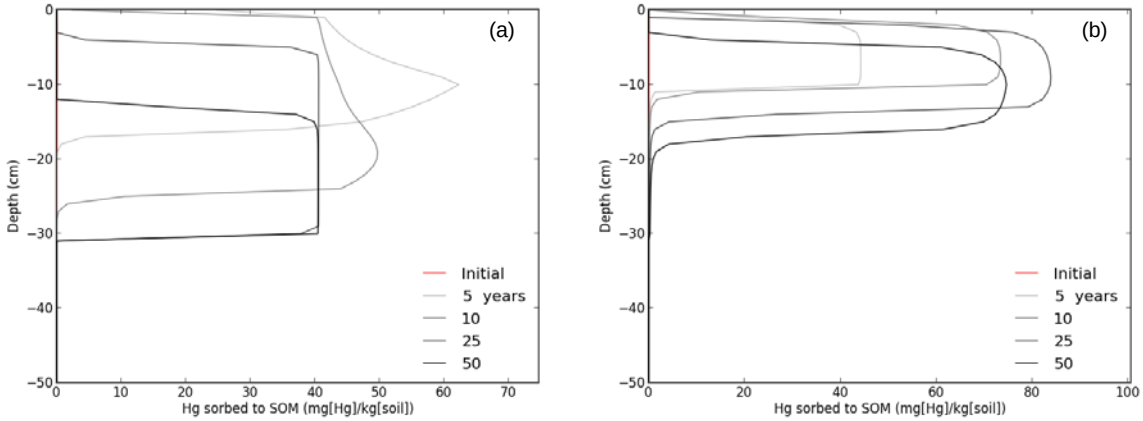

Figure 5. Depth distribution over time of Hg sorbed to SOM at t = 0, 5, 10, 25 and 50 years for two simulations with contrasting percentages of Hg in the top horizon after 50 years: 0% for (a) and 32.5% for (b). The initial contamination Hg NAPL was (135 mg[Hg]/kg[soil]).

Overall (i.e., including results not shown in this paper), parameter sensitivity for a given model output was found to depend on the type of mercury contamination. However, trends could be drawn by ranking the 13 parameters based on the sensitivity after 25 and 50 years for all types of contamination. For leaching, the most sensitive parameters were X_1, X_9 and X_4 (decreasing sensitivity ; see Table 2 for parameter names and ranges). For the percentage of Hg remaining in the topsoil, the ranking was: X_9, X_1 and X_4. For Hg below the horizon of contamination (11-30 cm), the most sensitive parameters were X_9, and X_1, X_4, X_2, X_{13}. Parameters that could generally be considered negligible based on the SA results were X_3, X_7, X_{11}, X_{12}.

Simulated Hg volatilization was found to be negligible (<0.1%). This is mainly due to the fact that the reduction rate depends on the total Hg^{II} concentration in the aqueous phase, i.e. the free species of Hg^{2+}, the inorganic and organic aqueous complexes of Hg^{II}, not being sorbed. Since

Hg^{II} concentration in the aqueous phase were relatively low at all times, Hg reduction and volatilization were consequently very limited.

4. Conclusions

The HP1 module of HYDRUS-1D was used to implement a numerical model of mercury fate and transport in soils. The processes included in the model are relevant for oxic conditions and pollution from anthropogenic sources. These simulated processes were Hg transport and speciation in the gaseous and aqueous phases, Hg sorption to SOM, cinnabar and Hg NAPL dissolution, Hg^{II} reduction and volatilization, and DOM sorption to minerals. Hg-DOM complexes in the aqueous phase were considered as a surrogate for colloid transport.

Three different phases of initial mercury contamination were tested: solid (cinnabar), non-aqueous phase liquid Hg, and aqueous mercuric chloride. The dominant processes for Hg fate in soils were identified by means of a parameter sensitivity analysis using the method of elementary effects. Overall, the most sensitive parameters were the equilibrium constant for Hg sorption to humic and fulvic acids (i.e., the most abundant sorption sites of SOM), the Hg initial concentration, and the DOM concentration of the infiltrating rainwater. Interactions between factors and nonlinear effects as measured by the elementary effect method were generally important. They depended on the type of contamination and on the time at which the indicators were evaluated.

More comprehensive modeling of the DOM cycle in soils should improve performance of the model, given the importance of DOM and SOM on Hg dynamics. Finally, we note that no model calibration was performed in the present study, but this is considered a necessary step in the future.

Acknowledgements
The present study is part of the IMaHg project (*Enhanced knowledge in mercury fate and transport for **I**mproved **Ma**nagement of **Hg** soil contamination*), which aims at providing recommendations to improve management of sites contaminated by mercury within the SNOWMAN funding framework. This particular work was done with financial support of the Public Waste Agency of Flanders (OVAM).

References

Bessinger, B. A., and C. D. Marks, Treatment of mercury-contaminated soils with activated carbon: A laboratory, field, and modeling study, *Remediation J.*, *21*(1), 115-135, 2010.

Blanc, P., Lassin, A., and P. Piantone, *THERMODDEM, A database devoted to waste minerals*, BRGM, Orléans, France, 2012. http://thermoddem.brgm.fr

Campolongo, F., J. Cariboni, and A. Saltelli, An effective screening design for sensitivity analysis of large models, *Environ. Modelling & Software*, *22*(10), 1509-1518, 2007.

Don, A., and E.-D. Schulze, Controls on fluxes and export of dissolved organic carbon in grasslands with contrasting soil types, *Biogeochemistry*, *91*(2), 117-131, 2008.

Gustafsson, J. P., Modeling the acid-base properties and metal complexation of humic substances with the Stockholm Humic Model, *J. Colloid and Interface Sci.*, *244*(1), 102, 2008.

Jacques, D., J. Šimůnek, D. Mallants, and M. Th. van Genuchten, Operator-splitting errors in coupled reactive transport codes for transient variably saturated flow and contaminant transport in layered soil profiles, *J. Contam. Hydrol.*, *88,* 197–218, 2006.

Jacques, D., J. Šimůnek, D. Mallants, and M. Th. van Genuchten, Modeling coupled water flow, solute transport and geochemical reactions affecting heavy metal migration in a podzol soil, *Geoderma*, *145*(3-4), 449-461, 2006.

Kothawala, D. N., T. R. Moore, and W. H. Hendershot, Adsorption of dissolved organic carbon to mineral soils: A comparison of four isotherm approaches, *Geoderma*, *148*(1), 43-50, 2008.

Mertens, J., J. Vanderborght, R., Kasteel, T. Pütz, R. Merckx, J. Feyen, and E. Smolders, Dissolved organic carbon fluxes under bare soil, *J. Environ. Qual.*, *36*(2), 597-606, 2007.

Morris, M. D., Factorial sampling plans for preliminary computational experiments, *Technometrics*, *33*(2), 161-174, 1991.

Parkhurst, D. L., and C. A. J. Appelo, User's guide to PHREEQC (Version 2), A computer program for speciation, batch-reaction, one-dimensional transport, and inverse geochemical calculations, *Water-Resources Investigations Report 99-4259*, U.S. Department of the Interior, U.S. Geological Survey, Denver, Colorado, USA, 1999.

Scholtz, M. T., B. J. Van Heyst, and W. H. Schroeder, Modelling of mercury emissions from background soils, *Sci. Total Environ.*, *304*(1-3), 185-207, 2003.

Sen, T. K., and K. C. Khilar, Review on subsurface colloids and colloid-associated contaminant transport in saturated porous media, *Adv. Colloid Interface Sci.*, *119*(2-3), 71-96, 2006.

Šimůnek, J., C. He, L. Pang, and S. A. Bradford, Colloid-facilitated solute transport in variably saturated porous media, *Vadose Zone J.*, *5*(3), 1035-1047, 2006.

Šimůnek, J., M. Šejna, H. Saito, and M. Th. van Genuchten, The HYDRUS-1D Software Package for Simulating the Movement of Water, Heat, and Multiple Solutes in Variably Saturated Media, Version 4.0. HYDRUS Software Series 3, Department of Environmental Sciences, University of California Riverside, Riverside, California, USA, 2008.

Skyllberg, U., Competition among thiols and inorganic sulfides and polysulfides for Hg and MeHg in wetland soils and sediments under suboxic conditions: Illumination of controversies and implications for MeHg net production, *J. Geophys. Res.*, *113*, G00C03, 2008.

Skyllberg, U., Chemical speciation of mercury in soil and sediment, In G. Liu, Y. Cai, and N. O'Driscoll (eds.), Environmental Chemistry and Toxicology of Mercury, John Wiley & Sons, Inc.: pp. 219-258, 2012.

Waples, J. S., K. L. Nagy, G. R. Aiken, and J. N. Ryan, Dissolution of cinnabar (HgS) in the presence of natural organic matter, *Geochimica Cosmochimica Acta*, *69*(6), 1575-1588, 2005.

Zhu, Y., L. Q. Ma, B. Gao, J. C. Bonzongo, W. Harris, and B. Gu, Transport and interactions of kaolinite and mercury in saturated sand media, *J. Hazardous Mat.*, *213-214*, 93-99, 2012.

Groundwater Recharge Modeling of the Nete Catchment (Belgium) Using the HYDRUS-1D – MODFLOW Package

Bertrand Leterme, Matej Gedeon, and Diederik Jacques

Performance Assessments, Institute Environment, Health and Safety, Belgian Nuclear Research Centre, Mol, Belgium, bleterme@sckcen.be, mgedeon@sckcen.be, djacques@sckcen.be

Abstract

The HYDRUS-1D and MODFLOW software packages were coupled to produce a groundwater model of the Nete catchment (northern Belgium) that would improve simulations of near-surface hydrological processes, including temporal and spatial variabilities in groundwater recharge rates. The present paper reports the practical implementation of the HYDRUS package for MODFLOW. Several issues are discussed: the choice and design of MODFLOW zones for coupling to one-dimensional HYDRUS profiles; time discretization of the MODFLOW and HYDRUS components, numerical oscillations and related warm-up periods; and the presence of seepage water in zones of shallow groundwater. In this study we delineated MODFLOW zones on the basis of groundwater depths as obtained with a calibrated steady-state version of the model. Transient simulations are then compared with observed groundwater depths derived from a piezometer network. We summarize a number of priorities and issues that need to be addressed in order to improve the model and achieve sound coupling of the two parts at the catchment scale, while keeping computation times reasonable.

1. Introduction

A groundwater model for the Nete catchment (Belgium) was previously developed assuming constant (in space and time) recharge (Gedeon and Wemaere, 2008). The model was calibrated for steady-state conditions using a uniform groundwater recharge rate of 289 mm y^{-1}. One way to introduce more realism in the spatial and temporal characterization of groundwater recharge is to couple the groundwater model to an unsaturated zone model. A review of surface-subsurface coupling methods and models is provided by Furman (2008). Recent examples using MODFLOW (Harbaugh et al., 2000) as the subsurface component include Xu et al. (2012) and Morway et al. (2013). Seo et al. (2007) developed a module that couples HYDRUS-1D (Šimůnek et al., 2008) to MODFLOW-2000, but until now only applications on synthetic cases have been documented (Twarakavi et al., 2008).

This case study documents the implementation of the HYDRUS-MODFLOW package for the Nete catchment in northern Belgium. The groundwater modeling domain for MODFLOW was discretized into cells of 400×400 m each (9644 active cells in the top layer; see Figure 1). The vertical thickness of active layers in the model varied between 0 and 200 m as some layers were wedged out.

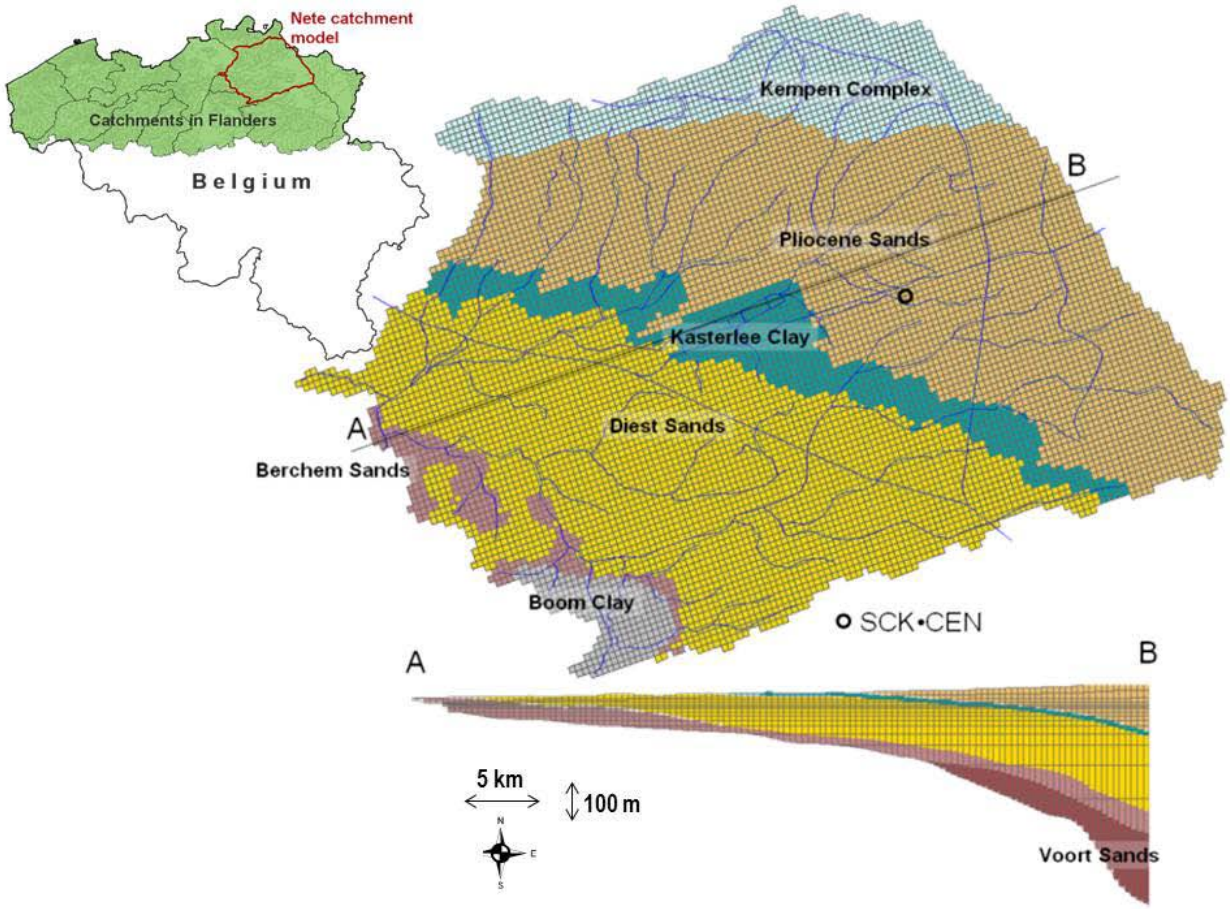

Figure 1. Surface discretization and cross-section of the groundwater model developed using MODFLOW.

2. Implementation of the HYDRUS Package for MODFLOW

2.1. Zone Definition

Zones within the MODFLOW discretization identify cells to which each unsaturated soil profile applies. In theory, the number of zones can vary between 1 and the total number of active cells in the top layer (9644 in the present case). In practice, a compromise is needed between increasing model realism (i.e., including more zones) and keeping reasonable CPU time (i.e., limiting the number of zones). For a given MODFLOW zone, the depth to groundwater in each cell is averaged to determine the hydraulic head at the bottom of the corresponding HYDRUS soil profile (details in Seo et al., 2007). The time-averaged flux at the bottom of the soil profile is applied to each cell in the zone as recharge during the time step. Therefore, the expected depth to groundwater should be taken as the first criterion for defining relatively homogeneous MODFLOW zones, in order to limit precision losses due to averaging between the MODFLOW and HYDRUS models. In our study, the expected groundwater depth was taken from the calibrated steady-state model of Gedeon and Wemaere (2008).

Other logical criteria for defining MODFLOW zones relate to surface processes. For given atmospheric input (i.e., precipitation time series), it is expected that different soil types and vegetation covers will significantly affect the fluxes calculated with HYDRUS, which then are applied to the MODFLOW cells. For this reason we used the soil association map (Maréchal and Tavernier, 1974) as a possible geographical criterion to define MODFLOW zones. Soil hydraulic parameters were taken from the AARDEWERK database (Van Orshoven and Vandenbroucke, 1993). Spatial information of land cover was extracted from a 2001 Landsat image (AGIV, 2011), which we further aggregated to obtain six main classes: surface water (1%), impervious (urban areas; 13%), grass (16%), deciduous trees (7%), coniferous trees (14%), and crop (maize; 49%).

We next developed a pre-processing script in Python that enables one to generate a zone array and HYDRUS soil profiles by specifying criteria of groundwater depth intervals, soil types, and land cover types (vegetation). The resulting number of zones can be easily tuned by changing the selection criteria.

For the work reported here, different simulations were performed using different numbers of zones obtained by changing only the groundwater depth intervals. Soil and land cover types were kept constant, being a typical podzol with a grass cover for the whole study area (except surface waters which were already included in the groundwater model). Despite the reduced complexity, several issues had to be addressed while coupling of the separate HYDRUS and MODFLOW models. These issues are discussed hereafter.

2.2. Seepage Water

A significant part of the study area can be characterized as a relatively shallow aquifer. This is illustrated in Figure 2 where zones 1 and 2 correspond to estimated groundwater depths being less than 2 m (on the basis of the calibrated steady-state model). For zones having shallow groundwater, it became apparent that the average groundwater depth transmitted from MODFLOW to HYDRUS frequently exceeded the soil surface. This may partly be a consequence of the spatial resolution (i.e., averaging of groundwater depths and/or topography), or could reflect a lack of precision of the calibrated groundwater model in certain areas. For example, the calibrated hydraulic conductivity of aquifer layers is closely linked to the imposed steady-state recharge rate.

The HYDRUS package could not properly handle this problem and produced convergence problems. We therefore modified the code to allow the excess water to be removed as seepage from the soil surface. For zones 1 to 3 (which accounted for approximately two thirds of the study area), Figure 3 shows the number of MODFLOW cells in which seepage was simulated during the last time step of the simulation (model with 20 zones). The simulated seepage was found to be very important for zone 1 (shallowest groundwater).

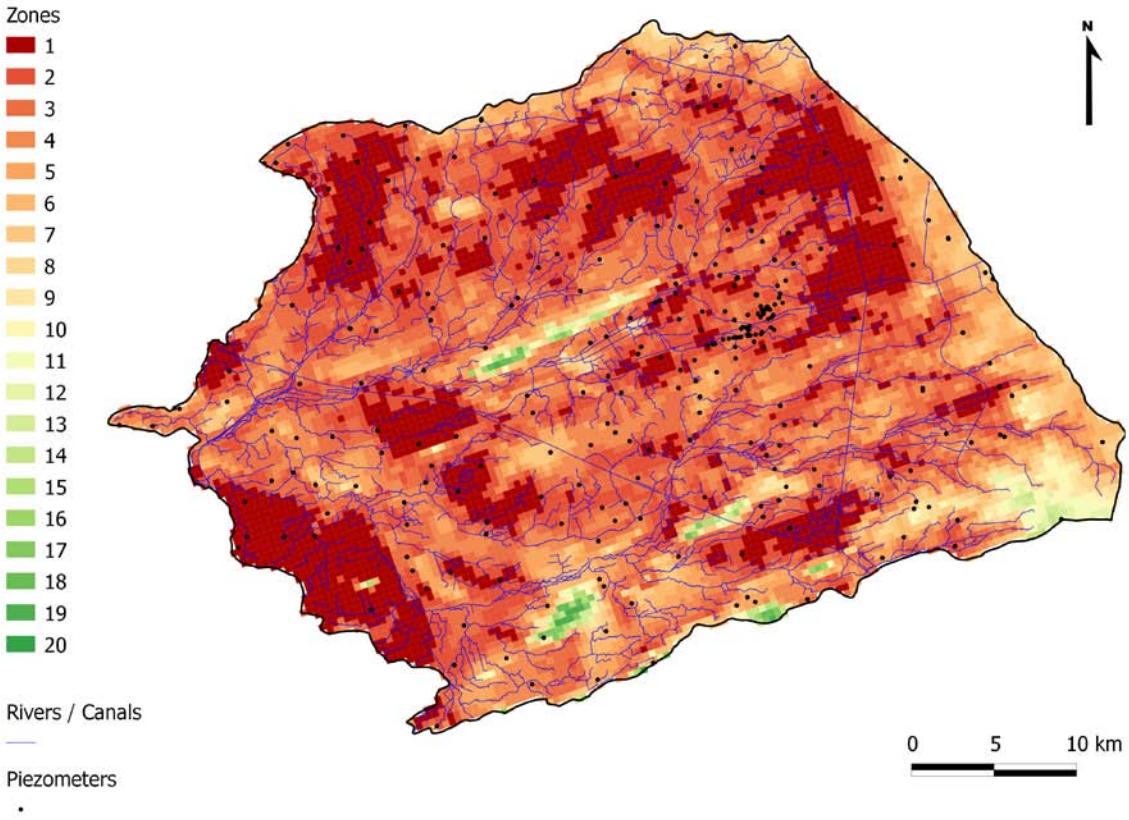

Figure 2. Map of the Nete catchment with 20 MODFLOW zones. Black dots represent locations of the piezometers available for comparison of simulated vs. observed groundwater depth.

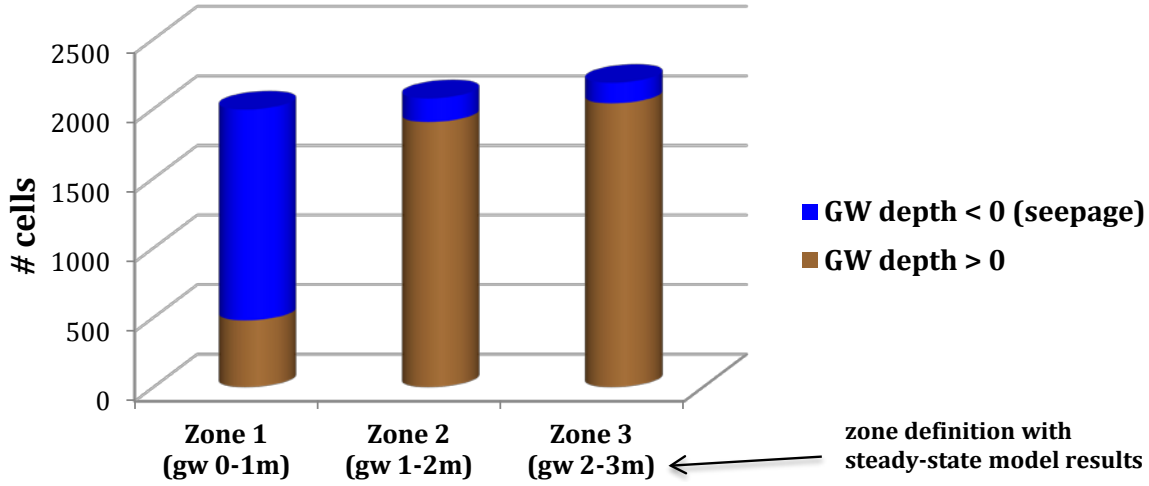

Figure 3. Total number of MODFLOW active cells with or without seepage during the last time step of a 10-year simulation (+10 years warm-up) for the coupled model using 20 zones. Only the first three zones are shown.

2.3. Warm-up Period

For all simulations tested (assuming a different number of zones, and using transient or steady-state atmospheric input), we noted oscillations in the fluxes being exchanged between HYDRUS and MODFLOW during some initial time period of the simulation (Figure 4). While this could be a consequence of the removal of seepage water, the oscillations were not limited to zones having shallow groundwater (e.g., see Figure 4(b)). The oscillations could eventually lead to non-convergence, especially when the number of zones was very low or the number of coupling time steps were insufficient during the early stress periods.

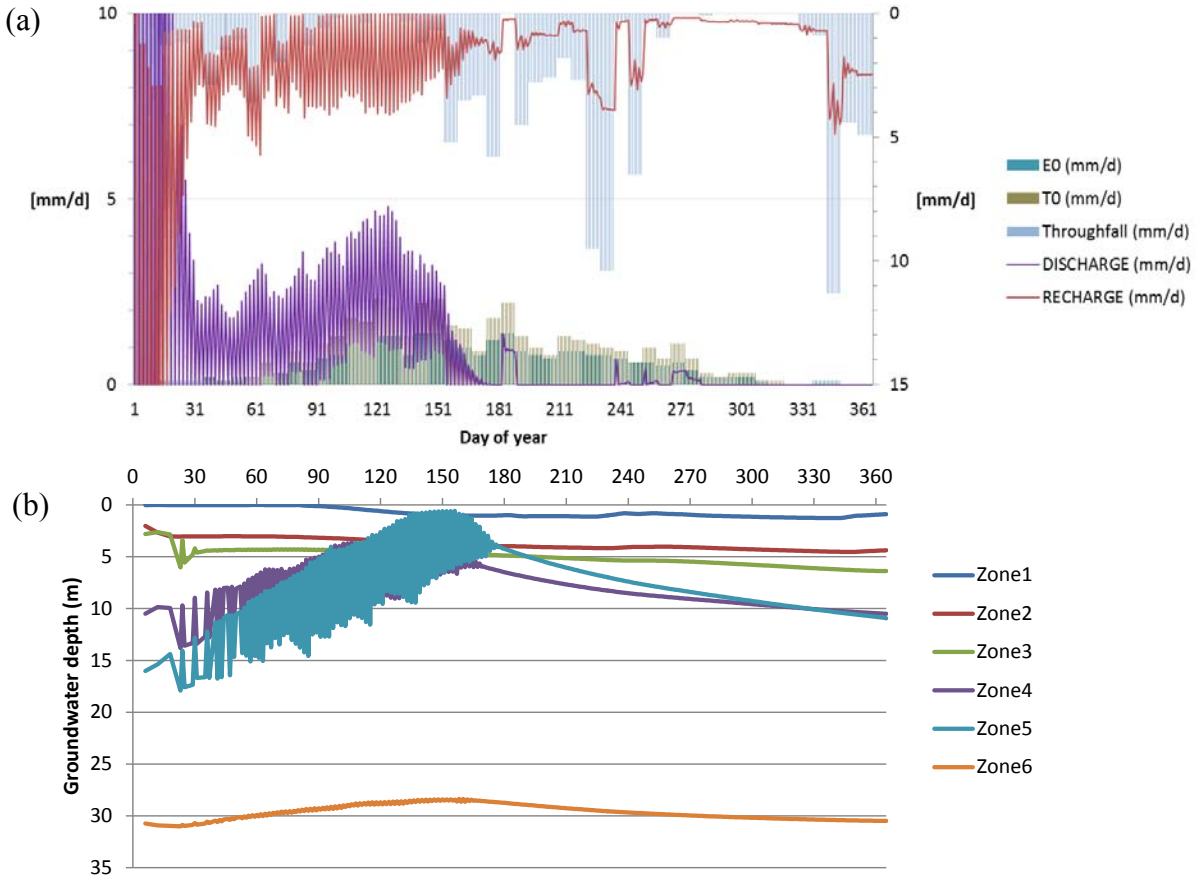

Figure 4. First year of transient simulation with the coupled HYDRUS-MODFLOW package using 6 zones, showing oscillations during approximately the first 180 days in (a) the total discharge rate (left vertical axis) and the potential evaporation (E0), transpiration (T0) and recharge rates (right axis), as well as the exchange flux between the unsaturated and saturated zones (right axis), all in mm d^{-1}, and (b) averaged groundwater depths (m) for each zone.

Even while the numerical solution eventually stabilized, we noted that relatively long warm-up periods were necessary to avoid oscillations (at least several years). This was partly due to the presence of zones with a deep groundwater table, which required several years before atmospheric input migrated through the unsaturated zone. This is illustrated in Figure 5, which compares HYDRUS profile water contents and fluxed at the bottom of the profile for two zones

with different groundwater depths. We therefore used a warm-up period of ten years in subsequent simulations (see section 2.4) to ensure results independent of the initial conditions.

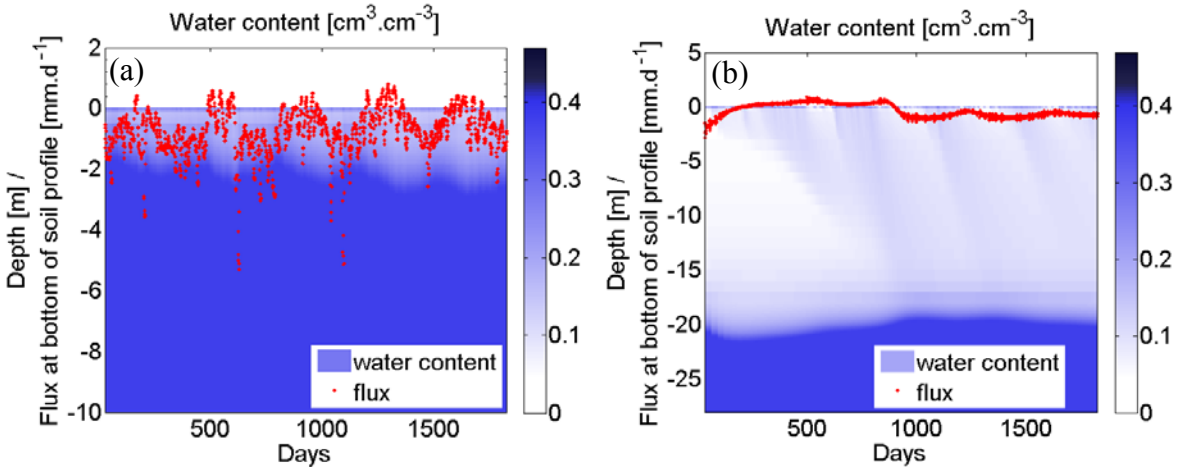

Figure 5. Water contents (blue color scale; $cm^3\ cm^{-3}$) and fluxes (red dots; mm d^{-1}) at the bottom of the HYDRUS profile during the first 5 years of a simulation with 10 zones. Results are for (a) zone 2 (initial groundwater depth between 2.5 and 5 m) and (b) zone 9 (initial groundwater depth between 20 and 25 m).

2.4. Comparison with Piezometer Data

For a 10-year simulation (plus a 10-year warm-up period) with 20 zones, the recharge rate varied between 226 and 392 mm y^{-1} for the different zones (Figure 6). In the present case, the variability between the zones was due only to variability in the groundwater depth translated to different positions of the bottom boundary condition in the HYDRUS profiles. This because a single combination of soil type, land cover and atmospheric boundary conditions was considered. For the entire Nete catchment, the average simulated recharge rate was 274 mm y^{-1}, and the average seepage rate 32 mm y^{-1} (mainly in zone 1 with initial groundwater table < 1 m). Net simulated recharge was thus 242 mm y^{-1}. Previous estimates of the groundwater recharge rate in the area ranged from 237 to 486 mm y^{-1} (see the review in Hardy et al., 2001).

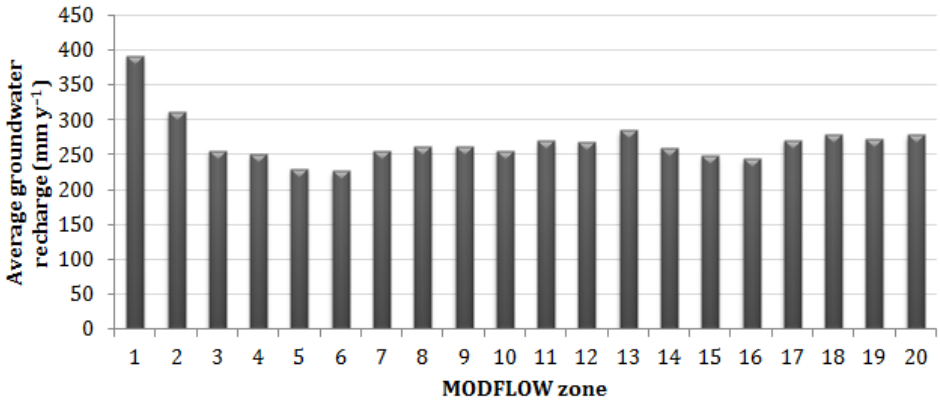

Figure 6. Average annual recharge rate in the period 2000-2009 for the 20 MODFLOW zones.

For each zone, simulated groundwater depths were compared with data available from a network of piezometers in the study area (Figure 2 indicates piezometer locations). This comparison is shown in Figure 7 for zones 1 to 3. Results indicate that the average simulated groundwater depths generally reflect seasonal fluctuations (higher water table at the end of winter). In zone 1, the simulated groundwater depth was close to zero due to seepage in many of the cells (cf. section 2.2), while piezometer data showed groundwater depths in the range 1.5-3.0 m most of the time. In zones 2 and 3, average calculated depths corresponded approximately to the observations.

We emphasize that until now no calibration was attempted with the model (which was previously calibrated for steady-state conditions using a single recharge rate). There are possibilities to improve the simulation by calibrating the number of zones and including more soil types and land covers. Also, the consistency and reliability of the piezometer observations need to be verified since different data sources were combined. Figure 7 shows that piezometric observations do not show an overall increasing groundwater depth from zone 1 to zone 3, contrary to the simulated groundwater depths. This may partly be due to the resolution of the MODFLOW cells and the corresponding DEM (400×400 m), which were too coarse compared to point measurements such as piezometers.

3. Conclusions and Perspectives

This paper presents a case study of coupling surface and subsurface models for the Nete catchment. A few practical issues during implementation of the HYDRUS-MODFLOW package are described. The main issues are related to the use of homogeneous MODFLOW zones (section 2.1), the occurrence of seepage in areas of shallow groundwater (section 2.2), and oscillatory behavior of the model during the initial time steps and the resulting need for a relatively long warm-up period (section 2.3). Results of a simulation with 20 zones were compared to piezometer data (section 2.4).

The main issue to address in the future is probably the treatment of seepage. Currently, this water is not routed to rivers, which makes it impossible to obtain a consistent water balance over the whole catchment. Moreover, currently simulated seepage rates seem too high and do not correspond to rates that have been observed in the catchment. This is probably due to the relatively large area covered by zones 1 and 2, and to assumed hydraulic parameters of the groundwater model. These parameters need to be re-calibrated to allow for more precise recharge drainage rates. The re-calibration will be done using transient groundwater level observations.

In parallel, the sensitivity of the model to the number of zones should be quantified. This would lead to an optimization of the number of zones. Important information for this is the variability in the simulated zone groundwater depth within a zone (cf., red shadowed area in Figure 7). A high standard deviation in a given zone indicates that splitting that zone may improve the results. On the other hand, analysis of HYDRUS sensitivities to groundwater depth prior to coupling could also provide valuable information. For example, having more zones may be beneficial in intervals of groundwater depth where the sensitivity is high (i.e., where actual ET is influenced by groundwater;Maxwell and Kollet, 2008), while having fewer zones may be possible in intervals with deeper groundwater (i.e., where groundwater is disconnected from the surface).

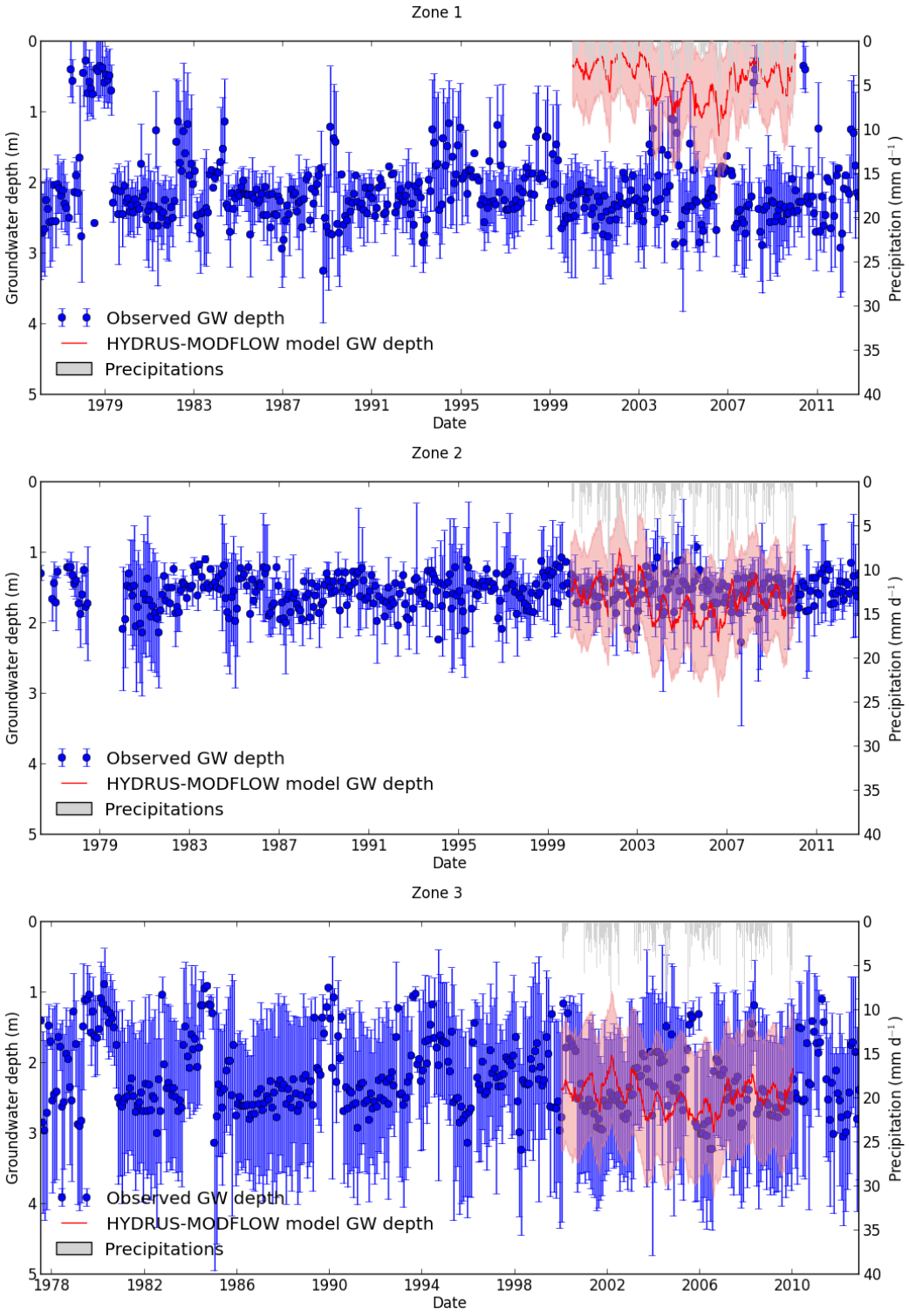

Figure 7. Comparison of observed (blue) and simulated (red) groundwater depths for zones 1 to 3 for a simulation with 20 zones. The shadowed red area is the average calculated depth (± 1 standard deviation) of all cells pertaining to a given zone.

Future simulations are planned, including for more soil types and land cover classes. This should improve model realism (e.g., having very low or no recharge in urbanized areas), but could require a (much) higher number of zones. One major issue here is the relatively long simulation time. The 10-year (plus 10-year warm up) simulation presented here took about 4 h on a standard computer. This is relatively high considering the need of multiple runs for calibration and/or sensitivity analyses. As such, an optimal design of the warm-up period, of MODFLOW stress periods and of the time steps could possibly improve CPU time. We also believe that the model eventually needs to be calibrated against observed piezometer data.

References

AGIV, *Bodemgebruiksbestand, opname 2001*, Agentschap voor Geografische Informatie Vlaanderen, 2011, available at www.agiv.be/gis (accessed March 15th, 2013).

Furman, A., Modeling Coupled Surface-Subsurface Flow Processes: A Review, *Vadose Zone J.*, *7*(2), 741-756, 2008.

Gedeon, M., and I. Wemaere, Conceptual uncertainty assessment for a catchment scale model, Calibration and Reliability in Groundwater Modelling. Credibility of Modelling, ModelCare 2007, Copenhagen, Denmark, 9-13 September 2007 IAHS, Wallington, United Kingdom, 2008.

Harbaugh, A. W., E. R. Banta, M. C. Hill, and M. G. McDonald, *MODFLOW-2000, The U.S. Geological Survey Modular Ground-Water Model User Guide to Modularization Concepts and the Ground-Water Flow Process*, USGS, Denver, CO., 2000.

Hardy, L., D. Mallants, and G. Volckaert, Hydrogeological model for the safety evaluation: groundwater flow and transport calculations for the nuclear zone Mol-Dessel, *R-3550*, Waste & Disposal Department, SCK-CEN Mol, Belgium, 2001.

Maréchal, R., and R. Tavernier, *Pédologie : commentaires des planches de la carte des associations de sols*, Livret explicatif des planches 11A et 11B de l'Atlas de Belgique du Comité National de Géographie, 4-64, 1974.

Maxwell, R. M., and S. J. Kollet, Interdependence of groundwater dynamics and land-energy feedbacks under climate change, *Nature Geosciences*, *1*, 665-669, 2008.

Morway, E. D., R. G. Niswonger, C. D. Langevin, R. T. Bailey, and R. W. Healy, Modeling variably saturated subsurface solute transport with MODFLOW-UZF and MT3DMS, *Groundwater*, *51*(2), 237-251, 2013.

Seo, H. S., J. Šimůnek, and E. P. Poeter, *Documentation of the HYDRUS Package for MODFLOW-2000, the U.S. Geological Survey Modular Ground-Water Model*. Golden, CO, Colorado School of Mines, 96 p., 2007.

Šimůnek, J., M. Šejna, H. Saito, M. Sakai, and M. Th. van Genuchten, The Hydrus-1D Software Package for Simulating the Movement of Water, Heat, and Multiple Solutes in Variably Saturated Media, Version 4.0, *HYDRUS Software Series 3*, Department of Environmental Sciences, University of California Riverside, Riverside, California, USA, 2008.

Twarakavi, N. K. C., J. Šimůnek, and S. Seo, Evaluating interactions between groundwater and vadose zone using the HYDRUS-based flow Ppckage for MODFLOW, *Vadose Zone J.*, *7(*2), 757-768, 2008.

Van Orshoven, J., and D. Vandenbroucke, Guide de l'utilisateur de Aardewerk, Base de données de profils pédologiques, K. U. L. IRSIA-COBIS Instituut voor Land-en Waterbeheer, Leuven, Belgium, 1993.

Xu, X., G. Huang, H. Zhan, Z. Qu, and Q. Huang, Integration of SWAP and MODFLOW-2000 for modeling groundwater dynamics in shallow water table areas, *J. Hydrol.*, *412-413*, 170-181, 2012.

Which Hydraulic Model to Use for Vertical Flow Constructed Wetlands?

Ania Morvannou[1], Nicolas Forquet[1], Marnik Vanclooster[2], and Pascal Molle[1]

[1] *Irstea, Freshwater Systems, Ecology and Pollution Research Unit, 5 rue de la Doua, CS70077, 69626 Villeurbanne cedex, France,* ania.morvannou@irstea.fr, nicolas.forquet@irstea.fr, pascal.molle@irstea.fr
[2] *Earth and Life Institute, Environmental Sciences, Université Catholique de Louvain, Croix du Sud 2 Box 2, B-1348 Louvain-la-Neuve, Belgium,* marnik.vanclooster@uclouvain.be

Abstract

Modeling water flow in a Vertical Flow Constructed Wetland (VFWC) is a prerequisite to simulate wastewater treatment using process based filtering models. The material used in a VFCW is often very susceptible to generate preferential flow. If this occurs, water will bypass much of the soil porous matrix in a largely unpredictable way. Even if it is possible to simulate water content variations within a VFCW, one cannot correctly model outflow using the standard van Genuchten-Mualem functions if preferential flow occurs. Various modeling approaches have been proposed to overcome this problem. These approaches mostly try to describe flow and transport separately in the preferred flow paths and in slow or stagnant pore regions. The objective of this study was to investigate and simulate the hydrodynamic behavior and solute transport through a simplified representation of a French VFCW by using both the classical equilibrium flow model and a non-equilibrium dual-porosity (mobile-immobile) type model with water content mass transfer as included in the HYDRUS-1D software package. Modeling results were compared to a solute breakthrough curve obtained from a tracer experiment carried out on an existing VFCW. Inlet concentrations were first corrected to account for tracer losses and experimental uncertainties. Both the hydraulic parameters of the mobile and immobile regions (θ_r^m / θ_s^m and $\theta_r^{im} / \theta_s^{im}$) and the transfer coefficient (ω) were optimized to fit the experimental tracer breakthrough curve. Comparison of measured and simulated tracer breakthrough curves indicates that the non-equilibrium approach seems to be more appropriate for simulating preferential flow.

1. Introduction

Constructed wetlands (CWs) provide an attractive wastewater treatment technology for small communities (< 2000 people-equivalents; p.e.) since their simplicity of operation, low cost and reliable treatment efficiency often fit with the limited resources of small communities for wastewater treatment. Irstea (formerly Cemagref) developed an innovative first-stage type system for vertical flow constructed wetlands (VFCWs) containing gravel instead of sand. The first-stage system directly accepts raw wastewater without needing a preliminary settling tank. Despite obtaining good treatment efficiencies, Molle et al. (2008) indicated that the treatment efficiency could be improved if the hydraulic behavior of the VFCW were better understood.

While a French VFCW initially contain only gravel, after some years of operation a sludge layer develops at the filter surface, with the filter medium slowly turning into a medium made up of gravel and organic matter. Water retention is then mainly caused by organic matter in the filter. Consequently, both gravitational and capillary flow due to gravel and the presence of organic

matter, respectively, must be considered (Maier et al., 2009). The macroporosity associated with the coarse material and the network of reed stalks may serve as preferential flow paths through which water can bypass much of the porous matrix. Moreover, during rest periods the sludge generally dries fast, often leading to visible cracks that facilitate preferential flow paths through the sludge layer, especially at the beginning of a feeding period (Molle et al., 2006). Non-equilibrium conditions in pressure heads are thus created between preferential flow paths and the matrix pore region. VFCWs thus far have been depicted as a porous medium with continuous properties. Variably saturated water flow is then usually modeled using the Richards equation assuming that the water content and pressure head are at equilibrium at each node. These equilibrium models cannot be used for simulating preferential flow in structured media (Gerke, 2006; Köhne et al., 2009). Moreover, even if it is possible to simulate water content variations within a VFCW using equilibrium models, outflow cannot be correctly modeled with the standard van Genuchten-Mualem functions (Morvannou et al, submitted). A model accounting for non-equilibrium water flow and solute transport would hence be more appropriate.

Preferential flow models thus far have not been applied to flow and transport processes in VFCWs. By comparison, many preferential flow studies have been carried out in the soil and hydrologic sciences for simulating water flow and/or solute transport in saturated and unsaturated porous media (Šimůnek et al., 2001; Haws et al., 2005; Köhne et al., 2006; Maier et al., 2009). Šimunek et al., (2003, 2008) carried out extensive literature reviews of existing models. Most of the models assume the simultaneous consideration of two or more domains for the same porous medium. Four different preferential flow models have been implemented in the HYDRUS software package (Šimůnek et al., 2006). These models have in common that water flow in the preferential flow paths is still simulated using the Richards equation and solute transport using the convection-dispersion equation. However, they differ in the way flow and transport in and between the ‘‘fast” (macropore domain) and “slow” or stagnant (matrix domain) pore spaces are modeled. A disadvantage of these approaches is that they increase the computational demand of the model as well as the number of required model parameters, some of which may be very difficult to estimate (Šimůnek and van Genuchten, 2008).

The purpose of this paper is to study and simulate the hydrodynamic behavior and solute transport in a simplified representation of a VFCW by using both the classical equilibrium and a non-equilibrium model formulation available in the HYDRUS-1D software package. We used the dual-porosity model since it represents the simplest non-equilibrium approach with the fewest possible parameters, while still facilitating both non-equilibrium flow and solute transport. Modeling results will be compared with a solute breakthrough curve obtained from a tracer experiment carried out on an existing VFCW to determine which approach is most appropriate. We also tried a more realistic approach for calibrating the dual-porosity model.

2. Materials and Methods

2.1. Tracer Experiment

The Evieu wastewater treatment plant (200 p.e.) in Ain, France, has been in operation since 2004. The first stage plant consists of three VFCWs receiving raw wastewater. A pump sump at the plant inlet is used for mechanical screening using a 5 cm mesh screen. Each filter is fed

according to a feeding/rest regime of 3.5/7 days. Effluent from the first stage is then routed to a second pump sump and separated between the second stage's vertical and horizontal flow constructed wetlands according to the experimental objectives (Molle et al., 2008). All beds are planted with *Phragmites australis*.

A fluorescein infiltration experiment was carried out from 04/15/2010 to 04/19/2010, corresponding to the entire feeding period, on one of the VFCW of the first stage of the wastewater treatment plant. The selected vertical filter (28 m², 2.9 m wide x 9.7 m long) was designed according to French recommendations. From the bottom to the top, the filter contains a 15-cm thick drainage layer (grain size of 30-60 mm), a 10-cm transition layer (grain size 15-25 mm) and a 60-cm gravel layer (d_{10} = 2.46 mm; $UC = d_{60}/d_{10}$ = 1.39; average porosity of 40.4%). Since the filter had been working at nominal load for 7 years, a sludge layer of about 20 cm had developed at the top of the filter. The VFCW is fed by raw wastewater in batches of 5 cm at a rate of 1.23 $m^3/h/m^2$ on average. During spells of dry weather, 8 separate batches are processed per day. Water is drained using a 160-mm diameter drainage pipe (0.42 m of pipe per m²), which allowed passive aeration from the bottom as well.

For the tracer experiment, 1.98 g of fluorescein was diluted in a batch volume (1973 L) and applied to the filter. This application was equal to 0.07 g/m², having a solution fluorescein concentration of 0.001 g/L. We note that not all the fluorescein was applied in only one batch as expected; some remained in the pump sump (despite attempts to empty the sump after each batch), which was then applied subsequently with the next batch. Unfortunately, the remaining concentration could not be determined. Some fluorescein after application also remained on top of the filter due to the low permeability and heterogeneity of the sludge deposit. After the fluorescein application, its concentration was recorded at the VFCW outlet (using an online fluorimeter PELI 1300 Case; Peli Products, USA) along with the outflow rate (measured with a venture flume) at time intervals of 1 minute throughout the tracer experiment.

Water contents were recorded at the same time using TDR probes, but only during the first batch of the tracer experiment. TDR probes were inserted at three different depths of the filter (13, 31 and 47 cm below the VFCW top surface) and connected through multiplexers to a signal generator/analyzer (model TDR100, Campbell Scientific™, Logan, UT). Results were recorded using a datalogger (model CR1000, Campbell Scientific™ Logan, UT). Measurements were made at 20 second time intervals.

2.2. Dual-Porosity Models

The aim of this section is not to provide a full mathematical description of various dual-porosity models. For this purpose readers are referred to Šimůnek et al. (2003, 2008). Our objectives are to emphasize how dual-porosity models can represent preferential flow and to highlight how complexity is increased by additional parameters. According to Šimůnek et al. (2003), preferential flow has two main characteristics: (1) an ability to quickly propagate by "bypassing a large part of the matrix pore-space", and (2) the presence of non-equilibrium between the water pressure head within the macropores and the water content in the matrix. Non-equilibrium is a key concept of preferential flow modeling. Classical descriptions of flow in variably saturated porous media based on the Richards equation presume that the water pressure head and water

content are always at equilibrium, and that they are linked by means of a certain water retention relationship (e.g., the van Genuchten function). This assumption does not hold in situations where preferential flow occurs.

Dual-porosity models do not aim to physically represent the paths of rapid flow (it would be very challenging to map every macropore at the scale of a VFCW), but rather attempt to incorporate their effects in a representative elementary volume (REV) to serve as a basis for modeling. Figure 1 comparatively shows how macropores can be observed in the filter and how they can be modeled at the REV scale.

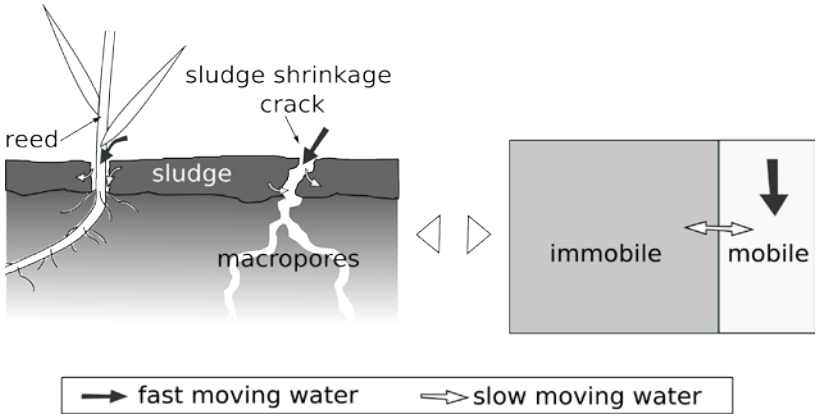

Figure 1. Schematic representation of macropores and preferential flow paths in a VFCW (left) and the corresponding conceptual physical non-equilibrium (mobile-immobile) model for water flow and solute transport (right).

Dual-porosity models assume that flow only takes place within the macropores (the mobile region), whereas flow in the remainder of the medium is neglected. Water in the matrix hence constitutes the immobile region. The hydraulic parameters (α, n and K_s) are representative of flow in the macropores and therefore must be adjusted, especially K_s, to produce rapid flow. The total porosity is divided between the mobile (θ_s^m) and the immobile (θ_s^{im}) regions. This brings additional complexity to the model. For example, for a given saturated hydraulic conductivity, the larger the mobile region, the slower the flow in the preferential flow path. For the sake of simplicity we considered the residual water content to be zero for both regions.

Non-equilibrium flow is modeled by adding a time-dependent parameter (ω) to the relationship between the water content in the immobile region and the water content in the mobile region (the latter being linked to the water pressure head). This is an important feature that allows water exchange to occur at a different time scale than the main gravitational drainage process. The parameter ω represents another increase in model complexity and needs to be calibrated for each material in the model.

2.3. Model Description

Because of significant ponding during the feeding process (~5 cm/m²), we assumed that the water distribution laterally was homogeneous. Consequently, we modeled water flow and solute

transport in one dimension with HYDRUS-1D. In contrast to previous studies carried out on the same VFCW where we considered four layers (a sludge layer, a first gravel-sludge layer, a second gravel-sludge layer, and a final layer consisting mostly only of gravel), in this study we limited the domain to only two layers: a sludge layer and a gravel-only layer. Since the number of parameters in the dual-porosity model is higher than in the equilibrium model, a simplified representation of the VFCW facilitates modeling and understanding of non-equilibrium flow.

The one-dimensional mesh used for the simulations consisted of 101 equidistant nodes. The top boundary condition was a time-dependent atmospheric condition with the threshold value for surface runoff set at 10 cm. The wastewater load duration and flow rate were specified, while evapotranspiration was neglected. When the incoming flow rate exceeded the infiltration capacity, ponding of water above the surface was taken into account until the level reached 10 cm. This value was never observed in our case. The bottom boundary condition was a seepage face. Initial conditions were set to hydrostatic equilibrium.

2.4. Tested Hydraulic Models

Water flow and solute transport were simulated using two different modeling approaches: the classical equilibrium model and a dual-porosity non-equilibrium model. Two dual-porosity models are available in HYDRUS-1D depending upon how the mass transfer rate (Γ_w) is modeled: either being proportional to the difference in effective water contents of the two regions, or to the difference in effective pressure heads (Gerke and van Genuchten, 1993). We used the first approach because it requires far fewer parameters. One then does not need to know the retention function for the matrix region explicitly, but only its residual and saturated water contents. The second approach should provide a more realistic description of the exchange rate since the difference in pressure heads between the macropore and matrix regions is the actual driving force. However, the mass exchange term may then become more unstable numerically (Šimůnek et al., 2003).

Using the first approach, the mass transfer rate Γ_w for water between the mobile and immobile regions is given by

$$\Gamma_w = \frac{\partial \theta_{im}}{\partial t} = \omega\left[S_e^m - S_e^{im}\right] = \omega\left[\frac{\theta^m - \theta_r^m}{\theta_s^m - \theta_r^m} - \frac{\theta^{im} - \theta_r^{im}}{\theta_s^{im} - \theta_r^{im}}\right] \tag{1}$$

which in our case simplifies to:

$$\Gamma_w = \omega\left[\frac{\theta^m}{\theta_s^m} - \frac{\theta^{im}}{\theta_s^{im}}\right] \tag{2}$$

where θ^m and θ^{im} are the mobile and immobile water content, respectively, θ_r^m and θ_r^{im} are the mobile and immobile residual water content, respectively, θ_s^m and θ_s^{im} are the mobile and immobile saturated water content, respectively, ω is a first-order rate coefficient (T^{-1}), and S_e^m and S_e^{im} are effective fluid saturations of the mobile and immobile regions, respectively.

For the equilibrium model we used hydraulic parameter values determined from a previous study (Morvannou, 2012), while for the dual-porosity model some of the hydraulic parameters (notably θ_s^m, α_m, n_m, λ, and θ_s^{im}) were adapted from Morvannou (2012), whereas others were arbitrarily fixed (θ_r^m, K_s, θ_r^{im}, and ω) (Table 1).

One major objective of this study was to obtain better insight into the hydrodynamic and solute transport processes taking place inside a VFCW. In a first attempt we simulated the tracer application for only one pulse. In order to evaluate if the observed multiple tracer peaks could be due to tracer remaining in the sump or at the surface of the filter, we also tested a case with seven pulses of decreasing concentrations. Modeling results obtained with the equilibrium and non-equilibrium models were compared in terms of concentrations and cumulative fluxes computed at the outlet.

2.5. Calibration of the Dual-Porosity Model

A second objective of our study was to calibrate the dual-porosity model. For this purpose we divided the gravel-sludge layer into two layers to be able to account for the decreasing gradient in organic matter content versus depth and to compare simulation results with water contents measured with TDR probes installed in the filter. The one-dimensional mesh and the top and bottom boundary conditions were the same as those used for the previous simulations. The setup of the initial conditions necessitated a prior initialization step. We could not use measured water contents (from TDR probes) since they did not provide a continuous water content profile at the initial time and caused convergence problems (Radcliffe and Šimůnek, 2010). Our prior initialization step consisted of repeating a batch simulation until the pressure heads reached a pseudo-permanent state. We then selected the time at which the simulated water content profile matched the measured initial water contents. The corresponding water pressure profile was considered as initial condition.

Inlet tracer concentrations were adapted from the tracer concentrations measured at the outlet. For this we applied four batches with decreasing tracer concentrations. Both the hydraulic parameters of the mobile and immobile regions (θ_r^m / θ_s^m and $\theta_r^{im} / \theta_s^{im}$) and the transfer coefficient (ω) were subsequently optimized to fit the experimental tracer breakthrough curve.

3. Results and Discussion

3.1. Tracer Experiment

Figure 2 presents the tracer concentration measured at the outlet of the VFCW and the cumulative percentage of the tracer recovery. The total tracer recovery was 62%, which indicates some loss of fluorescein. This loss could be due to photodegradation of the tracer in the ponded water above the surface, tracer retention on organic matter (adsorption) and uncertainties in the flow and concentration measurements.

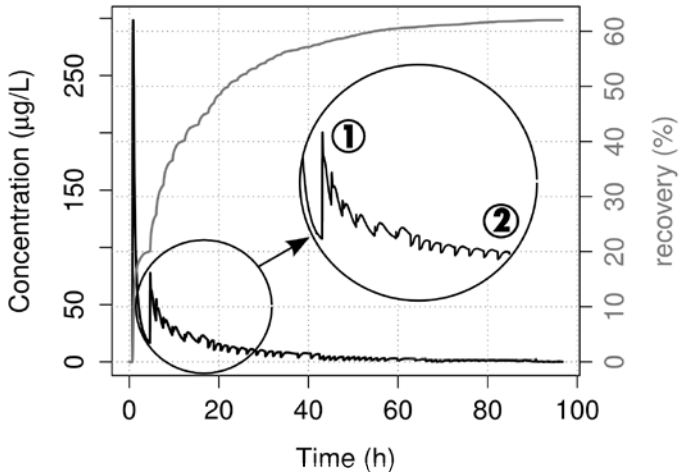

Figure 2. Tracer experimental breakthrough curve and cumulative tracer recovery percentage.

Figure 2 highlights two main issues. One is the presence of not just one but several peaks in the observed breakthrough curve (Fig. 2, (1)). Even if the tracer was mixed only once with the incoming wastewater, it seemed like the tracer application was carried out in several steps (e.g., remaining tracer in the sump and on filter surface). The tracer left the filter very quickly during the first batch, thus pointing out the presence of preferential flows in the filter. Another issue is a change in the shape of the breakthrough curve. After the first seven peaks, the tracer concentration decreased when a new batch arrived and then increased logarithmically towards a new equilibrium (Fig. 2; (2)).

3.2. Modeling Results

Table 1 presents the hydraulic parameter values used for the equilibrium and non-equilibrium models.

Table 1. Values of the hydraulic parameters of the VFCW used in HYDRUS-1D.

Equilibrium Model									
Layer	θ_r [-]	θ_s [-]	A [1/cm]	n [-]	K_s [cm/s]	λ [-]			
1	0.64	0.84	0.12	1.80	2.50	0.50			
2	0.00	0.44	0.50	3.20	100	0.50			
Dual-Porosity Model									
Layer	θ_r^m [-]	θ_s^m [-]	α_m [1/cm]	n_m [-]	K_s [cm/s]	λ [-]	θ_r^{im} [-]	θ_s^{im} [-]	ω [1/s]
1	0.00	0.05	0.12	1.80	5	0.50	0.20	0.79	0.05
2	0.00	0.10	0.50	3.20	100	0.50	0.20	0.34	0.00

Figure 3 shows the simulated concentrations and fluxes obtained with the equilibrium and non-equilibrium models. Also shown are results obtained with only one tracer pulse, and those with seven tracer pulses.

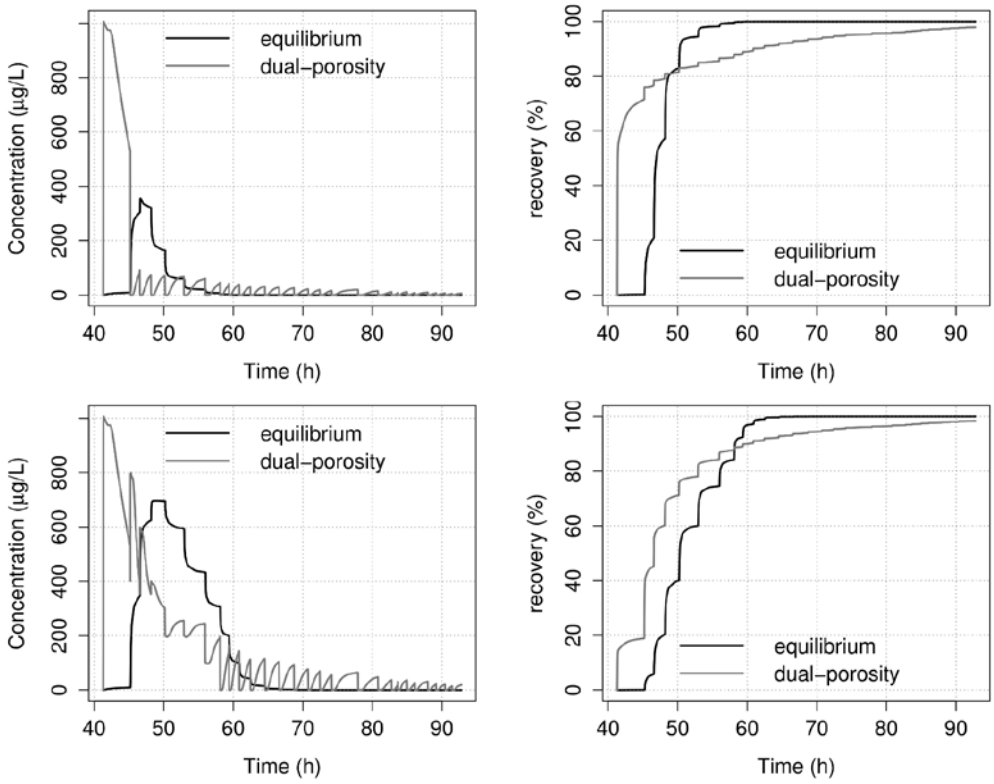

Figure 3. Simulated concentrations (left) and cumulative fluxes (right) for one pulse (top) and seven pulses (bottom) for the equilibrium and non-equilibrium dual-porosity models.

A comparison of the simulated tracer breakthrough curve obtained with the two models shows that the tracer left the filter faster when using the dual-porosity model than with the equilibrium model. Also, we note that the equilibrium model was not able to reproduce the shape inversion of the experimental tracer breakthrough curve (Fig. 2; (2)). The dual-porosity formulation on the other hand provided the same shape inversion due to tracer transfer into the immobile region and its release back into the mobile liquid after each batch. This suggests that preferential flow effects modeled in terms of mobile and immobile water are very important for matching the observed fluorescein tracer transport characteristics.

We further note that when only one batch with tracer was applied, it was not possible to simulate the multiple peaks of the tracer shown in Figure 2. It was necessary to apply the tracer several times to reproduce the tracer peaks observed at the beginning of the tracer experiment.

If one only compares the cumulative tracer fluxes from the outlet of the filter, no important differences can be seen between the equilibrium and non-equilibrium results. Indeed, cumulative fluxes are not sensitive enough for comparing the modeling results whereas tracer concentrations provide much more information about the non-equilibrium processes that occur in the filter.

Overall, the comparison of measured and simulated tracer breakthrough curves indicates that the non-equilibrium approach provides to the more appropriate model for simulating preferential flow paths.

3.3. Calibration Results

Table 2 presents the hydraulic parameter values of the dual-porosity model used for both the tracer concentrations obtained at the outlet of the filter and the water contents recorded in the VFCW.

Table 2. Hydraulic parameter values used for calibration of the dual-porosity model representing VFCW behavior in HYDRUS-1D.

Layer	θ_r^m [-]	θ_s^m [-]	α_m [1/cm]	n_m [-]	K_s [cm/s]	λ [-]	θ_r^{im} [-]	θ_s^{im} [-]	ω [1/s]
1	0.00	0.01	0.12	1.80	5	0.50	0.70	0.83	0.040
2	0.00	0.02	0.50	3.20	25	0.50	0.38	0.39	0.005
3	0.00	0.05	0.50	3.20	25	0.50	0.34	0.36	0.005

Figure 4 presents measured and simulated concentrations obtained from the tracer experiment and the dual-porosity model using parameter values shown in Table 2. Figure 5 compares simulated water contents presents using the dual-porosity model with measured values obtained with the TDR probes.

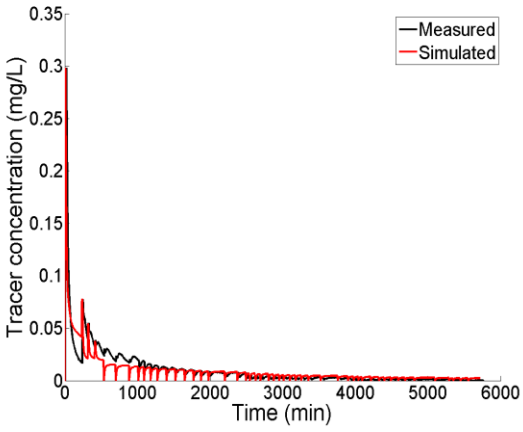

Figure 4. Measured (black line) and simulated (red line) concentrations from the tracer experiment and the dual-porosity model, respectively.

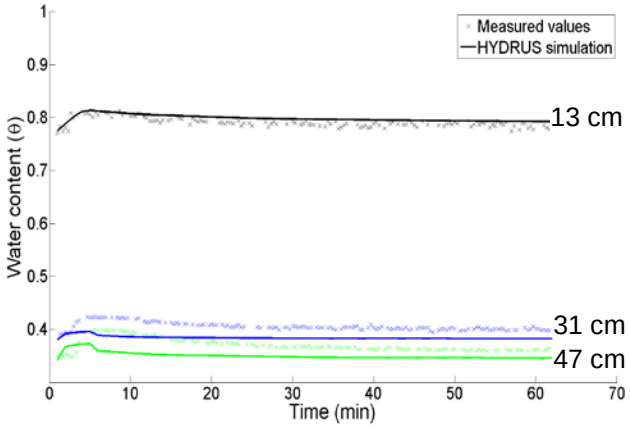

Figure 5. Measured (dots) and simulated (lines) water contents from the TDR probes and the dual-porosity model at different depths, respectively.

After adjusting some of the hydraulic parameters, the simulation using the dual-porosity model (Fig. 4) showed a good match with the measured data ($RMSE = 1.47.10^{-5}$). We could identify the four pulses corresponding to the four inlet concentrations at the beginning of the tracer experiment. After these four batches we observed the same tendency as seen in Figure 2 (2): the tracer concentration decreased immediately after each loading and then increased logarithmically to some equilibrium value until a new batch was applied.

The results in Figure 5 indicate that water retention decreased with depth, mostly because of lower organic matter contents deeper in the filter. Also, even with only having water contents recorded during the first tracer batch, Figure 5 shows that simulated water contents of the sludge layer (13 cm) where very close to the observed water contents ($RMSE = 9.1.10^{-3}$). While still reasonable, simulated water contents for the first (31 cm) and second (47 cm) gravel-sludge layers were far less accurate (RMSE values were 0.39 and 0.43, respectively). In all, the dual-porosity model hence was able to simulate both the tracer breakthrough curve and the water contents at different depths of the VFCW.

4. Conclusions

A comparison was carried out between the classical equilibrium flow model and a non-equilibrium (dual-porosity) type model for simulating the hydrodynamic behavior and the solute transport in a simplified representation of a French VFCW. The HYDRUS-1D software package was found used for modeling the flow and transport processes. Modeling results were compared to a solute breakthrough curve obtained from a tracer experiment carried out in an existing VFCW. This allowed us to determine the most appropriate modeling approach.

The comparison between measured and simulated tracer breakthrough curves indicates that the tracer left the filter faster when simulated with the dual-porosity model than with the classical equilibrium model. The dual-porosity results were consistent with the experimental tracer breakthrough data. Moreover, the dual-porosity model provided the same shape inversion due to the tracer transfer into the immobile region and its release back into the mobile region after each batch. The dual-porosity model also was able to closely match observed water contents at different depths of the filter. We conclude that the non-equilibrium approach is the more appropriate model for simulating preferential flow paths in a French-type VFCW.

References

Gerke, H. H., Preferential flow descriptions for structured soils, *Journal of Plant Nutrition and Soil Science*, *169*(3), 382-400, 2006.

Gerke, H. H., and M. Th. van Genuchten, A dual-porosity model for simulating the preferential movement of water and solutes in structured porous media, *Water Resources Research*, *29*(2), 305–319, 1993.

Haws, N. W., P. S. C. Rao, J. Šimůnek, and I. C. Poyer, Single-porosity and dual-porosity modeling of water flow and solute transport in subsurface-drained fields using effective field-scale parameters, *Journal of Hydrology*, *313*(3–4), 257–273, 2005.

Köhne, J. M., S. Köhne, and J. Šimůnek, Multi-process herbicide transport in structured soil columns: experiments and model analysis, *Journal of Contaminant Hydrology*, *85*, 1–32, 2006.

Köhne, J. M., S. Köhne, and J. Šimůnek, A review of model applications for structured soils: a) Water flow and tracer transport, *Journal of Contaminant Hydrology*, *104*, 4–35, 2009.

Maier, U., C. DeBiase, O. Baeder-Bederski, and P. Bayer, Calibration of hydraulic parameters for large-scale vertical flow constructed wetlands, *Journal of Hydrology*, *369*(3-4), 260-273, 2009.

Molle, P., A. Liénard, A. Grasmick, and A. Iwema, Effect of reeds and feeding operations on hydraulic behavior of vertical flow constructed wetlands under hydraulic overloads, *Water Research*, *40*(3), 606-612, 2006.

Molle, P., S. Prost-Boucle, and A. Liénard, Potential for total nitrogen removal by combining vertical flow and horizontal flow constructed wetlands: a full-scale experiment study, *Ecological Engineering*, *34*(1), 23-29, 2008.

Morvannou, A., Dynamic modelling of nitrification in vertical flow constructed wetlands. Sciences agronomiques et ingénierie biologique, *Université catholique de Louvain*, 184p, 2012.

Morvannou, A., N. Forquet, M. Vanclooster, and P. Molle, On the characterization of the hydraulic properties of the filter material of a Vertical Flow Constructed Wetland, (Submitted).

Radcliffe, D., and J. Šimůnek, Soil Physics with HYDRUS: Modeling and Applications, *CRC Press, Taylor and Francis Group*, 373 p, 2010.

Šimůnek, J., O. Wendroth, N. Wypler, and M. Th. van Genuchten, Non-equilibrium water flow characterized by means of upward infiltration experiments, *European Journal of Soil Science*, *52*, 13-24, 2001.

Šimůnek, J., N. J. Jarvis, M. Th. van Genuchten, and A. Gärdenäs, Review and comparison of models for describing non-equilibrium and preferential flow and transport in the vadose zone, *Journal of Hydrology*, *272*(1-4), 14-35, 2003.

Šimůnek, J., D. Jacques, M. Th. van Genuchten, and D. Mallants, Multicomponent geochemical transport modeling using the HYDRUS computer software packages, *Journal America Water Resources Association*, *42*(6), 1537-1547, 2006.

Šimůnek, J., and M. Th. van Genuchten, Modeling nonequilibrium flow and transport with HYDRUS, *Vadose Zone Journal*, *7*(2), 782–797, Special Issue "Vadose Zone Modeling", 2008.

Estimating the Soil Hydraulic and Thermal Properties of Unsaturated Porous Media Using HYDRUS-2D

Mohammad Nakhaei[1] and Jirka Šimůnek[2]

[1]*Department of Geology, Kharazmi University, Tehran, Iran, nakhaei@khu.ac.ir*
[2]*Department of Environmental Sciences, University of California Riverside, Riverside, USA, Jiri.Simunek@ucr.edu*

Abstract

The combined effects of soil temperature and water input on water flow and redistribution processes under field conditions have not been fully investigated. The objective of this study was to estimate the van Genuchten unsaturated soil hydraulic parameters and several heat transport parameters (the coefficients in the thermal conductivity functions) from observed temperature and infiltration data during a single ring infiltration field experiment. Real-time sensors built by the authors were used to monitor soil temperatures at depths of 40, 80, 120, and 160 cm during 10 hours. Water temperature in the single infiltration ring was simultaneously monitored at the same location. The soil thermal conductivity was estimated from cumulative infiltration and temperature measurements by solving the two-dimensional, inverse water flow and heat transport problem using HYDRUS-2D. Preliminary results are presented showing favorable agreement between simulated soil temperatures during the ring infiltration experiment and corresponding observed values.

1. Introduction

The importance of the unsaturated zone as an integral part of the hydrological cycle has long been recognized. The zone plays an important role in many aspects of hydrology, including infiltration, soil moisture storage, evaporation, plant water uptake, groundwater recharge, runoff, and erosion. Initial studies of the unsaturated zone focused primarily on water supply studies, inspired in part by attempts to optimally manage the root zone of agricultural soils for maximum crop production. The past several decades has seen considerable progress in the conceptual understanding and mathematical description of water flow and heat transport in the unsaturated zone.

Unsaturated water flow in porous media is generally described using the Richards equation. The solution of this equation requires knowledge of soil hydraulic functions, $\theta(h)$ and $K(h)$. Currently there are many laboratory and field methods to determine these nonlinear functions (e.g., Klute, 1986; Dirksen, 1991). Most methods require restrictive initial and boundary conditions, which can make measurements very time-consuming and expensive. When an inverse modeling approach is used, the unknown hydraulic parameters are estimated by minimizing deviations between observed variables and model-predicted output (e.g., Kool et al., 1987; Kool and Parker, 1988).

Models of the simultaneous movement of water and heat in the vadose zone are indispensable for evaluating the water and energy balance of subsurface environments for both agriculture and

engineering applications, especially in arid and semi-arid regions. Although it is widely recognized that the movement of water and heat are closely coupled and strongly affect each other, their mutual interactions are rarely considered in practical applications. The effect of heat transport on water flow is often neglected, arguably because of model complexity and a lack of data to fully parameterize the model, but partly also because user friendly simulation codes are not readily available. Exceptions are the HYDRUS codes (Šimůnek et al., 2006, 2008), which implement solutions for the coupled movement of water and heat in the subsurface. The HYDRUS programs numerically solve the Richards equation for saturated-unsaturated water flow and the convection-conduction equation for heat transport. The heat transport equation considers the transport due to conduction and convection with flowing water. The program may be used to analyze water and heat movement in unsaturated, partially-saturated, or fully-saturated porous media.

The objective of this study was to estimate soil hydraulic and heat transport parameters by collecting data during a ring infiltration experiment, including temperature data collected at several depths under the center of the ring, while using the parameter estimation options incorporated in the HYDRUS-2D software package (Šimůnek and Hopmans, 2002; Hopmans et al., 2002).

2. Material and Methods

2.1. Study Area

The study area is located at the campus site of the Kharazmi University in the city of Karaj of Alborz province, 48 kilometer outside Tehran, Iran. The altitude is 1,297 m above sea level, and the annual average precipitation approximately 300 mm. The annual average temperature is about 16°C. The geology is dominated by the Karaj tuff formations. Soils developed from this bedrock are ssandy loams with a low content of clay (40% sand, 55 % silt, 5% clay). The vegetation cover is very sparse.

2.2. Single Ring Infiltration Experiment

To study water movement and heat transport we instrumented the soil profile with a single 40 cm diameter infiltration ring (Fig. 1a) and 4 thermal sensors at depths of 40, 80, 120 and 160 cm (Fig. 1b). The measurement period was from 8.00 to 18.00 on 4th April 2012. Two soil samples were first collected to characterize soil texture, and then to measure bulk density and the initial water content. The soil samples were analyzed in the sedimentology laboratory of Kharazmi University. Water content was measured in the middle of the profile at a depth of 100 cm. Air temperature was 20^{o}C, and initial soil temperatures at the observation depths were 17.5 ^{o}C.

The temperature of the infiltration water was 61^{o}C during the whole experiment. The final steady-state infiltration rate was also measured and subsequently used for calculating the saturated hydraulic conductivity of the soil using the Wooding (1968) equation (cited from Radcliffe and Šimůnek, 2010, page 106).

Figure 1a. Single infiltration ring.

Figure 1b. Location of four thermal sensors.

2.3. Numerical Model

The HYDRUS-2D software package was used to model the soil water dynamics and heat transport assuming an axisymmetric transport domain (Šimůnek et al, 2006).

2.3.1. Soil Hydraulic Properties

HYDRUS implements the soil-hydraulic functions of van Genuchten (1980) who used the statistical pore-size distribution model of Mualem (1976) to obtain a predictive equation for the unsaturated hydraulic conductivity function in terms of soil water retention parameters. The expressions of van Genuchten (1980) are given by Eq. 1 and Eq. 2:

$$\theta(h) = \begin{cases} \theta_r + \dfrac{\theta_s - \theta_r}{[1+|\alpha h|^n]^m} & h < 0 \\ \theta_s & h \geq 0 \end{cases} \qquad (1)$$

$$K(h) = K_s S_e^l [1 - (1 - S_e^{1/m})^m]^2 \qquad (2)$$

in which θ_r and θ_s denote the residual and saturated water content [-], respectively; K_s is the saturated hydraulic conductivity [LT^{-1}], α is the inverse of the air-entry value (or bubbling pressure) [L^{-1}], n is a pore-size distribution index [-], and l is a pore-connectivity parameter assumed to be 0.5 [-].

2.3.2. Temperature Dependence of the Soil Hydraulic Functions

A scaling technique similar to one used to describe the spatial variability of soil hydraulic properties is used in HYDRUS to express the dependence of the soil hydraulic functions on

temperature. Based on capillary theory that assumes that the influence of temperature on the soil water pressure head can be quantitatively predicted from the influence of temperature on surface tension, Philip and de Vries (1957) derived the following equation:

$$\frac{dh}{dT} = \frac{h}{\sigma}\frac{d\sigma}{dT} \tag{3}$$

where T is temperature [K] and σ is the surface tension at the air-water interface [MT^{-2}]. From (3) it follows that:

$$h_T = \frac{\sigma_T}{\sigma_{ref}} h_{ref} = \alpha_h^* h_{ref} \tag{4}$$

where h_T and h_{ref} (σ_T and σ_{ref}) are pressure heads (surface tensions) at temperature T and reference temperature T_{ref}, respectively; and α_h^* is the temperature scaling factor for the pressure head. Following Constantz (1982), the temperature dependence of the hydraulic conductivity can be expressed as follows:

$$K_T(\theta) = \frac{\mu_{ref}}{\mu_T}\frac{\rho_T}{\rho_{ref}} K_{ref}(\theta) = \alpha_K^* K_{ref}(\theta) \tag{5}$$

where K_{ref} and K_T denote hydraulic conductivities at the reference temperature T_{ref} and soil temperature T, respectively; μ_{ref} and μ_T (ρ_{ref} and ρ_T) represent the dynamic viscosity [$ML^{-1}T^{-1}$] (density of soil water [ML^{-3}]) at temperatures T_{ref} and T, respectively; and α_{K^*} is the temperature scaling factor for the hydraulic conductivity.

2.3.3. Heat Transport

Neglecting the effects of water vapor diffusion, two- and three-dimensional heat transport can be described as (Sophocleous, 1979):

$$C_p(\theta)\frac{\partial T}{\partial t} = \frac{\partial}{\partial x_i}\left[\lambda_{ij}(\theta)\frac{\partial T}{\partial x_j}\right] - C_w q_i \frac{\partial T}{\partial x_i} \tag{6}$$

where $\lambda_{ij}(\theta)$ is the apparent thermal conductivity of the soil [$MLT^{-3}K^{-1}$] (e.g. $Wm^{-1}K^{-1}$) and C_p (θ) and C_w are the volumetric heat capacities [$ML^{-1}T^{-2}K^{-1}$] (e.g. $Jm^{-3}K^{-1}$) of the porous medium and the liquid phase, respectively. The volumetric heat capacity is defined as the product of the bulk density and the gravimetric heat capacity. The first term on the right-hand side of (6) represents heat flow due to conduction, while the second term accounts for heat being

transported by flowing water. In this study we did not consider the transfer of latent heat by vapor movement. According to de Vries (1963) the volumetric heat capacity can be expressed as:

$$C_p(\theta) = C_n\theta_n + C_o\theta_o + C_w\theta + C_a a_v \approx (1.92\theta_n + 2.51\theta_o + 4.18\theta)\ 10^6 \qquad (\text{J m}^{-3\,\text{o}}\text{C}^{-1}) \quad (7)$$

where θ refers to a volumetric fraction [L^3L^{-3}], and the subscripts *n, o, g, w* represent the solid phase, organic matter, gas phase and liquid phase, respectively.

2.3.4. Apparent Thermal Conductivity Coefficient

The apparent thermal conductivity, $\lambda_{ij}(\theta)$, combines the thermal conductivity $\lambda_0(\theta)$ of the porous medium (solid plus water) in the absence of flow, and the macro-dispersivity, which is assumed to be a linear function of the velocity (de Marsily, 1986). In analogy with the dispersion coefficient for solute transport, the apparent thermal conductivity $\lambda_{ij}(\theta)$ is given by (Šimůnek and Suarez, 1993):

$$\lambda_{ij}(\theta) = \lambda_T C_w |q| \delta_{ij} + (\lambda_L - \lambda_T) c_w \frac{q_j q_i}{|q|} + \lambda_0(\theta)\delta_{ij} \qquad (8)$$

where q is the absolute value of the Darcian fluid flux density [LT^{-1}], δ_{ij} is the Kronecker delta function, and λ_L and λ_T are the longitudinal and transverse thermal dispersivities [L], respectively. The volumetric heat capacity of the liquid phase is included here in the definition of the thermal conductivity in order to have the dimensions of the thermal dispersivities in length units (de Marsily, 1986). The thermal conductivity, $\lambda_0(\theta)$, accounts for the tortuosity of the porous medium, and is described with the simple equation (Chung and Horton, 1987):

$$\lambda_0(\theta) = b_1 + b_2\theta + b_3\theta^{0.5} \qquad (9)$$

where b_1, b_2 and b_3 are empirical parameters [$MLT^{-3}K^{-1}$] (e.g. $Wm^{-1}K^{-1}$).

2.4. Numerical Model

2.4.1. Transport Domain

The transport domain was 200 cm wide and 200 cm deep. The domain was discretized into 441 nodes and 400 triangular finite elements. Calculations were carried out over a period of 10 hours.

2.4.2. Initial and Boundary Conditions

The initial water content considered in the simulation (0.041 cm^3/cm^3) was measured in the field. A soil profile temperature of 17.5°C as measured in the field was used as the initial condition for heat transport.

All sides of the flow region were considered to be impervious, except for a small portion around the origin at the ponded surface inside the ring infiltrometer where a constant water content was imposed, and for the bottom of the soil profile where a free drainage condition was imposed (Fig. 2a). The volumetric water content of 0.43 cm^3/cm^3 was used as the water flow boundary condition under the single infiltration ring. A third-type heat transport boundary condition was used for nodes under the single infiltration ring with a constant temperature of 61°C, representing hot water infiltrating into the soil profile. A third-type heat transport boundary condition was also invoked at the bottom of the soil profile (Fig. 2b). No-flux boundary conditions were used for both water flow and heat transport along all other boundary nodes.

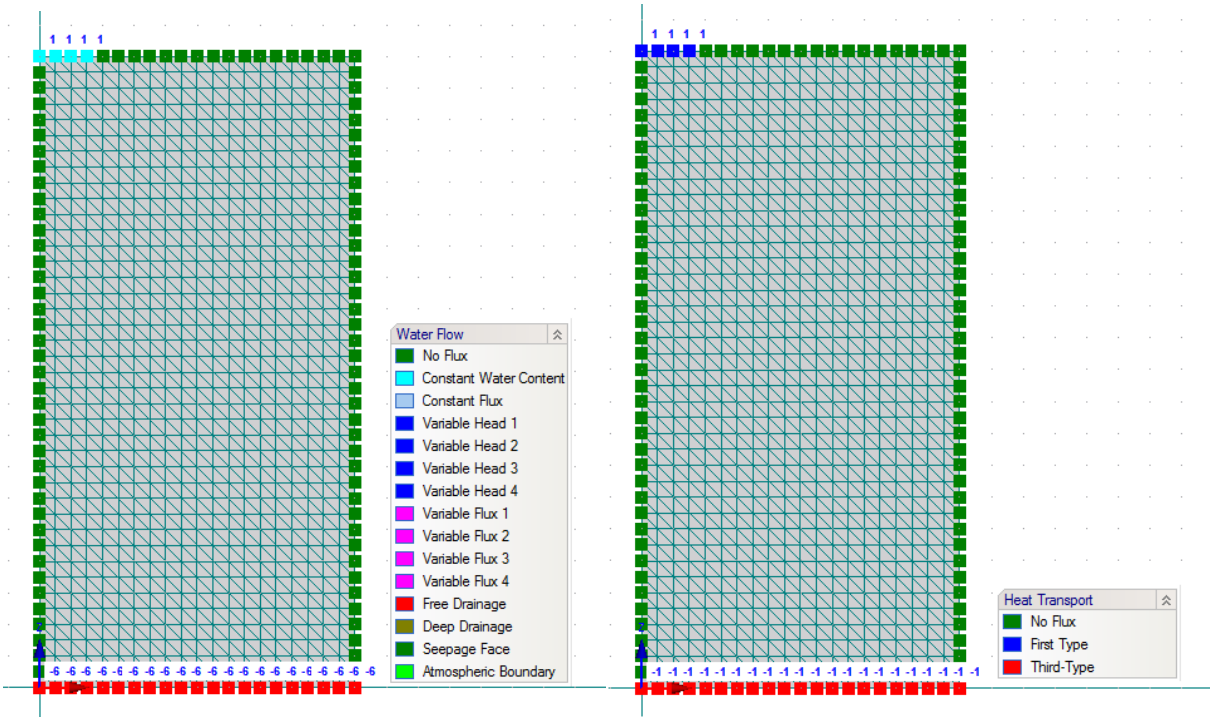

Figure 2. Imposed boundary conditions for water flow (left) and heat transport (right) for the single ring infiltrometer experiment investigated in this study.

3. Results and Discussion

The experimental infiltration data were used to estimate the soil hydraulic characteristics of the silt loam field soil profile. The steady-state infiltration rate from the ring was 0.00166 cm/s, while we used a macroscopic capillary length of 8.3 cm typical of a sandy loam (Radcliffe and Šimůnek, 2010). We subsequently used the predicted saturated hydraulic conductivity of 0.0011 cm/sec as an initial estimate in the inverse solution. Measured soil temperatures at four

observation depths and the cumulative infiltration were used to optimize selected soil hydraulic and heat transport parameters.

Figure 3 shows an example of the simulated output obtained with the HYDRUS-2D model. The plots show the final water contents and temperatures in the soil profile. Figure 4 compares simulated and measured cumulative infiltration rates (left) and simulated and measured temperatures in the soil profile at depths of 40, 80, 120 and 160 cm. Temperatures optimized with the model fitted the measured temperatures well. Also, the coefficient of determination indicated a good fit. We conclude that we were able to estimate selected soil hydraulic and thermal parameters quite well, although some questions remain about the uniqueness of the optimized values.

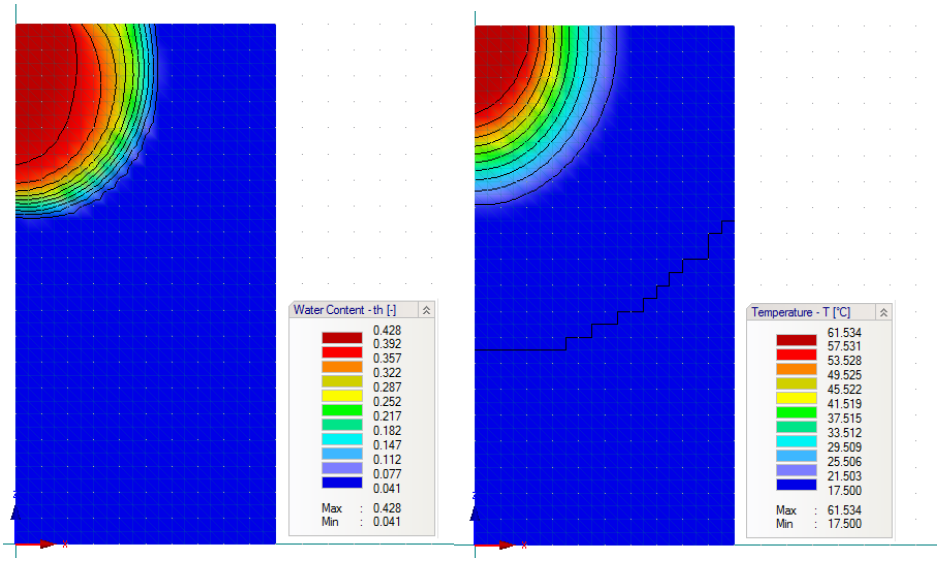

Figure 3. Final simulated water contents (left) and temperatures (right) in the soil profile.

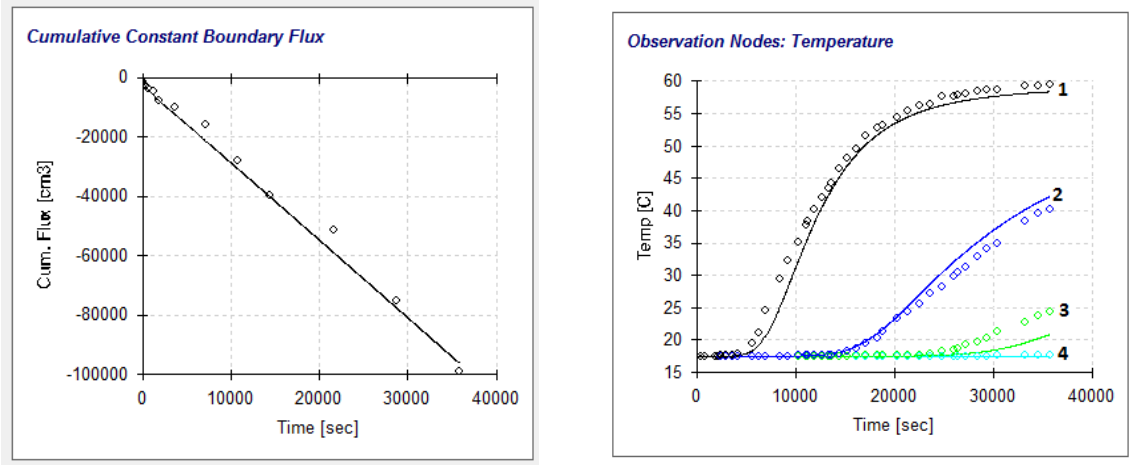

Figure 4. Simulated and observed cumulative fluxes (left) and temperatures (right).

Figure 6 shows the optimized soil characteristic curve, $\theta(h)$, and the unsaturated hydraulic conductivity function, $K(h)$, for the silt loam soil. Tables 1 and 2 show the initial estimates (for those parameters that were optimized) of the soil hydraulic and heat transport properties, respectively.

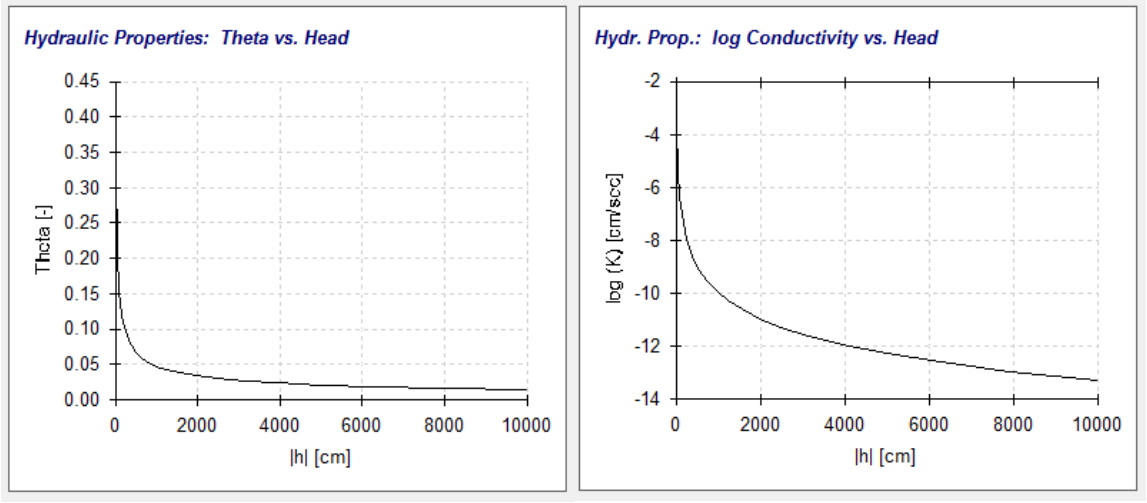

Figure 6. Optimized soil characteristic curve (left), $\theta(h)$, and hydraulic conductivity function (right), $K(h)$.

Table 1. Initial estimates of soil hydraulic parameters.

Residual moisture content	(WCR)	.001
Saturated moisture content	(WCS)	.43
First coefficient	(ALPHA)	.035
Second coefficient	(N)	1.5
Saturated conductivity	(CONDS)	.001067
Pore connectivity factor	(L)	.500

Table 2. Initial estimates of heat transport parameters.

Solid fraction	(Qn)	.600
Organic matter fraction	(Qo)	.001
Heat dispersivity longitudinal	(DisperHL)	2.000
Heat dispersivity transverse	(DisperHT)	.200
Parameter B1	(B1)	.2400E+02
Parameter B2	(B2)	.3000E+02
Parameter B3	(B3)	.1500E+03
Heat capacity - solid	(Cn)	.1920E+05
Heat capacity - organic matter	(Co)	.2510E+05
Heat capacity - water	(Cw)	.4180E+05

Finally, the optimized soil hydraulic and heat transport parameters obtained by solving the inverse problem using the HYDRUS-2D program are presented in Table 3. Figure 7 shows a comparison of the optimized thermal conductivity function $\lambda(\theta)$ for our silt loam soil with those for the three main textural classes of clay, loam, and sand (Chung and Horton, 1987). The results indicate that the optimized thermal conductivity function is very similar to the default functions, thus demonstrating the robustness of the numerical inverse solution when using only measured soil temperatures and cumulative infiltration during the field ring infiltration experiment.

Table 3. Final optimized soil hydraulic and heat transport parameters.

WCR, θ_r	WCS, θ_s	ALPHA, α [cm^{-1}]	n	CONDS, K_s [cm/sec]	b_1 [kg cm s^{-3} K^{-1}]	b_2 [kg cm s^{-3} K^{-1}]	b_3 [kg cm s^{-3} K^{-1}]
0.0	0.43	0.075	1.51	0.001322	43.3	29.6	106.0

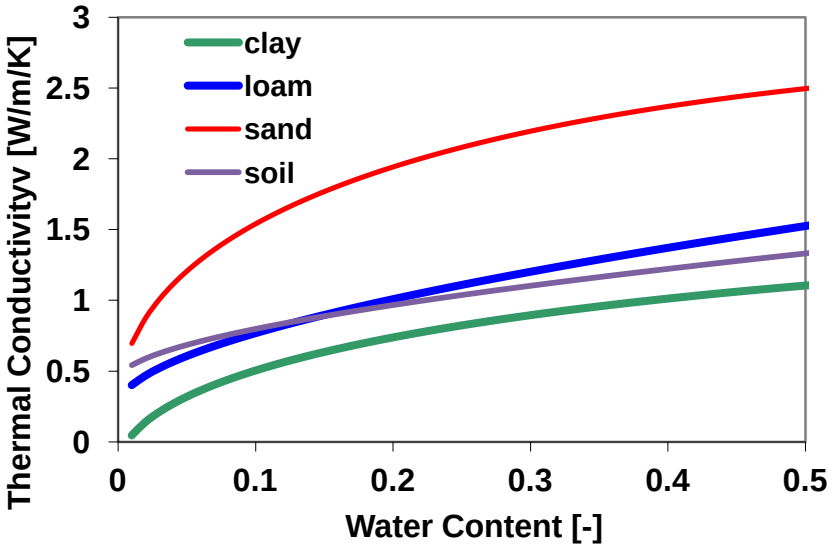

Figure 7. Comparison of the optimized thermal conductivity function $\lambda(\theta)$ with those for three main textural classes (clay, loam, and sand).

4. Conclusions

In this study we used HYDRUS-2D to simulate infiltration of relatively warm water from a single ring infiltrometer into a silt loam soil profile and to estimate the soil thermal and hydraulics properties by inverse solution from collected experimental data. We showed that temperatures collected at four sensors at four different depths with cumulative infiltration could provide the required information for simultaneous estimation of the soil thermal and hydraulic properties. However, using available collected data, we could prove the uniqueness of our estimated parameters. Therefore, in a subsequent study we will be collecting additional data (especially pressure heads and water contents at different locations, as well as independently measured retention and hydraulic conductivity functions) to be able to better evaluate results of our inverse analysis. We also plan to include nonreactive chemicals in the infiltrating warm water to study the possibility of inverse modeling for additionally estimate solute transport properties.

References

Chung S.-O., and R. Horton, Soil heat and water flow with a partial surface mulch, *Water Resour. Res., 23*(12), 2175-2186, 1987.

Constantz, J., Temperature dependence of unsaturated hydraulic conductivity of two soils, *Soil Sci. Soc. Am. J., 46*(3), 466-470, 1982.

de Marsily, G., *Quantitative Hydrogeology*, Academic Press, London, 1986.

de Vries, D. A., The thermal properties of soils, In: *Physics of Plant Environment*, edited by R. W. van Wijk, pp. 210-235, North Holland, Amsterdam, 1963.

Dirksen, C., Unsaturated hydraulic conductivity, In: *Soil Analysis: Physical methods*, K.A. Smith and C.E. Mullins (eds.), 209-269, Marcel Dekker, Inc., New York, 1991.

Hopmans, J. W., J. Šimůnek, N. Romano, and W. Durner, Inverse Modeling of Transient Water Flow, In: *Methods of Soil Analysis, Part 1, Physical Methods,* Chapter 3.6.2, Eds. J. H. Dane and G. C. Topp, Third edition, SSSA, Madison, WI, 963-1008, 2002.

Klute, A. (ed.), *Methods of Soil Analysis*, Part 1., 2nd ed., Agronomy Monograph, 9, 635-662, ASA and SSSA, Madison, WI, 1986.

Kool, J. B., and J. C. Parker, Development and evaluation of closed-form expressions for hysteretic soil hydraulic properties. *Water Resour. Res., 23*(1), 105-114, 1987.

Kool, J. B., J. C. Parker, and M. Th. van Genuchten, Parameter estimation for unsaturated flow and transport models - A review, *J. Hydrol., 91*, 255-293, 1987.

Mualem, Y., A new model for predicting the hydraulic conductivity of unsaturated porous media, *Water Resour. Res., 12*(3), 513-522, 1976.

Philip, J. R., and D. A. de Vries, Moisture movement in porous materials under temperature gradients, *Trans. Am. Geophys. Union*, *38*, 222-232, 1957.

Radcliffe D. E, and J. Šimůnek, *Soil Physics with HYDRUS*, CRC Press, Taylor & Francis Group, Boca Raton, FL, ISBN: 978-1-4200-7380-5, pp. 373, 2010.

Šimůnek, J., and D. L. Suarez, UNSATCHEM-2D code for simulating two-dimensional variably saturated water flow, heat transport, carbon dioxide production and transport, and multicomponent solute transport with major ion equilibrium and kinetic chemistry, Version 1.1, *Research Report No. 128*, U. S. Salinity Laboratory, USDA, ARS, Riverside, CA, 1993.

Šimůnek, J., and J. W. Hopmans, Parameter Optimization and Nonlinear Fitting, In: *Methods of Soil Analysis, Part 1, Physical Methods,* Chapter 1.7, Eds. J. H. Dane and G. C. Topp, Third edition, SSSA, Madison, WI, 139-157, 2002.

Šimůnek, J., M. Šejna, and M. Th. van Genuchten, The HYDRUS Software Package for Simulating Two- and Three-Dimensional Movement of Water, Heat, and Multiple Solutes in Variably-Saturated Media, User Manual, Version 1.0, PC Progress, Prague, Czech Republic, 2006.

Šimůnek, J., M. Th. van Genuchten, and M. Šejna, Development and applications of the HYDRUS and STANMOD software packages, and related codes, *Vadose Zone Journal*, *7*(2), 587-600, 2008.

Sophocleous, M., Analysis of water and heat flow in unsaturated-saturated porous media, *Water Resour. Res., 15*(5), 1195-1206, 1979.

van Genuchten, M. Th., A closed-form equation for predicting the hydraulic conductivity of unsaturated soils, *Soil Sci. Soc. Am. J.*, *44*, 892-898, 1980.

Wooding, R. A., Steady infiltration from large shallow circular pond, *Water Resour. Res.*, *4*, 1259-1273, 1968.

Simulation of Water and Salinity Dynamics under Different Irrigation Applications to an Almond Tree in Pulsed and Continuous Mode

Vinod Phogat[1,*], Mark A. Skewes[1], M. Mahadevan[1], and James W. Cox[1,2]

[1]*South Australian Research and Development Institute, G.P.O. Box 397, Adelaide, SA 5001*
Vinod.Phogat@sa.gov.au, Mark.Skewes@sa.gov.au, Mahalakshmi.Mahadevan@sa.gov.au, Jim.Cox@sa.gov.au
[2]*The University of Adelaide, PMB1 Glen Osmond SA 5064*
james.w.cox@adelaide.edu.au

Abstract

The quantification of the components of water balance is essential for designing strategies for improving irrigation efficiency and water productivity of crops under different irrigation systems and for minimizing the offsite movement of nutrients out of the rhizosphere. HYDRUS-2D was used to simulate seasonal water balance and salinity distribution under full pulsed (FI_p), sustained deficit pulsed (SDI_p; 65% ET_C), and full continuous (FI_c) irrigation of an almond tree using a surface drip. The weekly measured and predicted values of moisture content at different distances from the dripper and at different soil depths matched well, showing only a small variation in *RMSE* values. The sap flow underestimated almond water uptake by 31% as compared to the modeled value in SDI_p. Water uptake efficiency under SDI_p (68%) was higher compared to full water application conditions under FI_p and FI_c (54-55%). The leaching fraction was estimated to be 0.14 under SDI_p and 0.25 in FI_p and FI_c treatments. The higher irrigation amounts under 100% ET_C treatments (FI_p and FI_c) largely contributed to non-productive water fluxes (deep drainage losses and evaporation). The seasonal water uptake by almond under pulsed (FI_p) and continuous irrigation (FI_c) remained almost at par, indicating that pulsing didn't provide any added advantage, although it is a viable alternative to slow discharge continuous irrigation. The average modeled soil solution salinity (EC_{sw}) of the soil profile also remained below the threshold for the yield reduction during the growing season in all treatments. The irrigation water productivity (WP_I) increased substantially (37%), yield was reduced by 8% and about 35% of irrigation water was saved under sustained deficit irrigation (SDI_p) as compared to full irrigation (FI_p). It was concluded that SDI_p is a promising deficit irrigation strategy for almond cultivation in Australia. These outcomes can be utilized to improve irrigation efficiency and system design for drip irrigation of almond trees.

1. Introduction

Fierce competition among water users, frequent droughts, and scarce water resources in Australia put enormous pressure on irrigation systems and drive a requirement for more efficient irrigation practices. Hence, 90% of almond plantation in Australia is under a high efficiency drip system of irrigation. Various water saving interventions, like pulsing of irrigation and sustained deficit irrigation, are being followed for managing water efficiently and increasing the water productivity. However, dynamics of water fluxes above and in the soil exert a pronounced impact on plant water uptake, deep drainage, and solute distribution in the soil profile and thus significantly influence processes of water and solute movement in the rhizosphere (Phogat et al., 2013). Therefore, evaluating seasonal dynamics in plant water uptake and deep drainage is

needed, so that improvements in the usage of scarcely available water can be attained and to enhance water productivity.

The temporal and spatial dynamics of water fluxes through the soil-plant-atmosphere continuum can be better understood using numerical simulation models, provided that the precisely measured values of input parameters are used for modeling simulations. Out of the numerous models, varying in degree of sophistication and complexity and presently available for evaluating the soil water movement (Subbaiah, 2013), HYDRUS has been extensively used for the analysis of micro irrigation systems involving a varied range of soil, water, and crop conditions (Gardenas et al., 2005; Hanson et al., 2006; Kandelous et al., 2012; Phogat et al., 2012ab, 2013; Ramos et al., 2012). Although modeling has been done extensively for problems related to drip irrigation systems using the HYDRUS software, only a few studies have been substantiated with field validation.

The present study uses HYDRUS-2D modeling and the field data recorded for an almond tree over a season to evaluate the water balance and salinity dynamics under full irrigation and stress conditions, and to evaluate the impact of pulsing and continuous drip irrigation on the dynamics of water fluxes, including plant water uptake and deep drainage. Understanding the daily water fluxes during the crop season under high frequency irrigation would have large implications for devising the irrigation scheduling and improving water productivity of almond under stress conditions.

2. Materials and Methods

2.1. Details of Field Experiment

The experiment was conducted at Clark Taylor farms, a commercial almond [*Prunus dulcis* (Mill.) Webb] orchard in Berri, South Australia (34°20'S and 140°35'E) from July, 2009 to May, 2010. The orchard was planted in 1998 with the rows oriented north–south and a spacing of 6.7 m between rows and 6.1 m within a row. Since the soil was more or less uniform, a mean soil particle size distribution of 88.5% sand, 1.9% silt, and 9.6% clay, and a bulk density of 1,610 kg m^{-3} were considered in this study. The trees were managed and fertilized following current commercial practices. The total rainfall received during the study period was 220 mm. The daily ET_C for the irrigation purpose was calculated from E_{pan} values of the previous day multiplied with suitable crop factors.

The orchard was surface drip irrigated, with a pulsed irrigation treatment of 100% ET_C (FI_P), sustained deficit irrigation of 65% ET_C (SDI_p), and a continuous irrigation treatment of 100% ET_C (FI_c), covering an area of 1.89, 0.97, and 0.7 ha, respectively. The treatments were initiated from 20th August, 2009 after one month of a profile establishment stage. Profile establishment resulted in the application of an equal amount of irrigation (85 mm) in each treatment. The seasonal salinity of irrigation water ranged between 0.2 to 0.52 dS m^{-1}.

Each row of trees had two laterals, one on either side of the row at 1 m offset from the tree trunk. The pulsed treatments (FI_p and SDI_p) were irrigated with a cycle of one hour on and one hour

off, with an average flow rate of the drippers of 3.87 l h^{-1}. For continuous treatment (FI_c), the measured flow rate was 2.00 l h^{-1} per dripper. The number of drippers per tree was approximately 12 for the pulsed treatments and 15 for the continuous treatment, as the dripper distance in pulsed and continuous treatments was 100 cm and 80 cm, respectively.

Neutron probe access tubes were installed at a lateral distance of 0, 20, 40, 60, 80, and 100 cm from the dripper (Fig. 1) to a depth of 160 cm to monitor the profile soil water distribution at weekly intervals, at every 10 cm depth up to a depth of 100 cm, and then every 20 cm between depths of 100 and 160 cm.

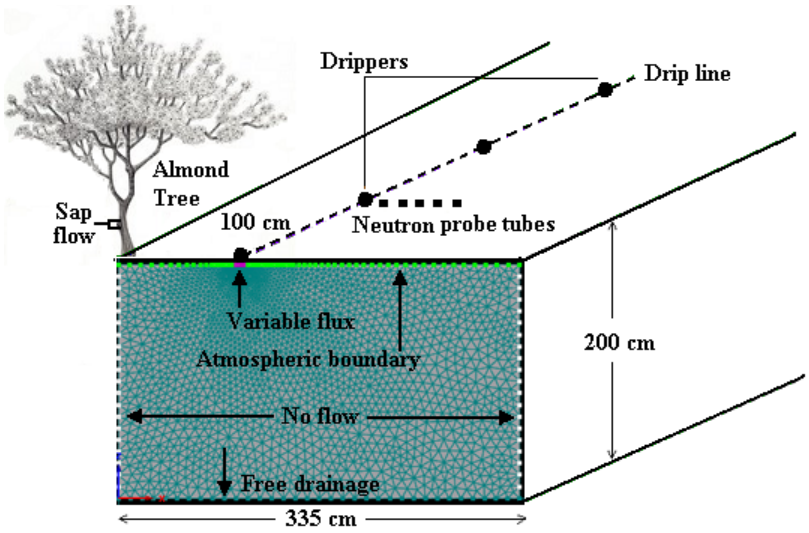

Figure 1. A schematic view of a model domain, plant spacing, and measuring gadgets.

Sap flow measurements were performed on two trees under pulsed treatments (SDI_p and FI_p) and were based on the heat pulse method outlined by Green et al. (2003) to quantify the water uptake by an almond tree. However, the sap flow installation was delayed and measurements were obtained only from 25th November onward.

2.2. Numerical Modeling

Soil water and soil water salinity distributions below the drip line were simulated with the version 2.x of the computer simulation model HYDRUS (2D/3D). This new HYDRUS software module can simulate two- and three-dimensional variably saturated water flow, heat movement, and transport of solutes involved in sequential first-order decay reactions. In addition, the model allows for specification of root water uptake, which affects the spatial distribution of water and soil water salinity between irrigation cycles. The details about the model can be obtained from Šimůnek et al. (2011) and Šejna et al. (2011).

2.3. Input Parameters

Though seasonal irrigations of almond were based on E_{pan} and crop factors, the potential ET_C was calculated from the reference evapotranspiration (ET_0) values collected from the

Bookpurong meteorological station, situated 150-200 m away from the experimental site, following the dual crop coefficient method (Allen et al., 1998), to serve as an input for the model. The seasonal potential transpiration (T_{pot}) amounts to 1,380 mm, and potential evaporation (E_s) for the same period was 414 mm. The estimates of optimized soil hydraulic parameters used for the modeling simulations were: $\theta_r = 0.06$, $\theta_s = 0.37$, $K_s = 276.6$ cm day^{-1}, $\alpha = 0.0316$ cm^{-1} and $n = 2.52$. The value of l was taken as 0.5 as recommended.

The almond root distribution was described using the Vrugt et al. (2001) two-dimensional model adapted in HYDRUS. The parameters used in the model for almond were: $z_m = 150$ cm, $z^* = 30$ cm, $x_m = 335$ cm, $x^* = 25$ cm, $p_x = 2.918$, $p_z = 3.214$. The values of empirical coefficients were taken from Vrugt et al. (2001), and were optimized for almond.

The reducing effects of both soil water pressure head and osmotic head on root water uptake were included, assuming their effects were multiplicative. The following parameters of the model were used: $h_1 = -10$, $h_2 = -25$, h_{3max}, $= -500$, $h_{3min} = -800$, $h_4 = -8000$ cm; $r_{2,high} = 0.5$ cm d^{-1}, and $r_{2,low} = 0.1$ cm d^{-1}. The threshold model was used to describe osmotic effects using a threshold $EC_e = 1.5$ dS m^{-1} and a slope of 19%.

Spatial distribution of salinity in the transport domain was simulated using the convection–dispersion equation for a nonreactive tracer. Such simulations cannot account for complex processes such as precipitation or dissolution of solid phases (e.g., gypsum or calcite) or cation exchange. Longitudinal dispersivity was considered to be 20 cm and transverse dispersivity was 2 cm.

The water content initial conditions were based on values measured by the neutron probe, which varied from 0.05 to 0.08 cm^{3}cm^{-3} in $F1_p$, 0.07-0.14 cm^{3}cm^{-3} in SDI_p, and 0.04-0.06 cm^{3}cm^{-3} in continuous ($F1_c$) drip irrigation. Similarly, the initial soil solution salinity (EC_{swi}) in the soil profile varied from 3.89 to 7.22 dS m^{-1}, 3.63-8.3 dS m^{-1}, and 4.55-7.95 dS m^{-1} in $F1_p$, SDI_p, and $F1_c$ treatments, respectively. Initial soil water salinities were based on field measurements made at the start of the experiment and estimated from measurements of the saturated soil extract (EC_e). The water flow boundary conditions are shown in Figure 1. In the case of solute transport, the boundary condition representing salinity is a third-type Cauchy boundary condition that prescribes the salt movement during defined irrigation intervals.

Simulations were made for hourly pulsed and continuous irrigation treatments during a period of 316 days. The simulated surface drip irrigation system design characteristics were typical of the drip systems used for the field experiment on almond, as shown in Figure 1. The model domain was 200 cm deep and 335 cm wide (one fourth of the bed spacing used for the almond production). The domain was discretized into 5,087 finite elements with a very fine grid around the dripper (0.3 cm) and gradually increasing elements farther from the drip (up to 9.8 cm). The measured salinity of irrigation water (EC_{iw}) was used as a time variable boundary condition. The drip irrigation was simulated assuming an infinite line source to be a good representation of the drip irrigation system. The root mean square error (*RMSE*) was calculated to compare the experimental and predicted values of water content.

3. Results and Discussion

The model-produced, weekly values of water content were compared with measured values at various horizontal and vertical locations in the domain in all treatments. For example, the measured and simulated water contents in full pulsed treatment (FI_p) at a distance of 20 cm from the dripper, averaged for all depths is shown in Figure 2. The simulated water content values matched the neutron probe measured data well, except within a short period during midseason of the crop. The *RMSE* values ranged from 0.01 to 0.08, 0.01-0.06, and 0.01-0.05 cm^3cm^{-3} in full pulsed ($F1_p$), pulsed deficit (SDI_p), and full continuous ($F1_c$) irrigation, respectively. Similar variations between measured and simulated moisture regimes have also been reported in other modeling studies (Phogat et al. 2012ab, 2013). This comparison confirms that the model successfully captured the dynamics of water movement in the soil throughout the cropping season under both scenarios of the water application. However, the small differences between measured and simulated water contents are likely due to model errors caused by restrictive assumptions regarding the geometry of the rooting system, homogeneity of soil hydraulic properties within the spatial domain, and the prescribed root water uptake model.

Simulated water balance components obtained for different treatments are shown in Table 1. Seasonal water uptake in sustained deficit treatment (SDI_p) was reduced by 13.9%, compared to full pulsed irrigation. However, water uptake under full pulsed ($F1_p$) and full continuous (FI_c) irrigations remained almost equal. On the other hand, root water uptake efficiency under stress treatment (68%) was much higher compared to normal water application conditions (54-55%) in FI_p and FI_c treatments.

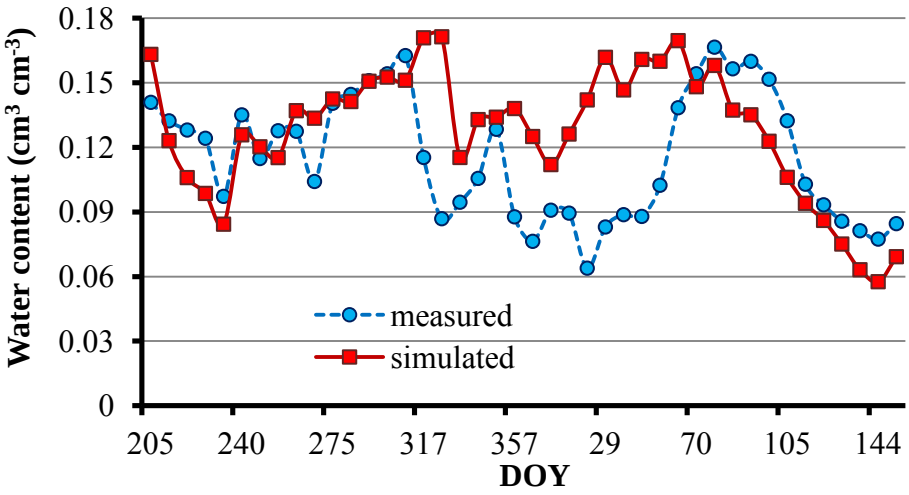

Figure 2. The comparison of weekly measured and simulated water contents in full pulsed irrigation (FI_p) at a distance of 20 cm from the dripper.

A significant reduction was observed in deep drainage flux for scenarios under stress, which was drastically reduced under SDI_p as compared to full irrigation (Table 1). Only 14% of total water applied escaped the crop root zone in SDI_p, compared to 25% in full irrigation treatments (FI_p and FI_c). However, among full irrigation scenarios, pulsing had a little impact on the deep drainage because it was slightly higher (13 mm) under pulsing (FI_p), and the soil storage was 20 mm higher under continuous irrigation (FI_c). Apparently, large changes in the soil storage (53

and 73 mm) reflected the depth of the soil in the model domain (200 cm) and the fact that the soil was quite dry at the beginning of the simulation, and uniformly wet across the model domain at the end of the simulation, as a result of irrigation and rainfall events.

Table 1. Water balance components in different treatments under pulsed and continuous irrigation.

Parameters	SDI_p	FI_p	FI_c	Difference (FI_p & FI_c)	
	----------(mm)----------				(%)
Irrigation	1104	1686	1668	18	1.1
Rainfall	220	220	220	-	-
Root water uptake	905	1051	1026	25	2.4
Evaporation	238	310	311	-1	-0.3
Deep drainage	190	489	476	13	2.7
Soil storage	(-) 8	53	73	-20	-37.7

Daily root water uptake rates calculated by HYDRUS-2D were compared with the sap flow measured transpiration by almond during 25th Nov, 2009 to 31st May, 2010 in full pulsed (FI_p), as well as for stress (SDI_p) treatments. The comparison for full irrigation has been illustrated in Figure 3. It can be seen that HYDRUS very well sensed the diurnal fluctuations in the water uptake driven by the evapotranspirational demand, and the model also predicted water uptake fluctuations very well, in accordance with the sap flow measurements. However, the magnitude of modeled water uptake was higher than the sap flow measurements until the almond harvest and, subsequently, both matched well. Sap flow measurements estimated 492 mm water uptake during this period, compared to 659 mm predicted by the model, and compared with the 1,167 mm of water applied through irrigation and rainfall. Hence, sap flow measurements underestimated water uptake by almond by about 25% under full irrigation and 31% under the stress treatment. We believe that the assumption of wood thickness, and wood and sap composition for the estimation of the correction factor may have resulted in the underestimation of water uptake by sap flow. Several other reasons for underestimations are also outlined in Phogat et al. (2013).

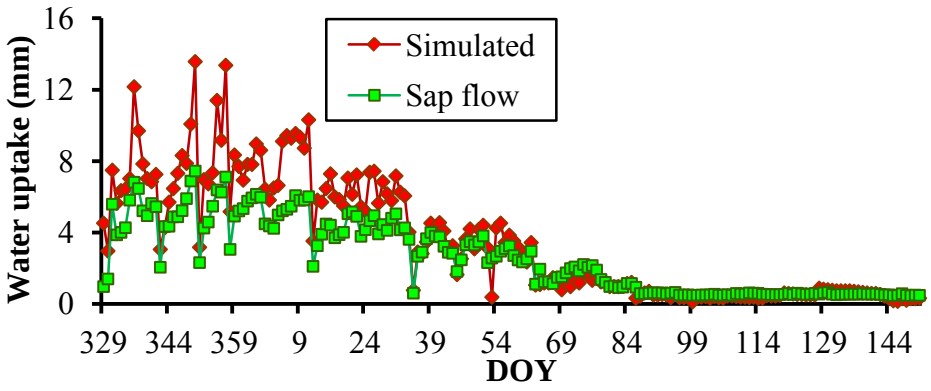

Figure 3. Comparison of simulated daily water uptake and sap flow water uptake by almond in full pulsed (FI_p) irrigation.

The deep drainage was not evenly distributed over the season (Figure 4). There was higher leaching early in the season (August) and after harvest in Feb-April, together amounting to 50% of the total seasonal leaching in FI_p and FI_c treatments, whereas more than 50% drainage in SDI_p occurred in July-August (a profile establishment stage), and thereafter the drainage volume was drastically reduced to negligible amounts during the midseason, increasing again during March-April after the harvest of kernels. Hence, during the July-August and Feb-April periods, the water requirement of almond was less than the water application. This implies that there is a need to revise the used crop coefficients (K_c), and reschedule irrigation applications during these periods so that these unnecessary water losses can be controlled.

Model simulations were also performed for the seasonal salinity distribution in the soil profile, and average soil solution salinity (EC_{sw}) data is presented in Figure 5. The EC_{sw} values remained similar in both full irrigation treatments (FI_p and FI_c) because the salt transport in a light-textured soil is predominantly governed by the dynamics of water movement, which was similar in both treatments. The average EC_{sw} values in the soil below the dripper ranged from 0.47 to 3.38 dS m^{-1} and 0.49 to 3.67 dS m^{-1} in FI_p and FI_c treatments, respectively.

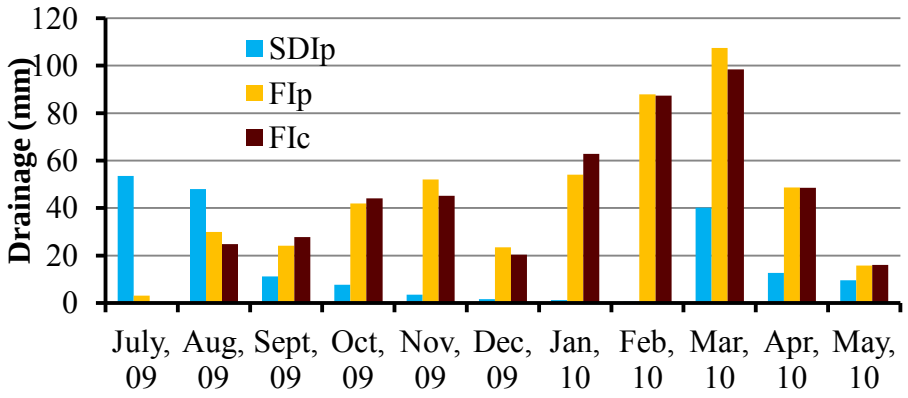

Figure 4. Simulated deep drainage (mm) under pulsed deficit (SDI_p), full pulsed ($F1_p$), and full continuous ($F1_c$) drip irrigation of almond.

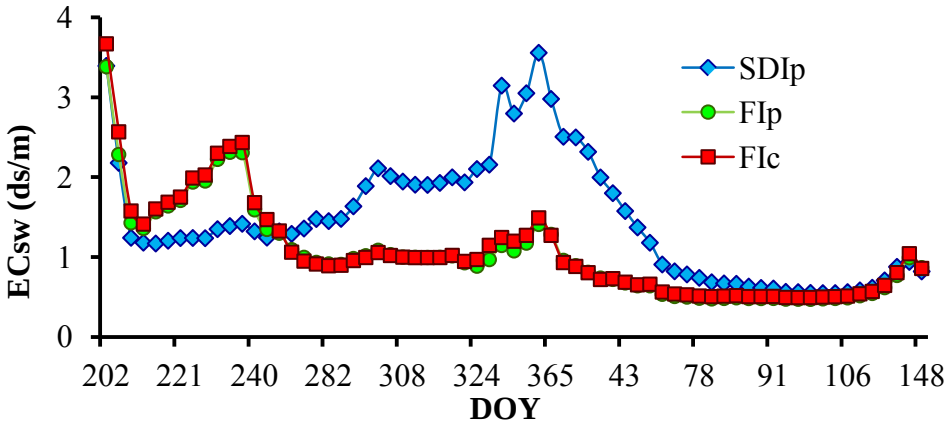

Figure 5: Simulated soil solution salinity (EC_{sw}) distribution in pulsed deficit (SDI_p), full pulsed (FI_p) and continuous (FI_c) drip irrigation of almond.

The soil solution salinity (EC_{sw}) under SDI_p was initially lower because the initial soil water content was substantially higher compared to FI_p and FI_c treatments and consequently, higher leaching was observed during the profile establishment and early growth period. However, from September onward the salinity in SDI_p was much higher and continued to increase until December, when it reached a maximum value of 3.55 dS m^{-1}, after which it decreased continuously until April, 2010. This occurred due to relatively lower water content in the soil under stress conditions in SDI_p up until December, and then dilution due to increased soil water contents after December, although little drainage was evident until March. However, the salinity remained below the threshold for almond (EC_e 1.5 dS m^{-1}) throughout the growing season in all the treatments.

HYDRUS-2D-calculated values of actual monthly evaporation and transpiration were summed up to calculate the monthly crop coefficients of almond (Figure 6). The midseason K_c's of 1.23, 1.22, 1.31, and 1.11 for October, November, December, and January, respectively, were significantly higher than the FAO 56 value of 0.9, which is applied to a temperate climate and no-stress conditions. However, the values of K_c obtained in the present study matched well with those reported by Stevens et al. (2012) for a sprinkler-irrigated almond in this region. They reported that higher K_c values for midseason were due to the prevalence of non standard weather conditions and high advective conditions in the region.

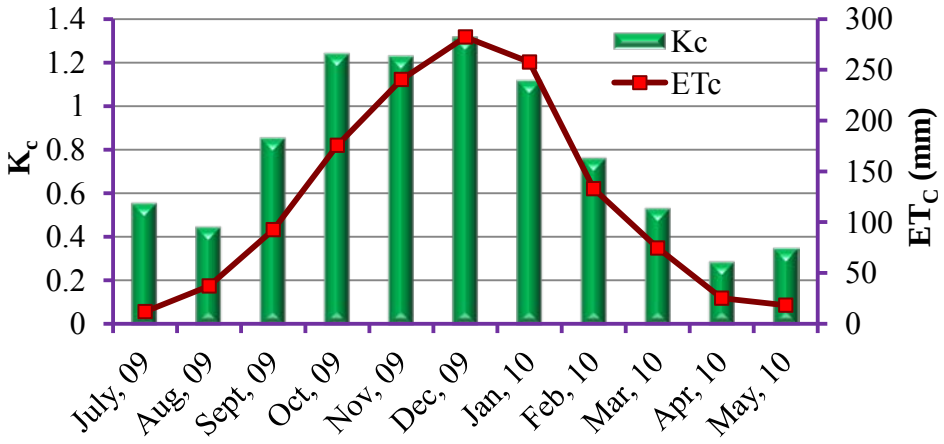

Figure 6. Estimated monthly crop coefficients (K_c) and crop evapotranspiration (ET_C) of almond.

Experimental and simulated values of water balance were utilized to calculate the water productivity of almonds under full and deficit irrigation (Figure 7). It can be seen that irrigation water productivity (WP_I) under stressed conditions (SDI_p) increased substantially (37%) as compared to full irrigation (FI_p). It is inferred that almonds are among the species capable of maintaining high gains in the water productivity under increasing soil water deficit (Girona et al., 2005). The estimated irrigation water productivity (WP_I) in this investigation was appreciably higher than that reported in several other studies, where it varied from 0.20-0.33 kg m^{-3} (Egea et al., 2010). The data indicates that, for regions with a severe water scarcity, SDI_p appears to be a promising deficit irrigation strategy for almond trees, as it increased WP_I by 37%, reduced yield only by 8%, and saved about 34.5% of irrigation water in comparison to full irrigation (FI_p).

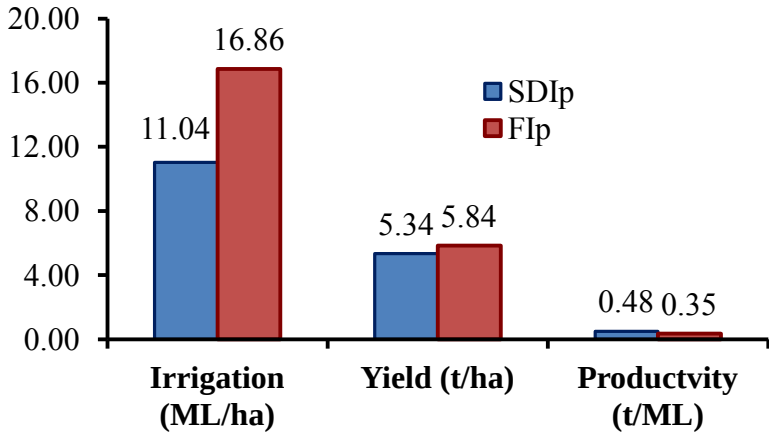

Figure 7. Almond water productivity under full irrigation (FIp) and stress conditions (SDI_p).

4. Conclusions

The study concludes that HYDRUS-2D simulated water fluxes and soil salinity dynamics under drip-irrigated almond very well. This work identifies significant drainage during the months of August and Feb-April, when the tree water demand was less than had previously been assumed. The model-produced values of evapotranspiration were utilized to evaluate the monthly crop coefficients and the crop water productivity. Recalculations of crop coefficients (K_c) as a result of this work have the potential to lead to significant water savings and water efficiency improvements. The study also revealed that SDI_p seems to be one of the most promising reduced irrigation application options available for improving irrigation efficiency.

Acknowledgements

The authors wish to thank Clark Taylor Farms for access to the orchard for field work and Jirka Šimůnek for modeling support. The financial support of the Almond Board of Australia is gratefully acknowledged.

References

Allen, R. G., L. S. Pereira, D. Raes, and M. Smith, Crop evapotranspiration guidelines for computing crop water requirements, *FAO Irrigation and Drainage Paper No. 56*, FAO, Rome, Italy, 1998.

Egea, G., P. A. Nortes, M. M. Gonzalez-Real, A. Baille, and R. Domingo, Agronomic response and water productivity of almond trees under contrasted deficit irrigation regimes, *Agricultural Water Management*, *97*, 171–181, 2010.

Gärdenäs, A. I., J. W. Hopmans, B. R. Hanson, and J. Šimůnek, Two-dimensional modeling of nitrate leaching for various fertigation scenarios under micro irrigation, *Agricultural Water Management*, *74*, 219–242, 2005.

Girona, J., M. Mata, and J. Marsal, Regulated deficit irrigation during the kernel-filling period and optimal irrigation rates in almond, *Agricultural Water Management*, *75*, 152–167, 2005.

Green, S., B. Clothier, and B. Jardine, Theory and practical application of heat pulse to measure sap flow, *Agronomy Journal*, *95*, 1371–1379, 2003.

Hanson, B. R., J. Šimůnek, and J. W. Hopmans, Evaluation of urea–ammonium–nitrate fertigation with drip irrigation using numerical modeling, *Agricultural Water Management*, *86*, 102–113, 2006.

Kandelous, M. M., T. Kamai, J. A. Vrugt, J. Šimůnek, B. Hanson, and J. W. Hopmans, Evaluation of subsurface drip irrigation design and management parameters for alfalfa, *Agricultural Water Management*, *109*, 81–93, 2012.

Phogat, V., M. Mahadevan, M. A. Skewes, and J. W. Cox, Modelling soil water and salt dynamics under pulsed and continuous surface drip irrigation of almond and implications of system design, *Irrigation Science*, *30*(4), 315-333, 2012a.

Phogat, V., M. A. Skewes, J. W. Cox, and M. Mahadevan, Modelling the impact of pulsing of drip irrigation on the water and salinity dynamics in soil in relation to water uptake by an almond tree, *WIT Transactions on Ecology and Environment*, *168*, 101-113, WIT Press, ISSN 1743-3541, doi:10.2495/SI120091, 2012b.

Phogat, V., M. A. Skewes, M. Mahadevan, J. W. Cox, Evaluation of soil plant system response to pulsed drip irrigation of an almond tree under sustained stress conditions, *Agricultural Water Management*, *118*, 1-11, 2013.

Ramos, T. B., J. Šimůnek, M. C. Goncalves, J. C. Martins, A. Prazeres, L. S. Pereira, Two-dimensional modeling of water and nitrogen fate from sweet sorghum irrigated with fresh and blended saline waters, *Agricultural Water Management*, *111*, 87-104, 2012.

Šejna, M., J. Šimůnek, and M. Th. van Genuchten, The HYDRUS software package for simulating two- and three-dimensional movement of water, heat, and multiple solutes in variably-saturated media, User Manual, Version 2, PC Progress, Prague, Czech Republic, pp. 280, 2011.

Šimůnek, J., M. Th. van Genuchten, and M. Šejna, The HYDRUS software package for simulating two- and three-dimensional movement of water, heat, and multiple solutes in variably-saturated media, Technical Manual, Version 2, PC Progress, Prague, Czech Republic, pp. 258, 2011.

Stevens, R. M., C. M. Ewenz, G. Grigson, S. M. Conner, Water use by an irrigated almond orchard, *Irrigation Science*, *30*(3), 189-200, 2012.

Subbaiah, R., A review of models for predicting soil water dynamics during trickle irrigation, *Irrigation Science*, *31*(3), 225-258, doi:10.1007/s00271-011-0309-x, 2013.

Vrugt, J. A., J. W. Hopmans, and J. Šimůnek, Calibration of a two-dimensional root water uptake model, *Soil Science Society of America Journal*, *65*, 1027-1037, 2001.

HYDRUS-1D Modeling Applications to Waste Disposal Problems in Brazil

Elizabeth M. Pontedeiro, Victoria Ottoni, and Martinus Th. van Genuchten

Departments of Nuclear, Civil and Mechanical Engineering, COPPE, Federal University of Rio de Janeiro, UFRJ, Rio de Janeiro, RJ, 21945-970, Brazil
bettinadulley@hotmail.com, viottoni@gmail.com, rvangenuchten@hotmail.com

Abstract

This paper summarizes three studies in which HYDRUS-1D was used to investigate the performance of different types of waste disposal sites in Brazil: a conventional mining installation containing naturally occurring radioactive materials (NORMs), a municipal landfill, and a radioactive waste repository. In the first application we used HYDRUS-1D to predict long-term (tens of thousands of years) radionuclide transport vertically through both the landfill and the underlying unsaturated zone, and then laterally in groundwater. The second study concerned water fluxes into and through a municipal solid waste (MSW) landfill in the city of Rio de Janeiro. We considered two cover systems that could minimize percolation through the landfill. One used a capillary barrier made from MSW compost, and the other one a vegetation cover using either grass or native vegetation. The third application involved a near-surface repository containing ^{137}Cs wastes resulting from decontamination of Goiania city in Brazil after the 1987 accident with a CsCl teletherapy source. Long-term simulations were carried out of ^{137}Cs transport from the repository through the concrete liner below the waste and the underlying vadose into groundwater. The examples show the flexibility of HYDRUS-1D to address different types of problems.

1. Introduction

Numerical models such as the HYDRUS codes (Šimůnek et al., 2008a) are increasingly used for predicting or analyzing water flow and contaminant transport processes in the subsurface, including the vadose zone. In this paper we summarize three recent applications of HYDRUS-1D to waste disposal problems in Brazil. One application involves the disposal of NORM mining wastes (i.e., wastes containing naturally occurring radioactive materials) in an industrial landfill. HYDRUS-1D (Šimůnek et al., 2008b) was used to predict long-term radionuclide transport vertically through both the landfill and the underlying unsaturated zone, and then laterally in groundwater. Calculations were carried out for both a best-case scenario assuming equilibrium transport in a fine-textured subsurface, and a worst-case scenario involving preferential flow.

The second study concerned water fluxes into and through a municipal solid waste (MSW) landfill in the city of Rio de Janeiro. Two different cover systems were considered that would minimize infiltration of rain water into the landfill. One used a capillary barrier made from MSW compost, and the other one a vegetation (evapotranspiration) cover using either grass or native vegetation from the area.

The third application considered a near-surface repository containing ^{137}Cs wastes resulting from decontamination of Goiania city in Brazil after the 1987 accident with a CsCl teletherapy source.

The study provided estimates of water fluxes through the soil cover into and through the repository and concrete liners of the repository towards underlying groundwater. Performance of the cover system and engineered barriers was followed for 400-years, which included accounting for the effects of concrete degradation. Simulations were further carried out of ^{137}Cs transport from the repository through the concrete liner below the waste and the underlying vadose towards groundwater below the site.

2. NORM Waste Disposal Site

The first application concerned the subsurface transport of radionuclide decay chains (notably the ^{238}U and ^{232}Th series) leached from a conventional mining installation in Amazonia processing ore containing natural occurring radioactive materials (NORMs). The disposal site contained slags having radionuclide concentrations many times higher as compared to the original ore. Dimensions of the disposal unit were 70 m wide by 100 m long and 6.0 m deep. Initial radionuclide concentrations were 71 Bq/g for ^{238}U and ^{234}U, 67 Bq/g for ^{230}Th, 63 Bq/g for ^{226}Ra and 4.8 Bq/g for ^{210}Pb. The slag waste layer had a measured bulk density (ρ_b) of 1.89 g/cm^3. Hydraulic properties of the waste were estimated from drainage experiments on large lysimeters containing slags from the site. Batch measurements produced radionuclide distribution coefficients (K_d) very close to those of a clay soil (ISAM, 1998), except for Ra, whose K_d value was closer to that of sand. For these reasons we used K_d values typical of clay for U, Th, and Pb (1.6, 5.8, and 0.54 m^3/kg, respectively), and the measured value (0.88 m^3/kg) for Ra. An impermeable liner under the waste layer (a requirement of the Brazilian regulatory agency) was not considered in our analysis.

The unsaturated zone below the waste layer consisted of reddish Belterra clay as described by Dennen and Norton (1977) and Truckenbrodt and Kotschoubey (1981). Soil texture, bulk density (1.3 g/cm^3) and the saturated hydraulic conductivity (K_s = 21 m/y) were locally measured. Other parameters of Belterra clay were taken from Belk et al. (2007), except for the soil hydraulic parameter α (we used a value of 4.5 m^{-1}). The saturated zone contained red saprolite interspersed with lighter-colored lenses derived from feldspars. The phreatic aquifer had an average thickness of 4.5 m, with a natural hydraulic gradient of 0.0562. Geotechnical essays produced K_s values between 4.2 x10^{-5} and 7.9x10^{-4} cm/s. For our calculations we used a value of 1.7 x 10^{-4} cm/s.

Average annual precipitation measured in the area was 2,430 mm, and the average evapotranspiration rate (as calculated with the Penman-Monteith equation) was 1,610 mm. Adjusted for runoff, the long-term average recharge rate at the site was estimated to be 657 mm/y. This recharge rate was used as a surface flux boundary condition for the steady-state simulations of water flow through the site and into groundwater.

We used HYDRUS-1D to first predict radionuclide transport vertically through both the landfill and the underlying unsaturated zone, and then one-dimensional laterally in groundwater. Calculations were carried out for both a best-case scenario assuming equilibrium transport, and a worst-case scenario with preferential flow as modeled using the physical nonequilibrium (dual-porosity) formulation of van Genuchten and Wierenga (1976). The performance assessment was carried out using a leaching and off-site small farm scenario (Pontedeiro et al., 2010).

Radionuclides transported in groundwater were assumed to be intercepted by a well 100 m down gradient of the landfill. For the safety analysis we used concentrations of the aquifer at the well.

Figure 1 shows the effect of preferential flow separately through the waste later, the vadose zone and the aquifer. For preferential flow we assumed a value of 0.5 for the fraction immobile water, and different values of the mass transfer coefficient (denoted here by the parameter β in year^{-1}). Results indicate that the highest U concentrations in the leachate leaving the waste were obtained for equilibrium transport. This shows that preferential flow (smaller value of β) of rain water through the waste leads to less pollution of the subsurface. This situation is reversed when preferential flow occurs in the unsaturated zone below the waste, or in the phreatic aquifer. Preferential flow then leads to more rapid transport and higher concentrations.

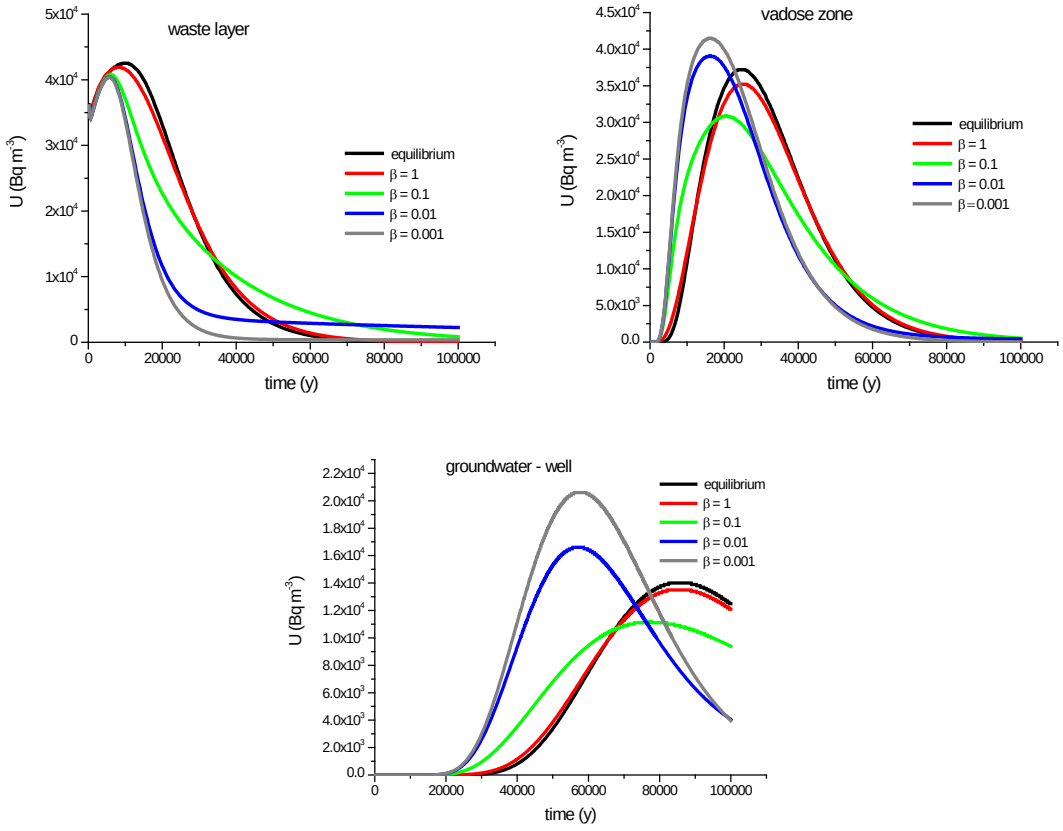

Figure 1. Calculated uranium concentrations versus time in the waste layer (upper right), the bottom of the vadose zone (upper right) and the downgradient well (bottom). Results are for different values of the mass transfer coefficient β (year^{-1}).

Figure 2 shows results of the safety assessment for both equilibrium transport and the situation where preferential flow would occur in all three regions simultaneously (waste, vadose zone, groundwater). A safety assessment is often used to provide evidence that human health and the environment are protected as much as possible in the future. The scenario used here assumes that the downgradient well was the only available source of water for direct consumption by residents, and for irrigation and animal use. We refer to Pontedeiro et al. (2010) for details. The results in Figure 2 show that preferential flow causes the risks to shift to much earlier times, but

that the maximum or annual risk is not much affected by preferential flow. Most of the risk in Figure 2 was caused by uranium followed by thorium.

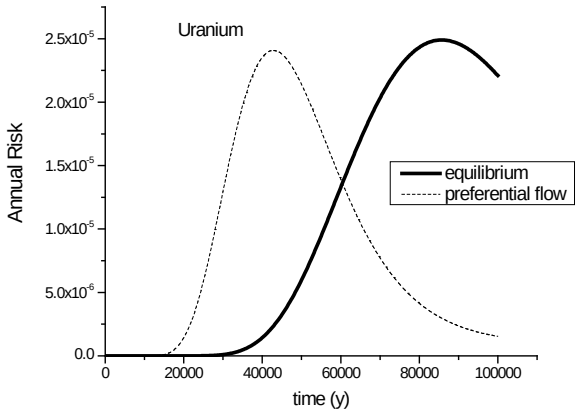

Figure 2. Calculated annual risk assuming equilibrium transport and preferential flow.

3. Municipal Solid Waste Landfill

The second case study concerned water flow into and through a municipal solid waste (MSW) landfill in the Nova Iguaçu suburb of Rio de Janeiro (Fig. 3). The landfill occupies an area of 1.2 million m^2 and contains mostly non-hazardous wastes (classified as Class IIA and IIB according to Brazilian standards). The location includes, among other things, a central treatment plant for the collected leachate and a biogas collection facility to generate electricity. Two studies were carried out to investigate the performance of a final cover that would minimize infiltration into the waste. One was a capillary barrier made from MSW compost, while a second scenario considered a vegetative cover using grasses or native species.

Figure 3. Aerial view of the Nova Iguaçu landfill showing four sub-landfills.

Table 1. Physical and soil hydraulic parameters of the waste.

ρ_b (g/cm^3)	K_s (cm/day)	θ_s cm^3/cm^3)	θ_r (cm^3/cm^3)	α (cm^{-1})	n (-)	l (-)
0.632	233	0.53	0.25	0.20	1.98	0.50

Local data were used as much as possible. The average saturated hydraulic conductivity (K_s) of the cover soil was measured to be 2.3 cm/day. Hydraulic parameters were estimated from measured soil texture data of the fines (on average 32% clay, 19% silt, and 49% sand) using the Rosetta pedotransfer functions in HYDRUS-1D, and adjusted for gravel (4%). Hydraulic parameters for the waste were taken from Breitmeyer (2011) and are listed in Table 1.

For all simulations we considered the intermediate (during operation) and final cover layers to have a thickness of 60 cm, and the waste layer to be 500 cm thick. In order to calibrate the model, we initially modeled each vertical landfill cell separately. For this we considered the influence of rainfall and evaporation on each cell independently, with the premise that the amount of liquid generated by each cell was fully captured by the drainage network of the landfill, and that the overall recharge rate was simply the sum of the deep drainage rates of all cells combined. It was estimated to be 0.257 m/y (0.0703 cm/day) using local weather data and potential evapotranspiration rates calculated with the equation of Hargreaves (1975). The simulations were performed for profiles varying from 1 to 10 meters, after which the individual cells were superimposed to cover the entire landfill. The total amount of leachate simulated for Sub-Landfill1 during 2010 was found to be 27,020 m^3, which compared well with the measured drainage volume of 33,100 m^3.

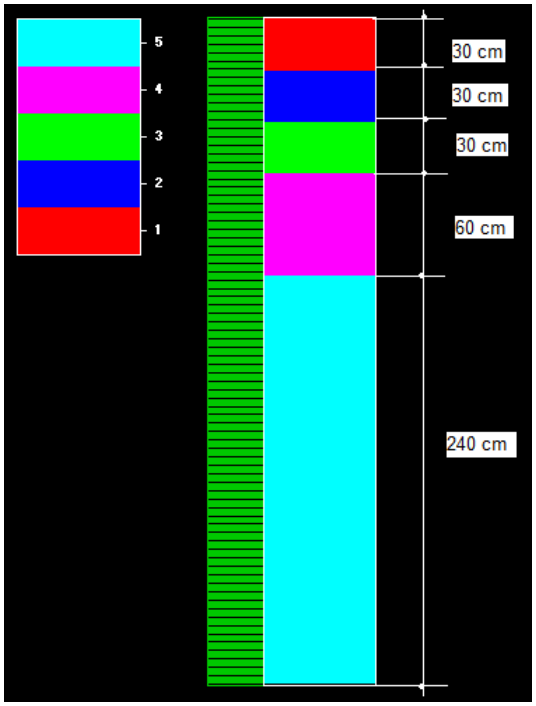

Figure 4. Composition of the capillary barrier system and underlying waste.

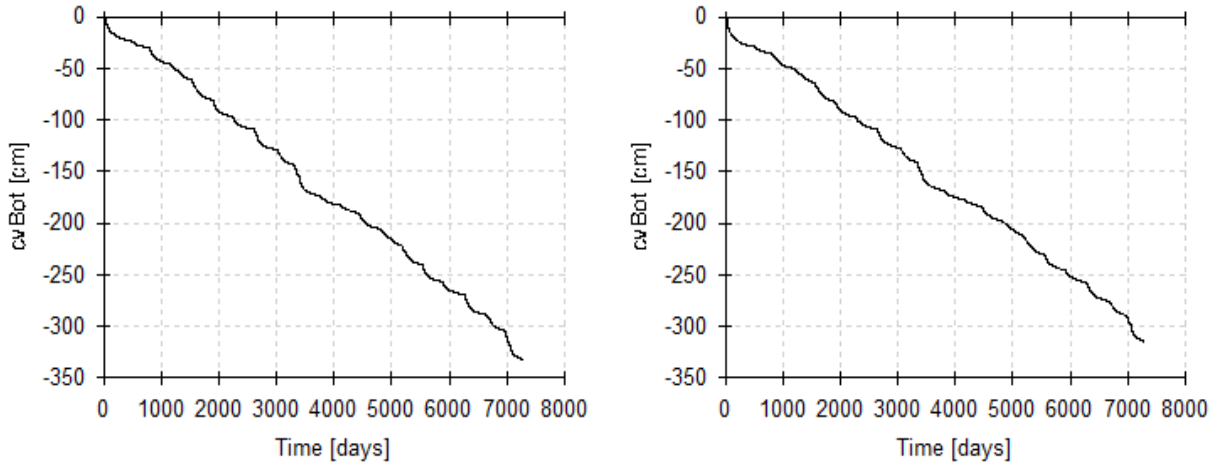

Figure 5. Cumulative drainage fluxes at a depth of 3 m assuming the capillary barrier to have a thickness of 30 cm (left) and 50 cm (right).

Another option we analyzed was the use of vegetation on the cover: either grass with roots uniformly distributed in the top 20 cm, or native vegetation (*brachiaria humidicola)* with roots having a distribution as reported by Costa (2002). The recharge rate with grass was estimated to be 0.0467 cm/day, as compared to 0.0367 cm/day for the native vegetation.

Figure 6 summarizes the drainage calculations. The use of a capillary barrier or vegetation on top of the landfill resulted in a water flux reduction of about 38% for a capillary barrier layer of 30 cm, 42% for a capillary barrier of 50 cm, 34% for grass and 48% for *brachiaria*. Our results confirm literature findings that vegetative covers (also referred to often as evapotranspiration covers) can significantly reduce water flow rates through a landfill by promoting root water uptake and hence evapotranspiration (e.g., EPA, 2003; McGuire et al., 2009), not only in arid and semi-arid regions but also in more humid areas. Additional details of this study are given by Ottoni (2010).

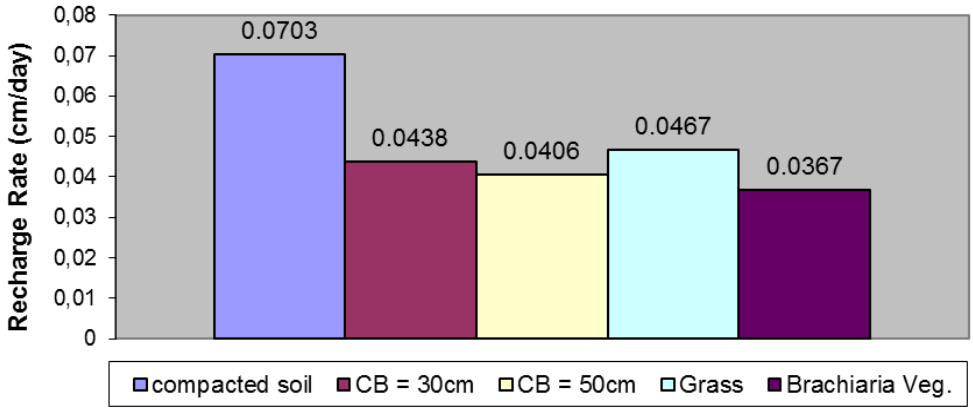

Figure 6. Comparison of calculated drainage rates from a landfill containing a compacted surface soil, capillary barriers (CBs) of 30 and 50 cm, and vegetative covers using grass and vegetation native to Rio de Janeiro, Brazil

4. The Goiania Repository

In September 1987 a major accident occurred with a ^{137}Cs teletherapy source in Goiania, Brazil (Paschoa et al., 1993; Heilbron et al., 2002). The accident caused widespread contamination of radioactive material (1375 Ci of ^{137}Cs) in the town of Goiania. Subsequent cleanup generated about 3,500 m^3 of solid radioactive wastes (about 6,000 tons of material). The wastes were disposed in a near-surface repository built in concrete. The purpose of this study was to perform a safety assessment of the low level radioactive waste deposit containing 137Cs over a time period of about 400 years.

The study was designed to provide estimates of water infiltrating through the soil cover above the repository into and through the repository and its concrete liners towards underlying groundwater. This was done by applying first a detailed water balance to the soil cover accounting for local precipitation and evapotranspiration rates, including root water uptake by grass on the cover. All calculations were carried out using HYDRUS-1D. Estimates were obtained of the infiltration of water from the cover through the concrete surface of the repository into and through the radioactive waste and underlying concrete liner. These flow rates were used next to simulate long-term ^{137}Cs transport from the repository through the bottom concrete liner into the underlying vadose zone until reaching the groundwater aquifer below the repository. Radionuclide transport calculations accounted for the effects of ^{137}Cs sorption and radioactive decay. Simulations provided estimates of possible future radionuclide fluxes into groundwater, thus permitting an evaluation of potential consequences to the environment and possible exposure to the public.

The subsurface repository was built in concrete, having dimensions of 19.6 m length, 60 m width and 6.20 m high, and with 20 cm thick concrete walls. A 50-cm thick uniform soil cover was placed on top of the repository and vegetated with grass. The waste inside the repository consisted mostly of compacted soil contaminated with ^{137}Cs (4.38 m). Figure 7 gives an above-ground view of the repository. A schematic cross-section of the facility and underlying vadose zone is shown in Figure 8. The repository is located at 16° 45′ 32″ S, 49° 26′ 16″ W, about 770 m above sea level.

Figure 7. View of the Goiania repository.

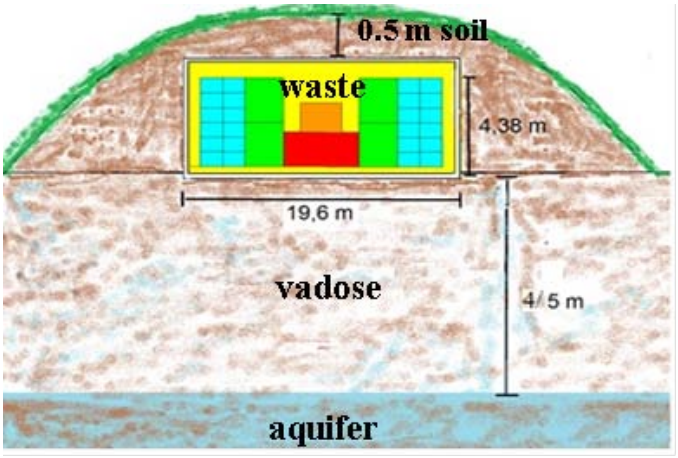

Figure 8. Schematic of the Goiania repository and underlying vadose zone.

CNEN, the Brazilian Nuclear Regulatory Agency, defined a maximum annual dose for the public of 0.25 mSv/y for a low-level radioactive waste repository. Two safety assessments were performed in the past (Heilbron et al., 2002). The present study was carried out 10 years later as part of the enforcement of national regulations. Modeling of the repository was done in two steps. First the behavior of the cover was studied assuming some degradation of the concrete liners with time (400 years). Fluxes through the upper liner into the repository obtained in this manner were used next to estimate ^{137}Cs transport rates from the waste vertically down towards the water table.

For the soil cover we used soil hydraulic parameters from a typical Cerrado soil (Batalha, 2010) containing 53% of sand, 10% of silt and 37% clay. The initial hydraulic properties for the concrete were taken from Schneider (2012). The soil cover above the upper concrete wall was modeled as a 50 cm layer covered by grass (30 cm rooting depth). Potential evapotranspiration rates (Fig. 9) needed for the simulations were obtained with the equation of Hargreaves (1975) using 10 years of temperature and precipitation data from a local weather station. These data were repeated 40 times to cover the 400 year total simulation period. For the root water uptake calculations we used the model of Feddes et al. (1978).

The saturated hydraulic conductivity (K_s) of the upper and lower concrete walls (liners) were assumed to decrease slowly due to natural degradation. We approximated this degradation process with a discrete function, using K_s=0.00315 m/year for the first 100 years, 0.0315 m/year for the next 100 years, and 0.315 m/year between 200 and 400 year. The porosity was simultaneously doubled after 100 and 400 years, while keeping the same values for the other hydraulic parameters of the concrete.

The contaminated waste layer in the repository was taken to be 4.38 m thick, situated over a 20-cm thick concrete liner and a 4 to 5 m thick vadose zone (Fig. 8) depending on fluctuations of the water table. Hydraulic properties of the waste layer were measured (Pereira, 1996), including the bulk density (1.7 g/cm^3) and for the calculations it was measured a value of 463 cm^3/g for the K_d in that layer. The relatively bulk density of the waste reflected compaction of the ^{137}Cs

contaminated soils. The concrete liner below the waste was assumed to have the same unsaturated hydraulic properties as the degraded upper concrete cover. A partitioning coefficient (K_d) of 10 cm^3/g was used for the concrete (Aguiar, 2006). Hydraulic properties and K_d of the vadose zone were measured (Pereira, 1996), with a bulk density of 1.3 g/cm^3 and mean value of 430 cm^3/g for the K_d.

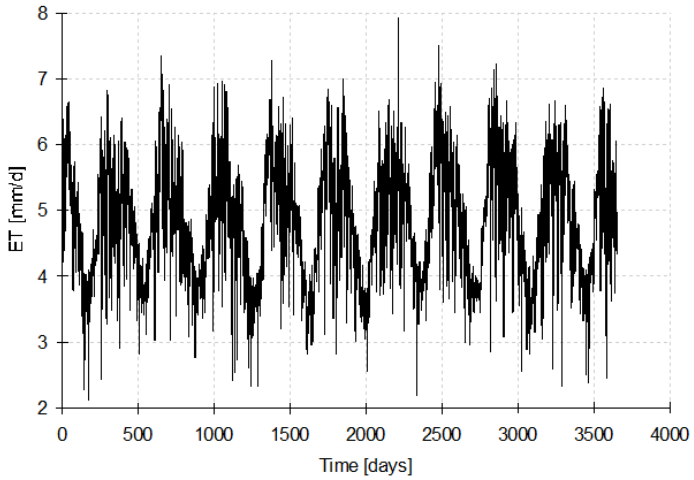

Figure 9. Calculated potential evapotranspiration rates.

Simulations for the infiltration of water from the cover through the upper concrete liner into the repository gave the following results: 0.00280 m/year for the initial period (0 to 100 years), 0.0290 m/year from 100 to 200 years, and 0.238 m/year for the period from 200 to 400 years. These infiltration rates were subsequently used for the ^{137}Cs transport equations. Figure 10 shows calculated ^{137}Cs concentrations of fluid leaving the waste layer and moving into the lower concrete liner. The three local concentration maxima in the curve are a consequence of the three conductivities used to approximate the concrete degradation process, leading to three flow rates and causing a different maximum during each for the three stages of concrete degradation. ^{137}Cs concentrations eventually approach zero because of radioactive decay.

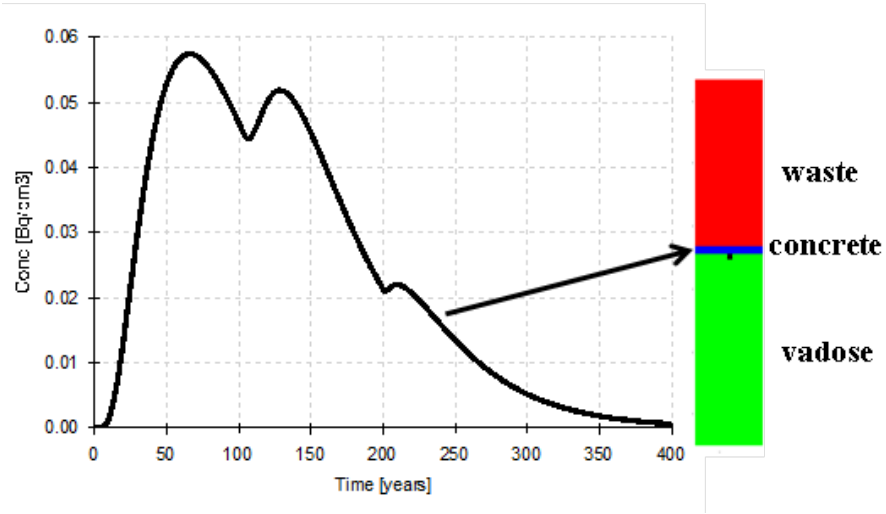

Figure 10. Calculated ^{137}Cs concentrations at the bottom of the waste layer.

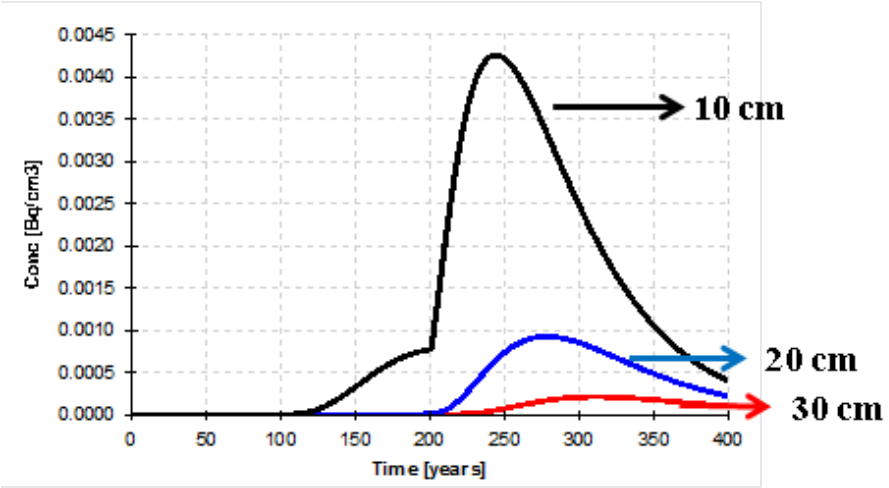

Figure 11. Calculated ^{137}Cs concentration at three locations in the vadose zone below the lower concrete liner.

5. Conclusions

In this paper we summarized three studies in which the HYDRUS-1D software package was used to investigate the performance of different types of waste disposal sites in Brazil: a conventional mining installation containing naturally occurring radioactive materials (NORMs), a municipal solid waste landfill, and a low-level radioactive waste repository. The three examples show the flexibility of HYDRUS-1D in being able to address different types of problems at involving different time and spatial scales. All calculations were based on the standard equilibrium formulation for variably-saturated flow (the Richards equation). Solute transport in the first example considered both equilibrium transport and some preferential flow as modeled with a dual-porosity type physical nonequilibrium transport formulation. The HYDRUS-1D code was found to be very appropriate and extremely easy to use for the required calculations.

References

Aguiar, L. A., Avaliação de Risco de um Repositório Próximo à Superfície na Fase Pós; Fechamento em Cenários de Liberação de Radionuclídeos por Infiltração de Água, DSc Thesis, Department of Nuclear Engineering, COPPE, Federal University of Rio de Janeiro, UFRJ, Rio de Janeiro, Brazil, 2006.

Batalhá, M. S., C. R. Bezerra, E. M. Pontedeiro, and M. Th. van Genuchten, Environmental fate of natural radioactive contaminants in fertilizers and phosphogypsum, *Proc. ENCIT 2010*, 13th Brazilian Congress of Thermal Sciences and Engineering, Dec. 5-10, 2010, Uberlandia, MG, Brazilian Soc. Mech. Sci. & Eng., ABCM, Brazil, 2010.

Belk, E. L., D. Markewitz, T. C. Rasmussen, E. J. M. Carvalho, D. C. Nepstad, and E. A. Davidson, Modeling the effects of through fall reduction on soil water content in a Brazilian Oxisol under a moist tropical forest, *Water Resour. Res.*, *43*, W08432, doi:10.1029/2006WR005493, 2007.

Breitmeyer, R. J., Hydraulic Characterization of Municipal Solid Waste, Ph.D. Dissertation, University of Wisconsin, Madison, WI, 192 p, 2011.

Costa, F. da; R. O. Pereyra, S. Paciomik, and J. B. R. de Abreu, Distribuição vertical de características morfológicas do sistema radicular de Brachiaria humidicola, *Pasturas Tropicales*, *24*(3), 14-20, 2012.

Dennen, W. D. and H. A. Norton, Geology and geochemistry of bauxite deposits in the lower Amazon basin, *Econ. Geol*., *72*, 82-89, 1977.

Feddes, R. A., P. J. Kowalik, and H. Zaradny, *Simulation of Field Water Use and Crop Yield*, John Wiley & Sons, New York, NY, 1978.

Felice, L. B., Aplicação do Código Computacional HYDRUS-1D na Avaliação de Segurança de Depósito de Rejeitos Radioativos; Estudo de Caso: Repositório de Rejeitos Radioativos de Abadia de Goiás, MSc Thesis, Department of Nuclear Engineering, Institute of Military Engineering, IME, Rio de Janeiro, Brazil, 2013.

Hargreaves, G. H., Moisture availability and crop production, *Trans. Am. Soc. Agric. Eng*., *18*(5), 980-984, 1975.

Heilbron, P. F., E. M. Pontedeiro, R. M. Cotta, J. P. Guerrero, and N. Ruperti, Reassessment of the safety of the Goiania repositories, Internal Report, CNEN, Rio de Janeiro, Brazil, 2002.

ISAM, Derivation of quantitative acceptance criteria for disposal of radioactive waste to near surface facilities: development and implementation of an approach, Safety Report, Version 3.0, IAEA, Vienna, Austria, 1999.

McGuire, P. E., B. J. Andraski, and R. Archibald, Case study of a full-scale evapotranspiration cover, *J. Environ. Eng*., *135*, 3, 316-332, doi:10.1061/(ASCE)1090-0241, 2009.

Pashoa, A. S., A. Tranjan Filho, and J. J. Rosenthal, Revisiting Goiânia: Toward a final repository for radioactive waste, Topical Report, *IAEA Bulletin, 1*, 28-31, 1993.

Roberts, L., Radiation accident grips Goiania, *Science*, 238, 1-28-1031, 1987.

Pereira, J. C. A, Determinação da Velocidade de Migração e das Razões de Partição de 137Cs em Solos da Região do Futuro Repositório de Rejeitos de Abadia de Goiás, Goiás. MS. Thesis, Pontifícia Universidade Católica do Rio de Janeiro, Departamento de Química, 1996.

Ottoni, V., Análise Numérica de Fluxo da Base de Aterros de Resíduos Solidos, MS Thesis, Department of Civil Engineering, COPPE, Federal University of Rio de Janeiro, UFRJ, Rio de Janeiro, Brazil, 2010.

Pontedeiro, E. M., M. Th. van Genuchten, R. M. Cotta and J. Šimůnek, The effects of preferential flow and soil texture on risk assessments of a NORM waste disposal site, *J. Hazard. Mater.*, *174*, 648-655, doi:10.1016/j.jhazmat.2009.09.100, 2010.

Schneider, S., D. Jacques, and D. Mallants, Determining hydraulic properties of concrete and mortar by inverse modeling, Mater. Res. Soc. Symp. Proc., *1475*, 367-372, Materials Research Society, DOI: 10.1557/opl.2012.601, 2012.

Šimůnek, J., M. Th. van Genuchten, and M. Šejna, Development and applications of the HYDRUS and STANMOD software packages and related codes, *Vadose Zone J.*, *7*, 587-600, 2008a.

Šimůnek, J., M. Šejna, H. Saito, M. Sakai, and M. Th. van Genuchten, The HYDRUS-1D Software Package for Simulating the Movement of Water, Heat, and Multiple Solutes in Variably Saturated Media, Version 4.0, *HYDRUS Software Series 3*, Department of Environmental Sciences, University of California, Riverside, California, USA, 315 pp., 2008b.

Truckenbrodt, W., and Kotschoubey, B., Cobertura terciária das bauxitas amazônicas, *Revista Braileira Geociências*. 11: 203-208, 1981.

van Genuchten, M. Th., and P. J. Wierenga, Mass transfer studies in sorbing porous media, I. Analytical Solutions, *Soil Sci. Soc. Am. J., 40*, 473-480, 1976.

Simulation of Groundwater Evapotranspiration with HYDRUS-1D in Desert Environments

Sergey Pozdniakov[1], Ping Wang[2], Sergey Grinevskiy[1], and Jingjie Yu[2]

[1]*Department of hydrogeology, Moscow State University, GSP-1, Leninskie Gory, Moscow, 119899, Russia*
sppozd@geol.msu.ru
[2]*Key Laboratory of Water Cycle & Related Land Surface Processes, Institute of Geographic Sciences and Natural Resources Research, Chinese Academy of Sciences, 11A, Datun Road, Chaoyang District, Beijing, 100101, P. R. China*
wangping@igsnrr.ac.cn

Abstract

It is well known that water tables fluctuate in many arid/semiarid areas both daily, seasonally, and annually in response to phreatophyte consumption of groundwater via evapotranspiration (Ridolfi et al., 2007). In this study the pattern of daily and seasonal groundwater fluctuations in a desert area of northwest China was analyzed. In addition, a one-dimensional saturated-unsaturated soil water flow model HYDRUS-1D (Šimůnek et al., 2008) was used to simulate daily and seasonal water table fluctuations induced by groundwater evapotranspiration (ET_G). Simulations were conducted for four different soil profiles (sand, loam, silt, and sandy clay) and two typical vegetation covers (*Populus* and *Tamarix*) with temporal variability of precipitation, potential evaporation, and transpiration input data, which was produced using special preprocessing code SurfBal 3.60. The results show that a strong linear relationship exists in all model settings between the ET_G values and the standard diversion of water table fluctuations. The proposed methodology is expected to provide a basis for assessment of groundwater evapotranspiration using diurnal water table fluctuations in arid and semi-arid areas.

1. Introduction

The lower Heihe River in northwestern China is characterized by a continental climate that is extremely hot in the summer and severely cold in the winter. According to observational data from 1960 to 2011 gathered at the local weather station, the mean annual air temperature was 8.95 °C, with a range from -35.3 °C (9 February, 1964) to +43.7 °C (28 July, 2010). The mean annual precipitation was only 34.5 mm, while the average annual potential evaporation (ET_0) was about 1413 mm, which was 40 times greater (Wang et al., 2013). The predominant natural plant species in this area is characterized by phreatophytes (e.g., *Populus euphratica* and *Tamarix ramosissiman*), which relies on groundwater for survival (Wang et al., 2011; Zhao et al., 2004). Groundwater evapotranspiration (ET_G) from the phreatophyte vegetation is an important part of the water balance in this area; however, the ET_G estimate still remains a challenge for the regional water resources assessment. Many studies have linked diurnal water table fluctuations to evapotranspiration resulting from groundwater use by phreatophytes, particularly in arid and semiarid areas (Bauer et al., 2004; Gribovszki et al., 2008; Loheide II, 2008; Soylu et al., 2012). In this paper, the daily and seasonal water table fluctuations in the riparian zone were analyzed by using monitoring of groundwater dynamics during the period of April, 2010 – March, 2012. Moreover, water table fluctuations induced by riparian

evapotranspiration were simulated with a one-dimensional, saturated-unsaturated soil water flow model.

2. Diurnal and Seasonal Water Table Fluctuations

The selected groundwater monitoring well, with a depth of 12 m, is located within a riparian zone of the lower Heihe River. The groundwater levels were recorded in 30-minute intervals by Schlumberger Mini-Diver pressure transducers with an uncertainty of ±5 mm (Fig. 1). Analysis of the groundwater levels showed that a diurnal fluctuation existed in the water table during the period from May to September; however, these diurnal fluctuations were smaller during winter. To test the hypothesis that groundwater evapotranspiration impacts diurnal water table fluctuations, the detrended analysis of water level time series was conducted using the BAYSEA procedure (Akaike, 1980). In this analysis, it is supposed that the fluctuation of the groundwater level depth Z_{gw} can be written as a superposition of a seasonal trend Z_y, a daily cycle z_d, and residual z_r fluctuations, i.e.:

$$Z_{gw} = Z_y + z_d + z_r \tag{1}$$

Then, the monthly standard deviation (Z_{sd}) of a detrended water level was analyzed. The increase of Z_{sd} in the summer and its decrease in the winter should indicate that the drawdown of the water table in the summer is related to groundwater evapotranspiration.

Figure 2 shows the amplitude of the diurnal water table fluctuation for typical summer (July) and winter (January) periods. There is a notable daily fluctuation in the water table during summer, with an amplitude of about 2 cm; however, such a diurnal fluctuation did not show in the winter. Analysis of the standard deviation of the water table (Z_{sd}) during the entire period showed that Z_{sd} is almost unchanged in winter (about 0.3 cm). It is noted that Z_{sd} increased significantly in May and obtained the maximum in June-July (Figure 2), indicating an increasing amplitude of diurnal fluctuations in the groundwater table during summer. Therefore, the analysis of daily fluctuations in the groundwater level indicates that the groundwater evapotranspiration during summer is the main cause of diurnal fluctuations in the water level and the cause of its seasonal decline.

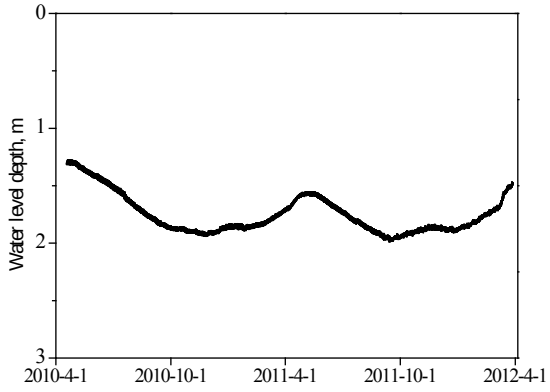

Figure 1. Water level depth in a riparian well for the period of 2010-2012.

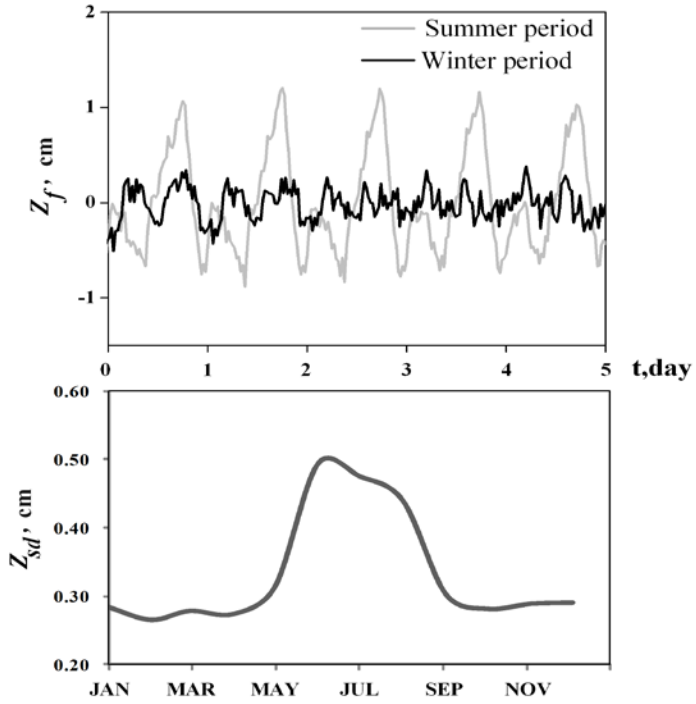

Figure 2. Diurnal fluctuations of the water table (Z_f, cm) and its monthly standard deviation (Z_{sd}, cm).

3. Simulation of Evapotranspiration

A one-dimensional, vertical saturated-unsaturated profile within the groundwater discharge zone due to evapotranspiration (Figure 3) was used to investigate the relationship between the mean groundwater depth, diurnal and seasonal water table fluctuations, and evapotranspiration. We consider a homogeneous soil with an active shallow root zone that extends from the soil surface to a depth Z_r (cm). A groundwater table occurs at a depth Z_g (cm) below the soil surface. The upper boundary of this profile is the soil surface and the lower boundary is located below the depth of seasonal groundwater level fluctuations within the zone of predominantly vertical flow. Let's suppose that the lower boundary of the profile is the boundary with a given flow rate $R(t)$. The root system is distributed along the profile and intakes water with a net rate $ET(t)$ that depends on the potential evapotranspiration and the root water uptake reduction according to the S-shape model (Šimůnek et al., 2008).

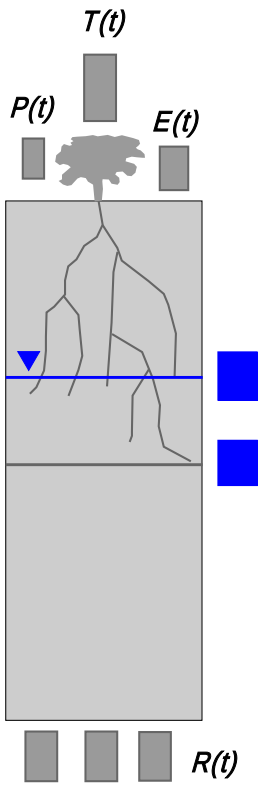

Figure 3. Sketch of the water table position and plant root distribution in the soil column.

Four typical soil profiles were selected for test: sand, loam, silt and sandy clay. The parameter values of the van Genuchten model used in the simulations are shown in Table 1.

Table 1. Mean textural and hydraulic properties of four typical sediment profiles (Loheide et al., 2005).

Sediment texture	θ_r	θ_s	α	n	K_s	S_y			
	-	-	1/cm	-	cm/day	$\theta_s - \theta_r$	Depth compensated	From Johnson (1967)	Readily available
Sand	0.045	0.43	0.145	2.68	710	0.385	0.38	0.34	0.32
Loam	0.078	0.43	0.036	1.56	25	0.352	0.19	0.095	0.075
Silt	0.034	0.46	0.016	1.37	6.0	0.426	0.11	0.06	0.026
Sandy clay	0.100	0.38	0.027	1.23	2.9	0.280	0.068	0.025	0.015

The species selected at this site were two drought-deciduous shrubs, *Populus* and *Tamarisk*, the dominant phreatophytes in the lower Heihe river basin. They all have dimorphic root systems that can reach a depth of 30 m and show the evidence of a hydraulic lift. Root distributions are fixed during the simulations and are used to weight the water uptake function. The root distribution of the *Populus* has the following normalized function (Zhu et al., 2009):

$$b(z_r)=\begin{cases}\dfrac{1}{3L_r}, & z_r \in (0;\quad 0.30L_r)\\ \dfrac{3}{L_r}, & z_r \in (0.30L_r;\quad 0.50L_r)\\ \dfrac{5}{8L_r}, & z_r \in (0.50L_r;\quad 0.90L_r)\\ \dfrac{1}{2L_r}, & z_r \in (0.90L_r;\quad 1.00L_r)\end{cases} \tag{2}$$

where z_r is the z coordinate of the soil surface, and L_r is the root depth.

Similarly, the following normalized function of the root distribution of the *Tamarisk* (Xu and Li, 2009) was used in the simulation:

$$b(z_r)=\begin{cases}0 & z \in (0;\ \ 0.12L_r)\\ \dfrac{13}{32L_r}(z-0.12L_r), & z \in (0.12L_r;\ \ 0.46L_r)\\ 0.13+\dfrac{32}{29L_r}(z-0.46L_r), & z \in (0.46L_r;\ \ 0.75L_r)\\ 0.45+\dfrac{50}{19L_r}(z-0.75L_r), & z \in (0.75L_r;\ \ 0.94L_r)\\ 0.95+\dfrac{5}{6L_r}(z-0.95L_r), & z \in (0.94L_r;\ \ 1.00L_r)\end{cases} \tag{3}$$

The groundwater table fluctuations were simulated using the HYDRUS-1D software package (Šimůnek et al., 2008), and the temporal variability of precipitation, potential evaporation, and transpiration input data were produced using the special preprocessing code SurfBal 3.60 (Grinevskii and Pozdnyakov, 2010) that creates an Atmosph.in input file for Hydrus-1D.

The first series of numerical experiments studied the relationship between the mean groundwater depth and groundwater evapotranspiration ET_G. Different constant head values were used on the lower boundary and the same atmospheric boundary conditions at the top in each simulation run. The meteorological variables that form the atmospheric boundary conditions were taken from observational data from 1960 to 2011. Thus, each simulation run covers 50-years total time with a daily resolution of atmospheric boundary conditions. The processing of simulation results by estimating average transpiration and plotting it versus the mean groundwater depth for a particular run shows the strong relationship between transpiration and the depth to groundwater level (Fig. 4). Taking into account that cumulative infiltration of precipitation for these conditions is too small in comparison with cumulative transpiration, the relationship shown in Figure 4 reflects the dependence of groundwater evapotranspiration on the mean groundwater depth. Figure 4 also shows the results of estimating groundwater *ET* by using data of a summer decline trend of the observed groundwater level in monitoring wells, using a precondition that the summer increase of the seasonal groundwater depth ΔZ_y is the result of evapotranspiration, i.e.:

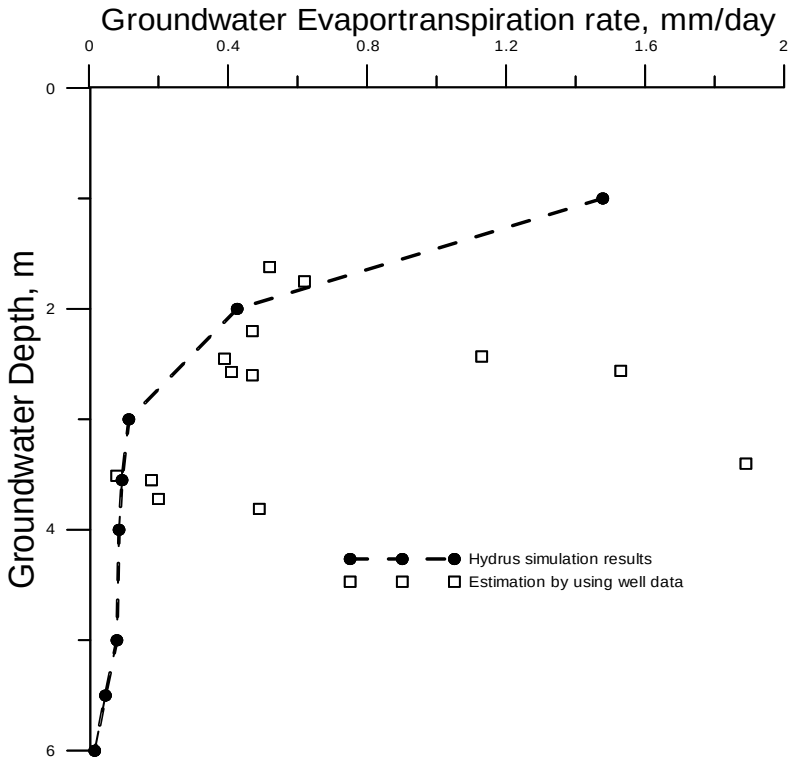

Figure 4. Simulated and estimated groundwater evapotranspiration rate.

$$ET_G = S_y \frac{\Delta Z_y}{\Delta t} \tag{4}$$

where Δt is the length of summer period.

One can see from this figure that simulations, as well as observations, show the decrease in the groundwater evapotranspiration with the increase of the mean groundwater depth.

In the second series of simulations we considered the relationship between daily groundwater level fluctuations and the evapotranspiration rate. The constant low boundary head that reflects the groundwater table depth of 200 cm below the soil surface and four different plant root depths (150 cm, 200 cm, 210 cm, and 250 cm) were used in this series of simulations. The simulation time for each run was three years with diurnal fluctuations of potential evapotranspiration. The diurnal fluctuation of potential evapotranspiration was simulated using the Fayer's model adopted in Hydrus-1D. To recognize small daily fluctuations of groundwater, the 5-m deep soil profile was discretized using a fine finite element mesh with 500 nodes. The simulation results were processed using the BAYSEA procedure to estimate the statistics of simulated diurnal groundwater level fluctuations.

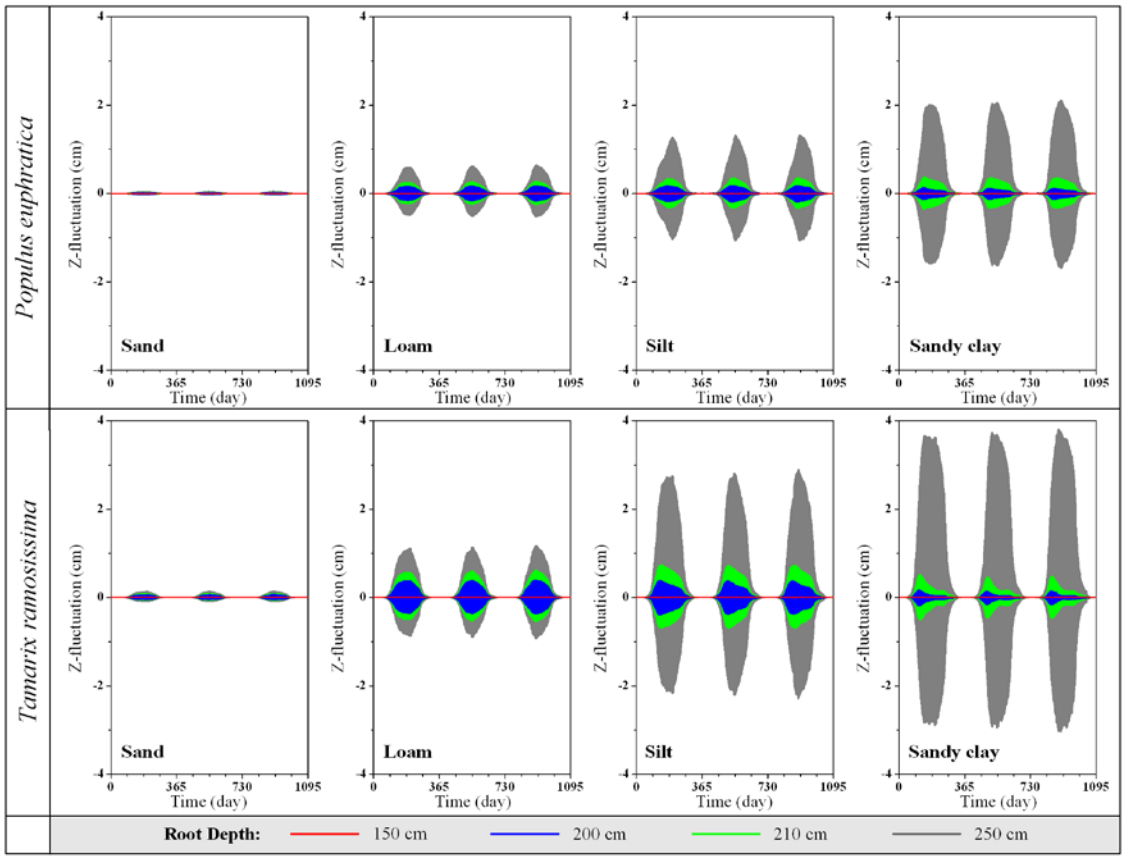

Figure 5. Water table fluctuations after the BAYSEA detrended analysis.

Figure 5 illustrates the diurnal fluctuation in groundwater levels in a 30-min simulation for different soil types and vegetation covers. Clearly, groundwater levels in all scenarios showed seasonal fluctuations. Strong diurnal fluctuations in the groundwater level could be found during summer, while such diurnal fluctuations were not observed during winter. In addition, for low hydraulic conductivity aquifers (silt and sandy clay), root water uptake induces a considerable water table depression. However, for coarse aquifers (sand and loam) the water table depression is lower because the decreasing storage can be readily recovered due to high hydraulic conductivities. To compare with the *Tamarix*, the root water uptake of *Populus* caused a smaller water table decline because of the difference in root distribution.

Figure 6 shows that a strong linear relationship exists in all model settings between the ET_G values and the standard deviation of water table fluctuations. This indicates that it is possible to estimate monthly groundwater evapotranspiration based on the analysis of the standard deviation of diurnal water table fluctuations.

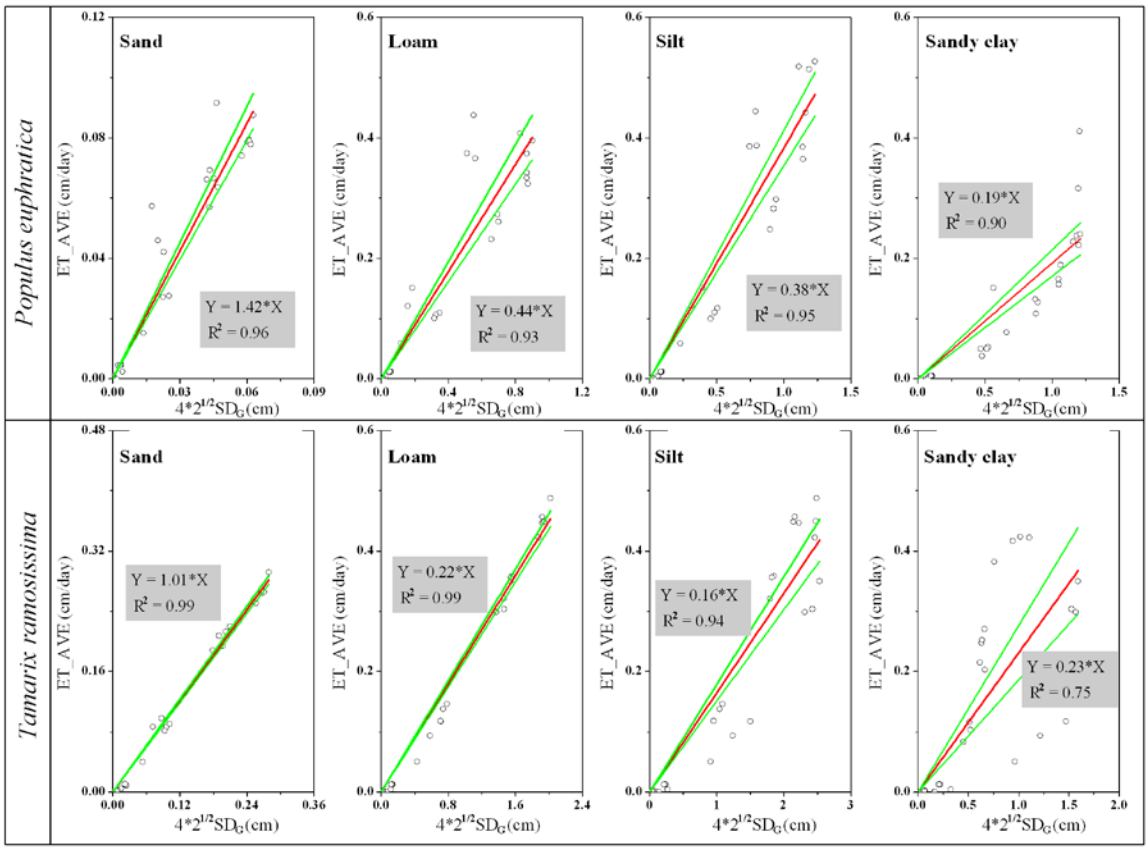

Figure 6. The relationship between daily average evapotranspiration (*ET_AVE*, cm/day) and the standard deviation of water table fluctuations (SD_G, cm).

4. Conclusion and Future Work

This study is an ongoing process report on developing the theoretical and numerical framework for estimating groundwater evapotranspiration using data about the mean groundwater depth, a seasonal groundwater trend, and diurnal water table fluctuations in the desert environments. The dynamic behavior patterns of the groundwater level at most wells are characterized by a declining trend during the period from spring to autumn and a slightly rising trend in the winter months, which relates to ET_G. Estimating ET_G by using seasonal trend and Hydrus simulations showed a strong dependence of ET_G on mean groundwater depths. The proposed method of estimating ET_G by using diurnal groundwater fluctuation statistics can be used for wells located in environments with the deep root zone, while the problem of how to take into account the dynamic of specific yield still remains. The potential for future work is to analyze the influence of the atmospheric evaporative demand, the soil hydraulic properties, and the vegetation parameters (e.g., leaf area index, root density distribution) on quantifying the relationship between groundwater evapotranspiration and water level fluctuations.

Acknowledgements
This work is supported by the Visiting Professorship for Senior International Scientists, Chinese Academy of Sciences (№ 2012T1Z0037), the NSFC-RFBR Program 2013 – 2014 (№13-05-91161), the National Natural Science Foundation of China (№ 91025023 and 41271049), the National Basic Research Program of China (973 Program) (№ 2009CB421305) and the Russian Federation Basic Research Foundation grant (№13-05-91161-ГФЕН_а)

References

Akaike, H., Seasonal adjustment by Bayesian modeling, *Journal of Time Series Analysis*, *1*, 1-13, 1980.

Bauer, P., G. Thabeng, F. Stauffer, W. Kinzelbach, Estimation of the evapotranspiration rate from diurnal groundwater level fluctuations in the Okavango Delta, Botswana, *Journal of Hydrology*, *288*, 344-355, 2004.

Gribovszki, Z., P. Kalicz, J. Szilágyi, and M. Kucsara, Riparian zone evapotranspiration estimation from diurnal groundwater level fluctuations, *Journal of Hydrology*, *349*(1-2), 6-17, doi:10.1016/j.jhydrol.2007.10.049, 2008.

Grinevskii, S. O. and S. P. Pozdnyakov, Principles of regional estimation of infiltration groundwater recharge based on geohydrological models, *Water Resources*, *37*(5), 638–652, 2010.

Loheide II, S. P, A method for estimating subdaily evapotranspiration of shallow groundwater using diurnal water table fluctuations, *Ecohydrology*, *1*(1), 59-66, doi:10.1002/eco.7, 2008.

Loheide, S. P., II, J. J. Butler, Jr., and S. M. Gorelick, Estimation of groundwater consumption by phreatophytes using diurnal water table fluctuations: A saturated-unsaturated flow assessment, *Water Resour. Res.*, *41*(7), W07030, doi:10.1029/2005wr003942, 2005.

Ridolfi, L., P. D'Odorico, and F. Laio, Vegetation dynamics induced by phreatophyte–aquifer interactions, *Journal of Theoretical Biology*, *248*(2), 301-310, doi:10.1016/j.jtbi.2007.04.025, 2007.

Šimůnek, J., M. Th. van Genuchten, and M. Šejna, Development and applications of the HYDRUS and STANMOD software packages, and related codes, *Vadose Zone Journal*, *7*(2), 587-600, doi:10.2136/vzj2008.0012, 2008.

Soylu, M. E., J. D. Lenters, E. Istanbulluoglu, and S. P. Loheide II, On evapotranspiration and shallow groundwater fluctuations: A Fourier-based improvement to the White method, *Water Resour. Res.*, *48*(6), W06506, doi:10.1029/2011wr010964, 2012.

Wang, P., J. Yu, S. P. Pozdniakov, S. O. Grinevsky, and C. Liu, Shallow groundwater dynamics and its driving forces in extremely arid areas: a case study of the lower Heihe River in northwestern China, *Hydrological Processes*, n/a-n/a, doi:10.1002/hyp.9682, 2013.

Wang, P., Y. Zhang, J. Yu, G. Fu, and F. Ao, Vegetation dynamics induced by groundwater fluctuations in the lower Heihe River Basin, northwestern China, *Journal of Plant Ecology*, *4*(1-2), 77-90, doi:10.1093/jpe/rtr002, 2011.

White, W. N., Method of estimating groundwater supplies based on discharge by plants and evaporation from soil – results of investigation in Escalante Valley, Utah, *Rep.*, 105 pp, Washington D.C, 1932.

Xu, G. Q., and Y. Li, Roots distribution of three desert shrubs and their response to precipitation under co-occurring conditions, *Acta Ecol Sin*, *29*(1), 130-137, 2009.

Zhu, Y., L. Ren, T. H. Skaggs, H. Lü, Z. Yu, Y. Wu, and X. Fang, Simulation of Populus euphratica root uptake of groundwater in an arid woodland of the Ejina Basin, China, *Hydrological Processes*, *23*(17), 2460-2469, doi:10.1002/hyp.7353, 2009.

Accounting for Solution Composition in a Plant Roots Active Nutrient Uptake Model

Iael Raij[1], Naftali Lazarovitch[1], Alan Ben-Gal[2], Uri Yermiyahu[2], and Diederik Jacques[3]

[1]*The Jacob Blaustein Institutes for Desert Research, Ben-Gurion University of the Negev, Sede Boqer Campus, Ben-Gurion, Israel*
[2]*Soil, Water and Environmental Sciences, Agricultural Research Organization, Israel*
[3]*Belgian Nuclear Research Centre, Belgium*

Abstract

The objective of this study was to include the nutrient uptake deficiency stress in the generic multicomponent transport model, HP1 (the geochemical code PHREEQC coupled to the transient water and solute transport model HYDRUS-1D). The first step was the incorporation of a combined passive-active root nutrient uptake model in HP1 (Jacques et al., 2006). The nutrient uptake model is based on the model of Silberbush et al. (2005). For example, Ca is taken up by passive and active processes, in which the parameters of the Michaelis-Menten active uptake model depend on the solution chemistry. Simulations were compared with experimental data from four irrigation treatments with different Na(-Cl) concentrations. The results are a preliminary attempt to predict uptake of different ions under varying conditions of salinity. Results for Na and K are promising.

1. Introduction

Plant nutrient uptake is controlled by both the plant and soil system (Feddes and Raats, 2004). Under saline conditions, plants are stressed through different processes, including reduced osmotic potential of the soil solution, specific ion toxicity, and ion competition (Taiz and Zeiger, 2002). Models can take into account the effects of general salinity characterized by electrical conductivity (*EC*) by decreasing water uptake as a result of a lower osmotic potential. In addition, models that calculate specific active uptake of solutes can decrease the uptake as a function of the concentration of specific toxic ions (Hopmans and Bristow, 2002). Generally, models that focus on water movement and solute transport in the soil will use the first approach, and plant based models will use the second approach. However, real field conditions are complex and their modeling demands integration of principles of soil and plant science (Hopmans and Bristow, 2002).

In this framework of coupling various soil and plant factors, Šimůnek and Hopmans (2009) presented an improvement to the classic macroscopic scale approach. In the classic approach (e.g., HYDRUS can serve as an example of the model for water movement and solute transport in unsaturated conditions), nutrient uptake is represented by a passive sink term based on root water uptake. The improved model includes active as well as passive nutrient uptake and uptake reduction due to salinity, in an attempt to connect soil modeling with root uptake modeling. A main limitation of this model is that uptake of a solute is independent of concentrations, activities, or speciation of the other solutes in the soil solution (Šimůnek and Hopmans, 2009).

Silberbush et al. (2005) proposed a root nutrient uptake model in which active uptake is specific for each solute according to Michaelis-Menten kinetics and takes into account salinity conditions (as a function of Na^+ and Cl^- concentrations) as well as passive nutrient uptake with water. This model is applied to a soilless culture of known hydraulic properties and follows a Darcy type flow.

The objective of the current study was to describe a model that combines the generic multi-component solute transport model, HP1 (geochemical code PHREEQC coupled to the transient water movement and solute transport model HYDRUS-1D), with a multi-component passive and active root solute uptake model (with parts taken from Silberbush et al. (2005)). The model integrates the strengths of both plant and soil approaches and will help explain and understand the root nutrient uptake deficiency stress under different salinity conditions. In addition, the model will help to separate the passive nutrient uptake reduction due to osmotic stress and the specific nutrient uptake reduction due to specific ion toxicity (Na-Cl, in this case).

2. HP1 Implementation of the Nutrient Uptake Model

The three subparts of the Silberbush et al. (2005) uptake model (passive uptake for Na, active uptake for K, and combined passive and active uptake for Ca) were implemented in HP1 (Jacques and Simůnek, 2005).

2.1. Passive Na root water uptake with maximum uptake flux controlled by solution chemistry

The generic passive uptake model is defined by Eq (1):

$$\begin{aligned} p_a(x,t) = \min[&s_w(x,t)\min\left[c(x,t), c_{\max}\right], \\ &A_{root}(x,t)\,J_{p,\max}\left(\omega(x,t)\right), \\ &p_p(x,t)] \qquad \text{if } c(x,t) > c_r \\ = 0 \qquad &\text{otherwise} \end{aligned} \tag{1}$$

where $p_a(x,t)$ is the actual passive nutrient uptake rate [$ML^{-3}T^{-1}$] for a given depth x [L] and time t [T], $s_w(x,t)$ is the root water uptake rate [$L^3L^{-3}T^{-1}$], $c(x,t)$ is concentration [ML^{-3}], $c_{\max}$ is the maximum allowed concentration for root uptake [ML^{-3}], $A_{root}(x,t)$ is the root surface area [L^2L^{-3}], $J_{p,\max}$ is the maximum allowed passive nutrient uptake rate [$ML^{-2}T^{-1}$], $\omega(x,t)$ is the geochemical condition at x and t, p_p is the potential passive nutrient uptake rate [$ML^{-3}T^{-1}$], and c_r is the critical concentration below which passive root uptake is zero [ML^{-3}]. This expression is generic as it limits uptake by (i) a maximum allowable concentration for uptake ($\min[c(.),c_{\max}]$), (ii) a maximum nutrient uptake flux ($\min[s_w(.)\min[c(.),c_{\max}]$, $A_{root}(.)J_{p,\max}(.)]$, and (iii) a maximum potential root uptake. Uptake below a critical value, c_r, equals zero.

Passive uptake of Na is controlled by the root water uptake rate (s_w) or by the coefficient of passive Na influx, P_m^{Na} (as in Silberbush et al. (2005)).

Three possible variants of this general equation are defined (in all variants, uptake is not limited by a potential uptake, i.e., $p_p = 4$ mol m^{-3} s^{-1} in Eq. (1)):

- *Variant 1*: Passive Na uptake is not limited (i.e., $c_{max} = 4$ mol m^{-3}, $J_{p,max} = 4$ m^{-2} s^{-1}, and $c_r = 0$ mol m^{-3} in Eq. (1)). The charge balance in the soil solution is controlled by an exudation of protons, which results in pH changes in the soil solution.
- *Variant 2*: Na uptake is only limited by a maximum Na concentration (i.e., $J_{p,max} = 4$ m^{-2} s^{-1} and $c_r = 0$ mol/m³ in Eq. (1)). The charge balance in the soil solution is controlled by an exudation of protons.
- *Variant 3*: Na uptake is only limited by a maximum allowable Na uptake flux and is zero below c_r (i.e., $c_{max} = 4$ mol m^{-3} in Eq. (1)). $J_{p,max}$ depends on the soil solution chemistry as shown in Eq. (2). In Silberbush et al. (2005), the Ca concentration will affect the active Na uptake. In this implementation to HP1, the uptake of Na is only passive, so this factor is included in the passive uptake according to Eqs. (1) and (2).

$$J_{p,\max} = 2.5\times10^{-11} c^{\mathrm{Na}} \left(c^{\mathrm{Ca}}\right)^{-0.24} \tag{2}$$

Note also that passive uptake is zero when $c_{max} = 0$ mol m^{-3}. In Eq. (2), c^{Na} and c^{Ca} are concentrations of Na and Ca, respectively.

2.2. Active K uptake with Michaelis-Menten kinetic rate parameters dependent on solution chemistry

Active nutrient uptake is described by the Michaelis-Menten rate equation:

$$a_a\left(x,t\right) = A_{root}\left(x,t\right) J_{a,\max}\left(\omega\left(x,t\right)\right) \frac{c(x,t) - c_{\min}}{K_m(\omega(x,t) + (c(x,t) - c_{\min})} \tag{3}$$

where $a_a(x,t)$ is the actual active nutrient uptake [ML^{-3}T^{-1}], $J_{a,max}$ is the maximum allowed active uptake [ML^{-2}T^{-1}], K_m is the Michaelis-Menten constant [ML^{-3}], and c_{min} is the minimum concentration below which active uptake is zero [ML^{-3}].

Both $J_{a,max}$ (mol m^{-2} s^{-1}) and K_m (mol m^{-3}) parameters depend on Na concentrations as described in Silberbush et al. (2005) (Eqs. (4) and (5), respectively).

$$J_{a,\max} = 5.12\times10^{-8} \exp(-0.023 c^{\mathrm{Na}}) \tag{4}$$

$$K_m = 0.0127 + 2.34\times10^{-4} c^{\mathrm{Na}} \tag{5}$$

2.3. Simultaneous passive and active Ca uptake with Michaelis-Menten parameters dependent on solution chemistry

In Šimůnek and Hopmans (2009), passive uptake is calculated first, and if it cannot supply the potential demand, active uptake is activated. In our HP1 implementation, passive and active uptake are calculated simultaneously as:

$$
\begin{aligned}
r_a(x,t) &= p_a + a_a \\
&= \beta s_w(x,t) c(x,t) + \\
&\quad + A_{root}(x,t) J_{a,\max}\left(\omega(x,t)\right) \frac{c(x,t) - c_{\min}}{K_m(\omega(x,t) + (c(x,t) - c_{\min})}
\end{aligned} \tag{6}
$$

where $r_a(x,t)$ is the actual root uptake [$ML^{-3}T^{-1}$], and β is he fraction of root water uptake active in Ca uptake [-]. $J_{a,\max}$ varies with Na concentrations as described in Silberbush et al. (2005) (Eq. (7) in mol cm^{-2} d^{-1}). K_m and β are constants.

$$
J_{a,\max} = 8.64 \times 8.90 \times 10^{-9} \left(1 - 2.56 \times 10^{-4} c^{\mathrm{Na}}\right) \tag{7}
$$

3. Numerical Example and Experimental Data

The nutrient uptake model was implemented in a generic problem described as:

- 1 m deep loamy soil. Soil hydraulic characteristics are described using the van Genuchten-Mualem model (van Genuchten, 1980).
- The bottom of the soil profile has a constant pressure head of 0 cm. The initial condition at the top is -10 cm with a linear decrease in pressure heads from the top to the bottom.
- A constant potential evaporation and transpiration of 0.01 and 0.15 cm day^{-1}, respectively. Between days 20 and 23, and between days 60 and 63, there is irrigation of 1 cm day^{-1}.
- The plant has a uniform root distribution down to a depth of 30 cm. The water stress reduction function of Feddes et al. (1978) is taken with values: P_0 = -10 cm, P_{Opt} = -25 cm, P_{2H} = -200 cm, P_{2L} = -800 cm, P_3 = -8000 cm, r_{2H} = 0.5 cm day^{-1}, r_{2L} = 0.1 cm day^{-1}. For simplicity, the area of the root surface is taken to be 1 $cm^2 dm^{-3}$ soil.
- The same four irrigation treatments used in the laboratory experiment are simulated (Table 1). Initial solution chemistry in the soil corresponds to the solution of Treatment 1.

Table 1. Solution composition for different treatments, concentrations in ppm.

	Treatment 1 (0 mM NaCl)	Treatment 3 (5 mM NaCl)	Treatment 5 (10 mM NaCl)	Treatment 7 (20 mM NaCl)
pH	5.7	5.7	5.7	5.8
Na	3.5	100.4	201.5	415.9
Cl	10.6	185.1	371.6	760.4
NH_4	6.6	6.6	6	5.9
NO_3	79.7	79.6	80.7	83.6
P	16.5	16.7	17.4	19
K	65.3	65	67.1	71.5
Ca	78.8	79.4	81.9	85.9
Mg	19.7	19.4	19.9	20.2

The dataset used to validate this model was from a laboratory experiment with sweet basil (Ocimum basilicum) grown in lysimeters. The controlled upper boundary conditions consisted of

different salinity treatments (Table 1). The bottom boundary conditions were measured to account for a complete water and macro-nutrient balance. Transpiration, growth, and nutrient uptake of sweet basil as a function of irrigation water amount, nutrient concentration, and salinity were measured over time, and compared with calculated data of K, Ca, and Na.

4. Numerical Results

As a first illustration, three different variants of passive uptake for the first subpart are shown in Figure 1. Because uptake is limited by a maximum concentration, cumulative uptake is smaller in variant 2 compared to variant 1, and also the differences between the treatments with higher Na concentrations is smaller compared to variant 1. Limiting the Na uptake by a maximum uptake flux has a large impact on the cumulative uptake (at least with the current parameter setting).

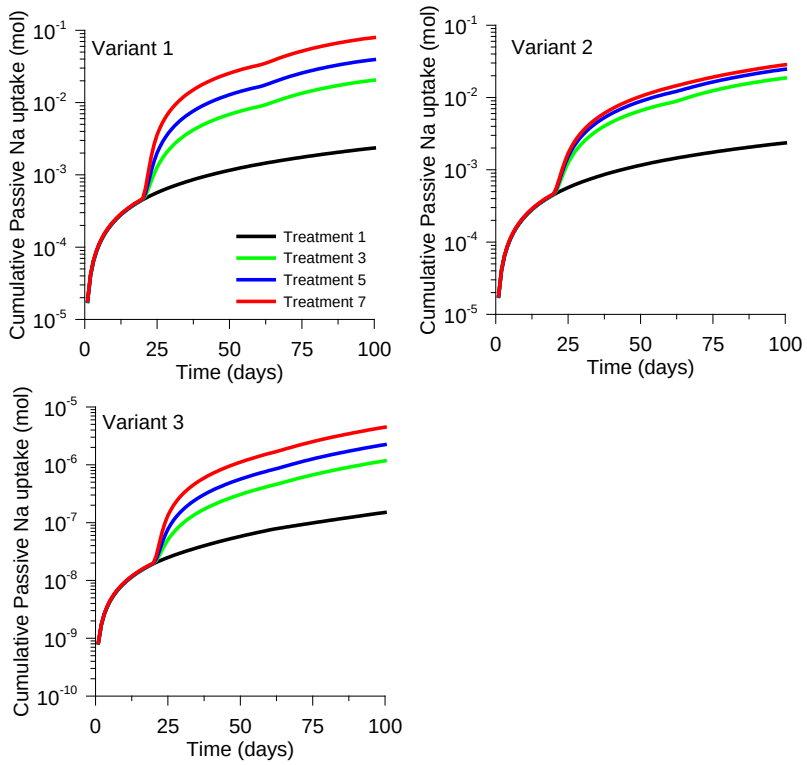

Figure 1. Cumulative passive Na for four salinity treatments simulated with three variants.

Numerical results from the combined implementation of the three subparts of the model of Silberbush et al. (2005) (with variant 3 for passive Na uptake) are shown in Figure 2, in which cumulative uptake of three specific ions under four different salinity treatments (Table 1) are shown. As salinity in irrigation water increases, Na uptake increases, K uptake decreases, and Ca uptake slightly increases.

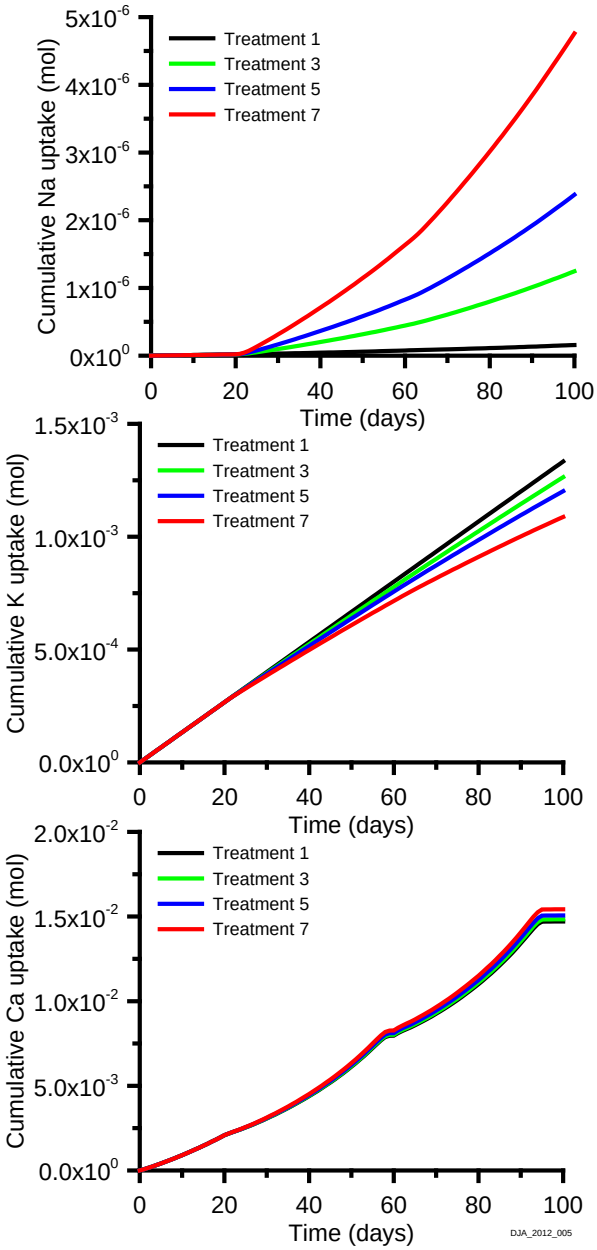

Figure 2. Cumulative Na, K, and Ca uptake for four salinity treatments.

The last result shows a comparison between the model and experimental data from basil grown in lysimeters (Figure 3). Relative uptake of Na, K, and Ca is plotted against four different *EC* values of irrigation water (differences in *EC* are due to different levels of NaCl added). Modeled values of Na and K are close to measured data. Ca shows disparities between measurements and model at high salinity values, indicating that not all parameters for simulations are accurate.

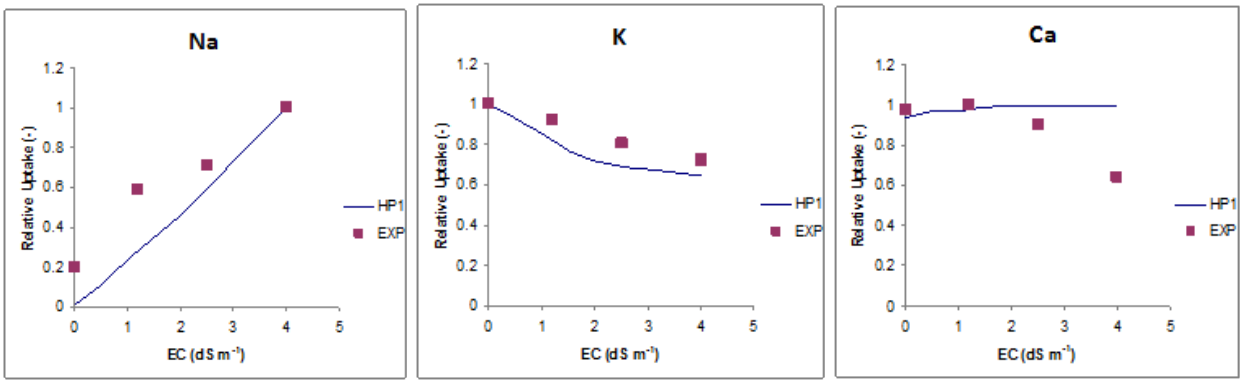

Figure 3. Relative uptake of Na, K, and Ca under various salinities. Comparison between the HP1 model simulations (lines) and experimental data (points) from basil plants grown in lysimeters.

5. Discussion and Conclusions

We have coupled a soil-focused model with a plant-focused model and have demonstrated the potential of linking the Silberbush et al. (2005) nutrient uptake model with HP1 (Jacques et al., 2006). Passive Na, active K, and passive and active Ca uptake with solution-dependent parameters were all integrated in a water movement and solute transport numerical model, as illustrated in the numerical experiment with HP1. Preliminary results are promising though parameters still need to be calibrated for different soils, climates, and crops.

What is ground-breaking in this model is the separation of the nutrient deficiency stress due to certain ions (e.g., Na or Cl) from the osmotic stress they pose. This will allow the functions describing water uptake reduction due to salinity (Maas and Hoffman, 1977; van Genuchten and Hoffman, 1984) to be strictly used to model osmotic stress (Ben-Gal et al., 2009), so that the additional stress due to the reduction in nutrient uptake and specific ion toxicity may then be quantified separately.

References

Ben-Gal, A., H. Borochov-Neori, U. Yermiyahu, and U. Shani, Is osmotic potential a more appropriate property than electrical conductivity for evaluating whole-plant response to salinity? *Envir. Exp. Bot.*, *65*, 232–237, 2009.

Feddes, R. A., P. J. Kowalik, and H. Zaradny, *Simulation of Field Water Use and Crop Yield*, John Wiley & Sons, New York, NY, 1978.

Feddes, R. A., and P. A. C. Raats, Parameterizing the soil-water-plat root system, in: R. A. Feddes, G. H. Rooij, and J. C. van Dam, (Eds.), *Unsaturated Zone Modeling: Progress, Challenges and Applications*, Kluwer Academic, Dordrecht, pp. 95–141, 2004.

Hopmans, J. W., and K. L. Bristow, Current capabilities and future needs of root water and nutrient uptake modeling, *Adv. Agr.*, *77*, 103–183, 2002.

Jacques, D., and J. Šimůnek, *User Manual of the Multicomponent Variably-Saturated Flow and Transport Model HP1: Description, Verification, and Examples*, Version 1.0, *SCK•CEN-BLG-998,* Waste and Disposal, SCK•CEN, Mol, Belgium, 79 pp., 2005.

Jacques, D., J. Šimůnek, D. Mallants, and M. Th. van Genuchten, Operator-splitting errors in coupled reactive transport codes for transient variably saturated flow and contaminant transport in layered soil profiles, *J. Cont.Hydrol.*, *88*, 197–218, 2006.

Maas, E. V., and G. J. Hoffman, Crop salt tolerance. Current assessment, *J. Irr.Drain. Div., 103*, 115–134, 1977.

Silberbush, M., J. Ben-Asher, and J. E. Ephrath, A model for nutrient and water flow and their uptake by plants grown in a soilless culture, *Plant and Soil*, *271*, 309–319, 2005.

Šimůnek, J., and J. W. Hopmans, Modeling compensated root water and nutrient uptake, *Ecol. Model.*, *220*, 505–521, 2009.

van Genuchten, M. Th., A closed-form equation for predicting the hydraulic conductivity of unsaturated soils, *Soil Sci. Soc. Am.*, *44*, 892–898, 1980.

van Genuchten, M. T., and G. J. Hoffman, Analysis of crop salt tolerance data, In: I. Shainberg, and J. Shalhevet, (Eds.), *Soil Salinity Under Irrigation: Processes and Management*, Springer Verlag, New York, pp. 258–271, 1984

Taiz, L., and E. Zeiger, *Plant Physiology*, 3rd ed., Sinauer, 2002.

Modeling Water and Nitrogen Fate in Plots with Sweet Sorghum Irrigated with Fresh and Blended Saline Waters using HYDRUS-2D

Tiago B. Ramos[1], Jiří Šimůnek[2], Maria C. Gonçalves[1,3], José C. Martins[3], Ângela Prazeres[3], and Luís S. Pereira[1]

[1]*CEER, Institute of Agronomy, Technical University of Lisbon, Lisbon, Portugal,* tiago_ramos@netcabo.pt
[2]*Department of Environmental Sciences, University of California Riverside, Riverside, CA, USA,* jiri.simunek@ucr.edu
[3]*National Institute of Agronomic and Veterinarian Research, INIAV, Oeiras, Portugal,* maria.goncalves@iniav.pt

Abstract

The Alentejo region in southern Portugal faces water scarcity and environmental problems as a result of high atmospheric demands and irregular rainfall. In the last few years, the HYDRUS software package has been calibrated and validated in order to minimize human-induced salinization, sodification, and non-point source pollution from agricultural fertilization in the region. This paper describes results from an experiment where HYDRUS-2D, while considering drip irrigation scenarios with different levels of nitrogen and salty waters, was used to assess the fate of nitrogen in a plot planted with sweet sorghum. HYDRUS-2D simulated water contents EC_{sw}, N-NH_4^+, and N-NO_3^- concentrations continuously between 2007 and 2010, while producing *RMSE* between simulated and measured data of 0.030 $cm^3\ cm^{-3}$, 1.764 $dS\ m^{-1}$, 0.042 $mmol_c\ L^{-1}$, and 3.078 $mmol_c\ L^{-1}$, respectively. Actual transpiration varied between 264 and 334 mm depending upon the crop season and the irrigation treatment. Sweet sorghum showed to be tolerant to saline waters only during one crop season. After that, the continuous use of saline waters led to soil salinization and to root water uptake reductions due to the increasing salinity stress. N uptake and leaching were dependent on the amount of water flowing through the root zone, the amount of N applied, the form of N in the fertilizer, and the timing and number of fertigation events. The effect of the osmotic stress on nitrogen leaching was only minimal. The yield function developed from N-NO_3^- uptake and dry biomass yield (R^2 = 0.71) estimated the N needs to be between 130 and 180 kg/ha. The simulations with HYDRUS-2D were thus useful to understand the best strategies toward increasing nutrient uptake and reducing nutrient leaching.

1. Introduction

The Alentejo region of southern Portugal normally exhibits high summer temperatures and very low rainfall that limits crop production. In this water scarce region, irrigation plays a fundamental economical and social role but has exacerbated several environmental problems as a result of poor irrigation and water management practices. Human-induced salinization, sodification, and non-point source pollution from agricultural fertilization are among the recognized problems. Therefore, a sound irrigation policy must be established to avoid and mitigate these risks. Such policy may include the adoption of less water and nutrient demanding

crops, and should be based on a quantitative understanding of the subsurface movement of water and dissolved chemicals.

Modeling of subsurface water flow and the transport of major soluble ions in and below the root zone is essential for predicting groundwater quality, implementing better irrigation and fertilization practices (Cameira et al., 2003), and quantifying salinization and alkalization hazards. Thus, the HYDRUS software package (Šimůnek et al., 2008) has been used in the last few years to better understand the main physical and chemical processes involved when irrigating with waters of different quality and to help establish sound irrigation practices for the soils in the region.

Gonçalves et al. (2006) first analysed transient water flow and solute transport in three soil lysimeters with waters of different quality over a period of 3 years using the UNSATCHEM module implemented in HYDRUS-1D. In this study, HYDRUS-1D successfully described water contents, overall salinity, concentration of major soluble cations (Ca^{2+}, Mg^{2+}, K^{+}, and Na^{+}), sodium adsorption ration, and exchangeable sodium percentage.

Later, Ramos et al. (2011) addressed the transport and reactions of salts and nitrogen species in the soil profile in an integrated way. The UNSATCHEM module was again used to simulate the overall salinity and major cations in two soils with coarse and medium textures during a long term experiment, while the general solute transport module of HYDRUS-1D was used to model nutrient fate ($N\text{-}NO_3^-$ and $N\text{-}NH_4^+$). This study allowed a better understanding of solute interactions between the solid and liquid phases and the complex reactions involved in solute transport. The study further allowed understanding of the basic relations between nutrient uptake, leaching and the salinity stress caused by the use of saline waters.

Although the modeling approaches carried out were successful in modeling soil water dynamics and solute transport in field conditions, these two studies were only one-dimensional and neglected water and solute fluxes and pressure head and concentration gradients in the horizontal direction. Additionally, one-dimensional models fail to adequately simulate micro-irrigation systems (such as drip emitters, drip tape, and micro-sprinklers), which can efficiently apply water and nutrients in the right amounts and precise locations throughout a field (e.g., Gärdenäs et al., 2005). Since drip irrigation is often used in Portugal, it seemed more appropriate to find modeling approaches that are better able to represent complex physical and chemical processes that take place in the soil profile under this irrigation system.

The main objective of this study was to use the HYDRUS-2D software package to model nitrogen fate in a field with sweet sorghum while considering different drip fertigation and water quality scenarios. Field data was used to calibrate and validate HYDRUS-2D for predicting (i) soil water contents and fluxes, (ii) the electrical conductivity of the soil solution (EC_{sw}), (iii) water uptake reductions due to the use of saline waters, and (iv) $N\text{-}NH_4^+$ and $N\text{-}NO_3^-$ concentrations in the soil and their leaching. Water and nutrient balances were calculated based on model predictions. A complete description of this study is reported by Ramos et al. (2012b).

2. Material and Methods

2.1. Field Experiment

The field experiment was conducted at the Alvalade Experimental Station (37º 56' 48'' N and 8º 23' 40'' W), southern Portugal, from May, 2007 to April, 2010. The field experiment involved irrigation of sweet sorghum (*Sorghum bicolor* (L.) Moench) with synthetic saline waters blended with fresh irrigation waters and waters with nitrogen (NH_4NO_3) during three crop seasons. The blended amounts varied between the 12 experimental plots, while the total amount of water applied per irrigation event and per crop season, as well as the quality of the irrigation waters before blending, remained identical in all plots.

The total amount of water applied was 425, 522, and 546 mm in 2007, 2008, and 2009, respectively. Application amounts averaged 15, 16, and 17 mm per irrigation event in 2007, 2008, and 2009, respectively. Nitrogen fertilization was applied in 4 (2007), 6 (2008), and 3 (2009) irrigation events during the vegetative stage (July). The *EC* of the fresh waters, saline waters, and waters with fertilizer was 0.8, 7.6-10.6, and 6.8-9.5 dS m^{-1}, respectively. $N\text{-}NH_4^+$ and $N\text{-}NO_3^-$ concentrations in the waters with fertilizer varied between 67.7-95.0 $mmol_c\ L^{-1}$.

In the plots with the highest application of synthetic saline waters, and in those irrigated only with the locally available fresh water, TDR probes with waveguides from the Trase System (Soil Moisture Equipment Corp., Goleta, CA) and ceramic cups were installed at depths of 20, 40, and 60 cm to measure soil water contents and collect soil solutions, respectively. The soil solution was monitored for EC_{sw} and the concentrations of $N\text{-}NH_4^+$ and $N\text{-}NO_3^-$. The dry biomass of sweet sorghum was determined at the end of each crop season by harvesting all sorghum plants in each experimental plot and oven drying them at 70 ºC to a constant weight.

2.2. Modeling Approach

Modeling of water flow and solute transport was carried out for all experimental plots irrigated with the highest application of synthetic saline waters and only with the water available in the region. The HYDRUS-2D software package (Šimůnek et al., 2008) was used to simulate the transient axisymmetrical (or radially symmetrical) three-dimensional movement of water and nutrients in the soil. The transport domain was set as a rectangle with a width of 37.5 cm (half the lateral spacing, i.e., the half-distance between triple joint laterals placed along the sorghum rows) and a depth of 100 cm (Figure 1). The flux boundary condition with the flux q was defined as:

$$q = \frac{volume\ \ of\ \ \ applied\ \ \ water}{surface\ \ \ wetted\ \ \ area\ \times\ duration} \tag{1}$$

where the volume of applied water [L^3] varied for different irrigation events, the surface wetted area [L^2] was approximately 1,256 cm^2 (i.e., 3.14 x 20^2), and the irrigation duration was adjusted to permit water to infiltrate into the soil without producing positive surface pressure heads and to allow for the application of irrigation waters of different qualities within a particular irrigation event.

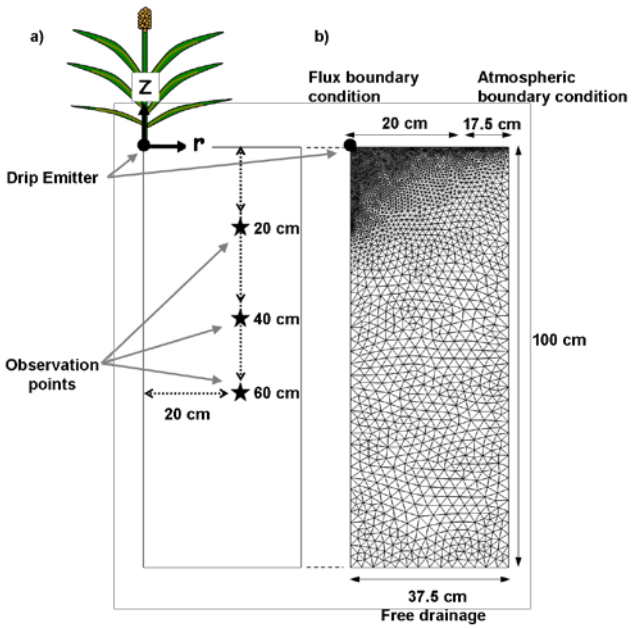

Figure 1. Location of observation points within the soil profile (a) and an axisymmetrical domain geometry with the finite element discretization used in HYDRUS-2D simulations (b).

HYDRUS-2D numerically solved the Richards equation for describing the variably-saturated water flow in a radially symmetric domain and the convection-dispersion equation for solute transport. The soil hydraulic properties were described using the van Genuchten-Mualem model (van Genuchten, 1980). Since the fertilizer used in our study was NH_4NO_3, nitrification ϕ [ML^{-3} T^{-1}] of the N-NH_4^+ species to N-NO_3^- was assumed to be the main N process occurring in the soil. This process was described by means of a sequential first-order decay chain as follows:

$$\phi_{N-NH_4^+} = -\phi_{N-NO_3^-} = -\mu_{w,N-NH_4^+}\theta \; c_{N-NH_4^+} - \mu_{s,N-NH_4^+}\rho \; \bar{c}_{N-NH_4^+} \qquad (2)$$

where c, and $\bar{c}$ are solute concentrations in the liquid phase [ML^{-3}] and solid phase [MM^{-1}], respectively, μ_w and μ_s (set to 0.2 d^{-1}) are the first-order rate constants for solutes in the liquid and solid phases [T^{-1}], respectively, θ is the volumetric water content [L^3L^{-3}], and ρ is the soil bulk density [ML^{-3}]. The first-order reaction terms, representing nitrification of N-NH_4^+ to N-NO_3^-, thus act as a sink for N-NH_4^+ and as a source for N-NO_3^-. The distribution of solutes between the solid and liquid phases was described by means of a linear adsorption isotherm. Only N-NH_4^+ was assumed to adsorb to the solid phase (K_d of 3.5 cm^3g^{-1}).

The Richards and the CDE equations incorporate a sink term to account for water uptake by roots. Water and salinity stresses were defined according to the functions proposed by Feddes et al. (1978) and the Maas (1990) salinity threshold and slope function, respectively. Soil evaporation and plant transpiration rates were obtained by combining the daily values of reference evapotranspiration (ET_0), determined with the FAO Penman-Monteith method and the dual crop coefficient approach (Allen et al., 1998). Nutrient uptake was simulated by considering unlimited passive uptake for nitrogen species (Šimůnek and Hopmans, 2009). Model validation was carried out by comparing field measured values with HYDRUS-2D simulations while using the root mean square error (*RMSE*) for quantifying model uncertainty.

3. Results and Discussion

Figure 2 compares the measured and simulated water contents at 40 cm depth in plots with the highest application of the saline and fresh waters. Water contents increased to full saturation near the emitter after an irrigation or rain event, and then decreased gradually during the following hours and days, until the next irrigation or rain event took place. Deeper depths showed smaller water content variations since root water uptake and soil evaporation were more pronounced at shallower depths. A *RMSE* of 0.030 cm^3 cm^{-3} was found between measured and simulated values.

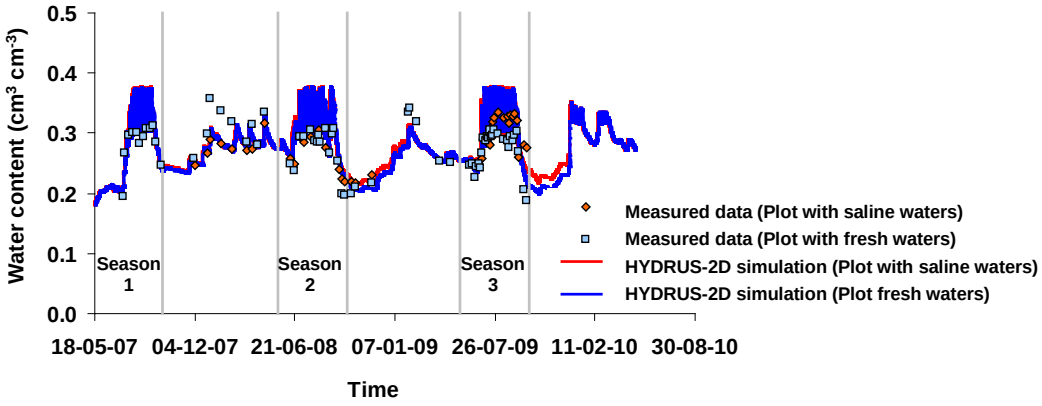

Figure 2. Measured and simulated water content at 40 cm.

Potential transpiration (T_p) varied between 360 and 457 mm. T_p values obtained in plots irrigated with saline waters were generally lower that those obtained in plots irrigated with fresh waters. However, the differences were found to be very small since sweet sorghum is moderately to highly tolerant to salinity (Maas, 1990). Actual transpiration (T_a) varied between 264 and 334 mm. T_p reductions due to water stress (21.9-27.4%) were a function of the adopted irrigation schedule. In plots irrigated with saline waters, T_p was further reduced by 2.3-7.0% due to salinity stress. The salinity stress became increasingly higher as a result of soil salinization and the continuous and increasing amount of synthetic saline waters being applied in each experimental plot (Figure 3). The *RMSE* obtained between measured and simulated EC_{sw} was 1.764 dS m^{-1}.

Nitrogen leaching was directly related to water flow through the bottom boundary of the soil domain. The movement of N out of the root zone also depended on the amount of applied N, the form of N in the fertilizer, and the time and number of fertigation events. Based on model simulations, most $N\text{-}NH_4^+$ was rapidly nitrified into $N\text{-}NO_3^-$, not reaching depths deeper than 20 cm (Figure 4). Leaching of nitrogen occurred mainly in the $N\text{-}NO_3^-$ form (Figure 5). The higher the number of fertigation events, the lower the amount of N applied per event, and thus the lower the amount of leached $N\text{-}NO_3^-$. Nutrient uptake by plant roots occurred mainly in the $N\text{-}NO_3^-$ form as well. The number of fertigation events also significantly influenced the amount of $N\text{-}NO_3^-$ taken up by plant roots. The effects of the salinity stress on nutrient uptake (and inversely on nutrient leaching) was relatively small since sweet sorghum has a medium to high tolerance to salinity, and consequently there were only small reductions in transpiration due to the increase of the osmotic stress.

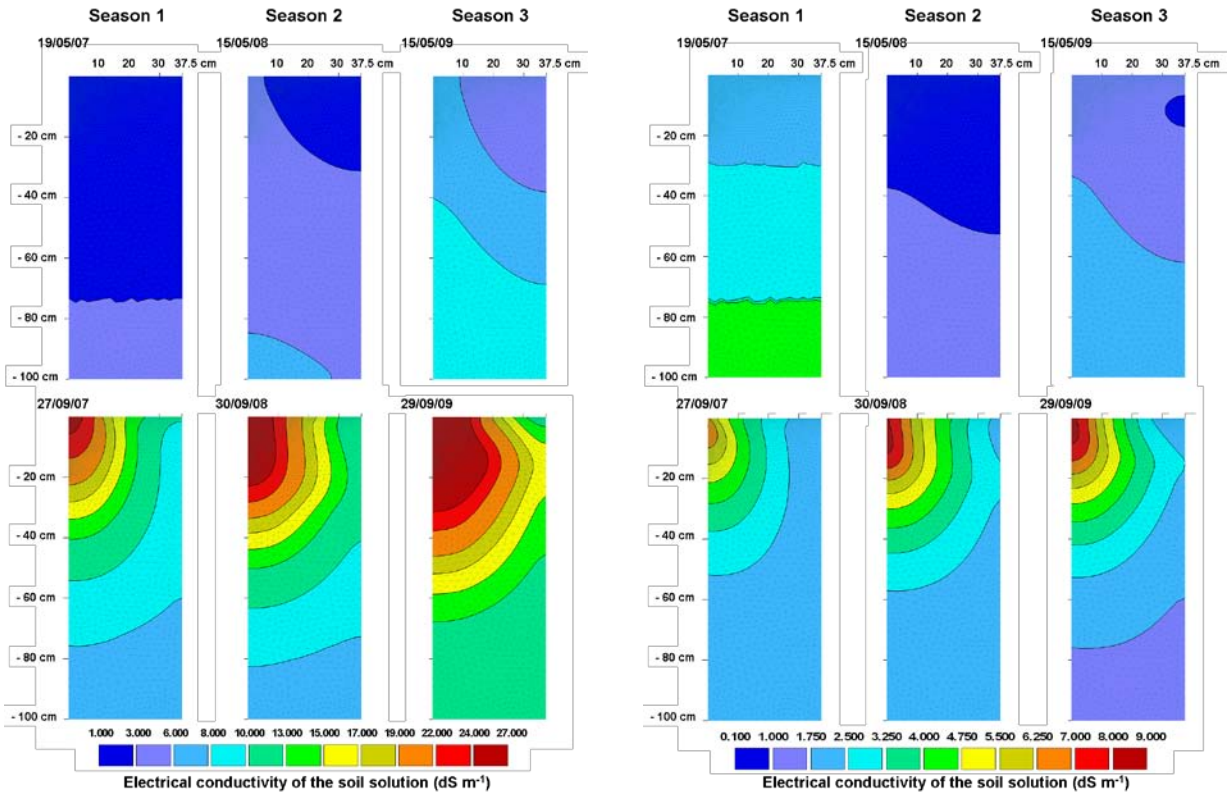

Figure 3. Simulated distributions of the electrical conductivity of the soil solution in plots irrigated with saline (left) and fresh (right) waters during sowing (top) and harvest (bottom) of each crop season. The drip emitter was located in the top left corner of each contour plot.

The *RMSE* obtained while comparing measured and simulated $N\text{-}NH_4^+$ and $N\text{-}NO_3^-$ concentrations were 0.042 and 3.078 $mmol_c\ L^{-1}$, respectively. Deviations between measured data and simulated variables were related to field measurements, model input and model structure errors. Here we would like to note that the approach followed for modeling the transport of the N species (eq. 2) is relatively simple, and can only consider N processes that are involved in a sequential-first order decay chain, such as nitrification, denitrification, and volatilization. Other

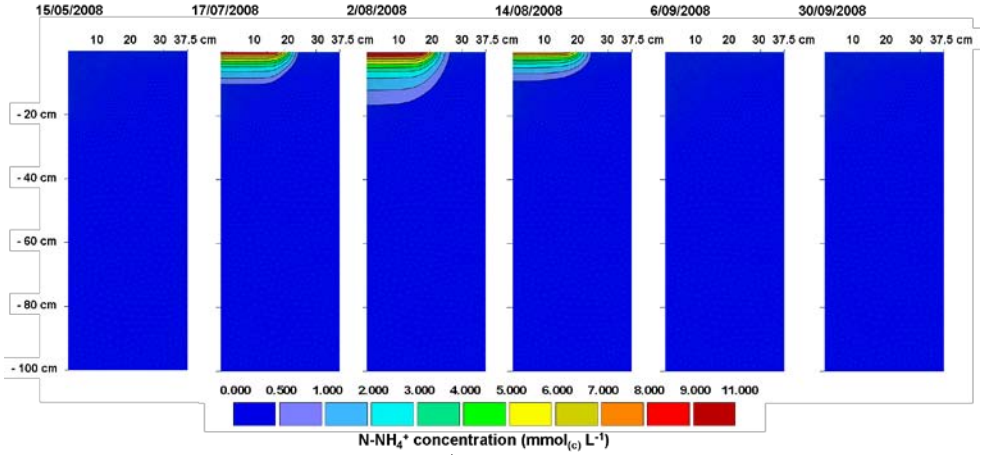

Figure 4. Simulated distributions of $N\text{-}NH_4^+$ concentrations in plot irrigated with saline waters during crop season 2. The dripper was located in the top left corner the contour plots.

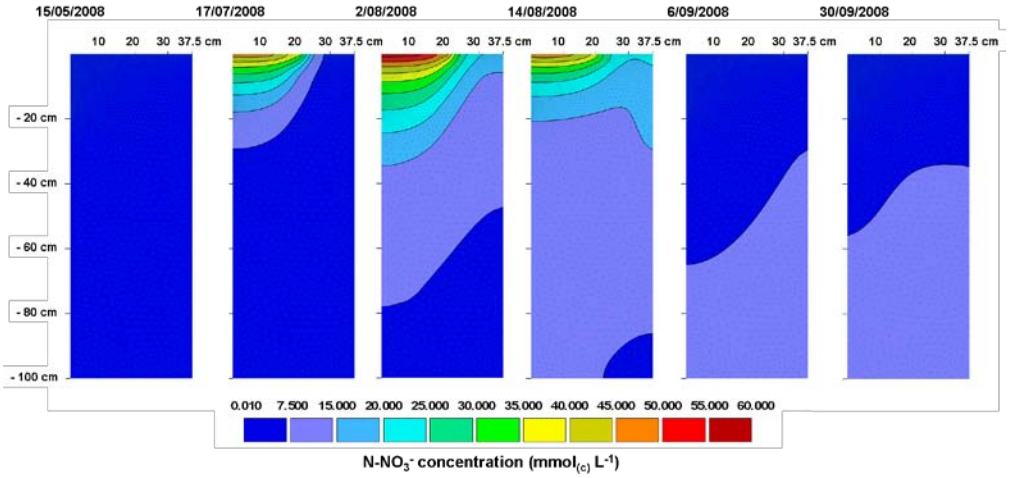

Figure 5. Simulated distributions of $N\text{-}NO_3^-$ concentrations in plot irrigated with saline waters during crop season 2. The dripper was located in the top left corner the contour plots.

nitrogen reactions, with probable relevance for long-term applications such as ours, simply cannot be accounted for using this approach. However, from an agronomical perspective where the efficient use of the fertilizer applied is one of the main objectives to achieve, the approach is adequate.

Figure 5 shows the relationship between the $N\text{-}NO_3^-$ plant uptake calculated using HYDRUS-2D and the experimentally determined dry biomass yield expressed using a logarithmic function with a R^2 of 0.71. This logarithmic function fitted to experimental data shows that an additional incremental increase of $N\text{-}NO_3^-$ uptake produced diminishing returns in the total dry biomass response, with optimum levels being reached at 130-180 kg/ha (Ramos et al., 2012a).

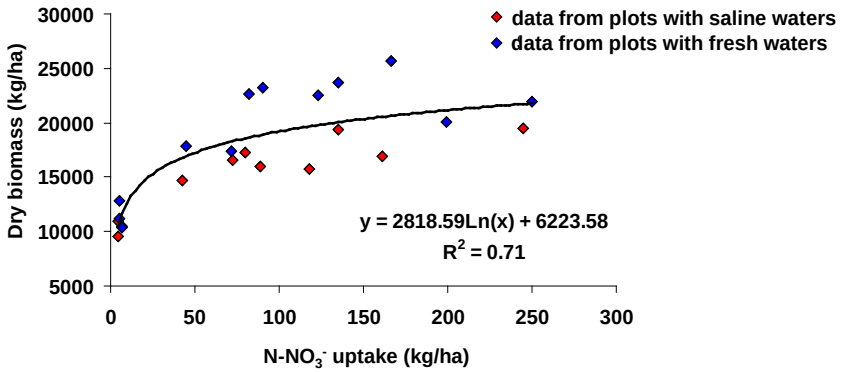

Figure 5. Relationship between the $N\text{-}NO_3^-$ uptake (x), as simulated by HYDRUS-2D, and the dry biomass yield (y).

4. Conclusions

HYDRUS-2D successfully estimated the fate of nitrogen in field plots grown with sweet sorghum in Alentejo. In this water-scarce region, where even saline waters can be viewed as an important source of irrigation water during drought seasons, the use of marginal waters showed

viability for irrigating sweet sorghum during a limited time period (one crop season). Furthermore, the relatively low water needs (360-457 mm) and N requirements (130-180 kg/ha) of sweet sorghum makes it a good alternative when compared to other traditional crops grown in the region. The leaching of N out of the root zone depended closely on drainage, the amount of N applied, the form of N in the fertilizer, and the time and number of fertigation events. The modeling approach helped us understand the best irrigation and fertigation management practices to be adopted in future practical applications for increasing nutrient uptake and reducing nutrient leaching.

Acknowledgments

This research was performed within the framework of the Project EUTROPHOS (PTDC/AGR-AAM/098100/2008) of the Fundação para a Ciência e a Tecnologia (FCT). T. B. Ramos was funded by the FCT grant SFRH/BD/60363/2009.

References

Allen, R. G., L. S. Pereira, D. Raes, and M. Smith, Crop Evapotranspiration – Guidelines for Computing Crop Water Requirements, Irrigation and Drainage Paper, 56, FAO, Rome, Italy, 1998.

Cameira, M. R., R. M. Fernando, and L. S. Pereira, Monitoring water and NO_3-N in irrigated maize fields in the Sorraia watershed, Portugal. *Agricultural Water Management*, *60*, 199-216, 2003.

Feddes, R. A., P. J. Kowalik, and H. Zaradny, Simulation of field water use and crop yield, Simulation Monographs Pudoc, Wageningen, The Netherlands, 1978.

Gärdenäs, A., J. W. Hopmans, B. R. Hanson, and J. Šimůnek, Two-dimensional modeling of nitrate leaching for various fertigation scenarios under micro-irrigation, *Agricultural Water Management*, *74*, 219–242, 2005.

Gonçalves, M. C., J. Šimůnek, T. B. Ramos, J. C. Martins, M. J. Neves, and F. P. Pires, Multicomponent solute transport in soil lysimeters irrigated with waters of different quality, *Water Resources Research*, *42*, W08401, 2006.

Maas, E. V., Crop salt tolerance, In: K. K. Tanji (Ed.), *Agricultural Salinity Assessment and Management*, Manual Eng. Pract., vol. 71, pp. 262–304, Am. Soc. of Civ. Eng., Reston, Va., 1990.

Ramos, T. B., J. Šimůnek, M. C. Gonçalves, J. C. Martins, A. Prazeres, N. L. Castanheira, and L. S. Pereira, Field Evaluation of a multicomponent solute transport model in soils irrigated with saline waters. *Journal of Hydrology*, *407*, 129-144, 2011.

Ramos, T. B., N. L. Castanheira, M. C. Gonçalves, M. L. Fernandes, M. I. Januário, M. E. Lourenço, F. P. Pires, and J. C. Martins, Effects of increasing levels of nitrogen fertigation and sodium on sweet sorghum yield components, *Pedosphere*, *22*, 785-794, 2012a.

Ramos, T. B., J. Šimůnek, M. C. Gonçalves, J. C. Martins, A. Prazeres, and L. S. Pereira, Two-dimensional modeling of water and nitrogen fate from sweet sorghum irrigated with fresh and blended saline waters, *Agricultural Water Management*, *111*, 87-104, 2012b.

Šimůnek, J. and J. W. Hopmans, Modeling compensated root water and nutrient uptake, *Ecological Modeling*, *220*, 505-521, 2009

Šimůnek, J., M. Th. van Genuchten, and M. Šejna, Development and applications of the HYDRUS and STANMOD software packages, and related codes, *Vadose Zone Journal*, *7*(2), 587-600, 2008.

van Genuchten, M. Th., A closed form equation for predicting the hydraulic conductivity of unsaturated soils, *Soil Science Society of America Journal*, *44*, 892-898, 1980.

Longitudinal Dispersivity Determination Using Conservative Tracer in the Field

Ružičić Stanko[1], Zoran Kovac[2], Marta Mileusnic[1], and Kristijan Posavec[2]

[1] *Department of Mineralogy, Petrology and Mineral Resources, Faculty of Mining, Geology and Petroleum Engineering, University of Zagreb, Pierottijeva 6, 10000 Zagreb, Croatia, sruzicic@rgn.hr*
[2] *Department of Geology and Geological Engineering, Faculty of Mining, Geology and Petroleum Engineering, University of Zagreb, Pierottijeva 6, 10000 Zagreb, Croatia*

Abstract

Determination of solute transport parameters in the unsaturated zone is of great importance for groundwater pollution risk assessment. The subject of this study was Fluvisol soil developed on the floodplain of the Sava River. The goal of the study was estimation of longitudinal dispersivity, one of the main solute transport parameters. A field experiment using conservative tracer calcium chloride was carried out. The investigated site is situated about eight hundred meters from the right bank of the Sava River at Kosnica regional well field. Longitudinal dispersivity was estimated by inverse modeling chloride concentration using HYDRUS-1D. Due to the collapse of the pedological pit during application of the tracer and sampling of percolating solution, the field experiment was not completed. Therefore, estimation of longitudinal dispersivity was performed on an incomplete data set.

1. Introduction

Solute transport at the field scale can be very complex because of the presence of several physical, chemical, and biological soil processes that may vary over space and time. Longitudinal dispersivity (λ), which is one of the main solute transport parameters, depends on the scale of measurement. This parameter is often determined in the field (e.g., Seuntjens et al., 2001; Stumpp et al., 2009; Severino et al., 2010). Common tracers are calcium chloride and potassium bromide. In this study, calcium chloride was used. The sorption potential of calcium chloride is relatively low and its suitability has been demonstrated in the unsaturated zone (Akhtar et al., 2003; Heilig et al., 2003; Dişli, E., 2010). Inverse optimization techniques, wherein differences between observed and predicted values are minimized, is increasingly used to estimate solute transport parameters (e.g., Jacques et al., 2002; Šimůnek et al., 2002; Moradi et al., 2005; Jacques et al., 2012). Numerical models for inverse modeling are STANMOD (Šimůnek et al., 1999b) and HYDRUS-1D (Šimůnek et al., 2008). STANMOD also includes several analytical models for solute transport problems. The CXTFIT code (Toride et al., 1999) is the most widely used (e.g., Fonseca et al., 2009; Zhang et al., 2011; Wang et al., 2013).

The goal of the study was estimation of longitudinal dispersivity which is one of the main solute transport parameters.

2. Materials and Methods

2.1. Site Description and Experimental Design

The study area is located near Zagreb, the capital city of Croatia, in the second zone of sanitary protection of the water abstraction site, Kosnica (45°46' N; 16°05' E). The soil is classified after FAO classification (FAO, 2006) as a Fluvisol (Horizons: A-AC-C-2C/Cl-3Cl-4Cl/Cr-5Cr). Separately, undisturbed and disturbed samples of investigated horizons were taken from the pedological pit for laboratory analyses. Undisturbed samples (soil-cores) were analyzed for bulk density, porosity, water capacity, air capacity, and sediment density. The soil particle size distribution was determined on disturbed samples using wet sieving and sedimentation. Soil bulk density was determined using the standard soil-core method. Analytical results are shown in Table 1. The texture of this type of soil is mainly loamy, in some parts clayey with loam. Results from grain size analysis and bulk densities of soil samples were used for prediction of soil hydraulic parameters. Soil hydraulic parameters (θ_s, θ_r, α, K_s, n and l) were calculated using Rosetta lite (Schapp et al., 2001) software (Table 1).

Table 1. Soil texture, bulk density and van Genuchten soil hydraulic parameters (Ružičić et al., 2012).

Soil horizons	Depth (cm)	Sand (%)	Silt (%)	Clay (%)	Bulk density (gcm^{-3})	θ_s ($cm^3\ cm^{-3}$)	θ_r ($cm^3\ cm^{-3}$)	K_s ($cm\ day^{-1}$)	α (cm^{-1})	n
A	0-19	24	66	10	1.04	0.428	0.055	30	0.0043	1.70
AC	19-68	14	77	9	1.36	0.466	0.055	36	0.0052	1.70
C	68-110	57	38	5	1.39	0.371	0.033	61	0.0218	1.44
2C/Cl	110-140	44	47	9	1.37	0.373	0.041	35	0.0096	1.54
4Cl/Cr	140-190	38	50	12	1.41	0.372	0.047	24	0.0077	1.58
5Cr	190-215	56	39	5	1.43	0.362	0.032	51	0.0223	1.444

Parameters such as water content, electrical conductivity and soil water tension are essential for modeling of solute transport. Therefore, a 2.1 m pedological pit, in which field measurement instruments were installed, was dug at the investigated location (Fig. 1). Two TDR (time domain reflectrometry) and two *EC* (electrical conductivity) probes (Fig. 1), as well as two tensiometers, were installed at different depths (TDR: 40 and 110 cm; *EC*: 50 and 120 cm; tensiometers: 40 cm and 110 cm). Furthermore, four suction lysimeters were installed at four different depths (40, 80, 150 and 190 cm).

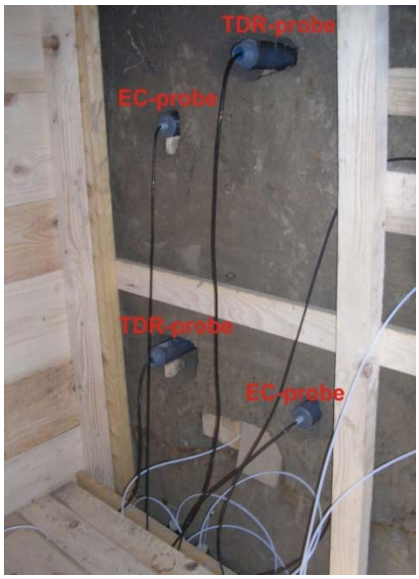

Figure 1. Investigative pedological pit with TDR probes and *EC*-probes.

The surface of the plot above the lysimeters and monitoring equipment to which the tracer was applied is approximately 0.7 m^2. Before application, the plot was leveled, cleaned of all vegetation and enclosed in order to prevent tracers run off. The plot was irrigated with a 200 l tracer solution over two hours. During the experiment, water content (using TDR probes) and electrical conductivity (using EC probes) were measured every twenty minutes. Due to unexpected problems with the suction lysimeters installed at deeper depths, the percolating solution was sampled only at a depth of 40 cm. Chloride concentrations in leachate were analyzed using ion chromatography (ICS–1000 Ion Chromatography System, Dionex).

2.2. Modeling

One-dimensional water flow in an unsaturated zone is based on the modified Richards equation (Richards, 1931):

$$\frac{\partial \theta(h)}{\partial t} = \frac{\partial}{\partial z}\left[K(h)\left(\frac{\partial h}{\partial z}+1\right)\right] \tag{1}$$

where z is the vertical coordinate (positive upward from water table) [L], t the time (s), h the pressure head [L], θ the volumetric water content [L^3L^{-3}] and K the hydraulic conductivity [LT^{-1}].

An empirical model of van Genuchten (1980) is used to describe the water retention characteristics, $\theta(h)$*:*

$$\theta(h) = \theta_r + \frac{\theta_s - \theta_r}{\left[1+\left|\alpha h\right|^n\right]^m} \qquad h<0 \tag{2}$$

where θ_r is the residual water content [L^3L^{-3}], θ_s the saturated water content [L^3L^{-3}], α [L^{-1}], n and m [-] are shape parameters.

In this study, conservative solute transport is described using the convection–dispersion equation (CDE) in the following form:

$$\frac{\partial \theta c}{\partial t} = \frac{\partial}{\partial z}\left(\theta D \frac{\partial c}{\partial z} \right) - \frac{\partial \theta v c}{\partial z} \tag{3}$$

where C is chloride concentration [$M\ L^{-3}$] in soil solution, v the average pore water velocity [LT^{-1}] and D the hydrodynamic dispersion coefficient [$L^2\ T^{-1}$].

Pore water velocity is calculated using Darcy's law:

$$v = \frac{q}{\theta} \tag{4}$$

where q is the Darcy flux [LT^{-1}] and θ the porosity [-].

The HYDRUS-1D model (Šimůnek et al., 2008) was used for estimation of the solute transport parameter, namely the longitudinal dispersivity.

A pressure head of 145 cm was set as the initial condition for water flow through the model domain. This pressure head presents average values from the tensiometer installed at 40 cm depth. The model domain is delineated by the water flux on the upper boundary and the known pressure head as the boundary condition on the bottom of profile (constant pressure head).

The initial chloride concentration (0.023 mg cm^{-3}) was set as input (tracer) concentration at the top of the model domain, while chloride contents through the soil profile were set as chloride concentrations in soil water (expressed in mg cm^{-3}). For the upper and lower boundary conditions, a third type condition, representing the flux concentration, was used.

3. Results

3.1. Field Experiment

Electrical conductivity and water content measured during the experiment are presented in Figures 2a and 2b. Electrical conductivity measured at 50 cm depth shows an immediate increase from 430 μS cm^{-1} to 550 μS cm^{-1} in the 20 minutes after the starting time of tracer application (9:00AM). Electrical conductivity measured at a deeper depth (120 cm) shows a slight increase from 230 μS cm^{-1} to 270 μS cm^{-1} after one hour and forty minutes. Water content measured at a depth of 40 cm also shows an immediate increase from 35.0 % to 36.4 % in 20 minutes after the starting time of tracer application. Water content measured at a deeper depth (110 cm) shows a slight increase from 27.8% to 29.1% after one hour and twenty minutes. Chloride concentrations of percolating water samples from the lysimeter installed at 40 cm are shown in Table 2.

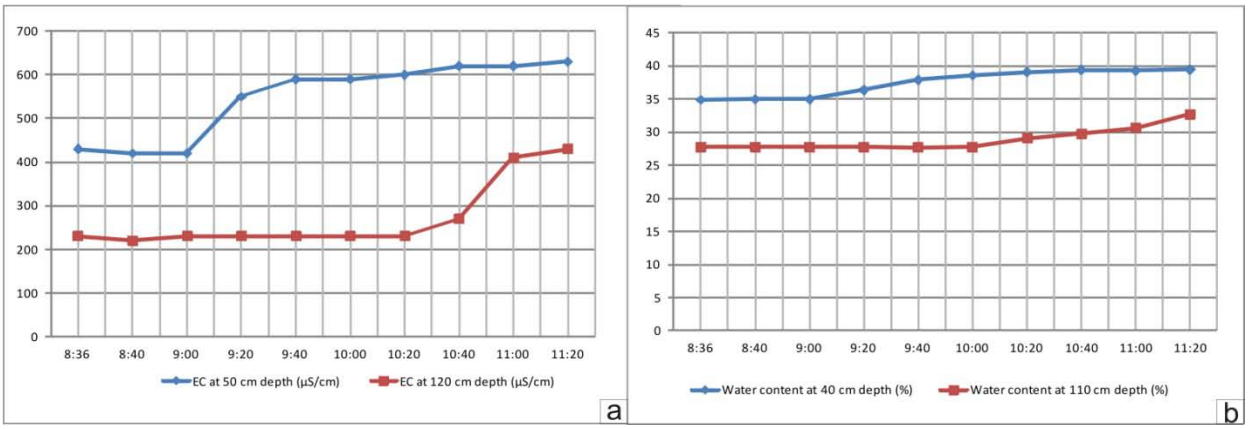

Figure 2. a) Diagram of water content for period of two hours and forty minutes, b) Diagram of electrical conductivity for period of two hours and forty minutes.

Table 2. Chloride concentrations of percolating water.

Sampled time (min)	**Observed concentration (mg cm^{-3})**
93	0.0212
98	0.0228
108	0.0232
110	0.0278
114	0.0294
116	0.0233
120	0.0262

Pore water velocity was analytically calculated using eq. 4. Table 3 presents estimated saturated hydraulic conductivity, porosity, hydraulic gradients, pore water velocities, and dispersivity.

Table 3. Estimated saturated hydraulic conductivity, porosity, hydraulic gradients, pore water velocities, and dispersivity.

$K_{avg.}$ (cm day^{-1})	$\theta_{avg.}$(-)	i (-)		v (cm min^{-1})		λ* (cm)
33	0.46	i_{min}	0.5	v_{min}	0.025	2
		i_{max}	4	v_{max}	0.2	

K_{avg} - average hydraulic conductivity for horizons A and AC, θ_{avg} - average porosity for horizons A and AC, i_{min} - minimal hydraulic gradient calculated from tensiometer readings, i_{max} - maximal hydraulic gradient calculated from tensiometer readings, v_{min} - minimal pore water velocity for i_{min}, v_{max} - maximal pore water velocity for i_{max}, λ* - estimated dispersivity with HYDRUS-1D.

3.2. Modeling

The diagram in Figure 3 shows that the calcium chloride concentration of 0.023 mg cm^{-3} (which is applied at the top of the soil) decreased to 0.013 mg cm^{-3} in 30 minutes. After that period, concentration rose to 0.025 mg cm^{-3} in 120 minutes. A longitudinal dispersivity of 2 cm gave the best fitting of simulated and observed values. The time that the lysimeter needed to intake enough water for the first sample was 93 minutes (Fig. 3). Due to collapse of the pedological pit during application of the tracer and sampling of percolating solution, the field experiment was not completed.

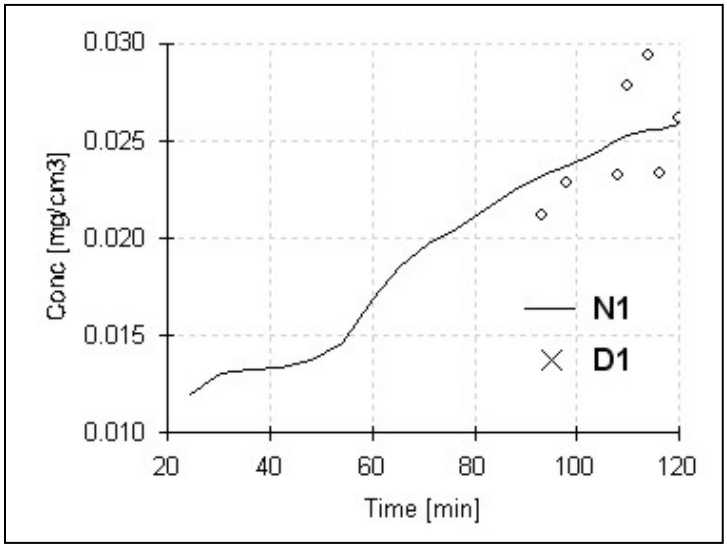

Figure 3. Diagram of concentration in time. Legend: - N1-predicted curve at 40 cm depth using HYDRUS 1D, x D1-observed values from suction lysimeter.

4. Conclusions

Longitudinal dispersivity was inversely estimated using data gained by a field experiment in Fluvisol using the HYDRUS-1D model. Calcium chloride was used as a conservative tracer. The percolating solution was sampled by a suction lysimeter installed at a depth of 40 cm. Monitoring equipment was used for input parameters and calculation of dispersivity. Pore water velocities were calculated using Darcy's law. Both velocities were used for estimation of dispersivity. The HYDRUS 1D model gave a dispersivity value of 2 cm. Due to collapse of the pedological pit during application of the tracer, estimation of longitudinal dispersivity was performed on an incomplete data set. The value of dispersivity is therefore doubtful.

Acknowledgments
The work was carried out as part of the GENESIS project on groundwater systems (http://www.thegenesisproject.eu) financed by the European Commission 7FP contract 226536 and Croatian Ministry of Science, Education and Sport (no. 195-1953068-2704 to G.D.).

References

Akhtar, M. S., T. S. Steenhuis, B. K. Richards, and M. B. McBride, Chloride and Lithium transport in large arrays of undisturbed silt loam and sandy loam soil columns, *Vadose Zone Journal*, *2,* 715–727, 2003.

Dişli, E., Batch and column experiments to support heavy metals (Cu, Zn and Mn) transport modeling in alluvial sediments between the Mogan Lake and the Eymir Lake Gölbaşi, Ankara, *Ground Water Monitoring & Remediation 30*(3), 125–139, 2010.

FAO, World reference base for soil resources 2006, A framework for international classification, correlation and communication, *World Soil Resources Reports No. 103*, FAO, Rome, 2006.

Fonseca, B., A. Teixeira, H. Figueiredo, and T. Tavares, Modelling of the Cr(VI) transport in typical soils of the North of Portugal, *Journal of Hazardous Materials*, *167*, 756–762, 2009.

Heilig, A., T. S. Steenhuis, M. T. Walter, S. J. Herbert, Funneled flow mechanisms in layered soil: field investigations, *Journal of Hydrology*, *279*, 210–223, 2003.

Jacques, D., J. Šimůnek, A. Timmerman, and J. Feyen, Calibration of Richards' and convection–dispersion equations to field–scale water flow and solute transport under rainfall conditions, *Journal of Hydrology*, *259*, 15–31, 2002.

Jacques, D., C. Smith, J. Šimůnek, and D. Smiles, Inverse optimization of hydraulic, solute transport, and cation exchange parameters using HP1 and UCODE to simulate cation exchange, *Journal of contaminant Hydrology*, *142-143*, 109-125, 2012.

Moradi, A., K. C. Abbaspour, and M. Afyuni, Modelling field-scale cadmium transport below the root zone of a sewage sludge amended soil in an arid region in Central Iran, *Journal of Contaminant Hydrology*, *79*, 187– 206, 2005.

Richards, L. A., Capillary conduction of liquids through porous mediums, *Physics*, *1*(5), 318–333, 1931.

Ružičić, S., M. Mileusnić, and K. Posavec, Building conceptual and mathematical model for water flow and solute transport in the unsaturated zone at Kosnica Site, *Mining-Geological-Petroleum Engineering Bulletin*, *25*, 21-31, 2012.

Schaap, M. G., F. J. Leij, and M. Th. van Genuchten, Rosetta: A computer program for estimating soil hydraulic parameters with hierarchical pedotransfer functions, *Journal of Hydrology*, *251*, 163-176, 2001.

Seuntjens, P., D. Mallants, N. Toride, C. Cornelis, and P. Geuzens, Grid lysimeter study of steady state chloride transport in two Spodosol types using TDR and wick samplers, *Journal of Contaminant Hydrology*, *51*, 13–39, 2001.

Severino, G., A. Comegna, A. Coppola, A. Sommella, and A. Santini, Stochastic analysis of a field-scale unsaturated transport experiment, *Advances in Water Resources*, *33,* 1188–1198, 2010.

Stumpp, C., G. Nützmann, S. Maciejewski, and P. Maloszewski, A comparative modeling study of a dual tracer experiment in a large lysimeter under atmospheric conditions, *Journal of Hydrology*, *375*, 566–577, 2009.

Šimůnek, J., M. Th. van Genuchten, M. Šejna, N. Toride, and F. J. Leij, The STANMOD computer software for evaluating solute transport in porous media using analytical solutions of convection-dispersion equation, Version 1.0, and 2.0, *IGWMC-TPS-71*, International Ground Water Modeling Center, Colorado School of Mines, Golden, Colorado, 32 pp., 1999.

Šimůnek, J., D. Jacques, J. W. Hopmans, M. Inoue, M. Flury, and M. Th. van Genuchten, Solute transport during variably–saturated flow – Inverse methods. Chapter 6.6 in *Methods of Soil Analysis: Part 1. Physical Methods*, 1435–1449, 3rd ed., J. H. Dane and G. C. Topp (eds.), Madison, Wisc., SSSA, 2002.

Šimůnek, J., M. Šejna, H. Saito, M. Sakai, and M. Th. van Genuchten, The HYDRUS-1D Software Package for Simulating the Movement of Water, Heat, and Multiple Solutes in Variably Saturated Media, Version 4.0, *Hydrus Software Series 3*, Department of Environmental Sciences, University of California Riverside, Riverside, CA, USA, pp. 315, 2008.

Toride N., F. J. Leij, and M. Th. van Genuchten, The CXTFIT code for estimating transport parameters from laboratory or field tracer experiments, Version 2.0, *Research Report No. 137*, U.S. Salinity Laboratory, USDA, Riverside, CA, 1999.

van Genuchten, M. Th., A closed form equation for predicting the hydraulic conductivity of unsaturated soils, *Soil Science Society of America Journal*, *44*(5), 892–898, 1980.

Zhang, S., M. Jin, and Q. Sun, Experiment and numerical simulation on transportation of ammonia nitrogen in saturated soil column with steady flow, *Procedia Environmental Sciences*, *10*, 1327 – 1332, 2011.

Wang, X., L. Zhao, X. Liu, A. Lili, and Y. Zhang, Temperature effect on the transport of nitrate and ammonium ions in a loose-pore geothermal reservoir, *Journal of Geochemical Exploration*, *124*, 59-66, 2013.

Predicting the Impact of Treated Wastewater Infiltration on Groundwater Recharge by Simulating Reactive Transport in the Unsaturated Zone

Cristina Sandhu, Thomas Fichtner, Issa Hasan, and Peter-Wolfgang Gräber

Faculty of Environmental Sciences, Institute for Waste Management and Contaminated Sites Treatment
Dresden University of Technology – Pratzschwitzer Straße 15, 01796 Pirna – Germany,
cristina.sandhu@tu-dresden.de,thomas.fichtner@tu-dresden.de,issa.hasan@tu-dresden.de,peter-wolfgang.graeber@tu-dresden.de

Abstract

Due to demographic increase and climate change, it is necessary to look at alternative ways to replenish groundwater resources. One possibility is to infiltrate treated wastewater directly into the ground and use the filtering capacity of the soil. To prevent the pollution of groundwater, one must ensure that not only the quality of treated wastewater is suitable for infiltration, but also that the soil has good filtration capacities. This is a sustainable alternative to groundwater recharge if natural precipitation is insufficient, especially in semi-arid and arid areas. This paper presents the results of a project investigating the infiltration of treated wastewater from small-scale wastewater treatment plants (WTPs) into the unsaturated soil zone. These small-scale WTPs use a preliminary sedimentation, followed by a biofilm reactor and secondary treatment. Consequently, the treated wastewater has a high quality and is therefore suitable for direct infiltration into the unsaturated soil zone. To forecast the transport and the transformation processes and the concentration of infiltrated treated wastewater into the unsaturated zone, different scenarios were modeled with the help of the software, PCSiWaPro®. For this purpose, the software tool PCSiWaPro® was further enhanced to include wastewater transport and transformation as well as the small-scale sewage treatment plants classes. To account for the relevant biogeochemical reactions, PCSiWaPro® was coupled to the geochemical software PHREEQC. To validate the enhanced simulation software, column experiments were conducted. The results from column experiments and from modeling have improved the understanding of the complex processes in the unsaturated zone and its relationship with the saturated zone. It is now possible to efficiently design and operate small-scale wastewater treatment plants and to predict groundwater recharge.

1. Introduction

According to the European Water Frame Directive (EU-WFD, 2000), all the member states must achieve a good chemical and ecological status for all water bodies until 2015. The EU-WFD establishes quality criteria that takes into account the local characteristics of the groundwater body and its chemical status and introduces measures to prevent or limit its pollution. As a large proportion of the groundwater recharge comes from the treated wastewater, important steps in collecting and disposing it have been taken. But there is still significant groundwater recharge originating from small-scale wastewater treatment plants (WTPs). Until now, the treated wastewater has been directly discharged via drainage pipes. Since both discharge methods are expensive, the concept of infiltrating the treated wastewater directly into the ground for small-scale individual systems is being investigated.

The main objective of this work is to develop a software tool for simulating the transport and transformation of contaminants in variable saturated porous media coming from WTPs, based on laboratory and field experiments. Thus, the results of the modeling and the experiments can further improve the designs of small-scale WTPs, increase their operational efficiency, and recharge groundwater.

2. Modeling Unsaturated Zone Processes

2.1. Theoretical Background

The water flow process in variably-saturated porous media can be described using the Richards equation (Richards, 1931), which considers both unsaturated and saturated regions simultaneously:

$$\frac{\partial \theta}{\partial t} = \frac{\partial}{\partial x_i}\left[K\left(K_{ij}^{A} \frac{\partial h}{\partial x_j} + K_{iz}^{A} \right)\right] - S \tag{1}$$

where θ is the volumetric water content [L^3L^{-3}], h is the capillary pressure head [L], x_i (i=1, 2) are the spatial coordinates [L], t is the time [T], K_{ij}^{A} are components of a dimensionless anisotropy tensor K^A, K is the unsaturated hydraulic conductivity function [LT^{-1}], and S is a sink/source term [T^{-1}], which is considered here as the amount of water removed by roots of plants. Since the capillary pressure head is a dependent variable and both the hydraulic conductivity K and the volumetric water content θ are dependent on the pressure head, the Richards equation is highly non-linear. Therefore, the solution process has to be conducted in an iterative manner. The unsaturated soil hydraulic properties are described by using the equations developed by van Genuchten (1980) and Mualem (1976). The water content in an unsaturated porous medium depends on the capillary pressure head in the pores, given by:

$$\theta(h_c) = \theta_s + \frac{\theta_s - \theta_r}{\left[1 + (\alpha \cdot h_c)^n\right]^{1-\frac{1}{n}}} \tag{2}$$

in which θ_r and θ_s denote the residual and saturated water contents, and the exponent n is the van Genuchten parameter.

The partial differential equation governing two-dimensional chemical transport during transient water flow in a variably-saturated porous media is given by:

$$\frac{\partial \theta c}{\partial t} + \frac{\partial \rho s}{\partial t} = \frac{\partial}{\partial x_i}\left(\theta D_{ij} \frac{\partial c}{\partial x_j} \right) - \frac{\partial q_i c}{\partial x_i} + \mu_w \theta c + \mu_s \rho s + \gamma_w \theta + \gamma_s \rho - S c_s \tag{3}$$

where c is the solute concentration [ML^{-3}], s is the sorbed concentration [ML^{-3}], q_i is the i^{th} component of the volumetric flux [LT^{-1}], and μ_w and μ_s are the first-order rate constants for

solutes in the liquid and solid phases [T^{-1}], respectively; γ_w and γ_s are zero-rate constants for the liquid [$ML^{-3}T^{-1}$] and the solid phases [T^{-1}]; ρ is the bulk density [ML^{-3}], S is the sink/source term in the water flow equation (1), c_s is the concentration of the sink/source term [ML^{-3}], and D_{ij} is the dispersion coefficient tensor [L^2T^{-1}]. The four zero-and first-order rate constants may be used to represent biodegradation, volatilization, precipitation and radioactive decay.

2.2. Software Tool PCSiWaPro®

The PCSiWaPro® is a software tool developed at the TU Dresden. It is based on a soil physical model implemented in the numerical code SWMS_2D, developed by Šimůnek et al., (1994). The PCSiWaPro® can simulate 1D and 2D vertical plane or axially symmetrical flow and transport processes in the unsaturated zone under steady-state and transient conditions. It numerically solves the Richards equation (1) and the convection-dispersion equation, using the finite elements method. Moreover, it has a flexible choice of boundary conditions, the consideration of hysteresis-like processes in the unsaturated zone, and a parameter identification algorithm. It considers sorption and zero- and first-order degradation. To account for hydrological conditions (e.g., precipitation, evapotranspiration, surface runoff, root water uptake), PCSiWaPro® is coupled with a Weather Generator module (WettGen) (Nitsch et al., 2007, Blankenburg, 2008).

As this numerical tool is intended for application by enterprises that investigate contaminant transport in groundwater and the degree of pollution of different contaminated sites, there is substantial demand to develop a complex software tool that covers all areas of interest (i.e., surface, unsaturated and saturated zone). Therefore, PCSiWaPro® is also coupled to the geochemical software PHREEQC (Appelo et al., 2005) to consider the relevant bio-geochemical reactions in the unsaturated zone (inter-dependent complexation reactions, cation exchange, precipitation-dissolution, volatilization, redox-reactions), and to the groundwater flow and contaminant transport simulation tool model PCGEOFIM (Boy et al., 2005) shown in Figure 1.

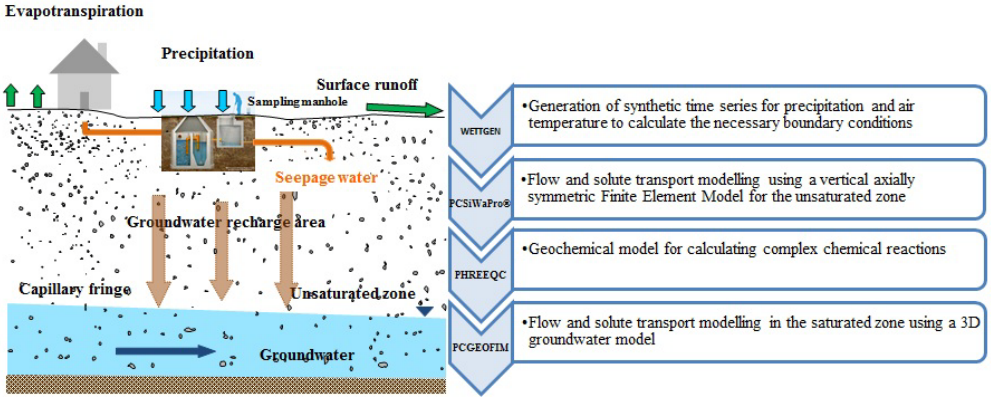

Figure 1. Conceptualization of coupled numerical codes for simulating surface, unsaturated and saturated zone processes.

2.3. Software Tool PHREEQC

The well known bio-geochemical program, PHREEQC (Parkhurst, 1995), is based on an ion-association aqueous model and is capable of a variety of chemical equilibrium reactions, kinetically determined reactions, solution and precipitation processes, and ion exchange

processes. In several databases, the chemical properties of the individual substances and the possible reaction equations are stored. In a control file, the definition of the solution and the resultant chemistry of the solution are calculated.

2.4. Coupling PCSiWaPro® and PHREEQC

PCSiWaPro® accounts for sorption, retardation, and zero- and first-order degree degradation, and in the case of wastewater, it is also necessary to consider biogeochemical reactions. The well known geochemical model PHREEQC was chosen to be coupled with PCSiWaPro® due to its modular structure and extensive geochemical databases.

While PCSiWaPro® simulates the transport of water and wastewater in the unsaturated soil zone, PHREEQC focuses on the bio-geochemical reactions. The simulation tool has to consider different soil types, small-scale sewage treatment plant classes, as well as a mixture of contaminants and their inter-relations. Therefore, a set of databases for soil types, typical organic and inorganic wastewater contaminants, sewage treatment plant classes, and boundary conditions have all been further implemented to make the tool more user-friendly (Figure 2).

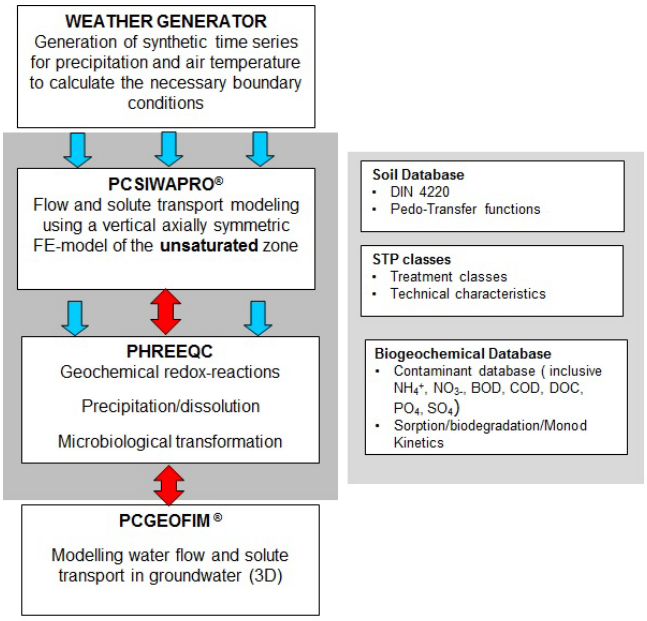

Figure 2. Coupling of numerical simulation codes and databases.

Figure 3 illustrates the program structure of the coupling between the two numerical models. In the discretized time domain of the numerical model, the three simultaneous and dependent processes of flow, transport and reaction are separated using a non-iterative splitting approach where Δt is the length of the coupling step. The coupling time step is further reduced in the case of geochemical reactions if necessary. As a result of decoupling, concentrations are assumed independent of reactions in the solute transport calculations. Likewise, the liquid phase saturation is considered independent of concentrations and reactions during flow calculation. During the geochemical step, performed by PHREEQC, the solution composition is considered independent of both flow and transport.

The coupling scheme between the PCSiWaPro® and PHREEQC takes places online, which means that for each time step, the codes exchange the following data:

1. Simulation of the water flow for the calculation of the convective transport performed by PCSiWaPro® (independent of concentrations and reactions)
2. Simulation of solute transport for each individual substance performed by PCSiWaPro® (independent of reactions)
3. Calculation of the bio-geochemical equilibrium and kinetics reactions for each node performed by PHREEQC (independent of flow and transport). The changes in the concentrations after the reactive step are the new initial concentrations for the next transport time step calculation. The concentrations in the immobile phase remain in the corresponding node and play no role for the mass transfer. A maximum one-day time step for the reaction is necessary to depict a realistic illustration of interactions between water and nutrient budgets.

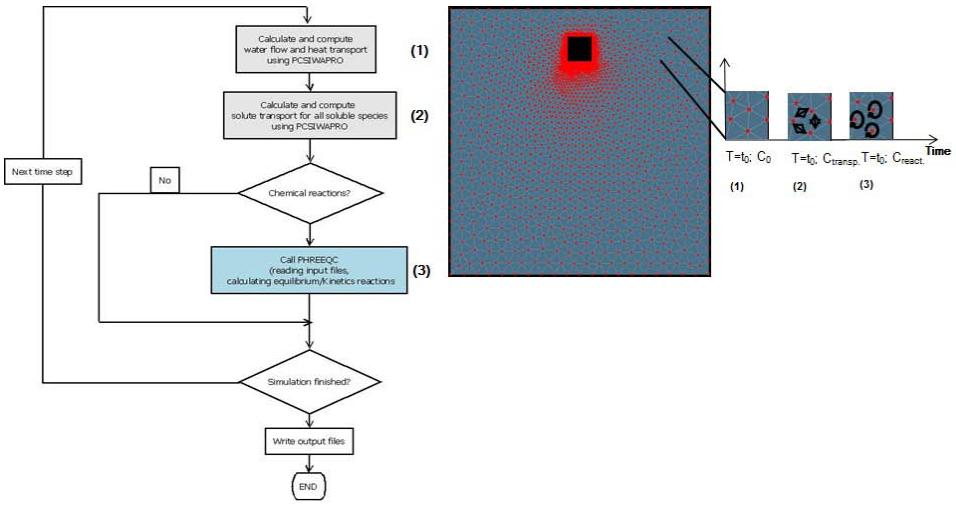

Figure 3. Coupling between the PCSiWaPro® and PHREEQC in a 2D cross-section.

3. Validation Through Column Experiments

As the software PCSiWaPro® is further developed to include small–scale WTPs, it is necessary to validate the results of the numerical simulations. Accordingly, a series of column experiments were performed in the laboratory to answer following:

- Which soil has the best natural attenuation capacity in order to ensure a good seepage water quality?
- How does the treated wastewater quality influence the infiltration capacity of soils (clogging aspect)?
- How do the infiltration rate characteristics (continuous/pulse, amount) influence the infiltration and natural attenuation capacity?
- Does the thickness of the unsaturated zone have a significant impact on the residence time of the seepage water and the natural attenuation capacity?

The experiments consisted of three columns, each with a different soil type described in Table 1. The in situ soil from the case study sites of Kleinopitz and Biehain in Saxony (Germany) was used for the column experiments. The 150 cm long columns were made of Plexiglas having an internal diameter of 15 cm. The treated effluent was infiltrated in the upper part of the column with the help of a peristaltic pump. Infiltration occurred eleven times daily, according to human diurnal water consumption. To determine the soil water potential in the column, two tensiometers were installed at different heights. Moreover, to have on overview of the temperature, a soil temperature sensor was attached. The measured data was directly recorded on a data logger.

Table 1. Soil parameters and initial conditions.

Soil type	van Genuchten parameters				Infiltration rate [$m^3 d^{-1}$]	Precipitation [mm y^{-1}]	Duration of experiments [d]
	θ_s [$cm^3 cm^{-3}$]	θ_r [$cm^3 cm^{-3}$]	α [cm^{-1}]	n [-]			
Coarse sand with gravel (KRB23)	0.38	0	0.15	1.34	0.1	676	365
Medium silty sand (KRB10)	0.38	0	0.2	1.23	0.1	676	365
Medium sandy silt (B5)	0.38	0	0.262	1.35	0.1	676	185

The quality of the inflow wastewater into the column and outflow was determined and compared to the legal limit for drinking water according to the German Drinking Water Directive (TWO: Die Trinkwasserverordnung, 2012) as listed in Table 2.

Table 2. Quality of some investigated parameters/contaminants and their legal limit.

	pH	COD	DOC	NO_2^-- N	NO_3^--N	NH_4^+-N	TKN	P_{ges}	E.coli
Unit	[-]	[mg L^{-1}]	[mg L^{-1}]	[mg L^{-1}]	[mg L^{-1}]	[mg L^{-1}]	[mg L^{-1}]	[mg L^{-1}]	/100 ml
Concentration in inflow	65	90	18.5	102	57.6	15.2	16.5	19.2	269
Legal limit TWO, 2012)	6.5-9.5	-	-	0.15	11.3	0.39	-		0

In the column with medium sandy silt (red line in Figure 4–left), a complete reduction of ammonium could be observed during the experimental duration of 185 days. However, an increase in the nitrate concentration was observed due to nitrification (Figure 4–right). The nitrate concentrations in the effluent were about 20 mg L^{-1} higher than the concentrations in the infiltrated wastewater. In the medium silty sand, a complete reduction of ammonium could be observed after 250 days. This result was achieved by decreasing the amount of infiltrated treated wastewater. An increase of nitrate could also be registered for this time. The reduction of the ammonium in the coarse sand with gravel was only between 25% and 50% and subject to major fluctuations. Due to the sufficient oxygen present in the soil column, denitrification was not observed.

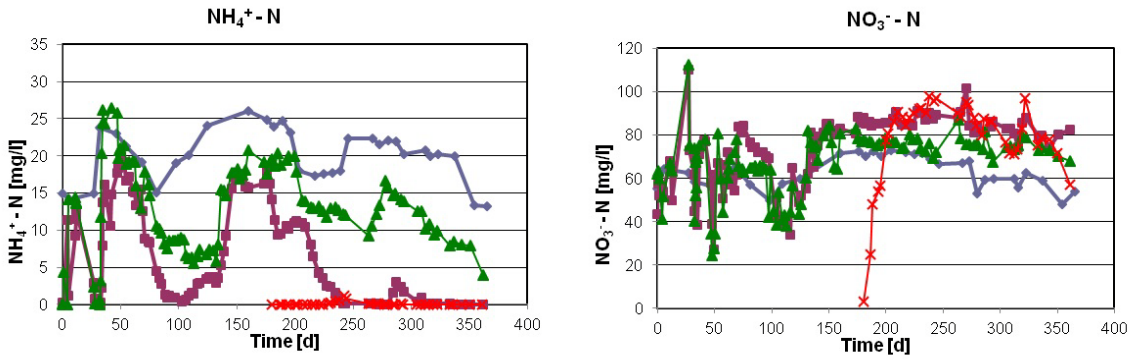

Figure 4. Ammonium Nitrogen (left) and Nitrate-Nitrogen (right) behavior in different soils (Blue- inflow; Green–coarse sand with gravel; Purple–medium silty sand; Red–medium sandy silt)

The reduction of COD and removal of DOC, TKN, and Total Phosphorous is presented in Table 3. It is observed that the highest removal of all parameters occurs in medium sandy silt. A higher removal was observed for COD and DOC in coarse sand with gravel, compared to medium silty sand. On the other hand a higher removal was observed for TKN and Total Phosphorous for medium silty sand, compared to coarse sand with gravel.

Table 3. Removal of COD, DOC, TKN, and Total Phosphorous observed during column experiments.

Soil class	COD	DOC	TKN	P_{Total}
	[%]	[%]	[%]	[%]
Coarse sand with gravel (KRB23)	70	40	30	0
Medium silty sand (KRB10)	50	20	70	75
Medium sandy silt (B5)	90	75	80	100

The reason for the low removal efficiency in the coarse sand with gravel and medium silty sand was the prevalent, non–optimal environmental conditions for the occurrence of biological degradation in the columns (low pH–value due to lower buffering capacity of soil). Another reason for low removal efficiency in the coarse sand with gravel and medium silty sand was the short residence time of the treated wastewater in the soil caused by the higher hydraulic conductivity. However, in the medium sandy silt, ideal conditions are present, as can be demonstrated by the highest removal of the concentrations of the infiltrated wastewater. Although the medium silty sand and the medium sandy silt have similar soil physical properties as shown in Table 1, the natural attenuation is more efficient in medium sandy silt due to the higher portion of fine grained silt compared to medium silty sand. Consequently, the finer grained soil type provides a larger specific surface area for the geochemical processes to occur.

4. Example Application

The PCSiWaPro® software was applied to the Kleinopitz case study site to predict the on-site transport of treated wastewater. A 2D numerical model was prepared (Figure 5) using input

parameters and data (Table 1) obtained from the field and laboratory experiments to simulate the seepage of the treated effluent from small–scale WTPs (Tomoda, 2012). The upper boundary condition was the atmosphere, while the lower boundary represents the groundwater table.

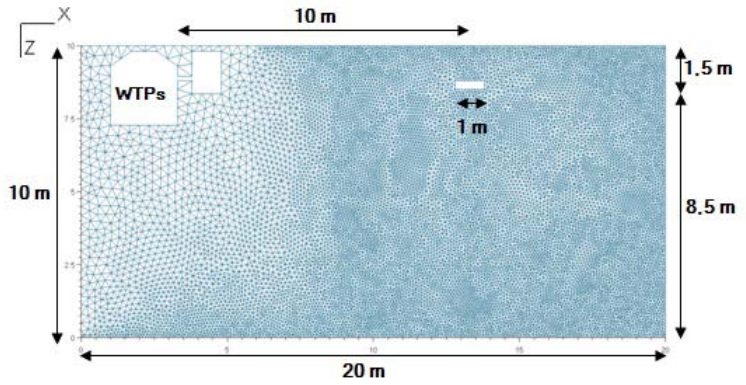

Figure 5. Graphical representation of the numerical model.

Several questions needed to be answered before performing a solute transport and reactions simulations, the most important being:

- Does the thickness of the unsaturated zone significantly impact the residence time of the wastewater and natural attenuation capacity?
- Where should the infiltration area be located to prevent contamination of any possible drinking water well?
- Which soil hydraulic parameters influence the seepage of the treated effluent?

The results in Figure 6 show the groundwater recharge from different scenarios, where the groundwater table depths of 10 m, 6.5 m, and 3.5 m have been used. Two different infiltration rates of 0.1 and 0.3 m^3d^{-1} for three different soil types were applied. When an infiltration rate of Q_{in} =0.1 m^3d^{-1} is applied (Figure 6–left) to all three different groundwater table depths, the travel time is always fastest for medium sand (compared to medium silty sand and medium sandy silt). As expected, the minimum travel time of 25 days to a GW table depth of 10 m is shortest for medium sand, compared to 27 and 33 days for medium silty sand and medium sandy silt, respectively. Irrespective of the depth of the GW table, a maximum groundwater recharge of 0.1 m^3d^{-1} is eventually attained for an equal infiltration rate of 0.1 m^3d^{-1}.

In case of medium sand and medium silty sand, when an infiltration rate of 0.3 m^3d^{-1} is applied, the minimum travel times are similar for both soil types. Thus the minimum travel time is 2, 6, and 10 days for a GW table depth of 3.5, 6.5 and 10 m, respectively. An eventual equivalent groundwater recharge rate (compared to the infiltration rate) of 0.3 m^3d^{-1} is also attained for these soil types but at a relatively faster rate compared to an infiltration rate of 0.1 m^3d^{-1} over a 60 day simulation period. The short travel time of water through the unsaturated zone to the groundwater table implies insufficient time for geochemical reactions to optimally occur. Only the medium sandy silt, with longer travel times, lower groundwater recharge rates, and greater depths to the groundwater table, could be a good candidate for infiltrating treated effluent from small scale WTPs, as also demonstrated by the column experiments.

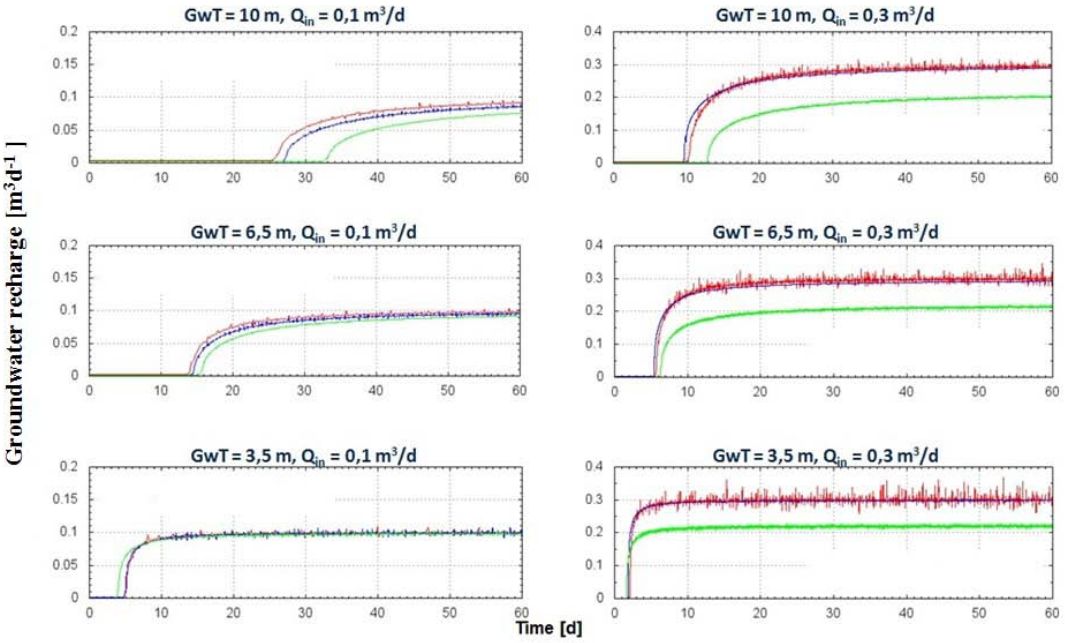

Figure 6. Groundwater recharge for different groundwater tables (GwT) and infiltration rates (Q_{in}) (blue–medium silty sand green–medium sandy silt, red–medium sand.

5. Conclusions

This paper presented a coupled finite element model that uses PCSiWaPro® for simulating water and solute transport in an unsaturated zone and the geochemical model PHREEQC for its capability of simulating chemical equilibrium and non–equilibrium reactions. The numerical model was validated by column experiments, where different soil types, infiltration rates and effluent qualities were considered. From the column experiments and the numerical simulation, one can conclude that medium sandy silt is the best suited soil type for infiltrating the treated effluent from small–scale WTPs because it has the longest travel time, and therefore sufficient time for bio–chemical reactions to take place. However due to the shallow depth to the GW table (up to 10 m), it is important to limit the infiltration rates to 0.1 $m^3\ d^{-1}$ or less.

The most difficult task in simulating the solute transport in unsaturated soils is the effective characterization and quantification of the effects of the chemical reactions on transport processes. In this context, one of the advantages of coupling is that PCSiWaPro® completely integrates the PHREEQC geochemical model, and thereby allows the user access to a large range of chemical reactions. It provides the ability to include the effects of a large number of different types of chemical processes on solution compositions on a per time–step basis. Another advantage is the extensive databases, which make the numerical PCSiWaPro® code a user-friendly software tool, especially when the necessary data collection cannot be performed through laboratory and field investigations. To demonstrate the robustness of the coupling scheme between the codes, the numerical software still needs to be extensively verified for more complex systems.

Acknowledgements
The authors thank the German Federal Ministry of Education and Research (BMBF) for the financial support of the research project "*RESS-199-016 ESEK –Ganzheitliches System zur Errichtung von Kleinkläranlagen; TP 3: Entwicklung eines Entscheidungshilfesystem und Validierung durch Laborversuche*" ("Integrated system for designing and operating a small-scale sewage treatment plant – Development of an expert system and validation using laboratory experiments"), whose results were presented in this paper.

References

Appelo, C. A. J., and D. Posma, *Geochemistry, Groundwater and Pollution*, CRC Press, Taylor & Francis Group, 2005.

Blankenburg, R., and O. Kemmesis, SiWaPro DSS a computer aided leaching forecast tool, *ConSoil Conference Abstract*, 2008.

Boy, S. and D. Sames, *PCGEOFIM®, Anwenderdokumentation*, Ingenieurbüro für Grundwasser Leipzig GmbH, (in German, internal use only), 2005.

EU Directive 2000/60/EC of the European Parliament and the Council of 23 October 2000 establishing a framework for Community action in the field of water policy, 2000.

Gräber, P.-W., et al., SiWaPro DSS, Beratungssystem zur Simulation von Prozessen der unterirdischen Zonen, *Simulation in Umwelt- und Geowissenschaften*, Buchverf, Wittmann Jochen und Müller Mike, Hrsg. Müller Mike. - Leipzig, Shaker Verlag, ISBN 3-8322-5132-4, (in German), 2006.

Jacques, D., J. Šimůnek, D. Mallants, and M. Th. van Genuchten, Modeling coupled hydrogeological and chemical processes in the vadose zone: a case study of long-term uranium transport following mineral P-fertilization, *Vadose Zone Journal*, *7*(2), 698-711, 2008.

Langergraber, G., and J. Šimůnek, Reactive transport modeling of subsurface flow constructed wetlands, *Vadose Zone Journal*, *11*(2), doi:10.2136/vzj2011.0104, 14 pp., 2012.

Mualem, Y, A new model for predicting the hydraulic conductivity of unsaturated porous media, *Water Resources Research*, *12*(3), 513-522, 1976.

Nitsch, B., and P.-W. Gräber, Anwendung synthetischer Niederschlagszeitreihen bei der Strömungs-modellierung der ungesättigten Bodenzone, *Simulation in Umwelt- und Geowissenschaften,* Workshop Berlin, Shaker Verlag, Bereich Umweltinformatik, (in German), 2007.

Parkhurst, D. L., and C. A. J. Appelo, User's guide to PHREEQ C (Version 2) – A computer program for speciation, batch-reaction, one-dimensional transport and inverse geochemical calculations, *Water-Resources Investigations*, *Report 99–4259*, Denver, Co, USA, 312 pp., 1999.

Radcliffe, D., and J. Šimůnek, *Soil Physics with HYDRUS: Modeling and Applications*, CRC Press, Taylor & Francis Group, Boca Raton, FL, ISBN: 978-1-4200-7380-5, pp. 373, 2010.

Richards, L. A., Capillary conduction of liquids through porous mediums, *Physics*, *1*(5), 318–333, 1931.

Šimůnek, J., T. Vogel, and M. Th. van Genuchten, The SWMS-2D code for simulating water flow and solute transport in two-dimensional variably saturated media, *Research Report No. 132*, U.S. Salinity Laboratory, USDA, ARS, Riverside, CA, 1994.

Šimůnek, J., and M. Th. van Genuchten, Modeling nonequilibrium flow and transport processes using HYDRUS, *Vadose Zone Journal*, *7*(2), 782-797, 2008.

Šimůnek, J., M. Th. van Genuchten, and M. Šejna, Development and applications of the HYDRUS and STANMOD software packages, and related codes, *Vadose Zone Journa*l, *7*(2), 587-600, 2008.

Tomoda, N., Sensitivitätssanalyse mittels Softwaretool PCSiWaPro® von hydrogeologischen und hydrologischen Kenngrößen bei Versickerung von gereinigten Abwassers aus Kleinkläranlagen (Bachelor Thesis, in German, internal use only), 2012.

Die Trinkwasserverordnung: Verordnung über die Qualität von Wasser für den menschlichen Gebrauch, Art. 1 ÄndVO vom 5. Dezember 2012, BGBl. I S. 2562, 2012.

van Genuchten, M. Th., A closed-form equation for predicting the hydraulic conductivity of unsaturated soils, *Soil Science Society of America Journal*, *44*, 892-898, 1980.

Temporal Variations of Soil Hydraulic Properties and its Effect on Soil Water Simulations

Andreas Schwen[1], Gernot Bodner[2], and Willibald Loiskandl[1]

[1] *Institute of Hydraulics and Rural Water Management, University of Natural Resources and Life Sciences (BOKU), Vienna, Austria; andreas.schwen@boku.ac.at*
[2] *Institute of Agronomy and Plant Breeding, University of Natural Resources and Life Sciences (BOKU), Vienna, Austria*

Abstract

Simulating water dynamics in the soil compartment close below the surface is challenging since this part of the soil profile inhibits large temporal dynamics as a response to climate and crop growth. For accurate simulations the soil hydraulic properties have to be properly known. These properties may be subject to temporal changes as a response to both tillage and natural impact factors. The impact of different tillage techniques – conventional (CT), reduced (RT), and no-tillage (NT) – on the soil hydraulic properties and their temporal dynamics were observed by repeated experiments using tension infiltrometers. The experimental data was analyzed in terms of the near-saturated hydraulic conductivity, inversely estimated parameters of the van Genuchten/Mualem (VGM) model, and the water-conducting porosity. In a second step, the inversely estimated VGM parameters were incorporated into a soil water simulation. By using temporally variable versus constant sets of VGM parameters, the impact on soil water balance components was tested. Simulated water dynamics were compared to observed data in terms of the soil water content and water storage in the near-surface soil profile (0-30 cm). The results show that the near-saturated hydraulic conductivity was in the order CT > RT > NT, with larger treatment-induced differences where water flow is dominated by mesopores. The VGM model parameter αVG was in the order CT < RT < NT, with high temporal variations under CT and RT, whereas the parameter n was hardly affected. The results give indirect evidence that NT leads to greater connectivity and smaller tortuosity of macropores, possibly due to biological activity and a better established soil structure. Simulations with temporally constant hydraulic parameters led to underestimations of soil water dynamics in winter and early spring and overestimations during late spring and summer. The use of temporally variable hydraulic parameters significantly improved simulation performance for all treatments, resulting in average relative errors below 13%. Since simulation results agreed with observed water dynamics in two seasons, the applicability of inversely estimated hydraulic properties for soil water simulations was demonstrated. Our results also showed that simulations addressing applied questions in agricultural water management can be improved by time-variable hydraulic parameters.

1. Introduction

For many applied questions in the fields of crop production and agronomy, soil water dynamics are of fundamental importance. Modeling can be a valuable tool to optimize its management (Roger-Estrade et al., 2009). Such soil water modeling requires an accurate description of soil hydraulic properties, i.e. the soil water retention function $\theta(h)$ and the hydraulic conductivity function $K(h)$. Generally, these constitutive functions are assumed to be unchanged over time in most simulation studies. However, there is extensive empirical evidence that soil hydraulic properties are subject to temporal changes particularly in the near-saturated range where soil structure essentially influences water flow characteristics (Daraghmeh et al., 2008; Or et al., 2000). The structure of soil top layers is especially subject to changes over time, caused by wetting/drying cycles, biological activity, and agricultural operations (Leij et al., 2002; Mubarak et al., 2009). Soil tillage and management affect the hydraulic properties with consequences for the storage and movement of water, nutrients and

pollutants, and for plant growth (Strudley et al., 2008; Xu and Mermoud, 2003). The temporal variability of hydraulic properties can even exceed differences induced by crops, tillage, or land use (Alletto and Coquet, 2009; Bodner et al., 2008; Bormann and Klaassen, 2008; Hu et al., 2009; Zhou et al., 2008).

Compared to deeper soil layers, soil moisture close to the surface (0-30 cm) is subject to rapid changes as response to rainfall, infiltration, evaporation, and root water-uptake. Despite its importance for the supply of water and nutrients for crops, simulation of this highly dynamic soil compartment is difficult and requires adequate sets of hydraulic parameters (Šimůnek et al., 2003). For modeling nutrient or contaminant transport and for the assessment of different tillage methods, soil water simulations should be introduced that account for time-variable hydraulic properties (Mubarak et al., 2009; Or et al., 2000). However, few studies have addressed this task. For instance, Or et al. (2000) introduced a model that describes temporal changes of the soil retention properties after tillage based on the pore-size distribution. Recently, Schwärzel et al. (2011) used the model to describe landuse-induced changes of the retention properties, but the model has not been applied to a more complex time series of measured hydraulic parameters.

To capture temporal variations in the soil hydraulic properties, suitable measurement methods have to be applied. As most of the temporal changes are expected to occur in the structural pores, due to changes in different groups of macro- and mesopores, field methods are preferable to laboratory methods (Angulo-Jaramillo et al., 2000; Hu et al., 2009; Yoon et al., 2007). To determine the near-saturated hydraulic properties of agricultural soils directly in the field, tension infiltrometry has become a commonly used method (Angulo-Jaramillo et al., 1997; Messing and Jarvis, 1993; Reynolds et al., 1995). Before now, hardly any study assessed the applicability of inversely estimated parameters in soil water simulations.

The main hypothesis underlying the presented study was that soil water simulations can be improved by accounting for temporal changes of near-surface soil hydraulic properties. Thus, the objectives of this study were 1) to capture temporal changes of soil hydraulic properties by repeated tension infiltrometer measurements, 2) to implement time-variable soil hydraulic properties in a soil water simulation. This study also aims to assess the feasibility of inversely estimated hydraulic parameters in soil water simulations. We acknowledge that this proceedings paper has been subject to previous publications (Schwen et al., 2011ab).

2. Materials and Methods

2.1. Experimental Site

Measurements were obtained on an arable field near Raasdorf, Lower Austria (48°N16°35′E). Climatic data have been recorded at the site since 1998 (Figure 1). The reference evapotranspiration ET_0 was calculated using the Penman-Monteith equation. The site has a mean annual precipitation R of 546 mm, a mean temperature of 9.8 °C, a mean relative humidity of 75%, and an annual reference evapotranspiration ET_0 of 912 mm. A field trial was established in 1997 to assess the following soil cultivation techniques: 1) Conventional tillage (CT) with moldboard ploughing and seedbed preparation using a harrow prior crop seeding; 2) Reduced tillage (RT) with a chisel plough to 10 cm for seedbed preparation; and 3) No-tillage (NT) using direct seeding technique.

The soil can be classified as Chernozem in the WRB (IUSS, 2007). The humous A-horizon (0-30 cm) is followed by an AC-horizon (30-60 cm) over the mature silty sediments (C-horizon, >60 cm). Due to particle size analysis (Table 1), the texture throughout the profile can be classified as silt loam according to the FAO classification (FAO, 1990). The organic carbon content was 24 g kg^{-1} in the topsoil. In the two seasons analyzed for this study (2008/09 and 2009/10) the site was cropped with winter wheat (*Triticum aestivum* L.) in mid October and harvested in mid July of the following year (Figure 1).

Soil water content in the field was continuously measured over two consecutive seasons using capacitance moisture sensors (C-Probe, Adcon Telemetry GmbH, Austria). For each treatment, three replicate probes were installed in depths of 10, 20, 40, 60, and 90 cm. The measurement interval was 15 min, and data was averaged to daily values. The probes were installed after seeding in November and removed from the field prior to harvest in July in both analyzed seasons. The water storage in the soil profile to a depth of 0.30 m *S* was derived from the water content measurement.

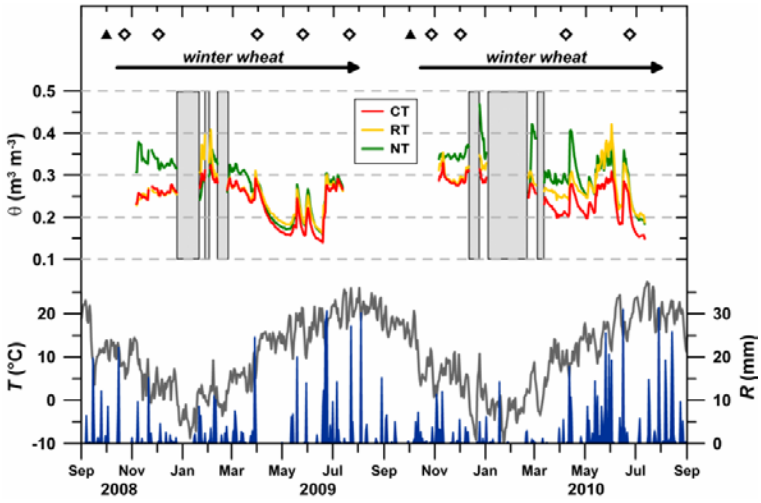

Figure 1. Soil water regime, climatic conditions, and times of measurements: Volumetric water content θ, measured in 10 cm depth for the different tillage treatments (mean of three replicate sensors), air temperature T (grey line); rainfall R (peaks), and times of infiltration measurements (diamonds), soil tillage (triangle), and crop growing period. The grey areas indicate frost periods.

2.2. Sampling and Infiltration Measurements

Infiltration measurements were made nine times, starting immediately before crop seeding in October 2008 and continuing until shortly before harvest in July 2010, using three tension infiltrometers (Soil Measurement Systems Inc., Tucson, AZ) of the design described by Ankeny et al. (1988). The supply pressure heads were −10, −4, −1, and 0 cm: the first two were maintained for approximately 50-60 min, and the last two for about 10-20 min. Preliminary tests found these durations to be sufficient to achieve steady-state infiltration. For each treatment, three replicate infiltration measurements were carried out. Before each infiltration measurement, soil samples were

taken with steel cores near the measurement location to obtain the initial water content θ_i. Immediately after each measurement, another core sample was collected directly below the infiltration disc to quantify the final water content θ_f, bulk density ρ_b, and total porosity φ. We used Wooding's solution (1968) as described by Reynolds and Elrick (1991) and Ankeny et al. (1991) to determine $K(h)$ from the infiltration measurements. More details can be found in Schwen et al. (2011).

One soil profile per treatment was excavated and sampled with soil cores in depths of 5 cm, 40 cm, and 70 cm with three replicates during July 2009. The hydraulic properties of the subsoil layers were determined using pressure plate extractors (Soil Moisture Inc., USA) at h = 0.2, 0.5, 1.0, 2.0 and 3.0 bar. The RETC code (van Genuchten et al., 1991) was used to fit the parameters of the van Genuchten/Mualem model (referred to as VGM, van Genuchten, 1980; Table 1).

Table 1. Physical soil properties and hydraulic parameters at the experimental site. Texture (content of sand, silt and clay), bulk density ρ_b, saturated water content θ_s, saturated hydraulic conductivity K_s, and the VGM model parameters α_{VG} and n are listed.

Depth	Tillage	Sand	Silt	Clay	ρ_b	θ_s	K_s	α_{VG}	n
cm		———	kg kg^{-1}	———	g cm^{-3}	m^3 m^{-3}	m d^{-1}	m^{-1}	-
0-30		0.27	0.54	0.20	1.38	0.48			
30-60	CT	0.35	0.47	0.18	1.27	0.52	0.40	6.77	1.168
60-90		0.31	0.57	0.12	1.36	0.49	0.31	1.15	1.571
0-30		0.27	0.54	0.20	1.38	0.48			
30-60	RT	0.35	0.47	0.18	1.23	0.54	0.30	5.57	1.234
60-90		0.31	0.57	0.12	1.38	0.48	0.31	1.55	1.452
0-30		0.27	0.54	0.20	1.42	0.47			
30-60	NT	0.35	0.47	0.18	1.27	0.52	0.30	12.34	1.169
60-90		0.31	0.57	0.12	1.39	0.48	0.31	1.40	1.575

2.3. Inverse Estimation of Soil Hydraulic Parameters

The inverse analysis of tension infiltrometer data required a numerical solution of the modified Richards' equation. The initial and boundary conditions were defined as proposed by Šimůnek et al. (1998). To describe the unsaturated soil hydraulic properties, we used the van Genuchten/Mualem model (van Genuchten, 1980). We formulated the objective function (OF) that is minimized during parameter estimation by combining the cumulative infiltration data, the $K(h)$ values calculated by Wooding's analysis, and θ_f. OF minimization was accomplished using the Levenberg-Marquardt nonlinear minimization method (Marquardt, 1963), as provided by the program HYDRUS 2D/3D (Šimůnek et al., 2006). For a numerical solution, a quasi-3D (axisymmetric) model geometry was chosen, as described by Šimůnek et al. (1998). Initial values for the parameters were derived from the soil's texture using the Rosetta pedotransfer package (Schaap et al., 2001; input parameters: soil texture and ρ_b). To reduce the amount of unknown variables, for all parameter estimations l was set constant at 0.5 (Ramos et al., 2006), and θ_r was fixed at 0.065 m^3 m^{-3}, as predicted by Rosetta (Lazarovitch et al., 2007). K_s was set to the value obtained by Wooding's analysis (Lazarovitch et al., 2007; Schwen et al., 2011ab; Yoon et al., 2007). The remaining parameters θ_s, α_{VG}, and n were inversely estimated.

Representative mean parameters for each cultivation treatment were derived using the scaling approach. Following the approach of Schwärzel et al. (2011) and Vereecken et al. (2007), a conventional scaling procedure was applied in which scaling factors were estimated by minimizing the residual sum of square differences between the data and the scaled $K(h)$ and $\theta(h)$ reference curves.

2.4. Simulation with Time-variable Hydraulic Parameters

Soil water dynamics were simulated with a daily temporal discretization for the wheat growing seasons (Oct. 2008 – July 2009 and Oct. 2009 – July 2010; Figure 1). The vertical 1D Richards' equation was solved numerically using the Earth Science Module within Comsol Multiphysics (Comsol AB). According to the observed soil horizons for the different tillage treatments, the geometry was divided into three layers: the surface soil (A-horizon) was between 0 and 0.15 m for RT and NT, and 0 - 0.30 m for CT, the AC-horizon down to 0.60 m, and the subsoil (C-horizon) from 0.60 m to 1.00 m.

Potential evaporation E_{pot} and transpiration T_{pot} were derived using the FAO 56 dual crop coefficient method (Allen et al., 1998). We used tabulated values for the crop coefficient K_c ($K_{c\ ini} = 0.4$, $K_{c\ mid} = 1.15$, $K_{c\ end} = 0.25$, Allen et al., 1998) and observed crop development stages. We acknowledge that we did not calculate E_{pot} and T_{pot} as treatment-specific but assumed them to be the same for the different tillage treatments. R and E_{pot}, the latter reduced by a h-dependent reduction function, were applied as the upper boundary condition (Bodner et al., 2007). T_{pot} was implemented via a sink term using a growth function, a linear decreasing root distribution function (Prasad, 1988), and a h-dependent reduction function according to Feddes et al. (2001) and Wu et al. (1999). The lower boundary was defined by a unit gradient condition.

Simulations were made with constant and time variable VGM parameters (α_{VG}, K_s, and θ_s) of the upper soil layer for all tillage methods. The measured parameter values were connected using cubic splines to allow a continous description. Since the temporal variability was expected to be negligible in the lower soil horizons, the hydraulic parameters were set constant (Table 1). To get a comparison between observed and predicted values, O_i and P_i, the average relative error (ARE) was calculated as follows (Popova and Pereira, 2011):

$$ARE = \frac{1}{N}\sum_{i=1}^{N}\left(\frac{|O_i - P_i|}{O_i}\right) \tag{1}$$

Here, N is the number of observations. For further comparison between O_i and P_i, regressions of the form $P_i = \text{slope} \times O_i + \text{intercept}$ were performed (Moret et al., 2007) and the determination coefficient R^2 was calculated. Root mean square errors ($RMSE$) were also calculated by (Ji et al., 2009; Popova and Pereira, 2011):

$$RMSE = \left[\frac{1}{N}\sum_{1}^{N}(P_i - O_i)^2\right]^{1/2} \tag{2}$$

To account for the spatial variability of the observed values, O_i used in the differences was defined as mean (O_i) ± standard deviation.

3. Results and Discussion

3.1. Climatic Conditions and Soil Water Content

For the present study two consecutive wheat growing seasons were analyzed. *R* between October 15, 2008 and July 13, 2009 was 398 mm, which is in line with the long-term average. Remarkably, there was hardly any rain during April and May 2009 (Figure 1). Between October 15, 2009 and July 12, 2010, the rainfall was 395 mm. Potential evapotranspiration Et_{pot} in the seasons 2008/09 and 2009/10 was 366 and 332 mm, respectively, which can be divided into E_{pot} (117 and 101 mm), and T_{pot} (249 and 231 mm). In the growing seasons 2008/09 and 2009/10 the climatic water balance resulted in a surplus of 32 mm and 63 mm, respectively.

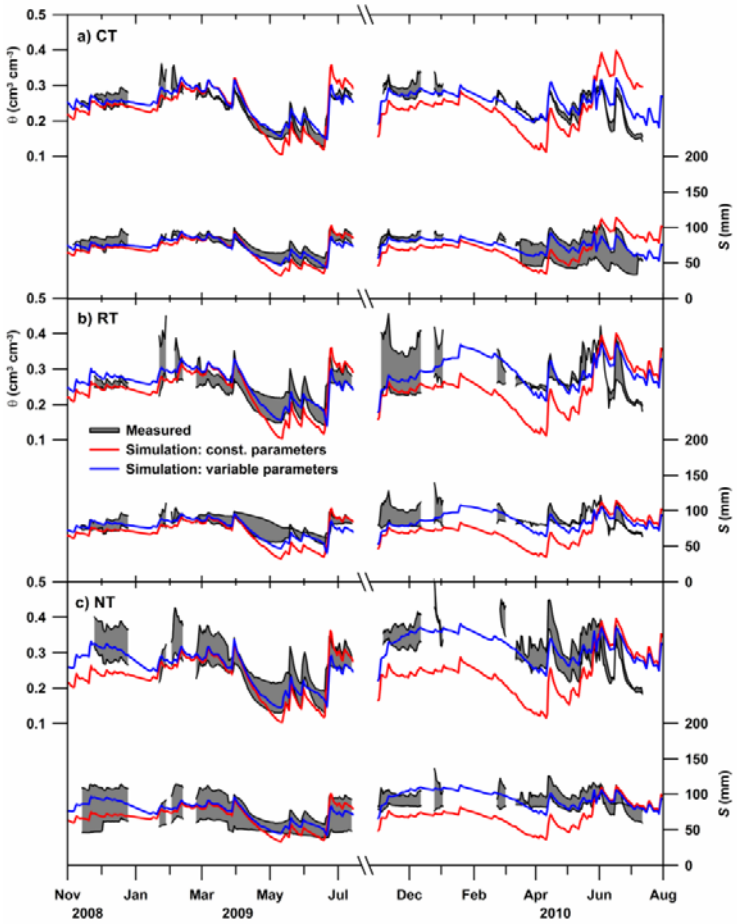

Figure 2. Simulated vs. measured volumetric soil water content θ in a depth of 10 cm (upper plots) and water storage *S* in the near-surface soil profile (0-30 cm; lower plots). θ and *S* (mean ± standard deviation) were measured using three replicate sensors per treatment in depths of 10, 20, and 40 cm (grey areas). The gaps in winter are due to frost periods (Figure 1). The results of simulations using constant and time-variable hydraulic properties are shown for the tillage treatments CT (a), RT (b), and NT (c).

In response to climatic conditions and crop growth, the soil water content varied over time (Figure 1). With high water contents in winter and early spring and dryer periods between April and June 2009, the first analyzed year shows a broad variety of soil moisture conditions. Since there was sufficient rainfall in spring 2010, the soil moisture in the season 2009/10 was more balanced. During frost periods in winter, the shallow sensors did not give meaningful values so they had to be excluded from further analysis (Figure 1). Only small differences in the near-surface water content occurred between treatments CT and RT, whereas NT resulted in significant higher soil moisture contents. This agrees with findings of Moret et al. (2007) and Moreno et al. (1997).

The variability within a treatment indicated by the replicate probes was considerably high (Figure 2). Since technical problems with the moisture sensors could be ruled out due to careful data processing, this variability might be attributed to the natural spatial variability in the hydraulic properties. As the variability was smallest for CT and slightly larger for RT, it reflects the effect of spatial homogenization of repeated tillage operations. Contrarily, considerable differences among the replicate sensors under NT indicate a high spatial variability, especially in the season 2008/09. Under NT, the variability was much smaller in the season 2009/10 than in 2008/09. This may be explained by the fact that the probes were removed before harvest in July and reinstalled at slightly different positions after seeding in October 2009.

3.2. Temporal Dynamics of Soil Hydraulic Properties

The temporal variability of soil hydraulic properties and its underlying water-conducting porosity at the experimental site has been discussed in detail by Schwen et al. (2011a). In both analyzed seasons, K_s and θ_s under CT and RT strongly decreased after tillage during winter (Figure 1), which might be due to rainfall-induced pore sealing and settling (Cameira et al., 2003; Mubarak et al., 2009; Xu and Mermoud, 2003). The decrease is followed by a gradual increase in spring and summer, possibly induced by biological activity, root development, and wetting / drying cycles, as proposed by Mubarak et al. (2009). Beside considerable higher K_s values in October 2009 and June 2010, NT showed only small temporal variability and no systematic dynamic. The high K_s values in the non-tilled soil may be due to the existence of preferential flow paths (earthworm burrows), as reported by Moreno et al. (1997).

Regarding the VGM model parameters, n showed only small temporal dynamic for all treatments. However, α_{VG} showed a considerable temporal dynamic. This dynamic was smallest for NT, indicating the relatively greater temporal stability of the hydraulic properties under this treatment (Schwen et al., 2011a). We found no systematic trend that reasonably explains the temporal dynamic of α_{VG} for both analyzed seasons. Possibly, this indicates that temporal dynamics of the VGM parameters are quite complex, even for the tilled treatments (CT, RT). Therefore, we did not apply a pore-size evolution model (e.g., Or et al., 2000), but used cubic splines to continuously describe the hydraulic parameters.

3.3. Performance of Near-Surface Water Simulations

The present study focuses on the simulation of water movement and storage in the highly dynamic near-surface soil compartment (0-30 cm). Therefore in the following, only the results for the uppermost soil layer are discussed. However, we acknowledge that we found a good agreement

between measured and simulated soil water contents in the deeper soil layers for all simulations. For quality assessment of the simulations, we compared simulated and measured values of θ_{10} and S using Eq. 9 and 10. Overall, the simulations resulted in soil water dynamics that agreed with the measured range for all treatments (Figure 2). Since the hydraulic parameters that were used in the topsoil were estimated inversely from tension infiltrometer measurements, this demonstrates the general applicability of this method for soil water simulations.

However, the degree of agreement between simulated and measured soil water dynamics differed among the tillage treatments and between simulations with temporally constant and variable hydraulic parameters. We observed that simulations with time-constant sets of hydraulic parameters tend to underestimate θ_{10} and S in winter and spring (November 2008 – March 2009 and November 2009 – April 2010), whereas they resulted in overestimations during late spring and summer (June and July 2009 and 2010). Contrarily, application of time-variable hydraulic parameters significantly increased the agreement of both θ_{10} and S for all tillage treatments in both seasons. This was also reported by Xu and Mermoud (2003). Compared to simulations with constant parameters, values of *ARE* for θ_{10} and S approximately halved and the *RSME* for S was reduced by up to 93% (Table 2). *RSME* values of θ_{10} for CT, RT, and NT were 0.042, 0.062, and 0.074 $m^3\ m^{-3}$, respectively (Table 2), and thus in the same range as reported by Moret et al. (2007). As the *ARE* values for θ_{10} and S were below 13%, the simulation results were satisfactory (Ji et al., 2009).

Within simulations with time-variable hydraulic parameters, the best agreement was found for CT with ARE and *RSME* values for θ_{10} of 0.09 and 0.042 $m^3\ m^{-3}$, respectively, (Table 2) and a correlation of $R^2 = 0.81$ (Figure 3), followed by NT (*ARE* = 0.09, $R^2 = 0.78$). Simulations for RT resulted in slightly larger differences and showed the weakest correlation (R^2 for $\theta_{10} = 0.65$, Figure 3). For all treatments, the agreement was better in the season 2008/09 than in 2009/10.

These results show that the accuracy of simulations of the near-surface soil water dynamics can be substantially improved by applying time-variable hydraulic parameters. The presented approach might help to improve the quality of soil water simulations, not only for the assessment of different tillage methods, but also for other applied questions in agricultural water management.

To capture temporal and management-induced dynamics in the near-surface soil hydraulic properties, adequate and expeditious methods have to be applied. As demonstrated by this study, repeated tension infiltrometer measurements followed by the described data analysis procedure can meet this requirement. However, to derive physically-based descriptions of the complex temporal and management-induced dynamics of soil hydraulic properties, more research is necessary. We suggest that future research should focus on measurements at different temporal scales that might be correlated to underlying changes in the soil's structure.

Table 2. Performance of the soil water simulation. Sums of relative differences *SRD* and root mean square differences *RSMD* are listed for the volumetric water content in 10 cm depth, θ_{10}, and the water storage S in the near-surface soil profile (0-30 cm). Results for simulations with constant and time-variable hydraulic parameters are shown for all tillage treatments.

Tillage	Season	θ_{10}				S (0-30 cm)			
		SRD (-)		*RSMD* (m^3 m^{-3})		*SRD* (-)		*RSMD* (mm)	
		const.	var.	const.	var.	const.	var.	const.	var.
CT	2008/2009	0.11	0.07	0.037	0.035	0.05	0.01	5.4	2.1
	2009/2010	0.32	0.11	0.080	0.049	0.16	0.02	14.3	2.8
	Overall	0.21	0.09	0.062	0.042	0.11	0.01	10.7	2.5
RT	2008/2009	0.13	0.08	0.065	0.072	0.09	0.03	10.0	4.0
	2009/2010	0.31	0.13	0.077	0.045	0.25	0.08	23.9	9.5
	Overall	0.21	0.10	0.072	0.062	0.17	0.05	18.1	7.2
NT	2008/2009	0.15	0.07	0.060	0.073	0.02	0.001	2.7	0.2
	2009/2010	0.35	0.12	0.101	0.073	0.20	0.03	22.3	3.9
	Overall	0.24	0.09	0.083	0.074	0.10	0.01	15.6	2.7

4. Conclusion

The present study reveals the applicability of repeated tension infiltrometer measurements to capture temporal and tillage-induced changes in soil hydraulic properties. As classical simulations of the soil water use temporally constant hydraulic parameters, we used a Richards' equation water simulation that enables the flexible definition of these important control quantities. Simulated water content and storage in the near-surface soil compartments under different tillage treatments were compared to measured data. The performance of the simulation could be improved significantly using time-variable hydraulic parameters, regardless the tillage. By giving meaningful results, our simulations demonstrate the applicability of inversely estimated hydraulic parameters for soil water simulations.

Acknowledgement
The content of this proceedings paper has been published previously in Schwen et al. (2011ab).

References

Allen, R. G., L. S. Pereira, D. Raes, and M. Smith, Crop evapotranspiration – Guidelines for computing crop water requirements, *FAO Irrigation and drainage paper 56*, Food and Agriculture Organization of the United Nations, Rome, 1998.

Alletto, L., and Y. Coquet, Temporal and spatial variability of soil bulk density and near-saturated hydraulic conductivity under two contrasted tillage management systems, *Geoderma*, *152*, 85-94, 2009.

Angulo-Jaramillo, R., J. P. Vandervaere, S. Roulier, J. L. Thony, J. P. Gaudet, and M. Vauclin, Field measurement of soil surface hydraulic properties by disc and ring infiltrometers - A review and recent developments, *Soil & Tillage Research*, *55*, 1-29, 2000.

Angulo-Jaramillo, R., F. Moreno, B. E. Clothier, J. L. Thony, G. Vachaud, E. FernandezBoy, and J. A. Cayuela, Seasonal variation of hydraulic properties of soils measured using a tension disk infiltrometer, *Soil Sci. Soc. Am. J.*, *61*, 27-32, 1997.

Ankeny, M. D., T. C. Kaspar, and R. Horton, Design for an automated tension infiltrometer, *Soil Sci. Soc. Am. J.*, *52*, 893-896, 1988.

Ankeny, M. D., M. Ahmed, T. C. Kaspar, and R. Horton, Simple field method for determining unsaturated hydraulic conductivity, *Soil Sci. Soc. Am. J.*, *55*, 67-470, 1991.

Bodner, G., W. Loiskandl, G. Buchan, and H.-P. Kaul, Natural and management-induced dynamics of hydraulic conductivity along a cover-cropped field slope, *Geoderma*, *146*, 317-325, 2008.

Bodner, G., W. Loiskandl, H.-P. and Kaul, Cover crop evapotranspiration under semi-arid conditions using FAO dual crop coefficient method with water stress compensation, *Agr. Water Management*, *93*, 85-98, 2007.

Bormann, H., and K. Klaassen, Seasonal and land use dependent variability of soil hydraulic and soil hydrological properties of two Northern German soils, *Geoderma*, *145*, 295-302, 2008.

Cameira, M. R., R. M. Fernando, and L. S. Pereira, Soil macropore dynamics affected by tillage and irrigation for a silty loam alluvial soil in southern Portugal, *Soil & Tillage Research*, *70*, 131-140, 2003.

Daraghmeh, O. A., J. R. Jensen, and C. T. Petersen, Near-saturated hydraulic properties in the surface layer of a sandy loam soil under conventional and reduced tillage, *Soil Sci. Soc. Am. J.*, *72*, 1728-1737, 2008.

FAO, Guidelines for Soil Description, 3rd ed. FAO/ISRIC, Rome, 1990.

Feddes, R. A, H. Hoff, M. Bruen, T. Dawson, P. de Rosnay, O. Dirmeyer, R. B. Jackson, P. Kabat, A. Kleidon, A. Lilly, and A. J. Pitman, Modeling root water uptake in hydrological and climate models, *Bulletin of the American Meteorological Society*, *82*, 2797-2809, 2001.

Hu, W., M. G. Shao, Q. J. Wang, J. Fan, and R. Horton, Temporal changes of soil hydraulic properties under different land uses, *Geoderma*, *149*, 355-366, 2009.

IUSS, World Reference Base for Soil Resources FAO, Rome, 2007.

Ji, X. B., E. S. Kang, W. Z. Zhao, Z. H. Zhang, and B. W. Jin, Simulation of heat and water transfer in a surface irrigated, cropped sandy soil, *Agr. Water Management*, *96*, 1010-1020, 2009.

Lazarovitch, N., A. Ben-Gal, J. Šimůnek, and U. Shani, Uniqueness of soil hydraulic parameters determined by a combined wooding inverse approach, *Soil Sci. Soc. Am. J.*, *71*, 860-865, 2007.

Leij, F. J., T. A. Ghezzehei, and D. Or, Modeling the dynamics of the pore-size distribution, *Soil & Tillage Research*, *64*, 61-78, 2002.

Marquardt, D. W., An algorithm for least-squares estimation of nonlinear parameters, *Journal of the Society for Industrial and Applied Mathematics*, *11*, 431-441, 1963.

McKnight, T. L., and D. Hess, Climate Zones and Types: The Köppen System. *In*: Physical Geography: A Landscape Appreciation. Upper Saddle River, NJ: Prentice Hall. ISBN 0130202630, 2000.

Messing, I., and N. J. Jarvis, Temporal variation in the hydraulic conductivity of a tilled clay soil as measured by tension infiltrometers, *Journal of Soil Science*, *44*, 11-24, 1993.

Middleton, N., and D. S. G. Thomas, World Atlas of Desertification. First Edition, United Nations Environment Programme (UNEP), Edward Arnold, London, ISBN 340691662, 1992.

Moreno, F., F. Pelegrín, J. E. Fernández, and J. M. Murillo, Soil physical properties, water depletion and crop development under traditional and conservation tillage in southern Spain, *Soil & Tillage Research*, *41*, 25-42, 1997.

Moret, D., I. Braud, and J. L. Arrúe, Water balance simulation of a dryland soil during fallow under conventional and conservation tillage in semiarid Aragon, Northeast Spain, *Soil & Tillage Research*, *92*, 251-263, 2007.

Mubarak, I., J. C. Mailhol, R. Angulo-Jaramillo, P. Ruelle, P. Boivin, and M. Khaledian, Temporal variability in soil hydraulic properties under drip irrigation, *Geoderma*, *150*, 158-165, 2009.

Or, D., F. J. Leij, V. Snyder, and T. A. Ghezzehei, Stochastic model for posttillage soil pore space evolution, *Water Resources Research*, *36*(7), 1641-1652, 2000.

Popova, Z., and L. S. Pereira, Modelling for maize irrigation scheduling using long term experimental data from Plovdiv region, Bulgaria, *Agricultural Water Management*, *98*(4), 675-683, 2011.

Prasad, R., A linear root water uptake model, *J. Hydrol.*, *99*, 297-306, 1988.

Ramos, T. B., M. C. Goncalves, J. C. Martins, M. Th. van Genuchten, and F. P. Pires, Estimation of soil hydraulic properties from numerical inversion of tension disk infiltrometer data, *Vadose Zone Journal*, *5*, 684-696, 2006.

Reynolds, W. D., and D. E. Elrick, Determination of hydraulic conductivity using a tension infiltrometer, *Soil Sci. Soc. Am. J.*, *55*, 633-639, 1991.

Reynolds, W. D., E. G. Gregorich, and W. E. Curnoe, Characterization of water transmission properties in tilled and untilled soil using tension infiltrometers, *Soil & Tillage Research*, *33*, 117-131, 1995.

Roger-Estrade, J., G. Richard, A. R. Dexter, H. Boizard, S. de Tourdonnet, M. Bertrand, and J. Caneill, Integration of soil structure variations with time and space into models for crop management. A review, *Agron. Sustain. Dev.*, *29*, 135-142, 2009.

Schaap, M. G., F. J. Leij, and M. Th. van Genuchten, ROSETTA: a computer program for estimating soil hydraulic parameters with hierarchical pedotransfer functions, *Journal of Hydrology*, *251*, 163-176, 2001.

Schwärzel, K., S. Carrick, A. Wahren, K.-H. Feger, G. Bodner, and G. D. Buchan, Soil hydraulic properties of recently tilled soil under cropping rotation compared with 2-years-pasture: Measurement and modelling the soil structure dynamics, *Vadose Zone Journal*, *10*(1), 354-366, 2011.

Schwartz, R. C., and S. R. Evett, Estimating hydraulic properties of a fine-textured soil using a disc infiltrometer, *Soil Sci. Soc. Am. J.*, *66*, 1409-1423, 2002.

Schwen, A., G. Bodner, P. Scholl, G. D. Buchan, and W. Loiskandl, Temporal dynamics of soil hydraulic properties and the water-conducting porosity under different tillage, *Soil & Tillage Research*, *113*(2), 89-98, 2011a.

Schwen, A., G. Bodner, and W. Loiskandl, Time-variable soil hydraulic properties in near-surface soil water simulations for different tillage methods, *Agricultural Water Management*, *99*, 42-50, 2011b.

Šimůnek, J., M. Th. van Genuchten, and M. Šejna, The HYDRUS Software Package for Simulating the Two- and Three-Dimensional Movement of Water, Heat, and Multiple Solutes in Variably-Saturated Media. Technical Manual PC Progress, Prague, Czech Republik, 2006.

Šimůnek, J., N. J. Jarvis, M. Th. van Genuchten, and A. Gärdenäs, Review and comparison of models for describing non-equilibrium and preferential flow and transport in the vadose zone, *J. Hydrol.*, *272*, 14-35, 2003.

Šimůnek, J., R. Angulo-Jaramillo, M. G. Schaap, J. P. Vandervaere, and M. Th. van Genuchten, Using an inverse method to estimate the hydraulic properties of crusted soils from tension-disc infiltrometer data, *Geoderma*, *86*, 61-81, 1998.

Šimůnek, J., and M. Th. van Genuchten, Estimating unsaturated soil hydraulic properties from tension disc infiltrometer data by numerical inversion, *Water Resources Research*, *32*(9), 2683-2696, 1996.

Šimůnek, J., and M. Th. van Genuchten, Estimating unsaturated soil hydraulic properties from multiple tension disc infiltrometer data, *Soil Science*, *162*(6), 383-398, 1997.

Strudley, M. W., T. R. Green, and J. C. Ascough, Tillage effects on soil hydraulic properties in space and time: State of the science, *Soil & Tillage Research*, *99*, 4-48, 2008.

van Genuchten, M. T., A closed-form equation for predicting the hydraulic conductivity of unsaturated soils, *Soil Sci. Soc. Am. J.*, *44*, 892-898, 1980.

van Genuchten, M. T., F. J. Leij, and S. R. Yates, The RETC Code for Quantifying the Hydraulic Functions of Unsaturated Soils, Version 6.0, US Salinity Laboratory, USDA, 1991.

Vereecken, H., R. Kasteel, J. Vanderborght, and T. Harter, Upscaling hydraulic properties and soil water flow processes in heterogeneous soils: A review, *Vadose Zone Journal*, *6*, 1-28, 2007.

Wooding, R. A., Steady infiltration from a shallow circular pond, *Water Resources Research*, *4*, 1259-1273, 1968.

Wu, J., R. Zhang, and S. Gui, Modeling soil water movement with water uptake by roots, *Plant and Soil*, *215*, 7-17, 1999.

Xu, D., and A. Mermoud, Modeling the soil water balance based on time-dependent hydraulic conductivity under different tillage practices, *Agricultural Water Management*, *63*, 139-151, 2003.

Yoon, Y., J. G. Kim, and S. Hyun, Estimating soil water retention in a selected range of soil pores using tension disc infiltrometer data, *Soil & Tillage Research*, *97*, 107-116, 2007.

Zhou, X., H. S. Lin, and E. A. White, Surface soil hydraulic properties in four soil series under different land uses and their temporal changes, *Catena*, *73*, 180-188, 2008.

HP2/3: Extensions of the HP1 Reactive Transport Code to Two and Three Dimensions

Jiří Šimůnek[1], Diederik Jacques[2], and Miroslav Šejna[3]

[1]*Department of Environmental Sciences, University of California Riverside, Riverside, CA, USA, jiri.simunek@ucr.edu*
[2]*Performance Assessment, Belgian Nuclear Research Institute, Mol, Belgium, djacques@sckcen.be*
[3]*PC-Progress, Ltd., Prague 2, Czech Republic, m.sejna@pc-progress.cz*

Abstract

A large number of interacting physical, chemical, and biological processes determine the fate of major cations and anions, contaminants (e.g., heavy metals, pesticides), and colloids in soil systems. Also, modeling of soil CO_2 sequestration requires consideration of water flow, heat transport, gas diffusion, and microbiological soil respiration processes. The HP1 simulator (Jacques et al., 2008) is a state-of-the-art model that was specifically developed to evaluate these and similar processes in the unsaturated zone. HP1 couples the one-dimensional variably-saturated flow and transport model HYDRUS-1D (Šimůnek et al., 2008) with the generic geochemical model PHREEQC (Parkhurst and Appelo, 1999). Although HP1 is a versatile code for implementing different geochemical and transport conceptual models in variably-saturated porous media, one of its main limitations is that flow and transport is restricted to one dimension. However, there are many applications that require consideration of various processes in either two- or three-dimensions. Typical examples are flow and transport in soil systems with tiled drains, or with drip and furrow irrigation, or in sloped, layered or heterogeneous systems. Therefore, PHREEQC has recently been coupled also with HYDRUS (2D/3D) (Šimůnek et al., 2011) to handle flow and transport problems, which require a higher dimensionality (HP2/3), and this manuscript describes the capabilities of this new tool. Typical two-dimensional flow and transport problems illustrating the capability of the HP2 simulator are presented in this manuscript. The HP2/3 code uses the graphical user interface of HYDRUS (2D/3D) (Šejna et al., 2011) for input and output processing, enabling definitions and finite element discretization of very complex flow domains.

1. Introduction

The one-dimensional program **HP1**, which couples the **PHREEQC** geochemical code (Parkhurst and Appelo 1999) with **HYDRUS-1D**, was first released in 2005 (Jacques and Šimůnek 2005). This comprehensive simulation tool (HP1 is an acronym for HYDRUS-PHREEQC-1D) can simulate (1) transient water flow, (2) the transport of multiple components, (3) mixed equilibrium/kinetic biogeochemical reactions, and (4) heat transport in one-dimensional variably-saturated porous media (soils). The code uses the Richards equation for simulating one-dimensional variably-saturated water flow and advection-dispersion type equations for heat and solute transport. However, the loosely coupled program can also simulate a broad range of low-temperature biogeochemical reactions in water, the vadose zone and in ground water systems, including interactions with minerals, gases, exchangers and sorption surfaces based on thermodynamic equilibrium, kinetic, or mixed equilibrium-kinetic reactions. HP1 uses the operator-splitting approach with no iterations during one time step (a non-iterative sequential modeling approach).

Jacques and Šimůnek (2005), and Šimůnek et al. (2006), and Jacques et al. (2008ab, 2013), demonstrated the versatility of HP1 in several examples, which included a) the transport of heavy metals (Zn^{2+}, Pb^{2+}, and Cd^{2+}) subject to multiple cation exchange reactions, b) transport with mineral dissolution of amorphous SiO_2 and gibbsite ($Al(OH)_3$), c) heavy metal transport in a medium with a pH-dependent cation exchange complex, d) infiltration of a hyperalkaline solution in a clay sample (this example considers kinetic precipitation-dissolution of kaolinite, illite, quartz, calcite, dolomite, gypsum, hydrotalcite, and sepiolite), e) long-term transient flow and transport of major cations (Na^+, K^+, Ca^{2+}, and Mg^{2+}) and heavy metals (Cd^{2+}, Zn^{2+}, and Pb^{2+}) in a soil profile, f) cadmium leaching in acid sandy soils, g) radionuclide transport, and h) long term uranium migration in agricultural field soils following mineral P-fertilization.

Although HP1 is a versatile code for implementing different geochemical and transport conceptual models in variably-saturated porous media, one of its main limitations is that flow and transport is restricted to one dimension. However, there are many applications, such as flow and transport in soil systems with tiled drains, or with drip and furrow irrigation, or in sloped, layered or heterogeneous systems, that require consideration of various processes in either two- or three-dimensions. Therefore, **PHREEQC** has recently been coupled also with **HYDRUS (2D/3D)** (Šimůnek et al., 2011) to handle flow and transport problems, which require a higher dimensionality (**HP2/3**), and this manuscript describes the capabilities of this new tool.

HP2/3 have, apart from the dimensionality (2D or 3D, respectively), the same capabilities as HP1. The HP2/3 module may be used to analyze water flow, solute movement, and biogeochemical reactions in unsaturated, partially-saturated, or fully saturated two- and three-dimensional porous media. HP2/3 can handle flow domains delineated by irregular boundaries. The flow region itself may be composed of nonuniform soils having an arbitrary degree of local anisotropy. Flow and transport can occur in the vertical plane, the horizontal plane, or in a three-dimensional region exhibiting radial symmetry about a vertical axis. The water flow part of the model considers prescribed head and flux boundaries, as well as boundaries controlled by atmospheric conditions.

The HP2/3 code uses the graphical user interface of HYDRUS (2D/3D) (Šejna et al., 2011) for input and output processing, enabling definitions and finite element discretization of very complex flow domains. Typical two-dimensional flow and transport problems illustrating the capability of the HP2 simulator are presented in this manuscript.

2. HYDRUS (2D/3D) Graphical User Interface for HP2/3

The HP2 code is fully incorporated into the HYDRUS (2D/3D) software package, and hence is installed automatically, together with selected examples, when one obtains HYDRUS (2D/3D) and HP2 licenses and downloads HYDRUS from the Hydrus website. Here, we focus mostly on the implementation of the HP2 module into HYDRUS (2D/3D). We will not discuss processes that are related to geometry design, finite element discretization, variably-saturated water flow, heat transport, solute transport, or initial and boundary conditions, which are described in detail in the HYDRUS (2D/3D) documentation (Šimůnek et al., 2011; Šejna et al., 2011). Nor will we discuss

processes and reactions related to biogeochemical reactions that are described in detail in the PHREEQC (Parkhurst and Apello, 1998] and HP1 (Jacques and Šimůnek, 2005, 2010) manuals.

2.1. Common Features with HP1

Similarly as HP1, the HP2 module is activated in the "Main Processes" window by selecting the "Solute Transport" check box and the "HP2 (Hydrus + Phreeqc)" radio button. The number of "Components" is again selected in the "Solute Transport - General Information" window. Large parts of this window (e.g., iteration criteria) are disabled, since they are not relevant to HP2 applications. Also the "HP2/3 Components and Database Pathway" window, in which users have to select the thermodynamic database to be used with HP2 calculations and to list all main components, is the same as in HP1.

2.2. HP2/3 Definitions Window

The main difference between HP1 and HP2 is in how PHREEQC-related inputs (i.e., those that are printed into the PHREEQC.IN input file) are handled. The "HP2/3 Definitions" window has been completely rewritten and reorganized. While in HP1, we had one "HP1 Definitions" window with four external text editors (Fig. 1), in HP2/3, the external text editors were converted into four Internal pages (Fig. 2) (1 - Additions to Thermodynamic Database, 2 - Definitions of Solution Compositions, 3 - Geochemical Model, and 4 - Addition Output), which can all be viewed directly in the "HP2/3 Definitions" window. One additional Page (5 - Database Viewer), in which one can view the selected thermodynamic database, has been added. The five pages can be selected in the top left corner ("List of Pages") of the "HP2/3 Definition" window (Fig. 2).

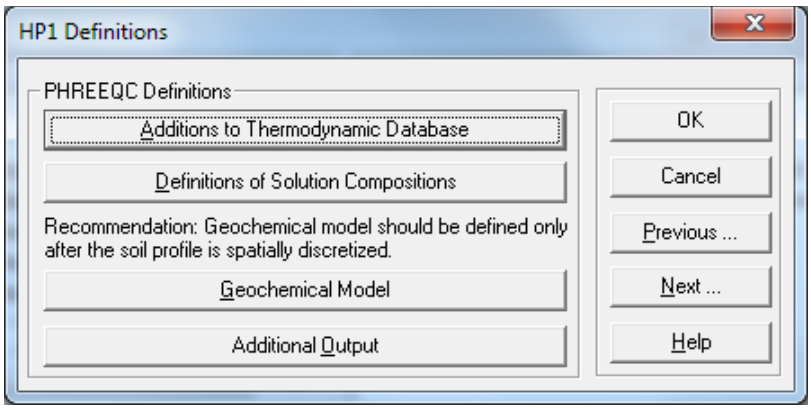

Figure 1. HP1 Definitions window with four external edit windows.

This allowed us to include a section called, "Keywords (double-click to insert)" (bottom left part), which offers the most commonly used PHREEQC Keywords that are used in the first four PHREEQC Pages. The Keywords are hierarchically organized in a tree-like structure in seven main groups: *Solution Definition*, *Geochemical Model*, *Output*, *Chemical/Physical Reaction*, *Database*, *Advanced*, and *Miscellaneous*. A single click opens a particular tree subsection and a double click copies the selected keyword to the Editor Window. This arrangement should dramatically simplify the work of HP2/3 users, and prevent many common errors that they may

have made with HP1. Note the most commonly used Solution Keywords in Figure 2 below - *-density*, *-isotope*, *-pe*, *-pH*, *-redox*, *-temperature*, *-units*, and *-water*.

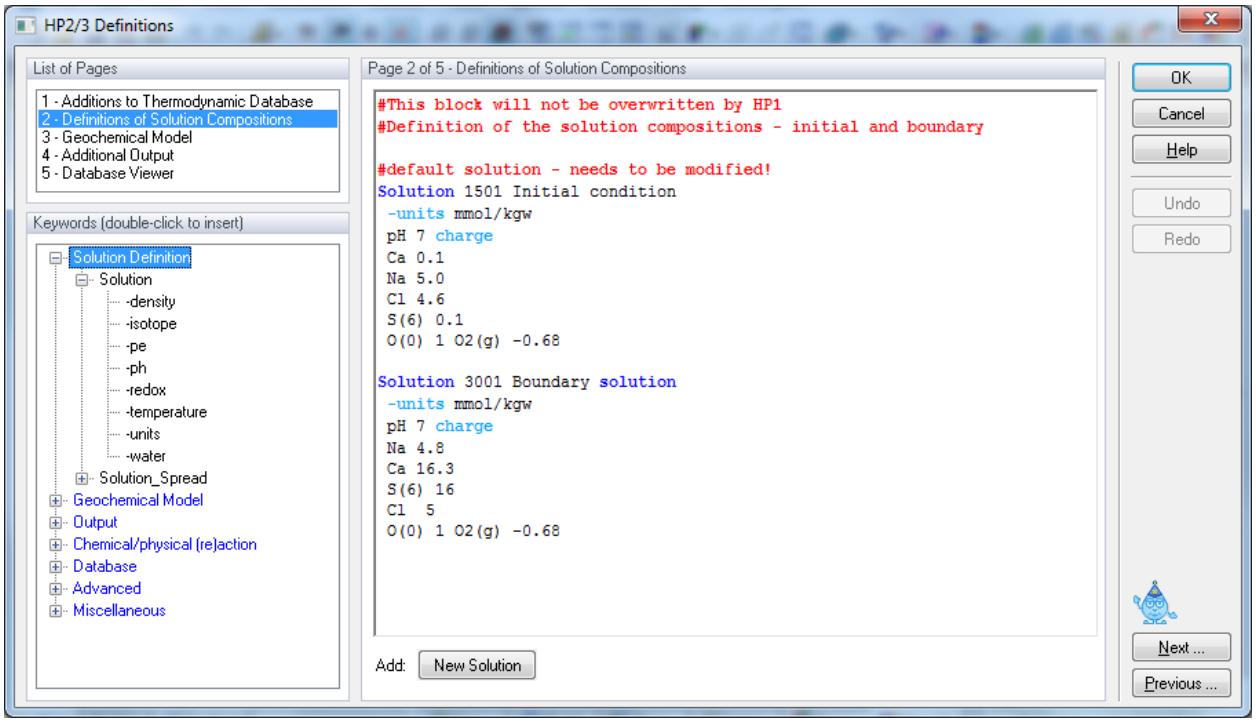

Figure 2. HP2/3 Definitions window with an open page Definitions of Solution Compositions.

Additional new commands were included below the Editor window. For example, the "New Solution" appears below the "*Definitions of Solution Compositions*" page in Fig. 2. Clicking this command will result in including a template for a new solution (Fig. 3). This solution will have a temperature of 25°C, a pH of 7, be in equilibrium with the atmospheric content of oxygen and have zero concentrations of Ca^{2+} and Cl^-.

```
solution 1001
-temp 25
-units mmol/kgw
-pH 7 charge
Ca 0
Cl 0
O(0) 1 O2(g) -0.68
```

Figure 3. A template for a New Solution.

Similar commands (e.g., Add *Exchange*, *Surface*, *Equilibrium Phases*, and *Kinetics*) appear below the "Geochemical Model" page. These commands can be used to include templates for defining cation exchange, surface complexation, and precipitation/dissolution reactions. For more details about the HP2/3 related GUI, see the HP2 Manual (Šimůnek et al., 2012a).

2.3. HP2/3 Output

The output for the HP2 module is similar to the output for the standard HYDRUS module and for standard variables, such as pressure head, water contents, and so on. Multiple variables can be displayed in the View window (Figure 4). Main components defined in the "HP2/3 Components and Database Pathway" window, variables selected in the "HP2 Print and Punch Controls" window, and variables specified in the "Additional Output" page of the "HP2/3 Definitions" window (Fig. 2) can be displayed this way.

Figure 4 below shows the "Results - Graphical Display" part of the Data Tab of the Navigator Bar for the *Leaching of the Uranium Tailings* example given below (Section 3.2). From the HP2 variables, the first seven are the main components (Total_H, Total_O, Ca, C, U, P, S, and Fe) defined in the "HP2/3 Components and Database Pathway" window, the next two (pH and pe) are variables selected in the "HP2 Print and Punch Controls" window, and finally the last four (calcite, gypsum, ratherfordine and siderite) are mineral phases specified in the "Additional Output" page of the "HP2/3 Definitions" window.

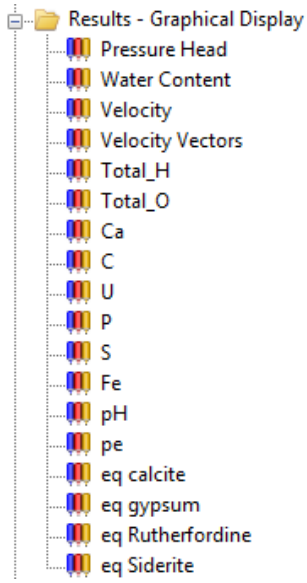

Figure 4. The "Results - Graphical Display" part of the Data Tab of the Navigator Bar for the HP2 module.

3. Example Problems with HP2

Most of the HP1 examples discussed above in the Introduction and provided with the HP1 installation have been rerun using HP2 to verify correct implementation of various components of the coupled program. Two additional two-dimensional examples are discussed below. All of these examples can be downloaded from the HYDRUS/HP2 website (the links are provided below).

3.1. Furrow Irrigation with Cation Exchange

A furrow irrigation problem, similar to the one used in the UNSATCHEM manual (Šimůnek et al., 2012b), was used to simulate two-dimensional infiltration of gypsum saturated water into a sodic soil. The example thus simulates a sodic soil reclamation problem and demonstrates the cation exchange feature of HP2. The schematic representation of the flow domain for the considered furrow irrigation is presented in Figure 5, together with the finite element mesh. It is assumed that every other furrow is flooded with water and that the water level in the irrigated furrow is kept constant at a level of 6 cm. Due to symmetry, it is necessary to carry out the simulation only for the domain between the axis of two neighboring furrows. Free drainage is used as the bottom boundary condition and zero flux is considered on the rest of the boundary. The initial pressure head condition is -200 cm, and the soil hydraulic properties for silt are used.

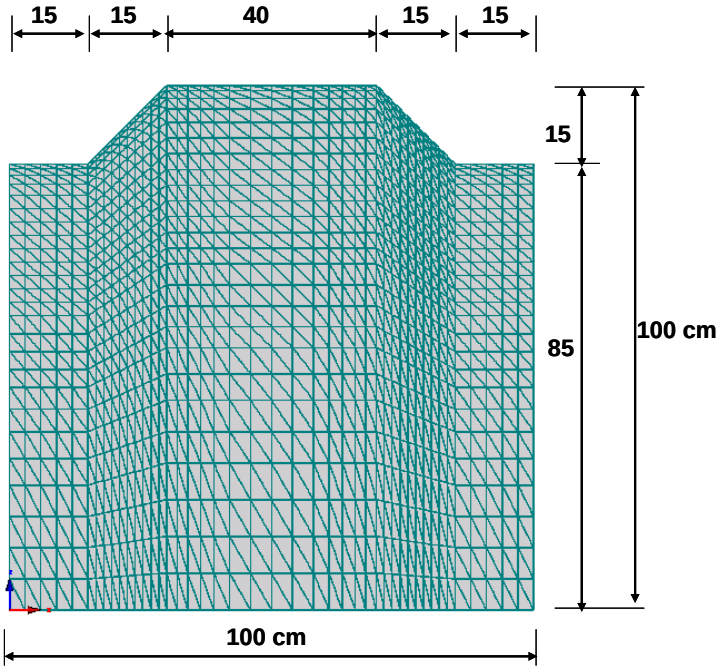

Figure 5. Schematic representation and finite element mesh of the flow domain for the furrow irrigation system.

The calculation was run at a constant temperature of 25 ^{o}C. The bulk density of the soil was taken as 1.4 g cm^{-3} and molecular diffusion as 2 cm^{2}day^{-1}. Longitudinal and transverse dispersivities were equal to 2 and 0.2 cm, respectively.

The solution composition of the water initially present in the soil profile is that of the following highly sodic water: Ca_T=1.0 Mg_T=0.0, Na_T=5.0, K_T=0.0, SO_{4T}=3.5, Cl_T=0.0 mmol L^{-1}. The cation exchange capacity is equal to 7.143 mmol kg^{-1} (10 mmol dm^{-3}) and is divided between exchangeable calcium and sodium (it is equilibrated with the solution). The solution composition of the irrigation water was almost gypsum saturated: Ca_T=16.3, Mg_T=0.0, Na_T=4.4, K_T=0.0, Cl_T=5.0, SO_{4T}=16.0 mmolL^{-1}. As a consequence of the reactions of the irrigation water with the

exchanger composition, cation exchange was the dominant chemical processes in the soil profile. Cation exchange is treated as an instantaneous process in the model.

Figure 6 below presents the exchangeable concentrations of sodium to demonstrate typical output of HP2. The exchange phase concentrations reflect the changes in aqueous Na and Ca concentrations.

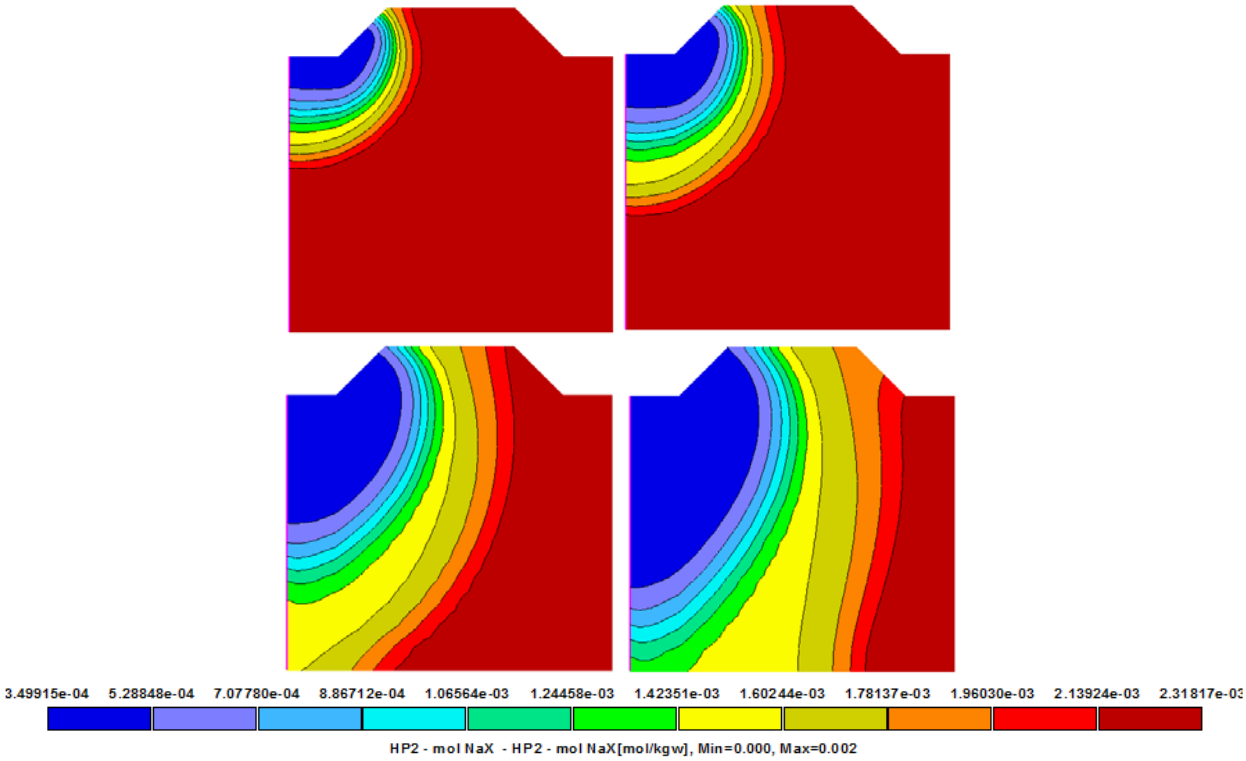

Figure 6. Exchangeable concentrations of sodium (mol kgw^{-1}) profiles at times: a) 0.5, b) 1, c) 3, and d) 5 days.

3.2. Leaching of the Uranium Tailings

This problem was inspired by one reported by Yeh and Tripathi (1991), and we have modified it to make it more realistic. The problem considers the release and migration of uranium from a simplified uranium mill tailings pile towards a river. The schematic of the transport domain is shown in Figure 7. The mill tailings pile is located adjacent to a surface that slopes down to a river. The medium has the hydraulic properties of a loam with the saturated hydraulic conductivity of K_s = 3.78 m/day.

The horizontal bottom of the region is impermeable. The vertical left edge has the Dirichlet boundary condition with a groundwater table 12 m above the bottom of the transport domain (exactly in the middle of the boundary). The top boundary (except for the mill tailing pile and the river) has a flux boundary condition with a net rainfall rate of 0.139 cm/day. The horizontal region on the top of the mill tailings pile is a Cauchy flow boundary with an infiltration rate of 1.39 cm/day. The nodes on the vertical line on the right side and the nodes on the river bottom

have the Dirichlet boundary condition reflecting the position of water in the river (4.5 m above the bottom of the transport domain). A hypothetical pumping well with a withdrawal rate of 271.58 cm^2/day is located at (x, z) = (400, 100). The region is discretized using a structured FE mesh with 1564 elements and 852 nodes.

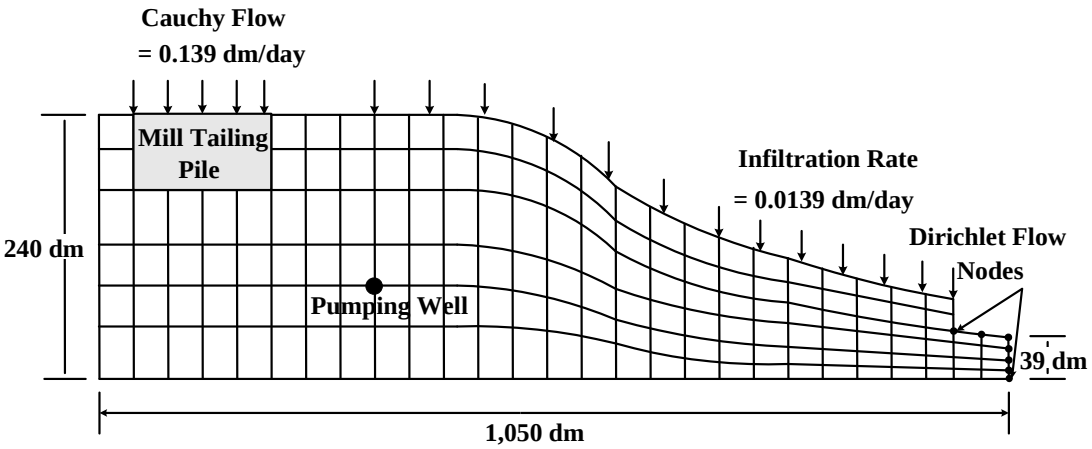

Figure 7. Problem description for the Uranium Tailing Problem (Yeh and Tripathi, 1991).

Chemical Reactions (35 Aqueous Complexation Reactions):

$CaCO_{3(aq)}$, $CaHCO_3^+$, $CaSO_{4(aq)}$, $CaH_2PO_4^+$, $CaPO_4^-$, $CaHPO_{4\,(aq)}$, $CaOH^+$, $FeSO_{4\,(aq)}$, $FeOH^+$, $Fe(OH)_{2\,(aq)}$, $Fe(OH)_3^-$, $Fe(OH)_4^{2-}$, $(UO_2)(OH)^+$, $(UO_2)_2(OH)_2^{2+}$, $(UO_2)_3(OH)_4^{2+}$, $(UO_2)_3(OH)_5^+$, $(UO_2)_4(OH)_7^+$, $(UO_2)_3(OH)_7^-$, $(UO_2)(CO_3)_{(aq)}$, $(UO_2)(CO_3)_2^{2-}$, $(UO_2)(CO_3)_3^{4-}$, $(UO_2)_2(CO_3)(OH)_3^-$, $(UO_2)(SO_4)_{(aq)}$, $(UO_2)(SO_4)_2^{2-}$, $H_2(UO_2)(PO_4)^+$, $H_3(UO_2)(PO_4)^{2+}$, $CaH_4(UO_2)(PO_4)_2^{2+}$, $CaH_5(UO_2)(PO_4)_2^{3+}$, HCO_3^-, $H_2CO_{3(aq)}$, HSO_4^-, HPO_4^{2-}, $H_2PO_4^-$, and H_3PO_4

and Precipitation-Dissolution Reactions (14):

$CaSO_{4(s)}$, $CaCO_{3(s)}$, $Ca_5(OH)(PO_4)_{3(s)}$, $FeCO_{3(s)}$, $Ca(UO_2)_2(PO_4)_{2(s)}$, $Ca_4H(PO_4)_{3(s)}$, $CaH(PO_4)_{(s)}$, $Ca(OH)_{2(s)}$, $Fe_3(PO_4)_{2(s)}$, $Fe(OH)_{2(s)}$, $(UO_2)(OH)_{2(s)}$, $(UO_2)(CO_3)_{(s)}$, $Fe(UO_2)_2(PO_4)_{2\,(s)}$, and $H(UO_2)(PO_4)_{(s)}$

and their thermodynamic equilibrium constants considered in this example are listed in Table 3 of the HP2 manual. For reactive hydrogeochemical transport, the problem consists of eight components: Total H, Total O, Ca, C, uranium, sulfate, phosphate, and Fe. A total of 35 species and 14 minerals is defined for the problem; redox reactions were not considered. Table 1 lists concentrations of the tailing and recharge waters.

Table 1. Initial and boundary compositions of recharge water and pore water in the tailings and regions outside of the tailing for the uranium tailing problem.

Species	Inside the Tailing	Outside the Tailing	Recharge Water
Ca2+	1.0 x 10-2	1.0 x 10-2	1.0 x 10-3
CO32-	1.0 x 10-2	1.5 x 10-3	1.5 x 10-3
UO22+	5.0 x 10-4	1.0 x 10-7	1.0 x 10-8
PO43-	1.0 x 10-6	1.0 x 10-6	1.0 x 10-6
SO42-	2.0 x 10-1	2.0 x 10-2	1.0 x 0-4
H+	2.0 x 10-1	1.0 x 10-3	1.ox 10-3
Fe2+	3.5 x 10-2	1.0 x 10-7	1.0x 10-7

The steady-state pressure heads and velocity fields are depicted in Figure 8. Uranium concentration profiles are shown in Figure 9. pH, calcite, and gypsum profiles are shown in Figure 10.

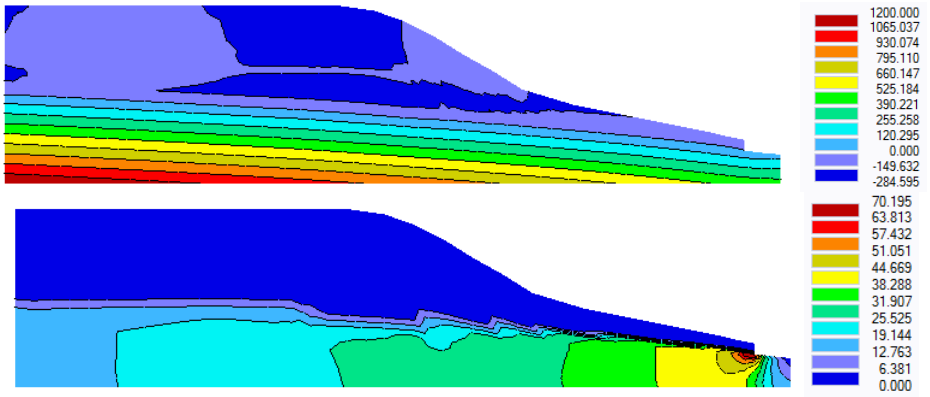

Figure 8. The steady-state pressure head (cm) (top) and flux (cm/d) (bottom) profiles for the Tailing Pile Leaching example.

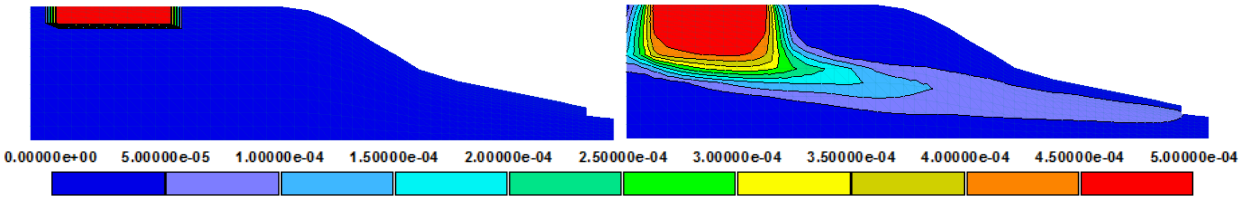

Figure 9. Uranium concentration profiles at time 0 (left), and 500 (right) d for the Tailing Pile Leaching example.

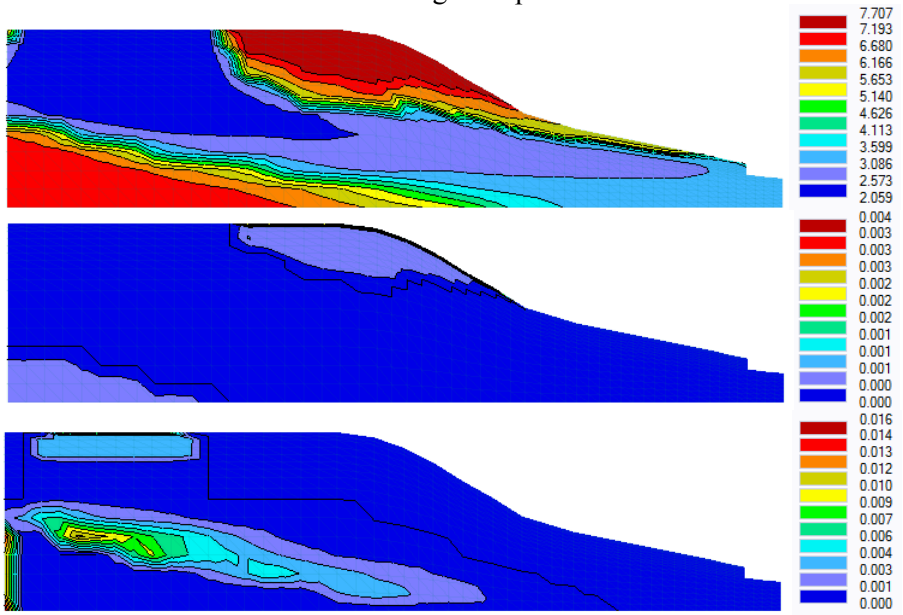

Figure 10. pH (top), calcite (mol/L) (middle), and gypsum (mol/L) (bottom) profiles after 1000 d for the Tailing Pile Leaching example.

4. Important Links

http://www.pc-progress.com/en/Default.aspx?h3d2-HP2: web page providing brief description of the HP2 module and listing all main documents (reports and manuscripts) related to this module.
http://www.pc-progress.com/en/Default.aspx?H3D2-lib-HP2: Examples demonstrating the HP2 program using one-dimensional (for comparison with HP1) and two-dimensional (those discussed above) problems.
http://www.pc-progress.com/Documents/HYDRUS3D_HP2_Manual.pdf: HP2 manual.

References

Jacques, D., and J. Šimůnek, User Manual of the Multicomponent Variably-Saturated Flow and Transport Model HP1, Description, Verification and Examples, Version 1.0, *SCK•CEN-BLG-998*, Waste and Disposal, SCK•CEN, Mol, Belgium, 79 pp., 2005.

Jacques, D., J. Šimůnek, D. Mallants, and M. Th. van Genuchten, Modelling coupled hydrogeological and chemical processes in the vadose zone: a case study of long-term uranium transport following mineral P-fertilization, *Vadose Zone Journal*, *7*(2), 698-711, 2008a.

Jacques, D., J. Šimůnek, D. Mallants and M. Th. van Genuchten, Modelling coupled water flow, solute transport and geochemical reactions affection heavy metal migration in a Podzol soil, *Geoderma*, *145*, 449-461, 2008b.

Jacques, D., J. Šimůnek, D. Mallants, M. Th. van Genuchten, The HPx reactive transport models: Summary of recent developments and applications, (this issue), 2013.

Parkhurst D. L., and C. A. J. Appelo, User's guide to PHREEQ C (Version 2) – A computer program for speciation, batch-reaction, one-dimensional transport and inverse geochemical calculations, Water-Resources Investigations, *Report 99–4259*, Denver, Co, USA, 312 pp., 1999.

Šejna, M., J. Šimůnek, and M. Th. van Genuchten, The HYDRUS Software Package for Simulating Two- and Three-Dimensional Movement of Water, Heat, and Multiple Solutes in Variably-Saturated Media, User Manual, Version 2.0, PC Progress, Prague, Czech Republic, pp. 280, 2011.

Šimůnek, J., D. Jacques, M. Th. van Genuchten, and D. Mallants, Multicomponent geochemical transport modeling using the HYDRUS computer software packages, *J. Am. Water Resour. Assoc.*, *42*(6), 1537-1547, 2006.

Šimůnek, J., M. Th. van Genuchten, and M. Šejna, Development and applications of the HYDRUS and STANMOD software packages, and related codes, *Vadose Zone Journal*, *7*(2), 587-600, 2008.

Šimůnek, J., M. Šejna, H. Saito, M. Sakai, and M. Th. van Genuchten, The HYDRUS-1D software package for simulating the one-dimensional movement of water, heat and multiple solutes in variably-saturated media, Version 4.08, *HYDRUS Software Series 3*, Department of Environmental Sciences, University of California Riverside, Riverside, California, USA, 2008.

Šimůnek, J., M. Th. van Genuchten, and M. Šejna, The HYDRUS Software Package for Simulating Two- and Three-Dimensional Movement of Water, Heat, and Multiple Solutes in Variably-Saturated Media, Technical Manual, Version 2.0, PC Progress, Prague, Czech Republic, pp. 258, 2011.

Šimůnek, J., D. Jacques, M. Šejna, and M. Th. van Genuchten, The HP2 Program for HYDRUS (2D/3D): A Coupled Code for Simulating Two-Dimensional Variably-Saturated Water Flow, Heat Transport, and Biogeochemistry in Porous Media, Version 1.0, PC Progress, Prague, Czech Republic, 76 pp., 2012a.

Šimůnek, J., M. Šejna, and M. Th. van Genuchten, The UNSATCHEM Module for HYDRUS (2D/3D) Simulating Two-Dimensional Movement of and Reactions Between Major Ions in Soils, Version 1.0, PC Progress, Prague, Czech Republic, 54 pp., 2012b.

Yeh, G. T., and V. S. Tripathi, A model for simulating transport of reactive multispecies components: Model development and demonstration, *Water Resour. Res.*, *27*, 3075-3094, 1991.

CO_2 Fluxes to Aquifers Beneath Cropland: Merging Measurements and Modeling

Eike M. Thaysen[1], Diederik Jacques[2], and Eric Laloy[2]

[1]*Department of Chemical and Biochemical Engineering, Center for Ecosystems and Environmental Sustainability, Technical University of Denmark, Kgs. Lyngby, Denmark, emth@kt.dtu.dk*
[2]*Institute for Environment, Health, and Safety, Belgian Nuclear Research Centre (SCK•CEN), Mol, Belgium, djacques@sckcen.be, elaloy@sckcen.be*

Abstract

Carbon dioxide (CO_2) fluxes in the vadose zone are influenced by a complex interplay of biological, chemical and physical factors. To determine the controls behind dissolved inorganic carbon (DIC) percolation to aquifers, CO_2 fluxes in planted soil mesocosms were described with the SOILCO2 model formulation (Šimůnek et al., 1993) that was implemented into the HP1 module of the Hydrus 1D software package. Water flow, cation exchange, and supersaturation for amorphous aluminum hydroxide were modeled. The model provided a good fit to measured water content and outflow time series. Also, the measured DIC efflux, CO_2 partial pressure (pCO_2), and CO_2 efflux were simulated well throughout most of the experimental period. However, alkalinity was significantly overestimated, indicating additional acidity production in the mesocosms. CO_2 fluxes were strongly influenced by a higher root growth in the mesocosms as compared to the field, which caused steep increases in pCO_2. The model showed that the high pCO_2 triggered weathering of calcite, leading to increases in alkalinity. DIC percolation lacked accompanying increases, indicating an overestimation of the DIC percolation estimated from measured pCO_2, alkalinity, and water flux.

1. Introduction

The global flux of carbon dioxide (CO_2) into the groundwater is less than 1% of the diffusion flux of CO_2 from soils to the atmosphere (Kessler et al., 2001). Although estimates of leaching losses of carbon are scarce, available estimates indicate that leaching of dissolved carbon from soils constitutes a significant fraction of the annual carbon (C) budgets of croplands (Kindler et al., 2011). C is leached from soils as dissolved organic carbon (DOC), dissolved methane (CH_4), and dissolved inorganic carbon (DIC). DIC originates from either soil respiration, dissolution of carbonate minerals, or atmospheric CO_2. The latter contribution is negligible because of the low atmospheric partial pressures of CO_2 (pCO_2) (Kindler et al., 2011). The amount of DIC varies with the soil pCO_2, pH, and temperature (Clark et al., 1997). However, our understanding of production and transport of CO_2 in the soil (Jassal et al., 2005) and of the exchange of CO_2 between soils, plants, and the atmosphere is incomplete (Sugden et al., 2004).

In this work, experimentally determined CO_2 fluxes in the vadose zone of large planted soil mesocosms were modeled using the HP1 module of the Hydrus-1D software package (Jacques et al., 2010) in order to identify the main drivers controlling DIC transport to aquifers.

2. Methodology

2.1. Experimental Data

Soil from the A and C horizons of a carbonated alluvial sediment was collected and packed into plexiglas cylinders (length: 83 cm, diameter: 19 cm) above a bottom plate with an embedded suction disc (Thaysen et al., in review). The hydraulic connection between the C horizon and the suction disc was optimized by means of a thin layer of quartz flour and a layer of quartz flour mixed with the C horizon.

Barley (*Hordeum vulgare L.* cv Anakin) was sown into the mesocosms at a seeding density of 280 plants m^{-2}. The mesocosms were incubated in climate chambers and maintained at mean daily air and night temperatures of 18 °C and 13 °C, respectively. Plants were irrigated with a 50% strength Hoagland solution (Hoagland et al., 1950) with an alkalinity of 0.05 meq L^{-1}. Root length was measured at five time points on the outside of the mesocosm walls.

Volumetric water content (VWC) and temperature within the mesocosms were logged at ten minute intervals with 5 TM and EC-TM sensors and EM50 (Decagon Devices, USA) and CR1000 loggers (Campbell Scientific, UK). To increase measurement accuracy, sensors were calibrated to the A and C horizon conditions according to the guidelines of the manufacturers.

Samples of soil air and soil water were collected weekly and analyzed for CO_2 partial pressure (pCO_2) and alkalinity, respectively. Soil air pCO_2 was measured on a 7890A GC System with a FID detector in combination with a methanizer (Agilent Technologies, DK). Alkalinity was determined using the Gran Titration method (Gran, 1952).

The exchange of CO_2 between the mesocosm and the atmosphere was measured at regular intervals using the static closed chamber technique (Ambus et al., 2007). During measurement, the concentration of CO_2 in the chamber space (V= 22.6 L) was continuously closed-loop sampled with an environmental gas monitor (EGM-2, PP-Systems, USA), and the flux was estimated from the concentration change, volume, and measurement time.

The DIC concentration in the percolating water was calculated from the pCO_2, the alkalinity in the soil solution, and the temperature at the mesocosm bottom (~62-76 cm) using PHREEQC software (Parkhurst et al., 2011), while assuming chemical equilibrium between gaseous CO_2, $CO_{2(g)}$, and solution H_2CO_3*, HCO_3^-, and CO_3^{2-}. The DIC concentration was multiplied by the water flux to obtain the DIC flux to the groundwater.

2.2. Modeling of Experimental Results

Results from only one planted mesocosm are discussed in this paper. The mesocosm consisted of three materials. The first and second layers were the A and C horizons located between 0-30 and 31-80 cm depths, respectively. The suction plate, the quartz flour layer, and the layer of quartz flour mixed with the C horizon were grouped in the third material between depths of 80-83 cm.

Model Setup

Water flow was described by the Richards equation and the constitutive relations of the van Genuchten-Mualem model without hysteresis (Mualem, 1978; van Genuchten, 1980). Upper boundary conditions for the water flow were atmospheric conditions with a surface boundary layer. At the bottom, a variable pressure head boundary condition was chosen. Maximum allowed pressure head at the soil surface was zero. Potential evapotranspiration was estimated using the Blaney Criddle formula (Blaney et al., 1962). Water retention parameters were obtained from inverse modeling of the water flow in an unplanted mesocosm (data not shown) using Hydrus-1D (Šimůnek et al., 2013) and a global stochastic optimization algorithm (Vrugt et al., 2009).

Heat transport was not included in the model as temperatures in the mesocosm were almost constant. Temperatures declined from the top to the bottom of the mesocosm due to the proximity of heat emitting lamps at the mesocosm top, high volumetric water content (VWC) in the A horizon and the higher heat capacity of water compared to air. Hence, constant boundaries of 22 and 18°C were used at the mesocosm top and bottom, respectively, with a linear interpolation in between. The model domain was discretized in 157 nodes with the highest node densities at the mesocosm top and at the interfaces of soil materials.

CO_2 production was modeled through implementation of equations and parameters for CO_2 production from SOILCO2 (Šimůnek et al., 1993; Suarez et al., 1993). The parameter a, describing the depth dependency of microbial respiration, was set to 0.04 cm^{-1}, and the boundary layer height (BLH) was set at 0.05 m. The dependency of CO_2 production on root growth was accounted for by 1) a distribution factor and (measured) root depth (as is done for root water uptake) and 2) by introducing a linear root biomass increase, RMI [M], (Eq. 2). The latter was added to account for a 2-5 times higher total root mass in mesocosms than in the field (Table 1) (Biscoe et al., 1975; Xu et al. 1992; Malhi 2002). It was anticipated that

$$RMI = R_{init} + r * time \tag{2}$$

where R_{init} [M] is the initial root mass at simulation time= 0 [T] and r is the growth rate [MT^{-1}]. For our simulations R_{init} was set to 0.1 g and r was 0.21 g day^{-1}.

Table 1. Root growth as a function of depth in mesocosms as measured 70 days after sowing.

Depth (cm)	**Root mass (g) (means ± SE)**	**Root mass per soil horizon (%)**	**Total root mass (g m^{-2})**
0-10	8.1 ± 0.5	91.7 ± 0.9	527.4 ± 14.7
10-20	3.5 ± 0.3		
20-30	2.6 ± 0.3		
30-42	0.5 ± 0.1	8.3 ± 0.9	
42-58	0.3 ± 0.1		
58-80	<0.01		

CO_2 transport in the gas and water phases and phase distribution were described as stated within HP1. For more details the reader is referred to Šimůnek et al. (2013). The measured pore water composition was supersaturated for amorphous aluminum hydroxide, $Al(OH)_{3(a)}$. Therefore, the saturation index (SI) of $Al(OH)_{3(a)}$ was set at 0.8 and 0.6 for the A and C horizons, respectively. The cation exchange capacity was estimated from the soil organic matter and clay content, resulting in values of $9.2*10^{-2}$ and $4.2*10^{-3}$ eq dm^{-3} for the A and C horizons, respectively. The exchanger composition was calculated from the soil water composition on day 40 and contained $3.90*10^{-2}$ Ca^{2+}, $6.51*10^{-3}$ Mg^{2+}, $6.62*10^{-4}$ K^{+}, $1.39*10^{-4}$ Na^{+}, $1.32*10^{-4}$ $Al(OH)_2^{-}$ and $4.04*10^{-5}Al^{3+}$ mol dm^{-3} in the A horizon, and $1.7*10^{-3}$ Ca^{2+}, $2.863*10^{-3}$ Mg^{2+}, $1.06*10^{-4}$ K^{+}, $1.52*10^{-4}$ Na^{+}, $2.4*10^{-5}$ $Al(OH)_2^{-}$ and $1.41*10^{-5}Al^{3+}$ mol dm^{-3} in the C horizon. To simplify the simulations, the influence of nutrients in the irrigation water was neglected.

3. Results and Discussion

3.1. Water Flow

Water flow throughout the soil profile was generally well described (forward simulation from fitted parameters in an unplanted mesocosm, Fig. 1). However, due to a pressure drop across the suction disc that offset boundary conditions and the lack of retention parameters for material three, outflow and VWC in the soil profile could not be matched with high accuracy at the same time. Water logging at the mesocosm bottom (76 cm) was overestimated but cumulative outflow was simulated correctly.

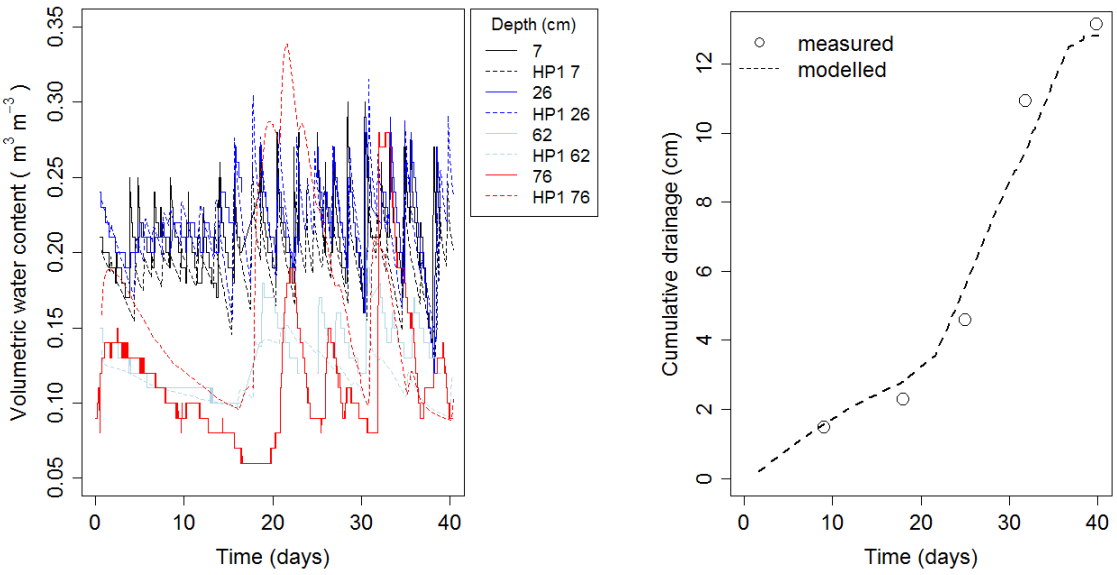

Figure 1. Measured and modeled water content profile and cumulative drainage.

3.2. Profiles of CO_2 and Alkalinity

The pCO_2 increased with plant growth. The magnitude of the pCO_2 could be simulated but the model could not capture all fluctuations in pCO_2 (Fig. 2). The diffusion gradient was matched quite well on days 7, 21 and 35. However, the measured gradients on days 27 and 40 were significantly steeper than the simulated ones. The addition of dependency of CO_2 production on the root biomass increase caused a steady increase in pCO_2 with root growth. On the other hand, the distribution of the production within the soil profile is defined by the normalized root distribution. However, the current implementation of the evolution of the normalized root distribution in HYDRUS simulates a downward shift of the center of mass of the roots (Šimůnek et al., 2013). This downward shift of the region of the highest root abundance seems to be an erroneous assumption for a mesocosm in which ~90% of the root biomass is found in the upper 30 cm after harvest, and root growth declines exponentially from the top (Table 1). Root mass always declines with soil depth (Malhi et al., 2002) and exponential decreases have often been reported (e.g., Xu et al., 1992; Mandal et al. 2003; Rong-hua et al., 2008).

The observed peak pCO_2 in mesocosms was 2-5% higher than observed at a corresponding field site (Voulund, Denmark, 56°2'35.7"N, 9°8'101.1"E). Peak pCO_2 levels were also 5-7% higher than in a previous field study addressing CO_2 dynamics under actively growing winter wheat in a silt loam soil at similar soil temperatures and VWC (Buyanovsky et al., 1983). The higher pCO_2 in mesocosms is probably caused by the higher root length in mesocosms as compared to the field.

The alkalinity increased throughout the experimental period (Fig. 2). Increases in alkalinity could be modeled, but simulated values were twice the measured values. Increases in alkalinity can be understood from 1) increased dissolution of $CO_{2(g)}$ into soil water as the pCO_2 in mesocosms increases (Eq. 2) and 2) the consumption of carbonic acid, H_2CO_3, during dissolution of calcite, $CaCO_3$, that causes 3) increases in $[HCO_3^-]$ (Eq. 3).

$$CO_{2(g)} + H_2O \leftrightarrow H_2CO_3 \leftrightarrow HCO_3^- + H^+ \qquad (2)$$

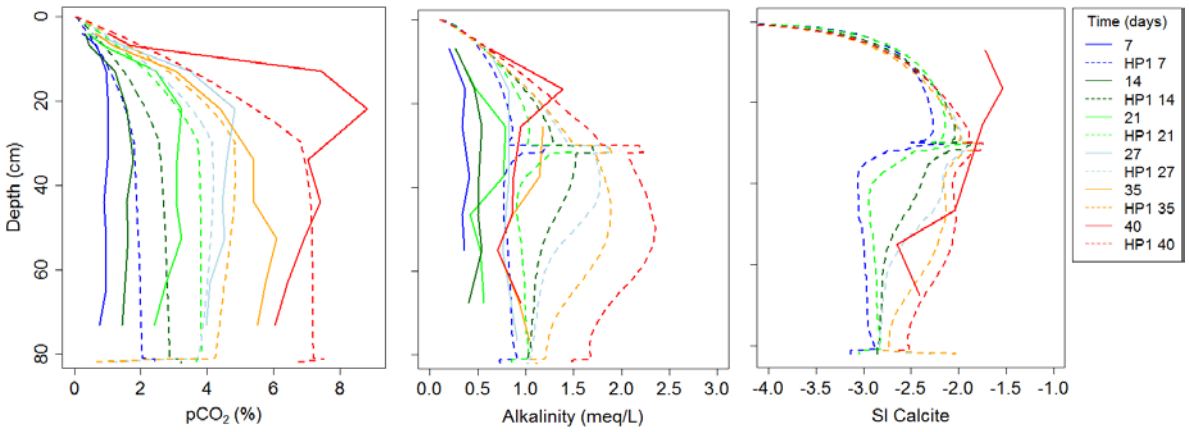

Figure 2. Measured and modeled time course of soil air pCO_2, alkalinity, and saturation index (SI) for calcite.

$$H_2CO_3 + CaCO_3 \leftrightarrow 2HCO_3^- + Ca^{2+} \quad (3)$$

Calcite dissolution on day 40 (Fig. 2) could be approximated by the model in the C horizon but was underestimated in the A horizon, which can be ascribed to the underestimation of pCO_2 on day 40. The larger increases in alkalinity in the simulation as compared to the measured values indicate additional alkalinity-consuming acid production in the mesocosm that is not covered by the model. This could be organic acids released by the roots although several authors have suggested that organic acid concentrations in nutrient-rich bulk soil are generally low (Drever et al., 1994; Ryan et al., 2001) to non-detectable (Baars et al., 2008). Alternatively, watering with a nutrient solution low in alkalinity might also have decreased the soil alkalinity due to the combined effects of flushing and cation exchange with sediment-bound base cations. It is also possible that modeling of proton exchange, which has been shown to act as a source of acid in $NaHCO_3$ water in which calcite dissolves (Appelo, 1994), could produce the measured profiles of alkalinity. The incorporation of additional acid-producing processes in future model work is planned and is expected to improve model fits to experimental data.

3.3. CO_2 Fluxes out of the Mesocosm

The simulated ecosystem respiration (ER) was slightly lower than the measured ER at days 0-30 (Fig. 3) although the diffusion gradients for pCO_2 were simulated well on days 7-21 and 35 (Fig. 2). Simulated ER was much lower than measured ER on days 30-40 (Fig. 3). This is due to the underestimation of the pCO_2 in the A horizon towards the end of the experiment as discussed in Section 3.2. Due to the much higher pCO_2 in mesocosms, measured ER was larger than what has been reported in the field under similar environmental conditions (Buyanovksy et al., 1986; Buyanovsky et al., 1983; Feizene et al., 2008). The simulated CO_2 efflux follows the applied irrigation pattern with lower efflux during irrigation events.

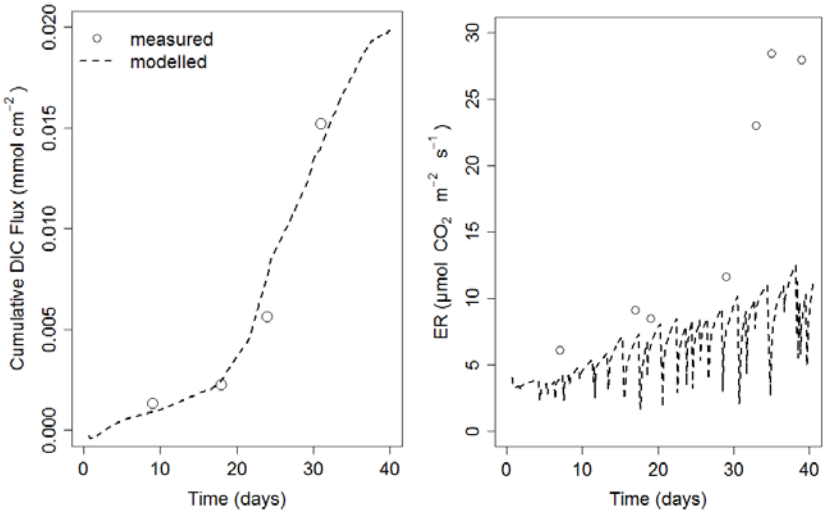

Figure 3. Measured and modeled time course of ecosystem respiration (ER) and DIC percolation.

DIC percolation was predicted well although alkalinity was largely overestimated (Fig. 3). According to theory (Appelo et al., 2005), the DIC concentration can be calculated from pCO_2

and soil alkalinity. DIC percolation is then described by the product of the [DIC] and the drainage flux (e.g., Kindler et al., 2011; Walmsley et al., 2011). As the drainage from the mesocosm was simulated well (Fig. 1), the large overestimation of alkalinity was expected to increase DIC percolation compared to the measured. While differences between the measured and simulated DIC percolation might be due to the fact that the measured DIC percolation was estimated from a weekly "snap shot" of the pCO_2 and the alkalinity, as has been suggested by Walmsley et al. (2011), these inconsistencies need further investigation. The average [DIC] of 2.5 ± 0.02 mmol L^{-1} was in the range of previously reported values for cropped carbonated soil: Luvisol with sand-loam texture ([DIC]: 1.90 mmol L^{-1}) (Siemens et al., 2012) and calcaric Cambisol with silt-loam texture ([DIC]: 5.9 mmol L^{-1}) (Kindler et al., 2011).

4. Conclusion

CO_2 fluxes in the vadose zone of planted mesocosms were strongly influenced by root growth that caused steep increases in CO_2, triggering the dissolution of calcite with subsequent increases of alkalinity. The applied simple model was able to simulate the main tendencies in the data and aided in the comprehension of the underlying biogeochemical processes. The model stressed that additional acid-producing processes occurred in the mesocosm that were not detectable from experimental results alone. Incorporation of the latter in future model work is planned and is expected to improve model fits to experimental data. Modeling results further indicated that pCO_2 profiles are strongly linked to the root distribution and that the downward shift of the center root mass with plant age (root growth) would need to be revised to improve the model.

Acknowledgements
The authors thank Rasmus Jakobsen, Søren Jessen, and Jirka Šimůnek for their support and discussion.

References

Ambus, P., S. O. Petersen, and J. F Soussana, Short-term carbon and nitrogen cycling in urine patches assessed by combined carbon-13 and nitrogen-15 labelling, *Agr. Ecosyst. Environ., 121*, 84-92, 2005

Appelo, C. A. J., Cation and proton exchange, pH variations, and carbonate reactions in a freshening aquifer, *Water Resour. Res., 30*, 2793-2805, 1994.

Appelo, C. A. J., and D. Postma, *Geochemistry, Groundwater and Pollution*, 2nd edition Edition. Balkema, 2005.

Baars, C., T. H. Jones, and D. Edwards, Microcosm studies of the role of land plants in elevating soil carbon dioxide and chemical weathering, *Global Biogeochem.*, *22* ,1-9, 2008.

Biscoe, P. V., R. K. Scott, and J. L. Monteith, Barley and its environment. III. Carbon budget of the stand, *J. Appl. Ecol*, *12*, 269-290, 1975.

Blaney, H. F., and W. D Criddle, Determining consumptive use and irrigation water requirements, In: "*USDA Technical Bulletin*", Beltsville, US Department of Agriculture, 1962.

Buyanovksy, G. A., G. H. Wagner, and C. J. Gantzer, Soil respiration in a winter wheat ecosystem, *Soil Sci. Soc. Am. J.*, *50*, 338-344, 1986.

Buyanovsky, G. A., and G. H. Wagner, Annual cycles of carbon dioxide level in soil air, *Soil Sci. Soc. Am. J.*, *47*, 1139-1145, 1983.

Drever, J. I., and G. F. Vance, *Role of Soil Organic Acids in Mineral Weathering Processes, Organic Acids in Geological Processes* (Eds. Pittman, E.D., and MD. Lewan), Springer, Berlin, 138-161, 1994.

Feizene, D., V. Povilaitis, and G. Kadziene, Springtime soil surface respiration and soil vapour flux in different long-term agro-ecosystems, *Ekologija*, *54*, 216-225, 2008.

Gran, G., Determination of the equivalence point in potentiometric titrations 2, *Analyst, 77*, 661-671, 1952.

Hoagland, D. R., and D. I. Amon, The water-culture method for growing plants without soil, Circ. 347. Univ. of Calif. Agric. Exp. Station, Berkley., Vol C347 rev 1950. College of Agriculture, University of California, Berkeley, 1950.

Jacques, D., and J. Šimůnek, Notes on HP1 – a software package for simulating variably-saturated water flow, heat transport, solute transport and biogeochemistry in porous media, *SCK•CEN-BLG-1068*, 2010.

Kessler, T. J., and C. F. Harvey, The global flux of carbon dioxide into groundwater, *Geophys. Res. Lett.*, *28*, 279-282, 2001.

Kindler, R., J. Siemens, K. Kaiser, D. C. Walmsley, C. Bernhofer, N., Buchmann, P. Cellier, W. Eugster, G. Gleixner, T. Grünwalds, A. Heim, A. Ibrom, S. Jones, M. Jones, S. Lehuger, B. Loubet, R. McKenzie, E. Moors, B. Osborne, K. Pilegaard, C. Rebmann, M. Saunders, M. W. I. Schmidt, M. Schrumpf, J., Seyferth, U. Skiba, J.-F. Soussana, M. A. Sutton, C. Tefs, B. Vowinckel, M. J. Zeeman, and M. Kaupenjohann, Dissolved carbon leaching from soil is a crucial component of the net ecosystem carbon balance, *Global Change Biol*., *17*, 1167–1185, 2011.

Malhi, S. S. and K. S. Gill, Fertilizer N and P effects on root mass of bromegrass, alfalfa and barley, *Journal of Sustainable Agriculture*, *19*(3), 51-63, 2002.

Mandal, K. G., K. M. Hati, A. K. Misra, P. K. Ghosh, and K. K. Bandyopadhyay, Root density and water use efficiency of wheat as affected by irrigation and nutrient management, *Jour. Agric. Physics*, *3*(1), 49-55, 2003.

Mualem, Y., Hydraulic conductivity of unsaturated porous media: Generalized macroscopic approach, *Water Resour. Res.*, *14*, 325–334, 1978.

Parkhurst, D., and C. A. J. Appelo, PHREEQC (Version 3)--A Computer Program for Speciation, Batch-Reaction, One-Dimensional Transport, and Inverse Geochemical Calculations (Denver, Colorado, USA, U.S. Geological Survey, Water Resources Division), 2013.

Rong-hua, L., Z. Zi-Xi, F. Wen-Song, D. Tian-Houg, and Z. Guo-Giang, Distribution pattern of winter wheat root system, *Shengtaixue Zazhi*, *27*(11), 2024-2027, 2008.

Ryan, P. R., E. Delhaize, and D. L. Jones, Function and mechansism of organic anion exudation from plant roots, *Annu Rev Plant Physiol Plant Mol Biol.*, *52*, 527-560, 2001.

Siemens, J., A. Pacholski, K. Heiduk, A. Giesemann, U. Schulte, R. Dechow, M. Kaupenjohann, and H.-J. Weigel, Elevated air carbon dioxide concentrations increase dissolved carbon leaching from a cropland soil, *Biogeochemistry*, *108*, 135-148, 2012.

Šimůnek, J., M. Šejna, H. Saito, M. Sakai, and M.Th. van Genuchten, The Hydrus-1D Software Package for Simulating the Movement of Water, Heat, and Multiple Solutes in Variably Saturated Media, Version 4.16, *HYDRUS Software Series 3* (Riverside, California, USA, Department of Environmental Sciences, University of California Riverside), 2013.

Šimůnek, J., and D. L. Suarez, Modeling of carbon dioxide transport and production in soil. 1. Model development, *Water Resour. Res.*, *29*, 487-497, 1993.

Suarez, D. L., and J. Šimůnek, Modeling of carbon dioxide transport and production in soil. 2. Parameter selection, sensitivity analysis, and comparison of model predictions to field data, *Water Resour. Res.*, *29*, 499-513, 1993.

Sugden, A., R. Stone, and C. Ash, Ecology in the underworld – Introduction, *Science*, *304*, 1613-1613, 2004.

Thaysen, E. M., S. Jessen, P. Ambus, C. Beier, D. Postma, and I. Jakobsen, Technical Note: Mesocosm aproach to carbon dioxide fluxes across the vadose zone in croplands, submitted to Biogeosciences.

van Genuchten, M. Th., A closed-form equation for predicting the hydraulic conductivity of unsaturated soils, *Soil Sci. Soc. Am. J.*, *44*, 892-898, 1980.

Vrugt, J. A., B. A. Robinson, and J. M. Hyman, Self-adaptive multimethod search for global optimization in real-parameter spaces, *IEEE Transactions on Evolutionary Computation*, *13*, 243-259, 2009.

Walmsley, D. C., J. Siemens, R. Kindler, L. Kirwan, K. Kaiser, M. Saunders, M. Kaupenjohann, and B. A. Osborne, Dissolved carbon leaching from an Irish cropland soil is increased by reduced tillage and cover cropping, *Agr. Ecosyst. Environ.*, *142*, 393-402, 2011.

Xu, J. G., and N. G. Juma, Above- and below-ground net primary production of four barley (Hordeum vulgare L.) cultivars in western Canada, *Can. J. Plant. Sci*., *72*, 1131-1140, 1992.

Fate and Transport of Nitrogen in Soils Based on a Coupled Nitrogen-Carbon Cycling Model Using the HP1 Code

Nobuo Toride and DaiWen Chen

Graduate School of Bioresources, Mie University, Tsu, 514-8507, Japan, ntoride@bio.mie-u.ac.jp

Abstract

In order to predict the fate and transport of nitrogen in soils as a result of decomposition of organic matter, we implemented within the PHREEQC program a coupled carbon and nitrogen cycling model based on the LEACHM code. Decay processes from organic carbon (Org-C) to biomass carbon (Bio-C), humus carbon (Hum-C), and carbon dioxide were described using first-order kinetics. Bio-C was recycled into the organic pool. Decomposition of Org-N was related to the carbon cycle using the C/N ratio. Mineralization and immobilization were determined based on available NH_4-N and the nitrogen demand for the formation of biomass and humus. Nitrogen transformations were also described with first-order chain reactions. The carbon and nitrogen cycling model described with PHREEQC was linked with HYDRUS-1D using the HP1 code. Various nitrogen transport scenarios were demonstrated for the application of organic matter to a variable-saturated soil under nonisothermal conditions.

1. Introduction

Nitrogen in soil can change its form through various microbial activities such as mineralization of ammonium from organic matter, nitrification from ammonium, and denitrification from nitrate. Nitrogen mineralization rates depend upon the rate of degradation of organic carbon, the N content of organic matter, and the carbon-to-nitrogen (C/N) ratio of the decomposition products. Because the biomass product usually has a higher C/N ratio than the parent manure, incorporation of biomass gradually increases the C/N ratio of the parent organic pool. The C/N ratios of humus and biomass determine how much N transforms to humus and biomass, while any excess N is released as mineral NH_4. If sufficient N for the production of humus and biomass is not released by mineralization, mineral N will be immobilized from the soil. In order to predict the dynamics and transport of nitrogen as a result of decomposition of organic matter in soils, it is necessary to link a coupled carbon and nitrogen cycling model with a water flow and solute transport model.

The LEACHM code (Hutson, 2005) used a coupled carbon and nitrogen cycling model developed by Johnsson (1987). Although LEACHM has been used widely for nitrogen transport problems, it is currently difficult to further modify the code for various applications. Furthermore, the basic properties of the coupled carbon and nitrogen cycling model have not been investigated thoroughly. In this study we firstly describe first-order kinetic equations for the carbon and nitrogen cycles in soils using the PHREEQC program (Parkhurst and Appelo, 1999). Then, the coupled cycling model is linked with the water flow and solute transport model of HYDRUS-1D (Šimůnek et al., 2005) within the HP1 code (Jacques and Šimůnek, 2010). Various nitrogen transport scenarios are demonstrated for the application of organic matters to a variable-saturated soil under nonisothermal conditions.

2. Coupled Nitrogen and Carbon Cycling Model

2.1. Degradation of Organic Matter

Figure 1 shows the coupled nitrogen and carbon cycling model of Johnsson et al. (1987) as implemented in LEACHM (Hutson, 2005). The blue lines are for the carbon cycle and the black lines for the nitrogen cycle. Numbers in the figure represent the reaction routes specified in the discussion that follows. Two types of principal organic matter were defined: a first cycling pool for litter and a slow cycling pool for stabilized humus. Separate litter pools were used for organic matter having different decay rates and carbon-to-nitrogen (C/N) ratios, such as plant residue and manure. Decay processes from organic carbon (Org-C) to biomass carbon (Bio-C), humus carbon (Hum-C), and carbon dioxide were described with a first-order kinetic. The biomass was recycled into a decomposable litter pool, forming a litter-decomposer complex. Decomposition from the Org-N to Bio-N and Hum-N were related to the carbon cycle using the C/N ratios of the organic matter, biomass and humus. Mineralization of ammonium (NH_4-N) from organic matter and immobilization of NH_4-N to organic matter were determined based on the available NH_4-N and the N demand for the formation of biomass and humus.

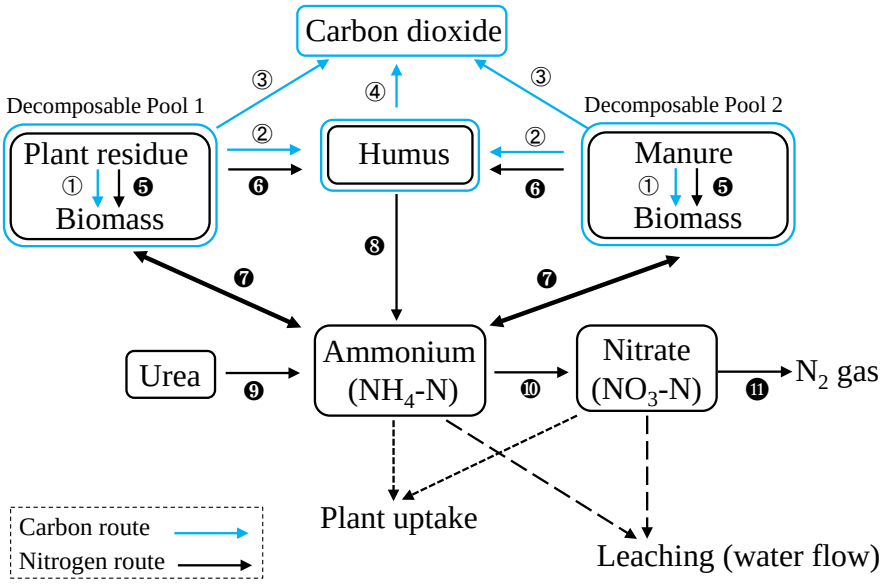

Figure 1. Coupled nitrogen and carbon cycling model based on the LEACHM code.

2.2. Carbon Cycle

Organic carbon (Org-C) in the organic pool *i* (= 1, 2) degrades into three components (routes 1, 2 and 3 in Figure 1): microbial biomass carbon (Bio-C), humus carbon (Hum-C), and carbon dioxide (CO_2):

$$\text{Org-C} \rightarrow \text{Bio-C} + \text{Hum-C} + CO_2 \qquad (1)$$

First-order kinetic is used for the degradation of organic carbon:

$$\frac{dC_{\text{Org-C}i(\text{d})}}{dt} = -k_{\text{Org}i} C_{\text{Org-C}} \tag{2}$$

where C is concentration, expressed as mass per volume of soil, and k_{Org} is the first-order rate coefficient. In order to distinguish the route and direction of the reactions in Figure 1, the subscript (d) is used for degradation while the subscript (p) is used for production in the rate equations. The rate coefficient depends on temperature and water content, with a correction factor according to Johnsson et al. (1987).

The fractions of three products in Eq. (1) are assumed to be invariant. The efficiency factor, f_e, determines the relative production of CO_2 and biomass plus humus while the humification factor, f_h, determines the split between biomass and humus as follows:

$$f_e = \frac{\Delta\text{Bio-C} + \Delta\text{Hum-C}}{\Delta\text{Bio-C} + \Delta\text{Hum-C} + \Delta\text{CO}_2} \tag{3}$$

$$f_h = \frac{\Delta\text{Hum-C}}{\Delta\text{Bio-C} + \Delta\text{Hum-C}} \tag{4}$$

The fraction of each mineralized product can be described with these two factors: $f_e\,(1 - f_h)$ for ΔBio-C, $f_e\,f_h$ for ΔHum-C, and $1 - f_e$ for ΔCO_2. Johnsson et al. (1987) used $f_e = 0.5$ and $f_h = 0.2$ in their examples, assuming fractions of ΔBio-C, ΔHum-C, and ΔCO_2 are 0.4, 0.1, and 0.5, respectively. The fraction of persistent humus production may depend on the type of organic matter (Brady and Weil, 2008). Since f_e and f_h can be different for the different organic pools, the subscript i (= 1, 2) is used in this paper to distinguish between these two factors.

The production rate of Bio-C, Hum-C, and CO_2 of the organic pool i (= 1, 2) can be related to the degradation rate of Org-C (routes 1, 2, 3):

$$\frac{dC_{\text{Bio-C}i(\text{p})}}{dt} = -f_{ei}\left(1 - f_{\text{h}i}\right)\frac{dC_{\text{Org-C}i(\text{d})}}{dt} \tag{5}$$

$$\frac{dC_{\text{Hum-C}i(\text{p})}}{dt} = -f_{ei}\,f_{\text{h}i}\,\frac{dC_{\text{Org-C}i(\text{d})}}{dt} \tag{6}$$

$$\frac{dC_{\text{CO2}i(\text{p})}}{dt} = -(1 - f_{ei})\frac{dC_{\text{Org-C}i(\text{d})}}{dt} \tag{7}$$

Hum-C further decomposes into CO_2 and the degradation rate is also described with first-order kinetics (route 4):

$$\frac{dC_{\text{Hum-C(d)}}}{dt} = -k_{\text{Hum}-\text{C}} C_{\text{Hum-C}} \tag{8}$$

Note that $k_{\text{Hum-C}}$ is much smaller than $k_{\text{Org}i}$ since humus is a persistent substance.

The net reaction rate for each carbon component can be described with a mass balance for all the routes in Figure 1. The net reaction rate for Org-C is the sum of degradation described using Eq. (2) and Bio-C production described with Eq. (5), which is recycled in the organic pool (routes 2, 3):

$$\frac{dC_{\mathrm{Org-C}i}}{dt} = -k_{\mathrm{Org}\,i} C_{\mathrm{Org-C}i} + f_{ei}\left(1 - f_{hi}\right) k_{\mathrm{Org}\,i} C_{\mathrm{Org-C}i} \tag{9}$$

The net reaction rate for Hum-C is the sum of degradation according to Eq. (8) and production from the organic pools according to Eqs. (2) and (6) (routes 2, 4):

$$\frac{dC_{\mathrm{Hum\text{-}C}}}{dt} = -k_{\mathrm{Hum-C}} C_{\mathrm{Hum-C}} + \sum_{i=1}^{2} f_{ei}\, f_{hi} k_{\mathrm{Org}\,i} C_{\mathrm{Org-C}i} \tag{10}$$

Carbon dioxide is produced from the organic pools according to Eq. (7) and Hum-C according to Eq. (8) (routes 3, 4):

$$\frac{dC_{\mathrm{CO2}}}{dt} = \sum_{i=1}^{2} \left(1 - f_{ei}\right) k_{\mathrm{Org}\,i} C_{\mathrm{Org-C}i} + k_{\mathrm{Hum-C}} C_{\mathrm{Hum-C}} \tag{11}$$

Note that since the biomass is recycled in the organic pool as shown by the second term on the right hand side of Eq. (9), Bio-C does not explicitly appear in the net rate equations.

2.3. Nitrogen Cycle

Organic nitrogen (Org-N) decomposes to microbial biomass nitrogen (Bio-N) and humus nitrogen (Hum-N) as in the case of carbon of Eq. (1):

$$\mathrm{Org-N} \rightarrow \mathrm{Bio-N} + \mathrm{Hum-N} \tag{12}$$

The C/N ratios, r, for organic matter, biomass and humus are defined as

$$r_{\mathrm{Org}\,i} = \frac{C_{\mathrm{Org-C}i}}{C_{\mathrm{Org-N}i}}, \quad r_{\mathrm{Bio}} = \frac{C_{\mathrm{Bio-C}i}}{C_{\mathrm{Bio-N}i}}, \quad r_{\mathrm{Hum}} = \frac{C_{\mathrm{Hum-C}}}{C_{\mathrm{Hum-N}}} \tag{13}$$

Note that $r_{\mathrm{Org}\,i}$ changes with time as the organic matter degrades, whereas r_{Bio} and r_{Hum}, are constant (≈ 10).

The degradation rate of Org-N in Eq. (12) can be related to the degradation rate of Org-C using $r_{\mathrm{Org}\,i}$ as

$$\frac{dC_{\mathrm{Org-N}i(\mathrm{d})}}{dt} = \frac{1}{r_{\mathrm{Org}\,i}} \frac{dC_{\mathrm{Org-C}i(\mathrm{d})}}{dt} \tag{14}$$

The production rates for Bio-N and Hum-N are also transformed to the carbon concentration rates and further related with the degradation rate for the organic carbon using Eqs. (5) and (6):

$$\frac{dC_{\mathrm{Bio-N}i(\mathrm{p})}}{dt} = \frac{1}{r_{\mathrm{Bio}}}\frac{dC_{\mathrm{Bio-C}i(\mathrm{p})}}{dt} = -\frac{f_{ei}\left(1-f_{\mathrm{h}i}\right)}{r_{\mathrm{Bio}}}\frac{dC_{\mathrm{Org-C}i(\mathrm{d})}}{dt} \tag{15}$$

$$\frac{dC_{\mathrm{Hum-N(p)}}}{dt} = \frac{1}{r_{\mathrm{Hum}}}\frac{dC_{\mathrm{Hum-C(p)}}}{dt} = -\frac{f_{ei}\,f_{\mathrm{h}i}}{r_{\mathrm{Hum}}}\frac{dC_{\mathrm{Org-C}i(\mathrm{d})}}{dt} \tag{16}$$

The difference between the nitrogen supplies from Org-N and the demands for Bio-N and Hum-N production gives the production rate of ammonium (NH_4-N):

$$\begin{aligned}\frac{dC_{\mathrm{NH_4}i(\mathrm{p})}}{dt} &= -\frac{dC_{\mathrm{Org-N}i(\mathrm{d})}}{dt} - \left(\frac{dC_{\mathrm{Bio-N}i(\mathrm{p})}}{dt} + \frac{dC_{\mathrm{Hum-N(p)}}}{dt}\right) \\ &= -\left(\frac{1}{r_{\mathrm{Org}\,i}} - \frac{f_{ei}\left(1-f_{\mathrm{h}i}\right)}{r_{\mathrm{Bio}}} - \frac{f_{ei}\,f_{\mathrm{h}i}}{r_{\mathrm{Hum}}}\right)\frac{dC_{\mathrm{Org-C}i(\mathrm{d})}}{dt} \\ &= \left(\frac{1}{r_{\mathrm{Org}\,i}} - \frac{f_{ei}\left(1-f_{\mathrm{h}i}\right)}{r_{\mathrm{Bio}}} - \frac{f_{ei}\,f_{\mathrm{h}i}}{r_{\mathrm{Hum}}}\right)k_{\mathrm{Org}\,i}C_{\mathrm{Org-C}i}\end{aligned} \tag{17}$$

In case of $r_{\mathrm{Bio}} = r_{\mathrm{Hum}} = r_0$, Eq. (17) can be simplified as

$$\begin{aligned}\frac{dC_{\mathrm{NH_4}i(\mathrm{p})}}{dt} &= -\left(\frac{1}{r_{\mathrm{Org}\,i}} - \frac{f_{ei}}{r_0}\right)\frac{dC_{\mathrm{Org-C}i(\mathrm{d})}}{dt} \\ &= \left(\frac{1}{r_{\mathrm{Org}\,i}} - \frac{f_{ei}}{r_0}\right)k_{\mathrm{Org}\,i}C_{\mathrm{Org-C}i}\end{aligned} \tag{18}$$

When the NH_4-N production rate described with Eq. (17) or (18) is positive, the surplus nitrogen is used for the mineralization of NH_4-N. On the other hand, when the production rate is negative, immobilization of NH_4-N occurs to compensate the nitrogen deficiency (route 7). If f_{ei} and r_0 are constant, the sign of the parenthesis in Eq. (18) simply depends on the $r_{\mathrm{Org}\,i}$ value. A negative production rate for $r_{\mathrm{Org}\,i} > r_0 / f_{ei}$ leads to immobilization while a positive production rate for $r_{\mathrm{Org}\,i} < r_0 / f_{ei}$ results in mineralization. In case $f_{ei} = 0.5$ and $r_0 = 10$, the immobilization occurs for $r_{\mathrm{Org}\,i} > 20$ while the mineralization for $r_{\mathrm{Org}\,i} < 20$.

The net reaction rate for each nitrogen component can be described with a mass balance scheme similarly as shown in Figure 1 for the carbon cycle. The net reaction rate for Org-N is the sum of reductions due to ammonium production as given by Eq. (18) and Hum-N production as given by Eq. (16) (routes 6, 7):

$$\frac{dC_{\text{Org}-\text{N}i}}{dt} = -\frac{dC_{\text{NH}_4(\text{p})}}{dt} - \frac{dC_{\text{Hum}-\text{N}(\text{p})}}{dt}$$
$$= -\left\{\frac{1}{r_{\text{Org}\,i}} - \frac{f_{ei}\left(1-f_{\text{h}i}\right)}{r_0}\right\} k_{\text{Org}\,i} C_{\text{Org}-\text{C}i} \tag{19}$$

Notice that Bio-N production does not explicitly appear in Eq. (19) since Bio-N is recycled in the organic pool (route 5). Although a similar expression can be obtained when $r_{\text{Bio}} \neq r_{\text{Hum}}$, for simplicity we assume in the discussion to follow that $r_{\text{Bio}} = r_{\text{Hum}}$ (= r_0).

Hum-N also produces ammonium as a result of first-order degradation (route 8):

$$\frac{dC_{\text{Hum}-\text{N}(\text{d})}}{dt} = -k_{\text{Hum-N}} C_{\text{Hum}-\text{N}} \tag{20}$$

The net reaction rate for Hum-N is degradation and production from the organic pools as described with Eq. (16) (route 6):

$$\frac{dC_{\text{Hum}-\text{N}}}{dt} = -k_{\text{Hum-N}} C_{\text{Hum}-\text{N}} + \frac{1}{r_0}\sum_{i=1}^{2} f_{ei}\, f_{\text{h}i} k_{\text{Org}\,i} C_{\text{Org}-\text{C}i} \tag{21}$$

As in the case of carbon, since $k_{\text{Hum-N}} << k_{\text{Org}i}$, it is possible to neglect Hum-N degradation as given by Eq. (20) for relatively short time periods.

2.4. Immobilization of Ammonium

If the C/N ratio for organic matter, $r_{\text{Org}i}$, is smaller than r_0/f_{ei}, mineralization of NH_4-N ammonium occurs according to Eq. (18). In that case, the NH_4-N concentration does not affect the degradation rate of organic matter. On the other hand, in case $r_{\text{Org}i}$ is larger than r_0/f_{ei}, the biomass and humus are produced using the immobilized NH_4-N. If the NH_4-N concentration is small enough for immobilization, the decay rate may slow down because of NH_4-N deficiency. According to the LEACHM program (Hutson, 2005), three immobilization stages can be defined depending upon the available amount of NH_4-N.

If the amount of Org-C_i degradation per day according to Eq. (2) is given as $\Delta C_{\text{Org-C}i}$, the amount of immobilized NH_4-N per day, ΔC_{NH4}, can be related with $\Delta C_{\text{Org-C}i}$ using Eq. (18):

$$\Delta C_{\text{NH4}} = \left(\frac{1}{r_{\text{Org}\,i}} - \frac{f_{ei}}{r_0}\right) \Delta C_{\text{Org}-\text{C}i} \tag{22}$$

It is assumed that not more than one tenth of the total NH_4-N concentration including solution and adsorbed phases, C_{NH4}, is available for each organic pool per day. The maximum amount of degradable Org-C_i per day can be defined as:

$$\Delta C_{\mathrm{Org-C}i,\,\mathrm{Max}} = \frac{C_{\mathrm{NH_4}}}{10}\frac{r_{\mathrm{Org}\,i}\,r_0}{r_0 - r_{\mathrm{Org}\,i}\,f_{ei}} \tag{23}$$

Three immobilization stages can be defined depending on the $\Delta C_{\mathrm{Org\text{-}C}i,\,\mathrm{max}}$ value:

Stage 1: $\Delta C_{\mathrm{Org\text{-}C}i,\,\mathrm{max}} > \Delta C_{\mathrm{Org\text{-}C}i}$
Since enough NH_4-N exists, immobilization does not affect the degradation rate of the organic pool.

Stage 2: $\Delta C_{\mathrm{Org\text{-}C}i} > \Delta C_{\mathrm{Org\text{-}C}i,\,\mathrm{max}} > 0.1\Delta C_{\mathrm{Org\text{-}C}i}$
The degradation rate of the organic pool is now reduced by multiplying Eq. (2) with $\Delta C_{\mathrm{Org\text{-}C}i,\,\mathrm{max}}/\Delta C_{\mathrm{Org\text{-}C}i}$ because of a deficiency in available NH_4-N. The reduction, however, is not less than 10 %.

Stage 3: $\Delta C_{\mathrm{Org\text{-}C}i,\,\mathrm{max}} < 0.1\Delta C_{\mathrm{Org\text{-}C}i}$
When the available NH_4-N is further reduced, $\Delta C_{\mathrm{Org\text{-}C}i,\,\mathrm{max}}$ becomes less than $0.1\Delta C_{\mathrm{Org\text{-}C}i}$. In this case, immobilization for biomass and humus production ceases. Degradation of Org-C now only produces CO_2 without biomass and humus production at the 10 % rate of Eq. (2). Degradation of Org-N according to Eq. (14) mineralizes only NH_4-N. Hence, the C/N ratio for the organic pool, $r_{\mathrm{Org}\,i}$, does not change since no immobilization of NH_4-N occurs. When the NH_4-N concentration increases, $\Delta C_{\mathrm{Org\text{-}C}i,\,\mathrm{max}}$ becomes greater than $0.1\Delta C_{\mathrm{Org\text{-}C}i}$. However, the immobilization of Stage 2 starts using the mineralized NH_4-N.

Since $\Delta C_{\mathrm{Org\text{-}C}i,\,\mathrm{max}}$ is defined for each organic pool, the immobilization stage can be different between the organic pools. Although we consider two organic pools as in the case of the LEACHM program, it is straightforward to increase the number of organic pools by simply letting i run from 1 to n in the summations of the above equations.

2.5. Nitrogen transformation

The inorganic N pools in Figure 1 consist of urea, ammonium and nitrate. The degradation processes of inorganic N are also described using first-order kinetics. Urea fertilizers are rapidly transformed to NH_4-N in soils:

$$\frac{dC_{\mathrm{Urea}}}{dt} = -k_{\mathrm{Urea}}C_{\mathrm{Urea}} \tag{24}$$

where k_{Urea} is the ammonification constant. The net reaction rate for NH_4-N is the sum of nitrification (route 10), mineralization from urea (route 9) and humus (route 8), and mineralization or immobilization for biomass and humus production as described with Eq. (18) (route 7):

$$\frac{dC_{\mathrm{NH4}}}{dt} = -k_{\mathrm{nit}}C_{\mathrm{NH4}} + k_{\mathrm{Urea}}C_{\mathrm{Urea}} + k_{\mathrm{Hum-N}}C_{\mathrm{Hum-N}}\,/\,r_0 + \sum_{i=1}^{2}\left(\frac{1}{r_{\mathrm{Org}\,i}} - \frac{f_{ei}}{r_0}\right)k_{\mathrm{Org}\,i}C_{\mathrm{Org-C}i} \tag{25}$$

where k_{nit} is the nitrification constant. When the available NH_4-N for immobilization is limited, the last term is modified for Stages 2 and 3 of the immobilization process. The net reaction rate for the nitrate is denitrification and production from NH_4-N:

$$\frac{dC_{NO3}}{dt} = -k_{den} C_{NO3} + k_{nit} C_{NH4} \tag{26}$$

where k_{den} is the denitrification constant.

2.6. Transport of Ammonium and Nitrate

Transport of nitrogen in soils can be predicted by coupling the first-order kinetic equations for the carbon and nitrogen cycles with the convective-dispersive equation (CDE). The total concentration, C, expressed as solute mass per volume of soil, can be related with the solute concentration, C_l, expressed as solute mass per volume of soil solution, and adsorbed concentration, S, expressed as adsorbed mass per mass of dry soil as follows:

$$C = \theta C_l + \rho_b S \tag{27}$$

where θ is the volumetric water content, and ρ_b is the soil bulk density. Adsorption of urea and ammonium is described with the Freundlich isotherm:

$$S = K_d C_l^{\,n} \tag{28}$$

where K_d and n are constants. Nitrate is assumed to be a nonreactive solute. The CDE for urea, ammonium, and nitrate are given by:

$$\frac{\partial C_{Uera}}{\partial t} = \frac{\partial}{\partial z}\left(\theta D_{Uera} \frac{\partial C_{l,Uera}}{\partial z} \right) - \frac{\partial q_w C_{l,Uera}}{\partial z} - k_{Urea} C_{Uera} \tag{29}$$

$$\begin{aligned} \frac{\partial C_{NH4}}{\partial t} = {} & \frac{\partial}{\partial z}\left(\theta D_{NH4} \frac{\partial C_{l,NH4}}{\partial z} \right) - \frac{\partial q_w C_{l,NH4}}{\partial z} - k_{nit} C_{NH4} + k_{Urea} C_{Urea} + k_{Hum-C} C_{Hum-C} / r_0 \\ & + \sum_{i=1}^{2} \left(\frac{1}{r_{Org\,i}} - \frac{f_e}{r_0} \right) k_{Org\,i} C_{Org-Ci} \end{aligned} \tag{30}$$

$$\frac{\partial \theta C_{l,NO3}}{\partial t} = \frac{\partial}{\partial z}\left(\theta D_{NO3} \frac{\partial C_{l,\,NO3}}{\partial z} \right) - \frac{\partial q_w C_{l,NO3}}{\partial z} + k_{nit} C_{NH4} - k_{den} \theta C_{l,NO3} \tag{31}$$

where D is the dispersion coefficient, q_w is the volumetric water flux density, z is the vertical position, and t is time.

The first-order kinetic equations for the carbon and nitrogen cycles can be described with the PHREEQC program, which can be readily implemented into HYDRUS-1D using the HP1 code for solute transport simulations.

3. Examples

We demonstrated the decomposition processes of organic matter and resultant nitrogen transport in soils for transient water flow and nonisothermal conditions. A constant flux of water of 0.5 cm d^{-1} was applied to the surface of a 100-cm deep silty soil profile having an initial pressure head h_i of -2000 cm. The soil bulk density, ρ_b, is 1.5 g cm^{-3}. Constant temperature boundary conditions were applied: 40 °C at the surface and 10 °C at the bottom. Four types of organic matter with different C/N ratios (= 5, 20, 30, and 100) were uniformly applied from the surface to 25 cm depth. The amount of carbon per volume of soil was 0.152 mg cm^{-3}, while the carbon content was taken to be the same for each type of organic matter. Linear adsorption was assumed for NH_4-N with K_d = 2.5. A negligible amount of NH_4-N initially existed and the initial C_{NH4} was set at 3.9 ×10-5 g kg^{-1}. A single carbon pool (i = 1) was used with k_{Org} = 0.04 d^{-1}, $k_{Hum\text{-}C}$ = $k_{Hum\text{-}N}$ = 0.0001 d^{-1}, f_e = 0.5, f_h=0.2, and r_0 = 10. Nitrification was neglected, k_{nit} = 0 d^{-1}. Figures 2 and 3 show volumetric water content and temperature profiles during infiltration. Results for low and high C/N rations with mineralization are presented below in sections 3.1 and 3.2, respectively.

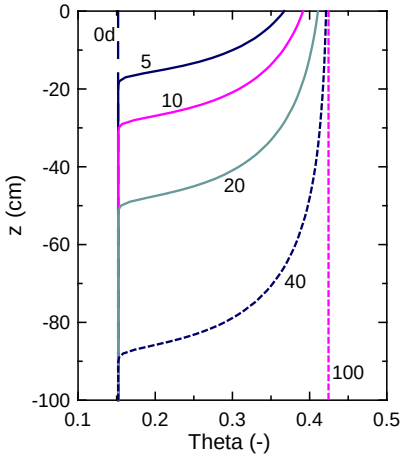

Figure 2. Volumetric water content profiles during infiltration into silt with a constant flux of 0.5 cm d^{-1}.

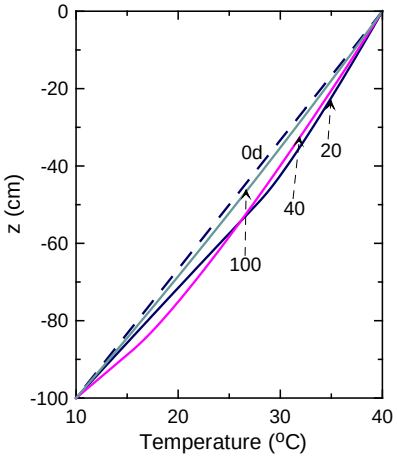

Figure 3. Temperature profiles during infiltration into silt with boundary conditions of 40 °C at the surface and 10 °C at the bottom.

3.1. Low C/N Ratio with Mineralization

When the C/N ratio of organic matter is below 20 (=r_0/f_e), sufficient N for humus and biomass production results in the mineralization of NH_4-N. Since the NH_4-N concentration did not affect the degradation rate of the organic matter, Org-C concentrations were identical for C/N = 5 and 20 (Fig. 2). Faster degradation near the surface was due to effects of temperature. At 40 days, Org-C and Org-N became almost negligible and the C/N ratio became close to 10 (=r_0). Increased mineralization resulted in higher NH_4-N concentrations for C/N = 5.

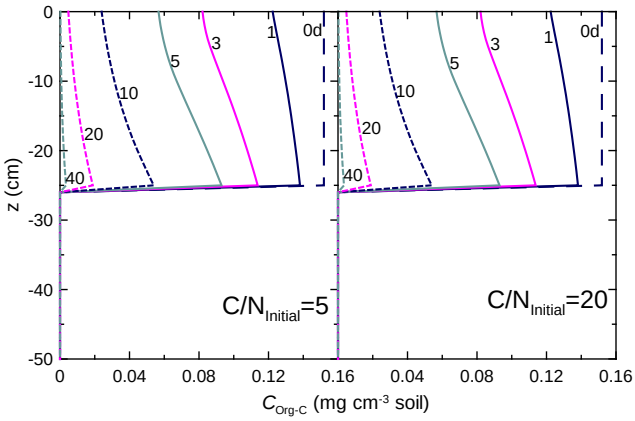

Figure 2. Organic carbon (Org-C) concentration profiles for C/N = 5 and 20 with mineralization of ammonium.

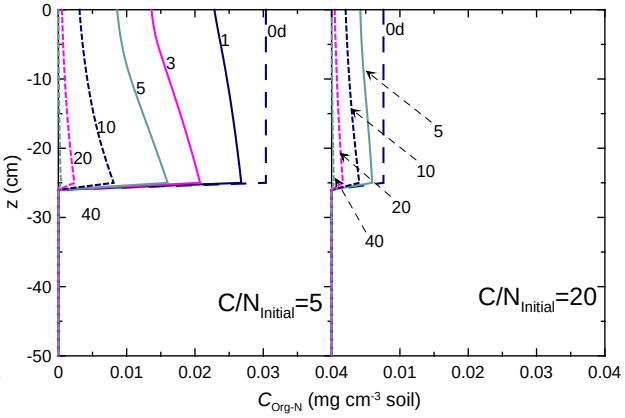

Figure 3. Organic nitrogen (Org-N) concentration profiles for C/N = 5 and 20 with mineralization of ammonium.

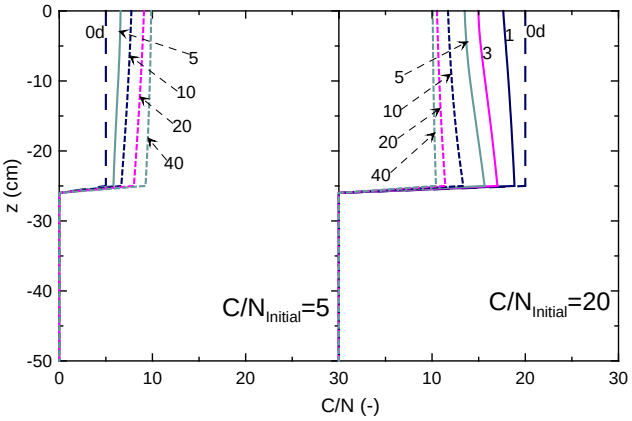

Figure 4. C/N ratio profiles in the organic pool for C/N = 5 and 20 with mineralization of ammonium.

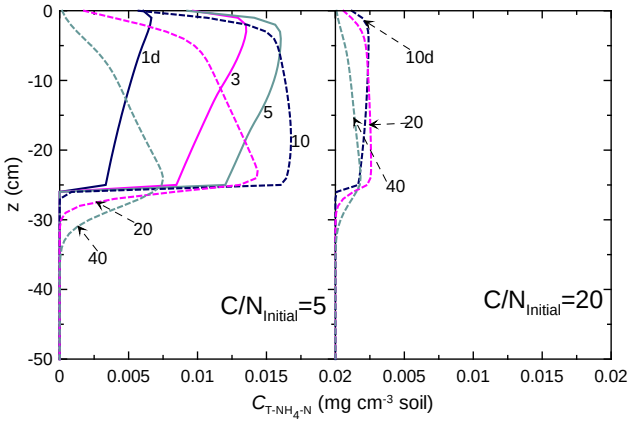

Figure 5. Total ammonium (NH_4-N) concentration profiles for o C/N = 5 and 20 with mineralization of ammonium.

3.2. High C/N Ratio with Immobilization

On the other hand, when the C/N ratio of organic matter was above 20 ($=r_0 / f_e$), NH_4-N in a soil is immobilized for humus and biomass production. The N deficiency now slowed down the degradation process in that it took more than 200 days until the degradation almost finished for C/N = 100. As shown in Figure 7, C/N became less than 20 near the surface in case of C/N = 30, indicating mineralization started near the surface whereas immobilization continued in the lower part of the soil. Stage 3 immobilization continued for C/N =100. During this stage, very slow degradation at a 90 % reduced rate produced only CO_2 and NH_4-N without biomass and humus production. Stage 2 stated in the lower part of the soil at 100 days because of NH_4-N supply from the upper part of the profile.

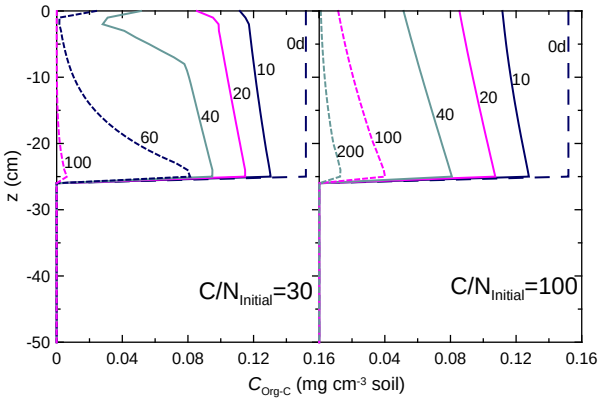

Figure 6. Organic carbon (Org-C) concentration profiles for C/N = 30 and 100 with immobilization of ammonium.

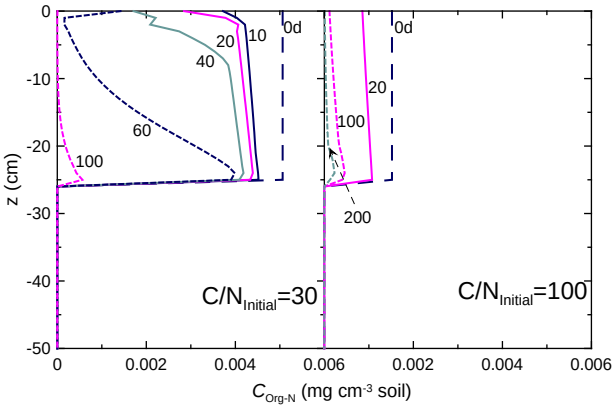

Figure 7. Organic nitrogen (Org-N) concentration profiles for C/N = 30 and 100 with immobilization of ammonium.

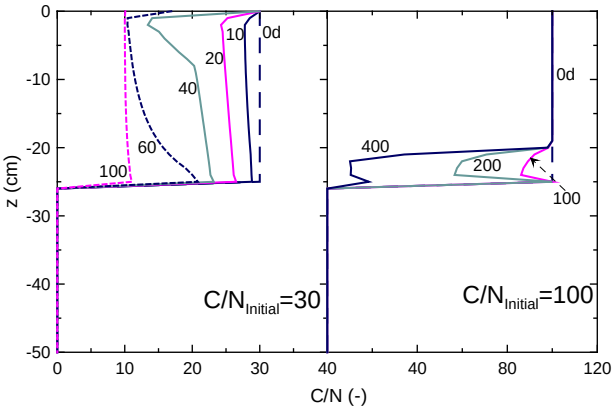

Figure 8. C/N ratio profiles in the organic pool for C/N = 30 and 100 with immobilization of ammonium.

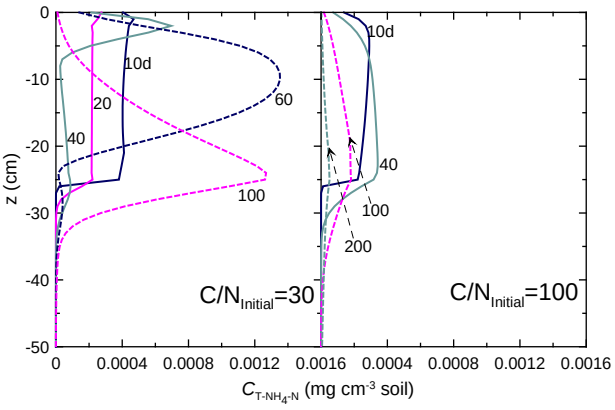

Figure 9. Total ammonium (NH_4-N) concentration profiles for C/N = 30 and 100 with immobilization of ammonium.

4. Conclusions

The carbon and nitrogen cycling model used in the LEACHM code was reformulated using the PHREEQC program and linked with HYDRUS-1D using the HP1 code. We confirmed that the HP1 code could accurately calculate carbon and nitrogen cycles and various nitrogen transport scenarios as a result of the application of organic matter to a variably-saturated soil profile under nonisothermal conditions. We further showed that coupled carbon and nitrogen cycling is especially important when organic matter with a high C/N ratio is applied to a soil. Although we only showed results for a single organic pool, it is possible to demonstrate various interactions between the different organic matter pools. We are planning to extend the program to include multiple organic pools, passive and active root uptake, CO_2 diffusion in the gas phase, cation and

anion exchange for ammonium and nitrate, and several other chemical reactions judged to be important.

References

Šimůnek, J., M. Th., van Genuchten, and M. Šejna, The HYDRUS-1D software package for simulating the one-dimensional movement of water, heat, and multiple solutes in variably-saturated media, Version 3.0, *HYDRUS Software Series 1*, Department of Environmental Sciences, University of California Riverside, Riverside, CA, 270 pp., 2005.

Hutson., J. L., Leaching Estimation and Chemistry Model, Version 4.1, School of Chemistry, Physics and Earth Sciences Flinders University Adelaide, Australia, pp. 135, 2005.

Jacques, D., and J. Šimůnek, Notes on HP1 – a software package for simulating variably-saturated water flow, heat transport, solute transport, and biogeochemistry in porous media, HP1 Version 2.2, SCK•CEN, Mol, Belgium, 2010.

Johnsson, H., L. Bergstörm, P.-E. Jansson, and K. Paustian, Simulated nitrogen dynamics and losses in a layered agricultural soil, *Agric. Ecosyst. Environ.*, 18, 333-356, 1987.

Parkhurst, D. L., and C. A. J. Appelo, User's guide to PHREEQC (Version 2): A computer program for speciation, batch-reaction, one-dimensional transport, and inverse geochemical calculations, *Water-Resour. Invest. Rep. 99-4259*, USGS, Denver, CO, pp. 312, 1999.

HYDRUS Application to Assess Possible Impacts of Non-Conventional Water Irrigation under Two Different Vadose Zone Monitoring Strategies

Javier Valdes-Abellan[1], J. Jiménez-Martínez[2], and L. Candela[3]

[1]*Department of Civil Engineering, University of Alicante, Alicante, Spain, javier.valdes@ua.es*
[2]*Geosciences Rennes, UMR 6118 CNRS, Université de Rennes I. Rennes, France, joaquin.jimenez-martinez@univ-rennes1.fr*
[3]*Department of Geotechnical Engineering and Geosciences, UPC-Barcelona, Jordi Girona 1-3, 08034 Barcelona, Spain, lucila.candela@upc.edu*

Abstract

Scarcity of water resources is one of the major problems that faces many arid and semi-arid areas where potential socio-economic development is often hindered by the lack of water. This has led to the use of non-conventional water sources such as desalinated brackish groundwater and/or seawater for urban and agricultural demands. Applications of non-conventional water to the vadose zone may produce various impacts such as changes in soil hydraulic properties, among others. In this context, monitoring vadose zone water dynamics is key to studying these possible impacts. According to the available literature, different monitoring systems and strategies have been carried out independently, while comparative studies between different monitoring techniques have received less attention.

In this study, an experimental plot was set with automatic and non-automatic sensors to measure the volumetric water content (θ) and the soil pressure head (h) down to a depth of 1.5 m. Water flow simulations for automatically and non-automatically collected data were carried out using HYDRUS-1D. A good agreement between simulated and experimental data was observed for both automatic and non-automatic data acquisitions. General trends were captured as expected, except for outlier values. Slight differences were found between hydraulic properties obtained from laboratory determinations and fitted by inverse modeling for both data acquisition strategies. Differences of up to 14% in the bottom drainage were obtained between both strategies. According to our results, automatic sensors were more accurate, and thus more appropriate, for detecting subtle changes in soil hydraulic properties as a consequence of non-conventional water use. Nevertheless, if the aim of the research is to control the general trend of water dynamics, then there are no significant differences between both data acquisition systems.

The current work presented here is the first part of the study carried out before the geochemical processes responsible for expected changes in the soil hydraulic properties as a consequence of non-conventional water use are analyzed. This second part will be carried out using the HP1 model, which couples the HYDRUS and PHREEQC models.

1. Introduction

In semi-arid regions with endemic water scarcity, which imposes constraints on socio-economic development (Lattemann and Höpner, 2008), the use of non-conventional resources (such as desalinated water, treated water, and waste-water) for agricultural purposes is increasing during recent years. The potential impacts of the use of non-conventional water on soil, plants, or

aquifer media may include changes in soil hydraulic properties due to mineral precipitation, root growth blockage and plant uptake of pollutants, and/or contaminant leaching to groundwater (Calderón-Preciado et al., 2011; Candela et al., 2007; Mandal et al., 2008). In addition, this irrigation water is usually characterized by high electric conductivity values while high evapotranspiration rates may prevail in arid areas. The combination of these two factors may enhance soil salinization, which ultimately causes damage to crop yield (Kanzari et al., 2012).

To assess these possible impacts, having a careful monitoring procedure of the vadose zone at a field scale is a very important issue. Field monitoring can be carried out using different devices, the number of which is continuously increasing following the latest technological developments. Among them, methods range from classical ceramic cup tensiometers and gravimetric determination of soil water contents from oven-dried samples to Time Domain Reflectometry (TDR) technology. These methods can be classified as manually managed, i.e., with non-automatic data acquisition, or with automatic data acquisition using more sophisticated sensors, which makes monitoring less time-consuming but with an increasing initial investment.

Although automatic and non-automatic monitoring strategies have been commonly used separately in the past in order to study different aspects of the vadose zone (Jiménez-Martínez et al., 2009; Wallis et al., 2011; Wollschläger et al., 2009), the selection of a monitoring strategy has not been completely justified in these studies. However, studies in which different monitoring strategies have been simultaneously set up and compared have not been carried out.

In this work, a comparative study between an automatic and non-automatic monitoring strategy for the same experimental plot is presented. Two different flow simulations were carried out using HYDRUS for different data sets (the monitoring period extended over 9 months). A conservative tracer test has also been modeled in order to validate the previous water flux results.

2. Methodology and Field Experiment

An experimental plot of 9 x 5 m located on the campus of the University of Alicante (Spain) was set up. On the plot, a mixture of turf grass (St. Agustine grass, *Stenotaphrum secundatum*, and ray grass, *Lolium perenne*) was grown to mimic the current management of the campus landscape. The plot was irrigated using micro-sprinklers, providing a quasi-uniform water input over the land surface.

Installed measurement devices included manual or non-automatic instruments, which consisted of ten Jet Fill tensiometers (Soil Moisture®) for h measurements installed at depths of 30, 45, 60, 90, and 120 cm (2 tensiometers in each depth), and two 44 mm (i.d.) polycarbonate access tubes installed down to a depth of 1.9 m for θ measurements using a TRIME FM TDR portable probe (IMKO®). The probe was previously calibrated in the lab following the manufacturer's recommendations and also specifically calibrated following previous study procedures (Laurent et al., 2001; Laurent et al., 2005; Varble and Chávez, 2011). Installation of non-automatic equipment was done from the plot surface, aided by hand auger equipment (Eijkelkamp®). Vertical installation was carefully performed in order to prevent preferential flows along the side walls of the equipment itself. Automatic data acquisition consisted of five 5TE sensors (Decagon

Devices ®) installed at depths of 20, 40, 60, 90, and 120 cm for θ measurements, and one MPS-1 sensor installed at a depth of 60 cm for h measurements. All automatic sensors were controlled by the data-logger, CR1000 (Campbell Scientific®). Installation of automatic sensors took place horizontally in an 80 cm wide and 150 cm deep excavated trench. Horizontal holes (40-50 cm long) were drilled in the trench walls for sensor installation in order to reduce the boundary effects. Subsequently, the holes were re-filled with the same soil material extracted during the excavation, in an attempt to keep the original soil conditions (e.g., bulk density). The side-wall of the trench was covered with a plastic film and finally, the trench was refilled with the soil material, creating a non-flow boundary condition for further modeling purposes.

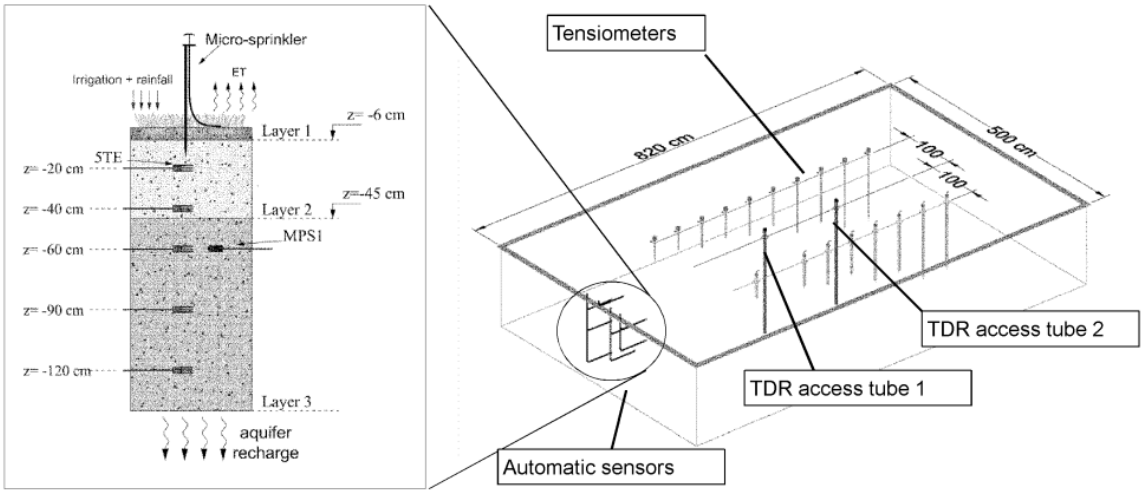

Figure1. Scheme of the experimental plot with the configuration of automatic and non-automatic devices.

2.1. Data Gathering

Data acquisition started on September 1st, 2011, five weeks after the devices' installation. Non-automatic θ measurements were taken twice per week, while h measurements were taken three times per week. An hourly measurement frequency was used regarding automatic data acquisition. A five-minute frequency was used in November, 2011, in order to capture the infiltration dynamics following extreme rainfall events that took place in this period. Meteorological data were recorded every 30 minutes by a meteorological station located 900 m away from the plot.

2.2. Numerical Modeling

Water flow through the vadose zone was modeled using HYDRUS-1D (Šimůnek et al., 2009), which numerically solves the governing Richards equation describing flow in partially-saturated porous media (Richards, 1931):

$$\frac{\partial \theta}{\partial t} = \frac{\partial}{\partial z}\left[K\left(\frac{\partial h}{\partial z} + 1 \right) \right] - S \qquad (1)$$

One dimensional modeling was selected based on the assumption of horizontal uniformity over the experimental plot and vertical flow being a dominant direction of flow in the experiment. Daily time steps were considered in the modeling process. Collected data in smaller time steps (as those values obtained with automatic data collection) were averaged over daily intervals.

The soil hydraulic properties were modeled using the van Genuchten-Mualem constitutive relationships (Mualem, 1976; van Genuchten, 1980):

$$\theta(h) = \begin{cases} \theta_r + \dfrac{\theta_s - \theta_r}{\left[1 + \left|\alpha h\right|^n\right]^{1-1/n}} & h < 0 \\ \theta_s & h \geq 0 \end{cases} \quad (2)$$

$$K(h) = K_s S_e^l \left\{1 - \left[1 - S_e^{n/(n-1)}\right]^{1-1/n}\right\}^2 \quad (3)$$

In order to reduce the number of free parameters, we considered l = 0.5, which is a common assumption regarding this model. The remaining parameters were estimated from laboratory data and by inverse fit.

Atmospheric boundary conditions (BC) were considered at the soil surface, and free drainage BC on the bottom of the soil profile. Daily evaporation and transpiration rates were computed following the Penman-Monteith method (Allen et al., 1998). A modified Feddes root water uptake model (Feddes et al., 1978; Wesseling and Brandyk, 1985) was considered for modeling the influence of the plants The key parameters of the model adopted for the current crop (grass) were: h_1= -10 cm, h_2= -25 cm, $h_{3.1}$= -240 cm, $h_{3.2}$= -360 cm, and h_4= -8000 cm. Root growth was not considered due to the selected species being completely developed at the beginning of the simulation period.

2.3. Tracer Test

A conservative tracer test with a LiBr solution was carried out in order to assess water flow and to estimate dispersivity coefficients for different soil layers. The Br^- tracer application was used due to the low background concentration of Br in the soil profile. On June 27th, 2012, a solution of LiBr (25 L with a LiBr concentration of 131.73 mmol/L) was sprinkled over 10 m^2 of the plot. Undisturbed soil samples were collected (7, 37 and 57 days after injection) at different depths. Subsequently, the total bromine concentration (Br) was determined using X-ray fluorescence, following the methodology proposed by Abderrahim et al. (2011). To simulate Br^- transport in the soil profile, soil hydraulic parameters obtained from the flow model with automatic data were used.

3. Results and Discussion

An important difference between the two monitoring strategies was the amount of collected data. 1489 versus 400 daily values were collected by an automatic and non-automatic monitoring strategy, respectively. Following identical and parallel procedures, θ and h measured values for

both data sets were simulated by means of HYDRUS-1D. Figure 2 shows the observed and simulated values of θ for the automatic and non-automatic equipment at different depths. A good agreement is observed between the experimental and modeled data for both collection strategies. Recorded and simulated h values are shown in Figure 3. Note that automatic sensors properly capture the peak events, while the non-automatic ones present a smoother behavior, which can be a consequence of the acquisition frequency. On the other hand, a greater dispersion of h data is found for the non-automatic acquisition system. Several statistics were calculated for pressure head (h) and volumetric water content (θ) data at all depths observed by both automatic and non-automatic devices. A summary of the results is provided in Table 1.

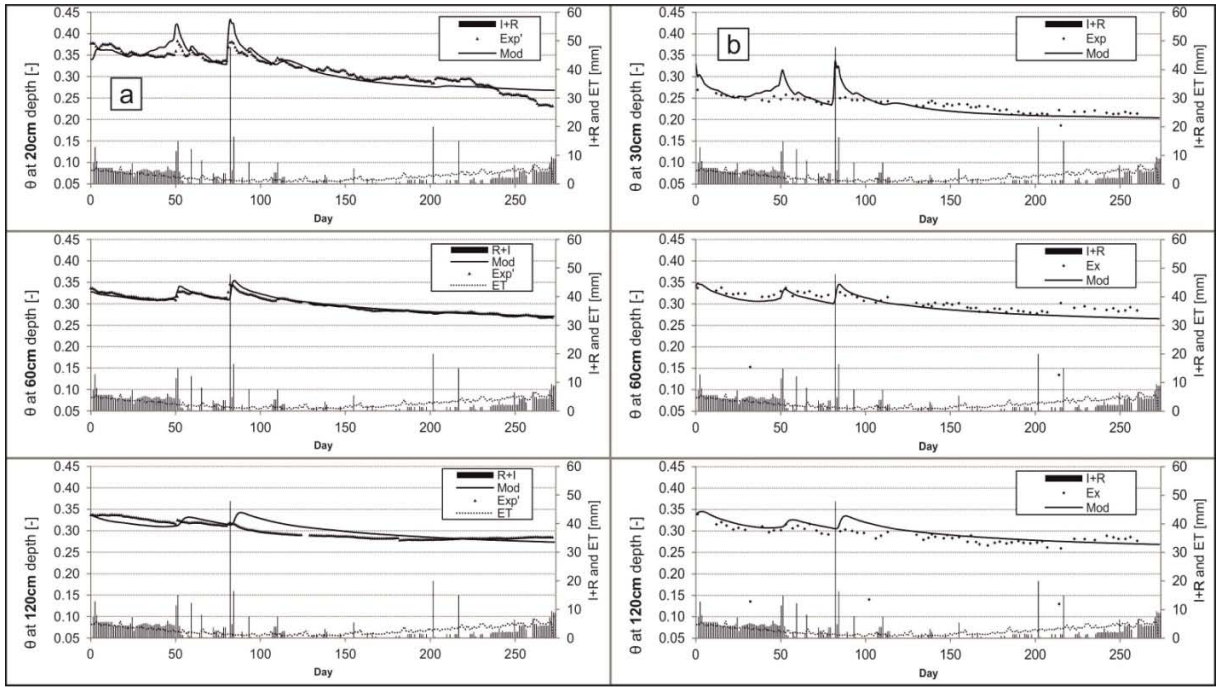

Figure 2. Observed and simulated θ values collected by an automatic (a) and non-automatic (b) monitoring strategy. Water input data (irrigation plus precipitation) is depicted on the secondary vertical axis.

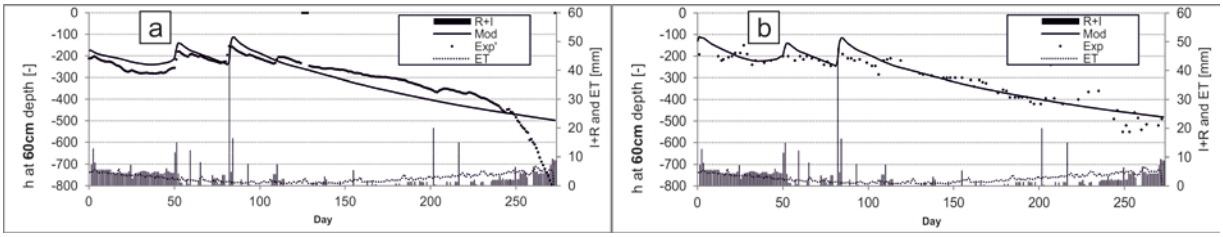

Figure 3. Observed and simulated h values collected by an automatic (a) and non-automatic (b) monitoring strategy. Water input data (irrigation plus precipitation) is depicted on the secondary vertical axis.

Table 1. Goodness of fit measures for simulations and experimental data.

Acquisition	Statistic	Pressure head, h	Volumetric water content, θ						
		60 cm	30 cm	45 cm	60 cm	90 cm	120 cm	All	All (h and θ)
Automatic	*RMSE*	0.21	0.05	0.04	0.02	-	0.05	0.04	
	EF	0.72	0.81	0.74	0.94	-	0.5	0.76	
	R^2								0.96
Non-automatic	*RMSE*	0.16	0.07	0.05	0.10	0.12	0.14	0.10	
	EF	0.80	0.00	0.43	0.24	-0.02	-0.37	0.44	
	R^2								0.98

Despite of good agreement between both simulations and experimental data, computed drainage flux through the bottom boundary was equal to 230 and 196 mm for automatic and non-automatic data acquisitions, respectively. This is a difference of 14.8% between both models, which is an important difference when attempting to assess groundwater recharge from a semi-arid area point of view.

The results of the tracer test performed to assess the flow model and to derivate transport parameters are shown Figure 4. A good agreement between measured and predicted total bromide (Br) concentrations along the soil profile was observed, which validates the flow model.

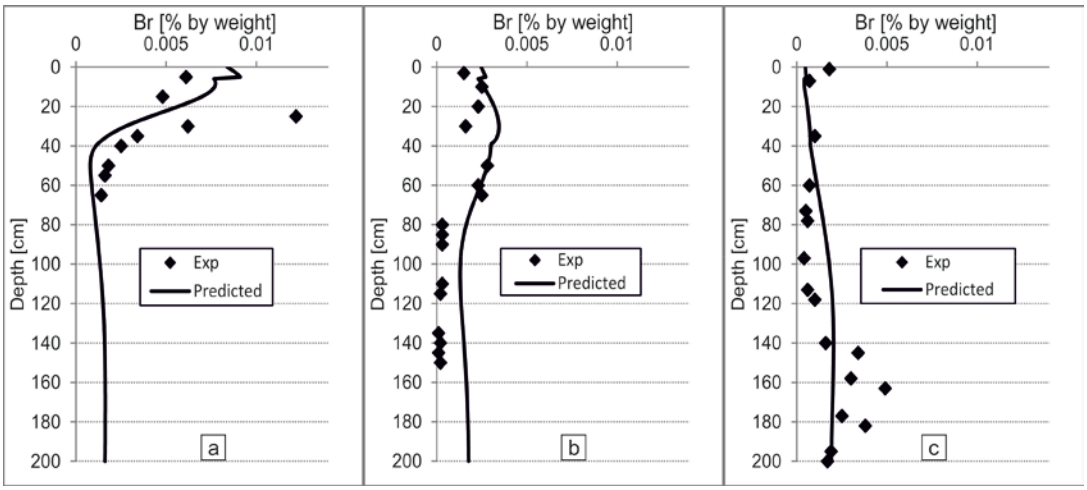

Figure 4. Measured and predicted values of total Br concentrations in soil at 7 (a), 37 (b), and 57 (c) days after the tracer application.

4. Conclusions

The analysis proposed in this study has provided insights into soil and vadose zone monitoring strategies to assess water dynamics and changes in soil hydraulic properties. However, monitoring results for hydraulic parameters were complex, indicating that one of the main limitations is the inability to measure the effective properties representing the overall system.

The instruments used normally explore a domain that is notoriously too small to describe average properties. Field measurements obtained with non-automatic (vertically-installed) instruments need to be carefully analyzed since the installation process can lead to preferential flow along the device walls, even when careful installation procedures are followed. It should be noted that if previously determined information on soil characteristics obtained in the laboratory is not taken into account, unrealistic soil hydraulic parameters can be obtained from simulated values of both automatic and non-automatic data.

The HYDRUS simulations were able to reproduce the behavior of a field-scale plot instrumented with automatic and non-automatic data acquisition systems. A good agreement between the predicted and measured soil water contents and pressure heads was obtained. However, the overall trend was predicted better than extreme episodes, which has been also observed by other researchers. Significant differences between the modeled parameters obtained from the non-automatic and automatic experimental data were observed. On average, the statistical evaluation revealed that fits of the θ data proved better than those of the h data. This fact could be related to the equilibration time required by the pressure head devices to obtain reliable measurements. For the tracer test, a good agreement between measured and predicted total bromine (Br) concentrations in the soil profile was obtained, which validates the flow model.

This work only represents the first step of the study, before the geochemical processes responsible for the expected changes in the soil hydraulic properties as consequence of the use of non-conventional water is analyzed. This purpose will be carried out using the coupled HYDRUS and PHREEQC model HP1.

References

Allen, R. G., L. S. Pereira, D. Raes, and S. Martin, Crop evapotranspiration: guidelines for computing crop water requirements. FAO Irrigation and Drainage Papers, Food and Agriculture Organization of the United Nations, Rome, 1998..

Calderón-Preciado, D., V. Matamoros, and J. M. Bayona, Occurrence and potential crop uptake of emerging contaminants and related compounds in an agricultural irrigation network, *Science of the Total Environment*, *412–413*, 14-19, 2011.

Candela, L., S. Fabregat, A. Josa, J. Suriol, N.Vigués, and J. Mas, Assessment of soil and groundwater impacts by treated urban wastewater reuse. A case study: Application in a golf course (Girona, Spain), *Science of the Total Environment*, *374*(1), 26-35, 2007.

Feddes, R. A., P. J. Kowalik, and H. Zaradny, Simulation of Field Water Use and Crop Yield, Wiley, 1978.

Jiménez-Martínez, J., T. H. Skaggs, M. Th. van Genuchten, and L. Candela, A root zone modelling approach to estimating groundwater recharge from irrigated areas, *Journal of Hydrology*, *367*(1-2), 138-149, 2009.

Kanzari, S., M. Hachicha, R. Bouhlila, and J. Battle-Sales, Characterization and modeling of water movement and salts transfer in a semi-arid region of Tunisia (Bou Hajla, Kairouan) - Salinization risk of soils and aquifers, *Computers and Electronics in Agriculture*, *86*, 34-42, 2012.

Lattemann, S., and T. Höpner, Environmental impact and impact assessment of seawater desalination, *Desalination*, *220*(1-3), 1-15, 2008.

Laurent, J.-P., P. Ruelle, N. Bréda, A. Chanzy, and C. Chevallier, On the use of the TDR TRIME-TUBE system for profiling water content in soils, TDR'01 Evanstons, Illinois, USA, pp. 1-10, 2001.

Laurent, J.-P. P. Ruelle, L. Delage, A. Zaïri, B. B. Nouna, and T. Adjmi, Monitoring soil water content profiles with a commercial TDR system, *Vadose Zone Journal*, *4*(4), 1030-1036, 2005.

Mandal, U. K., A. K. Bhardwaj, D. N. Warrington, D. Goldstein, A. Bar Tal, and G. J. Levy, Changes in soil hydraulic conductivity, runoff, and soil loss due to irrigation with different types of saline-sodic water, *Geoderma*, *144*(3-4), 509-516, 2008.

Mualem, Y., A new model for predicting the hydraulic conductivity of unsaturated porous media, *Water Resources Research*, *12*(3), 513-522, 1976.

Richards, L. A., Capillary conduction of liquids through porous mediums, *Journal of Applied Physics*, *1*(5), 318-333, 1931.

Šimůnek, J., M. Šejna, H. Saito, M. Sakai, and M. Th. van Genuchten, The HYDRUS-1D Software Package for Simulating the Movement of Water, Heat, and Multiple Solutes in Variability Saturated Media, Version 4.08. *HYDRUS Software Series 3*, Department of Environmental Sciences, University of California Riverside, Riverside, California, USA, pp. 315, 2009.

van Genuchten, M. Th., Closed-form equation for predicting the hydraulic conductivity of unsaturated soils, *Soil Science Society of America Journal*, *44*(5), 892-898, 1980.

Varble, J. L., and J. L. Chávez, Performance evaluation and calibration of soil water content and potential sensors for agricultural soils in eastern Colorado, *Agricultural Water Management*, *101*(1), 93-106, 2011.

Wallis, K. J., L. Candela, R. M. Mateos, and K. Tamoh, Simulation of nitrate leaching under potato crops in a Mediterranean area. Influence of frost prevention irrigation on nitrogen transport, *Agricultural Water Management*, *98*(10), 1629-1640, 2011.

Wesseling, J. G., and T. Brandyk, Introduction of the Occurrence of High Groundwater Levels and Surface Water Storage in Computer Program SWATRE, ICW, 1985.

Wollschläger, U., T. Pfaff, and K. Roth, Field-scale apparent hydraulic parameterisation obtained from TDR time series and inverse modelling, *Hydrology and Earth System Sciences*, *13*(10), 1953-1966, 2009.

Simulation of the Heavy Metal Transport in Unsaturated Soils: Use of Scale Factors to Quantify Variable Sorption Isotherms

Han Xiao[1], Jürgen Böttcher[2], and Jiří Šimůnek[3]

[1]*Institute of Soil Science, Leibniz University of Hannover, Hannover, Germany, xiao@ifbk.uni-hannover.de*
[2]*Institute of Soil Science, Leibniz University of Hannover, Hannover, Germany, boettcher@ifbk.uni-hannover.de*
[3]*Department of Environmental Sciences, University of California, Riverside, CA 92521, USA, jiri.simunek@ucr.edu*

Abstract

Heavy metals are toxic soil pollutants that are retarded in soils by sorption at the solid phase. At a small scale (of a soil sample), the sorption process can be observed and quantified using sorption isotherms. However, most environmental problems have to be treated and solved at large scales (e.g., a field scale). At the field scale, heavy metal sorption isotherms are commonly highly variable in space. This spatial variability makes a representative quantification of the sorption process (e.g., for the soil protection or for the management of soil functions) and its consideration in reactive transport modelling (e.g., for groundwater protection) difficult. Many transport simulation studies therefore treat soils as homogeneous to avoid the need for complex datasets and calculations. In this study we used a recently developed method of scale sorption factors to quantify the spatial variability of heavy metal sorption in soils at the field scale. This method reduces the variability of sorption isotherms into a single average relation while preserving their variation through the scale factors. We investigated the spatial variability of heavy metal sorption isotherms for an agricultural field on a Luvisol developed over a loess material near Hannover, Germany. Fifty samples were taken from A and B horizons along a 250-m transect. Sorption isotherms for heavy metals and soil properties, such as pH, CEC, and texture, were measured and scale factors were calculated. The heavy metal transport was simulated with the HYDRUS model using a unique reference sorption isotherm (derived using the scale procedure or mixed soil samples). Spatial variability of sorption at every sampling point was further represented using a scale factor, which was either directly calculated (using a scaling procedure) or indirectly estimated (using regression models with another heavy metal or from soil properties). For comparison, variability of sorption was also simulated using the original, measured Freundlich parameters.

The results show that scale factors are well suited for predicting spatially variable retardation and transport of heavy metals in soil, although a certain reduction of variability is to be expected. In the case of extreme situations, transport simulations with scale factors are not well suited to describe the depth distribution of heavy metal concentrations, especially when using indirectly calculated scale factors.

1. Introduction

Both agricultural (He et al., 2005; Nicholson, 2003) and environmental (Bradl, 2005) sciences treat heavy metals as an important environmental factor because of their negative impact on the ecosystem. Soils are either gradually contaminated by heavy metals due to their long-term depositions, or suddenly due to various industrial leaks or intentional applications of various compounds (e.g., sewage sludge, manure). The fate and transport of heavy metals in soils depends mainly on their reactive properties, with sorption reactions being the most important ones (Alloway, 1995). The soil can then act as a storage container for these contaminants. A lot

of studies reported spatial distributions of heavy metals in the subsurface (Yang, 1989; Camobreco, 1996; Ingwersen et al., 2006). However, much attention has been paid to transport processes in one-dimensional soil columns, without extending the transport into two or three dimensions. Soil spatial heterogeneity, which makes the sorption highly variable, is the main reason for the lack of extending transport studies into higher dimensions.

Sorption processes cause the retardation of heavy metals in soils (Sparks, 2003). Hence, the quantification of sorption isotherms and their spatial variability is a prerequisite to quantify the spatial variability of heavy metal transport in soils. To simulate heavy metal displacement at the field scale, Streck et al. (1997) used a parallel soil column approach. Altfelder et al. (2007) have studied the combination of uncertainty and variability to predict field-scale heavy metal transport. These authors have quantified sorption isotherms through pedotransfer functions (PTF). Deurer and Boettcher (2007) have compared PTF and a scaling method for sorption isotherms (Böttcher, 1997) to upscale the small scale transport variability and concluded that mean sorption behavior derived through scaling resulted in smaller uncertainty of heavy metal transport prognoses.

Scaling was used first in soil hydrology to quantify the variation of water retention (Miller and Miller, 1956, Russo and Bresler, 1980; Raats et al., 2006). Following the basic ideas and rules of scaling (Tillotson and Nielsen, 1984), Böttcher (1997) has developed a method to calculate scale factors for spatially variable sorption isotherms and successfully applied this method to Cd sorption in sandy soil. Furthermore, Böttcher (1997) showed that the scale factors for sorption isotherms were correlated with some soil physicochemical properties. Therefore, indirect calculation of scale factors for sorption from physicochemical soil properties (indirect scaling procedure) seems possible. If so, scale factors may be derived by direct or indirect procedures. This would extend the use of scale factors from statistical description of spatially variable sorption isotherms (direct scaling procedure) to a broadened application in the prediction of reactive transport processes in soil by the indirect scaling procedure.

In this study, scenarios of heavy metal (Cadmium, Zinc and Copper) transport in unsaturated soil using the direct and indirect scaling procedure were simulated with HYDRUS-2D (Šimůnek et al., 2011). The main objective was to prove the performance of the two scaling procedures in simulating spatially variable heavy metal transport compared to simulations with original sorption data.

2. Material and Methods

2.1. Soil Samples

The soil samples (undisturbed and disturbed) were taken from an agricultural field on a Luvisol developed in loess material near Hannover, Germany. 50 samples were taken along a 250 m transect at every five meters from 0 to 30 cm (topsoil) and 30 to 60 cm (subsoil). For each horizon, one mixed sample was made from the 50 soil samples to measure a mean sorption isotherm that is needed as a reference in the indirect scaling procedure (see 2.4.2).

2.2. Laboratory Analyses

The undisturbed soil samples were used to measure the bulk density and water content. The disturbed soil samples were air dried and sieved. Then the samples were used to measure the relevant soil physicochemical properties (Table 1).

Table 1. Soil physicochemical properties used to quantify the scale factors and the measurements method (source: Utermann et al., 2005).

Soil property [Unit]	Method
Texture [%]	Pipette method after Koehn (<63µm) Dry sieving (>63µm) DIN* 19683-2
pH($CaCl_2$) [-]	Potentiometric by use of a glass electrode in 0.001 M $CaCl_2$ DIN ISO^ 10390:1997
Total carbon [%]	C-N-S elementary analysis DIN ISO 10694
Total carbonate [%]	Gas volumetric DIN ISO 10693 (1997)
Total organic carbon (OC) [%]	Difference between Total carbon and total carbonate
Oxalate extractable oxide by Fe, Mn and Al (Fe_{ox}, Mn_{ox}, Al_{ox}) [mg/kg]	Extraction with oxalic acid ammonium oxalate DIN 19684-6 Measure with flame-AAS
Effective cation exchange capacity (CEC_{eff}) [mmol/kg]	Percolation with 0.1 M $BaCl_2$ Modified by DIN 19684-8 Measure of Ca, Mg, K, Na, Fe, Mn and Al with ICP-OES, determination of H^+-ions-concentration from pH-Value

* German Institute for Standardization
^ International Organization for Standardization

Sorption isotherms were measured in a batch experiment. Heavy metal solutions (concentrations range from 0 to 20 mg/L for Cadmium, 75 mg/L for Zinc and 40 mg/L for Copper) were added to the soil water suspensions. A $Ca(NO_3)_2$ electrolyte solution was also added to maintain the natural ionic strength. After 24 h of shaking, the suspensions were centrifuged for 15 minutes. Heavy metal concentrations were then measured in the supernatant by ICP-OES.

2.3. Parameterization of Heavy Metal Sorption Isotherm

From measured sorption data, sorption isotherms were calculated, and the Freundlich equation (Bradl, 2005) was used to describe the isotherms.

$$S = K C^n \tag{1}$$

In the Freundlich equation, S is the sorbed fraction [µg/kg], C is the solution concentration [µg/L], and K and n are parameters, adjusted by fitting the equation to the measured data.

2.4. Scaling of Sorption Isotherms

The scaling rule of sorption isotherms derived by Böttcher (1997) is:

$$C^* = \alpha^2 C_i \quad (2)$$

where C^* is the scaled concentration, C_i is a measured concentration, and α is the scale factor.

2.4.1 Direct Scaling Procedure

In the direct scaling procedure, mean concentrations describing the reference isotherm are first derived as scale means (Böttcher, 1997) from:

$$M_{r,j} = R^2 \left[\sum_{r=1}^{R} \left(\sqrt{C_{r,j}} \right)^{-1} \right]^{-2} \quad (1)$$

Second, scale factors are calculated under the constraint

$$\sum_{r=1}^{R} a_r R^{-1} = 1 \quad (2)$$

by minimization of the sum of squares (in logarithmic space)

$$SS = \sum_{r=1}^{R} \sum_{j=1}^{J} \left(\ln M_{r,j} - 2 \ln a_r - \ln C_{r,j} \right)^2 \quad (3)$$

to obtain α as:

$$\alpha = \exp \left[\left(2 J_r \right)^{-1} \sum_{r=1}^{J_r} \left(\ln M_{r,j} - \ln C_{r,j} \right) \right] \quad (6)$$

In the equations above, r is the number of soil samples (R = maxima) and j is the number of data points on the respective sorption isotherm (J = maxima). C represents the individual measured concentration, and M is the scale mean concentration.

The ratio $(SS_{before}\text{-}SS_{after})/SS_{before}$ is used to quantify the scaling efficiency. More details are given in Böttcher (1997).

2.4.2 Indirect Scaling Procedure

Both scale factors for sorption isotherms and scale factors for soil properties were calculated based on principles outlined in Tillotson and Nielsen (1984). Using correlations between heavy metal sorption and soil properties, an indirect scaling procedure was also developed.

The concept of indirect scaling is based on the assumption that the measured sorption isotherm of mixed samples is comparable with the mean sorption isotherm derived from the direct scaling

procedure, and that scale factors can be calculated from scale factors from soil properties relevant to sorption using multiple linear regression:

$$\alpha_{in} = \alpha^* + a\alpha_{pH} + b\alpha_{clay} + c\alpha_{OC} + ... \quad (7)$$

where α_{in} is the scale factor of indirect scaling and α^* is an intrinsic scale factor, α_{pH}, α_{clay} and α_{OC} are calculated scale factors of soil properties, and *a*, *b*, and *c* are fitting parameters of linear regression.

2.5. Simulation of Heavy Metal Transport with HYDRUS

In unsaturated soil, the water flow is usually vertical. Hence, the simultaneous heavy metal transport is also vertical and can be described by the widely used convection-dispersion equation (CDE) under steady flow conditions (Radcliffe and Šimůnek, 2010).

As sampling was carried out along a transect at every 5 m, the geometry in HYDRUS-2D was set as a rectangle with a length of 250 m and a depth of 0.6 m. The rectangles were divided into 50 columns, each with topsoil and subsoil horizons. Each column has a single set of water flow and solute transport parameters. The infiltration rate was 250 mm per year (Deurer, 2007). The input concentrations were set to 100 for Cd, 8000 for Zn, and 2000 µg/L for Cu. The simulation time was set to 500 years for Cd and Zn and 100 years for Cu.

Three scenarios were set up. Scenario I was simulated using the original measured sorption parameters. In scenario II, the reference isotherms (Table 3) for the soil horizons were used, and the scale factors from the direct scaling procedure were applied to calculate the sorption isotherms for the soil columns. In scenario III, sorption isotherms for the columns were calculated from the isotherm of the mixed soil sample, and the scale factors from the indirect scaling procedure.

3. Results

3.1. Sorption Isotherm Parameters and Physicochemical Soil Properties

Table 2 lists the mean and the coefficient of variation (CV) of the measured soil properties and the Freundlich parameters.

Differences between soil properties in topsoil and subsoil are low. The pH values are high, causing strong heavy metal sorption in topsoil and subsoil. The sorption parameter *K* of Cd and Zn in subsoil is much higher than in topsoil, possibly because of a higher pH in the subsoil, though *n* is more or less the same. *K* and *n* of Cu behave differently, which may be attributed to the higher OC content in the topsoil. Most *CV*s in Tab. 2 are low, except the *CV* of CEC_{eff} and *K*. This finding hints at a correlation between *CEC* and *K*, as already published by others (e.g., Buchter et al., 1989, Springob and Böttcher, 1998).

Table 2. Summary statistics of soil properties and isotherm parameters.

		pH	CEC_{eff}	OC	sand	clay	silt	Fe_{ox}	Al_{ox}	Mn_{ox}	K n (Cd)	K n (Zn)	K n (Cu)
		-	$\frac{mmol}{kg}$	%	%	%	%	$\frac{mg}{kg}$	$\frac{mg}{kg}$	$\frac{mg}{kg}$	[]^	[]	[]
Mean	Topsoil	6.9	96.8	1.18	3.8	11	85	2617	581	356	1407 0.81	7498 0.51	247 1.34
	Subsoil	7.2	72.9	0.31	3.3	12	85	2621	603	228	2271 0.80	13509 0.49	123 1.66
		%	%	%	%	%	%	%	%	%	%	%	%
CV^*	Topsoil	2	40	10	9	1	12	4	4	10	34 7	24 5	34 6
	Subsoil	2	42	17	13	2	10	5	6	17	33 6	17 7	49 9

* *CV* - Coefficient of Variation
^ Units of *K* are [$\mu g^{1-n}L^n/kg$], and units of *n* are [-]

3.2. Reference Isotherm and Scale Factors

A summary of sorption isotherm parameters and scale factors from direct and indirect scaling procedures and their statistics are presented in Table 3. Because the mean of scale factors is always 1 (compare to eq. 4), the range of scale factors with the coefficient of variation is given. *CV*s of scale factors α appear to be lower than *CV*s of *K* in Table 2, and higher than *CV*s of *n* in consideration of residual sum of squares. As shown in Table 3, the scaling efficiencies (derived for direct scaling) are mostly high. This confirms earlier findings of Böttcher (1997) and Deurer and Böttcher (2007), who showed that for sandy soils, successful scaling of sorption isotherms is possible.

Table 3. α and reference isotherms from direct and indirect scaling procedures, and statistical parameters.

Heavy metal	Horizon	Sample size	Direct scaling procedure			Indirect scaling procedure		
			α Range [-] *CV* [%]	R-SI*	*SE*^ %	α_{in} Range [-] *CV* [%]	Adj. R^2	SI_{mixed}#
Cd	topsoil	50	0.67 13	$S=1394C^{0.80}$	85	0.51 10	0.513	$S=1398C^{0.83}$
	subsoil	50	0.87 16	$S=2248C^{0.79}$	92	0.42 13	0.503	$S=2229C^{0.77}$
Zn	topsoil	50	0.71 14	$S=7482C^{0.51}$	88	0.55 11	0.505	$S=8709C^{0.49}$
	subsoil	50	0.81 14	$S=13638C^{0.49}$	75	0.29 7	0.248	$S=15612C^{0.44}$
Cu	topsoil	50	0.23 5	$S=245C^{1.33}$	78	0.13 3	0.443	$S=275C^{1.30}$
	subsoil	50	0.39 10	$S=118C^{1.64}$	89	0.32 8	0.612	$S=161C^{1.59}$

* Reference sorption isotherm, ^ Scaling efficiency, # Sorption isotherm derived from mixed sample

The values of "Adj. R^2" for indirect scale factors are low, indicating only weak correlation between measured soil properties and scale factors. The reasons could be a relatively small sample size and low *CV*s of soil properties, among other things. The reference sorption isotherms of the direct scaling procedure correspond quite well with sorption isotherms of the indirect scaling procedure (measured at mixed soil samples). This demonstrates that scale means are meaningful estimators to upscale soil sorption properties from point measurements to the field scale.

3.3. Evaluation of Heavy Metal Transport

The simulated heavy metal concentrations are shown in Figure 1. The spatial variation of concentration depth distributions along the transect between the different simulation scenarios is basically the same for each heavy metal. However, the extent of transport variability is in the order of Scenario I > II > III. These results indicate that the application of scale factors for sorption isotherms, especially indirect scale factors, causes a certain reduction of the variability of heavy metal retardation in soil, while the typical transport behavior of the metals is maintained.

Unlike Cd and Cu, Zn shows a very good match between model results simulated with the original topsoil sorption data or scale factors, regardless of the scaling procedure. This is very probably due to two reasons. First, Zn topsoil has a scaling efficiency of 88% (Table 3), which is higher than for Cd (85%) and Cu (78%). Second, Zn topsoil has low *CV*s of sorption isotherm parameters *K* (*CV*=24%) and *n* (*CV*=5%). Compared to Cd and Cu, these values are closer to the *CV*s of α and α_{in} (Table 3). Also, Nanos and Martín (2012) found that Zn concentrations in soil are not as spatially variable as Cd and Cu concentrations.

On the other hand, the simulation scenarios for the highly spatially variable heavy metal Cu demonstrate a disadvantage of sorption scale factors. Maximum Cu concentration has already been transported to a depth larger than 60 cm only in column 13 (from the left of the transect, Fig. 1) if simulated with the original sorption data (Scenario I). If simulated with direct scale factors (Scenario II) or indirect scale factors (Scenario III), respectively, Cu in column 13 traveled only slightly deeper or to a rather similar depth, compared to surrounding columns (Fig. 1). The reason for this behavior may be explained by comparing Freundlich parameters *K* and scale factors. The original Freundlich *K* at column 13 is 98.7 $\mu g^{1-n}L^n/kg$. Obviously, Cu retardation at this point (column 13) is relatively low. In contrast, the mean *K* of a directly calculated reference isotherm and *K* of a mixed sample are 244.8 and 274.8 $\mu g^{1-n}L^n/kg$, respectively. I.e., the ratios are 0.4 and 0.36, respectively. But the corresponding squared scale factors α^2 (eq. 2) are 0.82 and 0.91. Thus, using scale factors, a much stronger retardation of Cu is simulated in column 13. This shows that scale factors, and especially scale factors of the applied indirect scaling procedure (uncertain as indicated by low Adj. R^2, Table 3), are not well suited to describe extreme situations at single points in space.

Summarized, the simulated scenarios show that scale factors are well suited for predicting spatially variable retardation and transport of heavy metals in soil, although a certain reduction of variability is to be expected. In the case of extreme situations, transport simulations with scale factors are not well suited to describe the depth distribution of heavy metal concentrations.

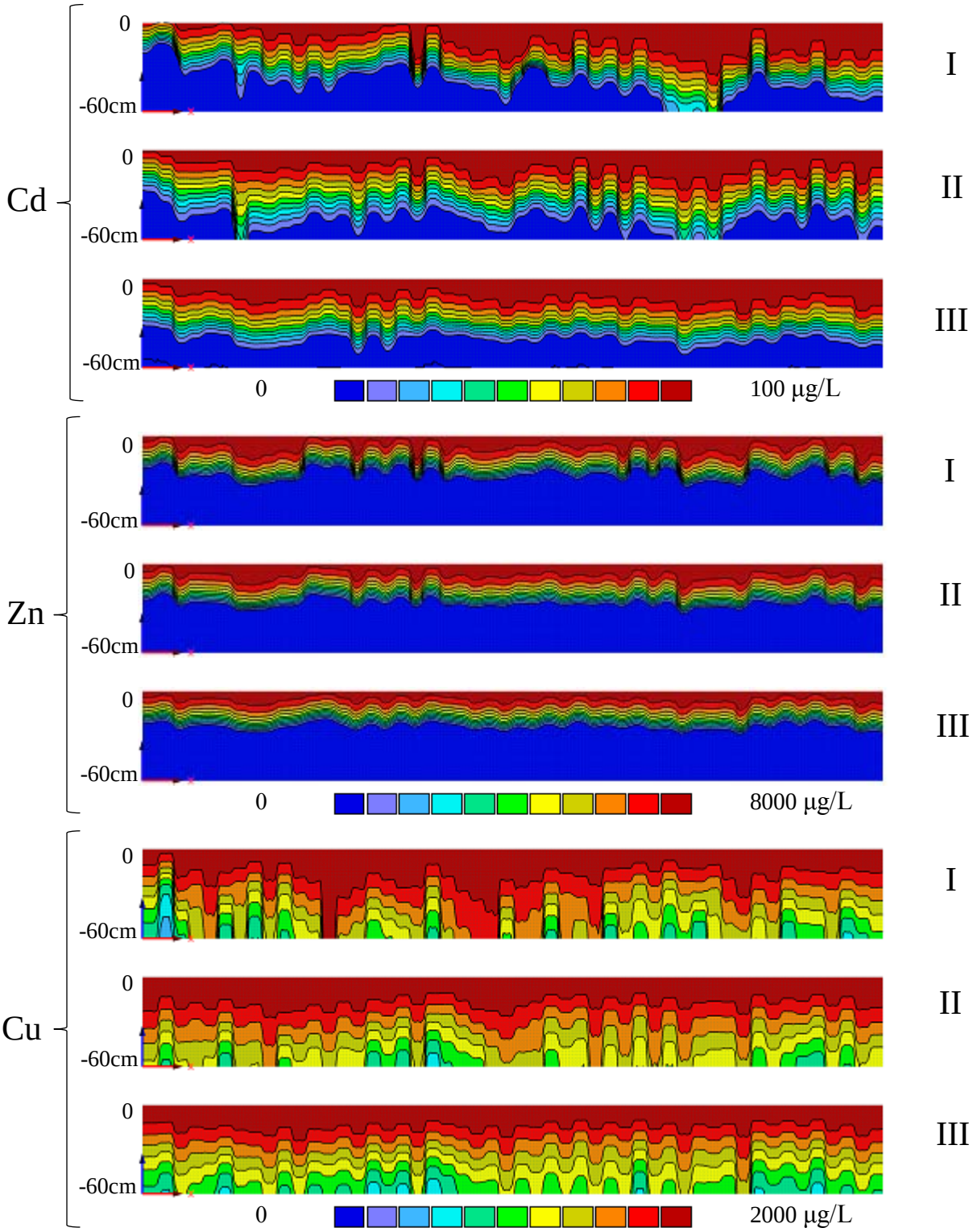

Figure 1. The simulation scenarios of heavy metal transport with I: the original sorption procedure, II: the direct scaling procedure, and III: the indirect scaling procedure.

4. Conclusions

We demonstrated that the calculation of scale factors is a convenient and effective method (due to high scaling efficiency) for deriving the mean sorption isotherm at the field scale. We conclude that scale factors have the potential to describe the spatial variability of heavy metal transport well if the variability of sorption isotherms is not too high, as it is, for example, in the case of Zn. In extreme situations (very week heavy metal sorption) at single points, scale factors may not be sufficiently effective to simulate sorption or retardation. In such a case, the indirect scaling procedure especially fails because of the high uncertainty of the multiple regression. However, in general, the applied indirect scaling procedure tends to even out the variability of heavy metal transport, and thus cannot be recommended as an effective tool for heavy metal transport prediction. Further studies should concentrate on developing an improved indirect scaling procedure, possibly including other sorption relevant soil properties such as a specific soil surface area.

References

Alloway, B. J., *Heavy Metals in Soils*, Blackie, Glasgow, ISBN: 978-94-007-4469-1, pp.18-24, 1995.

Altfelder, S., W. Duijnisveld, T. Streck, G. Meyenburg, and J. Utermann, Quantifying the influence of uncertainty and variability on groundwater risk assessment for trace elements, *Vadose Zone Journal*, *6*, 668-678. 2007.

Böttcher, J., Use of scaling factors to quantify variability of heavy metal sorption isotherms, *European Journal of Soil Science*, *48*, 379–386, 1997.

Bradl, H., *Heavy metals in the Environment: Origin, Interaction and Remediation*, Elsevier. Amsterdam. ISBN: 978-0-12-088381-3, pp. 47-73, 2005.

Buchter, B., B. Davidoff, M. C. Amacher, C. Hinz, I. K. Iskandar, and H. M. Selim, Correlation of Freundlich Kd and n retention parameters with soils and elements, *Soil Science*, *148*, 370-379, 1989.

Camobreco, V., B. Richards, T. Steenhuis, J. Peverly, and M. McBride, Movement of heavy metals through undisturbed and homogenized soil columns, *Soil Science*, *161*, 740-750, 1996.

Deurer, M., and J. Boettcher, Evaluation of models to upscale the small scale variability of Cd sorption in a case study, *Geoderma*, *137*, 269-278, 2007.

He, Z., X. Yang, and P. Stoffella, Trace elements in agroecosystems and impacts on the environment, *Journal of Trace Elements in Medicine and Biology*, *19*,125-140, 2005.

Ingwersen, J., and T. Streck, Modeling the environmental fate of cadmium in a large wastewater irrigation area, *Journal of Environmental Quality*, *35*, 1702-1714, 2006.

Miller, E., and R. Miller, Physical theory for capillary flow phenomena, *Journal of Applied Physics*, *27*, 324-332, 1956.

Nanos, N., and J. Martín, Multiscale analysis of heavy metal contents in soils: Spatial variability in the Duero river basin (Spain), *Geoderma, 189–190*, 554–562, 2012.

Raats, P., and M. Th. van Genuchten, Milestones in soil physics, *Soil Science*, *171*, 21-28, 2006.

Radcliffe, D., and J. Šimůnek, *Soil Physics with HYDRUS: Modeling and Applications*, CRC Press, Taylor & Francis Group, Boca Raton, FL, ISBN: 978-1-4200-7380-5, pp. 373, 2010.

Russo, D., and E. Bresler, Scaling soil hydraulic properties of a heterogeneous field, *Soil Science Society of America Journal*, *44*, 681-684, 1980.

Šimůnek, J., M. Th. van Genuchten, and M. Šejna, The HYDRUS Software Package for Simulating Two- and Three-Dimensional Movement of Water, Heat, and Multiple Solutes in Variably-Saturated Media, Technical Manual, Version 2.0, PC Progress, Prague, Czech Republic, pp. 258, 2011.

Sparks, D. L., *Environmental Soil Chemistry*, Academic Press, San Diego, ISBN: 978-0-12-656446-4, pp. 133-141, 2003.

Springob, G., and J. Böttcher, Parameterization and regionalization of Cd sorption characteristics of sandy soils. II. Regionalization: Freundlich k estimates by pedotransfer functions, *Journal of Plant Nutrition and Soil Science*, *161*, 689-696, 1989.

Streck, T., and J. Richter, Heavy metal displacement in a sandy soil at the field scale. II. Modeling, *Journal of Environmental Quality*, *26*, 56-62. 1997.

Tillotson, P., and D. R. Nielsen, Scale factors in soil science. *Soil Science Society of America Journal*, *48*, 953-959, 1984.

Utermann, J., G. Meyenburg, S. Altfelder, H. Gaebler, W. Duijnisveld, A. Bahr, and T. Streck, *Entwicklung eines Verfahrens zur Quantifizierung von Stoffkonzentrationen im Sickerwasser auf der Grundlage chemischer und physikalischer Pedotransferfunktionen*, BMBF Forschungsvorhaben 02WP0206, pp. 14, 2005.

Yang, C., Transport and transformation of some heavy metals in soil and research of their adsorption mechanism, *Environmental Science* (in Chinese), *3*, 2-8, 1989.

Comparison of HYDRUS-1D Simulations and Ion (Salt) Movement in the Soil Profile Subject to Leaching

Engin Yurtseven[1], Jiří Šimůnek[2], S. Avcı[3], and H. S. Öztürk[4]

[1]*Department of Farm Structures and Irrigation, Faculty of Agriculture, University of Ankara, 06110 Dışkapı, Ankara, Turkey, yurtsev@ankara.edu.tr*
[2]*Department of Environmental Sciences, University of California, Riverside, CA 92521, USA, jiri.simunek@ucr.edu*
[3]*Department of Farm Structures and Irrigation, Faculty of Agriculture, University of Ankara, 06110 Dışkapı, Ankara, Turkey, sertan.avci@gmail.com*
[4]*Department of Soil Science, Faculty of Agriculture, University of Ankara, 06110 Dışkapı, Ankara, Turkey, H.Sabri.Ozturk@agri.ankara.edu.tr*

Abstract

There is an increasing trend to require more efficient use of water resources, both in urban and rural environments. Drainage water can be beneficially reused for agricultural irrigation before being discarded after its use. The quality of the discarded water depends on many factors, including the irrigation water quality and irrigation management, i.e., the salt content and the quantity of irrigation water to be applied during the vegetation period.

A variety of analytical and numerical models have been developed during the past several decades to predict water and solute transfer processes between the soil surface and groundwater table. The HYDRUS-1D software package is one of such models simulating water movement and solute transport in the soil. In this study, we use HYDRUS-1D to analyze water flow and solute transport in soil columns 115 cm long and with a diameter of 40 cm, irrigated with waters of different quality at different leaching rates. Three different irrigation water salinities (0.25, 1.5, and 3.0 dS/m) and four leaching fractions (10, 20, 35, and 50% more water than required) were used in a fully randomized, factorial design experiment. Each experiment was run in three replicates, resulting in a total of 36 lysimeters. Following every irrigation, drainage waters were collected using the plastic pods situated under each lysimeter. Water fluxes, concentrations of individual ions (Na^+, K^+, Ca^{2+}, Mg^{2+}, Cl^-, SO_4^{2-}, CO_3^{2-}, and HCO_3^-), *EC* of the soil solution, and *SAR* were monitored at five depths (20, 40, 60, 80, and 100 cm) in all soil columns. The soil used for the experiments was SCL. In all leaching experiments, the salts accumulated in the profile due to irrigation with salty water could be leached out from the soil. More soluble salts, such as Cl^-, leached more easily than the less soluble salts, such as CO_3^{-2} and HCO_3^-.

The results showed that HYDRUS-1D was able to successfully simulate soil water salinity and movement of salts (ions) in the soil profile. The *RMSE* values for all treatments and for different soil depths varied for EC (dS/m) between 2.50-5.21 and 1.36-4.38 and for *SAR* between 1.26-3.18 and 1.45-1.88 during the first (2010) and second (2011) experimental year, respectively. The *RMSE* values for ions Ca^{2+}, Mg^{2+}, Na^+, K^+, SO_4^{2-}, and Cl^- were between 0.50-24.14 in 2010, and 0.28-14.25 in 2011. HYDRUS-1D proved to be a powerful tool for analyzing solute concentrations related to overall soil salinity.

1. Introduction

Salinization is, due to the presence of various ions in irrigation water, the most widespread problem in irrigated areas with arid and/or semi-arid climate throughout the world. Salinization

generally occurs when salts accumulate in the soil profile, depending on the relationship between irrigation applied by farmers, natural precipitation, evapotranspiration, and leaching. When the concentration of salts exceeds a level harmful to crops, crop yields decrease and fruit quality worsens. It is unavoidable that some salts accumulate in the root zone since all waters used for irrigation inevitably contain soluble ions, concentrations of which depend on the type of water source. The higher the content of salts in irrigation water, the faster the process of soil salinization. Evaporation and transpiration are the predominant mechanisms causing the accumulation of salts in irrigated agricultural soils. Both evaporation and transpiration processes remove water from the soil, while leaving salts behind and increasing their concentrations in remaining soil water (Corwin et al., 2007; Gonçalves et al., 2006). Therefore, the higher the evaporation and/or transpiration rates, the faster the soil salinization. The increase of salinity of water due to evaporation is often called evapoconcentration.

Salinity restrains root water uptake of plants by increasing the osmotic pressure in soil water and thus making it more difficult for plants to extract water from the soil. Some components of salinity may cause specific-ion toxicity and imbalance the nutritional stability of plants. In addition, the salt composition of soil water influences the composition of cations in the exchange complex of soil particles, which may significantly influence soil permeability and tilth (Yurtseven and Sönmez, 1992; Corwin et al., 2007).

Soils not only contain a mixture of salts, but the distribution of these salts is not uniform spatially, nor constant with a soil depth and/or time. Non uniformity within a field is caused in large part by irrigation systems that do not supply water evenly (Hoffman and van Genuchten, 1983). Excessive salts accumulated in soil profiles of irrigated lands can be leached out by adding more water than required to meet the evapotranspiration needs of the crops. The ratio of additional irrigation water, with respect to evaporation and transpiration, is usually expressed as a leaching fraction (*LF*) or a leaching requirement (*LR*), which are identical mathematical expressions, but with different meanings. The *LF* is simply a ratio of the total amount of water passing through the soil profile to the total amount of applied irrigation water. On the other hand, the *LR* is defined as the fraction of infiltrated water that must pass through the root zone to keep soil salinity from exceeding a level that would significantly reduce crop yield under steady-state conditions with associated good management and uniformity of leaching (USSL Staff, 1954; Rhoades, 1974).

Many methods are available to determine the impact of irrigation water quality and existing farm irrigation management in soil salinity. The most precise assessment of salinity is taking soil samples and carrying out laboratory analyses of salinity and its components using several types of laboratory instruments and methods. However, classical methods of evaluating soil salinity are time demanding, expensive, and require a lot of effort, yet cannot completely cover the spatial and temporal variability at the field scale (Rasouli et al., 2012). On the other hand, it is possible to use ground-based geophysical measurements of the apparent soil electrical conductivity (EC_a), such as electrical resistivity (ER) or electromagnetic induction (EM) surveys (Corwin and Lesch, 2003), to assess soil salinity across individual fields. However, even these types of methods are too time-consuming to be applied cost-effectively at larger scales, i.e., at regional scales (Lobel et al., 2010). For this reason, quicker and cheaper methods and tools are required to assess soil salinity for decision-making needs.

Mathematical models that can consider various soil, climate, and crop factors have been suggested as useful tools for evaluating the optimum management strategies for saline conditions (Ramos et al., 2011; Rasouli et al., 2012). A variety of analytical and numerical models have been developed during the past several decades to predict water and solute transfer processes between the soil surface and groundwater table. The HYDRUS-1D software package (Šimůnek et al. 2008) is one of such models simulating water movement and solute transport in the soil. The objective of this study is to use HYDRUS-1D to analyze water flow and solute transport in soil columns irrigated with waters of different quality at different leaching rates, and to assess its applicability for practical applications.

2. Material and Methods

2.1. Experimental Conditions

The experiment was carried out on soil columns 115 cm long and 40 cm diameter constructed from plastic pipes obtained by cutting 6 m long waste-water pipes. The soil columns were installed as outdoor lysimeters at the experimental field of the Agricultural College of Ankara University. The columns were filled with a sieved soil collected from the experimental field of the Agricultural College. The texture of the soil was classified as Silt Clay Loam with 58% sand, 21% silt, and 21% clay. The *CEC* (Cation Exchange Capacity) of the soil was 177.2 $mmol_c\ kg^{-1}$. Each column was equipped with TDR (Soil Moisture, TRACE) probes at four different depths (15, 35, 50, and 75 cm).

Large pots were placed below the bottom of the columns to collect drainage water after each irrigation application. Drainage waters and soil samples collected monthly during the irrigation period were analyzed for salt contents and individual components, i.e., *EC*, *p*H, Na^+, K^+, Ca^{2+}, Mg^{2+}, Cl^-, SO_4^{2-}, CO_3^{2-}, HCO_3^-, NO_2^-, NO_3^-, NH_4^+. Soil samples were taken at five different soil depths (20, 40, 60, 80, and 100 cm). The study was carried out on 36 soil columns using three irrigation water salinities (0.25, 1.5, and 3 dS m^{-1}; denoted below as treatments T_1, T_2, and T_3) with NaCl and $CaCl_2$ salts, four leaching rates (10, 20, 35, and 50% more water than required; denoted below as treatments Y_1, Y_2, Y_3, and Y_4), and three replicates in fully randomized, experimental design.

The soil was first irrigated at the seeding time of alfalfa (i.e., the soil was at the field capacity). Volumes of applied irrigation water and water drained from the bottom of the columns during each irrigation event were measured so that actual evapotranspiration of the crop could be obtained for each treatment. Actual evapotranspiration was calculated from the difference between irrigation and drainage depths. During a given time interval, the water balance is:

$$ET = I + P - D - \Delta S \tag{1}$$

where (all values are cumulative during a particular time interval) *ET* is evapotranspiration (cm), *I* is irrigation (cm), *P* is precipitation (cm), *D* is drainage (cm), and ΔS is the change in stored soil water (cm).

The experiments were conducted in the first year (2010) between May 1st and October 8th and in the second year (2011) between May 1st and October 13th. Irrigation times, amounts of applied and drainage waters, and the soil sampling dates are given in Table 1.

The amounts of irrigation water were calculated for the non-saline treatments and from gravimetrically measured soil water contents and TDR measurements. Total amounts of drainage water were measured during the experiments as well so that leaching fractions (*LF*) could be calculated. Leaching fractions were calculated using the formula below (Ayers and Westcot, 1985):

$$LF = \frac{\text{Drainage Water Amount}}{\text{Irrigation Water Amount}} * 100 \qquad (2)$$

Table 1. Irrigation and drainage water amounts (average of T1 - non-saline treatments), application times, and soil sampling dates for both the first (2010) and second (2011) year experiments.

	1	2	3	4	5	6	7	8	9
2010									
Irrig. time (Julian day)	18	38	49	67	79	96	110	127	143
Irrigation water (L)	12,88	12,88	12,88	25,25	25,25	30,9	30,9	30,9	30,9
Drainage water (L)	2,07	1,63	1,63	5,49	4,52	7,3	5,91	5,51	1,76
Soil sampling	June 1	July 2	Aug 2	Sept 1	Oct 4				
2011									
Irrig. time (Julian day)	67	86	100	117	131	149			
Irrigation water (L)	28,33	28,33	30,9	30,9	25,75	25,75			
Drainage water (L)	5,00	4,85	5,09	4,88	4,64	4,30			
Soil sampling	June 27	July 28	Aug 30	Sept 30					

2.2. Model Description

The HYDRUS-1D program numerically solves the Richards equation for variably-saturated water flow and the convection-dispersion equation for heat and solute transport. The flow equation incorporates a sink term to account for water uptake by plant roots. The heat transport equation considers transport due to conduction and convection with flowing water. The solute transport equations consider convective-dispersive transport in the liquid phase, as well as diffusion in the gaseous phase. The transport equations also include provisions for nonlinear and non-equilibrium reactions between the solid and liquid phases, linear equilibrium reactions between the liquid and gaseous phases, zero-order production, and two first-order degradation reactions: one which is independent of other solutes, and one which provides the coupling between solutes involved in sequential, first-order decay reactions. In addition, physical non-equilibrium solute transport can be accounted for by assuming a two-region, dual-porosity type formulation which partitions the liquid phase into mobile and immobile regions. Attachment/detachment theory, including the filtration theory, is included to simulate transport of viruses, colloids, and/or bacteria.

The program may be used to analyze water and solute movement in unsaturated, partially saturated, or fully saturated porous media. The soil profile itself may be composed of different

soil layers. The water flow part of the model can deal with prescribed head and flux boundaries, boundaries controlled by atmospheric conditions, and free drainage boundary conditions.

The UnsatChem module (Šimůnek and Suarez, 1994) of the HYDRUS-1D software package (Šimůnek et al., 2008), simulating the major ion chemistry/transport and carbon dioxide transport, is used in this study.

2.3. Statistical Analysis

In addition to a visual check, field measured values were compared with the results of the HYDRUS-1D simulations using the mean absolute error (*MAE*), the root mean square error (*RMSE*), and the relative error (*RE*). Which are defined as follows;

$$MAE = \frac{1}{N}\sum_{i=1}^{N}\left|O_i - P_i\right| \tag{3}$$

$$RMSE = \sqrt{\frac{\sum_{i=1}^{N}\left|O_i - P_i\right|}{N-1}} \tag{4}$$

$$RE = \frac{RMSE}{Obs_{avg}} \tag{5}$$

where O_i and P_i are observed and model-predicted values in units of a particular variable, N is the number of observations, and Obs_{avg} is the mean observed value. In general, $RMSE \geq MAE$. The degree to which the *RMSE* value exceeds *MAE* is usually a good indicator of the presence and extent of outliers, or the variance of the differences between the modeled and observed values (Legates and McCabe, 1999; Kobayashi and Salam, 2000). *RE* was used to evaluate the quality of the *RMSE* value. The simulation is considered to be excellent when a relative error is less than 10%, good if it is greater than 10% and less than 20%, fair if it is greater than 20% and less than 30%, and poor if it is greater than 30% (Loague and Green, 1991).

3. Results and Discussion

The HYDRUS-1D simulations were carried out for two experimental years of 2010 and 2011. A simulation time period started on May 1st of both 2010 and 2011 and ended on October 8th and 13th, 2010 and 2011, respectively, which corresponded to the irrigation period of alfalfa in relation with the climatological factors. Nine and six irrigations were applied during the first and second year, respectively. The leaching fractions, calculated (Eq. 2) using the ratio between irrigation and drainage water amounts, were 12, 17, 20, and 22 % in 2010, and 8, 16, 23, and 28 % in 2011, experimental years for Y_1, Y_2, Y_3, and Y_4 treatments, respectively.

The main physical and chemical parameters of the soil are given in Table 2. The solution concentrations of irrigation waters are given in Table 3.

The soil was sandy clay loam (SCL) with a water holding capacity of 74.4 mm m^{-1}, and a bulk soil density of 1.31 g cm^{-3}. At the beginning of the experiment, *p*H and the *EC* of the saturation extract were 8.18 and 0.816 dS cm^{-1}, respectively. *CEC* and exchangeable cations were measured in the laboratory on soil samples. *CEC* was 177.15 $mmol_c kg^{-1}$, and the exchangeable cations were Ca^{2+}=125.85, Mg^{2+}=41.35, Na^{+}=4.85, and K^{+}=4 $mmol_c kg^{-1}$. Actual crop *ET* and the total annual rainfall were 1595.7 and 136.7 mm in 2010, respectively, and 1124.1 mm and 189.4 mm in 2011, respectively.

Table 2. Physical and chemical soil characteristics (initial conditions).

Sand (%)	58	*SAR* ($(mmol_c L^{-1})^{0.5}$)	0.78
Silt (%)	21	Soil hydraulic parameters	
Clay (%)	21	K_s (cm day^{-1})	31.44
Texture	SCL	α (cm^{-1})	0.059
Bulk density (g cm^{-3})	1.31	n	1.48
EC (dS m^{-1})	0.816	θ_r	0.1
Soluble cations ($mmol_c L^{-1}$)		θ_s	0.39
Ca^{2+}	4.9	Exc. cations ($mmol_c kg^{-1}$)	
Mg^{2+}	2.265	Ca^{2+}	125.85
Na^{+}	1.48	Mg^{2+}	41.35
K^{+}	0.275	Na^{+}	4.85
Alk	4.595	K^{+}	4
SO_4^{2-}	3.045	*CEC* ($mmol_c kg^{-1}$)	177.15
Cl^{-}	1.28	Actual average *ET* (cm day^{-1})	0.985 (2010), 0.667 (2011)
		Total rainfall (cm)	13.67 (2010), 18.94 (2011)

Table 3. Ion contents of irrigation waters used in the experiments ($mmol_c L^{-1}$).

	Ca^{2+}	Mg^{2+}	Na^{+}	K^{+}	Alk	SO_4^{2-}	Cl^{-}	Tracer
Water 1 (T_1)	0.7	1.14	0.43	0.07	1.6	0.24	0.50	0
Water 2 (T_2)	13.24	0.56	1.94	0.04	1.9	0.35	13.08	0
Water 3 (T_3)	26.12	0.57	3.56	0.05	1.9	0.37	27.74	0

Simulation results were evaluated against measured data using several statistical measures (eqs. 3, 4, and 5), providing information about how well the model approximated collected experimental data. The results of the statistical analysis are given in Table 4. The statistical measures are given for each depth (20, 40, 60, 80, and 100 cm), as well as for the entire soil profile, as an average over the entire experimental year (2010 and 2011).

In general, the *MAE* and *RMSE* values increased and *RE* values decreased with the increasing soil depth. Also, almost in all experiments, the soil salt and ion concentrations increased with depth. As an example, the measured and simulated values of the soil Cl^{-} and *EC*, with depths of the soil profile for both years and for the T_2Y_4 and T_3Y_4 treatments, are shown in Figure 1.

Table 4. Results of the statistical analysis.

	2010					
Depth	**0**	**20**	**40**	**60**	**80**	**100**
	***EC* (dS m^{-1})**					
MAE	1.75	3.01	2.33	2.65	3.48	4.61
RMSE	2.50	4.07	2.76	3.24	3.93	5.21
RE	1.58	0.85	0.72	0.73	0.75	0.82
MAE	2.67					
RMSE	3.73					
RE	0.85					
	SAR					
MAE	0.94	1.72	1.46	1.47	2.33	2.60
RMSE	1.26	2.15	1.72	1.80	2.66	3.18
RE	1.74	0.60	0.44	0.42	0.49	0.56
MAE	1.75					
RMSE	2.22					
RE	0.56					
	Ca^{2+}					
MAE	10.90	15.11	11.46	12.08	12.67	14.62
RMSE	17.18	19.00	13.67	14.30	14.95	17.39
RE	1.29	0.90	0.87	0.78	0.75	0.77
MAE	12.82					
RMSE	16.20					
RE	0.88					
	Mg^{2+}					
MAE	1.97	8.60	6.74	8.06	9.49	11.65
RMSE	2.49	12.24	8.18	9.43	10.58	13.03
RE	3.29	1.14	0.93	0.95	0.95	0.97
MAE	7.74					
RMSE	9.94					
RE	1.09					
	Na^{+}					
MAE	3.00	10.67	9.16	10.93	16.09	19.51
RMSE	3.89	15.03	11.09	12.60	17.60	22.63
RE	1.97	0.98	0.79	0.78	0.82	0.91
MAE	11.56					
RMSE	14.97					
RE	0.96					
	SO_4^{2-}					
MAE	0.87	13.92	8.83	11.25	15.85	20.95
RMSE	1.10	24.09	12.42	15.55	19.77	24.14
RE	3.42	1.62	1.27	1.26	1.15	1.08
MAE	11.95					
RMSE	18.03					
RE	1.41					
	Cl^{-}					
MAE	15.54	12.87	10.20	7.03	8.25	11.79
RMSE	23.03	18.95	15.41	9.85	12.89	18.72
RE	1.67	1.16	1.20	0.66	0.70	0.79
MAE	10.95					
RMSE	17.03					
RE	1.02					

	2011					
Depth	**0**	**20**	**40**	**60**	**80**	**100**
	***EC* (dS m^{-1})**					
MAE	0.96	1.45	1.72	1.77	2.77	3.61
RMSE	1.36	1.64	2.04	1.99	3.35	4.38
RE	0.86	0.55	0.68	0.61	0.73	0.80
MAE	2.05					
RMSE	2.68					
RE	0.77					
	SAR					
MAE	1.03	1.36	1.35	1.54	1.24	1.30
RMSE	1.54	1.65	1.65	1.88	1.45	1.58
RE	2.12	1.02	0.83	0.90	0.47	0.46
MAE	1.30					
RMSE	1.63					
RE	0.76					
	Ca^{2+}					
MAE	7.35	8.38	9.34	9.52	8.06	8.19
RMSE	10.83	10.88	12.85	11.67	12.32	10.91
RE	0.81	0.68	1.02	0.82	0.85	0.70
MAE	8.47					
RMSE	11.60					
RE	0.81					
	Mg^{2+}					
MAE	0.93	2.62	3.20	4.35	5.40	5.60
RMSE	1.26	3.46	3.71	5.05	6.36	6.90
RE	1.66	0.93	0.85	0.85	0.90	0.96
MAE	3.68					
RMSE	4.85					
RE	1.00					
	Na^{+}					
MAE	1.33	2.39	2.11	2.91	4.71	6.30
RMSE	1.77	2.79	2.87	3.88	6.30	8.11
RE	0.89	0.55	0.50	0.57	0.64	0.72
MAE	3.29					
RMSE	4.82					
RE	0.71					
	SO_4^{2-}					
MAE	0.93	3.24	3.26	3.56	4.77	5.15
RMSE	1.60	4.25	4.71	4.65	9.52	6.85
RE	4.99	1.07	1.10	1.06	1.58	1.09
MAE	3.49					
RMSE	5.80					
RE	1.38					
	Cl^{-}					
MAE	9.09	6.91	9.60	8.67	7.99	8.53
RMSE	13.15	9.19	14.25	11.81	10.37	12.65
RE	0.95	0.56	1.00	0.69	0.52	0.59
MAE	8.47					
RMSE	12.02					
RE	0.70					

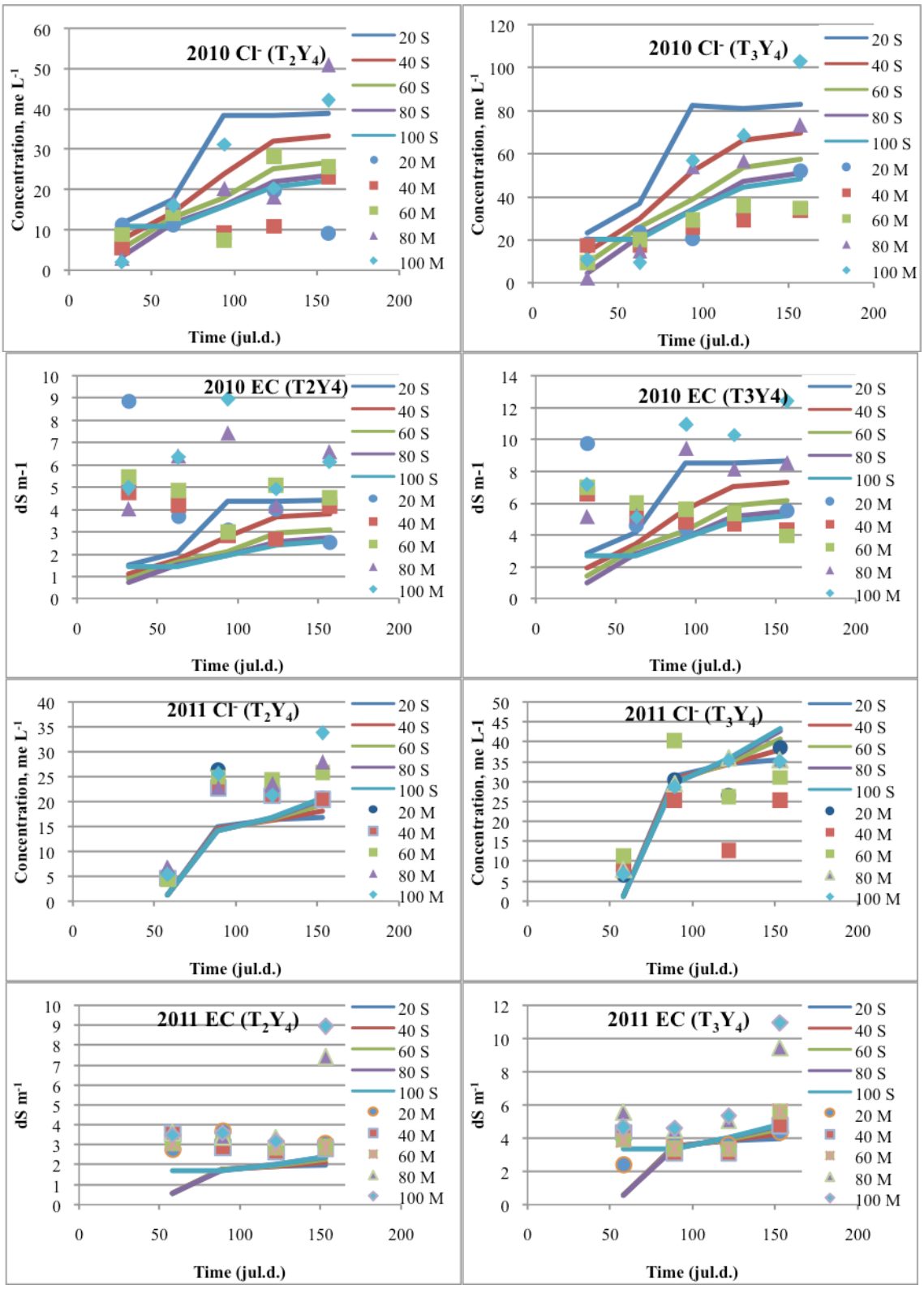

Figure 1. Measured (M) and simulated (S) Cl and soil *EC* values for both experimental years (2010 an 2011) and for the T_2Y_4 and T_3Y_4 treatments.

The *RMSE* values for all treatments and for different soil depths varied for *EC* (dS m^{-1}) between 2.50-5.21 and 1.36-4.38 and for *SAR* between 1.26-3.18 and 1.45-1.88 during the first (2010) and second (2011) experimental year, respectively. The *RMSE* values for ions Ca^{2+}, Mg^{2+}, Na^{+}, SO_4^{2-}, and Cl^{-} were between 0.50-24.14 in 2010, and 0.28-14.25 in 2011.

4. Conclusions

The results showed that HYDRUS-1D was able to successfully simulate soil water salinity and movement of salts (ions) in the soil profile. The model described better scenarios with lower values of salt concentrations (*EC*). Similar results were obtained for individual ion concentrations. The same results were reported by other researchers (e.g., Gonçalves et al., 2006; Ramos et al., 2011). HYDRUS-1D proved to be a powerful tool for analyzing solute concentrations related to overall soil salinity.

References

Ayers, R., and D. Westcot, Water quality for agriculture, *FAO Irrig. Drain. Pap., 29*, Rome, Italy, 1985.

Corwin, D. L., and S. M. Lesch, Application of soil electrical conductivity to precision agriculture: theory, principles, and guidelines, *Agron. J.*, *95*, 455–471, 2003.

Corwin, D. L., J. D. Rhoades, and J. Šimůnek, Leaching requirement for soil salinity control: Steady-state versus transient models, *Agric. Water Management*, *90*, 165-180, 2007.

Gonçalves, M. C., J. Šimůnek, T. B. Ramos, J. C. Martins, M. J. Neves, and F. P. Pires, Multicomponent solute transport in soil lysimeters irrigated with waters of different quality, *Water Resour. Res.*, *42*, W08401, doi:10.1029/2005WR004802, 2006.

Hoffman, G. J., and M. Th. van Genuchten, Soil properties and efficient water use: Water management for salinity control, Chapter 2C, in: Limitations to efficient water use in crop production, ASA-CSSA-SSSA, p.73-85, USA, 1983.

Kobayashi, K., and M. U. Salam, Comparing simulated and measured values using mean squared deviation and its components, *Agron. J.*, *92*, 345–352, 2000.

Legates, D. R., and G. J. McCabe Jr., Evaluating the use of ''goodness-of-fit'' measures in hydrologic and hydroclimatic model validation, *Water Resour. Res.*, *35*, 233–241, 1999.

Loague, K., R. E. Green, Statistical and graphical methods for evaluating solute transport models: overview and application, *J. Contam. Hydrol.*, *7*, 51–73, 1991.

Lobell, D. B., S. M. Lesch, and D. L. Corwin, Regional-scale assessment of soil salinity in the Red river valley using multi-year MODIS EVI and NDVI, *J. Environ. Qual.*, *39*, 35–41, 2010.

McNeal, B. L., J. D. Oster, and J. T. Hatcher, Calculation of electrical conductivity from solution composition data as an aid to in-situ estimation of soil salinity, *Soil Sci.*, *110*, 405–414, 1970.

Ramos, T. B., J. Šimůnek, M. C. Gonçalves, J. C. Martins, A. Prazeres, N. L. Castanheira, and L. S. Pereira, Field evaluation of a multicomponent solute transport model in soils irrigated with saline waters, *J. Hydrol.*, *407*(1–4), 29–144, 2011.

Rasouli, F., A. K. Pouya, and J. Šimůnek, Modeling the effects of saline water use in wheat-cultivated lands using the UNSATCHEM model, *Irrig.Sci.*, doi 10.1007/s00271-012-0383-8, 2012.

Rhoades, J. D., Drainage for salinity control, In: van Schilfgaarde, J. (Ed.), Drainage for Agriculture, *Agronomy Monographs No. 17*, SSSA, Madison, WI, pp. 433-461, 1974.

Šimůnek, J., and D. L. Suarez, Two-dimensional transport model for variably saturated porous media with major ion chemistry, *Water Resour. Res.*, *30*, 1115-1133, 1994.

Šimůnek, J., M. Th. van Genuchten, and M. Šejna, Development and applications of the HYDRUS and STANMOD software packages, and related codes, *Vadose Zone J.*, *7*, 587-600, 2008.

Šimůnek, J., and J. W. Hopmans, Modeling compensated root water and nutrient uptake, *Ecol. Model*., *220*, 505–521, 2009.

van Genuchten, M. Th., A closed form equation for predicting the hydraulic conductivity of unsaturated soils, *Soil Sci. Soc. Am. J.*, *44*, 892–898, 1980.

Yurtseven, E., and B. Sönmez, Sulama sularının değerlendirilmesi, Tarım ve Köy İşl.Bk., KHGM, *Toprak ve Gübre Araşt. Enst. Md. Yayınları No.181/T-63*, 62s., Ankara, 1992.

U.S. Salinity Laboratory Staff, Diagnosis and Improvement of Saline and Alkali Soils, U.S. Dept. Agriculture, *Handbook 60*, U.S. Government Printing Office, Washington DC, p.160, 1954.

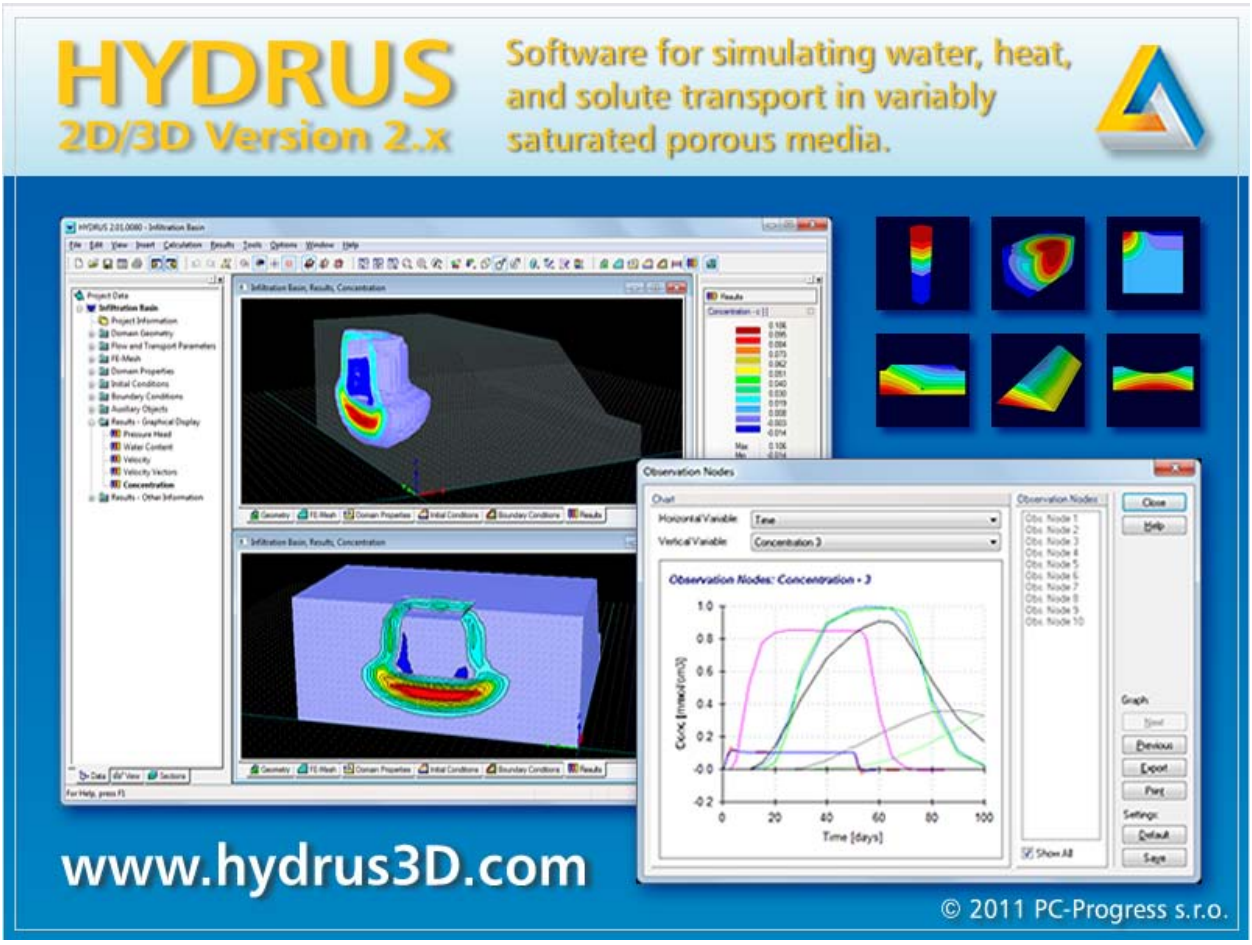

Proceedings of the 4th International Conference HYDRUS Software Applications to Subsurface Flow and Contaminant Transport Problems
Edited by J. Šimůnek, M. Th van Genuchten, and R. Kodešová
Czech University of Life Sciences Prague
Faculty of Agrobiology, Food and Natural Resources
Department of Soil Science and Soil Protection
Czech Republic
CD Proceedings
50
404 pages
First Printing
2013
ISBN: 978-80-213-2380-3